

ADVANCES IN
CHEMICAL ENGINEERING



VOLUME 17

ADVANCES IN CHEMICAL ENGINEERING

Volume 17

This Page Intentionally Left Blank

ADVANCES IN CHEMICAL ENGINEERING

Editor-in-Chief

JAMES WEI

*School of Engineering
Princeton University
Princeton, New Jersey*

Editors

JOHN L. ANDERSON

*Department of Chemical Engineering
Carnegie-Mellon University
Pittsburgh, Pennsylvania*

KENNETH B. BISCHOFF

*Department of Chemical Engineering
University of Delaware
Newark, Delaware*

JOHN H. SEINFELD

*Department of Chemical Engineering
California Institute of Technology
Pasadena, California*

Volume 17



ACADEMIC PRESS, INC.

Harcourt Brace Jovanovich, Publishers

**Boston San Diego New York
London Sydney Tokyo Toronto**

THIS BOOK IS PRINTED ON ACID-FREE PAPER. ♻

COPYRIGHT © 1992 BY ACADEMIC PRESS, INC.

ALL RIGHTS RESERVED.

NO PART OF THIS PUBLICATION MAY BE REPRODUCED OR
TRANSMITTED IN ANY FORM OR BY ANY MEANS, ELECTRONIC
OR MECHANICAL, INCLUDING PHOTOCOPY, RECORDING, OR
ANY INFORMATION STORAGE AND RETRIEVAL SYSTEM, WITHOUT
PERMISSION IN WRITING FROM THE PUBLISHER.

ACADEMIC PRESS, INC.

1250 Sixth Avenue, San Diego, CA 92101

United Kingdom Edition published by

ACADEMIC PRESS LIMITED

24–28 Oval Road, London NW1 7DX

LIBRARY OF CONGRESS CATALOG CARD NUMBER: 56-6600

ISBN 0-12-008517-8

PRINTED IN THE UNITED STATES OF AMERICA

91 92 93 94 9 8 7 6 5 4 3 2 1

CONTENTS

PREFACE	vii
-------------------	-----

Design Parameters for Mechanically Agitated Reactors

Y. T. SHAH

I. Introduction	1
II. Gas-Liquid Reactors.	10
II. Slurry Reactors.	32
IV. Catalytic Reactors.	68
V. Liquid-Liquid Reactors.	84
VI. Biological Reactors	110
VII. Polymerization Reactors	141
VIII. Special-Purpose Reactors	161
IX. Experimental Methods for Parameter Estimations.	169
Nonmenclature.	192
Greek Letters	195
Subscripts.	195
Superscript	196
References	196

Particulate Fluidization: An Overview

MOOSON KWAK

I. The Fluidized State	207
II. Idealization of the Fluidizing Process: Empirical Deductions from L/S Systems	216
III. Generalized Fluidization	223
IV. Fluidized Leaching and Washing.	238
V. Solids Mixing and Segregation	254
VI. Conical Fluidized Beds	264
VII. Application of the Moving Bed	275
VIII. Systems with Dilute Raining Particles	292
IX. Extension of Idealized Fluidization to G/S Systems	313
X. Powder Classification.	324
XI. Future Prospects	347
Notation	349
References	351
INDEX	361

This Page Intentionally Left Blank

PREFACE

The Frontier or Amundson Report of the National Research Council divided chemical engineering problems into three scales: the microscale of molecular dimensions, the mesoscale of equipment dimensions, and the macroscale of entire engineering systems. Electronics and optoelectronics engineers also classify their problems in three levels of organization: materials, devices, and systems/networks. Mesoscale activities such as unit operations and reaction engineering have been strongholds for chemical engineering from the beginning. In recent years, however, studies in the other two scales have been increasing in creativity and effectiveness.

Volume 17 of *Advances in Chemical Engineering* has two extensive chapters on the mesoscale, returning to this theme of historic and continuing importance. The chapter by Shah contains a comprehensive review of the subject of mechanical agitated reactors, which are important in a very large range of industries from large scale chemical manufacturing to small scale biotechnology. The chapter by Kwauk is an overview of particulate fluidization, which draws a great deal from the pioneering work of the author. These two chapters will provide the starting point for any chemical engineer who is seriously concerned with understanding or utilizing these two technologies.

James Wei

This Page Intentionally Left Blank

DESIGN PARAMETERS FOR MECHANICALLY AGITATED REACTORS

Y. T. Shah

**College of Engineering and Applied Sciences
The University of Tulsa
Tulsa, Oklahoma**

I. Introduction

A chemical reactor is a vessel in which reactants are converted to products through chemical reactions. This vessel takes many shapes and sizes depending upon the nature of the chemical reaction. The choice of a suitable laboratory reactor depends upon the nature of the reaction system (fluid–solid catalytic, fluid–solid noncatalytic, fluid–fluid, etc.), the nature of the required kinetic or thermodynamic data, or the feasibility of operation. The important parameters for a successful reactor design are the following:

- (1) construction difficulty and cost;
- (2) reliable sampling and analysis of products;
- (3) isothermality;
- (4) start-up and shut-down upsets;
- (5) accurate residence-contact time measurements;
- (6) roles of interphase mass and heat transfer, as well as intraparticle mass and heat transfer for fluid–solid systems;
- (7) selectivity time-averaging disguise; and
- (8) safety.

It is important to note that there is no global optimum reactor design that fits all purposes. There are always some trade-offs, and they should be evaluated on a case-by-case basis. Novel reactor designs have been constantly introduced to satisfy specific needs, some of which are outlined here.

One of the most widely used reactors is the mechanically agitated reactor. In this monograph, we examine the design parameters of various types of mechanically agitated reactors. These types of reactors are very popular because they offer the most flexibility in operation. They can be operated in

batch, semi-batch, or continuous modes. In multiphase systems, they provide the most flexibility in the mixing conditions in each phase. They can be conveniently used to measure intrinsic kinetics of catalytic and noncatalytic reactions. Compared to fixed-bed operation, they provide a higher space-time yield, because of smaller transport resistances under comparable conditions. They provide isothermal conditions, good temperature stability, simple heat recovery, and protection against the formation of hot spots in the reaction volume. They also provide the possibility of continuous catalyst regeneration without any interruption of production.

The mechanically agitated reactors, however, also require high energy consumption and stagewise operation to get a high degree of conversion and/or selectivity in continuous operation. They can also cause unwanted particle attrition and undesired homogeneous side reactions in catalytic operations. Stirring devices are subject to mechanical and sealing difficulties (mainly in pressurized operations) and may have high maintenance costs. In order to prevent gas leakage, the stirrer is often introduced at the bottom of the high-pressure mechanically agitated reactors.

We examine here various types of mechanically agitated reactors used in chemical, biochemical, polymer, and other industries. Both conventional and novel reactors are discussed. The reactors are divided in sections covering gas-liquid reactors, slurry reactors, catalytic (gas-solid or gas-liquid-solid) reactors other than slurry reactors, liquid-liquid reactors, and novel reactor applications in biological, polymer, electrochemical, photochemical, and chemical vapor deposition industries. Finally, experimental methods for design parameter estimations are evaluated. The major aim of the monograph is to evaluate the design parameters of various types of conventional and novel mechanically agitated reactors currently in use. Wherever necessary, strategies and the descriptions on the use of novel agitated reactors are also briefly outlined.

Finally, it should be noted here that the major purpose of mechanical agitation in a chemical reactor is to provide mixing. In recent years, attempts have been made to minimize mixing energy cost by replacing or supplementing traditional mechanical agitation with pneumatic (compressors) and hydrodynamic (pumps) energy inputs (Faust and Sittig, 1980). Some examples of the latter two types of reactor are air-lift loop reactors, pressure-cycle reactors, bubble-column pumped circuits, jet-propelled loop reactors, etc. These and other similar reactors carry a common feature of a recycle loop (most often external, but sometimes internal). While the recycling provides additional mixing just like mechanical agitation, it has some additional important effects (such as increased residence time, increased reactor phase holdup of recycling fluid, etc.) on the reactor performance. As such, the recycle

reactors form a different class of reactors, and they will not be evaluated in this monograph.

A. CONVENTIONAL AGITATED VESSELS AND INTERNALS

Although, as shown in this monograph, mechanical agitation is provided in a number of different ways, the most common method is by a stirrer in a standard vessel. In many mechanically agitated reactors, the vessel contains internals such as baffles (particularly for low-viscosity fluids), feed and drain pipes, heat transfer coils, and probes (e.g., thermometers or thermocouples, pressure transducers, level indicators). The degree of mixing and power requirement depend on the nature of the internals present in the vessel.

For an axially positioned stirrer in a vessel without internals, agitation causes rotational motion of the liquid and the formation of a vortex. At some critical stirrer speed, the vortex can reach the stirrer and cause gas entrainment in the liquid. This is generally undesirable because it results in a very high mechanical stress on the stirrer shaft, bearings, and seal. For a two-phase system with different phase densities, the centrifugal force produced in the vortex opposes the stirring motion, resulting in inefficient mixing.

For low-viscosity liquids, bulk rotation of the liquid can be reduced with the use of vessels having a rectangular cross-section, with the lateral insertion of the stirrer into the vessel, and with the use of baffles. When the stirring is weak, bulk rotation in cylindrical vessel can also be prevented by installing the stirrer off-center and/or at an angle to the axis, configurations resulting in an uneven mechanical stress on the stirrer shaft.

In cylindrical vessels, the bulk rotation of the liquid is generally prevented by the installation of baffles, which are usually attached to the vessel wall by means of welded brackets (see Fig. 1a). When this is not possible, they are either attached to the cover (e.g., in enamel-coated vessels) or are made in the form of a basket with pressure-fitted rings, as shown in Fig. 1b (e.g., glass vessels, wooden vats, etc.). Generally, fully effective baffling in a cylindrical vessel is achieved with four vertical baffles of width $d_T/10$. However, in recent years novel approaches (e.g., horizontal baffles) have been investigated. The dead volume behind the baffles is reduced by using baffles of width $d_T/12$ at a small clearance of $d_T/50$ from the wall.

The heat transfer (cooling or heating) in a stirred vessel is achieved in a number of different ways. The most conventional method is the use of a coil heat exchanger. The nature and positioning of the coil depends on the nature of the flow pattern created by the stirrer. For an axial flow stirrer, a spiral coil (see Fig. 2a) is effective because it provides good liquid circulation between the coil and the wall. For radial flow stirrers, spiral coils deflect the liquid

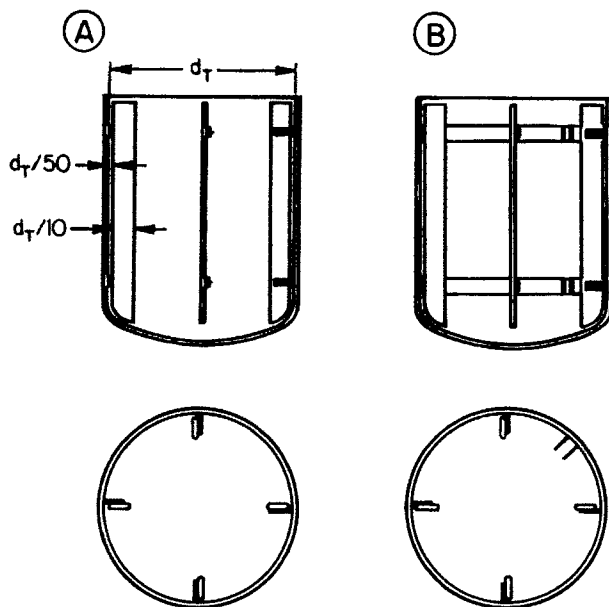


FIG. 1. Baffle designs. (a) Normal design; (b) design for glass and coated vessels (baffle basket with pressure-fitted ring). (Reprinted with permission from the publisher, VCH Publishers, Inc., after Zlokarnik and Judat, 1988.)

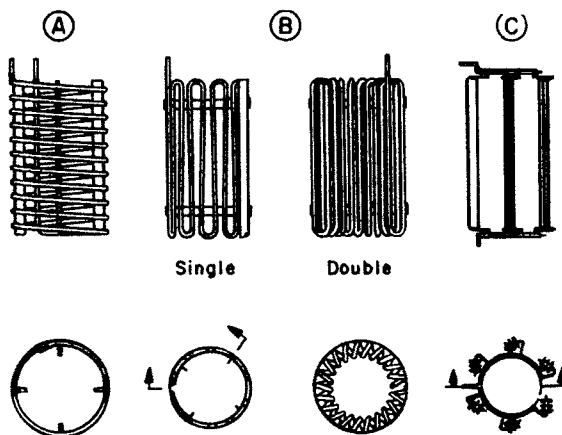


FIG. 2. Tube coil designs. (a) Spiral coil; (b) meander coils (cooling basket); (c) tube bundles. (Reprinted with permission from the publisher, VCH Publishers, Inc., after Zlokarnik and Judat, 1988.)

circulation, resulting in insufficient flow between the coil and wall. For this flow pattern, meander coil (see Fig. 2b) is more suitable since this arrangement does not deflect the radial flow pattern, but prevents bulk rotation of the liquid. The heat exchanger tubes can also be arranged into bundles and installed in place of baffles, as shown in Fig. 2c.

B. TYPES OF STIRRERS

The mixing is provided by a wide variety of stirrers, the choice of which depends on a specific mixing operation and given material system. The following discussion is limited to those stirrer types that are most widely used in the chemical industry, and for which established design guidelines exist (Zlokarnik and Judat, 1988). Various stirrers are illustrated in Fig. 3 according to the predominant flow pattern they produce, as well as the range of viscosities over which they can be effectively used. Typical flow patterns generated by stirrers are axial, radial, and sometimes tangential. The flow patterns and their influence on the design parameters are further evaluated in subsequent sections.

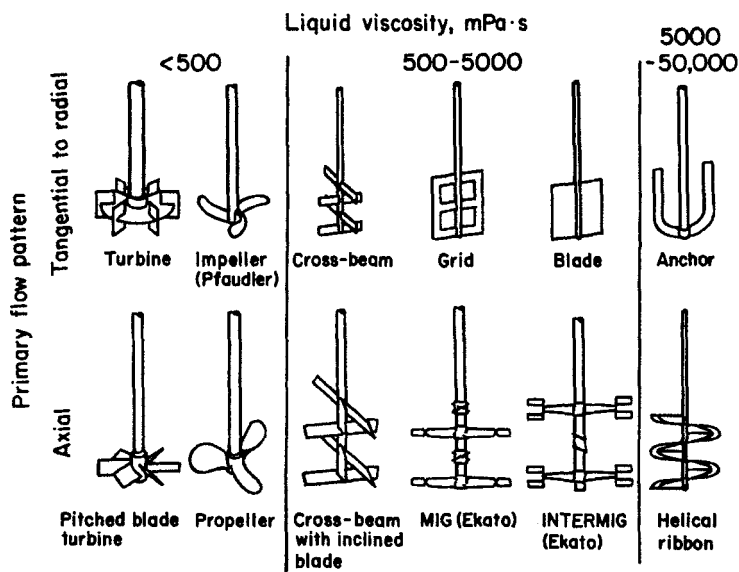


FIG. 3. Common stirrer types. (Reprinted with permission from the publisher, VCH Publishers, Inc., after Zlokarnik and Judat, 1988.)

1. *Radial Motion Stirrers*

a. Turbine Stirrer

The most common type is the Rushton turbine with six blades on a disk. It is the only high-speed stirrer that sets the fluids in radial motion—or, at higher viscosities, in tangential motion. This type is only effective with low-viscosity liquids and baffled vessels. In recent years, turbine stirrers with eight or 12 blades have also been employed. Generally, the stirrer diameter is such that the d_T/d_1 ratio ranges from 3 to 5. During rotation, the turbine stirrer causes high levels of shear and is well suited for the dispersion processes.

b. Impeller Stirrer

This type of stirrer was developed for use in enamel-coated vessels and thus has rounded stirring arms. The stirrer can be used in vessels with or without baffles. It is generally placed with a small clearance from the bottom, and its diameter is such that $d_T/d_1 = 1.5$. It can operate in a vessel with strongly fluctuating liquid levels because it mixes even a small amount of liquids very well.

c. Cross-Beam, Grid, and Blade Stirrers

These are low-speed stirrers and generally have diameters in the range $d_T/d_1 = 1.5-2$. For low-viscosity fluids, stirrers are used with baffles, and for high-viscosity fluids, they can be used without baffles. These stirrers are especially suited for liquid homogenization.

d. Anchor Stirrer

This low-speed stirrer is normally used for viscous fluids commonly encountered in biological and polymeric reactors. They are well suited for enhancing the heat transfer rate in viscous fluids. The stirrer is generally placed in a vessel with small clearances from the wall ($d_T/d_1-1.05$).

2. *Axial Motion Stirrers*

a. Paddle and Propeller Stirrers

Pitch-blade turbine (paddle stirrer with pitched blades) and propeller stirrers provide high mixing with an axial flow pattern. Both of these stirrers are normally used for low-viscosity liquids and in vessels with baffles. They are well suited for providing liquid homogenization and suspension of solids in slurry reactors. The stirrers can also be used in viscous fluids and for vessels with $H/d_T > 1$, which are generally encountered in fermentation processes. For these situations, axial flow is increased with the use of multistage stirrers with pitched stirring surfaces.

b. Cross-Beam Stirrer with Pitched Beams and MIG and INTERMIG Stirrers

The latter two types of stirrers are produced by Ekato Company, Schopfheim, Germany. These are low-speed stirrers with a d_T/d_I ratio of 1.5 in the presence of baffles and 1.1 in the absence of baffles. The stirrers are versatile and are used for liquid homogenization, gas–liquid or liquid–liquid dispersion, and solids suspension in slurry reactors.

c. Helical Ribbon Stirrer

This very low-speed stirrer is normally used for very viscous fluids. It is normally placed in a vessel with small wall clearance ($d_T/d_I \approx 1.05$) and operates in such a way that it drives the liquid downward along the wall. The stirrer is best suited for improving homogenization and heat transfer in very viscous fluids.

3. Novel Stirrers

In addition to the radial and axial flow stirrers described above, a large number of special designs exist. Of these, three need to be mentioned (Zlokarnik and Judat, 1988).

a. Rotor–Stator Stirrers

When a high degree of shear on small liquid volume is desired, a rotor–stator stirrer is used (see Fig. 4). This stirrer consists of a blade or paddle stirrer enclosed by a ring of baffles. This type of stirrer thus alleviates the need for separate baffles in the vessel. This stirrer is not useful for biological reactors, but finds special use in polymeric reactors containing non-Newtonian liquids.

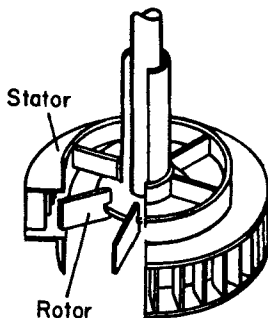


FIG. 4. A rotor–stator stirrer. (Reprinted with permission from the publisher, VCH Publishers, Inc., after Zlokarnik and Judat, 1988.)

b. Sawtooth-Disk Stirrer

This type of stirrer also provides high shear without a stator ring or baffles. A schematic of this stirrer is shown in Fig. 5. High shear rate is provided by liquid acceleration in a radial direction in a thin ring away from the center followed by quick deceleration. Both sawtooth-disk and rotor-stator stirrers are particularly suited for emulsification and dispersion over a wide range of viscosities, e.g., production of paint pigments, and polymerization, where the viscosity of the liquid changes significantly during the reaction process.

c. Hollow Stirrers

In this type of stirrer, the stirrer head is hollow and is connected through a hollow shaft to the gas-filled space above the liquid surface. The suction generated behind the stirrer edges during rotation can thus be used to supply a gas to the liquid. The stirrer thus provided internal recirculation of gas, which is needed for "dead-end" systems such as those used in biological waste treatment processes. As a single unit combining both stirrer and gas supply, hollow stirrers are well suited for enhancing mass transfer in gas-liquid systems. Various designs of hollow stirrers are available, and they are described in subsequent sections. The simplest design is the *tube stirrer*, which is schematically illustrated in Fig. 6. Other designs are described in Section 2. Hollow stirrers are not effective for very viscous systems. All hollow stirrers operate at high speeds and are used in baffled vessels with $d_T/d_1 = 3-5$. Hollow stirrers are useful for gas-liquid-solid reactors for hydrogenation and oxidation processes.

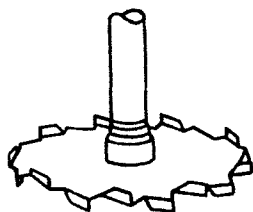


FIG. 5. Disperser disk. (Reprinted with permission from the publisher, VCH Publishers, Inc., after Zlokarnik and Judat, 1988.)

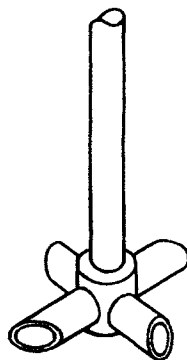


FIG. 6. Hollow stirrer (tube type). (Reprinted with permission from the publisher, VCH Publishers, Inc., after Zlokarnik and Judat, 1988.)

C. OTHER FORMS OF MECHANICAL AGITATION

In the previous two sections, we illustrated mechanical agitation by the use of various types of stirrers. This monograph also considers reactors wherein mechanical agitation is provided by means other than a stirrer. In several processes (e.g., the gas-liquid-solid catalytic reactor, the bubble column for viscous fluids, and reactors for latex formation), the agitation is provided by the rotation of the entire vessel. Mixing in such vessels, as well as in centrifugal film or pump reactors, is created by the centrifugal forces. In vibrating bed reactors, microreactors, or reciprocating sieve plate columns, mixing is provided by a vibrating motion of the whole reactor or a part of the reactor. Mixing can also be provided by a rotating belt or a plate such as in a rotary vertical batch reactor for chemical vapor deposition or reactions involving viscous, granular material. Finally, a high degree of mixing is also provided by rotating blades or screws, such as in the wiper blade catalytic reactor and thin film or double screw polymeric reactors. This monograph considers all of these reactors.

D. DESIGN PARAMETERS

The monograph evaluates design parameters for a variety of conventional and novel mechanically agitated reactors. Brief descriptions of the reactors and their operations are also outlined. The important design parameters examined in the monograph are the hydrodynamics (flow regime), phase holdups, macro- and micromixing, gas-liquid and liquid-solid mass transfer, fluid-wall or fluid-coil heat transfer, solids distribution, and power input by the stirrer. Various experimental methods for design parameter estimations are also examined. For those reactors used for intrinsic kinetic measurements, design conditions that allow such measurements are briefly evaluated.

It is important to note that the *issue of design* is much broader than the considerations of design parameters outlined here. The proper design strategies consider the nature of the reaction system. In a biological reactor, aseptic conditions and their implications for the reactor design are important. The nature of by-products and associated separation requirements are important in the detailed design of the mechanically agitated reactor. The use of a high-tech (automated) operation changes design requirements. Automated operation is desirable, when a high degree of selectivity is required or when high-purity products are needed. Automated operation is also justified when the unit price of the product is high. Safety, reliable performance, and cost are also important design considerations. When a reactor is scaled up, the power requirement is generally designed to be higher than the ones estimated

from the design correlations, but not so high that the power efficiency is reduced. Special considerations are given if a variable power instead of a constant power is required. For a large-scale system, safety plays an important role in the decision of how large a reactor system should be built, particularly for reactions involving high temperature and pressure. For large systems, mechanical considerations such as wear and tear of the agitation system also play important roles. For polymerization reactions, product quality significantly depends upon micromixing and effective heat transfer; the effects of scale-up on these parameters are, therefore, extremely important. For biological reactors, foaming is an important design issue.

Some of the above-mentioned design considerations are handled through the design of novel reactors. Few such novel reactors are discussed in this monograph.

II. Gas-Liquid Reactors

Mechanically agitated gas-liquid reactors are widely used because of their versatility. The liquid residence time in such reactors can be varied over a wide range, and semibatch operation can be adopted for systems that require long residence time. For gases, the unit can be designed to be a "dead-end" type, so that the amount of gas introduced into the reactor balances that consumed. It is used for a variety of reactions such as oxidation, hydrogenation, chlorination, carbonation, ozonation, etc.; some specific practical examples are outlined in Table I. In this section, we examine the design parameters for mechanically agitated gas-liquid reactors that are normally used in chemical and petrochemical industries. Discussions on slurry reactors, as well as those gas-liquid reactors for biological (including waste treatment) and polymeric systems, are outlined in subsequent sections.

A. CONVENTIONAL REACTORS

Conventional mechanically agitated gas-liquid reactors, wherein gas and liquid make contact in batch, semibatch, or continuous mode, are widely used in processes involving chlorination, sulfonation, hydrogenation, selective absorptions in amine solutions, etc. (Doraiswamy and Sharma, 1984). These reactors are popular for laboratory studies because of their simplicity in construction and low cost. As a rule of thumb with noncorrosive liquids, the mechanically agitated reactor is most economical when the overall reaction rate is five times greater than the mass transfer rate in a bubble column. If a

TABLE I
TYPICAL GAS-LIQUID REACTIONS^a

-
1. Liquid-phase processes such as oxidation, hydrogenation, sulfonation, nitration, halogenation, hydrohalogenation, alkylation, sulfonation, polycondensation, polymerization, etc.
 Examples: oxidation of acetaldehyde to acetic acid
 oxidation of ethylene to acetaldehyde
 oxidation of paraffins to acids
 chlorination of dodecane
 hydrogenation of olefins
 2. Biochemical processes
 Examples: aerobic fermentation
 oxidation of sludges
 manufacture of single cell proteins from hydrocarbons and other raw materials
 3. Gas scrubbing operations
 Examples: absorption of SO_3 in dilute sulfuric acid
 absorption of NO_2 in dilute nitric acid
 absorptions of CO_2 , H_2S , CO , SO_2 , NO , N_2O_y , HF , NH_4 , phosgene, etc.
 4. Manufacture of pure products
 Examples: manufacture of H_2SO_4 , BaCO_3 , BaCl_2 , adipic acid, phosphates, etc.
 5. Various processes in petroleum refining and recovery of nuclear materials.
-

^a Some of the examples contain three phases (biological or polymerization reactions).

large fraction of gas needs to be absorbed, stirred-tank reactors are not recommended. Over the years, significant effort has been made to understand the hydrodynamic, mixing, and mass- and heat-transfer characteristics of such reactors. The effectiveness of numerous types of agitators has also been investigated. Table II lists important characteristics of some of the agitators used for gas-liquid reactors.

1. *Hydrodynamics*

Flow patterns in a mechanically agitated reactor with disk turbine, pitched-blade turbine, and propeller types of agitator are schematically illustrated by Joshi *et al.* (1982). The flow pattern in the presence of gas is described later in the section on slurry reactors. In each of these cases, the dimensionless velocity profile with respect to the impeller tip velocity has been found to be independent of the impeller speed and has shown slight dependence on the impeller diameter.

The gas holdup in mechanically agitated reactors is a function of the geometric parameters, fluid properties such as viscosity and surface tension, the electrolyte nature of the solution, and the foaming characteristics of the liquid. The best correlations are those of Hughmark (1980) and Sridhar and

TABLE II

QUALITATIVE COMPARISON OF SOME DESIGN PARAMETERS FOR VARIOUS AGITATORS IN MULTIPHASE SYSTEMS^a (AFTER CARRA AND MORBIDELLI, 1987)

Stirrer Design	d_i/d_T	u_{AM} (m/s)	μ_{LM} (Pa s)	Baffled	Heat Transfer		Gas-Liquid Dispersion	Liquid-Solid Dispersion
					Wall	Coil		
Propeller	0.15-0.4	15	5	yes	gg	g	gg	gg
Disk flat-blade turbine	0.2-0.45	15	10	yes	gg	g	gg	g
Pitched-blade turbine	0.2-0.45	12	20	yes	gg	gg	gg	gg
Impeller	0.5-0.7	12	20	yes	gg	—	g	g
Paddle mixer	0.4-0.5	5	50	yes	gg	gg	g	bg
Anchor impeller	0.9-0.98	5	50	no	gg	—	g	bg
Helical mixer	0.9-0.98	1	1000	no	gg	—	—	—

^a gg, highly suitable; g, suitable; bg, conditionally suitable.

Potter (1980). Hughmark (1980) presented a relation

$$\epsilon_g = 0.74 \left(\frac{Q_g}{N V_\ell} \right)^{1/2} \left(\frac{N^2 d_1^4}{g w_1 V_\ell^{2/3}} \right)^{1/2} \left(\frac{d_b N^2 d_1^4 \rho_\ell}{\sigma_\ell V_\ell^{2/3}} \right)^{1/4}, \quad (2.1)$$

where

$$d_b = 2.5 \times 10^{-3} \text{ m}; \quad 10^{-2} < V_\ell < 51 \text{ m}^3; \quad u_g < 0.053 \text{ m/s}; \quad (2.2)$$

whereas Sridhar and Potter (1980) correlated gas holdup to power per unit volume as

$$\epsilon_g = \left(\frac{\epsilon_g u_g}{u_b} \right)^{1/2} + 0.000216 \left[\frac{(P_g/V_\ell)^{0.4} \rho_\ell^{0.2}}{\sigma_\ell^{0.6}} \right] \left[\frac{u_g}{u_b} \right]^{0.5} \left(\frac{P_T}{P_g} \right) \left(\frac{\rho_g}{\rho_a} \right)^{0.16}, \quad (2.3)$$

where

$$u_b = 0.265 \text{ m/s}; \quad \rho_a = \text{density of air at operating conditions};$$

$$P_T = P_g + P_K + P_q; \quad P_K = 0.5 Q_g \rho_g u_s^2;$$

$$P_g = \rho_\ell g H_L Q_g; \quad u_s = \text{gas velocity at sparger exit.}$$

Calderbank (1958) showed that the gas holdup varies inversely with the surface tension with a power of 0.55 to 0.65, and this has been supported by Hassan and Robinson (1977) and Luong and Volesky (1979). The most commonly used agitator for a gas-liquid reactor is the six-flat-blade turbine. Baffles improve gas-liquid dispersion. The baffling recommended is four 90°

baffles, $d_T/12$ in width; offset values such as $H/d_T = 1$, $d_i/d_T = 0.4$ to 0.5 , and $H_i/d_T = 0.33$ to 0.5 are recommended. Here, H_i is the height of the impeller from bottom of the reactor. The effective gas-liquid dispersion is achieved when the agitation speed exceeds a critical value N_0 (which corresponds to a tip velocity of 2.25 m/s) given by

$$N_0 d_i = \left(\frac{\sigma_l g}{\rho_l} \right)^{1/4} \left(a + b \frac{d_T}{d_i} \right), \quad (2.4)$$

where $a = 1.22$, $b = 1.25$ for turbine impellers; $a = 2.25$, $b = 0.68$ for two- and four-blade agitators.

The impeller speed at which gas above liquid is first entrapped by liquid is given by

$$N_c = 1.65 \frac{d_T^{1.1}}{d_i^{1.98}} \text{Ne}^{-0.125} \left(\frac{\sigma_l g}{\rho_l} \right)^{0.19} \left(\frac{\mu_l}{\mu_g} \right)^{0.031} \left(\frac{w_i}{d_i} \right)^{0.625}, \quad (2.5)$$

where Ne is the power number and w_i is the impeller blade width. Albal *et al.* (1983) have shown that this critical speed depends upon the liquid level above the stirrer, the impeller-to-vessel diameter ratio, and the nature of the stirrer arrangements. Further discussion and correlations for minimum impeller speed for gas entrapment are given in Section V.

Power consumption in a mechanically agitated reactor largely depends on the stirring rate and the physical properties of the fluids. The reported studies for power consumption are summarized by Joshi *et al.* (1982). Additional information is also given in Sections III, VI, and VII. The introduction of gas in mechanically agitated contactors reduces the power consumed by an impeller. This is due to the reduction in the local density of the dispersion as compared to that of pure liquid. Van't Riet and Smith (1973), Bruijn *et al.* (1974), and Van't Riet *et al.* (1976) have suggested that the formation of a stable cavity behind the impeller blade reduces the form drag and hence the power consumption. Several investigators have attempted to correlate the reduction in power consumption with parameters such as impeller diameter, speed, volumetric gas flow rate, and in some cases, physical properties of the gas/liquid system (Joshi *et al.*, 1982).

As mentioned earlier, the gas holdup in mechanically agitated contactors has been found to be, apart from geometric parameters, a function of liquid viscosity, surface tension, the electrolytic nature of the solutions, foaming character, etc. Hence, phenomenologically the reduction in power consumption should also depends on these characteristics of the system. Bruijn *et al.* (1974) concluded that the surface tension does not affect the mechanism of cavity formation and its shape to an appreciable extent. However, liquid viscosity influences the stability of the cavity. Hughmark (1980) presented the

following correlation for power consumption in the presence of gas:

$$\frac{P_g}{P_\ell} = 0.1 \left(\frac{NV_\ell}{Q_g} \right)^{1/4} \left(\frac{N^2 d_1^4}{g w_i V_\ell^{2/3}} \right). \quad (2.6)$$

This correlation covers a wide range of variables ($0.87 < \rho_\ell < 1.6 \text{ kg/m}^3$; $0.0008 < \mu_\ell < 0.028 \text{ PaS}$; $0.025 < \sigma_\ell < 0.072 \text{ N/m}$; $0.25 < d_i/d_T < 0.46$; $0.1 < d_T < 1 \text{ m}$; $0.31 < P_g/P_\ell < 0.8$) and is dimensionless in character. However, it fails at extreme values of gas flow rates.

The total power consumption is also correlated by Gray *et al.* (1982) as

$$\frac{P_T}{N^3 d_1^5 \rho_\ell} = 0.75 \left[\frac{g^2 H_i d_T}{(u_g/\varepsilon_g)^2 N^2 d_1^2} \right]^{1/4} \left(\frac{\sigma_\ell}{\sigma_w} \right)^{1/4}, \quad (2.7)$$

which is valid for $0.15 < d_T < 0.45 \text{ m}$; $0.25 < d_i/d_T < 0.45$; $0.75 < H_i/d_1 < 1.5$. In a dimensionless form, the power characteristics have the general form $Ne = f(N_A, Re, Fr, Ga, d_T/d_1)$. The aeration number N_A exerts the dominant influence on the power number Ne , and this relationship can be expressed as:

$$Ne = 1.5 + (0.5 N_A^{0.075} + 1.6 \times 10^3 N_A^{2.6})^{-1}, \quad (2.8)$$

which is valid for $Re > 10^4$, $Ga \geq 10^7$, $d_T/d_1 \geq 3.33$, and $Fr \geq 0.65$. The Froude number begins to have a slight effect for $Fr < 0.5$. The smallest values of Ne are observed shortly before flooding; under otherwise identical conditions, the stirrer power then is only about 40% of that in a nonaerated liquid.

For a given speed of rotation, every stirrer can thoroughly distribute a gas only up to a well-defined maximum flow rate. When this limit is exceeded, the stirrer is said to be flooded, i.e., it is completely surrounded by gas and ceases to work. For the turbine stirrer, the maximum gas flow rate that can be dispersed well is given by

$$N_A = 0.19 Fr^{3/4}, \quad 0.1 < Fr < 2.0. \quad (2.9)$$

The power requirements under these conditions can be calculated from the relationship $Ne = 1.36 Fr^{-0.56}$. Equation (2.9) is valid for $d_T/d_1 = 3.33$. Similar relations for other values of d_T/d_1 are given by Judat (1977). The power consumption and the maximum gas flow rate for two turbine stirrers on the same shaft are given by Kurpiers *et al.* (1985).

In the design of a gas-liquid agitated reactor, the depletion of the gaseous reactant concentration within the reactor is basically defined by the only parameter (a_L/Q_g) (Nagel *et al.*, 1973, 1978) for a given reacting system. This should be achieved with an efficient power consumption. A useful procedure for the selection of commercially available turbine agitators for this purpose has been presented by Hicks and Gates (1976).

2. *Mixing and R.T.D.*

The performance of a gas–liquid reactor depends on the extent of mixing in both the phases. A number of methods for measuring the mixer performance or mixing efficiency have been examined. Different criteria have been used to decide the degree of mixing or homogeneity, and based on these results, empirical correlations have been proposed for the prediction of dimensionless mixing time “ $N\theta$ ” for different types of agitators and vessel geometries. The experimental details of various reported studies on mixing time are summarized by Joshi *et al.* (1982).

While Norwood and Metzner (1960) and Biggs (1963) have found $N\theta$ to be proportional to $N^{0.34}$ and $N^{0.16}$, respectively, most reported studies indicate $N\theta$ to be constant for a particular impeller. The effect of impeller diameter is represented as

$$N\theta \propto (d_T/d_i)^\beta, \quad (2.10)$$

where β varies from 2 to 2.57 for flat-blade turbines and $\beta = 2$ for propellers. Brennan and Lehrer (1976) and McManamey (1980) have shown that the mixing time is minimum when the impeller is at mid-height. The effect of blade width on θ is dependent on the impeller speed, the impeller position, and the geometry of the vessel. The circulation model that can be used to predict the mixing time has the following features (Joshi *et al.*, 1982):

- (1) Mixing time is directly proportional to the longest loop length, which depends on the type of the impeller and the position.
- (2) Mixing time is inversely proportional to the average circulation velocity near the wall (in the case of the flat-blade turbine) or near the surface (upflow propeller) or, in other words, where the longest circulation loop exists,
- (3) Mixing time θ is taken to be equal to five times the circulation time (the length of the longest loop divided by the average circulation velocity). This assumption is based on the studies of Prochazka and Landau (1961) and Holmes *et al.* (1964), which indicate that after five circulations, 99% of the mixing is complete.
- (4) Flow is fully turbulent and the dimensionless velocity (v/Nd_i) is independent of the impeller speed.

Based on the circulation model, the following equations for $N\theta$ are obtained.

For propeller *downflow*:

$$N\theta = 6.0 \left(\frac{2H}{d_i} + \frac{d_T}{d_i} \right) \left(\frac{H_i}{d_i} \right); \quad (2.11)$$

upflow:

$$N\theta = 6.0 \left(\frac{2H}{d_i} + \frac{d_T}{d_i} \right) \left(\frac{H - H_i}{d_i} \right); \quad (2.12)$$

for pitched-blade turbine downflow:

$$N\theta = 5.0 \left(\frac{2H}{d_i} + \frac{d_T}{d_i} \right) \left(\frac{H_i}{d_i} \right); \quad (2.13)$$

upflow:

$$N\theta = 5.0 \left(\frac{2H}{d_i} + \frac{d_T}{d_i} \right) \left(\frac{H - H_i}{d_i} \right). \quad (2.14)$$

Mixing time predicted by the recirculation model agrees better with the measurements at higher d_i/d_T ratios than at lower ones.

In the presence of gas, the circulation model gives the mixing time for the flat blade turbine as

$$N\theta = 20.41 \left[\frac{H}{d_T} + 1 \right] \left(\frac{d_T}{d_i} \right)^{13/6} \left(\frac{w_i}{d_i} \right) \left(\frac{Q_g}{NV} \right)^{1/12} \left(\frac{N^2 d_i^4}{g w_i V^{2/3}} \right)^{1/15} \quad (2.15)$$

The above relation predicts $N\theta$ within 30% of experimental measurements.

Van de Vusse (1962) reported that when mixing time is less than one-tenth of the average residence time, the agitated vessel can be assumed to be completely backmixed. The micromixing in a mechanically agitated vessel is examined by Bourne *et al.* (1981a, 1981b) and Belevi *et al.* (1981). They used very fast reactions (fast enough to produce nonhomogeneous mixture at the molecular scale) to study the extent of segregation and developed a diffusion reaction formulation to represent inhomogeneity (or segregation) in mixtures and its influence on chemical reaction of a micromixing-dependent product distribution leaving a CSTR. According to the diffusion-reaction model, micromixing is characterized by the product distribution from two competitive and consecutive reactions. These distributions are functions of stoichiometric and volumetric ratios of reagents, the ratio of rate constants, a time parameter, and a Thiele-like modulus. Micromixing can play an important role in the selectivity of gas-liquid reactions in a mechanically agitated CSTR.

The liquid-phase dispersion coefficient, E_c , is given by Joshi *et al.* (1980) as

$$E_c = 0.116 \left[\frac{(d_T + H_L)^2 N}{(d_i/d_T)^2} \right], \quad (2.16)$$

where H_L is the clear liquid height. The above equation is valid for a disk turbine impeller. Liquid-phase backmixing is also studied by Sideman *et al.* (1966). Generally, both gas and liquid are considered to be completely backmixed for a stirrer speed greater than N_0 .

While very little information is available on gas-phase backmixing in a mechanically agitated CSTR, the extent of mixing increases with the impeller speed. If the reaction depends on the partial pressure of gas, an increased backmixing decreases the driving force for the absorption rate. An increase in impeller speed also increases $k_L a_L$, $k_g a_L$, etc. As a consequence, it is likely that an optimum impeller speed exists that gives maximum space-time yield ($\text{kmol/m}^3 \text{ s}$) and this optimum speed probably lies in the vicinity of critical impeller speed.

3. Gas-Liquid Mass Transfer

In many practical applications, gas-liquid mass transfer plays a significant role in the overall chemical reaction rate. It is, therefore, necessary to know the values of effective interfacial area (a_L) and the volumetric or intrinsic gas-liquid mass transfer coefficients such as $k_L a_L$, k_L , $k_g a_L$, k_g , etc. As shown in Section IX, the effective interfacial area is measured by either physical (e.g., photography, light reflection, or light scattering) or chemical methods. The liquid-side or gas-side mass-transfer coefficients are also measured by either physical (e.g., absorption or desorption of gas under unsteady-state conditions) or chemical methods. A summary of some of the experimental details and the correlations for a_L and $k_L a_L$ reported in the literature are given by Joshi *et al.* (1982). In most practical situations, $k_g a_L$ does not play an important role.

The volumetric gas-liquid mass transfer coefficient, $k_L a_L$, largely depends on power per unit volume, gas velocity (for a gassed system), and the physical properties of the fluids. For high-viscosity fluids, $k_L a_L$ is a strong function of liquid viscosity, and for low-viscosity fluids ($\mu < 50 \text{ mPa s}$), $k_L a_L$ depends on the coalescence nature of the bubbles. In the aeration of low-viscosity, pure liquids such as water, methanol, or acetone, a stable bubble diameter of 3–5 mm results, irrespective of the type of the gas distributor. This state is reached immediately after the tiny primary bubbles leave the area of high shear forces. The generation of fine primary gas bubbles in pure liquids is therefore uneconomical.

In salt solutions or mixtures of miscible liquids, the coalescence of tiny primary gas bubbles is suppressed significantly; the higher the concentration of the solution, the better the size of the primary gas bubbles is preserved. The stable bubble size in this case is 0.2–0.5 mm, an order of magnitude smaller than in pure liquids. As a result of coalescence suppression, the enhancement factor of physical sorption $\bar{m} = (k_L a)_{\text{sol}} / (k_L a)_{\text{solv}}$ rises to 7 or 8, which has been confirmed by measurements of $k_L a_L$ as a function of the concentration of various inorganic salts (both strong and weak electrolytes) as well as normal aliphatic alcohols (methanol to octanol) (Zlokarnik, 1980, 1985).

On the other hand, some substances, even in minute concentrations, promote coalescence. Some of the non-ionic surfactants often used as anti-foaming agents are so effective that a concentration of 3 ppm is sufficient to halve the $k_L a_L$ of pure water (Zlokarnik, 1979). Clearly the use of surfactants for foam prevention should be avoided whenever possible, and an efficient mechanical foam breaker should be used (Zlokarnik, 1986).

The foaming tendency of the liquid can affect the value of $k_L a_L$. Figure 7 illustrates the behavior of $k_L a_L$ for CO and H_2 in various fractions of F-T liquid (Deimling *et al.*, 1985). The results indicate that due to the pronounced foaming tendency of a medium fraction of F-T liquid, the effect of temperature on $k_L a_L$ for this fraction is the reverse of that for light and heavy fractions.

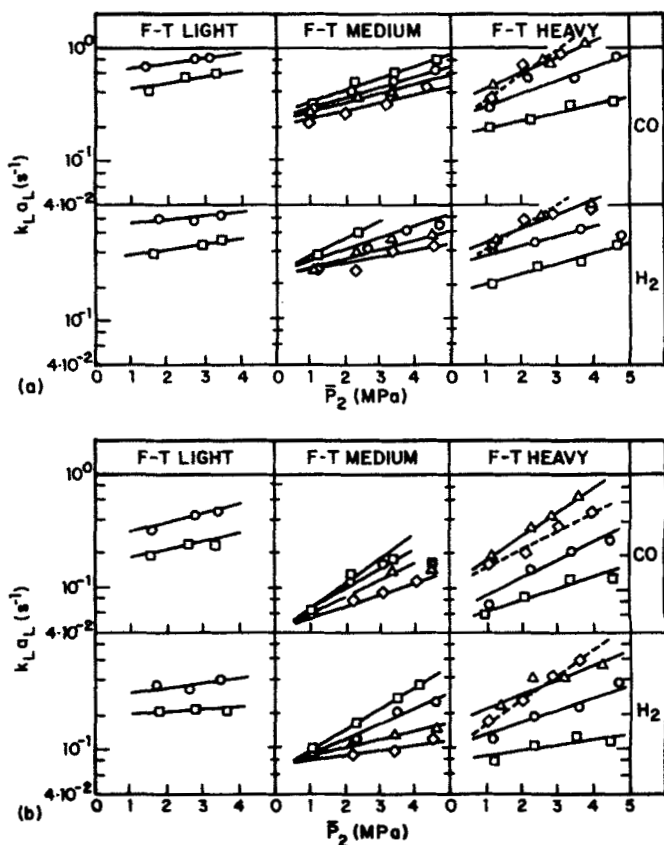


FIG. 7. Volumetric mass transfer coefficient $k_L a_L$ for CO and H_2 in various fractions of an F-T liquid as a function of pressure at different temperatures (\diamond , 523 K; \triangle , 473 K; \circ , 423 K; \square , 373 K) and two stirrer speeds: (a) 1,000 $rev\ min^{-1}$; (b) 800 $rev\ min^{-1}$. (After Deimling *et al.*, 1985.)

Deimling *et al.* (1985) showed that the data for all three fractions can be correlated to power input by the agitator in the vessel. Karandikar *et al.* (1986) showed that the addition of water in F-T liquids significantly changes $k_L a_L$ for CO, H₂, CO₂, and CH₄ in F-T liquid fractions.

The results shown in Fig. 7 indicate that $k_L a_L$ increases with pressure. On the other hand, for aqueous systems, Albal *et al.* (1983) showed both $k_L a_L$ and k_L to be independent of pressure. These investigators also showed that $k_L a_L$ decreases with an increase in viscosity and increases with a decrease in surface tension. The mass-transfer coefficient data for oxygen–CMC–water and oxygen–water–Triton CF-32 were correlated by the dimensionless equation

$$\text{Sh} = \frac{k_L a_L d_1^2}{\mathcal{D}} = 1.41 \times 10^{-3} \text{Sc}^{0.5} \text{Re}^{0.67} \text{We}^{1.29}, \quad (2.17)$$

where $\text{We} = \rho N^2 d_1^3 / \sigma$.

For an unaerated agitated vessel with a six-bladed turbine stirrer, the data for oxygen–water were also correlated using the relation

$$\frac{k_L a_L}{\mathcal{D}^{1/2}} = 2.579 \times 10^2 \left(\frac{P_g}{V_L} \right)^{0.6} \varepsilon_g^{0.6}. \quad (2.18)$$

Traditionally, $k_L a_L$ values measured in a given system have been correlated in a dimensional form,

$$k_L a_L = f(P_g/V, u_g), \quad (2.19)$$

where P_g/V is the stirrer power per unit volume and u_g the superficial velocity. Van't Riet (1979) proposed (SI units) the following relations:

for coalescing systems:

$$k_L a_L = 2.6 \times 10^{-2} (P_g/V)^{0.4} u_g^{0.5}, \quad (2.20)$$

for noncoalescing systems:

$$k_L a_L = 2.0 \times 10^{-3} (P_g/V)^{0.7} u_g^{0.2}. \quad (2.21)$$

Judat (1982) has compared the results of nine experimental works on the coalescing air–water system made in tanks with turbine stirrers with the volume varying from 2.5 L to 906 m³ ($0.15 \leq d_T \leq 12$ m). His correlation is

$$k_L a_L \propto (P_g/V)^{0.4} u_g^{0.6}. \quad (2.22)$$

Henzler (1982) was able to correlate the same experimental results by using the dimensionless group $Y \equiv (k_L a_L / \nu)(u_g^2 / g)^{1/3}$ as ordinate and $X' \equiv P_g / (V \rho g \nu)$ as abscissa. The dimensionless group Y represents the sorption number for bubble columns, while X' represents the ratio of the mechanical power of the stirrer to the hydraulic power of the gas throughput. The sorption number Y also allows comparison between mixing tanks and bubble columns (Henzler

and Kauling, 1985). The effect of viscosity seems to be appropriately taken into account by Y . The curves for different systems, however, do not coincide since each system exhibits a different coalescence behavior.

The reported correlations for $k_1 a_1$ and a_1 are summarized by Joshi *et al.* (1982). One of the most commonly used relations is that by Hughmark (1980), which gives

$$a_L = 1.38 \left(\frac{g \rho_\ell}{\sigma_\ell} \right)^{1/2} \left(\frac{Q_g}{N V_\ell} \right)^{1/3} \left(\frac{N^2 d_1^4}{g w_i V_\ell^{2/3}} \right)^{0.592} \left(\frac{d_b N^2 d_1^4 \rho_\ell}{\sigma_\ell V_\ell^{2.3}} \right)^{0.187} \quad (2.23)$$

for $d_b = 2.5 \times 10^{-3}$ m, $10^{-2} < V_\ell < 51$ m³, $u_g < 0.053$ m/s.

The gas-side mass-transfer coefficient was studied by Newman (1931). He presented a relation

$$k_g = 6.58 \left[\frac{\mathcal{D}_g}{d_{vs}(1-y)} \right], \quad (2.24)$$

where y is the gas mole fraction of diffusing components and d_{vs} is the sauter mean bubble diameter.

In recent years attempts have been made to improve the gas-liquid mass transfer by changing the design of the mechanically agitated vessel. Mann *et al.* (1989) evaluated the use of horizontal baffles mounted near the gas-liquid surface. Horizontal baffles prevent vortex formation, generate less shear than standard baffles, increase gas holdup, and improve gas-liquid mass transfer. The latter two results are due to the rotational flow below the baffles, which causes gas bubbles to move upward in a spiral trajectory and induces surface aeration. For a 12-inch i.d. and 18-inch-tall stirred vessel, they showed $k_L a_L$ to be improved by a factor of 1.6 to 2.3 with 30 to 50% lower agitation power compared to the standard vessel.

4. Heat Transfer

Several industrially important reactions, such as oxidation, hydrogenation, halogenation, etc., are accompanied by large heat effects. For maintaining the desired temperature, the heat is removed either through the vessel wall or through a coil or tube bundle immersed in the liquid. A knowledge of heat transfer coefficients for the different heat transfer elements is necessary for rational design. Some of the earlier reported studies on heat transfer in agitated vessels in the presence of gas are summarized by Joshi *et al.* (1982).

A more notable correlation for the heat-transfer coefficient at the wall of mechanically agitated contactors is given by Perry and Chilton (1973) as

$$\text{Nu} = 0.6 \text{Re}^{2/3} \text{Pr}^{1/3} \left(\frac{\mu}{\mu_w} \right)^{0.14} \quad (2.25)$$

for $40 < \text{Re} < 3 \times 10^5$ and a six-bladed disk (Rushton) turbine. Equation (2.25) is expressed in terms of average circulation velocity of liquid V_c by Shah *et al.* (1981) as

$$\text{Nu} = 0.4 \left(\frac{d_T V_c \rho}{\mu} \right)^{2/3} \text{Pr}^{1/3} \left(\frac{\mu}{\mu_w} \right)^{0.14}, \quad (2.26)$$

where $V_c = 3.72 N d_1^2 / (1 + H/d_T) d_T$.

The type of impeller appears to have little effect on the heat-transfer coefficient (Joshi *et al.*, 1982). At higher agitation speed, the effect of gas sparging on the heat-transfer coefficient is small. For very high stirring intensity ($N d_1^2 \rho \ell / \mu \ell > 10^5$), Steiff *et al.* (1981) report $\text{St} \propto (\text{Re}_g \text{Fr}_g \text{Pr}_g^2)^{1/3}$, a relation that was verified for the air–water system.

More recently, the heat-transfer characteristics are divided into two regimes the laminar flow regime and the turbulent flow regime, depending upon the value of the Reynolds number, $\text{Re} = N d_1^2 \rho / \mu$. Laminar flow prevails for $\text{Re} < 200$, and turbulent flow for $\text{Re} > 200$. For both flow regimes, the heat-transfer coefficient can be expressed in a dimensionless form of the type

$$\text{Nu} = c \text{Re}^a \text{Pr}^{1/3} \left(\frac{\mu}{\mu_w} \right)^m, \quad (2.27)$$

where the value of the constant c depends on the stirrer type and the nature of the heat-exchange surface. The values of c for various stirrer types and the heat transfer through the tank wall (w) or a spiral coil (s) are reported by Poggemann *et al.* (1980) and Zlokarnik and Judat (1988). The value of c also depends on the presence of baffles within the tank. A similar evaluation is also given by Edwards and Wilkinson (1972). For an anchor stirrer, Uhl and Voznick (1960) reported $c = 1.4$ for the laminar flow regime. For the turbulent flow regime, typical values of c for a variety of stirrers and vessels are summarized in Tabel III.

According to the reported literature, the exponent of the viscosity, m , for both heating and cooling varies between 0.14 and 0.24. For an anchor stirrer in the laminar flow regime, Uhl and Voznick (1960) report $m = 0.18$. The value of the constant a is generally $\frac{2}{3}$ for turbulent flow. For laminar flow, Uhl and Voznick (1960) report $a = 0.43$.

The heat transfer is particularly important for the laminar flow regime, which generally prevails for viscous (e.g., polymeric) systems. Zlokarnik (1969) showed that for a vessel with a low-clearance anchor stirrer, the effects of Re and Pr on Nu decrease steadily as the Reynolds number decreases. He suggested a two-parameter equation of the type

$$\text{Nu} = k_3 (\text{Re} \text{Pr}^{1/2} + k_4)^{2/3} \quad (2.28)$$

TABLE III
TYPICAL VALUES OF c IN THE TURBULENT FLOW REGIME ($Re > 200$)

Nature of Vessel	Stirrer Type	Range of Values of c
Unbaffled, any d_T/d_i	all	0.35–0.4
Baffled	axial flow (e.g., propeller stirrer)	0.5
Baffled	radial flow (e.g., bladed and turbine stirrers)	0.75–0.8
Vessels with spiral coils, without or with baffles; inside or outside the coil	radial flow stirrers	0.70–0.90

to correlate his data. For large Re (i.e., turbulent flow), Eqs. (2.27) and (2.28) are of similar form. Zlokarnik (1969) also suggested that for $0.5 < Re < 200$, a simplified relationship $Nu \propto Re^{0.1}$ can be used for cooling. Thus, for cooling in the laminar flow regime, the effect of Reynolds number on Nu is drastically reduced. For a helical ribbon mixer, Kuriyama *et al.* (1981) report

$$Nu \propto (Re Pr)^{1/3} (\mu/\mu_w)^{0.20}. \quad (2.29)$$

When wall clearances are small, the viscosity at the wall temperature should be used to calculate the Reynolds number.

For highly exothermic reactions, it is necessary to maintain the temperature at a desired level. In general, the heat-transfer coefficient is proportional to $(P_g/V)^{0.25-0.33}$, and the actual power cost varies linearly with (P_g/V) ; these dependencies lead to an optimum value of the reactor volume. For these reactions, when the demand for mass transfer is not important, the radial-flow turbine (curved blades) can be used for an efficient heat transfer. Optimum stirring conditions in the laminar flow regime have been evaluated by Zlokarnik and Judat (1988) and Pawlowski and Zlokarnik (1972).

B. MULTISTAGE MECHANICALLY AGITATED CONTACTORS

The single-stage mechanically agitated contactor suffers from the drawback of large gas- and liquid-phase backmixing, which results in low conversion per pass and low selectivity. Furthermore, with an increase in vessel diameter, the power input is ineffective in the wall region and gas dispersion becomes poor. This limitation can be greatly reduced by using multiple impellers and height-to-diameter ratios greater than one. In addition, these multistage units need thinner walls as compared to the single-stage units for the same contactor

volume, and thus can be used more favorably for high-pressure operations. In a typical multistage contactor, the ratio of the height of each compartment to the column diameter varies in the range of 0.5 to 1.5. The compartments are usually separated by radial baffles in order to reduce the extent of gas- and liquid-phase backmixing. The bottom paddle is generally kept at a height of $d_T/3$ from the vessel bottom.

1. Power Consumption

The power consumption in a multistage column depends upon the number of impellers and the distance between the impellers, along with all other parameters relevant for a single-stage system. Bates *et al.* (1966) reported that nearly five diameters of space between two consecutive propellers are required to consume twice the power of single impeller. Nienow and Lilly (1979), however, reported that for a six-bladed disk turbine, the power consumption of two impellers is twice that of a single impeller when the spacing is only one impeller diameter. The power reduction due to gas flow in the case of two impellers is not as great as that observed in a single-impeller vessel. This may be due to the fast dispersing action of the lower impeller, because of which the population of the gas bubbles near the second impeller is not the same.

2. Mixing

Sullivan and Treybal (1972) suggested the following correlation for the liquid-phase axial dispersion coefficient for a 0.15 m i.d., 12-stage column:

$$\frac{E_L}{HV_L} = 0.239 + 0.1405 \frac{Nd_1}{V_L} \quad (2.30)$$

Joshi (1980) proposed a relation on the basis of liquid circulation generated by an impeller (disk turbine) as

$$E_L = \frac{0.125d_T V_c}{n_s} \quad (2.31)$$

where V_c is the liquid circulation velocity at the column wall and n_s is the number of stages in the contactor. In the presence of gas, the axial mixing in the liquid phase increases. Sullivan and Treybal (1972) proposed

$$\frac{E_L}{d_1 NH_s} = 227.6 \left(\frac{d_1^2 N \rho_L \epsilon_L^2}{H_L} \right)^{-0.928} \quad (2.32)$$

where H_s is the height of each compartment in the multistage contactor.

$$\epsilon_L = 1 - \epsilon_g \quad (2.33)$$

and for $N = 0-8.33$ r/s,

$$\varepsilon_g = 6.876 \times 10^{-4}N + 1.874u_g + 2.31V_L + 0.052, \quad (2.34)$$

and for $N = 8.33-33.33$ r/s,

$$\varepsilon_g = 2.315 \times 10^{-2}N^{0.7} + 0.691 \times u_g^{0.3} + 0.137u_g^{0.2} - 0.234. \quad (2.35)$$

Paca *et al.* (1976) showed that for a 0.51 m i.d. multistage contactor with three impellers and for a non-Newtonian liquid with an apparent viscosity range of 0.001–0.05 Pa S, the mixing time decreases with an increase in gas velocity.

It is expected that an increase in the number of stages will decrease the gas-phase backmixing. Further experimental work is needed in this area.

3. Mass Transfer

The studies of Juvekar (1976) and Ramanarayanan and Sharma (1982) with a 0.2 m i.d. multistage contactor with $d_i/d_T = 0.5$ showed that both a_L and $k_L a_L$ are independent of superficial gas velocity above the critical speed of agitation, and they vary linearly with impeller speed. Both a_L and $k_L a_L$ were independent of the number of stages under otherwise identical conditions of d_i/d_T , N , u_g , and gas-liquid system. Thus, the results for a single stage are applicable to multistage systems. This conclusion needs to be verified for larger-diameter columns.

Nishikawa *et al.* (1984) measured the mass-transfer coefficient $k_L a_L$ for oxygen in sugar solutions in an aerated mixing vessel with multistage impellers. They used a two-region model, where the coexistence of the bubbling controlling-condition region and the agitation controlling-condition region in an aerated mixing vessel is assumed. For a turbine type impeller they presented

$$\begin{aligned} \frac{k_L a_L d_T^2}{\mathcal{D}} &= 0.115 \left(\frac{d_i^2 N \rho}{\mu} \right)^{1.5} \left(\frac{\mu}{\rho \mathcal{D}} \right)^{0.5} \left(\frac{\mu u_g}{\sigma} \right)^{0.5} \\ &\times \left(\frac{N^2 d_i}{g} \right)^{0.367} \left(\frac{N d_i}{u_g} \right)^{0.167} \left(\frac{d_i}{d_T} \right)^{0.4} \text{Ne}^{0.8} \\ &+ 0.112 P_{av} (P_{gv}/\text{Ne} + P_{av}) (u_g/\sqrt{g d_T}) \\ &\times \left(\frac{\mu}{\rho \mathcal{D}} \right)^{0.5} \left(\frac{g d_T^2 \rho}{\sigma} \right)^{0.66} \left(\frac{g d_T^3 \rho^2}{\mu^2} \right)^{0.42} \end{aligned}$$

where P_{gv} and P_{av} are agitation power per unit mass of liquid and aeration power per unit mass of liquid, respectively. Nishikawa *et al.* (1981) also

suggested the following impeller clearance to obtain high $k_L a_L$:

$$\Delta C/d_1 > 1.5 \quad \text{for turbine-type,} \quad (2.37)$$

$$\Delta C/d_1 > 1.6 \text{ or } \Delta C/d_1 < 0.1 \quad \text{for paddle-type,} \quad (2.38)$$

where ΔC is the clearance between two successive impellers.

The above relation implies strong dependence of $k_L a_L$ on N , u_g , d_1 , and the liquid properties (μ , ρ and σ).

C. GAS-INDUCING CONTACTORS

In several industrially important unit processes, such as hydrogenation, alkylation, ozonolysis, oxidation with molecular oxygen, ammonolysis, addition halogenation, etc., it is desirable to have complete utilization of the solute gas. However, the gas-phase conversion per pass in a large number of gas-liquid reactions is low in the case of conventional mechanically agitated contactors because of the limited residence time of the gas and/or the low rate of the chemical reaction. The external recycle of the gas can be eliminated by using self-inducing impellers. The gas-inducing type of agitated contactor (see Fig. 8) is very popular in flotation, hydrometallurgy operations and in biological waste water treatment. In the latter process, pure oxygen is often used. When using oxygen, it is desirable that the system should be a "dead-end" type with respect to oxygen. Since the solubility of oxygen is low, the mass conversion of oxygen is low and the unreacted oxygen is required to be recycled.

Many designs of self-inducing impellers are reported in the literature. Figure 9 illustrates some of the designs. Zlokarnik (1966) suggested a design (see Fig. 9a) that contains a hollow shaft and a hollow impeller. The impeller consists of a hollow tube, which at the center is connected to a hollow shaft. At the two ends of the impeller, cuts at 45° are taken so that while the impeller is rotating, the open portions are kept at the near side. Hollow stirrers operate on a principle similar to that of water-jet ejectors. The tube stirrer appears to be the most effective hollow stirrer, as well as the simplest to construct. The stirrer can draw either external air or recirculating gas of the tank's gas head, depending on whether the inlet holes in the shaft are located above or below the vessel cover. Recirculation is particularly useful, since bubbling the gas once through the liquid does not use it completely (particularly for slow reactions). Hollow stirrers are particularly suitable in operations under pressure, since no pumping is required for gas recirculation in chemical reaction at constant pressure.

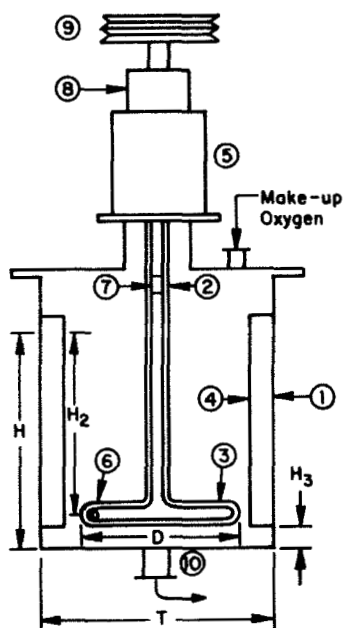


FIG. 8. Inducing type of agitated contactor. 1, vessel; 2, hollow shaft; 3, hollow impeller; 4, baffles; 5, gland and stuffing box; 6, orifice on the impeller; 7, gas inlet; 8, bearing housing; 9, pulley; 10, liquid drain. (After Joshi *et al.*, 1985.)

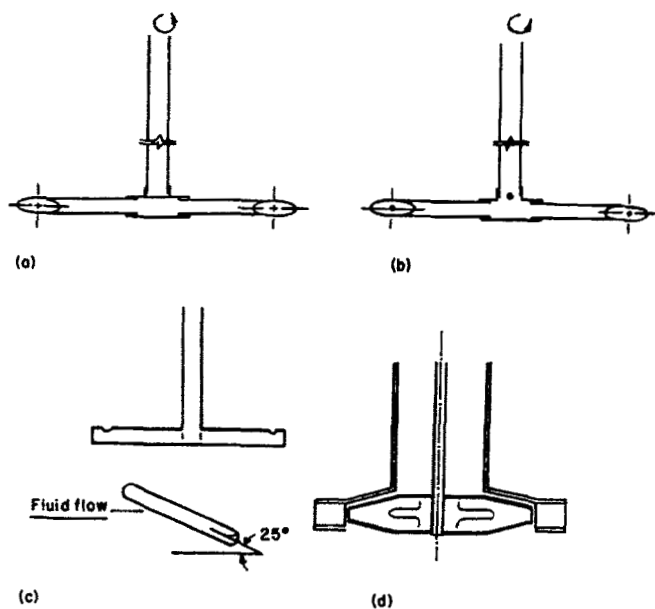


FIG. 9. Different designs of gas-inducing agitators. (a) Gas-inducing type pipe impeller; (b) gas-inducing type modified pipe impeller; (c) gas-inducing type flattened cylindrical impeller; (d) turbo aerator. (After Joshi *et al.*, 1985.)

Joshi (1980) modified the pipe impeller design. Holes were drilled near the tip of the impeller and on the hub (Fig. 9b). In this design, the increase in the liquid flow increases the rate of gas induction by 30–60% at practically the same power consumption. Martin (1972) used a flattened cylindrical tube so as to simulate the aerofil design (Fig. 9c). In flotation applications, the Denver and Wamco type of self-inducing impellers has been widely used for several decades. Zundelovich (1979) has modified the Denver design so as to increase the rate of gas induction by about 100% (Fig. 9d).

In all of these different types of gas-inducing agitated vessels, the pressure drop required for the flow of gas is provided by the impeller and no external gas pumping device is necessary. Both liquid and gas phases are considered to be completely backmixed.

1. Critical Impeller Speed for Gas Induction

When the gas-inducing impeller rotates in a fluid, the sudden acceleration of the fluid elements causes reduction in the static pressure. In all the designs, the reduced pressure area is connected to the gas space, and the gas is induced if the reduction in pressure is sufficient to overcome all the resistance in the path of the gas.

It is desirable to know *a priori* the minimum (or critical) impeller speed, N_{cy} , at which the onset of gas induction occurs. The onset of induction will occur when the static pressure at the point of gas induction equals the static pressure in the gas space. For pipe and flattened cylindrical impellers, Joshi and Sharma (1977) proposed

$$\frac{N_{cy}^2 d_1^2}{gH_L} = -\frac{2}{\Pi^2 K}. \quad (2.39)$$

The value of K lies in the range -0.9 to -1.3 . For the liquid viscosity range 1 to 80×10^{-3} Pa S, Sawant and Joshi (1979) proposed the following relationship for the Denver and Wamco type of flotation cell:

$$\frac{N_{cy}^2 d_1^2}{gH_L} \left(\frac{\mu_w}{\mu} \right)^{0.11} = 0.21. \quad (2.40)$$

The previous relationship indicates strong dependence of N_{cy} on d_1 and H_L .

2. Rate of Gas Induction

Because the gas is aspirated through a hollow stirrer in a gas-inducing impeller, the gas must overcome the hydrostatic pressure of the liquid above the stirrer, $H^* \rho g$. The liquid head over the stirrer, $H^* \equiv (H_L - H_i)$, therefore has a significant influence on the gas flowrate q . A uniform aeration of

the vessel contents can be achieved at $H_i/d_i = 1$, where H_i is the stirrer clearance from the bottom. For $d_T/d_i \simeq 3$, the d_T/d_i ratio has no effect on aeration. In order to minimize the pressure drop in the hollow shaft, the shaft and the inlet openings are usually generously dimensioned.

The surface tension σ and the dynamic viscosity of the liquid μ (as long as it is low) do affect gas flowrate. For viscosities greater than 0.5 PaS, however, the use of hollow stirrers for aeration becomes meaningless. Since aeration deals with a material system with large density differences, the operation is strongly influenced by the parameter $g \Delta \rho / \rho \simeq g$ at normal pressure, and therefore by the Froude number.

The gas throughput characteristic of a hollow stirrer generally has the form $N_A = f(\text{Fr } d_i/H^*, \text{Ga}, d_T/d_i, H_i/d_i)$, where $N_A \equiv q_g/(Nd_i^3)$ is the dimensionless flowrate number, $\text{Fr} \equiv Nd_i/g$ the Froude number, and $\text{Ga} \equiv d_i^3 g / \nu^2$ the Galileo number. For liquids with viscosities close to that of water and for $H_i/d_i = 1$, the gas throughput characteristics for the tube stirrer shown in Fig. 9 are as follows:

$$\frac{1}{N_A} = 33(\text{Fr } d_i/H^*)^{-1.47} + 180(d_T/d_i)^{-4.1}, \quad \text{Fr } d_i/H^* \leq 1.80; \quad (2.41)$$

$$\frac{1}{N_A} = 15.5(\text{Fr } d_i/H^*)^{-0.19} + 180(d_T/d_i)^{-4.1}, \quad \text{Fr } d_i/H^* \geq 1.80. \quad (2.42)$$

The optimum operating conditions under which the desired gas flow rate is attained at the minimum stirrer power (per unit of gas flow) can be found by combining the dimensionless number N_A , Ne , and Fr . The appropriate dimensionless group in this case is $\text{Ne Fr}/N_A \equiv P/(q_g \rho g d_i)$, and is likewise a function of $\text{Fr } H^*/d_i$. The optimum operating condition for the tube stirrer is given by $\text{Fr } d_i/H^* = 1.80$; here $H^* = H_L - H_i$ (i.e., liquid height above the stirrer).

For an air–water system with a liquid volume of 0.05 m³ and a height of 0.4 m, Joshi *et al.* (1982) have compared the gas induction rate for a variety of impellers. Their analysis indicates that for a power consumption per unit liquid volume greater than approximately 2 KW/m³, the turbo-aerator gives the maximum rate of gas induction for a given power consumption. The procedures for the calculations of gas induction rate for pipe, Denver, and turbo impellers are given by Zlokarnik (1966), Zundeleovich (1979), and Sawant and Joshi (1979), respectively.

3. Gas–Liquid Mass Transfer

The gas–liquid interfacial area and the volumetric mass transfer coefficient for pipe and flattened cylindrical impellers are given by Joshi and Sharma

(1977) as

$$a_L = 112(P_g/V)^{0.4}u_g^{0.5}, \quad u_g < 5 \text{ mm/s}, \quad (2.43)$$

$$a_L = 36.7(P_g/V)^{0.4}u_g^{0.25}, \quad u_g > 5 \text{ mm/s}, \quad (2.44)$$

and

$$k_L a_L = 6.8 \times 10^{-3}(P_g/V)^{0.55}u_g^{0.5}, \quad u_g < 5 \text{ mm/s}, \quad (2.45)$$

$$k_L a_L = 3.26 \times 10^{-3}(P_g/V)^{0.55}u_g^{0.25}, \quad u_g > 5 \text{ mm/s}. \quad (2.46)$$

These correlations were developed from experimental results obtained in agitated contactors of diameters 0.41, 0.56, and 1.0 m i.d., with other ranges of operating conditions as follows: $0.35 < d_i/d_T < 0.75$, $H_B/d_T < 0.5$, $0.1 < B/d_i < 0.3$, $3 < N < 11.7$, and $0.3 < u_g < 32 \text{ mm/s}$. Joshi and Sharma (1977) and Sawant and Joshi (1979) showed that all gas-inducing aerators provide comparable values of a_L and $k_L a_L$ for the same value of P_g/V .

4. Heat Transfer

For a 0.4 m contactor containing a triangular hollow gas-inducing stirrer, Zlokarnik (1966) proposed the following correlation for the heat-transfer coefficient to a heating coil:

$$\text{Nu} = 0.185(\text{Re}_{g,T})^{0.733}(\text{Fr}_{g,T})^{-0.267}(\text{Pr})^{0.466}, \quad (2.47)$$

where

$$\text{Re}_{g,T} = \frac{\rho_L u_g d_T}{\mu_L}, \quad \text{Fr}_{g,T} = \frac{u_g}{gd_T}, \quad \text{Pr} = \frac{\mu_L C_P}{\lambda_L}.$$

More experimental work on this subject is needed. The above relation implies strong dependence of the heat transfer coefficient on the gas velocity and the liquid properties (ρ_L , μ_L , λ_L , and C_P).

D. CYCLONE SPRAY REACTOR

In a cyclone spray reactor, liquid is sprayed in the center of a gas cyclone. The centrifugal field created by the rotating gas accelerates the droplets in the radial direction toward the wall. Liquid–gas slip velocities are high, and gas-side mass-transfer coefficients are far in excess of those for conventional, gravity-controlled contactors. The reactor was used by Schrauwen and Thoenes (1988) for selective absorption of hydrogen sulfide in an amine solution from a mixture of hydrogen sulfide and carbon dioxide. The reactor is thus useful for the separation of gaseous compounds depending on their intrinsic rates of reaction with a dissolved reactant.

Another type of cyclone reactor was developed by Beenackers (1978) to study selectivity of the reaction between benzene and benzene + 1,2-dichloroethane and sulfur trioxide. In this reactor, liquid is fed tangentially, and a gas mixture of SO_3 and N_2 is introduced into the reactor via a porous section of the cylindrical wall. The liquid phase is the continuous phase in the reactor, except near the cyclone axis. Here a gaseous core is found, due to a strong centripetal field generated by the rotating liquid. This field causes gas bubbles to spiral from the wall to the cyclone axis. Gas leaves the reactor via the upper outlet, which is known as the vortex. Liquid leaves the reactor via the bottom outlet, which is referred to as the apex. A cone at the bottom prevents gas entrainment with the liquid. Liquid entrainment through the vortex varies between 12 and 20%, depending on gas and liquid velocities. Because of centripetal forces on gas bubbles, k_L for cyclone reactors is found to be considerably larger than that for tubular reactors. Beenackers (1978) found that because of the high k_L , the cyclone reactor gave superior selectivity (nearly 100%) compared to tubular and stirred-cell reactors.

E. SUMMARY

Mechanically agitated gas-liquid reactors are widely used in laboratories, although their use in large-scale operations is somewhat limited due to the required energy cost of mixing. Large-scale operations are possible in the production of fine chemicals, pharmaceutical products, or high-priced chemicals.

The design parameters for gas-liquid reactors depend on the nature of the reaction system, as well as on the design of the stirrer. The suitability of various stirrer designs is outlined in Table II.

While a number of good correlations for the gas holdup in mechanically agitated reactors are available (Joshi *et al.*, 1982), the best correlations are those by Hughmark (1980) and Sridhar and Potter (1980), and they are recommended. The critical impeller speed, N_0 , required for effective gas-liquid dispersion, and the impeller speed at which gas above liquid is first entrapped, N_c , can be reasonably well calculated using Eqs. (2.4) and (2.5), respectively.

For aerated, agitated vessels, the power consumption is best described by the dimensionless relationship $Ne = f(N_A, Re, Fr, Ga, d_T/d_I)$. The aeration number N_A exerts the dominant influence on the power number (see Eq. 2.8). The effect of Fr can be neglected for $Fr < 0.5$.

The mixing time ($N\theta$ in the dimensionless form) is mainly dependent upon the geometrical parameters of the stirrer and vessel. $N\theta \propto (d_T/d_I)^\beta$, where β varies from 2 to 2.57 for flat-blade turbines and $\beta = 2$ for propellers.

Circulation models indicate $N\theta$ to be also dependent upon the heights of the impeller from the bottom of the vessel and the heights of the unagitated liquid level (see Eqs. (2.11)–(2.14). For an aerated vessel, the use of Eq. (2.15) for $N\theta$ is recommended. Generally, both gas and liquid are considered to be completely backmixed for a stirrer speed greater than N_0 . While more information on gas-phase backmixing is needed, if the reaction depends on the partial pressure of gas, an optimum impeller speed to achieve the maximum space–time yield lies in the vicinity of critical impeller speed.

The volumetric gas–liquid mass transfer coefficient, $k_L a_L$, depends upon physical properties such as viscosity, density, and surface tension of liquid. In general, $a_L \propto \rho_L^{0.2}/\sigma_L^{0.6}$. The coalescence characteristics of the vessel have a pronounced effect on a_L and $k_L a_L$. The correlation presented by Judat (1982) is recommended for this purpose. Foaming characteristics can also influence $k_L a_L$. In general, the use of $k_L a_L = f(P/V, u_g)$ relationship is recommended for a given aerated vessel. The diameters of stirrer and vessel and the heights of stirrer and liquid level also affect $k_L a_L$. The work of Calderbank and co-workers in this area is most worth noting.

The fluid–coil and fluid–wall heat transfer have been extensively studied (Joshi *et al.*, 1982; Zlokarnik and Judat, 1988). The best relationship is $Nu \propto c Re^a Pr^b (\mu/\mu_w)^m$, where the values of c , a , b , and m largely depend on the nature of the stirrer and the agitated vessel. Generally, relationships are divided into two flow regimes: laminar for $Re < 200$, and turbulent for $Re > 200$. For $Re > 10^5$ (very intense stirring), the relationship $st \propto (Re_g Fr_g Pr_g^2)^{1/3}$ is recommended. Strategies for optimum heat transfer operations outlined by Zlokarnik and Judat (1988) are recommended for viscous systems.

Novel gas–liquid mechanically agitated reactors such as multistage mechanically agitated reactors, gas-inducing contactors, and cyclone reactors should find an increasing number of applications.

The liquid-phase mixing in a multistage mechanically agitated reactor is best correlated by Eq. (2.31) in the absence of gas flow and by Eq. (2.32) in the presence of gas flow. The mixing time can be estimated from the study of Paca *et al.* (1976). Experimental work is needed to estimate gas-phase backmixing. The use of Eq. (2.36) for the calculation of the gas–liquid volumetric mass transfer coefficient in a multistage mechanically agitated column is recommended.

In a gas-inducing reactor, both gas and liquid phases are generally considered to be completely backmixed. The use of Eqs. (2.39) and (2.40) for the calculations of the critical speed for gas induction is recommended. The rate of gas induction can be expressed by a dimensionless relation $N_A = f(Fr d_i/H^*, Ga, d_T/d_i, H_i/d_i)$. The most important parameters are $Fr d_i/H^*$ and d_T/d_i . For a given power input per unit volume, the turbo aerator appears

to give the best rate of gas induction. The volumetric gas-liquid mass-transfer coefficient, $k_L a_L$, (as well as a_L) is best related to the parameters (P_g/V) and u_g (see Eqs. 2.43–2.46). The use of Eq. (2.47) for the heat transfer calculation is recommended.

The cyclone reactors will provide a large gas-liquid mass-transfer coefficient. However, these reactors are most useful only in small-scale operations and for kinetic study of very fast reactions.

Finally, some remarks on the operation of mechanically agitated gas-liquid reactors are worth mentioning. The mode of operation (i.e., batch, semibatch, continuous, periodic, etc.) depends on the specific need of the system. For example, the level of liquid-phase backmixing can be controlled to any desired level by operating the gas-liquid reactor in a periodic or semibatch manner. This provides an alternative to the tanks in series or plug flow with recycle system and provides a potential method of increasing the yield of the desired intermediate in complex reaction schemes. In some cases of industrial importance, the mode of operation needs to be such that the concentration of the solute gas (such as Cl_2 , H_2S , etc.) as the reactor outlet is kept at a specific value. As shown by Joshi *et al.* (1982), this can be achieved by a number of different operational and control strategies.

F. FUTURE WORK

The future work should include:

- development of design parameter correlations for a mechanically agitated gas-liquid reactor containing non-Newtonian and/or viscoelastic liquids;
- development of design parameter correlations for a mechanically agitated gas-liquid reactor operating near critical temperature and pressure conditions of the reactions; and
- development of novel methods to improve gas-phase residence time, gas-liquid mass transfer, and heat transfer with a minimum increase in power consumption, particularly for viscous liquids.

III. Slurry Reactors

Mechanically agitated slurry reactors have a wide range of applications in the chemical, biochemical, and pharmaceutical industries and, in particular, catalytic processes (see Table IV). They are commonly used for catalytic hydrogenation, oxidation, halogenation, or polymerization reactions such as

TABLE IV
SOME APPLICATIONS OF MECHANICALLY AGITATED SLURRY REACTORS

System	Catalyst	Pressure (atm)	Temperature (°C)
Hydrogenation of soybean oil	Cu-chromite or supported Ni	2.0	170–200
rapeseed oil	Nickel	0.3–10	140–220
2,4-dinitrotoluene	Pd-alumina	1–5	25–70
butynediol	Pd-Zn-CaCO ₃	10–20	50–90
Oxidation of SO ₂	Activated C	1	25

edible oil hydrogenation, olefin oxidation or hydroformylation, SO₂ oxidation, etc. Some fermentation processes also use slurry reactors. These reactors can be operated with both gas and liquid phases fed continuously, with only the gas phase fed continuously, and as batch reactors. Thus, they are suitable for both bulk and fine chemicals production.

The well-known advantages of the slurry reactor over other types of three-phase reactors (such as trickle bed or fixed bed upflow reactor) are the following:

- (1) intraparticle diffusional resistance is less compared to trickle or packed bubble column reactors because of the use of smaller catalyst particles;
- (2) there can be better control of thermal behavior of slurries; the possibility of hot spot formation and temperature runaway is also minimized;
- (3) it is not necessary to shut down plants for catalyst replacement, as it can be removed continuously or added while the plant is in operation;
- (4) the problem of partial wetting of catalyst (as observed in trickle bed reactors) is not encountered in slurry reactors, which leads to better utilization of the catalyst surface; and
- (5) under comparable conditions, the space-time yield is often higher in slurry reactors.

In spite of these advantages of slurry reactors, some technical difficulties are involved in the operation of these reactors. For example, separation of the catalyst and handling of the slurry is difficult; the solids can produce erosion of the equipment; and significant backmixing of the liquid phase does not allow operation in a plug-flow manner.

The important design parameters for a stirred slurry reactor are the power input by the stirrer, the pumping flow rate of the stirrer, which affects the

homogenization of various phases; gas holdup; macro- and micromixing within the slurry, gas-liquid and liquid-solid mass transfer rates; and the slurry-wall heat transfer rate. These design parameters are affected by the physical properties (slurry density, viscosity, and interfacial tensions), operating parameters, such as gas and liquid flow rates, liquid volume, catalyst size, concentration, density, stirrer speed, and geometrical parameters such as stirrer shape and size, number of stirrers, vessel diameter, height of liquid, bottom shape, clearance of the stirrer, number and width of baffles, etc.

In this section, we first evaluate the design of conventional nonaerated and aerated stirred slurry reactors. Since the design of mechanically agitated gas-liquid reactors has already been discussed in Section II, here the main emphasis is placed on the effects of solids on the design parameters. We subsequently illustrate some special-purpose slurry reactors used in the chemical and petrochemical industries. Novel slurry reactors used in biological or polymeric industries are discussed in Sections VI and VII, respectively.

A. CONVENTIONAL MECHANICALLY AGITATED REACTORS

The mechanically agitated aerated slurry reactors, used in hydrogenation of unsaturated oils, production of aluminum alkyls, hydroxylamine synthesis, and fermentation processes, are the oldest types of slurry reactors. Technical dimensions of these reactors range from $< 1 \text{ m}^3$ up to several hundred cubic meters of reaction volume. The operating pressure is usually less than 100 bar in order to avoid design problems. The energy needed for solids suspension depends mainly on the geometry of the agitator and reactor, and to a lesser extent on the specific gas load. Turbines seem to be more effective as agitators than paddles. In the usual range of operation, the gas flow rate and the type of gas distributor have only a minor influence on fluid dynamics if the agitator speed is high. On the other hand, the gas flow rate and the gas distributor are important in the case of smaller stirrer speeds. Typically, the gas is fed below the stirrer through a suitable device such as a toroidal sparger. Gas flow rates in the range of 0.5 m/s and higher are in use, and values of the gas holdup between 0.2 and 0.4 have been measured. For catalytic reactions, typical solid concentrations are in the range of 10–20 g/L. An agitator diameter of $\frac{1}{3}$ of the reactor diameter seems to be optimal. The agitator is most often installed approximately at half the impeller (or $\frac{1}{6}$ the reactor) diameter distance from the bottom. But it should be noted that the optimal location in two-phase systems does not necessarily coincide with that in a three-phase system; it is also dependent on the solid concentration and the gas supply system (Nagata, 1975). In the case of pressure aeration, gas throughput and stirrer speed are independent process variables, whereas in surface aeration or gas suction

through the stirrer shaft, both are coupled. The height-to-diameter ratio of the reactor is close to one, preferentially in high coalescing systems, but also H/d_T ratios of 2.5 are to be found in practice; in the latter case, very often several agitators are mounted on the same shaft.

Although, as shown in Section I, a number of different types of stirrers are used in practice, one widely used stirrer is the so called Rushton six-blade turbine, suggested by Rushton and coworkers (Rushton *et al.*, 1950). The disk of this turbine prevents gas from short-circuiting along the stirrer shaft. Recently, improvements in performance have been obtained by changing to 12 or 18 blades, or employing perforated or hollow blades. Axial stirrers, like pitched-blade turbines and marine propellers, are seldom used for gas-liquid dispersion, even though they are particularly effective for suspending solids.

With a gas sparger and a radial turbine of the Rushton type, gas loads of up to $500 \text{ m}^3/(\text{m}^2\text{h})$ can be achieved with reasonable energy consumption. This method of dispersing the gas phase is usually employed for fast reactions or in situations where the hourly demand for the gaseous reactant is high, as in industrial fermenters. With such high gas-feed rates, the gas reactant may not react completely, so that eventually the unreacted gas may be recycled externally.

When the reaction is slow, surface aeration (described later in Section VI) becomes practical. Surface aeration can be improved by using gas-inducing agitators. One version of this agitator consists of a hollow shaft with a hollow impeller. Rotating the impeller reduces the static pressure behind the blades, drawing gas down the shaft and into the liquid. In the region of reduced pressure, holes are drilled in the blade wall, through which the gas flows out into the liquid. Surface aeration permits gas loads of up to $100 \text{ m}^3/(\text{m}^2\text{h})$.

1. Hydrodynamics

The most important fluid dynamic parameters of aerated stirred slurry reactors are the energy dissipation and pumping efficiency of the agitator, gas throughput, gas holdup, mean bubble diameter (i.e., interfacial area), and flooding characteristics. As mentioned earlier, these parameters are affected by the physical properties of the slurry, as well as the operating and geometrical parameters of the system. For low solids loading, the suspended solids do not significantly affect the hydrodynamics.

Wiedmann *et al.* (1980) studied the flow regimes and the flooding characteristics of a slurry reactor. They found that at low gas velocity, the gas stream does not change the flow pattern significantly, and the bubbles and particles are essentially carried along by the circulation flow produced by the stirrer. With increasing gas flow rate, however, the liquid circulation gets more and more pronounced. A further increase in the gas rate leads to the so-called flooding point, at which the gas breaks through in the middle of the vessel

without dispersing. Under such conditions, the radial flow from the stirrer declines drastically and the escaping gas determines the flow in the vessel. Also, in this situation, the particles tend to settle down at the bottom because of reduced effect of the stirrer.

Although, as pointed out by Smith (1981), a distinction must be made between the flow field in the vicinity of the stirrer and that in the whole vessel, there is a strong interaction in the flow fields in these two regions. When the turbine is used in a low-viscosity liquid, two spinning vortices arise behind each blade (Van't Riet and Smith, 1973, 1975; Bruijn *et al.*, 1974). Large centrifugal forces created by these vortices result in a low-pressure region near the blades, causing bubbles to flow near them and form a cavity in the eye of the vortices. This is region (a) in Fig. 10, generally formed at low gas flow rates. As gas flow increases, the cavity volume increases and a clinging cavity is formed (region (b) in Fig. 10), which adheres to the blade. The liquid flow in this region is mainly radial. A further increase in gas flow rate leads to the formation of large streamline cavities (region (c) in Fig. 10), and the liquid flow shifts from radial to tangential. Region (c) is more stable than region (b) and is more effective for gas dispersion. Region (c) also causes a decrease in the drag coefficient at the blade and thereby leads to a decrease in power dissipation. As gas flow is further increased, cavities behind each blade of the stirrer become very large, and they are bridged to cause flooding or selective gas flow near the

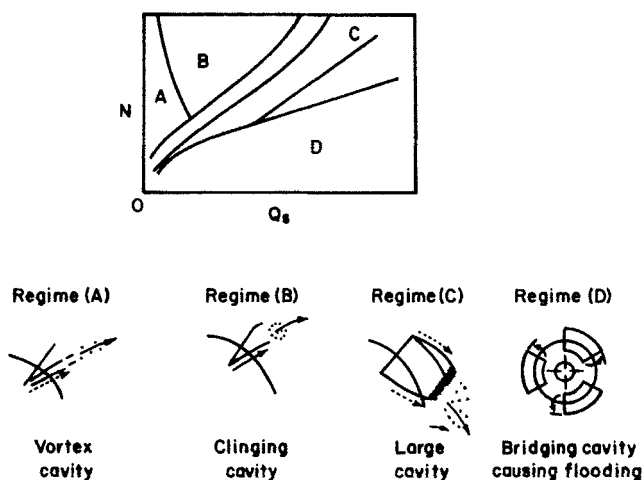


FIG. 10. Qualitative diagram of stirrer zone hydrodynamic regimes for a Rushton turbine. (Adapted from Bruijn *et al.*, 1974.)

TABLE V

LITERATURE CHARACTERIZATION OF THREE FUNDAMENTAL HYDRODYNAMIC REGIMES^a

Regime a	Regime b	Regime c
By pass (Sicardi <i>et al.</i> , 1982; Loiseau <i>et al.</i> , 1977)	Loading (Sicardi <i>et al.</i> , 1982; Loiseau <i>et al.</i> , 1977)	Total aeration (Sicardi <i>et al.</i> , 1982)
Flooding of the stirrer (Bruxelmann, 1978)	Flooding of the vessel (Nienow <i>et al.</i> , 1977; Rushton and Bimbinet, 1968)	Total gas circulation and secondary circulation loops (Nienow <i>et al.</i> , 1977)
Slightly aerated liquid (Wiedmann <i>et al.</i> , 1980)	Aerated liquid (Wiedmann <i>et al.</i> , 1980)	Flooding (Loiseau <i>et al.</i> , 1977)
No gas dispersion (Nienow <i>et al.</i> , 1977; Rushton and Bimbinet, 1968; Westerterp <i>et al.</i> , 1963; Van Dierendonck <i>et al.</i> , 1968)		

^a For any regime: $N_{A, \max} = \frac{Q_{g, \max}}{d_i^3 N} = f(\text{Fr}, d_T/d_i)$ (Judat, 1976).

middle of the vessel (region (d) in Fig. 10). Thus, flooding is initiated by the flow field near the stirrer.

In principle, various hydrodynamic regimes can also be set up by changing stirrer speed for a fixed gas flow rate. Unlike in Wiedmann's experiments, if, at a constant gas feed rate, the stirrer speed is increased, three fundamental hydrodynamic regimes arise, which, as shown in Table V, are referred to by various names in the literature. For our discussion, we will refer them as regimes a, b, and c. A schematic of these three regimes is shown in Fig. 11. At low stirrer speed (Fig. 11a), bubbles rise around the shaft following a helical path. In regime b, bubbles begin to disperse in the zone above the stirrer. In regime c, bubbles are dispersed in the whole vessel, and recirculation of gas to the stirrer takes place (Fig. 11d), and as the stirring rate increases further, secondary recirculation loops are observed. In regime c, recirculation of gas bubbles to the stirrer allows the gas flow through the agitator to be greater than that fed to the sparger. Near the stirrer zone, regime a corresponds to flooding, regime b corresponds to the formation of large cavities behind the stirrer blades, and regime c corresponds to small clinging cavities. Similar flow regimes are obtained for viscous and non-Newtonian fluids (Ranade and Ulbrecht, 1977), except for high N , where a reverse flow (liquid enters

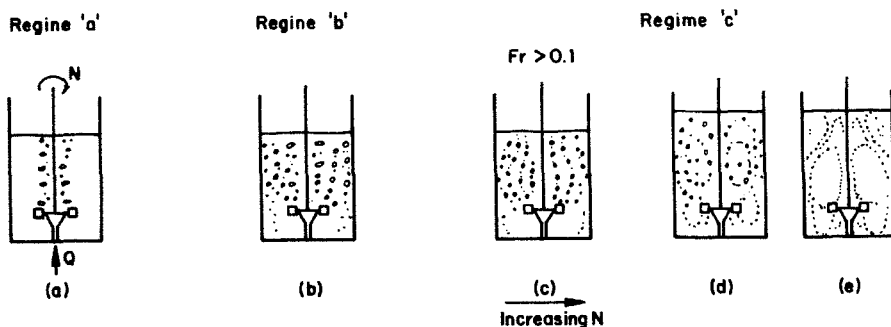


FIG. 11. Vessel hydrodynamic regimes and the evolution of dispersion as stirrer speed increases at a constant gas feed rate.

zone from a radial direction and is pumped axially) appears for viscoelastic fluids.

The flow rate required for the transition from regimes a to b or b to c is correlated to the Froude number and other system parameters, as shown in Table VI. The flowrate for the a–b transition depends on the direction in which N is changed, as well as on the reactor scale (Zlokarnik and Judat, 1967). Van't Riet and Smith (1975) showed that the dispersion does not occur if $Fr < 0.1$. The aeration number for the b–c transition is mainly a function of the Froude number.

2. Power Consumption

Power or energy dissipated in the aerated suspension has to be large enough (a) to suspend all solid particles and (b) to disperse the gas phase into small enough bubbles. It is essential to determine the power consumption of the stirrer in agitated slurry reactors, as this quantity is required in the prediction of parameters such as gas holdup, gas–liquid interfacial area, and mass- and heat-transfer coefficients. In the absence of gas bubbling, the power number P_{0l} is defined as

$$Ne_\ell = P_{0l} = \frac{P_l}{\rho_l N^2 d_l^5}, \quad (3.1)$$

where P_l is the power dissipated by a stirrer, d_l the stirrer diameter, and N the stirrer speed. This power number depends on the stirrer and vessel geometry. For fully baffled tanks, P_{0l} is constant for values of stirrer Reynolds number greater than 10,000.

In the presence of gas bubbling, power dissipation decreases because of the reduction of form drag of the blades as a result of the formation of streamline

TABLE VI

AERATION NUMBERS FOR REGIME TRANSITIONS (RUSHTON TURBINE)

Authors	Relationships	Transition Type
Bruxelmane (1978)	$N_A = \frac{Q_g}{Nd_i^3} = 3.93 \text{ Fr}^{0.72} (d_i/d_T)^{1.9} (\ell/d_i)^{0.47} (w_i/d_i)^{1.30} n_p^{1.50}.$	a-b
Van Dierendonck <i>et al.</i> (1968)	$\frac{1}{N_A} = \frac{0.07 d_i (g d_T^3)^{0.5}}{Q_g}; \quad d_T < 1 \text{ m}, u_g < 0.03 \text{ m/s.}$ $\frac{1}{N_A} = 2 \left(\frac{\sigma_\ell^3 \rho_\ell}{\mu_\ell^4} \right)^{-0.25} \left(\frac{H - H_i}{d_T} \right)^{0.5} \left(\frac{d_T d_i \sigma_\ell}{Q_g \mu_\ell} \right); \quad d_T > 1 \text{ m}, u_g < 0.03 \text{ m/s.}$	a-b
Bruxelmane (1978)	$N_A = \frac{Q_g}{Nd_i^3} = 2.45 \text{ Fr}^{0.78} (d_i/d_T)^2 (\ell/d_i)^{0.41} (w_i/d_i)^{1.20} n_p^{1.35},$ <p>ℓ = length of blade; w = height of blade; n_p = number of blades.</p>	b-c
Nienow <i>et al.</i> (1977)	$\frac{1}{N_A} = \frac{4 d_i d_T^{0.2}}{Q_g^{0.5}}.$	b-c

cavities. In this case, one can similarly define

$$Ne_g = P_{0g} = \frac{P_g}{\rho_g N^3 d_1^5}. \quad (3.2)$$

The power number Ne_g depends on the aeration number N_A . The aeration number represents the ratio between the gas feed rate that must be handled by the stirrer and a quantity proportional to the delivery rate of the stirrer. The behavior of Ne_g as a function of the aeration number (varied by changing the stirrer speed) at different gas feed rates is illustrated in Fig. 12. As N increases, the power number first decreases and then rapidly increases. The maximum at very high speeds corresponds to the development of a secondary recirculation loop (Nienow *et al.*, 1977), and the minimum in P_{0g} is very close to the transition between b and c regimes (Sicardi *et al.*, 1982).

For the gas-liquid systems, Michel and Miller (1962) proposed the following correlation to predict the power consumption:

$$P_g = \alpha \left(\frac{P_\ell^2 N d_1^2}{Q_g^{0.56}} \right)^m, \quad (3.3)$$

where α and m are constants specific to a given vessel and stirrer geometry. For turbine stirrers and pure liquids, $m = 0.45$, and

$$\alpha = 0.34 n_p \quad (\text{S. I. units}), \quad (3.4)$$

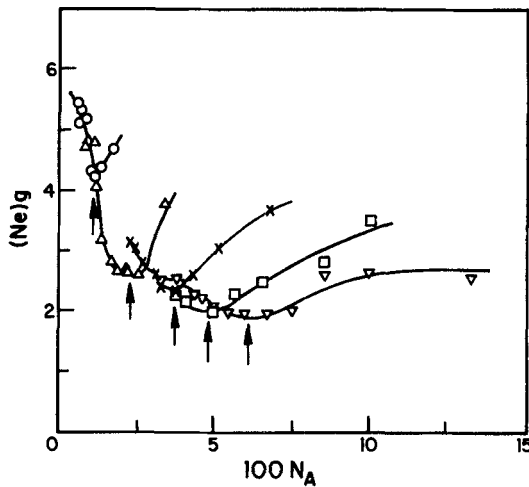


FIG. 12. Power number as function of aeration number. $d_T = 0.230$ m; $d_1 = 0.054$ m; tube sparger. Q_g (10^{-4} m³/s): \circ , 0.17; \triangle , 0.33; \times , 0.67; \square , 1.00; ∇ , 1.33. (After Sicardi *et al.*, 1981; also, Baldi, 1986.)

where n_p is the number of stirrer blades. For solutions, especially saline aqueous solutions, m may have values as low as 0.33 (Midoux and Charpentier, 1979). Sicardi *et al.* (1982) observed that the P_g calculated from Eq. (3.3) best fit the experimental data in regime c. For $m = 0.45$, Eq. (3.3) also shows that

$$P_g/P_t = (N_A)^{-0.25} N^{-0.1} d_t^{0.1}. \quad (3.5)$$

This relation suggests that P_g/P_t is largely influenced by the aeration number.

Loiseau *et al.* (1977) found that their data for nonfoaming systems agreed well with Eq. (3.3). Calderbank (1958), Hassan and Robinson (1977), and Luong and Volesky (1979) have also proposed correlations for power consumption in gas-liquid systems. Nagata (1975) suggested that power consumption for agitated slurries can be reasonably predicted from these correlations by the correction factor ρ_{sl}/ρ_L , where ρ_{sl} is the density of the slurry. Power consumption for a gas-liquid-solid system has also been studied by Wiedmann *et al.* (1980). They examined the influence of gas velocity, solid loading, type of stirrer, and position of the stirrer blades on power consumption; plots of power numbers vs. Reynolds numbers for propeller and turbine type impellers proposed by them are shown in Fig. 13.

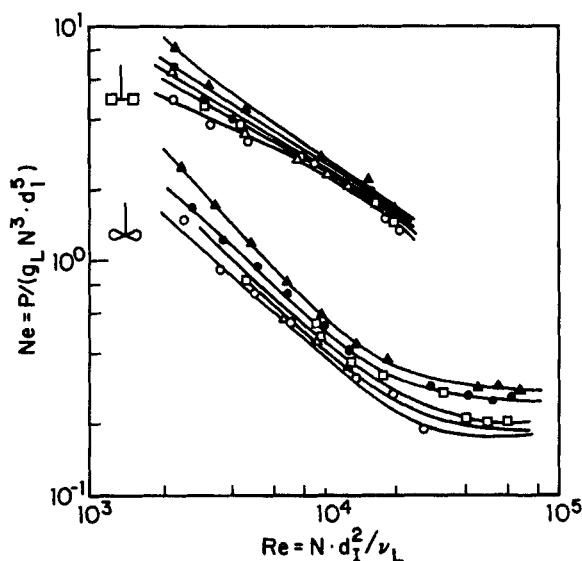


FIG. 13. Effect of solid content on power number vs. Reynolds number plot. Tank: $d_T = 0.45$ m; $H_R/d_t = 0.5$; sintered plate. System: air; $u_g = 0.025$ m/s; glass beads, $298 \mu\text{m}$; 60 wt % glycerol solution. ϵ_s : \circ , 0; \triangle , 0.05; \square , 0.10; \bullet , 0.20; \blacktriangle , 0.30. (Reprinted by permission of VCH Publishers, Inc., 220 East 23rd St., New York, NY 10010, from Wiedmann, J. A., Steiff, A., and Weinspach, P. M., *Ger. Chem. Eng.* 3, 303, 1980.)

They found that optimal conditions of the position of the stirrer exist in the range of $0.25 < H_i/d_1 < 0.75$ for both turbine and propeller stirrers. Their work suggests that beyond a Reynolds number of 20,000, the power number becomes constant. An increase in solid content increases the power consumption, while an increase in gas velocity reduces the power consumption. Kurten and Zehner (1979) examined the effect of gas velocity on the power consumption for suspension of solids and found that because of simultaneous aeration, a higher power input is required for suspension in the presence of gas. This is mainly due to the reduced liquid circulation velocity in the presence of gas bubbles. Most recently, Albal *et al.* (1983) evaluated the effect of liquid properties on power consumption for both two- and three-phase systems. They found that power consumption per unit volume increases with solid concentration. The influence of particle size on power consumption increases with the solids concentration. For an unconventional arrangement of a stirrer, they also found different $Ne-Re$ curves for glycerine and CMC solutions.

Besides Eq. (3.3), several other correlations are proposed for predicting power consumption in gas-slurry systems; some of these are summarized by Baldi (1986). Since power depends significantly on both operating and geometrical parameters of the system, the use of the correlation that is best applied to a given system is recommended.

3. Suspension of Solid Particles

The suspension of fine solid particles can be characterized by two limiting states:

- (1) "complete" suspension, i.e., the state where just all particles have been brought into motion; and
- (2) homogeneous suspension, i.e., the state where all the solid particles are uniformly distributed throughout the entire vessel volume.

As homogeneous suspension in *nonaerated* stirred vessels can hardly be achieved, even with very high stirrer speeds, mainly N_c , needed for "complete" suspension, is of interest for the design purposes. This value, by definition, is characterized by the "just-suspended" criterion, i.e., the state where only a small fraction of the solids remains at the bottom of the reactor for one second at maximum (Einenkel, 1979). Zwietering (1958) proposed the following correlation to predict N_c , the minimum rotational speed of agitation required for the complete suspension:

$$N_c = \frac{\beta d_p \mu_L^{0.1} g^{0.45} (\rho_p - \rho_L)^{0.45} w'^{0.13}}{\rho_L^{0.55} d_1^{0.85}}, \quad (3.6)$$

where w' is the percentage loading and β is a constant dependent on the ratio d_T/d_I . In general, axial stirrers and dished bottoms give smaller minimum speeds than radial stirrers and flat bottoms. Nienow (1968, 1975) suggested that β can be approximated for a disk turbine impeller as

$$\beta = 2 \left(\frac{d_T}{d_I} \right)^{1.33} \quad (3.7)$$

Herringe (1979) proposed a general correlation for N_c in geometrically similar systems as

$$N_c \propto \left(\frac{\Delta \rho g}{\rho_l} \right)^{\alpha_1} \left(\frac{\mu_l}{\rho_l} \right)^{\alpha_2} d_p^{\alpha_3} d_I^{\alpha_4} w'^{\alpha_5} \quad (3.8)$$

The α_j values of different researchers are compared by Baldi (1986). With the exception of the values of Nagata (1975) and Narayanan *et al.* (1969), the agreement of different researchers for α values is remarkable. For eight blade turbine stirrers, Baldi *et al.* (1978) reported $\alpha_1 = 0.42$, $\alpha_2 = 0.17$, $\alpha_3 = 0.14$, $\alpha_4 = -0.89$, and $\alpha_5 = 0.13$.

From the above correlation, it is clear that the critical stirrer speed N_c mainly depends on the geometry of the stirrer d_I and the vessel (H/d_T), the type of stirrer, the density (ρ_L) and viscosity (ν_L) of the liquid, the solids mass ratio $\psi_s = m_s/(m_s + m_L)$, and the particle diameter (d_p) and density (ρ_p). On the basis of a dimensional analysis, one gets the dimensionless relation

$$\text{Re}_c = f(\text{Ar}, d_p/d_I, \psi_s), \quad (3.9)$$

where $\text{Ar} = d_I^3 g \Delta \rho_{LS} / \rho_l \nu_l^2$ is the so-called Archimedes number (also called the expanded Froude number Fr). In most practical design cases, one is interested only in turbulent flow conditions, where $\text{Re}_c(d_p/d_I) > 10^2$. Zlokarnik (1969) has shown that in this case,

$$\text{Re}_c = f(\text{Ar}, d_p/d_I, \psi_s), \quad (3.10)$$

or as $\text{Ar} = \text{Re}^2 / \text{Fr} \cdot (\Delta \rho_{LS} / \rho_s)$, with $\text{Fr} = N^2 \cdot d_I / g$,

$$\text{Fr}_c = b(\Delta \rho_{LS} / \rho_L) \psi_s^{0.5} \quad (3.11)$$

Zwietering (1958) has shown that for (radially acting) Rushton turbines,

$$\text{Fr}_c = b(\Delta \rho_{LS} / \rho_L)(w / \rho_L)^{0.29}, \quad (3.12)$$

where w is the mass of catalyst per unit volume of slurry, and

$$b = (d_T/d_I)^{2.59} (d_p/d_T)^{0.44} \text{Re}^{-0.22} \quad (3.13)$$

For reactor design, it is most important to know the power consumption corresponding to "complete" suspension. Power consumption is correlated

either per unit volume of suspension ($[P/V]_{sp}$ in W/m^3) or in a dimensionless way as the power number (Newton number),

$$Ne = P/\rho_L N^3 d_i^5 = f(Re), \quad (3.14)$$

which is related to the stirrer Reynolds number (Chapman *et al.*, 1981). The power consumption for "complete" suspension therefore can be calculated according to

$$P_c = Ne_c \cdot N_c^3 \cdot d_i^5 \cdot \rho_L. \quad (3.15)$$

From the dimensionless correlation between the power number and the expanded Froude number (Zlokarnik, 1972), one obtains

$$Fr \cdot (\rho_L/\Delta\rho_{Ls}) \frac{N_c d_i}{u_{ss}} \psi_s^{-1} = K(V/d_i^3) Ne^{-1} \quad (3.16)$$

(with V as total volume of the slurry, u_{ss} as terminal setting velocity of the solid particles, and K a constant whose value depends upon the geometry of stirrer and vessel). The preceding relations are verified for paddles by Einenkel (1977) and Zehner (1979), for propellers by Pavlushchenko (1957), for paddle ejector combinations by Zlokarnik (1972), and for Rushton turbines by Baldi *et al.* (1978).

Joosten *et al.* (1977) and Kolar (1967) also studied suspension of solids in stirred vessels. The correlations of Baldi *et al.* (1978) and Zwietering (1958) are based on data over a wide range of conditions and are also in good agreement with each other. Baldi *et al.* (1978) also proposed a new model to explain the mechanism of complete suspension of solid particles in cylindrical flat-bottomed stirred vessels. According to this model the suspension of particles at rest on certain zones of the tank bottom is mainly due to turbulent eddies of a scale of the order of the particle size. The model leads to an expression

$$\Pi = \left(\frac{\Delta\rho_g}{\mu_t} \right)^{1/2} \frac{d_T d_p^{1/6}}{Ne^{1/3} d_T^{5/3} N_c} = -f \left(Re, \frac{d_T}{d_i}, \frac{H_i}{d_i} \right). \quad (3.17)$$

With the help of experimental data in three (12.2, 19.0, and 22.9 cm diameter) flat-bottom vessels with an eight-flat-blades disk turbine stirrer and four baffles, they obtained a relationship

$$\Pi \propto Re^{-0.2} \psi_s^{-0.15}, \quad (3.18)$$

where

$$Re = \left(\frac{\mu_t d_T}{\rho_L d_i^3 N_c} \right).$$

Albal *et al.* (1983) have shown that the Zwietering correlation does not work well in an unconventional agitated vessel. Zlokarnik and Judat (1969) studied

suspension in a stirred vessel with a self-inducing hollow propeller stirrer for air–water–solid (quartz, iron powder, and galena) system. They showed that the minimum stirrer speed for complete suspension also depends on the design and positioning of the stirrer. They presented a relation for critical Reynolds number as

$$Re_c = 7.08[Ar(\Delta\rho/\rho_f)(B/d_I)^{1/3}\psi_s^{1/3}]^{1/2}e^{(0.58\,d_T/d_I - 2.27)}, \quad (3.19)$$

where B is the thickness of the baffles and Ar the Archimedes number. A summary of some of the studies on suspension of solids in stirred vessels is given in Table VII.

Kneule and Weinspach (1967) divided suspension characteristics into two regimes. They postulated

$$Re_c \propto Ar^{0.4}(\psi_s d_p/d_I)^{0.2} \quad (3.20)$$

for

$$Ar(d_p/d_I)^2\psi_s^{0.5} < 5 \times 10^4,$$

and

$$Re_c \propto Ar^{0.5}\psi_s^{0.25} \quad (3.21)$$

TABLE VII
SUMMARY OF STUDIES OF SUSPENSION IN AGITATED GAS–LIQUID REACTORS

Reference	System	Impeller Type	Particle Size, μm	
Zwietering (1958)	Sand–water, acetone, carbon tetrachloride	Paddle, six-blade turbine, and propeller	125–850	
Nienow (1975)	Sand–water, aq. MgSO_4 soln.	Disk turbine	153–600	
Baldi <i>et al.</i> (1978)		Disk turbine (eight blades)	50–545	
Zlokarnik and Judat (1969)	Air–water–quartz, iron powder, galena	Hollow propeller, self-induced	quartz	60–600
			iron	50–315
			galena	< 33
Sabbarao and Taneja (1979)	Air–water, sand, glass beads	Propeller	sand	70–600
			glass beads	3070
Wiedmann <i>et al.</i> (1980)	Air–water–iron, glass beads	Rushton turbine, propeller	iron	313
Chapman <i>et al.</i> (1981)	Air–water, polystyrene, glass powder	Rushton turbine, propeller	glass	71–1,800
Albal <i>et al.</i> (1983)	Air–water– glass beads	Turbine with six blades, conventional and unconventional	180–355	
			100–600	

for

$$\text{Ar}(d_p/d_i)^2\psi_s^{0.5} > 5 \times 10^4.$$

Since $\text{Ar} = \text{Re}^2/\text{Fr}'$, Fr' being $N_c^2 d_i \rho' g \Delta \rho$, the second relationship is also described by

$$\text{Fr}'_{\text{crit}} = b\psi_s^{0.5}, \quad (3.22)$$

which defines Fr' which is often used for scale-up purposes.

Kneule and Weinspach (1967) also measured the suspension characteristics of numerous stirrer types and agitated vessels. They found the optimum stirrer diameter d_i and distance from the bottom H_i to be given by $d_T/d_i = 3.0\text{--}3.5$ and $H_i/d_i = 0.3\text{--}0.5$. The optimum shapes for the vessel bottom are hemispherical and elliptical; a flat vessel bottom is unsuitable for particle suspension. For a vessel with an elliptical bottom, baffles, and a propeller stirrer installed at $H_i/d_i = 0.2\text{--}0.8$ pumping the liquid toward the floor, the constant b in Eq. (3.22) has the value $b = 3.06$. For a turbine stirrer with six paddles and $H_i/d_i = 0.3$, the value is $b = 1.21$. In order to keep the particles in the same material system in suspension, the propeller stirrer must therefore operate at a rotational speed $(3.06/1.21)^{1/2} = 1.59$ times higher than a turbine stirrer of the same size.

Voit and Mersmann (1986) showed that for small particles, $d_p/d_T \leq 10^{-3}$; $\text{Fr}' d_p/d_i = \text{constant}$. For large particles, $d_p/d_T \geq 10^{-3}$; $(\text{Fr}') d_p/d_T = \text{constant}$. These predictions are supported by the experimental results of several authors. In the turbulent regime, the scale-up rule is that either the tip speed u is constant or Fr is constant, depending on the value of d_p/d_T . This results in the following rules for the critical speed of rotation in an industrial-scale facility:

$$u = \text{constant}, \quad N_c^L = N_c^s \bar{\mu}^{-1}, \quad (3.23)$$

$$\text{Fr}' = \text{constant}, \quad N_c^L = N_c^s \bar{\mu}^{-1/2}, \quad (3.24)$$

where $\bar{\mu}$ is the scale factor; N_c^L and N_c^s are the critical speeds for the large- and the small-scale vessels respectively. Since the results are considerably different for the two regimes, knowledge of the appropriate regime is particularly important for scale-up purposes.

The optimum stirrer, from the point of view of energy efficiency, is the one that requires the least power at the critical speed of rotation. In terms of a dimensionless relation, this can be expressed as the condition where $\text{Ne Fr}'_{\text{crit}}^{3/2}$ is minimum. For a propeller stirrer with $\text{Ne} = 0.50$ and a turbine stirrer with $\text{Ne} = 10.0$, and with the values of b already given for the two stirrers, the propeller stirrer requires only 20% of the power needed by the turbine stirrer. Mixing Equipment Co, CA, has recently introduced a new impeller design that consists of a pitched blade turbine (three blades). At the tips of the

vertical pendant plates are attached. It has been claimed that with this impeller, solids are suspended at a lower value of power consumption as compared to conventional impellers.

a. Aerated Suspension

In aerated stirred slurry reactors, the suspension characteristics behaves more like a two-phase system (Wiedmann *et al.*, 1981). Einkenkel (1979) gives design guidelines for cases where the stirrer must distribute the solid quasi-homogeneously in the vessel; for example, this may be required to allow the transport of solids from stage to stage in continuous processes. Multistage stirrers are better suited for this operation than single mixers, with the cross-beam stirrer (beam angle $\alpha < 45^\circ$) being especially effective (Muller and Rysall, 1986). Suspension characteristics for enameled stirrers with rounded edges are outlined by Lamade (1977).

Experiments (Weinspach, 1967) have shown that the flow behavior of suspensions with solid volume fractions ψ_s up to 0.25–0.30 approximates that of a Newtonian fluid. In this range of ψ_s values, the stirrer power required for suspension can be calculated from the corresponding power characteristics $Ne = f(Re)$ for homogeneous fluid (see Section II), only the physical properties ρ and μ must be replaced with the effective values ρ_s and μ_s for the suspension:

$$\rho_s = \rho + \psi_s \Delta \rho \quad (3.25)$$

and

$$\mu_s = \mu [1 + 1.25\psi_s / (1 - \psi_s / \psi_{s,\max})]^2. \quad (3.26)$$

For spherical particles of the same size, $\psi_{s,\max} = 0.74$ and therefore, $\mu_s = \mu [1 + 0.926\psi_s / (0.74 - \psi_s)]^2$. The increasing particle concentrations have a similar effect on the state of “complete suspension” in aerated and nonaerated systems, i.e.

$$\begin{aligned} N_c &\propto \psi_s^{0.1} & \text{with } d_1 &= d_T/2, \\ N_c &\propto \psi_s^{0.14} & \text{with } d_1 &= d_T/3. \end{aligned} \quad (3.27)$$

Nagata (1975) showed that in aerated suspensions, a significantly higher stirrer speed and thus power consumption per unit volume is required to establish the state of “complete” suspension. Furthermore, the propeller normally requires a higher stirrer speed for “complete” suspension than the turbine. Arbiter *et al.* (1969) reported that drastic sedimentation of suspended particles occurs when the aeration number $N_A = Q_g / N \cdot d_1^3$ (here Q_g is the volumetric gas flow rate) exceeds a critical value. This critical gas flow coincided with the point where the power drawn by the agitator decreased suddenly with a small increase in the gas sparger rate. Thus, an increase in gas

impellers, rate or a decrease in impeller speed have a similar sedimenting effect, while decreasing gas rate or increasing stirrer speed tends to homogenize the suspension.

In order to achieve simultaneous suspension of solid particles and dispersion of gas, it is necessary to define the state when the gas phase is well dispersed. Nienow (1975) defined this to be coincident with the minimum in Power number, Ne , against the aeration number, N_A , relationship (see Fig. 12 [Sicardi *et al.*, 1981]). While Chapman *et al.* (1981) accept this definition, their study also showed that there is some critical particle density (relative to the liquid density) above which particle suspension governs the power necessary to achieve a "well-mixed" system and below which gas dispersion governs the power requirements. Thus, aeration at the critical stirrer speed for "complete" suspension of solid particles in nonaerated systems causes partial sedimentation of relatively heavy particles and aids suspension of relatively light particles. Furthermore, there may be a similar (but weaker) effect with particle size. Wiedmann *et al.* (1980), on the other hand, define the "complete" state of suspension to be the one where the maximum in the $Ne-Re_n$ diagram occurs for a constant gas Reynolds number.

b. Suspension of Large or Light Particles

A criterion for the prediction of minimum stirrer rotation speeds for the suspension of coarse-grain particles (Archimedes number > 40) is derived by Molerus and Latzel (1987). They showed that the minimum stirrer rotation speeds can be predicted by the evaluation of two diagrams: the drag of fluidized particles as a function of concentration, and the pressure-head volumetric flow-rate characteristics of the agitated vessel. The latter can be obtained using the similarity of fluid-kinetic machines and can be expressed as $\psi_{av} = f(\phi_{av})$, where

$$\psi_{av} = \frac{(1 - \phi_v)^2 \Delta P_{stat}}{[(1 - \phi_v)\rho_F + \phi_v\rho_s]u_{f0}^2} \quad \text{and} \quad \phi_{av} = \frac{u_{f0}}{(1 - \phi_v)d_i\omega_c}.$$

Here ΔP_{stat} is the static pressure drop, ϕ_v the volume fraction of solid, u_{f0} the fluid velocity, and ω_c the critical impeller velocity for the complete suspension. All the parameters in this relation (except ω_c) can be obtained from the graphical representation of the drag of fluidized particles as a function of the concentration. Molerus and Latzel (1987) verified their results in two geometrically similar vessels equipped with a marine propeller ($d_T = 0.19$ and 1.5 m, $d_i/d_T = 0.315$, $H/d_T = 1$) and for solids concentration $0.5\% \leq \phi_v \leq 30\%$. They also suggested that $\omega_c \propto d_T^{-0.64}$, with the proportionality constant increasing with the solids concentration.

In a continuous stirred-tank slurry reactor, when the solid particles are large (particle size greater than approximately 0.1 mm), heavy, and in high concentration, a significant vertical concentration profile for the solid phase may occur (Baldi *et al.*, 1981). Because of stratification, the locations of the feed and discharge points are important design considerations for the control of catalyst residence time distribution in such a reactor. Baldi *et al.* (1981) showed that for a given agitation system geometry and for constant physical properties and flow rate of suspending liquid, the concentration profile depends upon the stirrer speed and the particle size and density, but is independent of the mean concentration (especially when $N > N_c$). As N increases, the homogeneity increases; good homogeneity is achieved for $N/N_c \geq 2$. The data also indicate that for achieving solids homogeneity, the best discharge point is near the middle of the reactor.

One of the most difficult mixing operations is to stir into the liquid a nonwettable solid that is lighter than the liquid. The usual method consists of using a high-speed stirrer (propeller, turbine, sawtooth disk) in an unbaffled vessel and provide mixing in the solid through the vortex that extends to the stirrer. Another possibility is the use of self-aspirating rotor-stator systems, although design guidelines for these operations are not yet available (Joosten *et al.*, 1977a).

4. Gas Holdup

Gas holdup is an important hydrodynamic parameter in stirred reactors, because it determines the gas-liquid interfacial area and hence the mass transfer rate. Several studies on gas holdup in agitated gas-liquid systems have been reported, and a number of correlations have been proposed. These are summarized in Table VIII. For a slurry system, only a few studies have been reported (Kurten and Zehner, 1979; Wiedmann *et al.*, 1980). In general, the gas holdup depends on superficial gas velocity, power consumption, surface tension and viscosity of liquids, and the solid concentration. The dependence of gas holdup on gas velocity, power consumption, and surface tension of the liquid can be described as

$$\epsilon_g \sim u_g^{0.36-0.75} P^{0.26-0.47} \sigma^{0.36-0.65} \quad (3.28)$$

For a low solids concentration, the correlations of Calderbank (1958) and Loiseau *et al.* (1977) agree reasonably well with most literature data and are hence recommended. These correlations, however, do not account for the effect of solid concentration on ϵ_g . Kurten and Zehner (1979) studied the effect of solid content on gas holdup in a stirred vessel with a six-blade turbine impeller using an air-sulfite solution-glass beads system. They found

TABLE VIII

SUMMARY OF CORRELATIONS FOR GAS HOLDUP IN MECHANICALLY AGITATED REACTORS (LOW SOLIDS CONCENTRATION)

Reference	Correlations for ε_g
Calderbank (1958)	$\varepsilon_g = \left(\frac{u_g}{u_c}\right)^{0.5} + \frac{0.0126(P/V_L^{0.4})\sigma_\ell^{0.2}}{\sigma_\ell^{0.5}}.$
Loiseau <i>et al.</i> (1977)	$\varepsilon_g = 0.011u_g^{0.38}\sigma_\ell^{0.058}\left(\frac{p}{V_L} + \frac{P_g}{V_L}\right)^{0.27} \quad \text{for nonfoaming systems,}$ $\varepsilon_g = 0.051u_g^{0.24}\left(\frac{p}{V_L} + \frac{P_g}{V_L}\right)^{0.57} \quad \text{for foaming systems.}$
Yung <i>et al.</i> (1979)	$\varepsilon_g = 6.8 \times 10^{-3} \left(\frac{Q_g}{Nd_1^3}\right)^{0.5} \left(\frac{\rho_1 N^2 d_1^3}{\sigma_\ell}\right)^{0.65} \left(\frac{d_T}{d_1}\right)^{1.4}.$
Miller (1974)	$\varepsilon_g = \left[\frac{u_g \varepsilon_g}{v u_g + u_l}\right]^{0.6} + 2.6 \times 10^4 \left[\frac{(P_1/V)^{0.4} \rho_\ell^{0.2}}{\sigma_\ell^{0.6}}\right] \left[\frac{u_g}{u_g + u_l}\right]^{0.6},$ <p>where $Pr = P_G + C_1 P_E + C_0 P_k$</p> <p>$C_1$ and C_2 are empirical constants. Generally the contribution of P_k is negligible compared to other contributions.</p> <p>Expansion power P_E is provided by rising bubbles and is expressed as</p> $P_E = \rho_g Q_g \frac{RT}{M} - \log\left(\frac{P_1}{P_c}\right).$ <p>P_1 and P_c are the gas pressure at the sparger and at the liquid surface.</p>
Sicardi <i>et al.</i> (1982)	$\varepsilon_g = (P_g/V)^{\alpha_1} u_g^{\alpha_2},$ <p>α_1 and α_2 depend on the liquid systems examined</p>
Van Dierendonick <i>et al.</i> (1968)	$\varepsilon_g = 0.31 \left[\frac{u_l u_g}{\sigma_\ell}\right]^{2/3} \left[\frac{\rho_\ell \sigma_\ell^3}{g \mu_\ell^4}\right]^{1/8} + 0.45 \frac{(N - N^4) d_1}{\sqrt{g d_T}} \left(\frac{d_T}{d_1}\right),$ <p>valid for $\varepsilon_g < 0.2$, $0 < \mu_g < 0.05$ m/s, $H/d_T = 1$, $(H - H_i)/d_T = 0.5$. N^4 is the critical stirrer speed when surface incorporation begins.</p>
Warmoeskerken <i>et al.</i> (1981)	<p>For $N_A < 0.025$ (no large cavities), $\varepsilon_g = 0.62 Q_g^{0.45} N^{1.6}$.</p> <p>For $N_A > 0.025$ (large cavities present), $\varepsilon_g = 1.167 (Q_g)^{0.75} (N)^{0.7}$</p>
Sridhar and Potter (1980)	$\varepsilon_g = \left[\frac{\varepsilon_g u_g}{u_l}\right]^{0.5} + 2.16$ $\times 10^{-4} \frac{(P_g/V)^{0.4} \rho_\ell^{0.2}}{\sigma_\ell^{0.5}} \left[\frac{u_g}{u_l}\right]^{0.5} \left[\frac{P_1}{P_g}\right] \left[\frac{\rho_g}{\rho_s}\right]^{0.18}.$ <p>ρ_s is the density of air at atmospheric pressure. This relation is valid for pressures above atmospheric.</p>

that ε_g is reduced with an increase in solid concentration. In an independent study, Wiedmann *et al.* (1980) reported similar observations on ε_g variation with solid loading. The effect of solid loading was particularly significant at higher gas velocities.

The typical effect of flow regime on the gas holdup is illustrated by Sicardi *et al.* (1982). The liquid viscosity also plays an important role in determining the magnitude of ε_g . Rushton and Bimbinet (1968) found an increase of ε_g with the liquid viscosity, μ_l , until a maximum value is reached; a further increase in μ_l leads to a decrease in gas holdup. These findings, however, have not been confirmed by other authors (Van Dierendonck *et al.*, 1968; Calderbank, 1958), so that the influence of viscosity still remains uncertain. Interfacial phenomena that affect the bubble size and coalescence rate depend on local physical properties that may differ considerably from the bulk properties. It is well known that the state of a gas-liquid dispersion is very sensitive to the presence of minute amounts of surfactants that may give rise to foaming, ionic substances that hinder coalescence, and even very fine suspended solids which can absorb on the gas-liquid interface (Ganguli, 1975). Consequently, a pure liquid and a liquid solution with the same "bulk" physical properties may produce quite different degrees of gas dispersion even under the same operating conditions.

5. Mixing

The flow pattern of a liquid in a standard agitated vessel equipped with a radial turbine is characterized by two recirculation loops, one below and the other above the stirrer. These circulation loops are responsible for the macromixing of the liquid; the greater the recirculation flow rate, the more homogeneous is the liquid. The degree of mixing can be evaluated from the residence time distribution function in continuously fed systems, and from the recirculation time (time interval between successive passes of an element of fluid through a fixed point in the vessel) or the mixing time in batch systems. A great number of data are available on the mixing of liquids in a vessel. Much less has been published for aerated systems. The presence of a gas decreases the pumping capacity of the stirrer, and this in turn reduces the recirculation rate and mixing of the liquid. Middleton (1979) found a remarkable increase of the recirculation time in aerated systems as the gas flow rate was increased. This was also found by Bryant and Sadeghzadeh (1979); they observed, however, that the mixing time was unaffected by Q_g . On the other hand, for viscous liquids an increase in the mixing time with the gas flow rate was observed by Einsele and Finn (1980).

The mixing in agitated vessels has been extensively studied, and this subject is well reviewed by Naga (1975) and Uhl and Gray (1966). In slurry reactors, it

is important to consider mixing in the presence of both gas bubbles and suspended solid particles. In mechanically agitated vessels, the liquid phase is completely backmixed, but the gas- and solid-phase dispersion may not be complete. Gas-phase mixing has been studied by Galor and Resnick (1966), Hanhart *et al.* (1963), Van't Riet *et al.* (1976), and Westerterp *et al.* (1963). It is reported that gas-phase mixing depends on the design of the impeller and the nature of the bubbles, as well as the superficial gas velocity. The maximum interaction between the bubbles is found to be near the impeller. Juvekar (1976) found that the gas mixing is influenced by the presence of solid particles, and the gas phase tends to move in a plug flow. Similar observations have also been made by Komiyama and Smith (1975).

Wiedmann *et al.* (1980) have compared the mixing of nonaerated liquids, aerated liquids, and slurries in a turbulent flow. They found that the torque required for stirred, aerated liquids is lower than that for nonaerated stirred liquids because of the decrease in the density of the gas-liquid mixture. The concentration distribution of the particles in aerated suspension becomes more uniform with increasing impeller speed, whereby the torque is higher than that for aerated liquids but lower than that for nonaerated slurries. For gas-liquid-solid systems, very limited data on dispersion of solids and gas phase are available, and further studies are necessary with different designs and for systems with different physical properties. The available literature has been reviewed by Stiegel *et al.* (1978), Shah *et al.* (1982), and Shah and Sharma (1986).

The micromixing state in an agitated vessel is connected with coalescence of bubbles. Coalescence occurs mainly in the stirrer zone, where the recirculated gas bubbles partially mix with fresh gas in the cavities. It also occurs to a lesser extent in the highly turbulent stream leaving the stirrer, but it is virtually absent in other parts of the vessel because the low kinetic energy of the bubbles cannot stretch out the liquid film between a pair of bubbles to reach the coalescence thickness.

Coalescence is a difficult phenomenon to measure directly; usually it is dealt with as a rate or frequency. The coalescence rate (or coalescence frequency) is expressed as the number of coalescences of a bubble during the mean residence time of the gas. Few published results (Reith, 1970; Hassan and Robinson, 1980a, 1980b) show a sharp increase of the coalescence frequency as N increases. The frequency decreases notably when a saline solution is used in place of water.

The mixing time for three-phase systems (oxygen-water-150 micron glass beads) as a function of solids concentration was studied by Albal *et al.* (1983). The results of this study for two stirrer speeds are illustrated in Table IX. As shown, the mixing time increases with the solids concentration.

The subject of micromixing is important for many gas-liquid biological and polymerization reaction systems as well. For instantaneous reactions

TABLE IX
MIXING TIME REQUIRED FOR HOMOGENEOUS DISPERSION
(STIRRER ARRANGEMENT UNCONVENTIONAL)

Solids Concentration (vol %)	800 rev min ⁻¹ θ (s)	1,000 rev min ⁻¹ θ (s)
0	1.0	0.75
0 ^a	1.45 ^a	1.2 ^a
3.0	1.0	0.75
6.7	1.25	1.0
10.0	1.5	1.25
15.0	2.0	1.5
20.3	2.5	2.0
28.62	— ^b	2.5

^a Values calculated by Joshi *et al.* (1982) for the conventional arrangement.

^b Critical stirring speed for suspension was higher than 800 rev min⁻¹.

where intimate mixing is required, the manner in which reactants are introduced and products are removed to a mechanically agitated reactor has important effects on the reactor performance (Pohorecki and Baldyga, 1988). Bourne has made a significant contribution in the evaluation of micromixing effects on stirred-tank reactor performance. In biological and polymeric systems, particularly for highly viscous fluids, segregation of fluids often occurs, which affects the reactor performance. The micromixing in polymerization reactors has important effects on the nature of the product (e.g., molecular weight distribution, etc.) and the product selectivity. Similarly, the performance of fermenters operated in a fed-batch mode is affected by the mixing (both micro in the immediate vicinity of impeller and macro in the rest of the reactor) efficiency because the concentrated solution of the carbon source or other nutrient can not *a priori* be considered to be diluted instantaneously in the whole liquid phase (Engasser, 1988). The micromixing is affected by the size and nature of the agitator, the size of the reactor vessel, the presence of baffles, the positions of the feed inlet and product outlet, etc. An appropriate design of the agitated reactor must, therefore, consider the role of micromixing in the reactor performance. Some experimental techniques to determine micromixing in an agitated vessel are discussed in Section IX.

6. Gas-Liquid Mass Transfer

Gas-liquid mass transfer in the absence of solids has been widely studied (Shah *et al.*, 1982). In these studies, both physical and chemical methods for the determination of the volumetric mass-transfer coefficient and the gas-liquid

interfacial area have been used (see Section IX). Chapman *et al.* (1982) and Niiyama *et al.* (1978) used a dynamic response technique for the measurement of $k_L a_L$ that allows incorporation of the effect of gas residence-time distribution. Early studies on the effect of solid particles on $k_L a_L$ have been reported by Bern *et al.* (1976), Joosten *et al.* (1977a, 1977b), Slesser *et al.* (1968), Yagi and Yoshida (1975), Mehta and Sharma (1971), and Komiyama and Smith (1968), Yagi and Yoshida (1975), Mehta and Sharma (1971), and Komiyama and Smith (1975). Important studies of $k_L a_L$ in mechanically agitated vessels and available correlations are summarized in Table X. In general, it was observed that $k_L a_L$ is strongly dependent on agitation speed, impeller diameter, linear gas velocity, surface tension, and viscosity of the liquid phase. The design of the stirrer, bubble dynamics, and the position of the blades also affect $k_L a_L$ values. Andrews (1982) showed that for P_g/V (kW/m³) less than unity, $k_L a_L/\epsilon_q$ is constant at about 0.4 and for $P_g/V > 1$, $k_L a_L/\epsilon_g \propto (P_g/V)^{5/6}$. Bern *et al.* (1976) and Calderbank (1958) found that $k_L a_L$ is proportional to $N^{-0.2}$, but Yagi and Yoshida (1975) observed that $k_L a_L$ is proportional to $N^{2.2}$. The exponent with respect to impeller diameter is in the range of 1.5–2.0, while that for u_g is in the range of 0.28–0.5. Thus, the correlations reported in these studies differ markedly, which could be due to the variation in system properties and design of the equipment used.

Joosten *et al.* (1977b) studied the effect of solids on $k_L a_L$ and found that up to 10% catalyst loading, values of $k_L a_L$ were not affected by the presence of solid particles; however, at higher concentrations, $k_L a_L$ values decreased significantly. Bern *et al.* (1976) and Komiyama and Smith (1975) measured $k_L a_L$ using a slurry reaction system under gas–liquid mass-transfer controlled conditions. They also found that in a low solid concentration range, $k_L a_L$ values were in the same range as those for the gas–liquid systems. Lee *et al.* (1982) found $k_L a_L$ to decrease with an increase in solids concentration (for concentrations > 10 wt%). A nonmonotonic trend of $k_L a_L$ with solids concentration was observed by Mehta and Sharma (1971). More recently, Albal *et al.* (1983) reported $k_L a_L$ for both conventional and unconventional mechanically agitated vessels. The effects of liquid properties, solid concentration, particle size, and the nature of the solids on $k_L a_L$ were evaluated. The results were in general agreement with those reported by Joosten *et al.* (1977). They showed that for an aqueous system, both $k_L a_L$ and k_L are independent of pressure. The presence of small amounts of solids increases $k_L a_L$, but as the concentration of solids further increases, the $k_L a_L$ value declines. For both Newtonian and non-Newtonian liquids, an increase in viscosity decreases $k_L a_L$. A decrease in surface tension increases the value of $k_L a_L$.

The mass transfer in a Fischer–Tropsch slurry under reaction conditions has been extensively evaluated by Albal *et al.* (1984), Deimling *et al.* (1985), and Karandikar *et al.* (1986). These studies report that the mass transfer coefficient

TABLE X
SUMMARY OF $k_L a_L$ STUDIES IN MECHANICALLY AGITATED REACTORS

References	Method	Impeller Type	System	Correlation for $k_L a_L$
Calderbank (1958)	Physical absorption	Turbine	—	—
Mehta and Sharma (1971)	Chemical absorption	Turbine propeller	—	—
Yagi and Yoshida (1975)	Physical desorption of O ₂	Six-blade		$0.06 \frac{d_T}{d_i^2} \left(\frac{d_i^2 N \rho_L}{\mu_L} \right)^{1.5} \left(\frac{d_i N^2}{g} \right)^{0.19} \left(\frac{\mu_L}{\rho_L \mathcal{D}} \right)^{0.5}$
		Turbine		$\left(\frac{\mu_T u_g}{\sigma_f} \right)^{0.5} \left(\frac{N d_i}{u_g} \right)^{0.32}$
Bern <i>et al.</i> (1976)	Chemical-catalytic hydrogenation in slurry reactor	Turbine	Supported Ni catalyst	$1.099 \times 10^{-2} N^{1.18} d_i^{1.979} u_g^{0.32} v_L^{0.521}$
Komiyama and Smith (1975)	Chemical-catalytic oxidation in slurry reactor	Turbine	Activated carbon	—
Joosten <i>et al.</i> (1977)	Physical desorption of He	Turbine	Glass beads, sugar and polypropylene	—
Chandrasekharan and Calderbank (1981)	Physical absorption	Turbine	—	$\frac{0.0248}{d_T} \left(\frac{P}{V_L} \right)^{0.55} (x \sigma_f^2 u_g)^{0.551} \sqrt{d_T}$
Niyama <i>et al.</i> (1978)	Dynamic absorption			
Albat <i>et al.</i> (1983)	Dynamic absorptions	Turbine (six-blade)	Glass beads	$\frac{k_L a_L}{\mathcal{D}^{1/2}} = 2.579 \times 10^2 \left(\frac{P}{V_L} \right)^{0.5} \varepsilon_g^{0.6}$ $Sh = \frac{k_L a_L d_i^2}{\mathcal{D}} = 1.41 \times 10^3 Re^{0.67} Sc^{0.5} We^{1.29}$

$k_L a_L$ decreases with an increase in solids concentration for both CO and H₂ in various fractions of F-T liquid. Alper *et al.* (1980) and Pal *et al.* (1982) showed that the fine porous particles enhance the mass transfer rate considerably because of adsorption on the particles.

Philadelphia Gear Co. has recently introduced a mechanically agitated contactor wherein the impeller is surrounded by a draft tube. The company claims higher values of the mass-transfer coefficient in this equipment, presumably as a result of increased gas holdup. The higher gas holdup is, however, expected to decrease the heat-transfer coefficient and the extent of mixing.

Most recently, Oguz *et al.* (1987) and Oguz and Brehm (1988) carried out extensive studies of gas-liquid mass-transfer coefficients in aqueous and organic slurries. They proposed

$$k_L a_L [\text{in s}^{-1}] = 3.07 \times 10^{-3} (u_G)^{0.5 \sqrt{\sigma_{\text{H}_2\text{O}}/\sigma_L}} \times \sigma_L^{-3.0} \mu_{sL}^{-0.34} (P_T/V_{sL})^{0.75} \mathcal{D}_L^{0.5}. \quad (3.29)$$

The above correlation was obtained from the experimental data in a 14.5 cm diameter flat-bottom tank with four baffles over its entire height and a four-blade impeller with $d_i = d_T/2$ and with an off-bottom clearance of $d_T/3$. Oguz and Brehm (1988) also proposed the Yagi-Yoshida correlation for both aqueous and organic liquid systems as

$$\text{Sh} = 0.162 \text{Re}^{1.5} \text{Sc}^{0.5} \text{Fr}^{0.19} (G_F)^{-0.6} N_A^{0.09 \sqrt{\sigma_{\text{H}_2\text{O}}/\sigma_L}}, \quad (3.30)$$

where

$$\text{Sh} = k_L a_L d_i^2 / \mathcal{D},$$

$$\text{Re} = N d_i^2 \rho_{sL} / \mu_{sL},$$

$$\text{Sc} = \nu_{sL} / D,$$

$$\text{Fr} = d_i N^2 / g,$$

$$G_F = \sigma_L / \mu_{sL} u_g,$$

$$N_A = d_i N / u_g.$$

The above correlations are recommended for calculations of gas-liquid mass transfer coefficients in conventional stirred slurry reactors.

The intrinsic gas-liquid mass transfer coefficient k_L depends on the physical properties of liquid and on the bubble diameter. In regime c, $k_L \propto P_g^\alpha$, where $\alpha = 0.14-0.25$ (Calderbank and Moo-Young, 1961; Linek *et al.*, 1970; Yoshida and Miura, 1963). Nevertheless, in general k_L is independent of N (Reith and Beek, 1968; Mehta and Sharma, 1971). For low-viscosity liquids, $k_L = 2.4 \times 10^{-4}$ m/s may be assumed. Furthermore, $k_L \propto \sigma_L^{1/2}$ (Linek *et al.*,

1970); an increase in viscosity decreases k_L , but the data for agitated vessels are incomplete.

The gas-liquid interfacial area depends on the coalescing nature of the system. The most widely used correlation of Calderbank (1958) shows

$$a_L = 1.44 \left[\frac{(P_g/V)^{0.4} \rho_l^{0.2}}{\sigma_l^{0.6}} \right] \left(\frac{u_g}{u_i} \right)^{0.5} \quad (3.31)$$

Equation (3.31) is valid for $a_L < 120 \text{ m}^{-1}$ and $\varepsilon_g < 0.08$. Miller (1974) introduced the total power P_T and proposed

$$a_L = 1.44 \left[\frac{(P_T/V)^{0.4} \rho_l^{0.2}}{\sigma_l^{0.6}} \right] \left(\frac{u_g}{u_g + u_i} \right)^{0.5} \quad (3.32)$$

For electrolyte solutions, the relationship is

$$\frac{a_L}{1 - \varepsilon_g} = 0.21(P_T/V)^{1.03} \quad \text{for } 0.0022 < u_g < 0.158 \text{ ms}^{-1}. \quad (3.33)$$

A decrease in liquid-phase surface tension increases a_L ; $a_L \propto \sigma_l^{-\alpha}$, where α varies from $\frac{1}{3}$ to 1.

7. Liquid-Solid Mass Transfer

Several studies on liquid-solid mass transfer in a mechanically agitated reactor have been reported in the literature, and this subject has been reviewed by Miller (1971) and Chaudhari and Ramachandran (1980). The last authors compared the predictions of k_s from various correlations for identical conditions and found that the variation in the predictions of different correlations was significant. The values of k_s depend mainly on the agitation speed, particle size, and physical properties of the system. The effect of agitation speed on k_s is, however, mild compared to that observed for the gas-liquid mass transfer coefficient k_L . The correlations of Levins and Glastonbury (1972) and Sano *et al.* (1974) suggest that the dependency of k_s on N changes with particle size, while Boon-Long *et al.* (1978) reported that $k_s \propto N^{0.28}$.

Hixon and Baum (1941) observed that at rotational speeds lower than N_{crit} , not only k_s changes, but also the effective interfacial area a_s of the heap of solids lying more or less at the bottom of the vessel. Above the critical rotational speed, only k_s changes. Weinspach (1967) showed that $k_s \propto (\mathcal{D}/\nu)^{0.44} (\Delta \rho g \nu / \rho)^{1/3}$. For $N > N_{\text{crit}}$, the relationship $\text{Sh} - 2 = a(Pd_p^4/\nu^3)^\alpha \text{Sc}^{1/3}$, where a can be as high as 0.55 and $\alpha = 0.21-0.26$, is applicable. For $100 < \text{Sc} < 50,000$, following Kolmogoroff's theory, a relation

$$\text{Sh} - 2 = 0.55(Pd_p^4/\nu^3)^{0.25} \text{Sc}^{1/3} \quad (3.34)$$

is recommended for the estimation of the liquid–solid mass-transfer coefficient.

8. Heat Transfer

For exothermic reactions in slurry reactors, it is often necessary to design an efficient heat removal system. A knowledge of heat transfer through the reactor walls, to the following gas phase, and to inserted rods, cooling coils, etc., is therefore most essential. Heat transfer in mechanically agitated reactors has been studied by Hovas *et al.* (1982), Maerteleire (1978), Rao and Murthy (1973), Steiff and Weinspach (1978), and Zlokarnik (1966). A summary of published data on heat-transfer coefficients for both stirred vessels and bubble columns is presented by Steiff and Weinspach (1978). The reported studies of heat-transfer coefficients in bubble-column slurry reactors have been reviewed by Shah (1979), Shah *et al.* (1982), and Shah and Sharma (1986). For the low solids concentration and fine particle size normally used in catalytic slurry reactors, the correlations presented in Section II are applicable if fluid properties (μ , ρ , c_p , etc.) are replaced by the corresponding slurry properties.

B. ADIABATIC SLURRY REACTOR

This type of laboratory reactor is designed to measure the thermal characteristics of the slurry reaction system. In this reactor (Bhattacharjee *et al.*, 1986), heat losses from the body of the reactor are minimized by surrounding the reactor with insulation and then placing the insulated reactor inside a thick copper vessel. Electric heaters are placed outside the copper vessel and are controlled so as to make the temperature difference between the copper and the reactor as close to zero as possible. All connections to the reactor are insulated and heated to keep heat losses small. A digital computer continually monitors temperatures on the reactor, the copper vessel, and the transfer lines and adjusts the heaters to maintain small heat losses. A cooling coil is provided in the reactor to remove the heat generated by the reaction. The flow rate of coolant and the entering and leaving temperature of coolant are measured accurately and are used to measure the rate of heat generation. The flow rate of coolant is controlled to keep the temperature of the reactor at the desired value.

A detailed drawing of the reactor assembly is shown in Fig. 14. It is a stainless steel, 1-L autoclave equipped with a Magnedrive stirrer and a cooling coil. A special shaft extension was made to provide extra room for insulation heating tapes. It can be operated at a high stirrer speed so as to have all phases completely backmixed. The Magnedrive is cooled by house air.

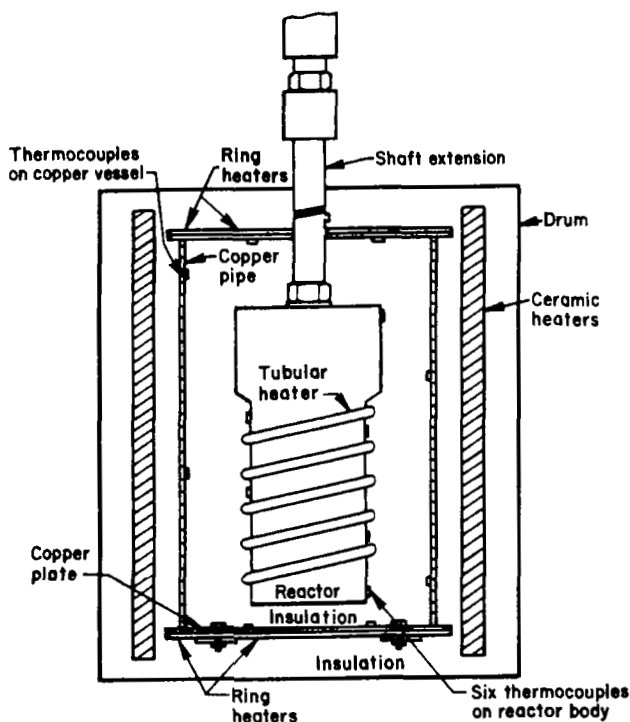


FIG. 14. Cross-section of the adiabatic reactor assembly. (Reprinted with permission from Bhattacharjee, S., Tierney, J. W., and Shah, Y. T., *Ind. Eng. Chem. Process Des. & Dev.* **25**, 117, copyright 1986, American Chemical Society.)

A 1500-W tubular heater is wrapped around the reactor. The autoclave is placed inside a copper pipe, with Fiberfrax bulk fiber insulation packed between the copper pipe and the reactor. Four 1000-W quarter-circle ceramic heaters are placed around the copper pipe. The space between the copper pipe and the ceramic heaters is filled with aluminum balls for efficient and uniform heat transfer from the heaters to the copper pipe. The bottom of the copper vessel is closed with a copper plate. Beneath the copper plate, there are two heaters (a small one of 500 W and a larger one of 1000 W), which are tightly clamped to the bottom copper plate. The top of the copper pipe is similarly covered with another copper plate, and two slots are provided for the feed and product gas lines, coolant inlet and outlet lines, thermocouple extension wires, and the lead wires of the tubular heater. Two ring heaters (660 and 1000 W) are placed on the top copper plate. One thermocouple and a tape heater are placed on the shaft extension to minimize the heat loss through the shaft. No insulation is placed around the ceramic heaters to achieve better control of

the temperature of the copper vessel. A DECLAB-23 MINC digital computer was used for data acquisition, data manipulation, process monitoring, and on-line control.

The above described reactor is useful for the measurements of heat of reaction as well as thermal behavior of gas-liquid or gas-liquid-solid, high-pressure, high-temperature reactions. Since the reactor can be operated under adiabatic conditions, it simulates the commercial operation. The reactor was successfully utilized by Bhattacharjee *et al.* (1986) for investigating thermal behavior of slurry phase, catalytic synthesis gas conversion.

C. MULTIPLE-AGITATOR SLURRY REACTORS

In some cases, a slurry reactor with multiple agitation is used. For example, Bern *et al.* (1976) used the reactor shown in Fig. 15 for the hydrogenation of oils. In this reactor type, horizontal partitions are also introduced at various stages to reduce the extent of backmixing. These authors proposed the following correlation for the gas-liquid mass transfer coefficient, $k_L a_L$, in this type of reactor based on pilot-plant data (30 and 500 L capacity):

$$k_L a_L = 1.099 \times 10^{-2} N^{1.16} d_1^{1.98} u_g^{0.32} u_r^{-0.52}. \quad (3.35)$$

The above correlation indicates a strong dependence of $k_L a_L$ on stirrer diameter and speed.

Double or multi-impeller tanks are quite often used for practical purposes, both to get high volumetric mixing or high heat transfer and to reduce the floor area occupied by the equipment. Takeda *et al.* (1986) showed that a multi-impeller stirred tank does not always have high mixing efficiency. Magelli *et al.* (1986) and Komori and Murakami (1988) measured mixing time and power consumption in multi-impeller baffled stirred tanks. The qualitative relation between the placement of single and double paddles and mixing efficiency or energy consumption is described by Komori and Murakami (1988). These authors also concluded that turbulent mixing in both single- and double-impeller tanks is strongly dominated by large-scale recirculating flows, which prevail in the radial and axial directions. Higher mixing is attained by creating larger-scale recirculating flows and by reducing the number of recirculating flows. A double-impeller tank has more recirculating flows than a single-impeller tank, and thus mixing efficiency in double-impeller agitation is inferior to that in single-impeller agitation. The circulation time, defined as the traveling time of a tracer on the flow patterns, is a useful parameter in estimating the magnitudes of mixing time and energy consumption (or mixing efficiency). A smaller circulation time can generate more effective mixing in both single- and double-impeller tanks.

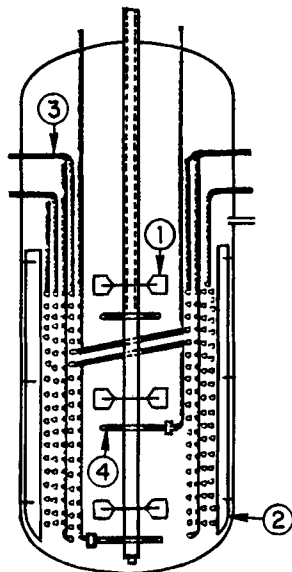


FIG. 15. Reactor with a multiple-agitator arrangement. 1, turbine impeller; 2, baffle; 3, cooling and heating coils; 4, perforated ring for hydrogen supply. (Bern *et al.*, 1976; also from Chaudhari *et al.*, 1986, by courtesy of Marcel Dekker, Inc.)

D. GAS-INDUCED AGITATED SLURRY REACTOR

Another way to improve the performance of the continuous stirred tank reactor is to use a gas induced agitator. In several hydrogenation processes, a dead-end type of agitated reactor is used wherein the gas is supplied at the rate of consumption. The advantage of this system is that the recycle of unreacted gas is eliminated. When the build-up of by-product gases is negligible, as in the case of hydrogenation reactions, this operation is useful. The mass transfer in this type of reactor is, however, poor because of very low gas velocities, and in order to improve the mass-transfer efficiency, a gas-inducing agitator is often used. This allows for the efficient recirculation of the gas from the head space back into the slurry phase. Martin (1972), Zlokarnik (1966), Joshi (1980), and Zundelovich (1979) proposed different designs for gas-inducing agitators that were illustrated earlier in Section II for gas-liquid systems. It is, however, important to know that the gas-inducing method is useful only for small-scale operations. Gas inducing is not effective for large-scale operations because of the large liquid height above the impeller, and in such cases the multiple stirrer/multistage reactor systems as described earlier can be used.

E. NOVEL CATALYTIC SLURRY REACTORS

In a conventional slurry reactor, the reaction kinetics during the initial heat-up period complicates the determination of the exact kinetic expressions. Furthermore, the so-called induction period causes inaccuracy in the kinetic measurements of catalytic reactions.

In order to alleviate these problems, the reactions in well-stirred batch or continuous slurry reactors are often initiated using two different groups of techniques: (1) injection of one of the reactants, generally the gaseous one, into the suspension containing the remaining reactants and the solid catalyst, and (2) insertion of the catalyst into the mixture of gaseous and liquid reactants in a manner such that the effects of the initial heat-up period and/or induction period on the kinetic measurements are minimized.

In the first group of techniques, the reactor containing all the reactants except one and the catalyst is taken to reaction conditions either under vacuum or under an inert atmosphere. The remaining reactant is then added to start the reaction. Both vacuum and inert atmosphere, however, prevent *in situ* activation of the catalyst prior to the start of the reactions (e.g., hydrogenation reactions). In vacuum techniques, minute leaks may cause a partial or total oxidation of the catalyst upon heating. This problem is avoided with the second alternative by using positive pressures of inert gases. In this case, however, a continuous replacement of the inert gas with, say, hydrogen is required, which adds uncertainties in defining its partial pressure at zero reaction time.

The second group of techniques is more widely used. In this section we describe five different types of reactors that consider different ways of catalyst addition, induction, and heat-up in gas-liquid mixtures. These reactors attempt to (1) minimize the effect of the "induction period" or catalyst pretreatment on kinetic measurement; (2) minimize the effects of the "heat-up" period and homogeneous reaction on the catalytic reaction rate; and (3) minimize the time for the "heat-up" period.

1. *Cup-and-Cap Reactor* (Grau *et al.*, 1987)

In earlier studies, the problem of induction was handled by pre-activating the catalyst inside the reactor in glass ampules and breaking these fragile glass ampules at zero reaction time to mix the catalyst with the rest of the reacting mixture. While this method solves the problem, it is cumbersome, and the catalyst and its coating are not exposed to an actual pre-activation and saturation with high-pressure hydrogen gas.

The novel cup-and-cap reactor allows kinetic determination of small catalyst loadings, accurate control, and stability of process operating condi-

tions, *in situ* pre-activation of the catalyst at any pressure and temperature without external devices for injection or introduction of solids, and zero-induction-time determinations of reaction rates. This reactor was successfully used by Grau *et al.* (1987) to study catalytic hydrogenation of vegetable oils. The reaction conditions were temperature in the range of 393–473 K, pressure in the range of 140–1,300 kPa, and solids concentration 0.04–0.40 wt fraction. The liquid–solid mass-transfer coefficients measured in this reactor agreed well with those calculated from the literature correlations.

The reactor consists of a fixed cover (cap) and a loose vase (cup) mounted on the reactor shaft. A helicoidal groove on the shaft allows the descent of the cup by means of a follower pin. Two horizontal grooves allow the positioning of the cup either at the upper part of the helix in the gas phase or at the lowest position on top of the impeller blades submerged into the liquid phase.

The cup contains the solid catalyst and prevents its contact with the liquid reactants while exposing the catalyst to pretreatment at real process temperature and pressure conditions. Thus, activation of the catalyst with simultaneous gas (hydrogen) saturation of both the protective coating and the liquid (oil) phase can be achieved. An excellent and quick stabilization of the temperature and pressure can be obtained.

The cap prevents the liquid reactants from splashing into the cup whenever the liquid (oil) is mechanically agitated. Its internal diameter is slightly greater than that of the vase. A conical upper external face avoids accumulation of liquid or slurry portions. The cup interior has to be carefully designed to prevent catalyst spills due to centrifugal forces and to guarantee a complete, fast mixing of the solid with the liquid reactants. A detailed description of the reactor and its operational procedure has been given by Grau *et al.* (1987).

2. *Falling-Basket Reactor* (Alcorn *et al.*, 1974)

This reactor is a modification of the conventional moving-basket Carberry reactor. In the design of a falling-basket reactor for coal liquefaction, Alcorn *et al.* (1974) set five requirements:

- (1) Batch operation for rapid screening;
- (2) pre-activate the catalyst *in situ* with H_2/H_2S ;
- (3) use formed catalyst (tablets and extrudates), rather than powder;
- (4) avoid contact of catalyst with slurry during heat-up; and
- (5) separate thermal from catalytic conversion experimentally.

The falling-basket reactor was developed to meet these requirements. With this device, the catalyst is suspended in the gas phase during the initial stages of the run, then lowered into the liquid for the catalytic reaction portion. Catalyst (25 cc) is loaded in the four arms of the basket assembly, which moves

along a grooved sleeve attached to the agitator shaft. In operation, the basket is held at the top of the shaft by a horizontal notched groove as long as the shaft is rotated at a constant rpm. When rotation is stopped and momentarily reversed, the basket travels down the groove to the bottom position, where it remains for the rest of the run. The point at which the basket drops is recorded by a temporary drop in batch temperature.

Pre-activation of the catalyst, heat-up, pressurization, and a period of thermal reaction are accomplished after the reactor is sealed, but before there is contact between catalyst and slurry. The catalytic period starts when the basket is dropped into the liquid and stops when the heater is removed from the autoclave.

3. *Reactors with Induction Heaters*

Shinn (1982) developed a mechanically agitated slurry reactor with induction heaters for coal liquefaction. While the induction heaters required large power input, they allowed the slurry to heat up to 400–450°C in few minutes, thus cutting down the heat-up period. In the use of such reactors, the effects of induction heating on the metal degradation and failure need to be carefully considered. Except for the induction heating system, the rest of the reactor was a conventional slurry reactor. The concept of induction heating is more practical for smaller-size reactors.

4. *Rapid-Injection Reactor*

In recent years concentrated efforts have been made to evaluate novel batch reactors to examine the kinetics of high-pressure and high-temperature hydroprocessing reactions, in particular coal conversion processes. The conventional batch reactors require large heat-up and cool-down times and have large temperature overshoots. Thus, residence time at a particular temperature is not accurately known. In complex hydroprocessing systems in which multiple reaction steps with different activation energies occur, variations in heat-up and cool-down times may have a significant influence on conversion and product distribution. Processes such as direct coal liquefaction have high initial rates, and thus the gathering of meaningful data requires the design of a reactor that will allow measurements at short contact times.

In order to overcome these problems, a number of investigators have developed rapid-injection reactors. In such systems, coal and/or catalyst are injected into the reactor once the gas and liquid reactants are heated to the desired reaction temperature. The coal and/or catalyst may be mixed with liquid reactant (to form a slurry) and preheated to an allowable temperature where significant reaction does not occur before injecting into the reactor. This minimizes the amount of the coal and/or catalyst left in the injection tube

and the reactor temperature perturbation upon the injection. The reactors have been developed by Whitehurst and Mitchell (1977), Abichandani *et al.* (1984a, 1984b), and Foster *et al.* (1983, 1984a, 1984b); all are for the kinetic study of direct coal liquefaction, particularly for the short-contact-time liquefaction. The reactor used by Foster *et al.* was a 0.30-L autoclave (Autoclave Engineers, Model No. 15-1 5k-A28A) reactor. This design is suitable for the injection of finely divided solids (such as coal and catalyst) as well as slurries and emulsions.

The rapid-injection reactor is particularly suitable for applications involving catalysts that require specific pretreatment procedures. For example, in applications with catalysts requiring presulfiding, the catalyst treatment can be undertaken in the injection tube. Upon completion of pretreatment, the injection tube can be attached to the reactor and the contents added to the reactor when desired.

5. Microreactors

When the catalyst is available in a small amount, a microreactor assembly is often used (Miller, 1987). This is a simple T-type reactor heated by a fluidized sand bath. The mixing is provided by mechanical agitation that shakes the reactor up and down within the fluidized bed. Because of the small amount of slurry, and an effective heat transfer in the fluidized sand bath, the heat-up period in such a reactor is small. The nature of mechanical agitation is, however, energy-efficient. The reactor provides only a small sample for the product analysis, which makes the usefulness of the reactor for detailed kinetic measurements somewhat limited. The reactor has been extensively used for laboratory catalyst screening tests in coal liquefaction.

F. SUMMARY

Mechanically agitated slurry reactors are widely used in three-phase catalytic and noncatalytic reactions. In aerated slurry reactors, the three regimes outlined in Table V prevail. These regimes are schematically illustrated in Fig. 11. The gas flow rate and stirrer speed where the transition from regimes a to b or b to c with a Rushton turbine stirrer occurs can be estimated from the relationships described in Table VI.

The power in aerated slurry reactors in regime c can be calculated using Equation (3.3). In general, relations summarized by Baldi (1986) can be used for the calculation of power consumption. The most widely used correlation for the minimum rotational speed of agitation required for complete suspension of solids is that of Zweitering (Equation (3.6)). The most versatile

correlation is, however, that by Herringe (1979) (Equation (3.8)). In dimensionless form, the relationship $Re_c = f(Ar, d_p/d_i, \psi_s)$ applies for turbulent flow, where $Re_c(d_p/d_i) > 10^2$. Here Ar is the Archimedes number and ψ_s the weight fraction of solids in slurry. Kneule and Weinspach (1967) divided suspension characteristics into two regimes. For $Ar(d_p/d_i)^2\psi_s^{0.5} < 5 \times 10^4$,

$$Re_c \propto Ar^{0.4} \left(\psi_s \frac{d_p}{d_i} \right)^{0.2},$$

and for $Ar(d_p/d_i)^2\psi_s^{0.5} > 5 \times 10^4$, $Re_c \propto Ar^{0.5}\psi_s^{0.25}$. These relationships are valuable for scale-up purposes. The optimum stirrer diameter d_i and distance from bottom H_i are given by $d_T/d_i = 3.0-3.5$ and $H_i/d_i = 0.3-0.5$. The optimum shapes for the vessel bottom are hemispherical and elliptical bottom; a flat vessel bottom is unsuitable for particle suspension. The flow regime is also divided in terms of d_p/d_T ratio. For $d_p/d_T \leq 10^{-3}$; $Fr'(d_p/d_i) = \text{constant}$; for $d_p/d_T > 10^{-3}$, $Fr'(d_p/d_T) = \text{constant}$. The optimum stirrer is the one that requires the least power at the critical speed of rotation. This can be expressed as the condition where $Ne Fr_{crit}^{3/2}$ is minimum.

For complete suspension in a given aerated slurry reactor, Ne is a function of the aeration number as well as the Reynolds number. For both aerated and nonaerated systems, $Ne \propto \psi_s^{0.1}$ for $d_i = d_T/2$ and $Ne \propto \psi_s^{0.14}$ for $d_i = d_T/3$. For large particles ($Ar > 40$), the criterion for minimum stirrer rotation speed outlined by Molerus and Latzel (1987) is recommended. The homogeneous suspension, where the particles are uniformly distributed in the entire vessel, is difficult to achieve, particularly for large particles and high solids concentration. Generally $N/N_c \geq 2$ and a withdrawal location at mid-height are recommended for homogeneous suspension.

The gas holdup in a slurry reactor depends upon superficial gas velocity, power consumption, the surface tension and viscosity of the liquids, and the solids concentration. For the first three parameters, the relationship $\epsilon_g \propto u_g^{0.36-0.75} P^{0.26-0.47} \sigma^{0.36-0.65}$ holds. For low solids concentration and waterlike liquids, the relationship $\epsilon_g = f(P/V, u_g)$ is useful, although the nature of such a relationship depends upon the foaming characteristics of the liquids. An increase in solids concentration decreases gas holdup, whereas an increase in viscosity first increases and then decreases the gas holdup. A decrease in surface tension and an increase in stirrer speed increases the gas holdup.

In slurry reactors, the liquid phase is completely backmixed, whereas backmixing in the gas and solid phases may not be complete. The gas-phase mixing depends on the design of the impeller and the nature of the bubbles, as well as the superficial gas velocity. The presence of gas reduces liquid-phase mixing; however, an increase in gas flow increases the mixing. The mixing is also dependent upon the coalescence rate of the bubbles.

The gas-liquid volumetric mass-transfer coefficient strongly depends on the agitation speed, the impeller diameter, the linear gas velocity, and the surface tension and viscosity of the liquid phase. The design of the stirrer, bubble dynamics, the position of the blades, and the solids concentration and size also affect $k_L a_L$ values. In general, the relationship $k_L a_L \propto N^{2.2} d_1^{1.5-2.0} u_g^{0.25-0.5}$ applies. $k_L a_L$ decreases with an increase in solids concentration, an increase in liquid viscosity, and a decrease in surface tension. For low-viscosity liquids, $k_L a_L$ can be related to (P/V) , and its value depends upon the foaming nature of the liquids. The most generalized relationship for $k_L a_L$ is given by Oguz and Brehm (1988), as illustrated by Eq. (3.30). Both k_L and a_L are related to power per unit volume. The relationships $k_L \propto P_g^\alpha$ where $\alpha = 0.14-0.25$ and $a_L = f((P/V), u_g, \rho_l, \sigma_l)$ are recommended. The exponent on P/V in the last functionality is generally 0.4.

The liquid-solid mass-transfer coefficient depends mainly on the agitation speed, the particle size, and the physical properties of the system. While $k_s \propto N^{0.28}$, this relationship may depend on the particle size (Sano *et al.*, 1974). In a dimensionless form, $Sh \propto Re^m Sc^{0.5}$; however, the value of m changes at some critical Reynolds number when all particles are suspended. The most generalized relationship is given by Eq. (3.34), and its use is recommended.

Heat transfer in slurry reactors follows the same behavior as that described for, gas-liquid systems as long as liquid properties are appropriately substituted by the slurry properties.

Multiple-agitator slurry reactors can be designed in a manner similar to a multiple-agitator gas-liquid reactor. The use of Eq. (3.35) for $k_L a_L$ in such a reactor is recommended. For a vessel with two impellers, higher mixing is attained by creating larger-scale recirculating flows and by reducing the number of recirculating flows. A double-impeller tank has more recirculating flows than a single impeller tank, and thus, mixing efficiency in double-impeller agitation is inferior to that in single-impeller agitation. The mixing efficiency is measured by circulation time, and its dependence on the position of two impellers is illustrated by Komori and Murakami (1988). Gas-induced slurry reactors behave very much like gas-induced gas-liquid reactors. Mass transfer in such reactors is generally poorer than that in gas-sparged systems. Gas-induced slurry reactors are not effective for large-scale systems.

Slurry reactors are often used for intrinsic kinetic measurements. In order to alleviate the effects and complications of the initial heat-up period, as well as the induction period, on the kinetic measurements, novel designs have been introduced. Cup-and-cap reactors, falling-basket reactors, rapid-injection reactors, reactors with induction heaters, and microreactors are five such novel designs. Each of these reactors has been found to be successful; the first three, however, consider both induction and heat-up periods. The last two reactors alleviate the complications due to the heat-up period only. All of these

reactors can operate under high-pressure, high-temperature conditions and are applied for hydrogenation processes. When the slurry sample is small, microreactors are effectively used for kinetic measurements as well as catalyst screening. Because of their small reaction volume, the flexibility for product analysis for such reactors is, however, limited.

G. FUTURE WORK

Future work should include:

- development of techniques for complete and homogeneous suspension of very light particle (i.e., particles that float on the liquid surface) and very heavy particles;
- estimations of design parameters for slurry reactors with very light, very heavy, or large particles;
- development of new configurations of stirrers and baffles to provide enhanced mixing and transport rates with low power consumption;
- development of experimental techniques (preferably nonintrusive) to detect solids distribution in actual reactor at both high and low pressures and temperatures with both organic and aqueous liquid phases and wettable and nonwettable solids;
- estimations of design parameters for a mechanically agitated vessel with multiple agitators.

IV. Catalytic Reactors

In this section we consider mechanically agitated reactors that are largely used to study intrinsic kinetics of catalytic reactions. It is clear that the nature of a reactor used for this purpose will depend on the type of kinetic data required, the nature of the reaction system, the nature and amount of catalyst, and safety considerations. Some of the mechanically agitated reactors used for kinetic measurements are illustrated in Table XI. In this section, we will not consider previously discussed conventional slurry reactors and their modifications.

A. GENERAL CONSIDERATIONS

Various types of mechanically agitated catalytic reactors outlined here have their own specific advantages, and no *a priori* decision on the choice of reactor is often possible or desirable. The major function of the mechanically agitated

reactors is to provide a large amount of mixing in the reaction system so that heat and mass transfer resistances to the reaction are minimized. The mixing should, however, be provided with a minimum possible power input and without any harmful effects to the catalyst. Safety can also be an important consideration. Among other factors, the choice is dependent on the catalyst form, on prior knowledge of the homogeneous reactions (which dictates the maximum allowable ratio of free volume to catalyst volume), and on the thermodynamics of the reaction. For example, a rotating basket reactor should be used for studying catalytic reactions involving low heats of reaction because of the uncertainty in the knowledge of the catalyst surface temperature. When the homogeneous reactions are important, the reactor with catalyst lined at the wall should not be used. The reactors with stationary cylindrical baskets and internal recycle are versatile and may be used for studying any gas–solid or gas–liquid–solid reactions. These reactors, however, operate better under high pressure and for higher stirrer speeds. Novel reactors serve the purpose of satisfying specific needs of reaction systems.

Three problems affecting the design of mechanically agitated reactors are worth noting: (1) overheating of the shaft bearings when high-temperature reaction systems are studied; (2) leakage along the shaft, and (3) contamination of the catalyst due to possible poisons produced by the mixer hardware. The shaft bearings may be protected from overheating by cooling them or by using a long shaft with the bearings at one end safely removed from the high-temperature zone. The problem of leakage along the shaft may be solved by using a hydraulic seal at atmospheric pressure or a magnetically coupled drive system. If necessary, the mixing hardware should be coated with a material that is nonpoisonous to the catalyst.

The mechanically agitated catalytic reactor is often operated in a batch mode. The basic mixing characteristics of such a reactor are similar to those of a continuous flow reactor, except that the reactor is operated under transient conditions. The use of such a reactor for kinetic measurements requires a continuous sampling of the reaction mixture. The separation of the product from the catalyst must be accompanied by the sampling system. It must also provide rapid quenching to prevent further reaction in the sampling system itself. Although with enough agitation, isothermality can be achieved, the reaction occurring during the heat-up period and the quench time can be a problem. Accurate residence time measurements should be possible. For a three-phase reaction, since all three phases are contained in the reactor, this type of reactor could provide the most accurate measurement of contact time of all mechanically agitated reactors, provided the reaction can be quenched rapidly at the end of the experiment. Because of the decaying nature of the catalyst, this type of reactor gives poor selectivity disguise. The reactor is very simple to construct and at a reasonable cost.

TABLE XI
TYPES OF MECHANICALLY AGITATED REACTORS USED FOR KINETIC MEASUREMENTS

Type	Major Applications	Major Advantages	Major Drawbacks
Agitated slurry reactor Single stage	Catalytic and noncatalytic operations Polymerization reactions	Transport rates are high Convenient to operate	Catalyst erosion, sintering Internal temperature gradients can be high
Multistage		Ease of variation or parameters	
Basket-type reactors	High-pressure, high-temperature catalytic operations	Transport rates are high Parameters can be easily varied	Used for limited particle size Catalyst erosion and sintering may be a problem High equipment cost Difficult to operate under a wide range of conditions without creating flow maldistribution
Berty reactor	High-pressure, high-temperature petroleum and chemical operations	Can provide intense mixing and high transport rates	Not useful for low-pressure operations Ease of variation of parameters can be limited
Short-contact-time reactor	Catalytic and noncatalytic operations	Useful for kinetic measurements when solid is a reactant.	Leakage can be problem Representative product sampling and parameter

		Particularly useful for high-temperature, high-pressure, exothermic reactions	variations may be problem Requires very high mixing in coal and polymeric operations
Adiabatic slurry reactor	Catalytic and noncatalytic operations	Used for thermal parameters, i.e., heat of reaction, multiple thermal steady states	Internal temperature gradient has slow time response for high-pressure operation
Rotating-disk type reactors	Catalytic processes	Fluid–solid mass transfer known Kinetic parameters can be correlated to surface properties	Equipment cost can be high Convenience of operation and ease of variation of parameters poor
Resonant bubble slurry	Catalytic and noncatalytic operations	High mass transfer rates	Not very convenient to operate Ease of variation of parameters can be limited
Wiper-blade reactor	Moderate temperature and pressure, catalytic and noncatalytic operations	Extremely high transport rates	Equipment cost can be high High temperature and pressure may be problems
Amoco internal recycle reactor	High-pressure, high-temperature coal, petroleum, and chemical-related operations	Intense mixing	Ease of variations of parameters can be limited

B. BASKET-TYPE REACTOR

Basket-type reactors are well known and are used extensively for laboratory studies for gas–solid and gas–liquid–solid reactions. The two designs commonly used are rotating basket and stationary basket reactors. A schematic design of a rotating basket reactor is shown in Fig. 16. Detailed descriptions of this reactor type are given by Carberry (1964), Doraiswamy and Tajbl (1974), Shah (1979), and Weekman (1974). The rotating basket reactors lead to experimental difficulties at high rotation speeds (which are necessary to eliminate the external gradients) and for studies at higher pressures. Another disadvantage of the basket reactor is that the actual temperature of the surface of the catalyst, or even in the field immediately external to it, cannot be directly measured. Bennett *et al.* (1972) and Brisk *et al.* (1968) showed that higher turbine speed is needed to mix higher gas feed flows, a result opposite to the one observed by Tajbl *et al.* (1966). Germain (1973) proposed the replacement of the reactor peripheral baffles by fixed baskets (see Fig. 17). Caldwell (1983) recently described an improvement to the traditional Berty and Carberry-type (rotating basket) reactors. Significantly higher mass-

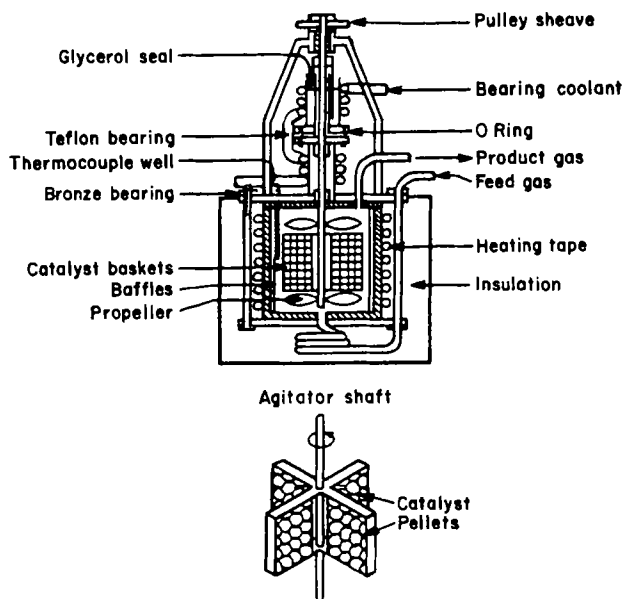


FIG. 16. Schematic of a rotating-basket type reactor. (After Chaudhari *et al.*, 1986, by courtesy of Marcel Dekker, Inc.)

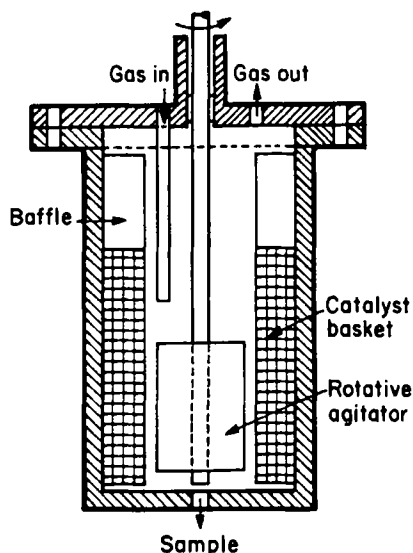


FIG. 17. Stirred-tank gas-liquid-solid basket reactor; fixed basket. (Germain, 1973; also from Chaudhari *et al.*, 1986, by courtesy of Marcel Dekker, Inc.)

transfer coefficients were obtained using larger and more effective impeller. This improvement was achieved at the cost of greater diameter and gas-volume-to-catalyst ratio. Tikhonov *et al.* (1966) designed a special type of spinning basket reactor for high-pressure multiphase reactions, which was also used by Mahoney *et al.* (1978) and Nijiribeako *et al.* (1977) for a kinetic study of hydrotreating reactions.

Basket-type reactors provide good mixing and are easy to maintain under isothermal conditions. The major use of these reactors has been for the determination of intrinsic kinetics. They are also ideal for studying the influence of intraparticle diffusion effects in the absence of external mass transfer effects. In several catalytic reactions, the kinetics evaluated after crushing the catalyst particles may not be useful for design purposes because of nonuniform distribution of the metal in the pellet. In such cases, determination of the kinetics without crushing the catalyst particles is essential, and this can be achieved using the basket-type reactors. Relatively small particles are, however, inappropriate for study in rotating basket reactors.

In gas-solid catalytic reactions, the question of whether or not all of the catalyst is uniformly involved in the reaction in a rotating basket reactor was addressed by Smith (1970). He showed that when the reactor had no baffles,

there was a distribution of contacting within the baskets. However, when the baffles were installed, the contacting was in fact quite uniform. Baffles are thus essential in the stirred basket reactor. The gas phase is certainly well mixed, but there may be some doubt as to how fast the gas actually goes past the catalyst particles. Gelain (1969) has described a number of reactors with a turbine incorporated into the recirculation path of the reactor. In these designs there is still a large free gas volume, which is generally undesirable.

In a stationary cylindrical basket reactor, catalysts of any form and size or even a single pellet are placed in a cylindrical basket (provided with a fine wire mesh) that is fitted at the center of the bottom of the reactor. The mixing is provided either by a rotating special impeller or by a rotating reactor with baffles around the basket. The ratio of the free volume to the catalyst volume can be minimized by proper design of the reactor, impeller, and basket. In this reactor, the catalyst temperature can be measured directly. The ratio of free volume to catalyst volume is low, and the reactor can be used as a single pellet reactor and can also be employed for rapid catalyst evaluations. The reactor can also be used with catalyst impregnated on a surface of the closed cylinder, thus minimizing free volume as compared to the reactors with catalyst impregnated on the reactor walls. Costa and Smith (1971) followed a similar approach to study the noncatalytic hydrofluorination of uranium dioxide.

Halladay and Mrazek (1973) used a unique glass backmix reactor to study hetero-homo decompositions of nitrous oxide. The gold ribbon catalyst was mounted on support racks that were rotated at rates sufficient to insure perfect mixing. With the use of this reactor, the authors separated the rates of homogeneous and heterogeneous reactions. Trifiro *et al.* (1973) studied the oxidation of butenes to maleic anhydride in a stirred gas-solid reactor in which the catalyst was placed in a cylindrical basket mounted on the rotating shaft between two propellers. Their data indicated that perfect mixing prevailed at rotating speeds greater than about 2,200 rpm.

For gas-liquid-solid systems, studies on gas-liquid and liquid-solid mass transfer in basket reactors have been rather limited. For the rotating basket reactor, gas-liquid mass-transfer coefficient data are needed. Liquid-solid mass transfer has been studied by Teshima and Ohashi (1977), and their data are correlated by

$$\frac{k_s d_p}{\mathcal{D}} = 2.0 + 0.012 \left[\frac{e d_p^4 \rho_L^3}{\mu_L} \right]^{0.41} \left[\frac{\mu_L}{\rho_L \mathcal{D}} \right]^{0.64} \quad (4.1)$$

In the case of a stationary basket-type reactor, $k_L a_L$ correlations proposed for conventional agitated slurry reactors by Ramachandran and Choudhari (1983) can be used. No experimental data for liquid-solid systems are, however, available.

C. INTERNAL RECYCLE REACTOR

Internal recycle reactors are designed so that the relative velocity between the catalyst and the fluid phase is increased without increasing the overall feed and outlet flow rates. This facilitates the interphase heat and mass transfer rates. A typical internal flow recycle stirred reactor design proposed by Berty (1974, 1979) is shown in Fig. 18. This type of reactor is ideally suited for laboratory kinetic studies. The reactor, however, works better at higher pressure than at lower pressure. The other types of internal recycle reactors that can be effectively used for gas-liquid-solid reactions are those with a fixed bed of catalyst in a basket placed at the wall or at the center. Brown (1969) showed that imperfect mixing and heat and mass transfer effects are absent above a stirrer speed of about 2,000 rpm. Some important features of internal recycle reactors are listed in Table XII. The information on gas-liquid and liquid-solid mass transfer coefficients in these reactors is rather limited, and more work in this area is necessary.

D. WIPER-BLADE REACTOR

Recently, Manor and Schmitz (1984), Carberry *et al.* (1985), and Tipnis and Carberry (1984) illustrated a wiper-blade reactor for gas-liquid and gas-liquid-solid reactions. The reactor is a continuous flow reactor and incorporates a multibladed rotor that contacts the gas-liquid interface

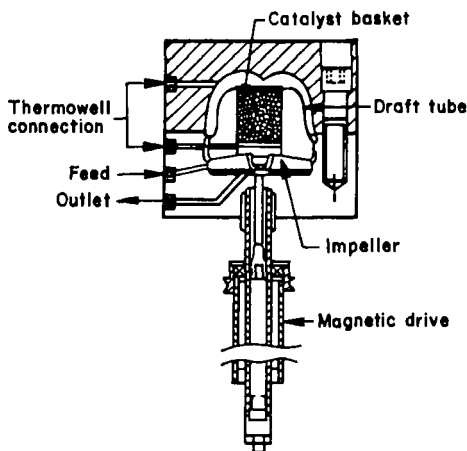


FIG. 18. Flow recycle reactor (Berty type). (Berty, 1974; also from Chaudhari *et al.*, 1986, by courtesy of Marcel Dekker, Inc.)

TABLE XII

KEY FEATURES OF AN INTERNAL RECIRCULATION REACTOR [AFTER SHAH, 1979]

-
1. Well-mixed, isothermal conditions are achieved.
 2. Sampling and product analysis are good. They are the same as those for rotating-basket reactors.
 3. Residence-time distribution can be accurately measured.
 4. Combines advantages of both differential and integral reactors. The integral recycle rate can be accurately measured and controlled.
 5. Heat- and mass-transfer rate correlations obtained in a fixed-bed reactor can be applied to this type of reactor.
 6. Steady-state operation, unless the catalyst is decaying.
 7. Construction difficulty and cost are close to those for the rotating-basket and other similar continuously stirred tank reactors.
 8. Internal recirculation would give better mixing in the catalyst baskets.
 9. It can be used for process studies conducted into the flow and mass-transfer regimes on the commercial scale. One can use it to examine the phenomena occurring at a specific point in the commercial fixed-bed reactor.
 10. Heat- and mass-transfer resistances in the catalyst basket could be significant. They may make data analysis difficult.
-

directly. Mass transfer rates greater than 30 times those of previously used conventional gas-liquid reactors were obtained. Mixing tests indicated that the bulk fluid phases were gradientless. The reactor is schematically shown in Figure 19.

In conventional thin-film evaporators, the liquid film is spread on the wall by the rotor while flowing downward by gravitation. In the reactor of Manor and Schmitz (1984), however, the liquid is forced to the wall by the rotor against a backpressure created on the liquid outlet. According to Manor and Schmitz (1984), the liquid phase is confined to the gap between the rotor blades and the cooling jacket. It rotates around the circumference of the cooling jacket wall while being vigorously mixed. The liquid is continuously fed and withdrawn from the reactor. The reactor is therefore operated as a continuous-flow backmixed device, as opposed to the typical plug-flow operation of thin-film evaporators.

Semicircular grooves, oriented diagonally from the bottom to the top of the jacket while turning half the circumference, were cut deep into the inside wall of the cooling jacket. These grooves facilitated liquid mixing in the vertical direction. The gas phase was mixed by baffles that prevented the gas from turning with the rotor, while producing flow currents between the rotor blades. A high absorption rate of the gaseous reactant into the liquid was achieved by the unique formation and stirring of the liquid phase.

Tracer measurements have indicated that the liquid in the reactor is well mixed on a macroscopic scale. Mass-transfer parameters were determined by

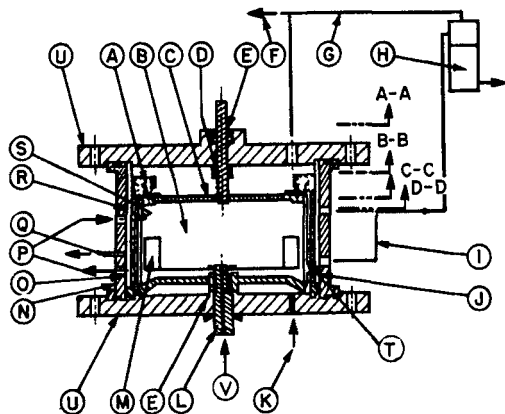


FIG. 19. Vertical cross-section of the wiper-blade reactor. A, Sealing arrangement; B, gas phase; C, rotor; D, sealing; E, bearing; F, excess gas flow; G, gas collected from the liquid exit; H, overflow vessel; I, liquid exit; J, rotor blades; K, gas feed; L, adjustable shaft; M, baffles; N, reactor shell; O, cooling jacket; P, cooling water feed and exit; Q, sampling port; R, grooves; S, liquid phase; T, gas-liquid interface; U, top and bottom plates; and V, liquid feed. (After Manor and Schmitz, 1984; also from Chaudhari *et al.*, 1986, by courtesy of Marcel Dekker, Inc.).

monitoring the chemical absorption of oxygen into a concentrated sodium sulfite solution, and these data indicate that $k_L a_L$ for this type of reactor is at least 100 times better than that for any other type of gas-liquid reactor. The reactor, in addition, provides adequate heat removal so that isothermal operation can be maintained over a wide range of conditions.

Tipnis and Carberry (1984) and Carberry *et al.* (1985) used this concept to design, construct and demonstrate a gradientless gas-liquid-solid catalytic reactor of well-defined interface. With the use of high-speed "wipers," a continuously fed liquid film is sustained upon a catalytic wall in the presence of a continuously fed, well-stirred gas phase. This design allows the measurement of intrinsic kinetics of gas-liquid-solid catalytic systems.

E. REACTORS WITH CATALYST IMPREGNATED ON REACTOR WALLS OR PLACED IN AN ANNULAR BASKET

In some cases, a thin layer of the desired catalyst can be directly coated on the inner walls of the reactor (Ford and Perlmutter, 1964) or on a removable liner fitted snugly inside the reactor (Lakshmanan and Rouleau, 1969), or the reactor wall itself can have catalytic properties (Wentzheimer, 1969). The reactor is then provided with an efficient stirrer to ensure thorough mixing. Since the catalyst layer is thin, in the presence of intense mixing both external and interparticle diffusional effects are small. Thus intrinsic kinetics can be

measured in any desired temperature range. The reactor can be used for gas–solid, liquid–solid, and gas–liquid–solid reactions. However, for each of these systems, the use of the reactor is limited to the situations where homogeneous side reactions are not important. The reactor provides very large gas and/or liquid holdups compare to catalytic surface area. The temperature of the catalyst (that is, the reactor wall) can be directly measured.

A small modification of the above design, in which the catalyst in the form of granules or pellets is placed in an annular basket made of wire mesh fitted close to the reactor wall, has also been examined. The use of such an annular basket-type reactor has been reported by Tajbl *et al.* (1967), Relyea and Perlmutter (1968), and Lakshmanan and Rouleau (1970). The basic features of this reactor are the same as the ones described above. The reactor has been used to carry out high-pressure, high-temperature catalytic methanation of mixtures of carbon monoxide/hydrogen and carbon dioxide/hydrogen.

A reactor developed by Bennett *et al.* (1972) to reduce the mixed gas volume to a minimum was used to study the kinetics of methanol synthesis at 200 atm, between 300 and 400°C. In this reactor, the turbine motor is contained in a cool, high pressure vessel; the drive shaft for the turbine enters the reactor through the gas inlet tube. The turbine throws the gas outward, and it travels upward between vertical baffles, inward radially through the catalyst basket, and down through the central space to the turbine again. The turbine shaft in this reactor is sealed by a conventional gland; a small leak is of no consequence if the flow rate is measured upstream. However, for vacuum operation a more elaborate arrangement is required (Bennett *et al.*, 1972). In this case, the turbine is driven by samarium–cobalt magnets, which retain most of their strength up to 400°C.

A turbine-mixed reactor with an internal motor has also been described by Geranin *et al.* (1967).

F. FLUIDIZED BED REACTOR WITH AGITATION

A fluidized bed can be made fully mixed by providing suitable baffles or by using a stirrer. A stirrer fluidized bed reactor of this design has been used by Trotter (1960). Shah *et al.* (1977) examined the pressure drop and the gas-phase backmixing in a stirred fluidized bed. They found that the pressure drop through a solid bed below incipient fluidization decreased with an increase in stirrer speed. The torque on the stirrer under the same conditions increased with an increase in stirrer speed. Both pressure drop and torque on the stirrer remained essentially independent of both gas flow rate and stirrer speed once the incipient fluidization conditions were reached. The gas phase backmixing coefficient remained essentially independent of stirrer speed once the incipient

fluidization conditions were reached, and it increased with an increase in gas velocity (dispersion coefficient α (gas velocity)^{0.85}). The main disadvantage of this reactor is the attrition of the catalyst due to mechanical agitation. This disadvantage was overcome by Ramaswamy and Doraiswamy (1973), who employed external agitation through a pulsator operating independently of the feed device.

The pulsed fluidized bed gives better mixing than a conventional fluidized bed, allows use of a wider range of particle sizes, and provides better solid–gas contacting. Instead of using an independent pulsator, the feed itself can be introduced through a pulse pump. In the use of this reactor, caution must be exercised in the use of proper range of pulsation parameters, and suitable baffles should be provided in the reactor.

The vibrating fluidized bed is useful for processing particles that are difficult to fluidize because of stickiness, wide polydispersity, agglomerating tendency, large size, and extreme friability. High-frequency (10–100 Hz) and small-amplitude (1–10 mm) vibrations imparted to relatively shallow beds of particulate solids have been found to facilitate fluidization of difficult-to-fluidize solids. The use of such a fluidized bed for the chemical reactor has been evaluated by Mazumdar (1984). The detailed transport characteristics of a vibrating fluidized bed were recently outlined by Endesz *et al.* (1989).

G. BALL-MILL AND TRAVELING-GRATE REACTORS

Barrett (1971) has illustrated a rotating mixer reactor that is based on the concept of a ball mill. It provides good solids mixing. The reactor can be used for both catalytic and noncatalytic systems, and it is particularly useful for systems with high solids concentration (or highly viscous polymeric systems). Mixing of solid and gas is obtained by rotating the reactor, which causes “cascading” of the solid particles. The temperature difference between the particles and the gas is also reported to be low (less than 2°C). When the reaction requires short contact time and continuous flow of solids and gas, a traveling-grate or belt-dryer type of reactor can be used.

H. ADSORBER REACTOR FOR TRANSIENT STUDIES AT MILLISECOND RATES

Stolk and Syverson (1978) described an adsorber-reactor that is capable of carrying out transient studies at millisecond rates. They presented a high-temperature, high-speed constant volume adsorber reactor that is capable of measuring adsorption rate in the presence of a chemical reaction. The reactor provides rapid gas–solid contact in a constant-volume cell with transient rates for temperature and pressure measurements in the millisecond region. Using

catalytic dehydration of *tert*-butanol as an experimental system, they showed that adsorption studies can provide a better insight into transport mechanisms and the role of adsorption in heterogeneous catalysis, thereby assisting the development of an improved kinetic model for complex reactions.

The primary reactor design consideration was the arrangement of reactor components to insure rapid gas–solid contact. The measuring devices had to be capable of operating at high temperatures, and they had to have millisecond time constants. The internal reactor volume must be minimized. Catalyst volume was chosen to cause a detectable pressure change in the system during the experiment.

In order to achieve rapid gas–solid contact followed by effective mixing, a combination “flywheel/fan” was designed to crush the glass capsule and to provide gas circulation. An inclined grid and screen were added to separate the catalyst particles from the capsule before contact with the flywheel to reduce attrition. Clear plastic prototypes were built for evaluation at ambient conditions. High-speed (4000 fps) motion pictures permitted observation of a capsule being broken inside the reactor. Examination of the pictures showed that gas–solid mixing was effective in the millisecond range and that very little disintegration of the catalyst occurred. The reactor components included a capsule holder, a flywheel, a rotary feedthrough, a grid and screen, a pressure transducer, and a thermocouple. The capsule holder contained the activated catalyst in a sealed glass capsule at the start of the test. The reaction was initiated by manually rotating the holder 180 degrees and releasing the capsule into the flywheel.

Adsorber reactors to measure adsorption at reaction conditions have also been reported by Winfield (1953), Macarus and Syverson (1966), Edwards (1961), Keller (1962), and Haering and Syverson (1974).

I. VIBRATION-MIXED REACTOR

Sunderland and El Kanzi (1974) used a novel vibration-mixed reactor to study oxidation of *o*-xylene over a supported vanadium pentoxide catalyst. A schematic of this reactor is shown in Fig. 20; Table VIII presents the key to Fig. 20. The design is unusual in that mixing within the reactor is carried out by a piston reciprocating at high speed rather than the more normal rotary devices. The frequency and amplitude of reciprocation can be varied over a wide range, but 50 cps with an amplitude of 0.6 cm provided adequate mixing for Sunderland and El Kanzi (1974). This mode of agitation, where the catalyst bed is swept and the direction of flow is altered for each stroke, provides better mixing than a system in which the flow is always in the same direction.

The piston was driven by means of a coil oscillating at 50 cps in the annulus of a powerful pot magnet. The amplitude of vibration and hence the

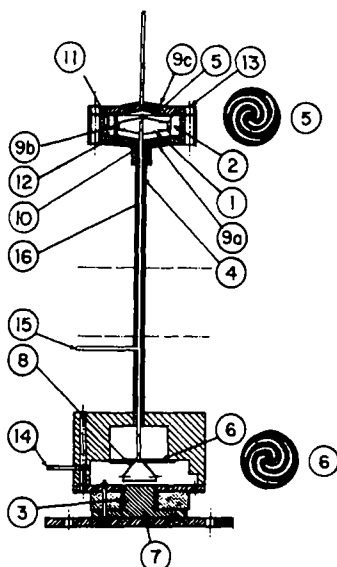


FIG. 20. Vibration mixed reactor. (Reprinted with permission from Sunderland, P. and El Kanzi, E. M. A., "A Vibration Mixed Reactor for Chemical Kinetics in Gas/Solid Catalyzed Reactors," *Chem. Reaction Eng. 11, ACS Symposium Series 133*, pp. 3, Copyright 1974, American Chemical Society.)

TABLE XIII
KEY TO FIG. 20

Item	Name	Composition
1	Piston	18/8 stainless steel
2	Catalyst bed	
3	Moving coil ^a	
4	Piston road	18/8 stainless steel
5	Upper spring	Nimonic 75
6	Lower spring	Be/Cu alloy
7	Pot magnet ^a	soft iron
8	Conneting cone	aluminium
9a	Main body of reactor	18/8 stainless steel
9b	Piston sleeve	18/8 stainless steel
9c	Upper portion of reactor	18/8 stainless steel
10	Space between piston rod and sheath	
11	Thermocouple well	
12	Grooves to hold piston sleeve	
13	Holes to allow free movement of gases	
14	Reactant inlet	18/8 stainless steel
15	Reactant inlet	18/8 stainless steel
16	Piston road sheath	18/8 stainless steel

^a Moving coil and magnet supplied by Rank-Wharfedale Ltd., Idle, U.K.

degree of mixing was varied by varying the applied voltage. Operation with amplitudes > 0.6 cm is possible using either a more powerful moving coil and magnet assembly or a less bulky piston and rod. Frequencies other than 50 cps are possible if the drive unit is coupled to a frequency oscillator and power amplifier.

For minimum power requirements and efficient operation, it was necessary to center the coil, piston, and rod, and then balance all the vibrating parts dynamically. This was done by flat Archimedian-type spiral springs at top and bottom. Since the top spring had to withstand the hot corrosive reactor environment, it was made from Nimonic 75, an 80/20 nickel/chromium alloy; the bottom spring, in a less demanding environment, was a beryllium/copper alloy. By varying the thickness of the springs, the vibrating parts could be tuned to any desired frequency.

Because the piston was magnetically driven, the drive unit and reactor were made leakproof and suitable for operation at elevated pressure. The coil and magnet were outside the constant-temperature bath and far enough from the bath not to require any cooling. The reactor was made from 18/8 stainless steel in three parts. The piston and rod were made from the same type of steel, hollowed to reduce their mass. The main body of the reactor was shaped to take the piston at maximum displacement and yet keep the total free space to a minimum. The reactor inlet was at the base, and a thermocouple well at the top allowed measurement of the gas temperature. There were eight holes, slightly larger than 0.635 cm in diameter, drilled at regular intervals into the body of the reactor around its perimeter, each hole able to admit two 0.635 cm diameter catalyst spheres. The loosely mounted spheres allowed free access of gaseous reactants to all the available surface area.

Sunderland (1974) showed that for a frequency of reciprocation of 50 cps, the reactor demonstrated nonideal macromixing only for amplitudes of reciprocation approaching zero. Experiments with the oxidation of *o*-xylene indicated that the reactor effectively minimized heat and mass transfer contributions to overall reaction rate, but the proper evaluation of extent of effectiveness requires further experimental measurements of heat and mass transfer coefficients (fluid-solid) for varying rates of reciprocation of the piston.

J. ROTATING PACKED-BED REACTOR

In this type of three-phase catalytic reactor, centrifugal force is employed to vary the hydrodynamics and transport characteristics of the conventional gas-liquid-solid reactor. Interphase transport of momentum and mass in such a reactor is governed by the centrifugal forces. Dudukovic and co-

workers (1989) evaluated the design parameters for such a reactor. They used Davidson's statistical approach (1959) to model behavior of liquid holdup in such a reactor. Dudukovic (1989) also evaluated short-contact-time mass transfer in the laminar liquid film of such a reactor. He devised a simple expression,

$$\frac{1}{\text{Sh}(L)} \cong \frac{1}{\mathcal{D}a} + 1.238L^{1/3}, \quad (4.2)$$

which gives a value for average mass transfer coefficient $\bar{k}(L)$, defined as

$$\overline{\text{Sh}(L)} = \mathcal{D}a \left(\frac{\bar{k}(L)}{k'_s} \right), \quad (4.3)$$

where $\mathcal{D}a = k'_s Y / \mathcal{D}$; here k'_s is the rate constant for the first-order heterogeneous surface reaction, Y the characteristic distance in the y direction (normal to the interface), \mathcal{D} the binary diffusion coefficient, and L the dimensionless distance along the solid surface. Further experimental and theoretical studies to examine liquid distribution, mixing, and transport characteristics in this type of reactor are being carried out in the chemical reaction engineering laboratory of Dudukovic (1989).

K. SUMMARY

Mechanically agitated catalytic reactors are frequently used to measure the intrinsic kinetics of gas–solid or gas–liquid–solid catalytic reactions. The main objective here is to provide high enough mixing so that the apparent reaction rate is largely controlled by the intrinsic kinetics. High mixing generally provides large heat and mass transfer rates.

The true intrinsic kinetic measurements require (1) negligible heat and mass transfer resistances by the fluids external to the catalyst; (2) negligible intraparticle heat and mass transfer resistances; and (3) that all catalyst surface be exposed to the reacting species. The choice of the reactor among the ones described in this section depends upon the nature of the reaction system and the type of the required kinetic data. Generally, the best way to determine the conditions where the reaction is controlled by the intrinsic kinetics is to obtain rate per unit catalyst surface area as a function of the stirrer speed. When the reaction is kinetically controlled, the rate will be independent of the stirrer speed. The intraparticle diffusional effects and flow uniformity (item 3, above) are determined by measuring the rates for various particle sizes and the catalyst volume, respectively. If the reaction rate per unit surface area is independent of stirrer speed, particle size, and catalyst volume, the measurements can be considered to be controlled by intrinsic kinetics. It is possible

that even when the overall reaction rate is kinetically controlled, parts of a given reaction network may have diffusional limitations. Thus, the validity of intrinsic kinetics-controlled operation needs to be checked for each product species and each reaction path in a complex reaction network.

The advantages and disadvantages of various types of reactor outlined in this section are summarized in Table XI. The choice of a suitable reactor generally depends upon these characteristics, as well as cost, safety, and availability considerations.

L. FUTURE WORK

Future work should include the further development of catalytic reactors

- for sticky catalyst and/or reactant particles;
- to measure the dissolution rate of the solid reactant, e.g., catalytic coal liquefaction;
- to measure accurately the kinetics of reactions involving volatile reactants and/or products, e.g., hydrocracking;
- to measure accurately the kinetics of retrogressive or deactivation reactions, e.g., coking, demetallization, etc.;
- to measure accurately the kinetics and thermochemistry of highly exothermic or endothermic reactions; and
- to measure accurately the kinetics of reactions in viscous liquids.

V. Liquid-Liquid Reactors

Liquid-liquid reactions may involve reactions between two miscible or immiscible liquids. When the reactions involve two miscible liquids, homogenization of liquid mixtures is important. Homogenization deals with the mixing of miscible liquids to obtain the desired degree of homogeneity, or with the maintenance of homogeneity for the purpose of carrying out a reaction under well-defined conditions. For this purpose, it is important to evaluate the type of stirrer and mixing conditions that allow the desired mixing operation to be achieved with minimum expense (i.e., an inexpensive stirrer and a low energy of mixing). This evaluation requires a knowledge of the mixing time and power characteristics of various available stirrers and vessel configurations. When the reactions involve two immiscible liquids, the liquid-liquid dispersion characteristics, the power required for homogeneous dispersion, the droplet size distribution, and liquid-liquid mass

transfer are important design parameters. Before evaluating different types of liquid-liquid reactors, we examine the design parameters for conventional mechanically agitated vessels.

A. MIXING OF TWO MISCIBLE LIQUIDS

1. Correlation of Mixing Time

In the homogenization of liquids having the same density ρ and kinematic viscosity ν , the mixing time θ for a given stirrer type and vessel inserts depends on the rotational speed N , the stirrer diameter d_1 , and the kinematic viscosity. In terms of dimensional analysis, this can be expressed as $N\theta = f(\text{Re})$. Since mixing time and the associated power characteristics are valid for the particular stirrer and vessel geometry, various types of commonly used agitated vessels are illustrated in Fig. 21. The relationship between $N\theta$ and Re obtained from the chemical decolorization method (see Section IX) for various configurations shown in Fig. 21 are illustrated in Fig. 22. This figure

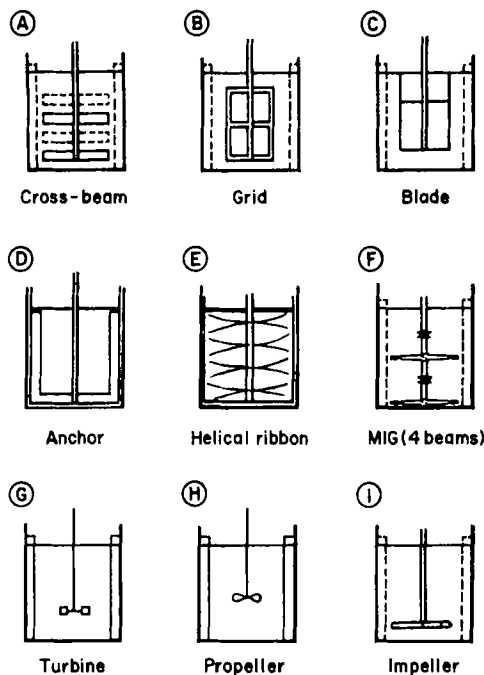


FIG. 21. Various types of agitated vessels with $H/d_1 = 1$ (baffles drawn with dotted lines indicate that the stirrer can be used in baffled or unbaffled vessels).

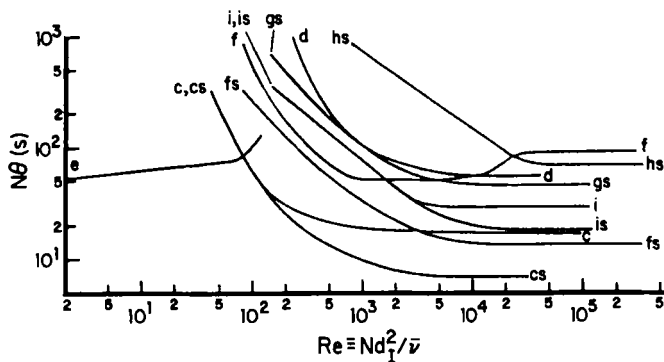


FIG. 22. Mixing-time characteristics of the stirrer types in Fig. 21 (curve *h* for 21h without baffles; curve *hs* for 21h with baffles, etc.). (Reprinted with permission from the publisher, VCH Publishers, Inc., after Zlokarnik and Judat, 1988.)

provides the values of $N\theta$ needed to homogenize the mixture under given flow conditions (Re) and for $H/d_T = 1$. As the ratio H/d_T increases, the mixing time becomes longer. For example, for a baffled vessel with a cross-beam stirrer, the following relationship is valid for the range $10^3 < Re < 10^5$ (Zlokarnik, 1967):

$$N\theta = 16.5(H/d_T)^{2.6}. \quad (5.1)$$

In the development of the above equation, it is assumed that the number of stirrer beams increases with vessel height in accordance with Fig. 21a. Homogenization and power characteristics for enamel-coated stirrers with rounded edges are described by Gramlich and Lamade (1973); a number of other mixer types and insert configurations are treated by Henzler (1978).

In the homogenization of liquids with different densities and viscosities, coarse mixing is affected by the specific weight difference of the two components, $g\Delta\rho$. However, the elimination of the final concentration gradients also depends on the properties $\bar{\rho}$ and $\bar{\nu}$ of the homogeneous mixture. Thus, in this case, the mixing time depends on the following parameters: $\theta = f(N, d_T, \bar{\rho}, \bar{\nu}, g\Delta\rho)$. In the dimensionless form, this can be expressed as $N\theta = f(Re, Ar)$, where $Re \equiv Nd_T^2/\bar{\nu}$ is the Reynolds number based on the viscosity of a homogeneous mixture, and $Ar \equiv d_T^3 g\Delta\rho/(\bar{\nu}^2 \bar{\rho})$ is the Archimedes number. The mixing time characteristics of the cross-beam stirrer shown in Fig. 21a, operating in a baffled vessel with $H/d_T = 1$, can be expressed as (Zlokarnik, 1970)

$$N\theta = 51.6 Re^{-1} (Ar^{1/3} + 3). \quad (5.2)$$

This relationship is valid for $10 < Re < 10^5$ and $10^2 < Ar < 10^{11}$. Similar relationships for $N\theta$ for other configurations would also depend on both Reynolds and Archimedes numbers.

The mixing time for viscous liquids was examined by Hoogendoorn and Den Hartog (1967). The types of mixers examined in this study are illustrated in Fig. 23. The mixing time was measured by a decoloration and a thermal response technique (see Section IX). In truly viscous flow, the mixing time was inversely proportional to the stirrer speed. The performance of the various mixers were compared using the two dimensionless correlations $\theta^2 P / (d_1^3 \mu)$ and $\rho d_1^2 / (\mu \theta)$. The turbine and anchor mixers were found to be unsatisfactory for viscous mixing.

Most recently, novel fluid foil impellers have been used to create efficient mixing in viscous fluids, particularly in the transition flow regime (Weetman and Coyle, 1989). Although these impellers were originally designed to maximize the flow in terms of pumping capacity and axial flow direction in the turbulent flow regime, recently they have been effectively used for viscous mixing in the transitional flow regime. Using Newtonian glycerine and non-Newtonian carbopol systems, Weetman and Coyle (1989) showed that fluid

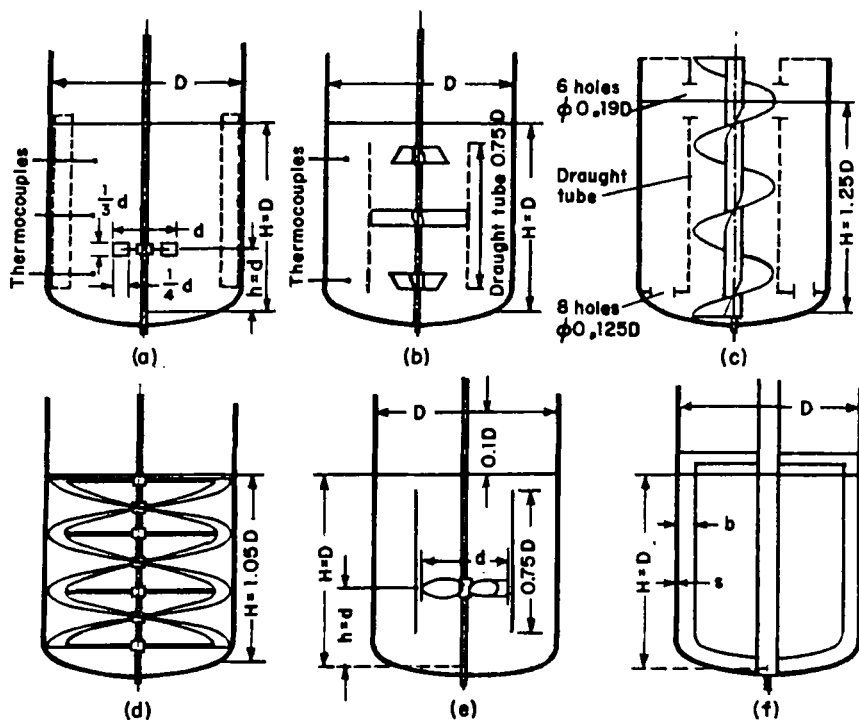


FIG. 23. Some mixers for viscous liquids. (a) Six-blade turbine; (b) three inclined-blade paddles; (c) helical screw; (d) helical ribbon; (e) propeller in draught tube; (f) anchor. (Reprinted with permission from *Chemical Engineering Science*, 37, 813, C. J. Hoogendoorn and A. P. Den Hartog, © 1967 Pergamon Press plc).

foil impellers show equal blend times at one-half of the power consumption of pitched-blade turbines.

2. Power Consumption

The power required for a given stirrer type and associated vessel configuration depends on the speed of rotation N , the stirrer diameter d_1 , the density ρ , and the kinematic viscosity ν of the medium. In vessels without baffles, the liquid vortex, and therefore the acceleration due to gravity, g , is immaterial, as long as no gas is entrained in the liquid. Thus, $P = f(N, d_1, \rho, \nu)$, and in the dimensionless form, $Ne = f(Re)$, a relationship generally known as the power characteristics of the stirrer. Here, $Ne \equiv P/(\rho N^3 d_1^5)$ is the Newton or Power number, and $Re \equiv Nd_1^2/\nu$ the Reynolds number. This relationship was described in Sections II and III for gas-liquid and gas-liquid-solid systems.

An early study of power consumption in a homogeneous liquid in the absence of an air-liquid interface was reported by Laity and Treybal (1957). They examined agitation in unbaffled vessels as well as baffled vessels with four radial baffles, each 16.7% of the vessel diameter, and concluded that dynamic similarity is obtained in geometrically similar, unbaffled vessels by operating with no air-liquid interface and equal Reynolds numbers. For both unbaffled and baffled vessels, unique relations between Ne and Re can be obtained. Continuous flow of liquid through an unbaffled vessel has a small effect on the power characteristics of the impeller. For baffled vessels, the effect of continuous flow is negligible. For unbaffled vessels and $10^3 < Re < 10^5$,

$$Ne = 14.86(Re)^{0.2545}. \quad (5.3)$$

The power characteristics of various stirrers and associated vessel configurations illustrated in Fig. 21 are presented in Fig. 24. Three flow regimes can be identified:

(1) Laminar regime ($Re \leq 10^2$). For stirrers with very small wall clearances, such as the anchor or helical ribbon mixer, the laminar regime prevails for $Re \leq 100$. In this regime, the viscous force dominates. The effect of inertial forces (density) is negligible, and thus the baffles are unnecessary. In this regime,

$$Ne \propto Re^{-1},$$

or

$$Ne Re = \text{constant},$$

which leads to

$$P = k_1 N^2 d_1^3 \mu, \quad (5.4)$$

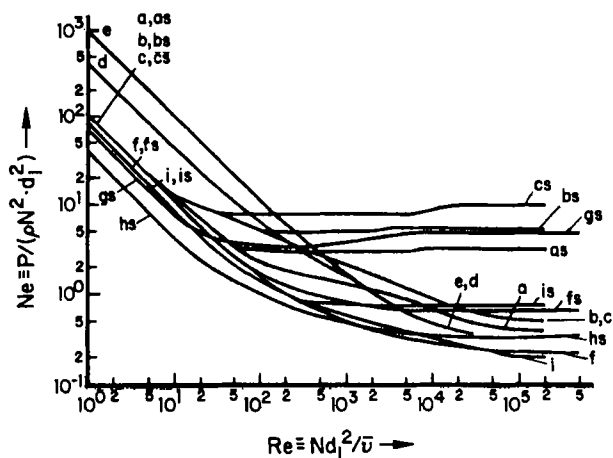


FIG. 24. Power characteristics of the stirrer types in Fig. 21 (Zlokarnik, 1967), except g (Bates *et al.*, 1963) and h (Rushton *et al.*, 1950). (Reprinted with permission from the publisher, VCH Publishers, Inc., after Zlokarnik and Judat, 1988.)

where μ is the dynamic viscosity, and k_1 is the constant whose value depends on the stirrer and vessel configuration.

(2) Turbulent flow regime ($Re \geq 10^2$ for baffled vessels and $Re \geq 5 \times 10^4$ for unbaffled vessels) In this regime, viscosity and Reynolds number have no effect on power consumption. Thus,

$$Ne = \text{constant}$$

which leads to

$$P = k_2 N^3 d_1^5 \rho. \quad (5.5)$$

In this regime, baffles are fully effective and they can increase the required stirring power by a factor as great as 10. This is illustrated in Fig. 24 for a vessel containing the blade stirrer with (curve cs) and without (curve c) baffles.

(3) Transition regime ($10 \leq Re \leq 5 \times 10^4$) This regime arises only in vessels without baffles. In this case, both viscosity and density have significant effects on power consumption. The relationship $Ne \propto Re^{-1/3}$ applies in this regime.

The constants k_1 and k_2 for various types of stirrers are reported by Zlokarnik and Judat (1988). In general, the Reynolds number is first determined and the corresponding value of Ne is obtained from Fig. 24. Using this value, the power can be evaluated using the expression

$$P = Ne N^3 d_1^5 \rho. \quad (5.6)$$

As shown in Fig. 24, the Newton number for most vessels without baffles decreases monotonically over a wide range of flow conditions. For liquid-liquid polymerization reactions, this offers the possibility of determining the viscosity of a reaction mixture and therefore the conversion, or the degree of polymerization, as a function of time if the mixing power is measured during the reaction process. If large differences in density or viscosity exist at the start of mixing, it is advisable to calculate the mixing power using the larger of the two values. Values of Newton numbers for various turbine and paddle stirrer vessels are given by Bates *et al.* (1963). Zlokarnik (1967), Gramlich and Lamade (1973), and Henzler (1978) have also discussed power characteristics of a variety of agitated vessels.

Hoogendoorn and Den Hartog (1967) examined power requirement for viscous liquids. As indicated earlier, they compared the performance of various mixers using modified power and mixing numbers (based on 75% of the total mixing time, i.e., θ_{75}). They found that the modified dimensionless power required to reach a certain mixing time was lowest for a helical screw in a draught tube, with inclined blades or propellers in a draught tube a close second; an anchor required the largest power. The Newton number-Reynolds number relationship for viscous liquids is similar to those described in Fig. 24, except that turbulent flow cannot be achieved with viscous liquids.

The minimum power consumption or work of mixing can be obtained from the results shown in Figs. 22 and 24 by defining the modified power number $Ne Re^3(d_T/d_I) = Pd_T\rho^2/\mu^3$ and the modified mixing number $N\theta Re^{-1}(d_T/d_I)^{-2} \equiv \theta_\mu/d_T^2\rho$ and representing them as illustrated in Fig. 25 (Zlokarnik and Judat, 1988). The stirrer whose curve lies lowest in Fig. 25 gives the desired mixing time with the least power consumption. For the sake of clarity, only the curves for the optimum stirrers and their corresponding ranges of Reynolds numbers are included in Fig. 25. For a given mixing number, the best stirrer type and the optimum rotational speed are obtained from the abscissa of this figure, and the optimum mixing power is obtained from the corresponding ordinate in the figure.

Figure 25 also indicates that the minimum mixing number is of the order of 10^{-4} . Thus, for liquids with a viscosity similar to that of water and for large vessels, $\theta_{\min} = 10^{-4}d_T^2\rho/\mu$. Mersmann *et al.* (1975) correlated Fig. 25 by a cubic expression,

$$\frac{Pd_T\rho^2}{\mu^3} \cong 700 \left(\frac{\theta_\mu}{d_T^2\rho} \right)^{-3}. \quad (5.7)$$

This relationship is valid for the turbulent flow regime, and Mersmann *et al.* indicate that (1) at constant P/V , θ increases as $d_T^{2/3}$, and (2) at constant d_T , θ decreases as $(P/V)^{-1/3}$. Thus, for the homogenization of liquid mixtures in

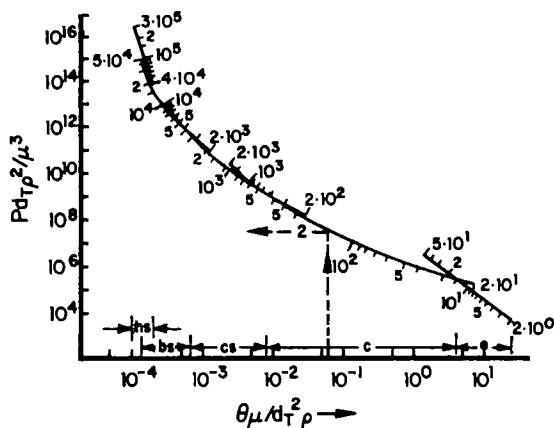


FIG. 25. Curves for determining the optimum stirrer type and the operating conditions that minimize the mixing work. The numbers along the curves are the Reynolds number, $Re = Nd_T^2 \rho / \mu$. (Reprinted with permission from the publisher, VCH Publishers, Inc., after Zlokarnik and Judat, 1988.)

the turbulent flow regime, vessels cannot be scaled up assuming constant P/V . Mersmann *et al.* (1975) reported a similar relationship for the helical ribbon mixer in the laminar flow regime as

$$\frac{P\theta^2}{d_T^3 \mu} = 5.8 \times 10^5. \quad (5.8)$$

This indicates that in the laminar flow regime, a vessel can be scaled up assuming constant P/V . It also shows that under this condition, $\theta \propto (P/V)^{-1/2}$.

3. Pumping Capacity of Stirrers

The liquid flow rate that is displaced through the area swept by the stirrer is termed the liquid throughput of the stirrer, or its pumping capacity q' . This area is given by $\pi d_T^2/4$ for axially operating stirrers, and by $\pi d_T b$ for radial flow stirrers, where b is the paddle height. In continuously stirred tanks, homogenization can only be achieved if $q' > q$, where q is the liquid flow rate through the vessel. Under these conditions, the mixing time is $\theta \propto V/q'$, where V is the liquid volume.

The throughput characteristic of a given stirrer is defined by the dimensionless relation $Q' = f(Re, d_T/d_1, H_i/d_1)$, where $Q' \equiv q'/(Nd_T^3)$ represents the dimensionless throughput number; $Re \equiv Nd_T^2/\nu$ is the Reynolds number;

and d_T/d_1 , H_i/d_1 are the pertinent geometric parameters of the stirrer and associated vessel.

In the turbulent flow regime ($Re > 10^3$), Q' is mainly a function of the parameter d_T/d_1 . This relationship for typical stirrers is defined as

$$Q' = 0.654(d_T/d_1)^{-0.16}, \quad d_T/d_1 > 3, \quad (5.9)$$

for a propeller stirrer with $H/d_T = 1$ and pitch $s = 1$ (pitch $s = \tan$ of the blade angle a) operating in a baffled vessel, and

$$Q' = 1.29(d_T/d_1)^{-0.20}, \quad 2 < d_T/d_1 < 33, \quad (5.10)$$

for paddle stirrers with six pitched paddles ($\alpha = 45^\circ$, $b/d_1 = 0.2$) (Fort *et al.*, 1969).

Cooper and Wolf (1968) examined the velocity profile and pumping capacity for turbine stirrers with six paddles (Fig. 21g). They concluded that the normalized radial velocity profiles of the turbine jet are independent of turbine speed and independent of turbine diameter for geometrically similar turbines. The radial velocity profile is parabolic but becomes increasingly plug in shape with greater radial distance. The tangential profile is somewhat flat in nature. The pumping capacity can be expressed as

$$Q' = \mathcal{K} \quad \text{for constant } w_i/d_1, \quad (5.11)$$

and

$$Q' \propto W_i/d_1 \quad \text{for } w_i/d_1 \text{ around } \frac{1}{3}. \quad (5.12)$$

The constant \mathcal{K} was independent of turbine speed but varied with turbine diameter and fluid used. For water, \mathcal{K} varied from 0.73 to 0.89 for turbine diameters ranging between 3 and 6 in.

Sano and Usui (1985) found that for both paddle and turbine stirrers with various dimensions, Q' is independent of the Reynolds number. They presented the relationships

$$Q' = 1.3(d_i/d_T)^{-0.86}(w_i/d_T)^{0.82}n_p^{0.60} \quad (5.13)$$

for paddle stirrers, and

$$Q' = 0.80(d_i/d_T)^{-0.70}(w_i/d_T)^{0.65}n_p^{0.60}. \quad (5.14)$$

for turbine stirrers. Here, n_p is the number of impeller blades. Sano and Usui (1985) also correlated Q' with power number as

$$Ne = 4.3 Q'^{1.34} \quad \text{for paddles,} \quad (5.15)$$

and

$$Ne = 6.6 Q'^{1.34} \quad \text{for turbines.} \quad (5.16)$$

Sano and Usui (1985) recommended that in turbulent flow, impellers with larger diameter, larger breadth, and a greater number of blades will give better energy savings.

4. Vortex Depth in Unbaffled Stirred Tanks

For liquid-liquid mixtures, the calculations of mixing time and power (or Newton) number outlined above are valid for unbaffled vessels only as long as the vortex created by the stirrer does not reach the stirrer head. Otherwise, gas entrainment occurs and the physical properties of the system change. The depth of the liquid-gas interface at the vessel axis with respect to static liquid surface level, H_L , can be related to the Froude and Galileo numbers. Some of the reported relationships are summarized in Table XIV. The value of H_i at which the vortex reaches the upper impeller blades level can be expressed as

$$\frac{H_{icr}}{d_i} = \frac{H_L - H_i - w_i}{d_i} \quad (5.17)$$

The corresponding impeller speed is N_{max} . For commonly used propeller (Fig. 21h) and turbine (Fig. 21g) stirrers, the highest allowable rotation speed is given in terms of the Froude number, as

$$\frac{N_{max}^2 d_i}{g} = Fr_{max} = 0.072(H^*/d_i)^{1.33}/(0.25 - Ga^{0.1}) \quad (5.18)$$

for a propeller stirrer with $d_T/d_i = 3.33$, $H_i/d_i = 1.50$, and

$$Fr_{max} = 0.016(H^*/d_i)^{1.16}/(0.10 - Ga^{0.18}) \quad (5.19)$$

for a turbine stirrer with $d_T/d_i = 3.33$, $H_i/d_i = 1.0$. Here $Ga = d_i^3 g / \nu^2$, and $H^* = H_L - H_i$ is the liquid height above the stirrer; the expressions are valid for $2.3 < H'/d_i < 5.7$, $10^6 < Ga < 10^{10}$. Rieger *et al.* (1979) reported

$$N_{max} \sim \left(\frac{H_{icr}}{d_i}\right)^{0.42-0.48} \left(\frac{d_T}{d_i}\right)^{(0.69-0.85)} (d_T)^{-(0.53-0.67)} \nu^{(0.06-0.07)} \quad (5.20)$$

for a high Ga number, or

$$N_{max} \sim \left(\frac{H_{icr}}{d_i}\right)^{0.27-0.5} \left(\frac{d_T}{d_i}\right)^{(0.87-1.98)} (d_T)^{(0.55-1.4)} \nu^{(0.18-0.33)} \quad (5.21)$$

for a low Ga number.

Similar expressions can be obtained from the correlations of Zlokarnik (1971) and Le Lan and Angelino (1972), and they are outlined in Table XIV. All of these relations indicate a strong dependence of N_{max} on the impeller diameter.

TABLE XIV
CORRELATIONS FOR H_i

Investigator	Type of Stirrer	Other Relevant Dimensions	Correlations
Zlokarnik (1971)	Turbine impeller	$\frac{d_T}{d_i} = 3.33, \frac{H_i}{d_i} = 0.9,$ $\frac{H_L}{d_i} = 1-1.75$ $2.7 \times 10^6 < Ga < 1.7 \times 10^{10}$	$\frac{H_i}{d_i} = 62.0 Fr(0.1 - Ga^{-0.18}) \left(\frac{H^*}{d_i} \right)^{-0.16},$ where H^* = distance between the static liquid surface and the disk of the turbine impeller.
Le Lan and Angelino (1972)	Six-blade disk turbine	$\frac{d_T}{d_i} = 1.39 \text{ to } 4.55$ $\frac{H_i}{d_i} = \frac{1}{2} \text{ to } \frac{2}{3}$ $Re = 5,000 \text{ to } 7 \times 10^4$	$\frac{H_i}{d_i} = \Pi^2 \left(\frac{Re}{3.27 Re + 4,400} - 0.05 \frac{d_T}{d_i} \right)$ $Fr \frac{d_T}{d_i}$
Rieger <i>et al.</i> (1979)	See Table XIVa	See Table XIVa	$\frac{H_i}{d_i} = B_1 Ga^{0.069} \left(\frac{d_T}{d_i} \right)^{-0.38} Fr^{1.14} Ga^{-0.008(d_T/d_i)^{0.006}}$ for high Galileo number and $\frac{H_i}{d_i} = \bar{B}_1 Ga^{0.33} \left(\frac{d_T}{d_i} \right)^{-1.18} Fr^{3.38} Ga^{-0.074} \left(\frac{d_T}{d_i} \right)^{0.14}$ for low Galileo number range.

TABLE XIVa

VALUES OF CONSTANTS B_1 , \bar{B}_1 FOR CORRELATIONS OF RIEGER *et al.* (1979)

Impeller Type	H_i/d_i	Ga Range	Constant	B_1 or \bar{B}_1
Six-blade disk turbine	1	$(3 \times 10^7, 5 \times 10^{10})$	B_1	1.51 ± 0.03
		$(2.6 \times 10^5, 3 \times 10^7)$	\bar{B}_1	0.055 ± 0.002
	1/3	$(3.10^7, 5 \times 10^{10})$	B_1	1.43 ± 0.03
		$(3.4 \times 10^5, 3 \times 10^7)$	\bar{B}_1	0.046 ± 0.002
Flat six-blade turbine	1	$(8 \times 10^6, 10^{10})$	B_1	1.52 ± 0.02
		$(4 \times 10^5, 8 \times 10^6)$	\bar{B}_1	0.073 ± 0.002
	1/3	$(8 \times 10^6, 10^{10})$	B_1	1.57 ± 0.03
		$(4.1 \times 10^5, 8 \times 10^6)$	\bar{B}_1	0.071 ± 0.004
Pitched six-blade turbine	1	$(10^8, 2 \times 10^{10})$	B_1	1.13 ± 0.03
		$(5.6 \times 10^5, 10^8)$	\bar{B}_1	0.037 ± 0.002
	1/3	$(10^8, 2 \times 10^{10})$	B_1	1.04 ± 0.02
		$(7.5 \times 10^5, 10^8)$	\bar{B}_1	0.029 ± 0.002
Pitched three-blade turbine	1	$(10^8, 10^{10})$	B_1	0.84 ± 0.04
		$(1.2 \times 10^5, 10^8)$	\bar{B}_1	0.019 ± 0.002

B. DISPERSION IN IMMISCIBLE LIQUID-LIQUID SYSTEMS

As described later, liquid-liquid reactors are mechanically agitated in order to achieve a good dispersion and large interfacial area between two immiscible liquids. The increase in interfacial area due to stirring enhances the reaction rate (e.g., saponification, bead polymerization, etc.). It should be noted that the interfacial area is also increased by the addition of surfactants. This process is called emulsification and is governed by completely different principles than the ones described here.

Liquid-liquid dispersion involves two phases: a continuous phase (one with large volume), and a dispersed phase (one with small volume). When the volume fractions of both phases are nearly the same, phase inversion occurs. In this case, which of the two phases becomes a continuous one depends on the starting conditions as well as the physical properties of the system. The range of volume fraction within which either of two immiscible liquids may be continuous is primarily a function of the viscosity ratio; it is not strongly dependent upon vessel characteristics or stirring speed (Selker and Sleicher, 1965). Here we briefly evaluate the minimum speed of rotation required to disperse one phase completely into the other, the interfacial area, and the mass-transfer coefficient in liquid-liquid dispersion.

1. Dispersion Characteristics

In liquid-liquid dispersion, a steady state is established in which the formed droplets continuously coalesce into larger ones and are broken up by

the stirrer into new droplets. The droplet size distribution of a dispersion generated by stirring is characterized by a mean droplet size d_{sv} , $d_{sv} \equiv \sum n_i d_{svi}^3 / \sum n_i d_{svi}^2$ (n_i = number of droplets in class i ; d_{sv} is referred to as the Sauter mean diameter. According to this definition, a simple relationship exists between d_{sv} and the interfacial area per unit volume of the dispersed phase a_L as $a_L = 6/d_{sv}$.

For a given stirrer type and associated vessel, the steady-state values of d_{sv} and a_L are functions of the following variables: $d_{sv} = f(N, d_1, \Delta\rho g, \rho', \nu', \nu, \sigma, \phi')$. In this expression, N is the speed of rotation of the stirrer, d_1 the stirrer diameter, $g \Delta\rho$ the specific weight difference between the two phases, ρ' and ρ the densities, ν' and ν the kinematic viscosities, σ the interfacial tension, and ϕ' the volume fraction of the dispersed phase (the prime indicates the dispersed phase). In the dimensionless form, the above relationship can be stated as follows: $d_{sv}/d_1 = f(\text{Re}, \text{Fr}', \text{We}, \rho'/\rho, \nu'/\nu, \phi')$, where $\text{Re} \equiv Nd_1^2/\nu$, $\text{Fr}' \equiv N^2 d_1 \rho / g \Delta\rho$ (modified Froude number), and $\text{We} \equiv \rho N^2 d_1^3 / \sigma$ is the Weber number.

The relationship for d_{sv}/d_1 for the turbine stirrer shown by Fig. 21g can be expressed as (Coulaloglou and Talvarides, 1976; Mersmann and Grossmann, 1980)

$$d_{sv}/d_1 = a \text{We}^{-0.6} (1 + b\phi'), \quad (5.22)$$

where a lies between 0.05 and 0.08 and $b = 4.47$. Emulsion droplets can be disrupted in various mixers by an addition of polymer. According to Kolmogoroff's theory, the turbulent eddies set up pressure fluctuations that disrupt the globules so that their final size is determined by the size of the smallest eddies. This theory has been experimentally verified for different types of stirrers (Hinze, 1955; Shinnar and Church, 1960; Sprow, 1967) and also has been shown to be applicable to high-pressure homogenizers (Walstra, 1969). The coalescence frequency is a strong function of impeller speed N (frequency $\propto N^{2.85}$) when compared to d_{sv} dependence on N ($d_{sv} \propto N^{-1.2}$). Average drop size correlations reported in the literature before 1976 are summarized by Coulaloglou and Talvarides (1976).

The minimum rotational speed required to mix the dispersed phase completely is given by Van Heuven and Beek (1970) as

$$\text{Fr}' = 36.1(\text{Re We})^{-0.2} (1 + 3.5\phi')^{2.34}. \quad (5.23)$$

Skelland and Seksaria (1978) correlated the minimum rotation speed in both dimensional and dimensionless forms. In the dimensional form, they presented

$$N_m = C_0 d_1^{\alpha_0} \mu_c^{1/9} \mu_d^{-1/9} \sigma^{0.3} \Delta\rho^{0.25}, \quad (5.24)$$

where C_0 and α_0 depend upon the type of impeller, and its location and their

TABLE XV
VALUES OF C_0 AND α_0 IN EQ. (5.24) AND C_1 AND α_1 IN EQ. (5.25)
(SKELLAND AND SEKSARIA, 1978)^a

Set No.	C_0	α_0	C_1	α_1
1	0.348148	-1.38272	15.3244	0.28272
2	0.151858	-1.65355	9.9687	0.55355
3	0.293388	-1.49329	15.3149	0.39329
4	0.044722	-2.02317	5.2413	0.92317
5	0.047382	-2.15120	6.8231	1.05120
6	0.063248	-1.91877	6.2040	0.81877
7	0.009150	-2.69010	2.9873	1.59010
8	0.031193	-1.97371	3.3545	0.87371
9	0.009103	-2.72474	3.1780	1.62474
10	*	*	•	*
11	0.036654	-1.98099	3.9956	0.88099
12	•	•	*	*
13	0.013292	-2.56244	3.6108	1.46244
14	*	*	*	*
15	0.048231	-1.90056	4.7152	0.80056
16	0.066748	-1.64010	4.2933	0.54010

^a Asterisks indicate that there were insufficient data to correlate results. Sets 1, 5, 9, 13: impeller midway in denser phase, $H/4$. Sets 2, 6, 10, 14: impeller midway in lighter phase, $3H/4$. Sets 3, 7, 11, 15: impeller at organic-water interface, $H/2$. Sets 4, 8, 12, 16: two impellers, one midway in each phase, $H/4$, $3H/4$. (Reprinted with permission from Skelland, A.H.P., and Seksaria, R., *Ind. Eng. Chem. Proc. Des. Dev.* 17 (1), Copyright 1978, American Chemical Society.)

values are described in Table XV. In the dimensionless form, they presented

$$\frac{N_m d_1^{1/2}}{g^{1/2}} = C_1 \left(\frac{d_r}{d_1} \right)^{\alpha_1} \left(\frac{\mu_c}{\mu_d} \right)^{1/9} \left(\frac{\Delta \rho}{\rho_c} \right)^{0.25} \left(\frac{\sigma}{d_1^2 \rho_c g} \right)^{0.3}, \quad (5.25)$$

where the values of C_1 and α_1 are once again described in Table XV. It is clear from these relations that N_m is a strong function of the impeller diameter and the nature of the impeller.

2. Stirrer Power in Dispersion

The power characteristics are the same for homogeneous systems and liquid-liquid dispersion as long as the liquid density is replaced by the mean density of the dispersion, $\rho_d = \rho + \phi' \Delta \rho$, and the viscosity is replaced by the weighted geometric mean of the viscosities of the two phases, $\mu_d = \mu' \phi' \mu^{(1-\phi')}$

or $\mu_d = [\mu/(1 - \phi')][1 + 1.5\phi'\mu'/(\mu' + \mu)]$. The latter is more easily interpreted on a physical basis (Vermeulen *et al.*, 1955; Laity and Treybal, 1957).

Laity and Treybal (1957) showed that with the above definitions of ρ_d and μ_d for two-phase mixtures, the correlations for Ne for two-phase and single-phase liquids can be identical. Laity and Treybal (1957) also showed that the impeller height in relation to the liquid-liquid interface of two-phase systems has little effect between one and two impeller diameters from the bottom of an unbaffled vessel. Impeller height in baffled vessels is important in the agitation of two-phase liquids. For more effective agitation, the vessel should be operated, if possible, with the impeller in the low-viscosity phase.

3. Scale-up of the Dispersion Process

The dispersion characteristic $d_{sv}/d_i \propto We^{-0.6}$ yields the following scale-up criterion:

$$(d_{sv}/d_i)We^{0.6} = d_{sv}(\rho/\sigma)^{0.6}(N^3d_i^2)^{0.4} = \text{constant}. \quad (5.26)$$

This results in the scale-up rule, $(N_{\text{large}}/N_{\text{small}}) = \bar{\mu}^{-2/3}$ (where $\bar{\mu}$ is the scale-up factor) for the speed of rotation. Replacing the term $N^3d_i^2$ with the equivalent expression $P/\rho V$ in Eq. (5.26), which is valid in the turbulent regime, produces the relationship

$$d_{sv}(\rho^{0.2}/\sigma^{0.6})(P/V)^{0.4} = \text{constant}. \quad (5.27)$$

Therefore, the mean droplet size and the volumetric interfacial area a_L remain unaltered if the same power per unit volume (P/V) is used in the scale-up.

Skelland and Seksaria (1978) showed that $(P/V) \propto d_i^{-1.3}$; i.e., the power consumption per unit volume decreases as the apparatus size increases to achieve the minimum impeller speed for complete dispersion. Thus the "rule" of equal power input per unit volume, although incorrect here, is on the safe side. When physical properties are constant and full geometric similarity prevails between two different-sized vessels, the relation

$$\frac{(N_m)_1}{(N_m)_2} = \left(\frac{d_{i,2}}{d_{i,1}}\right)^{1.1} \quad (5.28)$$

applies. The power consumption per unit volume at minimum mixing speed varies with the geometric ratio d_T/d_i as

$$(P/V) \propto \left(\frac{d_T}{d_i}\right)^{3\alpha_1 - 1.7} d_T^{-1.3}, \quad (5.29)$$

where values for $3\alpha_1 - 1.7$ for various types of impeller and their positions are listed in Table XVI.

TABLE XVI
VALUES OF $3\alpha_1 - 1.7$ IN EQ. (5.29)
(SKELLAND AND SEKSARIA, 1978)

	Set No.	$3\alpha_1 - 1.7$
Propeller	1	-0.85184
	2	-0.03935
	3	-0.52013
	4	1.06951
Pitched-blade turbine	5	1.45360
	6	0.75631
	7	3.07030
	8	0.92113
Flat-blade turbine	9	3.17422
	10	* ^a
	11	0.94297
	12	•
Curved-blade turbine	13	2.68732
	14	•
	15	0.70168
	16	-0.07970

^a Asterisks indicate insufficient data. Set numbers are as in Table XV. (Reprinted with permission from Skelland, A.H.P., and Seksaria, R., *Ind. Eng. Chem. Proc. Des. Dev.* 17 (1), Copyright 1978, American Chemical Society.)

4. Mass Transfer in Dispersion

The mass-transfer coefficient k_L at the liquid-liquid interface between the dispersed and the continuous phase can be described by the dimensionless relation $Sh = f(Ar, Re, Sc, d_{sv}/d_i)$, and the heat-transfer coefficient can be described by the relation $Nu = f(Ar, Re, Pr, d_{sv}/d_i)$. Calderbank and Moo-Young (1961) showed that these two characteristics are the same for all disperse systems.

As the speed of rotation is increased, smaller droplets are formed, and the interfacial area per unit volume a_L increases. As long as d_{sv} is greater than 2.5 mm, the mass-transfer coefficient k_L remains practically constant. As soon as the droplet size becomes less than 2.5 mm, the k_L value begins to decline. In the transition range $0.8 \text{ mm} < d_{sv} < 2.5 \text{ mm}$, the value of k_L falls by a factor of approximately four and then remains constant, although further increase in the stirrer power results in smaller droplets. The reason for the large drop in k_L values for $d_{sv} < 2.5 \text{ mm}$ is the increasing hindrance of turbulence in the boundary layer. The small droplets behave like rigid spheres.

For $d_{sv} > 2.5$ mm, $Sc > 1$ and $Pr < 10^5$, the following relationships apply for pure coalescing liquids:

$$Sh/Ar^{1/3} = 0.42 Sc^{1/2}. \quad (5.30)$$

When Eq. (5.30) is expressed in terms of k_L , this gives

$$k_L \propto (\mathcal{D}/v)^{1/2} (vg \Delta\rho/\rho)^{1/3}. \quad (5.31)$$

Equation (5.31) shows that k_L is independent of both the flow conditions and d_{sv} and is determined exclusively by the physical properties of the system.

For $d_{sv} < 2.5$ mm, $Sc > 1$, $Pr < 10^5$, the following relationships apply for liquid-liquid noncoalescing systems:

$$Sh/Ar^{1/3} = 0.31 Sc^{1/3}. \quad (5.32)$$

The mass-transfer characteristic in terms of k_L becomes

$$k_L \propto (d_T/v)^{2/3} (vg \Delta\rho/\rho)^{1/3}. \quad (5.33)$$

Therefore,

$$k_L \propto d_T^{2/3}. \quad (5.34)$$

For $Ar > 0.1$, $Sc < 10^{12}$, the mass transfer characteristic for $d_{sv} < 2.5$ mm can be expressed by the relation

$$Sh = 2 + 0.31(Ar Sc)^{1/3}. \quad (5.35)$$

This relationship indicates that the Sherwood number takes the value 2 for $\Delta\rho \simeq 0$, as is the case in natural convection. A generalized correlation for mass and heat transfer coefficients is recommended by Calderbank and Moo-Young (1961). This correlation relates the mass-transfer coefficient to the power per unit volume and Schmidt number. The relationship is mainly applicable to low-viscosity liquids.

C. INDUSTRIAL LIQUID-LIQUID REACTORS

As mentioned earlier, the basic objective of liquid-liquid reactors is to create a fairly high specific area of contact, and at the same time ensure that the phase separation is conveniently achieved. A liquid-liquid system gives high values of specific interfacial area because of low interfacial tension. While small density differences in a liquid-liquid system give a large interfacial area, too small a density difference is detrimental to the quick separation of the two phases, and this may lead to operational difficulties.

Here we examine commonly used mechanically agitated industrial liquid-liquid contactors. Table XVII describes mixing and mass transfer parameters for mechanically agitated liquid-liquid contactors. The most commonly

TABLE XVII

TYPICAL VALUES OF MIXING AND MASS-TRANSFER PARAMETERS IN
MECHANICALLY AGITATED CONTACTORS (REPRINTED FROM
DORAISWAMY AND SHARMA, 1984, COURTESY OF MARCEL DEKKER, INC.)

Dispersed phase	Partially mixed
Continuous phase	Mixed
ε_d (fractional dispersed-phase holdup)	0.05–0.4
$k_L \times 10^2$ (cm/s)	0.3–1
a_L (cm ² /cm ³)	1–800
$k_L a_L \times 10^2$ (s ⁻¹)	0.3–800
Residence time of the continuous phase	Can be varied over a wide range

used contactor is the mixer-settler. Others include symmetric and asymmetric rotating disk columns, mixed columns, pulsed packed columns, and Podbielniak centrifugal extractors. Some of the practical applications of these reactors are outlined in Table XVIII. Typical characteristics of these contactors are described in Table XIX.

TABLE XVIII

PRACTICAL APPLICATIONS OF MECHANICALLY AGITATED INDUSTRIAL
LIQUID-LIQUID REACTORS

Type of Reactor	Practical Applications
Mixer-settler	<ul style="list-style-type: none"> • Removal of free fatty acids from fats using aqueous or alcoholic caustic soda • Removal of HCl from organic substitution chlorination reactions by extraction into aqueous soda ash or caustic soda solutions • Batch nitrations and sulfonations, e.g., reactions of toluene or chlorobenzene with a mixture of sulfuric and nitric acids • Alkylation of isobutane with isobutylene or butene with sulfuric acid as a catalyst
Columns agitated with rotating stirrers	<ul style="list-style-type: none"> • Organic liquid-liquid reactions with high interfacial tension • Suitable for dirty systems and for systems with extreme phase ratios
Pulsed column	<ul style="list-style-type: none"> • Extraction of metals from radioactive solutions and slurries • Oximation of cyclohexanone
Centrifugal extractor	<ul style="list-style-type: none"> • Extraction of penicillin • Recovery of vanadium by a hydrometallurgical route—extraction of vanadic acid anion by a tertiary amine that is insoluble in water • Treatment of waste liquors from nuclear energy systems

TABLE XIX
TYPICAL CHARACTERISTICS OF MECHANICALLY AGITATED INDUSTRIAL
LIQUID-LIQUID REACTORS

Type of Reactor	Characteristics
Mixer-settlers	<ul style="list-style-type: none"> • Simple, easy maintenance and highly flexible • Any ratio of two phases can be handled, no hydrodynamic limitation on flooding • Can be operated batchwise or continuously • Agitation conditions can be varied from stage to stage • Can be highly efficient and easy to scale up • Can handle solids • Can require large space, and power consumption can be high • Undesirable side reactions are possible because of long residence time
Columns agitated with rotating stirrers	<ul style="list-style-type: none"> • Particularly useful for systems with high interfacial tension and small overall driving force—RDC is well suited for high throughputs at low separations performance • RDC suited for dirty systems • RTD for both phases in droplet-size distribution are important for scale-up purposes—backmixing is a problem for scale-up • ARDC is a relatively expensive contactor
Pulsed column	<ul style="list-style-type: none"> • Particularly useful for contacting two hazardous (e.g., radioactive) liquid phases with high interfacial tension values • Show good efficiencies • Generally not used for diameters greater than 180 cm • Baffles are used to reduce axial mixing
Centrifugal extractors	<ul style="list-style-type: none"> • Useful for liquids having a very small difference in densities and/or very much lower interfacial tension • Useful for systems requiring short residence time to avoid degradation of desired species • Useful when both liquid phases are viscous and gravity separation is difficult • Large handling capacity • Floor space requirement is low • Rather expensive in capital as well as recurring costs compared to other types of extractors • Maintenance will require close attention • Generally useful for special operations

1. Mixer-Settler

The mixer-settler unit shown in Fig. 26a is usually considered to be approximately equivalent to one theoretical stage. Some of the typical characteristics of the mixer-settler are shown in Table XIX. For many applications outlined in Table XVIII, a large number of stages (more than five)

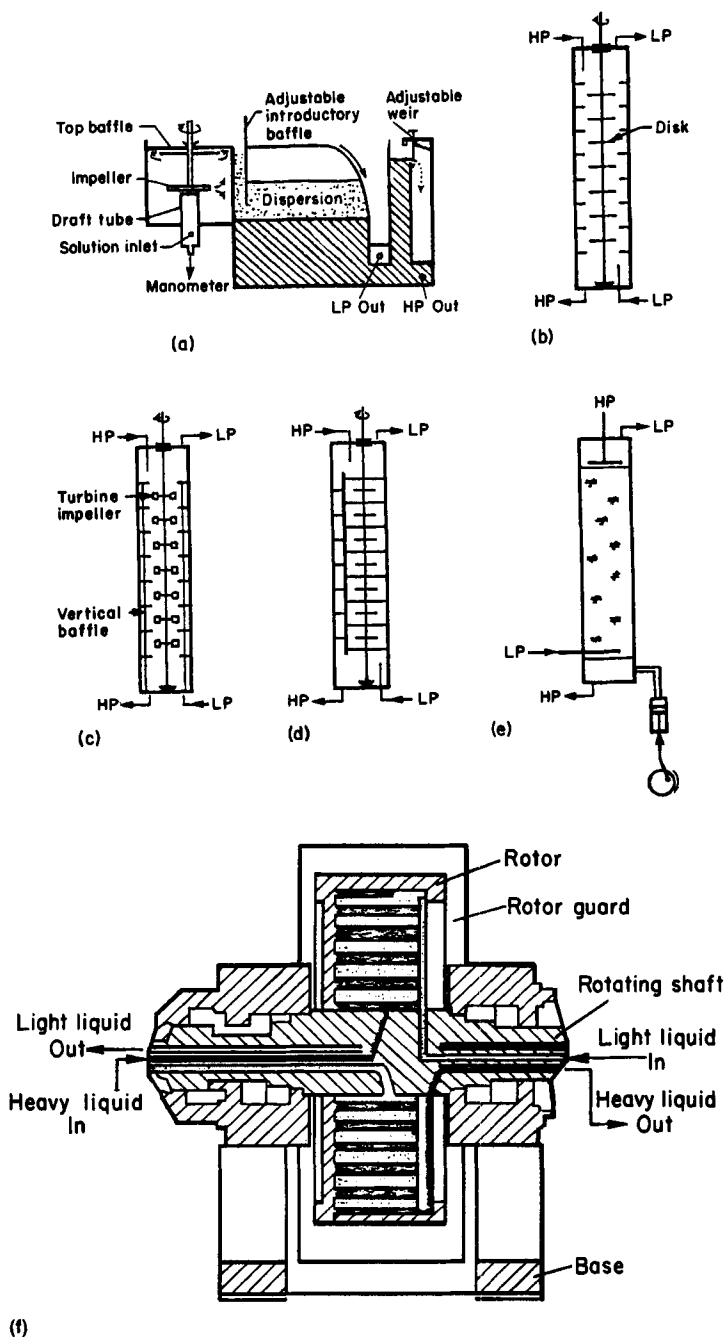


FIG. 26. Mechanically agitated industrial contactors. (a) mixer-settler; (b) rotating-disk column; (c) mixco column; (d) asymmetric rotating-disk column; (e) pulsed packed column; (f) Podbielniak centrifugal extractor. (Reprinted from Doraiswamy, L. K., and Sharma, M. M., *Heterogeneous Reactions: Analysis, Examples and Reactor Design, Vols. 1 and 2*, © 1984, John Wiley and Sons.)

are often required, and this makes the space requirement for such a reactor somewhat excessive. New designs requiring less space, based on the box configuration, have been suggested. The efficiency in the individual stages of the box unit is suspected to be as low as 50%. Furthermore, pumps are required to transfer liquid from one stage to the next, and the overall power consumption is relatively high. Because of large holdup and residence times, such units are not satisfactory for radioactive materials, materials that are expensive or sensitive, or for systems that produce large numbers of undesirable side reactions. In order to overcome these drawbacks, in recent years the vegetable oil industry has implemented a combination of a set mixer and a centrifugal separator for the removal of fatty acids.

The mixer-settler system can be operated either in cocurrent or counter-current mode, depending upon the need for a particular reaction system. The choice of continuous phase vs. dispersed phase also depends on the nature of the reaction. It is possible to design a multistage mixer-settler system without external pumping by use of impellers that have pumping characteristics. This design is particularly relevant where the recycle of one phase within a stage is required. Figure 26a shows the design conceived by Power Gas Company of England incorporating these features (Warwick, 1973). The flow from one stage to the next can also be induced by the hydrostatic head created by the difference in the densities caused by mixing.

The Lurgi Company of Germany has developed a stacked settler unit, which results in a marked reduction in the floor-space requirement. A centrifugal stirrer is attached to the side of the settling column. This mixer is responsible for mixing, mass transfer, and pumping, and contains baffles for fast reactions. The efficiency of such a unit is adversely affected by entrainment. One motor can be used to drive three to five mixer pumps. The optimal speed for mixing often differs from that for pumping, and a suitable combination of mixer and pump is needed to obtain the optimal results (Reissinger and Schröter, 1978).

Horizontal vessels are normally used as settlers in order to provide a large area of phase interface. It is generally necessary to conduct experiments to ascertain the coalescence rate. The settling area can usually be reduced by the use of coalescing aids such as mesh and metal swarf. In recent years, attempts have been made to use an electrostatic field as a coalescence aid. Mumford and Thomas (1972) and Jeffreys and Mumford (1974) have described various methods for reducing the overall size of the settlers. In many instances, differential contact (DC) packings are used that are claimed to act as excellent coalescence aids.

In settlers having a diameter of more than 1 m, recirculating flow caused by the density gradient in the flow direction within the heavy phase is likely to cause an uncontrolled backmixing. This problem can be circumvented to a

considerable extent by increasing the length of the settler; settling aids can be used only downstream of this zone. In a Graesser contactor, a cylinder rotating with a horizontal axis is used, and vertical partitions are provided. The dispersion and mixing are achieved by using dippers. The throughput of this type of contactor is relatively low.

2. *Pump Reactors*

An extreme case of the mixer-settler is the pump reactor, wherein the reaction occurs within the pump itself. The pump provides mixing and short contact time. These reactors are useful for fast reactions requiring high mixing and short time, as in some aromatic nitration reactions. As indicated later, pump reactors are also useful for some polymeric reactions.

3. *Columns Agitated with Rotating Stirrers*

Spray, packed, and sieve-plate columns give poor mass-transfer rates for consequently require greater height. The mass transfer in such columns can be significantly improved by providing mechanical agitation. Remen (1951) and Oldshue and Rushton (1952) introduced the rotating-disk contactor (see Fig. 26b) and the mixed column (see Fig. 26c).

These mechanically agitated columns are particularly useful in processing fluids with high interfacial tension values, such as those found in several industrially important organic reactions. The height equivalent to a theoretical stage (HETS) in an RDC varies from 100 to 200 cm. An RDC is well suited for high throughputs with low separation efficiency. RDCs have been built of different materials, including fiberglass-reinforced plastics, and with diameters of up to 6–8 m, but with a height of only 10–12 m. The height is restricted because the shaft should be continuous, and if intermediate bearings are employed, these provide centers for flooding. The residence-time distribution in both phases and the droplet size distribution are important for scale-up purposes (Olney, 1964; Bibaud and Treybal, 1966; Landau and Houlihan, 1974; Laddha *et al.*, 1968; Marr, 1978).

In order to control backmixing in both phases, a modified form of the RDC, called the asymmetric rotating-disk contactor (ARDC), has been devised (see Fig. 26d). In this design, the shaft with agitator disks is located asymmetrically to the column axis, and nonperforated plates are used to separate the agitating zones. The HETS in an ARDC varies from about 35 to 100 cm, and unlike the RDC, the rotor shaft can be made with couplings so that taller columns can be used. Multiple agitators can be employed. However, an ARDC is a relatively expensive contactor.

In another modification, namely the Kuehni column, centrifugal agitators are used and stator disks are perforated, and their free cross-sectional area

can be adopted to suit the specific requirements. Here, HETS as low as 10 cm can be used. This column is particularly useful as a reactor for systems with extreme phase ratios.

4. Pulsed Column

In certain operations, such as the extraction of metals from radioactive solutions (produced in atomic energy operations), mechanical agitation may be highly undesirable because of health hazards. In these circumstances, pulsed columns can be satisfactorily used. The pulsations can be introduced in a number of ways. For instance, in a perforated column the plate assembly can be mechanically moved up and down while the liquids pass through the contactor. Alternatively, liquids can be "pulsed" by an outside mechanism (Reissinger and Schröter, 1978). One such unit is shown in Fig. 26e. Baird *et al.* (1968) suggested a new design by which liquid pulsations are produced with the use of an air column. By ensuring operation under conditions of resonant frequency, the power requirement can be reduced significantly.

Bender *et al.* (1979) have discussed the operating characteristics of pulsed packed columns, wherein the efficiency can be improved by a factor of two through the introduction of pulsations. Raschig rings are not recommended, since the droplets of the dispersed phase are likely to adhere to the packings. Pulsed columns work well in situations where the liquid properties do not change substantially in the column. On the whole, a pulsed packed column is not a very efficient column, and it requires that the density difference between the two phases be more than 0.08 g/cm^3 .

Pulsed sieve-plate columns have shown good efficiencies for frequencies between 60 and 150 strokes/min and amplitudes under 1 cm. In general, a plate spacing of 10 cm is considered most favorable. However, these columns operate well in only a limited load range and are also susceptible to fouling, particularly with sticky products. To some extent, the reduction in efficiency at underload can be compensated by changing the pulsation characteristics; the load can also be artificially increased by recycling the raffinate.

5. Reciprocating Sieve-Plate Column

Reciprocating sieve-plate columns, where a reciprocating motion is imparted to the plate assembly, have been suggested by Karr and Lo (1976). In such columns, a baffle plate can be employed to minimize axial mixing, and reciprocation speed can be varied over a wide range. Karr and Lo have discussed procedures for scale-up and have tested this procedure with columns up to 90 cm in diameter. HETS increases with column diameter and shows an optimum with respect to reciprocation speed. For a column 90 cm in diameter,

an HETS value of around 50 cm for a system such as *o*-xylene–acetic acid–water is possible.

Pulsed columns are generally not used for column diameters greater than 180 cm because of problems with mechanical support and pulse generation. The great amount of backmixing also causes uncertainties in column performance. Small pulsed columns have been successfully used for the extraction of metals from slurries (Warwick, 1973).

6. *Vibrating-Plate Extractors*

For some applications, instead of pulsed sieve-plate columns, vibrating-plate extractors have been recommended (Rod, 1976). Rod has pointed out some advantages of this type of contactor for the oximation of cyclohexanene.

7. *Centrifugal Extractors*

For liquids having a very small difference in densities and/or very low interfacial tension, centrifugal extractors offer a good alternative. Typical characteristics of such extractors are outlined in Table XIX. The Podbielniak extractor or a rotating sieve-tray extractor is the most commonly used centrifugal extractor (see Fig. 26f). It contains a number of concentric sieve trays located around a horizontal axis through which the two liquid phases flow in a countercurrent pattern. Each extractor can provide three to five theoretical stages and throughputs of the order of 130,000 L/h. However, this extractor is not suitable for emulsions and requires that the density difference between the two phases be greater than 0.05 g/cm^3 (Reissinger and Schröter, 1978).

Rosenbaum *et al.* (1971) have reported that centrifugal extractors can be used for the recovery of vanadium by a hydrometallurgical route. Centrifugal extractors have also been considered for the treatment of waste liquors from nuclear energy systems.

Centrifugal extractors are rather expensive (in capital as well as maintenance costs). The maintenance of the equipment requires the removal of solid particles from the feed. Use of centrifugal extractors is therefore restricted to special operations.

D. SUMMARY

Mechanical agitation is very prevalent in liquid–liquid reactors because it provides the required high interfacial area, interphase mass transfer, and good dispersion in the case of reactions between two immiscible liquids or

homogenization in case of reactions between two miscible liquids. Generally, heat transfer is less important in liquid-liquid systems.

The factors affecting the design of mechanically agitated liquid-liquid reactors are the miscibility of the liquid phases, the interfacial tension, and the densities and viscosities of the liquid phases, as well as the density and viscosity differences between the two liquids. As shown in Fig. 21, a variety of stirrer configurations are available to carry out liquid-liquid reactions.

When liquids are miscible, the mixing time required to achieve homogenization is the most important design parameter. When the densities and viscosities of the two liquids are very close, this mixing time depends only on the mixing Reynolds number. The relationship between mixing time and mixing Reynolds number for a variety of stirrers is described in Fig. 22. A higher Reynolds number gives a smaller mixing time. When the densities and viscosities of two liquids are significantly different, mixing time depends on both the Reynolds and the Archimedes numbers. For given Reynolds numbers, a smaller Archimedes number (i.e., a smaller density difference between the two liquids) gives a smaller mixing time.

Another important design parameter for miscible liquids is the power consumption, which can be obtained from Fig. 24. For viscous liquids, flow is in most part laminar. When the agitated vessels contain baffles, turbulence is achieved at a lower Reynolds number. Once the flow becomes turbulent, the power number attains a constant value.

The optimum stirrer configuration for providing mixing can be obtained from Fig. 25. This optimum depends upon the Reynolds number and the required modified mixing number. For scale-up purposes, it should be noted that in turbulent flow (i.e., $Re > 10^3$), at constant power per unit liquid volume, mixing time $\theta \propto d_T^{2/3}$, and for constant vessel diameter, $\theta \propto (P/V)^{-1/3}$. In this flow regime, vessels cannot be scaled up assuming constant P/V . In laminar flow, vessels can be scaled up assuming constant (P/V) , and $\theta \propto (P/V)^{-1/2}$.

For an open system, the homogenization can only be achieved if the pumping capacity of the stirrer is greater than the liquid flow rate through the vessel. This pumping capacity expressed in a dimensionless form $Q' = q'/Nd_1^3$ is a function of the Reynolds number and the vessel geometrical parameters (d_T/d_1) and H_i/d_1 . In turbulent flow ($Re > 10^3$), Q' is independent of the Reynolds number. The nature of the relationship also depends upon the nature of the stirrer and the agitated vessel.

The relationships for mixing time and power consumption discussed above assume no gas entrainment. For unbaffled vessels, this occurs only below a certain maximum stirrer speed. This maximum stirrer speed, defined in terms of the dimensionless Froude number ($Fr_{\max} = N_{\max}^2 d_1/g$), depends upon the

Galileo number, Ga , and other geometrical parameters of the vessel, such as H^*/d_i where H^* is the height of liquid above the stirrer, and the ratio d_T/d_i . The dependence of N_{\max} on the kinematic viscosity of the liquid is stronger at larger values of Ga .

When two liquids are immiscible, the design parameters include droplet size distribution of the disperse phase, coalescence rate, power consumption for complete dispersion, and the mass-transfer coefficient at the liquid-liquid interface. The Sauter mean diameter, d_{sv} , of the dispersed phase depends on the Reynolds, Froudes and Weber numbers, the ratios of density and viscosity of the dispersed and continuous phases, and the volume fraction of the dispersed phase. The most important parameters are the Weber number and the volume fraction of the dispersed phase. Specifically, $d_{sv} \propto We^{-0.6}(1 + b\phi')$, where b is a constant that depends on the stirrer and vessel geometry and the physical properties of the system. Both d_{sv} and the interfacial area a_L remain unaltered, if the same power per unit volume (P/V) is used in the scale-up.

For the same physical properties, the minimum speed for complete dispersion (N_m) depends on $d_i^{1.1}$. Furthermore, the relationship $N_{\text{large}}/N_{\text{small}} = \bar{\mu}^{-2/3}$, where $\bar{\mu}$ is the scale-up factor, applies. The power consumption at minimum mixing speed varies as

$$(P/v) \propto \left(\frac{d_T}{d_i}\right)^{3\alpha_1 - 1.7} d_T^{-1.3},$$

where values for $3\alpha_1 - 1.7$ for various types of impellers and their positions are listed in Table XVI.

The range of volume fraction within which either of two immiscible liquids may be continuous is primarily a function of the viscosity ratio, but is only weakly dependent upon vessel characteristics or stirring speed. The coalescence frequency for the dispersed drops is, however, a strong function of impeller speed (i.e., frequency $\propto N^{2.85}$).

The liquid-liquid mass transfer coefficient k_L depends strongly on the drop size d_{sv} . For $d_{sv} > 2.5$ mm, $k_L \propto$ fluid properties, and for $d_{sv} < 2.5$ mm, $k_L \propto d_T^{2/3}$. In general, the Sherwood number depends on the Schmidt and Archimedes numbers. For $d_{sv} < 2.5$ mm, $Sh \propto (Ar \cdot Sc)^{1/3}$, and for $d_{sv} > 2.5$ mm, $Sh \propto Ar^{1/3} Sc^{1/2}$. The mass-transfer coefficient can also be related to the power per unit volume and the Schmidt number.

As shown above, design parameters for liquid-liquid reactors are well known, and scale-up of these reactors can be reasonably carried out. Viscous systems cause the most uncertainties in the estimations of design parameters. Practical applications and typical characteristics of several industrial liquid-liquid reactors are described in Tables XVIII and XIX, respectively.

E. FUTURE WORK

Future work should include:

- evaluations of design parameters for a mechanically agitated reactor containing two immiscible liquids, at least one of which is non-Newtonian or viscoelastic; and
- evaluations of design parameters for a mechanically agitated reactor containing two immiscible liquids and solids.

VI. Biological Reactors

A bioreactor is a vessel in which biochemical transformation of reactants occurs by the action of biological agents such as organisms or *in vitro* cellular components such as enzymes. This type of reactor is widely used in food and fermentation industries, in waste treatment, and in many biomedical facilities. There are two broad categories of bioreactors: fermentation and enzyme (cell-free) reactors. Depending on the process requirements (aerobic, anaerobic, solid state, immobilized), numerous subdivisions of this classification are possible (Moo-Young, 1986).

In fermentation reactors, cell growth is promoted or maintained to produce metabolite, biomass, transformed substrate, or purified solvent. Systems based on macro-organism cultures are usually referred as "tissue cultures." Those based on dispersed non-tissue forming cultures of micro-organisms are loosely referred as "microbial reactors." In enzyme reactors, substrate transformation is promoted without the life-support system of whole cells. Frequently, these reactors employ "immobilized enzymes," where an enzyme is supported on inert solids so that it can be reused in the process. Virtually all bioreactors of technological importance deal with a heterogeneous system involving more than two phases.

General design considerations for mechanically agitated gas-liquid and gas-liquid-solid mechanically agitated reactors described earlier in Sections II and III are applicable here. In this section, however, we evaluate additional design considerations that are specific to bioreactors. Novel reactors to overcome specific needs of biological processes are also evaluated in this section. The characteristics of the bioreactors and other chemical/petrochemical gas-liquid and slurry reactors are compared in Table XX.

As an illustration of the complexity of a bioreactor design, consider the critical need of an adequate oxygen supply in aerobic fermentations. In order to prevent irreversible cell damage, oxygen must be supplied continuously to

TABLE XX

COMPARISON BETWEEN CHARACTERISTICS OF CHEMICAL/PETROCHEMICAL AND BIOLOGICAL REACTORS

Chemical/Petrochemical Reactors	Biological Reactors
<ul style="list-style-type: none"> • Liquid phase is organic. • Basic nature of reacting mixture generally remains unchanged during the reaction; constant amount of catalyst. • Catalyst particles are generally heavier than the liquid phase. • Catalyst particle size varies from tens and hundreds of microns to millimeters. • Reaction mixture is generally Newtonian and has reasonably low viscosity. • Catalyst particles generally remain segregated. Flocs of particles are not formed under well-mixed conditions. • Clean environment is not generally required. • Foaming problem can be important for some reactions. • Larger shear stress caused by mechanical agitation does not damage catalyst except for attrition. • Chemical reaction rates are reasonably fast, not requiring excessive reactor volume or fluid residence time. • Generally driving forces for mass and heat transfer rates in chemical/ petrochemical reactors are substantial. • Catalyst activity is not very strongly dependent upon the reactant concentrations, temperature, pressure, and pH of the reaction medium. 	<ul style="list-style-type: none"> • Liquid phase is aqueous. • Complex and time varying reaction mixture. Microbial biomass increases, and the catalyst is synthesized as the biochemical reaction proceeds. • Microbial cells and substrate particles often have densities closer to that of the liquid phase. The relative flow between the dispersed (solid) and continuous (liquid) phases is generally small. • Microbial cells are in the range of a few microns. Small particles give smaller velocities and a low degree of turbulence. • Mycelial growth and polymeric substrates or metabolites often produce a highly viscous and sometimes pseudoplastic non-Newtonian mixture. • Multicellular microbial growth, especially fungal, often forms large cell aggregates such as mycelia, clumps, or pellets. Intraparticle diffusional resistances in these systems may be important and can lead to anaerobiosis. • Aseptic conditions are required. The requirement of a clean environment makes large-scale mechanically agitated operation more difficult. • The conventional mechanically agitated reactors are generally susceptible to foaming for the fermentation reactors. The foaming causes an additional barrier to effective transport rates and reactor operation. • Large shear stress caused by the mechanical agitation may be harmful to live cells. Pronounced mixing is, therefore, harmful. • Microbial growth rates are substantially slower than chemical reaction rates, requiring large reactor volumes and fluid residence times. • Generally, driving forces for mass and heat transfer rates in biochemical reactors are small. This is because concentrations of reactants and/or products in the aqueous phase are generally small, and the reactions generally require low temperatures. • Very close control of solute concentrations, temperature, pressure, and pH of the reaction medium is required in order to avoid damage or destruction of live or labile catalytic components.

the fermentation medium in such a way that the oxygen absorption rate at least equals the oxygen consumption rate of the cells. Furthermore, the same microbial species may show large variations in their oxygen requirements, depending on the oxygen concentration to which they have been adapted. Oxygen requirements also vary with carbon and energy source for the microorganisms, which could frequently change with time.

In contrast to chemical and petrochemical reactors, biochemical reactors invariably contain *aqueous phase* at low pressures. This aqueous phase generally controls the overall interparticle mass-transfer rate and provides four different types of resistances to the overall mass-transfer rate (Moo-Young, 1986):

- (1) Resistance at the gas-liquid interface: This resistance is often rate-controlling in aerobic fermenters because of the relatively low solubility of oxygen in aqueous solutions and the absorption inhibition effects of absorbed materials at the interface.
- (2) Resistance in the bulk aqueous medium separating the dispersed phases: This resistance is insignificant provided good mixing is insured, as is the case in most practical reactor systems.
- (3) Resistance near the solid-liquid interface: This resistance can be significant because of the small relative velocity differences resulting from the low density difference between the continuous aqueous medium and a dispersed phase such as microbes, gel-entrapped enzymes, etc.
- (4) A liquid-phase resistance inside a dispersed solid phase such as cell flocs, immobilized enzymes, etc.

Because of the dominant role of these resistances, mechanical agitation and a high degree of mixing are important to bioreactors.

Many factors must be considered in the design of mechanically agitated biological reactors. For a fermentation reaction, the desired environment for the microbial population may be accomplished at reasonable cost with a conventional fermenter or by design of a novel fermenter. The use of a conventional mechanically agitated fermenter requires the appropriate selections of the agitation rate, the gas flow rate, the operating pressure in the fermenter, the liquid volume, the nutrient composition of the feed, pH, temperature, method of foam control, and mode of operation (batch, fed batch, or continuous). For a novel fermenter, an appropriate equipment design specific to the needs of the given fermentation process must be considered. In both cases, the rate of oxygen transfer in aerobic fermentations is usually one of the important concerns.

A. CONVENTIONAL REACTORS

Well-stirred reactor systems have traditionally been employed for carrying out the great majority of fermentation processes. In these processes, providing a homogeneous reactor environment has been a difficult task. Large residence times in continuous or batch operation help maintain a liquid phase that is well mixed with respect to the nutrients. On the other hand, the large size of these reactors and the complex and time-varying rheological behavior of a multiphase reaction system make homogenization in these reactors energy-consuming and, in general, difficult. Nevertheless, very large ($2,000 \text{ m}^3$) fermentation vessels have been built and operated in the pharmaceutical, food, and chemical industries, mainly because of the relative simplicity of their design and operation. Configuration of a typically mechanically stirred fermenter is shown in Fig. 27. In many cases the stirrer, however, is introduced from the bottom.

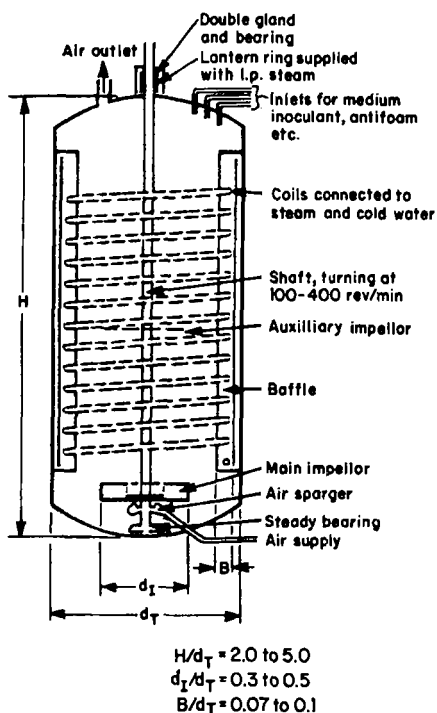


FIG. 27. Configuration of a typical mechanically stirred fermenter. (After Moo-Young, 1986.)

Typical mechanical mixing means in a fermenter consist of various designs of impellers to achieve efficient distribution of the gaseous phase into the fermentation liquor and to provide adequate flow characteristics of the liquid nutrient medium, which is necessary for the physiology of the cultivated microbial, plant, or animal cells. The mass-transfer capabilities of such equipment can be improved by such modifications as the use of baffling systems, draft tubes, or air lift methods. However, each of these conventional methods requires a great deal of mechanical energy to distribute the gaseous phase through the liquid phase and to provide the necessary mixing in large industrial-scale equipment, resulting in both technical and economic problems. In addition to the high energy consumption of these systems, the mechanical agitation of the fermentation liquor in many fermenters creates high shear stresses on the cells, which limits or inhibits cell growth.

Another problem with conventional fermenters concerns foaming. In traditional systems, the introduction of large quantities of gas into the vigorously agitated fermentation liquor often produces great quantities of foam in the reaction vessel. Biological reactors are particularly susceptible to foaming because of the surfactant properties of most biomolecules. This foam severely limits the usable volume of the vessel and can render the fermentation process inoperable and microbially contaminated when the gas flow exit lines become filled with foam. All of these problems have a substantially adverse influence upon the yield and cost-effectiveness of conventional fermentation processes.

Because of the need to avoid mutations and maintain the superior qualities of the genetically developed strain, batch or fed-batch operations are used in most applications. Continuous culture operations, however, provide a time-invariant environment that facilitates greatly the study of a biological process in research laboratories. Moreover, some industrial operations employ continuous reactors, such as the single-cell protein facility of ICI in Billingham, England (total reactor volume of about 2,300 m³), all waste treatment processes, and others. It should be noted that it is relatively common to follow a batch process with a period of fed-batch or continuous operation. Also, in most cases batch cultivation is the optimal start-up procedure for continuous or fed-batch cultivation (Yamane *et al.*, 1977).

Recently, many batch operations have been transformed into fed-batch (semicontinuous) operations by the gradual introduction of nutrient into the reactor. The rationale is to control the feed optimally to maximize a composite performance index. For the case of penicillin fermentation, for example, for which the specific growth rate and the specific penicillin formation rate are mutually disposed, the optimal feed policy is carried out in two phases. During the first phase, cell biomass is quickly built up to the allowable maximum level. During the second product formation phase, the feed is controlled such that

high penicillin production and sufficient biomass growth to make up for the dilution effects take place.

As microbial cultures are very sensitive systems, they pose high demands on the monitoring and control capabilities of a bioreactor. On-line, automated microanalytical methods, as well as various enzyme probes, are presently being developed for the purpose of providing the means for monitoring many other reactor variables on-line. Bioreactor control is presently concerned with the control of the abiotic culture environment as the latter is described by the temperature, the pH, the dissolved O_2 concentration, and the presence of foam. In fed-batch operation, the feed rate of nutrients is also controlled. A certain interaction exists among the various control actions, but the multivariable control characteristics of these systems have not been studied. Most of the control is presently carried out by local analog controllers. However, as the reactor systems and processes grow more complex and the monitoring-estimation capabilities increase, more sophisticated control policies are expected to be introduced in bioreactor operation.

1. Design Parameter Estimations for Conventional Mechanically Agitated Reactors

a. Power Consumption

Ungassed System From dimensional analysis, as shown in earlier chapters, one obtains

$$Ne = \frac{P}{d_1^5 N^3 \rho} = f\left(\frac{d_1^2 N \rho}{\mu}, \frac{d_1 N^2}{g}, \text{geometric factor}\right), \quad (6.1)$$

or

$$\psi = \frac{Ne}{(Fr)^n} = C_3 (Re)^m, \quad (6.2)$$

where C_3 depends on geometrical considerations. $(Fr)^n$ often approaches 1 (particularly for $Re < 300$). In the turbulent flow regime,

$$Ne = \text{constant}, \quad (6.3)$$

$$P \propto \rho N^3 d_1^5 \quad (P \text{ depends on density and is independent of viscosity}). \quad (6.4)$$

In laminar flow,

$$Ne \propto 1/Re, \quad (6.5)$$

$$Ne \propto \mu N^2 d_1^3 \quad (P \text{ depends on viscosity and is independent of density}). \quad (6.6)$$

The relationship between Ne and Re for various impellers is described in Fig. 25. Similar relations for non-Newtonian viscous liquids have been outlined by Schügerl (1981).

For power-law fluids, the above equations can be used if Re is defined as

$$Re = \frac{d_1^2 N \rho}{\mu_{app}}, \quad (6.7)$$

$$\text{where } \mu_{app} = \frac{k}{(B_2 N)^{1-n}} \left(\frac{3m+1}{4m} \right)^m. \quad (6.8)$$

B_2 is a geometric factor that is equal to 11 for the usual bioreactor design with $d_T/d_1 = 1.5$ and $m < 1$.

Gassed System Here, as shown earlier,

$$P_g P_c = f(N_A), \quad (6.9)$$

where N_A is the aeration number, Q_g/Nd_1^3 ; P_g is the power for a gassed system, and P_c is the power for an ungassed system. This relationship is graphically illustrated in Section III. For bioreactors, the relationship of Michel and Miller (1962),

$$P_g = C(P_c^2 \mu d_1^3 / Q_g^{0.56})^{0.45}, \quad (6.10)$$

is also applicable. The details of these relations are discussed in Section III.

Taguchi and Miyamoto (1966) showed that for non-Newtonian fermentation broth, the power requirement in the turbulent flow regime was well correlated by the above correlation of Michel and Miller (1962). Broth from the production of gluco-amylase by *Endomyces* species and carboxymethyl-cellulose solutions were used as non-Newtonian fluids. For non-Newtonian fluids in laminar and transition regions, particularly for fluids with apparent viscosities greater than 300 cP, the impeller diameter and impeller blade width had considerable effects on power consumption in a non-gassed system. They proposed

$$Ne = P_0 g_c / \rho N^2 d_1^5 = 32(Re')^{-0.9} (d_1/d_T)^{-1.7} (w_i/d_T)^{0.4}, \quad Re' < 10, \quad (6.11)$$

$$Ne = 11(Re')^{-0.4} (d_1/d_T)^{-1.7} (w_i/d_T)^{0.5}, \quad 10 < Re' < 50, \quad (6.12)$$

$$Ne = 9(Re')^{-0.05} (d_1/d_T)^{-1.2} (w_i/d_T)^{0.9}, \quad Re' > 50, \quad (6.13)$$

where

$$Re' = (d_1^2 N^{2-m} \rho / 0.1k)(m/(6m+2))^m. \quad (6.14)$$

Here, k is the fluid consistency index and m the flow behavior index. While no data for a gassed system under laminar and transition flow were reported, P_g is expected to depend on impeller dimensions in these regimes.

Hughmark (1980) presented the following relationship of P_g/P_ℓ for flat-blade turbine impellers:

$$\frac{P_g}{P_\ell} = 0.10 \left(\frac{Q_g}{NV_\ell} \right)^{-0.25} \left(\frac{N^2 d_1^4}{g w_i V_\ell^{0.667}} \right)^{-0.20} \quad (6.15)$$

Other relations have been presented by Luong and Volesky (1979), Hassan and Robinson (1977), and Oyama and Endoh (1955). Luong and Volesky (1979) and Schugerl (1981) investigated non-Newtonian CMC solutions, while Hassan and Robinson (1977) investigated electrolytic solutions. Joshi *et al.* (1982) recommend the use of Hughmark's correlation. A reliable correlation for the gas holdup is also reported by Hughmark (1980) as

$$\varepsilon_g = 0.74 \left(\frac{Q_g}{NV_\ell} \right)^{0.5} \left(\frac{N^2 d_1^4}{g w_i V_\ell^{0.667}} \right)^{0.5} \left(\frac{d_b N^2 \rho_\ell d_1^4}{\sigma_\ell V_\ell^{0.667}} \right)^{0.25} \quad (6.16)$$

where, following Calderbank (1967), d_b is related to the physical properties of liquids as

$$d_b = 2.25 \frac{\sigma^{0.6} \rho_g^{0.4}}{(P/V)^{0.4} \rho_\ell^{0.2}} \left(\frac{\mu_\ell}{\mu_g} \right)^{0.25} \quad (6.17)$$

b. Gas-Liquid Mass Transfer

For baffled agitators, sparged with submerged impellers, some of the useful correlations for the gas-liquid interfacial area a_L and the volumetric gas-liquid mass-transfer coefficient are outlined in Table XXI. The correlations are liquid mass-transfer coefficient are outlined in Table XXI. The correlations are valid under nonflooding conditions (i.e., low gas flow rate).

Volumetric mass-transfer coefficients for mechanically agitated fermenters with air sparged into the vessel below the agitator are also reviewed by Joshi *et al.* (1982) and Schugerl (1981). The effects of physical properties of fluids on the volumetric mass-transfer coefficient have been investigated by Miller (1974), Zlokarnik (1978), Yagi and Yoshida (1975), and Henzler (1980). Yagi and Yoshida (1975) developed the correlation

$$\begin{aligned} \frac{k_L a'_L d_1^2}{\mathcal{D}} &= 0.060 \left(\frac{d_1^2 N \rho_L}{\mu_a} \right)^{1.5} \left(\frac{d_1 N^2}{g} \right)^{0.19} \left(\frac{\mu_a}{\rho \mathcal{D}} \right)_L^{0.5} \\ &\times \left(\frac{\mu_a u_g}{\sigma} \right)^{0.6} \left(\frac{N d_1}{u_g} \right)^{0.32} [1 + 2(\lambda N)^{0.5}]^{-0.67}, \end{aligned} \quad (6.18)$$

where $a'_L = a_L/(1 - \varepsilon_g)$, using the data for both Newtonian and non-Newtonian liquids. In Eq. (6.18), the dimensionless groups are the Sherwood number, the impeller Reynolds number, the Froude number, the Schmidt number, the gas flow number, the Aeration number, and the Deborah number.

TABLE XXI

GAS-LIQUID MASS TRANSFER CORRELATIONS FOR CONVENTIONAL MECHANICALLY AGITATED BIOREACTORS

Parameter	Correlations	References
Interfacial area	(a) "Coalescing" air-water dispersions	Moo-Young (1986)
	$a_L = 0.55 \left(\frac{P}{V} \right)^{0.4} u_g^{0.5}$	
	$d_b = 0.27 \left(\frac{P}{V} \right)^{-0.17} u_g^{0.27} + 9 \times 10^{-4} \text{ (mm)}$	
	(b) "Noncoalescing" air-electrolyte solution dispersion	
Volumetric gas-liquid mass-transfer coefficient	$a_L = 0.15 \left(\frac{P}{V} \right)^{0.7} u_g^{0.3}$	Smith <i>et al.</i> (1977)
	$d_b = 0.89 \left(\frac{P}{V} \right)^{-0.17} u_g^{0.17}$	
	Here P/V is in W/m^3 ; u_g is m/s .	
	(a) "Coalescing" air-water dispersion	
	$k_L a_L = 0.01 \left(\frac{P}{V} \right)^{0.475} u_g^{0.4}$	
	(b) "Noncoalescing" air-electrolyte solution dispersion	
	$k_L a_L = 0.02 \left(\frac{P}{V} \right)^{0.475} u_g^{0.4}$	
	VISCOUS SYSTEMS	
General	$\text{Sh} = \frac{k_L a_L d_1^2}{D} = A \left(\frac{\mu_a}{\rho D} \right)^a \left(\frac{\mu_a \mu_s}{\sigma} \right)^b \left(\frac{d_1^2 N \rho}{\mu_a} \right)^c \left(\frac{\mu_d}{\mu_a} \right)^d$	Sideman <i>et al.</i> (1966)
Case a ^a	$k_L a_L = C_1 (d_T/H_L) N d_1^{0.5} + C_2$	Loucaides and McManamey (1973)
	$k_L a_L \propto (P/V)^{0.9-1.2} u_g^{0.3}$, low (P/V)	
	$k_L a_L \propto (P/V)^{0.55} u_g^{0.3}$, high (P/V)	

^a Two types of viscous fermentations exist: (a) Mycelial fermentations; viscosity is due to microbial network structure dispersed in a continuous phase. (b) Polysaccharide fermentation; viscosity is due to polymer in an aqueous phase-homogeneous viscous liquid.

Henzler (1980) presented the relation

$$\frac{k_L a'_L V_L}{Q_g} Sc^{0.3} = 0.045 \left[\frac{P_g}{Q_g \rho_L (g\nu)^{0.667}} \right]^{0.5} \quad (6.19)$$

using the data for water, glucose, and glycerine. For aqueous CMC solutions, he presented

$$\frac{k_L a'_L V_L}{Q_g} Sc^{0.3} = 0.082 \left[\frac{P_g}{Q_g \rho_L (g\nu)^{0.667}} \right]^{0.6} \quad (6.20)$$

Zlokarnik (1978) examined the effect of coalescence on the volumetric mass-transfer coefficient in agitated vessels.

Euzen *et al.* (1978) measured interfacial area by the oxidation of sodium sulfite in three 5 L, 200 L, 1,000 L mechanically agitated fermenters. In all fermenters, the flat-blade turbine stirrer was introduced from the bottom. Various other geometrical parameters were $1.2 < H/d_T < 2$, $1/3.1 < \bar{\delta}/d_T < 1/2.3$, and $1.1 < L/d_i < 1.5$, where $\bar{\delta}$ is the baffle diameter and L the height between turbines. The results indicated that the cylindrical baffles provided a negative effect on oxygen transfer. For a given energy source and given strain,

$$a_L = K(P/V_L)^\alpha, \quad (6.21)$$

where $0.6 < \alpha < 0.7$, $100 < K < 200$.

For $\alpha = 0.65$, $K = 200$,

$$k_L a_L = 360(P/V_L)^{0.65} \quad (\text{h}^{-1}). \quad (6.22)$$

For mold pellets and other suspended particles with densities close to that of the continuous phase, the agitation in a stirred mixing vessel creates the dominant force for relative fluid motion between the two phases. The intrinsic gas-liquid mass-transfer coefficient under these conditions is given by Calderbank (1967) as

$$k_L = 0.13 \frac{[(P/V)\mu_c/\rho_c^2]^{1/4}}{Sc^{2/3}}. \quad (6.23)$$

Surfactants are frequently present in fermenters. The mass-transfer coefficient may decrease significantly because of surfactant.

Mass transfer into viscous fermentation media was examined by Loucaides and McManamey (1973). The rates of oxygen mass transfer into simulated fermentation medium, made up of 16 kg of paper pulp per cubic meter of aqueous sodium sulfite solution with a cupric ion catalyst, were determined in vessels of 0.187, 0.291, and 0.451 m diameter using flat-bladed turbine impellers. As was found for gas-liquid systems (Mehta and Sharma, 1971;

Westerterp *et al.*, 1963), there is a minimum impeller speed for efficient operation; above this, $k_L a_L$ can be expressed as the sum of two terms, one related to impeller speed and diameter and vessel dimensions, and the other depending on the power per unit volume and the gas rate. The correlations for $k_L a_L$ presented in this study are outlined in Table XXI.

Mechanical agitation and gas-liquid mass transfer are very important in viscous fermentation media. Most recently, Lim and Yoo (1989) and Lee and Wang (1989) have examined mixing effects in the fermentation of Xanthan gum. Aunins *et al.* (1989) evaluated the effects of paddle geometry on power input and mass transfer in small-scale animal cell culture, 500 mL Corning spinner vessels. The results indicate that power dissipation dependency differs from literature correlations and may compromise scale-up at constant power input from these vessels.

c. Liquid-Solid Mass Transfer Coefficient

The best correlation for bioreactors is proposed by Calderbank and Moo-Young (1961) as

$$\text{Sh} = 0.13(\text{Re}_\ell)^{3/4}(\text{Sc})^{1/3} \quad \text{for rigid spheres (small particles),} \quad (6.24)$$

where

$$\text{Sh} = \frac{k_s d_p}{\mathcal{D}}, \text{Sc} = \frac{\mu}{\rho \mathcal{D}}, \text{Re}_\ell = \frac{d_p^{4/3} \rho_L^{2/3} (P/V)^{1/3}}{\mu_\ell}.$$

Thus, $\text{Sh} \propto (P/V)^{1/4}$. For particles with a mobile interface (large particles), alternate relations need to be used. These are

$$\text{Sh} = 0.65 \left[\frac{\mu_\ell}{\mu_\ell + \mu_d} \right]^{1/2} \text{Pe}^{1/2} \quad \text{for } \text{Re} < 1, \quad (6.25)$$

and

$$\text{Sh} = 1.13 \text{Pe}^{1/2} \quad \text{for large Re.} \quad (6.26)$$

For liquids with $\mu > 70$ cP, a more appropriate correlation is

$$\text{Sh} = 1.31 \text{Pe}^{1/2}, \quad (6.27)$$

where

$$\text{Pe} = \text{Re} \cdot \text{Sc}.$$

For gravitationally induced flow (large particles), the relation $\text{Sh} = 0.42 \text{Sc}^{1/2} \text{Gr}^{1/3}$ holds.

B. MAGNETICALLY STIRRED PLANT-CELL SUSPENSION CULTURE REACTORS

Suspension cultures are the most widely used method of plant-cell cultivation (Kargi and Rosenberg, 1987). The major advantage of the suspension culture reactor is that it provides a rather uniform cultivation environment for plant cells. Although the environment of growth changes in a dynamic form during batch cultivation, suspension of cells is uniform with proper aeration and agitation. One of the major disadvantages of suspension cultures is the relatively low level of control over cell aggregate size. A certain degree of cell aggregation (cell-cell contact) and cell differentiation seems to be essential for secondary metabolite formation (Lindsey and Yeoman, 1983). However, when large aggregates are formed, microenvironmental conditions inside aggregates are difficult to control, and the nutrient concentration at the center core of aggregates may not be high enough to support metabolic activities. Moreover, cell aggregate size may change during the course of batch growth depending on the shear field and other environmental parameters (e.g., Ca^{2+} and C-compound concentrations).

Mechanically agitated reactors have been used for cultivation of plant cells (Kato *et al.*, 1972; Tanaka, 1981). A jar fermenter with a six flat-blade turbine and a modified paddle has been used by Tanaka (1981) and a similar jar fermenter with two disk turbine impellers has been used by Kato *et al.* (1972) at about 50 rpm with no significant shear damage to plant cells. Paddle-type impellers were found to be more appropriate (less shear damage) than flat-blade turbine type impellers (Kato *et al.*, 1972). The only production-scale reactor used for shikonin production in Japan is also an agitated vessel.

Two major types of magnetically agitated and aerated laboratory reactor types are the V-fermenter (Wilson, 1980; Kurz and Constabel, 1979) and the phytostat developed by Miller *et al.* (Kurz and Constabel, 1979). The V-fermenter consists of a conical glass reactor that was developed by Kurz and Constabel (1979) and later used by Wilson (1980) and Sahai and Shuler (1982) for continuous cultivation of plant cells. The fermentation medium is agitated by a Teflon-coated magnetic bar stirrer. Forced air is supplied to the fermenter for aeration and further agitation. Temperature control is achieved by circulating constant-temperature water through an external jacket surrounding the fermenter. Aeration and agitation in the fermenter is gentle enough not to lyse the cells. The V-fermenter can be operated in batch and continuous modes. Imperfect mixing in the V-fermenter at low aeration rates has been reported (Sahai and Shuler, 1982).

The phytostat fermenter developed by Miller, *et al.* is a spherical glass reactor that is aerated by forced air and agitated using a magnetic bar. Air is

passed through an aqueous CuSO_4 solution before filtration for sterilization purposes. The fermenter is equipped with needle valves for the automatic collection of samples. A similar reactor was used by Wilson for continuous cultivation purposes. This type of reactor geometry is likely to have a more uniform pattern than the V-fermenter.

Although the design is not normally used, Lombrana *et al.* (1989) demonstrated the use of a magnetically stirred cylindrical bubble column for the experimental study of agricultural reclamation of residuals from waste-water treatment plants. The magnetic stirrer provided gentle additional mixing in the bubble column, which is needed for the uniform suspension of residual material.

C. NOVEL BIOREACTOR DESIGNS

Although the stirred tank reactor described earlier has been employed extensively in the past, it is considered inadequate for more demanding applications. The main factors against it are technical, but there are also economic and biological reasons for developing novel bioreactor schemes. Schügerl (1982) summarizes the main reasons for the introduction of new bioreactors as (1) the difficulty of stirred-tank scale-up to very large size because of design difficulties and heat removal problems, often accompanied by high power requirements and high energy and utility costs; (2) the reduction of specific energy and capital costs; (3) the avoidance of cell damage; and (4) the increase of yields and reduction of substrate losses. The basic requirements of a desirable bioreactor are summarized in Table XXII.

TABLE XXII
REQUIREMENTS OF BIOREACTORS

-
- Aseptic conditions
 - Low foaming
 - Simplicity of design
 - Uniform reaction conditions for all microorganisms
 - Large and uniform concentration of microorganisms
 - Continuous operation with narrow residence time distribution for all components involved in the process
 - Uniform concentration of reactants
 - Low and uniform distribution of energy for the process
 - Simple and efficient method for oxygen supply
 - Low shear rates to microorganisms
 - Efficient heat removal
 - Low substrate loss
-

The energy situation of a bioreactor can only be improved by reducing the rotational and increasing the axial fluid motion in the mixing vessels. To accomplish this demand, the development of new types of mixing systems is necessary. Besides mixing, foaming is also another problem in bioreactors. A novel design must also reduce foaming for smoother and more efficient operation. Most of the available knowledge of novel bioreactors comes from laboratory and pilot plant units, and some of this is summarized in a comprehensive review by Schügerl (1982). Various novel designs for traditional submerged-culture mechanically agitated reactors outlined by Schügerl (1982) are illustrated in Fig. 28. The novel designs include various types of

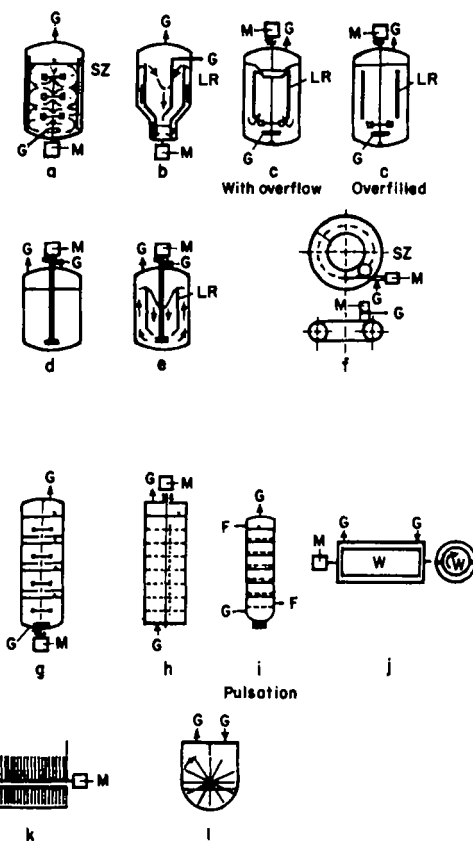


FIG. 28. Biochemical reactors in which energy input is by mechanically moved internals. M, motor; G, gas (air); SZ, baffles (in (f), foam breaker); LR, conduit tube; 1, self-gas agitator; W, roller. (From Schügerl, 1982; also, reprinted from Erickson and Stephanopoulos, 1987, by courtesy of Marcel Dekker, Inc.).

TABLE XXIII
 $k_L a_L$, P/V , AND MASS TRANSFER ECONOMY (MEC) FOR
 VARIOUS NOVEL REACTORS

Reactor	$k_L a_L$ (h^{-1})	P/V (kW/m^3)	MEC
Multistage agitator	200	10	20
Agitator, draft tube	220	11	20
Agitator, self-aspirating	150	4	38
Blade wheel or paddle reactor	1,000	9	111

agitation without (28a) and with (28b) a loop; other types are mechanically stirred loop reactors (28c); self-aspirated aerated reactors without (28d) and with (28e) loops; mechanically stirred, self-aspirated, aerated, horizontal loop reactors (28f); cascade reactors with rotating mixing elements (28g), with axially moving mixing elements (28h), or with pulsating liquid (28i); and finally surface reactors such as thin-layer reactors (28j), disk reactors (28k), and paddle wheel reactors (28l). The reported mass transfer efficiencies, presumably at maximum levels, in terms of $k_L a_L$ values and power consumption and values of MEC (mass-transfer economy capability) as the ratio of $k_L a_L$ to P/V for some of these novel reactors are given in Table XXIII. Brief descriptions of some of these and more recent novel reactors are given below. Gas-inducing agitated reactors are described in detail in Section II.

1. Centrifugal Film Fermenter

Numerous chemical and mechanical devices have been proposed to solve the foaming problem in industrial biosynthesis processes. Most of the existing methods are founded upon chemical or mechanical defoaming of a developed foam. Chemical treatment currently used for defoaming involves silicones and other water-immiscible additives that substantially decrease the rate of oxygen transfer, thus interfering with an effective process of aerobic biosynthesis. The mechanical defoamers that are sometimes used in fermentation processes typically require an additional power source and a particular fermenter design to accommodate the defoaming equipment. Mechanical defoamers are not uniformly reliable or feasible, especially in large fermentation vessels. In addition, the conventional design has a high cost of mixing and aeration, high shear stress on cells, and frequent incidents of contamination in aerated systems.

A laboratory device that eliminates or greatly diminishes some of these disadvantages has been described by Long *et al.* (1988). In this device, an improved mass transfer is achieved by generating a thin film of liquid that

flows upward along a rotating truncated conical surface, exposing a large area of flowing liquid to a substantially static gaseous phase. This equipment is useful in promoting efficient molecular transfer of gases with a low solubility in the liquid, for example, the transport of oxygen into an aqueous phase, typical of conventional aerobic fermentation processes. The principle of this system can alternately be employed in the reverse direction of transfer, as is with gases leaving a liquid phase, such as the one that occurs in stripping, defoaming, and deodorization. An important feature of this equipment is the fact that the thin-film process prevents the formation of foam. Long *et al.* (1988) showed that a value of $k_L a_L \sim 10 \text{ h}^{-1}$ for O_2 in water can be observed for a power input equivalent to less than 0.2 kW per m^3 for a single rotating cone. Furthermore, a vessel with a smaller height-to-diameter ratio showed higher $k_L a_L$ values. For the rotational speed below about 160 min^{-1} , a continuous film in the cone was not formed. As the depth of immersion decreases, the angular speed required for continuous film formation increases.

A more elaborate design of centrifugal film fermenter is shown in Fig. 29 (Feres and Roubicek, 1988). This comprises a typical sterilizable fermentation vessel, on the top of which drive means are flange-mounted and connected to a central shaft that is further attached to a central distributor. The central distributor is open at its lower end and attached to rotating multiple conical surfaces. Alternatively, the cones are spaced a short distance away and are attached to each other and to the drive means. Below the central distributor, a cylindrical heat exchanger is provided, having an axially mounted propeller, operated by drive means located at its lower end. With the central distributor rotating and having its lower end submerged in the liquid phase, liquid is drawn up along the inner surface of the central distributor, ejected through a set of openings, and distributed onto the rotating conical surfaces. Simultaneously, a flow of gas over the thin liquid film on the conical surfaces is created by the same centrifugal force that is moving the liquid along the conical surface. When the cones are attached to the central distributor, this gas flow is through nozzles in the central distributor that are arranged to prevent the ingress of liquid. These nozzles create a forced flow of the gaseous phase across the thin film of flowing liquid. When the cones are spaced apart from the central distributor, the gas flow is between the cones and the central distributor.

The flow of the liquid phase to the inlet of the central distributor is enabled by raising the liquid level within the heat exchanger cylindrical guide tube with the help of an axial propeller pump. The flow to the central distributor can be controlled by varying the level of the liquid in the heat exchanger tube, or by adjusting the vertical position of the central distributor. When desired, the gaseous phase is supplied at the bottom of the fermenter through a gas sparging system, contributing to the versatility of the fermenter equipment. This equipment has been successfully used for cell cultivation.

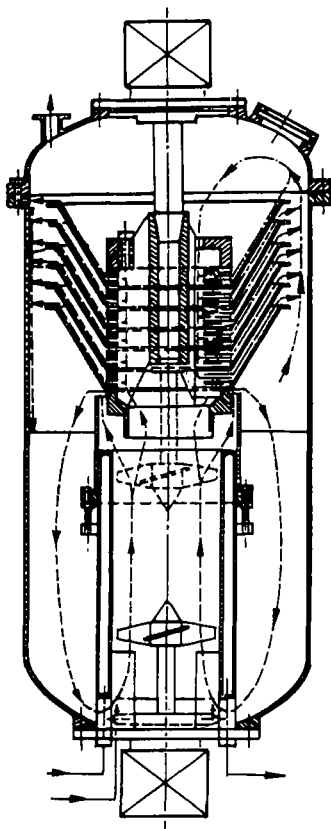


FIG. 29. Schematic of multistage centrifugal film fermenter. (Feres and Roubicek, 1988.)

2. *Three-Stage Rotating Disk Reactor*

The three-stage rotating disk reactor is illustrated in Fig. 30. Each stage consists of one cylindrical and two conical elements and is connected to the next stage by another cylindrical element with a relatively small diameter. Fluid motion and gas dispersion are achieved by a rotating flat plate that contains holes at its outer edge to generate gas bubbles. The reactor can be used for cocurrent and countercurrent flow of gas and liquid or slurry.

In each stage, the bottom part provides the gas supply to the rotating disk, the central cylindrical element provides the gas dispersion for mass transfer and biochemical reaction, and the upper part separates gas and liquid (or slurry). The flat rotating plate imparts very little mixing energy to the fluid, i.e., only 4% of that for turbine stirrers. As a result, the microorganisms do not

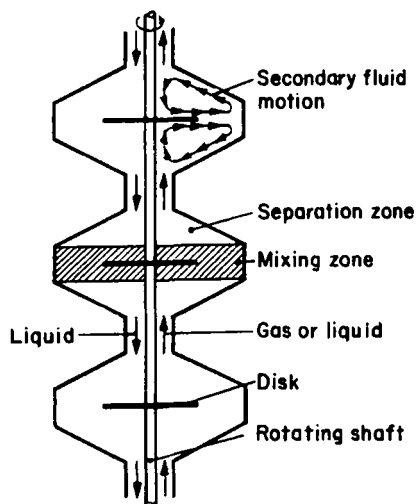


FIG. 30. Schematic diagram of three-stage rotating-disk reactor. (After Brauer, 1982, reprinted with permission from the Institute of Chemical Engineers.)

suffer any damage from this element. The important design characteristics of this new bioreactor are summarized in Table XXIV.

The efficiency of this type of reactor was examined by Maruoka (1982) and Stichlmayr (1979) using the CO_2 desorption from water in air as a case study. The mass transfer efficiency for each stage was defined as

$$n_f = \frac{x_{i-1} - x_i}{x_{i-1} - x_{ip}}, \quad (6.28)$$

where (x_{i-1}) is the mole fraction of the diffusing component in the liquid in the stage being considered; x_i is the mole fraction of the diffusing component in the liquid in the stage above the one being considered; and x_{ip} is the mole fraction on the liquid side of the interface.

For a fixed fluid Reynolds number (based on cylindrical column diameter d_T of the stage) of 1982, and $d_i/d_T = 0.62$, the efficiency n_f decreases with a decrease in the stirrer Reynolds number (Nd_i^2/ν) and the Aeration number, u_g/Nd_i^3 , and with an increase in the stage number (i.e., the highest in stage 1 and the lowest in stage 3). A large number of stages would produce poor efficiency.

3. Stagnation Jet Reactor

In this reactor, two jets are generated and directed towards each other so that they collide in a stagnation plane. This plane is fluid-mechanically unstable and produces stochastic fluctuations and intense mixing in liquid.

TABLE XXIV

IMPORTANT DESIGN CHARACTERISTICS OF THREE-STAGE ROTATING-DISK REACTOR
(AFTER BRAUER, 1982)

- Simplicity of design
- Continuous throughflow of all phases in either cocurrent or countercurrent manner
- Wide range of flow rates for gas and liquid
- Large gas holdup in each stage, up to five times that in conventional gas-liquid reactors
- Large interfacial area due to large gas holdup and to smaller-diameter bubbles, generated by the rotating disk
- Renewal of interfacial area when gas bubbles rise to the next stage, and also when they follow the secondary liquid motion in the same stage
- Very efficient mass-transfer process due to the large interfacial area and its periodic renewal
- Very low energy dissipation, since the flat plate has a lower resistance to flow than any other dispersing element; only 4% of that for turbine stirrers
- Very low mechanical stress in the rotating liquid mass; normal stress, which is dangerous to microorganisms, is practically absent

Figure 31 presents a schematic of the stagnation jet reactor. The reactor is a slim cylindrical vessel with diameter D and length $2h$. In each half of the reactor, there is a propeller fitted inside a draft tube. The only function of the impeller is the generation of a jet with a large axial momentum. The rotational motion of the jet should be as small as possible.

When the two jets meet at a free stagnation plane, the strength of the generated stochastic fluctuations depend directly on the axial momentum of

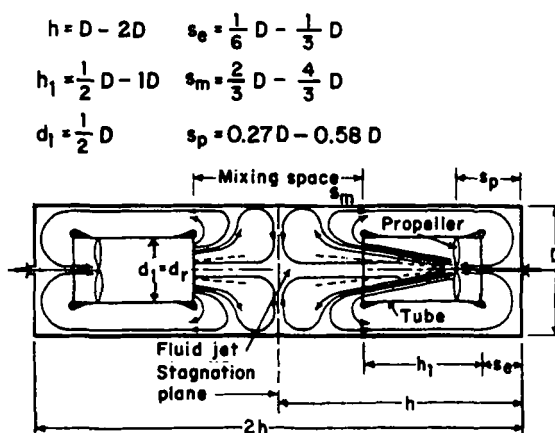


FIG. 31. A diagram of fluid flow in a stagnation jet reactor. (After Brauer, 1982, reprinted with permission from the Institute of Chemical Engineers.)

the jets. The rotational motion of the liquid within the jets enhances the stochastic fluctuations, particularly because of the countercurrent rotational liquid motion in the jets. After leaving the mixing and reaction space between the two draft tubes, the liquid (or slurry) flows through the outer annular space of the vessel and is then sucked into the draft tube by the propeller.

The power P or the rate of transfer of energy from the propeller to the liquid is expressed in terms of the dimensionless Newton or Power number as

$$Ne = \frac{P}{\rho N^3 d_i^5}. \quad (6.29)$$

For a given Reynolds number, the Newton number for a reactor with $h/D = 2$ is somewhat higher than the one for $h/D = 1$. The data for both h/D values compare reasonably well with those reported by Zlokarnik (1967) for a conventional mixing vessel with a propeller stirrer. For high Reynolds numbers $Ne \rightarrow 0.3$, which is considerably smaller than $Ne \rightarrow 5$ to 6 under similar conditions for conventional reactors with turbine stirrers.

The reactor is particularly useful for fast reactions where good micromixing is essential. The efficiency for micromixing can be characterized by the mixing time t or the mixing number $\mu t/D^2 \rho$. Brauer (1982) showed that the stagnation jet reactor gives considerably lower values of the power function ($= Ne Re^3 D/d_i$) for given mixing numbers than those obtained in conventional mixing vessels containing propeller or cross-blade stirrers with and without baffles.

4. *Reciprocating Reactor*

The reciprocating bioreactor is a slim cylindrical vessel with a height/diameter ratio of the order of 4 to 5 (Brauer and Sucker, 1979). The reactor contains a package of sieve plates attached to five rods. In the reactor of Brauer and Sucker (1979), the plate spacing is 42 mm, the diameter of the holes in the plates is 12 mm, and the hole spacing is 29 mm. This element undergoes a reciprocating motion up and down the reactor with an amplitude of 100 mm.

The reciprocating motion of the sieve plate generates vortices in the biosuspension. Each vortex region represents the elementary volume of the bioreactor. When the gas dispersion element moves upwards, the biosuspension is forced to pass through the holes of the sieve plates: From each hole, a jet of biosuspension flows downward into the space between two sieve plates. The jet reverses direction as the element reverses direction. Very effective dispersive action is due to the periodic generation of bubbles, which renews the larger interfacial area on each reversal of direction. The important design characteristics of this reactor are summarized in Table XXV.

TABLE XXV
 IMPORTANT DESIGN CHARACTERISTICS OF A RECIPROCATING REACTOR
 (AFTER BRAUER, 1982)

-
- Generation of a large interfacial area
 - Periodic renewal of the interface
 - Formation of small agglomerates of microorganisms
 - Uniform distribution of air bubbles and microorganisms in the bioreactor
 - Small resistance to oxygen transfer in the biosuspension
 - No dead volume and sedimentation in the bioreactor
-

The design characteristics outlined in Table XXV allow this reactor to treat various kinds of waste water biologically in extremely short periods. For example, a waste water of initial $BOD_t = 850 \text{ mg/l}$ had its value reduced to 30 mg/l during a mean residence time of 17 min. Compared with a conventional concrete basin, the volume of the reciprocating bioreactor required for purification of a given flow rate can be reduced to approximately $1/30$ or $1/60$.

A comparison between the performance of conventional biological wastewater treatment basins and the reciprocating bioreactor is given in Table XXVI. As shown, the conversion rate in the reciprocating reactor can be as high as more than four times that obtained in a conventional bioreactor.

5. Plug Flow Bioreaction Processing

Plug flow is normally achieved by using a reactor with a large length-to-diameter ratio. Two types of tubular systems behavior need to be distin-

TABLE XXVI
 COMPARISON OF THE PERFORMANCE OF A
 RECIPROCATING REACTOR WITH THAT OF A
 CONVENTIONAL REACTOR

	Reciprocating Reactor Conventional Reactor
Capacity per unit volume	6.6 - 10
Capacity per unit mass	10 - 65
Mass of dry substance	2.14
Conversion rate	7.4 - 74

guished. Some systems reported show plug flow behavior of the liquid phase with respect to gas-liquid mass transfer, but over the time scale of a biological reaction, they are well mixed. Others are plug flow with respect to the biological reaction. The time scale for mass transfer is generally in seconds, whereas, except for immobilized-enzyme systems, the time scale for reaction is generally of the order of hours.

Based on the above-described principles, in several novel plug flow bioreactors, the liquid phase is mechanically agitated but the reactors are designed so that overall, the plug flow of various phases prevails. Three such designs are illustrated in Fig. 32. In staged vessels, staging and the perforated plates in between two stages reduces the overall backmixing. Falch and Gaden (1969) measured the gas-liquid mass-transfer coefficient in such a vessel and

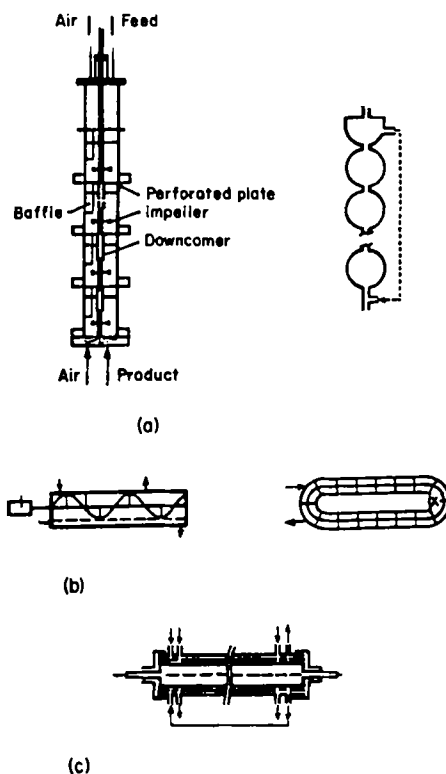


FIG. 32. Examples of plug-flow bioreactor processing. (a) Staged vessels; (b) tubes with moving compartments; (c) annulus around rotating cylinder. (After Moo-Young, 1986.)

found that $k_L a_L$ was dependent on the level of power supplied through mechanical agitation. The superficial gas velocity had little effect on $k_L a_L$.

Moser (1973) examined small annular-flow tubular devices in which agitation was provided by a second cylinder placed within the tube, the liquid volume being confined to the annular region. Agitation was provided by rotation of the liquid flow. Liquid backmixing was a function of the rate of rotation of the inner cylinder. Moser (1973) reported oxygen transfer rates in the range of 50–250 nmol/L h, and these rates increased linearly with increasing rotational speed of the inner cylinder.

Moo-Young *et al.* (1979) developed two novel tubular bioreactors. One design consists of a horizontal tube containing an internal mechanical wall-scraper that partially segregates the medium in the tube into moving compartments. Aeration is provided in a cross-flow manner by orifices at the bottom of the tube. This design keeps the wall growth to a minimum. The second novel reactor was a pneumatically scraped plug flow device consisting of a vertical array of vessels interconnected by single orifices. The plug-flow behavior of both reactors, with respect to biological reaction, was tested for two fermentation processes: a lipase-producing yeast growth and a cellulase-producing fungal growth. Both fermentations are subject to catabolite repression, and hence, the reactors performed better than more conventional reactors.

6. Novel Reactors for Waste Treatment

a. Surface Aerators

Surface aeration is usually employed for slow reactions or for batch processes. It can be used in semicontinuous systems when it is desirable to recirculate the gas from the headspace. This is frequently the case in hydrogenation and is referred to as "dead-end hydrogenation." In this system, gas is fed continuously to the reactor at the rate at which hydrogen is being consumed; no compression costs to overcome the static head of liquid or external recirculation is needed. Feeding gas from the headspace may be preferred when there is a possibility of plugging sparger holes with reaction products. Surface aerators are also extensively used for waste-water treatment. There are two types of surface aerators: the brush aerator, and the most commonly used turbine aerator.

In surface aeration, bubbles are generated at the surface because of the turbulence in the liquid phase. These bubbles are entrained into the bulk liquid by the liquid flow generated by the impeller. For a six-bladed turbine, Van Dierendonck *et al.* (1968) proposed the following correlation for the minimum impeller speed needed for surface aeration in the absence of gas

sparging ($u_g = 0$):

$$\frac{N_s d_i}{\left(\frac{\sigma_g}{\rho_L}\right)^{1/4}} = 1.55 \frac{d_T}{d_i} \left(\frac{H - H_i}{d_T}\right)^{1/2}, \quad (6.30)$$

where H is the liquid height and H_i is the height of the stirrer from the bottom of the vessel. For hydrogenation of oils, Wisniak *et al.* (1971) found that the optimal value of C for a Rushton impeller is about $\frac{3}{4}$. The rate of gas incorporation is greatly improved when two impellers are used: an axial one just at the surface of the liquid, and a submerged radial one (Oldshue, 1980). Several gas-inducing impellers have also been proposed (Zlokarnik, 1966; Zlokarnik and Judat, 1967; Martin, 1972; Koen and Pingaud, 1977).

Surface aeration in the presence of gas sparging was studied by Calderbank (1958) for a six-bladed disk turbine in 0.3, 0.375, and 0.5 m i.d. mechanically agitated contactors. He suggested the correlation

$$\left(\frac{N_s d_i^2 \rho}{\mu}\right)^{0.7} \left(\frac{N_s d_i}{N_G}\right)^{0.3} = 15,000. \quad (6.31)$$

The critical stirrer speed can also be predicted on the basis of the liquid flow generated by the impeller. For a six-bladed disk turbine, the average liquid circulation velocity in the bulk can be expressed as

$$V_c = 0.53 \left(\frac{d_i}{w_i}\right) N d_i \left(\frac{d_i}{d_T}\right)^{7/6} \quad (6.32)$$

The terminal bubble rise velocity can be expressed as

$$u_{b\infty} = 0.71 \sqrt{g d_B}, \quad (6.33)$$

where, from Bhavaraju *et al.* (1978),

$$d_B = 1.21 \frac{\sigma_\ell^{0.6}}{(P/V)^{0.4} (\rho_\ell)^{0.2}} \left(\frac{\mu_\ell}{\mu_g}\right)^{0.1}. \quad (6.34)$$

The surface aeration starts when $V_c = u_{b\infty}$. Thus,

$$\frac{N_s d_i^{1.98}}{d_T^{1.1}} = \frac{1.65}{N_p^{0.125}} \left(\frac{\sigma g}{\rho_L}\right)^{0.19} \left(\frac{\mu_\ell}{\mu_G}\right)^{0.031} \left(\frac{w_i}{d_i}\right). \quad (6.35)$$

For an air - water system, $N_p = 5$, and the above equation becomes

$$\frac{N_s d_i^{1.98}}{d_T^{1.1}} = 1.34 \left(\frac{\sigma g}{\rho_L}\right)^{0.19}. \quad (6.36)$$

In the presence of sparging, the average liquid circulation velocity is reduced by 30% (Joshi *et al.*, 1982). This reduction should be factored in the calculation of N_s .

The extent of gas entrainment depends on the turbulence at the liquid surface and the downward volumetric flow rate. Thus, the impeller design, diameter, and location are very important. Matsumura *et al.* (1977) proposed the following correlation for a 0.218 in. diameter vessel using a disk turbine:

$$\frac{\bar{\eta}}{(1 - \bar{\eta})^2} = 1.913 \times 10^{-10} \left(\frac{u_g}{Nd_1} \right)^{-2.2} \left(\frac{Nd_1^2}{\mu_L} \right)^{0.1} \left(\frac{N^2 d_1^3 \rho_L}{\sigma_L} \right)^{1.38} \\ \times \left(\frac{N^2 d_1}{g} \right)^{0.07} \left(\frac{d_1}{d_T} \right)^{6.4}, \quad \text{where } \bar{\eta} = \frac{Q_E}{Q_E + Q_g}. \quad (6.37)$$

Q_E and Q_g are the volumetric flow rates of entrained and sparged gases. Matsumura *et al.* (1978) also proposed the following correlation for power consumption in the presence of gas entrainment:

$$\frac{P_g}{P_L} = 0.26 \left(\frac{u_g}{Nd_1} \right)^{-0.2} \left(\frac{N^2 d_1}{g} \right)^{0.055} \quad (6.38)$$

The mass-transfer rate in surface-aerated vessels was investigated by Mehta (1970) in 0.125, 0.20, 0.40, and 0.70 m i.d. vessels using a six-bladed disk turbine as the surface aerator. The values of a_L and $k_L a_L$ were found to be in the range of 125 to 325 m^2/m^3 and 0.08 to 0.2 s^{-1} , respectively, when P_g/V varied in the range of 0.017 to 41.11 kW/m^3 . Teramoto *et al.* (1974) found $k_L a_L$ to be independent of pressure in an aqueous system.

The surface aerator has been used for decades in biological waste-water treatment with $H < 4$ m. For various sizes of turbine stirrers whose disks were positioned exactly in the surface of the liquid, the mass-transfer coefficient can also be related as

$$k_L = G/A \Delta C, \quad (6.39)$$

and

$$Y = \left[\left(\frac{k_L}{A d_1^3} \right) (v/g^2)^{1/3} \right] = \text{sorption number} \\ = 1.41 \times 10^{-4} \text{Fr}^{1.2} \text{Ga}^{0.115}, \quad (6.40)$$

where

$$\text{Fr} = N^2 d_1 / g,$$

$$\text{Ga} = d_1^3 g / \nu^2$$

for $0.02 < Fr < 0.34$; $1.5 \leq Ga \leq 200$; $H_i/d_1 = 0.2$. H_i is the immersed height of the stirrer blades.

The power characteristics of a turbine-type surface aerator are given by

$$Ne = P/(\rho N^3 d_1^5) = f(Fr), \quad (6.41)$$

which leads to

$$(Y_1 Ne^{-1} Fr^{-1.5}) Ga^{-0.115} = f(Fr). \quad (6.42)$$

The quantity in parentheses represents the dimensionless efficiency number E^* (which is a measure of mass-transfer rate per unit power input). The experiments indicate that

$$E^* \propto Fr^{-0.35}. \quad (6.43)$$

Thus, to get large E^* , Fr should be as low as possible. If $Fr = \text{constant}$, Eq. (6.42) gives

$$E^*(Ga)^{-0.155} = \text{constant}. \quad (6.44)$$

b. UNOX Oxygenation Reactor

In the aerobic biological treatment of waste water, often pure oxygen is used instead of air. In the presence of pure oxygen, the level of dissolved oxygen (DO) in the waste water can be maintained at a higher level than with air. All the advantages of using pure oxygen can be attributed to the high levels of DO. The UNOX process (marketed by Union Carbide Corporation) uses pure oxygen. The UNOX biological reactor (Joshi *et al.*, 1985) is divided into stages by interior walls and is completely covered to provide a gas-tight enclosure. The tank is usually a rectangular concrete structure with common wall construction. The dimensions and the number of stages depend on the application.

The liquid and gas phases flow concurrently through the reactor. The liquid waste, oxygen gas at a slight pressure (0.2 to 1 kN/m²), and recycled sludge enter the first stage. The flow rate of oxygen is controlled on the basis of a constant-pressure operation of the first stage. The gas and liquid flow from stage to stage through the openings in each interstage wall above and below the liquid surface respectively. The vent from the last stage contains mainly generated CO₂, stripped N₂, and unused O₂. The treated effluent and the activated sludge flow from the last stage to a sedimentation unit from which the activated sludge is recycled and the clarified water is discharged.

The agitator in each stage is provided with two impellers. The impeller that is located at the liquid surface causes surface aeration. It creates turbulence at the liquid surface and generates liquid flow in the downward direction. Because of this impeller action, the oxygen from the gas space is dispersed

into the liquid in the form of small bubbles. The other impeller is located approximately at the center of the liquid. This impeller keeps the biomass in suspension and provides the energy necessary for the mixing of the bulk liquid, which keeps the DO level uniform throughout the reactor.

c. Horizontal Agitated Contactors

In the conventional mechanically agitated reactors, poor dispersion is likely to occur in large units, particularly near the bottom. This can be overcome by using a large L/d_T ratio with a horizontal arrangement and multiple impellers.

Horizontal contactors are essentially bubble columns with an aspect ratio less than one, and the gas is sparged at the bottom as turbulent jets. In order to get fairly uniform gas-liquid dispersion, multiple injection points are employed for the gas. The gas-liquid contact can be further improved using impellers (Fig. 33). The impellers are of a modified propeller type and are mounted on a horizontal shaft.

Because of the vertical downward motion of liquid created by the impellers, substantial amounts of surface aeration occur. In addition, an axial flow of liquid is also generated that gives better gas-liquid dispersion. These horizontal sparged and agitated units provide very low pressure drops as compared with those of vertical sparged and agitated contactors. Further, the extent of backmixing in horizontal contactors is much lower, by at least a factor of five, as compared with that in the vertical designs.

Joshi and Sharma (1976) also evaluated interfacial area and liquid-side mass-transfer coefficients using chemical methods in columns of 0.38, 0.57, and 1.0 m diameters. The optimum liquid submergence ratio (H/d_T) and impeller spacing ratio (L_i/d_T) were found to be in the range of 0.6–0.7 and 1.4–1.6, respectively. The following correlations were proposed:

$$a_L = 0.3 N d_T^{0.6}, \quad (6.45)$$

$$k_L a_L = 1 \times 10^{-5} N^{1.3} d_T^{0.6}, \quad (6.46)$$

where $d_i/d_T = 0.5$, $W/d_T = \frac{1}{6}$, $H/d_T = 0.65$, $L_i/d_i = 1.6$.

They also presented the correlations for $k_L a_L$ in terms of power input per unit volume as, for horizontal sparged contactors,

$$k_L a_L = 0.03(P/V)^{0.47}, \quad (6.47)$$

and for horizontal agitated contactors,

$$k_L a_L = 0.036(P/V)^{0.45}. \quad (6.48)$$

A comparison between a horizontal sparged contactor and a bubble column has been made, and it appears that for a variety of situations, horizontal sparged contactors may prove to be more attractive than bubble columns.

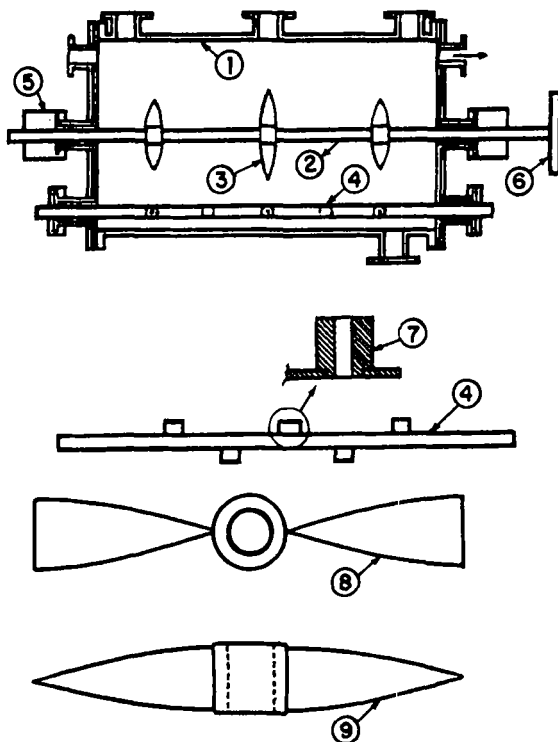


FIG. 33. Horizontal contactor and various types of impeller. 1, vessel; 2, impeller shaft; 3, impeller; 4, sparger assembly; 5, gland and stuffing box; 6, pulley; 7, nozzle; 8, plan; 9, elevation. (After Joshi *et al.*, 1985.)

Further, the liquid-phase backmixing is considerably lower in horizontal sparged contactors compared to that in bubble columns. Some comparison may be valid between horizontal and vertical agitated contactors.

d. Rotating Disk Reactors

These consist of a series of flat parallel disks (Joshi *et al.*, 1985; also, Fig. 28k) that are rotated (0.01–0.5 r/s) while partially immersed in the waste water being treated. Sometimes wire mesh disks are employed. Even engineering plastics can be used as a material of construction, and in such cases different designs that provide a larger surface area and promote turbulence can be used. Initially, a film of biological slime develops on these disks; the excess slime generated by the synthesis of waste material is wiped off gradually and is subsequently separated by settling. Rotating disks carry a film of waste water into the air where it absorbs the oxygen. Yamane and Yoshida (1972) and

Ravetkar and Kale (1981) have shown that Higbie's surface-renewal theory can be successfully employed for the calculation of the liquid-side mass-transfer coefficients for Newtonian and non-Newtonian liquids as

$$\frac{k_L \delta}{\mathcal{D}_A} = 0.063 \left(\frac{\delta (N d_T)}{\mathcal{D}_A} \right)^{0.5} \left(\frac{N^2 d_T^3 \rho}{\sigma} \right)^{0.125}, \quad (6.49)$$

where δ is the liquid film thickness formed over the rotating disk.

No information is available in the published literature pertaining to the gas-liquid interfacial area, a_L . It may be assumed that a_L equals the disk area exposed to the air. The thickness of the liquid film on a vertically rotating disk partially immersed in a Newtonian liquid has been evaluated by Vijayraghvan and Gupta (1982). They also showed that the measured liquid holdup on the disk compares well with the values predicted from the flat-plate withdrawal theory. The gas-phase pressure drop is very low. The liquid and the gas phases are partially backmixed. The extent of backmixing is reduced by providing baffles.

7. Rotating Bubble Column Biological Reactor

Mersmann (1988) has developed a rotating bubble column reactor for processing highly viscous fluids, such as Xanthan, often used in bioprocessing. Centrifugal forces created by the rotation create smaller bubbles that provide a large interfacial area and a better gas-liquid mass transfer rate. In the absence of rotation, bubble columns processing highly viscous fluids operate under the slug flow regime with large bubbles and low gas-liquid interfacial area. Such conditions make the reaction mass-transfer-controlled and the reactor inefficient. The rotating bubble column reactor is thus most useful for mass-transfer-controlled gas-liquid reactions. The reactor can be vertical or inclined.

D. SUMMARY

The design of conventional biological reactors is very similar to those of gas-liquid, slurry, and polymerization reactors outlined in other chapters. As a matter of fact, biological reactors are the most versatile of all reactors, since such a reactor can carry two or three phases, the liquid can be Newtonian or non-Newtonian, the solids can be heavy or light, and the reaction mixture can be simple or complex. A biological reactor, however, carries certain distinct features:

- (1) It always contains an *aqueous* phase;
- (2) oxygen mass transfer in the aqueous medium is the paramount design problem;

- (3) it is generally a low-temperature and low-pressure system;
- (4) careful control of reaction conditions is very important;
- (5) the purity of the reactor (aseptic conditions) is very important;
- (6) foaming is an important problem in many biological processes;
- (7) good mixing should be provided without high shear stress on living cells; and
- (8) the reactor dynamics are generally time-dependent.

These features have encouraged the development of many novel biological reactors.

For a conventional mechanically agitated biological reactor, the information provided for aqueous gas-liquid and gas-liquid-solid systems in Sections II, III, and VII is applicable here. For power consumption, the most noteworthy works are those by Hughmark (1980) (see Eqs. (6.15) and (6.16)) and Schügerl (1981). For gas-liquid mass transfer, the relationship $k_L a_L = (P/V, u_g)$ is applicable for biological systems. The relationships (6.19) and (6.20) are also valuable, and their use is recommended. The most generalized relation for $k_L a_L$ is provided by Eq. (6.18). The intrinsic gas-liquid mass transfer coefficient is best estimated by Eq. (6.23). For liquid-solid mass transfer, the use of the study by Calderbank and Moo-Young (1961) (Eqs. (6.24)–(6.26)) is recommended. For viscous fluids, Eq. (6.27) should be used.

Relationships for mixing time discussed in Sections II, III, V, and VII are applicable to biological systems; the appropriate relationship for *aqueous systems* and corresponding rheological properties should, however, be considered. Heat-transfer parameters can be similarly obtained from the literature described in Sections II, III, V, and VII.

Novel reactors are developed to take care of some of the distinct features outlined above. The centrifugal film fermenter reduces foaming and provides renewed gas-liquid interfaces. The reactor is somewhat complex and may not be economical on a large scale for all applications. The three-stage rotating-disk reactor provides flexible operation and offers large gas holdup and efficient mixing operation. The use of secondary flow to obtain a high degree of mixing with low shear energy is a very important idea for biological applications. The number of stages that can be practically used is limited because of the reduction in efficiency with increased stages. The stagnation jet reactor is useful for fast reactions where a high degree of mixing eliminates mass-transfer resistances at the reaction plane. The operation is, however, not very efficient, particularly at a high Reynolds number. The reciprocating reactor provides efficient mixing. It also generates a large and constantly renewed gas-liquid interface, prevents settling of microorganisms, and provides a good bubble-size distribution. It is a useful reactor for waste treatment; however, it would have limited usefulness for reactions requiring a

clean environment. The design of very large-scale systems may also have mechanical difficulties.

Plug-flow bioreactors provide an important concept of high mass transfer with a low degree of backmixing. This is achieved by using a reactor with a large length-to-diameter ratio. To some extent this is the same principle as the one used in staged reactors. The reactors described in Fig. 32 are more useful in laboratory or medium-size units than in commercial-scale operations. Power consumption in these units is not very efficient. Finally, the rotating bubble column biological reactor is an important new concept. The use of centrifugal force to break down bubbles and provide a large gas-liquid interfacial area in viscous system is an interesting concept. The reactor can be used at laboratory scale and in medium-size units. However, the power requirement is large, and this restricts its use for medium- to high-priced products. Mechanical limitations will also restrict the size of such a reactor.

In waste-water treatment, the energy-efficient transfer of oxygen in the aqueous phase is very critical. Since reactions are slow, a long contact time is required. Both of these can be achieved by a conventional surface aerator or novel UNOX surface aeration system. The minimum impeller speed needed for surface aeration in the absence of gas sparging can be obtained from Eq. (6.30). Similar calculations in the presence of gas sparging can be carried out using either Eq. (6.31) for a turbine stirrer or Eq. (6.36) for other stirrers. The gas entrainment and the power consumption in the presence of gas entrainment can be obtained using Eqs. (6.37) and (6.38), respectively.

The mass-transfer coefficient, k_L , or in the dimensionless form, the sorption number

$$Y = \frac{k_L}{A d_i^3} \left(\frac{v}{g^2} \right)^{1/3}$$

is a function of the Froude and Galileo numbers. The efficiency for the mass-transfer rate per unit power input is proportional to $Fr^{-0.35}$. Thus, greater efficiency is obtained at a smaller Froude number. If $Fr = \text{constant}$, greater efficiency is obtained at a higher Galileo number.

In conventional mechanically agitated reactors, poor dispersion is likely to occur in large units, particularly near the bottom. This can be overcome by using a large L/d_T ratio with a horizontal arrangement and multiple impellers. Both $k_L a_L$ and a_L in such a reactor can be expressed either in terms of stirrer speed and column diameter, or preferably in terms of power per unit volume. The use of Eq. (6.48) for the calculation of $k_L a_L$ is recommended. The optimum liquid submergence ratio (H/d_T) and impeller spacing ratio (L_i/d_T) are estimated to be in the range of 0.6–0.7 and 1.4–1.6, respectively (Joshi and Sharma, 1976). This type of reactor provides lower liquid-phase backmixing

than conventional mechanically agitated reactors. Power consumption and mechanical difficulties may limit the size of such vessels.

Finally, the rotating-disk reactor provides efficient gas-liquid mass transfer by constant renewal of the gas-liquid film on the rotating disk. The mass-transfer coefficient in such a reactor can be calculated using Eq. (6.49). The reactor provides a low pressure drop and partially backmixed gas and liquid phases. The extent of backmixing can be further reduced by the use of baffles. Once again, power consumption and mechanical difficulties may limit the size of such vessels.

E. FUTURE WORK

Future work should include:

- novel designs of mechanically agitated reactors, particularly at large scale, that carefully control aseptic conditions, temperature, and micro-mixing in the reactor;
- novel designs of mechanically agitated reactors that provide good micromixing at low shear rates on enzymes or other living cells; and
- development of novel designs, as well as evaluations of design parameters, for liquids with time-dependent rheological properties.

VII. Polymerization Reactors

A. GUIDELINES FOR REACTOR SELECTION

Selection of a polymerization reactor depends on production costs, simplicity, and energy efficiency, all of which depend on the viscosity and the non-Newtonian rheological properties of the reaction mixture (Oldshue *et al.*, 1982; Middleman, 1977). Flow properties significantly influence the nature of the reactor, agitator size, power, and design (Gerrens, 1982).

From an operational point of view, the choice of an appropriate polymerization reactor depends on six requirements: temperature control; mixing; product accumulation and reactor foul-up; follow-up separation processes; the desired form of the product; and safety. Heats of polymerization are typically high, so that maintaining the reactor at a desired temperature level is not always a simple task. Temperature can become spatially nonuniform and globally out of control (causing inconsistency of the reaction medium). Nonuniformity in temperature can lead to localized zones of poor mixing or even dead zones. In a polymerization reactor, temperature, mixing, viscosity,

and product molecular-weight distributions are all interdependent. Large heat transfer areas provided by coils and corrugated surfaces are not appropriate for polymerization reactors since they affect mixing and the product molecular-weight distribution. This can lead to localized accumulation of materials and fouling of the heat-transfer surfaces, and in general make the reactor very difficult to operate in a clean manner. For these reasons, polymerization reactions require smooth heat-transfer surfaces with the best possible agitation to sweep the fluid cleanly over the surface. Mechanical agitation is, therefore, essential for many polymerization reactions.

High-pressure ethylene polymerization is commercially carried out in both tubular and mechanically agitated reactors. While tubular reactors provide a high ratio of surface area to volume for good heat transfer, they also provide poor mixing, which may lead to segregation and a nonhomogeneous mixture, both of which are undesirable. Mechanically agitated reactors have a comparatively low surface-to-volume ratio for heat transfer, and the reactor temperature is often manipulated by controlling the feed temperature. These reactors, however, provide better mixing and more homogeneous products and are preferred when throughput rates are not high.

Many polymerization reactions start out in a low-viscosity medium. As polymerization proceeds, the viscosity of the reaction medium increases, and in many cases the product agglomerates and deposits on the reactor wall and on the stirrer, causing product accumulation and subsequent reactor foul-up. The steady-state operation of a polymerization reactor thus requires constant cleaning of the reactor and stirrer walls and the product outlets under varying viscosity conditions.

A polymerization reaction is normally followed by two principal separation processes: elimination of monomers or diluents, and separation of solid polymers. The residual monomer content is often removed by the devolatilization. When this is important, extruders, tower, and wiped-film reactors are used (e.g., for certain step-growth polymerizations to very high conversion).

The nature of the polymerization reactor also depends upon the desired form of the product (pellet, powder, bead, etc.). For example, extruder reactors (Stuber and Tirrell, 1985) are best suited to producing pellets, sheets, and coatings. The beads that may be directly useful in processing are best produced by the suspension polymerization process. The round beads, however, may not have suitable bulk-flow properties and are dangerous if spilled. Alternate shapes and the appropriate methods of production are, therefore, often employed.

Finally, safety is always a prime consideration in the selection of an appropriate polymerization reactor. Venting to the atmosphere in a safe and environmentally sound manner should always be a part of polymerization reactor design. Some additional useful information and insight into the

practical aspects of the reactor selection are given by Platzer (1970) and Gerrens (1982).

B. MECHANICALLY AGITATED CONTINUOUS STIRRED-TANK REACTOR

Since mixing and good heat transfer are of vital importance in viscous polymerization reactions, a mechanically agitated continuous stirred-tank reactor is widely used in polymerization processes. Solution polymerization, emulsion polymerization, and solid-catalyzed olefin polymerization are all carried out in a mechanically agitated slurry reactor.

The key problems in a polymerization CSTR are the determination and characterization of micro- and macromixing, and the possibility of multiple steady states due to the exothermic nature of the reactions. Recent studies of CSTRs for bulk or solution free-radical polymerization indicate the possibility of multiple steady states due to the large heat evolution and difficult heat transfer that are characteristic of the reactors. Furthermore, even in simple solution polymerization (for example, in methyl methacrylate polymerization in ethyl acetate solvent), autocatalytic kinetics can lead to "runaway" conditions even with perfect temperature control for certain combinations of solvent concentration and reactor residence time. In practice, the heat evolution can be an additional source of autocatalytic behavior.

Emulsion polymerization is usually carried out isothermally in batch or continuous stirred-tank reactors. Temperature control is much easier than for bulk or solution polymerization because the small ($\sim 0.5 \mu\text{m}$) polymer particles, which are the locus of the reaction, are suspended in a continuous aqueous medium. This complex, multiphase reactor also shows multiple steady states under isothermal conditions. In industrial practice, such a reactor often shows sustained oscillations. Solid-catalyzed olefin polymerization in a slurry batch reactor is a classic example of a slurry reactor where the solid particles change size and characteristics with time during the reaction process.

1. *Fluid Rheological Considerations*

Both polymeric and some biological reactors often contain non-Newtonian liquids in which viscosity is a function of shear rate. Basically, three types of non-Newtonian liquids are encountered: power-law fluids, which consist of pseudoplastic and dilatant fluids; viscoplastic (Bingham plastic) fluids; and viscoelastic fluids with time-dependent viscosity. Viscoelastic fluids are encountered in bread dough and fluids containing long-chain polymers such as polyamide and polyacrylonitrile that exhibit coelastic flow behavior. These

flow characteristics generate secondary flow patterns opposite to the flow pattern caused by the inertial forces. Viscoelasticity is modeled by a combination of Newtonian viscosity and Hookian elasticity (Skelland, 1968).

The most common non-Newtonian fluid characterization in polymeric and biological applications is the power-law model

$$\tau = k(\dot{\gamma})^m, \quad (7.1)$$

where τ is shear stress, $\dot{\gamma}$ the shear rate, k the "consistency coefficient," and m the flow behavior index. $m < 1$ corresponds to pseudoplastic fluids, and $m > 1$ corresponds to dilatant fluids. This model fails to predict the Newtonian behavior frequently observed at very high and very low shear rates, and the equations are not dimensionally sound, since

$$\mu_{\text{app}} = \tau/\dot{\gamma} = k\dot{\gamma}^{m-1}. \quad (7.2)$$

The apparent viscosity decreases with increasing shear rate for pseudoplastic and Bingham plastic fluids, but increases for dilatant ones.

Viscoelastic fluids can be further subcategorized as (1) thixotropic fluids, which show a reversible decrease in shear stress with time at a constant rate of shear, and (2) rheopectic fluids, which show an opposite effect. In normal reactor operation, these time dependencies usually become important for start-up conditions and for significant system perturbations.

2. *Hydrodynamics and Stirrer Power in Non-Newtonian Fluids*

The dispersion characteristics in an agitated reactor may be profoundly affected by the fluid behavior. It is possible that the conventional mass-transfer equipment used for low-viscosity Newtonian fluids may prove to be practically useless for non-Newtonian fluids. Further, the scale-up of contactors will pose problems in view of the rheological complexities. In mechanically agitated contactors, a nonuniform shear distribution exists for non-Newtonian fluids. The shear rates will be highest near the tip of the impeller and will decay rapidly as the contactor wall is approached. Thus, gas will have a strong tendency to channel through the impeller region in view of the low apparent viscosity in this region and, as a result, the dispersion characteristics in the contactor will be very poor. Loucaides and McManamey (1973) have reported such behavior in the case of a fermentation broth that exhibited pseudoplastic behavior. For situations where the apparent viscosity is very high, the conventional mechanically agitated contactors cannot be used because of the poor gas-phase dispersion.

In the case of the Bingham plastic type of fluids, if the yield stress is higher than the characteristic shear stress in the contactor, the gas bubbles may not have any relative motion with respect to the rest of the fluid. For viscoelastic

fluids, the elasticity of the fluids may result in a situation, in which the fluid, instead of being thrown away from the impeller, is sucked in toward the impeller. Viscoelastic liquids reduce the rate of coalescence and also dampen the turbulence. Joshi and Kale (1979) have shown that the addition of 50 ppm of polyethylene oxide to aqueous solutions results in about a 50% increase in the effective interfacial area and a 20% reduction in the liquid-side mass-transfer coefficient.

Metzner and Otto (1957) were the first to examine the power consumption of a turbine stirrer in liquids whose viscosities are adequately described by the power law. They found the mean shear rate to be proportional to the speed of rotation of the stirrer $\dot{\gamma} = kN$, $k = 13$. Therefore, the Reynolds number becomes $Re' = N^{2-m} d_1^2 \rho / K$, and the power characteristic can be expressed in a dimensionless form $Ne = f(Re', m)$.

An analogy between the drag characteristics for pipe flow of a non-Newtonian fluid and the power characteristic suggests the function $f(Re', m)$ to be

$$f \left[\frac{N^{2-m} d_1^2 \rho}{k} 8 \left(\frac{m}{6m+2} \right)^m \right]. \quad (7.3)$$

For $k = \mu$ and $m = 1$, the expression reduces to $f(Re = Nd_1^2 \rho / \mu)$. Calderbank determined the value of the rheological constant $k = 1.25$ for $m < 1$. He extended the measurements for blade and propeller stirrers and published the relationship $\dot{\gamma} = 10N$ for pseudoplastic and Bingham plastic fluids; however, for dilatant fluids he found that $\dot{\gamma} = 12.8N(d_T/d_1)^{0.5}$. For anchor stirrers operating in the region $Re < 100$, Beckner and Smith (1965) developed a relationship $Ne = 8[Re' f(m)]^{-0.93} (1 - d_T/d_1)^{-1/4}$, wherein $f(m) = [a(1 - m)]^{m-1}$ and a is a function of d_T/d_1 .

The power characteristic for viscoelastic fluids (Reher, 1969; Schümmer, 1970) can also be described accurately by a relationship of the type $Ne(Re')$. Additional parameters to account for viscoelastic properties are needed only when the ratio of tangential to normal stresses is less than two (Reher, 1969). Power characteristics for the turbine stirrer in *aerated* non-Newtonian fluids (carboxymethylcellulose [CMC] and polyacrylamide [PAA] solutions) have been presented by Hocker and Langer (1962).

3. Mixing and RTD

Homogenization characteristics of a mechanically agitated polymerization reactor in terms of $N\theta = f(Re_{\text{eff}} = Nd_1^2 \rho / \mu_{\text{eff}})$ have been published for various stirrer types and pseudoplastic liquids with power-law behavior (Opara, 1975; Tebel *et al.*, 1986). The homogenization time is compared to that for Newtonian fluids (Opara, 1975), and the homogenization properties of a

propeller stirrer in agitated tanks are compared with those in loop reactors (Tebel *et al.*, 1986). The subject of micromixing is also extensively discussed by Oldshue (1980, 1983).

Along with micromixing, the control of macromixing or RTD is also important for efficient operation of the polymerization reactor. For continuous polymerization, the reactor should accomplish the following requirements:

- (1) narrow residence time distribution to achieve high conversions;
- (2) good mixing of the two phases to obtain polymers with proper particle size distribution;
- (3) no dead space and gas phase within the reactor to avoid coating of the reactor wall; and
- (4) large specific surface of the reactor to remove the heat of polymerization.

These requirements indicate that a narrow RTD but a high degree of micromixing are desirable. Reichert and Moritz (1981) illustrated a stirred-tube reactor that can carry out the continuous polymerization of vinyl acetate with high conversions and the desired mean particle size of the polymer. Tai *et al.* (1989) evaluated the effectiveness of various stirrer designs outlined in Fig. 34, both continuous and reciprocating, on narrowing the RTD of fluids in laminar flow in pipes. They showed that at the optimum rpm of stirrers, all six designs shown in Fig. 34 give approximately same value of L/nd_T , where

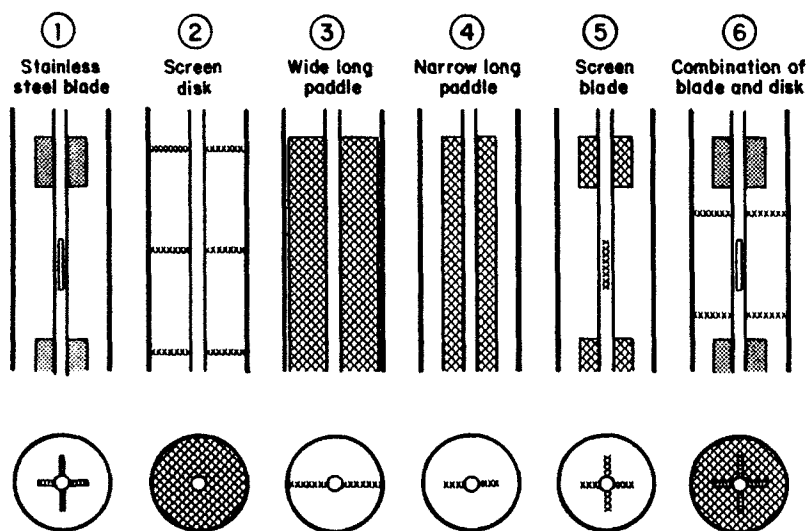


Fig. 34. Different stirrers used for narrowing RTD. (Tai *et al.*, 1989.)

L is the length of the vessel, n the number of stages, and d_T the column diameter. The optimum rpm is in the range of 10 to 60 rpm and is rather flat. At the optimum, each half pipe-diameter of pipe length behaves as an ideal stirred tank. At much higher rpm, the RTD of the fluid broadens drastically. Reciprocating and continuous operation of the stirrers given roughly the same optimum.

4. Gas-Liquid Mass Transfer

Hocker *et al.* (1981) have determined the liquid-side mass-transfer coefficient using unsteady physical absorption of oxygen. A 0.4 m i.d. vessel was employed, and aqueous solutions of carboxymethylcellulose and polyacrylamide were used as the liquid phase. They found that the same value of liquid-side mass-transfer coefficient is obtained as in the systems having Newtonian liquids at the same value of P_g/V and u_g . $k_L a_L$ was independent of the impeller design. Nishikawa *et al.* (1981) have also used the unsteady absorption of oxygen in 0.15, 0.20, 0.30, and 0.60 m i.d. vessels to measure $k_L a_L$. They have reported two correlations for $k_L a_L$, one for below the critical impeller speed, and the other for above the critical impeller speed.

Perez and Sandall (1974) studied the absorption of carbon dioxide in aqueous carbopol solution. The rheological behavior of the solution was described by the power law model with flow behavior indices varying from 0.91 to 0.59. For an agitated vessel with a turbine impeller, the mass-transfer coefficient across the unbroken interface was correlated as

$$\frac{k_L d_i}{\mathcal{D}} = 5.11 \times 10^{-3} \left(\frac{d_i^2 N \rho}{\mu_{app}} \right)^{0.926} \left(\frac{\mu_{app}}{\rho \mathcal{D}} \right)^{0.5}, \quad \text{standard deviation } 8.5\%, \quad (7.4)$$

where $\mu_{app} = \tau(\gamma_a)/\gamma_a$; γ_a is the average shear rate (s^{-1}) and τ the shear stress (dynes/cm²). It is related to the power-law model parameter by the relation

$$\mu_{app} = k(11N)^{m-1} \left(\frac{3m+1}{4m} \right)^m, \quad (7.5)$$

where k is the consistency index in g/cms² - m .

For absorption in a mechanically agitated gas-liquid dispersion in the absence of surface foam, they proposed

$$\frac{k_L a_L d_i^2}{\mathcal{D}} = 21.2 \left(\frac{d_i^2 N \rho}{\mu_{app}} \right)^{1.11} \left(\frac{\mu_{app}}{\rho \mathcal{D}} \right)^{0.5} \left(\frac{d_i u_g}{\sigma} \right)^{0.447} \left(\frac{\mu_g}{\mu_{app}} \right)^{0.694},$$

standard deviation 5%. (7.6)

where u_g is the superficial gas velocity through the sparge tube, in cm/s.

The gas-liquid mass-transfer coefficient for non-Newtonian and viscoelastic solutions has been extensively studied by Yagi and Yoshida (1975). The

correlations presented by these investigators are outlined in Table XXVII. For the power-law type of fluids, the effective viscosity can be obtained from Eq. (7.5). Hubbard *et al.* (1989) indicated that the sparger design is very important for gas-liquid mass transfer in non-Newtonian liquids. The desired values of Q and N for scale-up can be determined by keeping $k_L a_L$ and Q/Nd_1^3 the same for all reactor volumes.

5. Heat Transfer

Edney and Edwards (1976) have given a correlation to predict the heat-transfer coefficient in a non-Newtonian aerated system. They found no effect of the rate of aeration on the heat-transfer coefficient.

For a six-bladed turbine stirrer, they reported

$$\frac{h_c d_1}{k} = 0.036 \left(\frac{Nd_1^2}{\mu} \right)^{0.641} \left(\frac{\mu_A C_p}{k} \right)^{0.353} \left(\frac{d_1}{d_T} \right)^{-0.375} \left(\frac{\mu_A}{\mu_{Aw}} \right)^{0.2} \quad (7.7)$$

The non-Newtonian systems used were carboxymethylcellulose (0.5–2.0%) and polyacrylamide (0.5–1.5%) solutions.

The heat transfer between pseudoplastic fluids and the tank wall with a paddle stirrer (four paddles at 45°) can be well characterized with the usual

TABLE XXVII

MASS-TRANSFER COEFFICIENT CORRELATION OF YAGI AND YOSHIDA (1975)

$$Sh = 0.060 \frac{Re^{1.5} Sc^{0.5} Fr^{0.19} (\mu_c u_g / \sigma)^{0.6} (Nd_1 / u_g)^{0.32}}{[1 + (4Deb)^{0.5}]^{0.67}},$$

where $Sh = k_L a_L d_1^2 / \mathcal{L}$,

$Re = d_1^2 N \rho / \mathcal{L}$,

$Sc = \mu_c / \rho \mathcal{L}$,

$Fr = d_1 N^2 / g$,

$Deb = \lambda N$.

Alternate Forms

$$Sh = 0.056 (d_T / d_1)^{0.64} \frac{Re^{1.5} Sc^{0.5} Fr^{0.19} (\mu_c u_g / \sigma)^{0.6} (Nd_1^3 / Q)^{0.32}}{[1 + (4Deb)^{0.5}]^{0.67}},$$

or

$$Sh = 0.060 \frac{Re^{0.9} Sc^{0.5} Fr^{0.19} We^{0.6} (Nd_1 / u_g)^{-0.28}}{[1 + (4Deb)^{0.5}]^{0.67}},$$

where $We = d_1^3 N^2 \rho / \sigma$.

relationship $Nu = a[Re' f(m)]^{2/3} Pr^{1/3}$, where $a = 3.41$ for heating and 1.43 for cooling. The expression given by Metzner and Otto (1957) must be used for $Re' f(m)$, while the Prandtl number $Pr \equiv C_p \mu / \bar{k}$ must be calculated with the constant viscosity value at high shear rates. The heat-transfer rates, however, can be better correlated by defining the Prandtl number in a way analogous to $Re' f(m)$; corresponding relationships for various stirrer types and non-Newtonian fluids are reviewed by Edwards and Wilkinson (1972).

C. REACTION CALORIMETER

The design of chemical plants for the production of polymers require a knowledge of the thermodynamic and kinetic parameters of the reaction, as well as the heat-transfer rate and stirrer power of the agitated reactor. The calorimetric method is a useful tool to determine such data quickly and with high accuracy. Since viscosity increase of the reaction mass and fouling at the reactor wall are typical features of many polymerizations, a heat-transfer-independent calorimetric analysis is necessary. Schmidt and Reichert (1988) and Regenass (1978) have developed a laboratory-scale polymerization calorimeter that allows the measurement of heat flux of the reaction independently from the heat-transfer coefficient through the reactor wall, which often changes during the course of the polymerization. This polymerization calorimeter consists of a 1.5 l jacket-cooled, stirred-tank reactor. The cooling medium (water) is circulated in a loop including the reactor jacket (jacket loop) with high speed by a centrifugal pump. The reactor as well as the jacket loop are housed in a temperature-controlled air bath. For calibration of the calorimeter, a power-controllable electric heater is inserted into the reaction mass. The on-line data of all temperatures, the flow rate of the cooling medium, the stirrer speed, and stirrer torque, as well as the mass of the feed, are collected by a microcomputer that also serves as a controller. A similar type of heat-flow calorimeter is also described by Regenass (1978). The detailed operational procedures for such calorimeters are described in their publications. The heat-transfer coefficient can be calculated from the overall heat balance on the calorimeter.

Schmidt and Reichert (1988) used the above-described calorimeter to study the behavior of an exothermic emulsion polymerization reaction. Using experiments with cross-linking of an aqueous polyvinyl alcohol solution with strong viscosity increase, data for the specific power consumption of the stirrer and the heat-transfer coefficient over a range of $20 < Re_m < 2000$ were obtained. The data for an anchor-type agitator were correlated using the expressions $Nu = 0.41 Re_m^{0.67}$, $Pr^{0.33}$ and $Ne = 14.38 \exp(27.17/Re_m) - 12.45$, where $Re_m = \rho N d_I^2 / \mu$, $Pr = \mu C_p / \lambda$, $Nu = h_i d_T / \lambda$, and $Ne = P / \rho N^3 d_I^5$. Schmidt

and Reichert (1988) also showed that if the appropriate operating parameters are used, a semibatch technique with partial monomer storage increases operational safety by reducing reactant accumulation. Experimental results also showed the strong influence of the operation parameters on the viscosity of the reaction mass during emulsion polymerization. Regenass (1978) used his heat-flow calorimeter to measure heats of reaction, specific heats, and heat-transfer coefficients for industrial organic reactions. This calorimeter is useful for reactions below a temperature of about 250°C and a pressure of 50 bar.

D. ROTATING-CYLINDER REACTOR

A rotating-cylinder reactor is often used where the entire polymerization reaction chamber is rotated horizontally about its long axis while immersed in a constant-temperature bath. This requires only a minimum amount of stirring, or possibly no stirring at all. The particles would be kept in suspension strictly through the rotation of the reactor, which is variable over a small rpm range.

The rotating-cylinder reactor is basically a piston/cylinder dilatometer. It can be filled completely with a swollen latex, eliminating any air-liquid interface. The variation of the latex volume as a function of temperature and degree of polymerization can be monitored continuously. A thermocouple is used to follow the latex temperature within the reactor.

A cutaway drawing of the rotating-cylinder reactor is shown in Fig. 35. The mechanical aspects of the reactor system were designed to provide temperature control, fluid containment, and process measurements. The apparatus consists of a stainless steel (SS) holder and glass cylinder in which rides an SS piston, sealed by two Viton O-rings. Piston movements is monitored by a linear variable differential transformer (type 250 HCD, Schaevetz Engineering) attached to the piston and fixed relative to the cylinder.

The rotating cylinder reactor is used by Kim *et al.* (1988) for the preparation of large-particle-size monodispersed latexes in a simulated microgravity environment. The gravitational effects of creaming and settling can be eliminated by carrying out polymerization in a microgravity environment. In this case, the emulsifier concentration can be kept at a low enough level to ensure no new particle generation while maintaining the stability of the latex, and agitation is only necessary to prevent significant temperature gradients within the polymerizing latex. Rotational speed is also important to prevent flocculation. A rotational speed of 8 rpm was chosen for the polymerization of polystyrene particles in the size range of 6–60 μm . Improved particle-size uniformities were obtained when compared to more conventional poly-

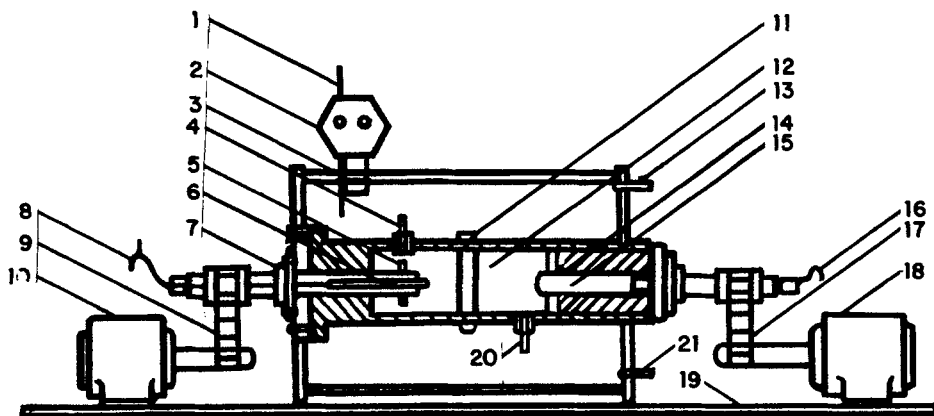


FIG. 35. Schematic diagram of the rotating-cylinder reactor. 1, thermometer; 2, temperature controller; 3, housing; 4, reactor inlet bolt; 5, stirrer; 6, temperature sensor; 7, bearing; 8, temperature sensor wire leads; 9, stirrer shaft belt; 10, stirrer motor; 11, reactor holder; 12, reaction chamber; 13, water jacket inlet; 14, O-ring; 15, volume sensor; 16, volume sensor wire leads; 17, rotating chamber belt; 18, rotating chamber motor; 19, base plate; 20, reactor outlet bolt; 21, water jacket outlet. (Reprinted with permission from *Chem. Eng. Sci.* 43, 2025, J. H. Kim, E. D. Sudol, M. S. El-Aasser, J. W. Vanderhoff, Copyright 1988, Pergamon Press plc.)

merization techniques. Improved seeded emulsion polymerization and the latex prepared from it are thus obtained from this novel agitated reactor.

E. THIN-FILM REACTORS

A number of industrially important polymerization reactions involve viscous, heat-sensitive substances and the evolution of a large quantity of heat. For such reactions, a thin-film reactor can be effectively used (Schütz, 1988). This reactor consists of a cylindrical or conical vessel, and the liquid film is agitated by means of blades fixed onto a central shaft. There is a close clearance between the blade and the wall of the vessel. Thus, highly viscous liquids can also be agitated efficiently. Furthermore, the vessel can be jacketed and a heating or cooling medium can be circulated through the jacket. Because of efficient agitation of the liquid film, large transport rates between gas and fluid can be obtained (Mützenberg, 1965). Typical Peclet numbers for axial mixing range from 3 to 15. This reactor is thus capable of handling highly exothermic reactions involving heat-sensitive substances. The reactor can be operated continuously with no backmixing in the liquid film. Consistent product quality and yield can be obtained, and with appropriate modification

of the design, the residence time of the liquid can also be accurately controlled. Finally, with the use of an alternative rotor design, the reactor can also handle a slurry. The suitability of this reactor for multiple reactions is discussed by Schütz (1988). An improved version of such a thin-film reactor is produced by Votator Processing Equipment with the trade name "Turba-Film" Processor. This reactor is capable of continuous single-pass operation of products having viscosities in excess of 500,000 centipoises at high heat and mass transfer rates. The heat-transfer coefficient decreases with an increase in mean bulk viscosity, with a value of about $250 \text{ kcal/m}^2\text{h}^\circ\text{C}$ at a viscosity of about 1000 cP. The contact time is short, and the Peclet number is of the order of 10.

For very highly viscous fluid (viscosities exceeding 10,000 poises) the Luwa thin-film agitated reactor has been found to be very effective (Widmer, 1973). A schematic of this reactor is shown in Fig. 36. The reactor has a small clearance between the heated wall and the rotor blade. This clearance results in high shear gradients and considerably reduced apparent viscosity. The apparatus

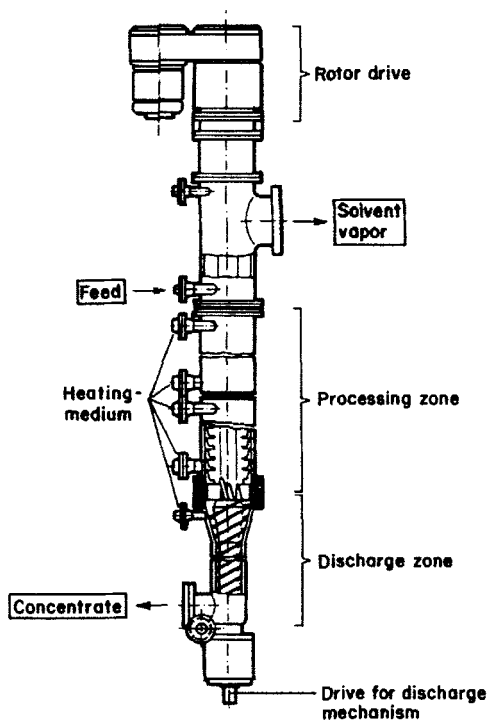


FIG. 36. Schematic layout of high-viscosity machine (Luwa Filmtuder) with discharge mechanism. (Reprinted with permission from Widmer, F., *Polymerization Kinetics & Technology* 51, *Advances in Chemistry Series* 128, Copyright 1973, American Chemical Society.)

can also be used to remove solvents from polymers and polycondensation processes. The residence-time distribution characterized by the Peclet number depends on the rotor blade arrangement. Straight blades give more plug flow and lower mean residence time than pitched blades. Under a high shear gradient, this apparatus is useful for a threefold variation in viscosity. The reduction in apparent viscosity at higher temperatures improves the efficiency of mass and heat transfer operations. According to penetration theory, $h \sim (\Delta t)^{0.5}$, where Δt is the contact time of every film element. If one assumes that in the agitated film, the surface of the film is renewed after every passage of a blade, one finds $\Delta t \sim 1/uz$ and $h \sim (uz)^{0.5}$, where z is the number of blades and u the peripheral speed. The validity of the penetration theory, as shown by Widmer (1973), points out that heat and mass transfer in an agitated viscous thin film (even in the case of evaporation) are mainly affected by forced convection and continuous surface renewal. For low-viscosity products, some correlations for the heat transfer coefficient are given by Penny and Bell (1967).

F. SCREW REACTOR

Highly viscous polymeric reactions (e.g., the hydrolytic polyamide reaction) are often carried out in a gear-pump reactor (Tadmor and Klein, 1970). This type of reactor is often difficult to operate because the clearance of the gear teeth is increased by wear caused by flow and the reaction process. For smaller viscosity of the melt, a screw reactor or a twin-screw extruder is often used. Sterbecsek *et al.* (1987) used a twin-screw extruder (i.e., Werner-Pfleiderer extruder ZSK 83) for studying fast ion-catalyzed polymerization (6-caprolactam) in a melt. They indicated that power input and quality of product in such a reactor depends on the slot width between reactor wall and impeller in a twin screw extruder. They provided an optimum design of a twin-screw reactor for a fast ion-catalyzed polymerization in a melt.

The twin-screw reactor is useful for polymeric operations because it provides

- intense shear mixing, such as that required for degradation of gels;
- dampening of feed irregularities to produce a homogeneous product;
- intimate blending of different constituents;
- surface exposure for removal of a component; and
- molecular-scale mixing for reaction.

When the mixer's task is primarily blending of different constituents and dampening of feed irregularities, an agitator that causes a fair amount of axial mixing is desirable. In simple twin-screw extruders, this may be achieved by

imposing a restriction on the output that causes the discharge to be less than the forwarding capacity of the screws and brings some internal cycling within the flow channel. Other mixing effects can be accomplished by modification of the screw cross-section, such as providing compounding sections to enhance gel breakdown. For many process applications, too much axial mixing may be undesirable, such as for a polycondensation reaction or for a reaction where devolatilization is important.

The mechanical features of several other types of twin-screw extruders were compared by Prause (1968). The effects of viscosity and rotor speed on axial mixing for this reactor compare well with those for a single-screw extruder. The study of Todd and Irving (1969) indicates that a continuous screw design leads to excessive axial mixing, and this can be reduced by an order of magnitude with proper blade design. The Peclet number for this reactor can be varied by a factor of four to five, depending upon the configuration of screw.

Finally, in the operation of a polymerization reactor, the viscosity of the reaction mixture can sometimes change from close to that of water (in the beginning) to a highly viscous melt as the reaction proceeds. The reactor, in this situation, should be able to provide variable mixing characteristics. For this purpose, a screw reactor is often equipped with a helical ribbon so that the reactor has more flexibility for providing variable mixing characteristics that are required during the reaction process. Some other novel reactors designed for this purpose are illustrated in Table XXVIII.

G. PROPELLER LOOP REACTOR

A schematic of the propeller loop reactor is shown in Fig. 37. In this case, the circulation flow of the fluid phases is created by a hydromechanical propeller flow drive. The use of a draft tube often improves the mass and heat transfer efficiency in these reactors (Blenke, 1967). This type of reactor involves complicated construction and leads to operating problems related to the sealing of the shaft. It is not suitable for biosystems due to possible damage to sensitive organisms in the high shear fields at the propeller. However, it is especially suitable for highly viscous polymeric fluids and for medium-size units.

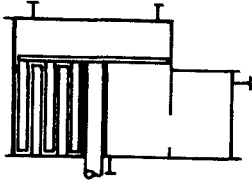
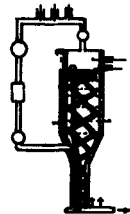

H. MULTIDISKS REACTOR

Nylon salt polymerization in the presence of monobasic acid can be carried out in a multidisk reactor shown in Fig. 38. The holdup in this vessel can be expressed by the relation (Murakami *et al.*, 1972)

$$\frac{\epsilon_L}{d_1^2 L} = 0.6 \left(\frac{\mu N d_1}{\sigma} \right)^{1/7}. \quad (7.8)$$

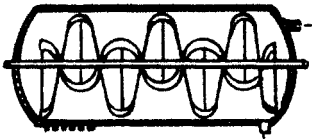
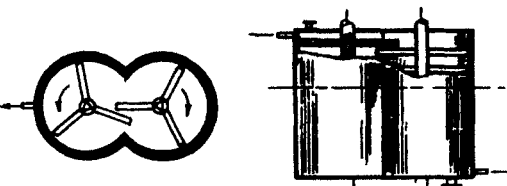

TABLE XXVIII

NOVEL REACTORS FOR POLYMERIZATION REACTIONS^a

Reactor Configuration	Reactron System	Remarks	U.S. Patent No.
	Polymerization in concentrated systems	<p>The reactor has a cylindrical body having vertical axis with upper and lower heads; in correspondence of a generatrix of the cylinder an opening with vertical axis is provided, which puts the interior of the cylinder in communication with the body of an extruder, it too with vertical axis, and solid with the reactor.</p>	4,748,219 Gordini and Elastomeri (1988)
	slurry co-polymerization process for ethylene	<p>Suitable for elastomeric copolymers which tend to agglomerate.</p> <p>Vessel fouling is prevented and occluded liquid is removed. This is achieved at high reaction rate.</p>	4,021,600 Dupont
		<p>Copolymer may be removed from the interior surfaces of the vessel, either (a) with an open-cage, double-flighted spiral ribbon with a rod inside to remove copolymer from the inside periphery of the spiral ribbon; or (b) with two intermeshed spiral helices which remove co-polymer from surfaces of the vessel and from each other.</p>	

(continues)

TABLE XXVIII (continued)

Reactor Configuration	Reactron System	Remarks	U.S. Patent No.
	Continuous solution polymerization of ethylene	<ul style="list-style-type: none"> Improved mass transfer Good for solution viscosity above 500 cp. Two phases are agitated by pitched helical blades on a horizontal rotatable shaft. 	3706719-S Dupont
	Graft copolymers of vinyl aromatic compounds and stereo specific rubbers.	Self cleaning screw extruder type reactor	3,243,481 Ruffing et al. (1966)
	Polymerization vessel for polyethylene terephthalate or polycarbonate	<ul style="list-style-type: none"> Annular structure cuts down viscous material moving with blades and interlocking flow paths gives good mixing and surface renewal on free upper surface. Close wall contact cuts down scaling. 	4,776,703 Hitachi



Manufacture of
polymers or copoly-
mers of trioxane

•Mixture is treated by the paddles
at the slurry stage during
polymerization and therefore
produces few large block polymers
and so requires little further reduction
in particle size, while the paddles
also reduce deposit of polymer scale
on the wall surface of the barrel allow-
ing rapid removal of heat.

4,727,132
Polyplastic Co.



Vinyl chloride
polymerization

•Avoid fouling during a low shear
secondary polymerization stage.

4,045,185
Rhône-Poulenc

•The design avoids stagnant or eddy
pockets near the function of the blade
and the shaft. The flow over the
spreading blade roots tends to keep
the surface scoured clean.

^a Courtesy of a patent literature search by Exxon Chemical (1989).

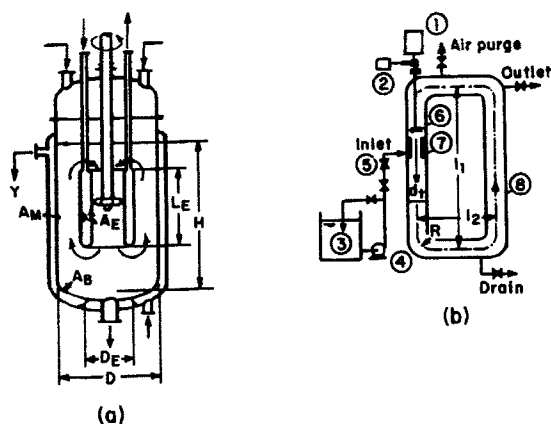


FIG. 37. Schematic of propeller loop reactor designs. Dimensions: $L = 280$ cm, $d_1 = 10$ cm, $l_1 = 100$ cm, $l_2 = 50$ cm, $R = 11.7$ cm, $V = 22$ L. 1, dc motor; 2, tachometer; 3, reservoir; 4, pump; 5, Venturi meter; 6, impeller; 7, baffle; 8, loop reactor. (After Chaudhari *et al.*, 1986, by courtesy of Marcel Dekker, Inc.)

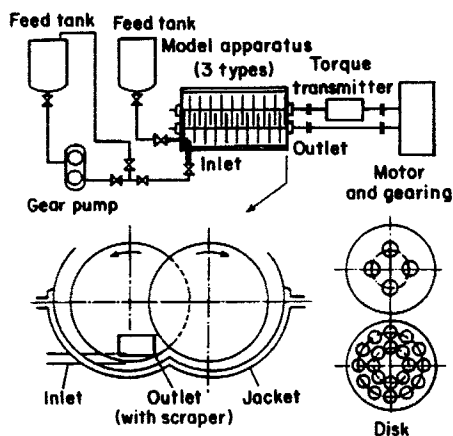


FIG. 38. Schematic diagram of experimental apparatus. (After Y. Murakami, Fujimoto, K., Kakimoto, S., and Sekino, M., *J. Chem. Eng. of Jpn.* 5 (3), 257, 1972.)

The power input in this reactor can be related to the Reynolds and Froude numbers as (Murakami *et al.*, 1972)

$$Ne = \frac{Pg_c}{\rho N^3 d_1^4 L} = 42.1 \left(\frac{\rho N d_1^2}{\mu} \right)^{-1} \left(\frac{N^2 d_1}{g} \right)^{-0.13} \left(\frac{\ell}{d_1} \right)^{-1}, \quad (7.9)$$

where ℓ is the distance between the two successive disks. No effect of the clearance between the disk tip and the vessel wall on power consumption was recognized. The mixing time is independent of Reynolds number and can be correlated as

$$N\theta = 47(\ell/d_1)^{0.12}. \quad (7.10)$$

The degree of axial mixing can be correlated in terms of the number of perfectly mixed tanks n . For the present reactor, this is correlated as

$$n = 4.52(\text{Re}_F/\text{Re}_M)^{1/4}(\ell/L)^{-1}. \quad (7.11)$$

Based on the above relation, for most practical operations, this reactor behaves much like the plug-flow reactor, where $\bar{\text{Re}}_F = \rho d_1 L / \mu \bar{\theta}_T$, $\text{Re}_M = \rho d_1^2 N / \mu$. Here, $\bar{\theta}_T$ is the average residence time. The relationship between power consumption and mixing time reveals the similarity of this vessel to the double helical-ribbon mixer. The fraction of dead space in this apparatus appears to be small. The relationships described above are valid for the fluids in the viscosity range of 50–5000 poises.

Karandikar and Kale (1981) have given the following correlation for the liquid-side mass-transfer coefficient for Newtonian and non-Newtonian liquids based on the data obtained in 125, 175, and 500 mm diameter disks:

$$\frac{k_L \delta}{\mathcal{D}} = 0.063 \left\{ \frac{\delta(N d_1)}{\mathcal{D}} \right\}^{0.5} \left\{ \frac{N^2 d_1^3 \delta}{\sigma} \right\}^{0.125}, \quad (7.12)$$

where δ is the liquid film thickness formed over the rotating disk.

The rotating-disk reactor is applicable for bulk polycondensation reactions such as those for the productions of Nylon 66 and 610, polyethylene terephthalate, polyurea, and polycarbonate. High agitation and multidisks provide a high rate of surface renewal, which increases the efficiency of the reaction process.

I. NOVEL REACTORS

The reactor foul-up due to the depositions of viscous and sticky polymer products on the walls of the reactor and stirrer, as well as at the reactor outlet, has led to many special designs of mechanically agitated reactors. These designs are largely published in the patent literature. Some of these novel

designs are summarized in Table XXVIII. The design parameters for these novel reactors are only available in the patent literature outlined in this table. It is clear that this subject is still under intense industrial investigation.

J. SUMMARY

The major characteristic of a polymeric reactor that is different from most other types of reactors discussed earlier is the viscous and often non-Newtonian behavior of the fluid. Shear-dependent rheological properties cause difficulties in the estimation of the design parameters, particularly when the viscosity is also time-dependent. While significant literature on the design parameters for a mechanically agitated vessel containing power-law fluid is available, similar information for viscoelastic fluid is lacking.

Conventional stirred-tank polymeric reactors normally use turbine, propeller, blade, or anchor stirrers. Power consumption for a power-law fluid in such reactors can be expressed in a dimensionless form, $Ne = g(Re', f(m), d_T/d_i)$, where Re' is the Reynolds number based on the "consistency coefficient" for the power-law fluid. Various forms for the function $f(m)$ in terms of the power-law index have been proposed. Unlike that for Newtonian fluid, the shear rate in the case of power-law fluid depends on the ratio d_T/d_i and the stirrer speed N . For anchor stirrers, the functionality g developed by Beckner and Smith (1962) is recommended. For aerated non-Newtonian fluids, the study of Hocker and Langer (1962) for turbine stirrers is recommended. For viscoelastic fluids, the works of Reher (1969) and Schümmer (1970) should be useful. The mixing time for power-law fluids can also be correlated by the dimensionless relation $N\theta = f(Re_{eff} = Nd_i^2\rho/\mu_{eff})$ (Tebel *et al.*, 1986).

The gas-liquid volumetric mass-transfer coefficient for the agitation of power-law fluid in an aerated vessel can be expressed in the form $k_L a_L = f(P_g/V, u_g)$ (Hocker *et al.*, 1981). For the mass transfer in a vessel with an unbroken interface, the relationship $Sh = f(Re, Sc)$ given by Eq. (7.4) is recommended.

Gas flow has little effect on heat transfer in a mechanically agitated vessel containing power-law fluid. While for turbine stirrers the heat-transfer coefficient for a power-law fluid can be obtained from Eq. (7.7), a more generalized form $Nu = a[Re' f(m)]^{2/3} Pr^{1/3}$ should be preferred. Here the expression given by Metzner and Otto (1957) for $Re' f(m)$ should be used and the viscosity in Prandtl number must be the constant viscosity value at high shear rates.

Design parameters for novel reactors such as rotating-cylinder reactors, thin-film reactors, propeller loop reactors, screw reactors, and multidisk reac-

tors are reasonably well established. Of these, thin-film and screw reactors are the most widely used, largely because they offer the most operational flexibility. Thin-film reactors can be used for threefold variations in the viscosity of fluids. Screw reactors offer intense mixing, intimate blending of different constituents even at the molecular scale, surface exposure for removal of components and homogeneous product formation. Significant knowledge on the proper design of blades in a screw reactor is also available.

Multidisk reactors are most useful when significant renewal of fluid surface is required for the reaction. The rotating cylinder reactor offers a microgravity environment, which is required during the production of large particle-size monodispersed latexes. Centrifugal forces in a horizontal reactor prevent settling that would occur in other gravity-forced reactors. Propeller loop reactors provide high mass and heat transfer rates in highly viscous systems. These reactors are, however, most suitable in medium-size units.

K. FUTURE WORK

Future work should include

- development of correlations for design parameters for a mechanically agitated reactor containing viscoelastic liquids;
- development of novel reactors to handle viscous, sticky, and heat-sensitive materials; and
- development of novel reactors to handle mass-transfer-controlled gas-liquid (or gas-liquid-solid) reactions in a high-viscosity liquid medium.

VIII. Special-Purpose Reactors

In this section we briefly discuss the use of mechanically agitated reactors in the electrochemical, photochemical, and chemical vapor deposition industries. While the use of mechanical agitation is not very common in the reactors used in these industries, it does provide special advantages in specific instances.

A. ROTATING-DISKS ELECTROCHEMICAL REACTORS

Explorations of new electrochemical routes to traditional as well as specialty chemicals via electro-organic synthesis have given rise to a search for more efficient electrochemical reactors. The radial flow reactors or cells show promise compared to the conventional parallel plate configurations. A typical radial flow reactor is schematically shown in Fig. 39, which includes the

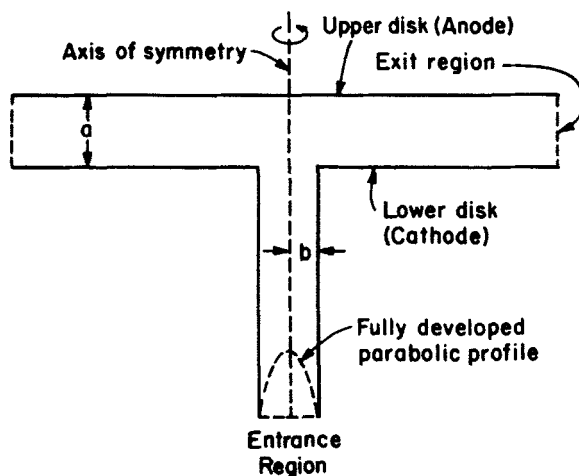


FIG. 39. Schematic of radial flow electrochemical cells, also showing the enclosed boundary for flow simulation. (Reprinted with permission from *Chem. Eng. Sci.* **43**, 2013, F. B. Thomas, P. A. Ramchandran, M. P. Dudukovic, and R. E. W. Jansson, Copyright 1988, Pergamon Press plc.)

configuration of the pump cell (PC) with one rotating disk and the rotating electrolyzer (RE) with both disks rotating.

The radial flow cells offer many advantages: (1) The gap width between the electrodes can be changed with ease. This alters the ratio between the electrode surface area and the cell volume and allows good control over the relative magnitudes of the electrode reaction and the homogeneous reactions, which is especially important in an electro-organic synthesis where product selectivity often depends on the relative magnitude of these steps. (2) The flow pattern in the rotating cells can be changed by variation of the rotational speed. In some processes, an intermediate is generated at the electrode surface and reacts homogeneously with a substrate in the region near the wall. With control of the "convective transport" of this precursor, it may be possible to fine-tune the residence time of the precursor and thereby improve reactor selectivity. (3) The rotating electrolyzer causes a flow separation between cathodic and anodic regions, and this can be used for a membraneless separation of products in a paired synthesis. (4) The increased mass transfer provided by the rotation may be advantageous in many situations.

The effectiveness of RE and PC electrochemical reactors for methoxylation of furan was examined by Thomas *et al.* (1988). The performance of various types of reactors is compared in Table XXIX. As shown, both RE and PC with cathode spinning gave better performance than a capillary gap cell. For the pump cell, the results differ depending on whether the cathode is spinning or

TABLE XXIX
PERFORMANCES OF VARIOUS ELECTROLYZERS
FOR METHOXYLATION OF FURAN

Reactor Type	Conversion Percent
CGC	5.66
RE	5.71
PC: Cathode spinning	13.5
PC: Anode spinning	2.01

(Reprinted with permission from *Chem. Eng. Sci.* 43 (8), 2013, Thomas F. B., Ramchandran, P. A., Dudukovic, M. P. and Jansson, R. E. W., Copyright 1988, Pergamon Press plc).

the anode is spinning. In this case, the cathodic reaction was rate-limiting. These results show that the velocity patterns in the cells influence the reactor performance.

Thomas *et al.* (1988) also showed that for both CGC and RE, the velocity profiles become fully developed after a certain radial entry length. The fully developed velocity profile has a parabolic shape for the CGC and the shape of two wall jets with a nearly stagnant region in between for the RE. For the pump cell, no asymptotic velocity profile is reached. The fluid continues to accelerate in the radial direction near the spinning electrode, while significant reverse flow is obtained near the stationary electrode.

Because of the strong effects of plate rotations on the reactor performance for both RE and PC electrolyzers, the critical design parameters for these reactors are the Taylor number $(a^2w/4\nu)^{0.5}$ and the Reynolds number (aV_f/ν) . Here a is the gap width between the plate, w the angular velocity of rotation (in radians per second), ν the kinematic viscosity of the fluid, and V_f the velocity in the feed pipe. Since no asymptotic velocity profile is reached for PC, the length of the cell will be an important design parameter in a pump-cell electrolyzer. Detailed mathematical models for RE and PC electrolyzers are given by Thomas *et al.* (1988), Jansson (1978), Jansson *et al.* (1978) and Simek and Rousar (1984).

B. PHOTOCHEMICAL REACTORS

When dealing with the design of the equipment for carrying out a photochemical reaction, several aspects must be considered. Some of them are common to the design of conventional thermal reactors, such as the kinetic characteristics of the reactions involved, the phases of the system, the necessity

of temperature control, the requirements about the material of construction, and so on. Others arise specifically from the selection of the appropriate radiation source for the reaction under study (i.e., the spectral distribution of the emitted light and the geometrical configuration of the reactor lamp arrangement). In addition, a certain number of important photochemical reactions share the common characteristic of presenting products and reactants with highly corrosive or dissolving properties; a typical example is the chlorination of hydrocarbons, where the presence of chlorine, hydrochloric acid, and chlorinated solvents creates difficulties in the selection of materials for equipments and seals. In the case of heterogeneous systems, the mixing pattern of the reactor is extremely important. Another important aspect in the design is the requirement for temperature control in strongly exothermic or endothermic reactions. Finally, in some particular cases the design can be improved by adding a reflecting device.

Many of these difficulties can be overcome by choosing an appropriate configuration of the photoreactor system. One such a system is the mechanically agitated cylindrical reactor with parabolic reflector. In this type of reactor, the reaction system is isolated from the radiation source (which could also simplify the solution of the well-known problem of wall deposits, generally more severe at the radiation entrance wall). The reactor system uses a cylindrical reactor irradiated from the bottom by a tubular source located at the focal axis of a cylindrical reflector of parabolic cross-section (Fig. 40). Since the cylindrical reactor may be a perfectly stirred tank reactor, this device is especially required. This type of reactor is applicable for both laboratory- and commercial-scale work and can be used in batch, semibatch, or continuous operations. Problems of corrosion and sealing can be easily handled in this system.

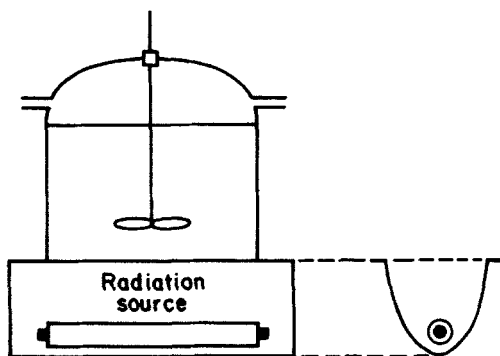


FIG. 40. Cylindrical photoreactor with parabolic reflector. (After Cassano *et al.*, 1986, by permission of Gordon and Breach, Science publishers S.A.)

Another type of mechanically agitated photoreactor used for industrial applications is a multilamp reactor (De Barnardes *et al.*, 1987). This reactor can be recommended for liquid-phase reactions with small-to-medium heat-transfer requirements, which could be improved by adding cooling coils inside the vessel. The walls of the tank could have reflecting properties, increasing the efficiency of the radiation emitted by the lamps. Again, it can be used for low and medium reaction pressures, since restrictions are placed in the diameter of the tubes surrounding the radiation sources. This reactor is very appropriate for reactions where energy requirements are rather high or if, in spite of having low energy requirements, the optical thickness of the medium is great. In the second case, the same input energy could be distributed in several radiation sources, obtaining a more useful radiation field distribution inside the tank. It is also suitable for multiphase reactions since very good stirring is easily achieved. It is not appropriate for gas-phase reactions.

The main difference between photochemical and thermal reaction is the presence of a radiation-activated step. The rate of reaction of this step is proportional to the local volumetric rate of energy absorption (LVREA). For any emission model, the LVREA is a function of the spatial variables, of the physical properties and geometrical characteristics of the lamp-reactor system, and some physicochemical properties of the reacting mixture. The most important design parameter that is pertinent in photochemical and photocatalytic reactions is the effective attenuation coefficient.

When the agitated reactors are used for gas-liquid systems, several correlations have been proposed to evaluate the effective attenuation coefficient. Otake *et al.* (1981) proposed a simple empirical expression that accounts for the absorption effects produced by the liquid phase and the reflection, refraction, and transmission effects provoked by the gaseous phase. Considering that the latter are proportional to the specific surface area (a'_L), $\mu_{\text{eff},v}$ may be represented by the correlation

$$\mu_{\text{eff},v} = \mu_v(1 + \varepsilon_g) + ka'_L, \quad (8.1)$$

where μ_v is the attenuation coefficient of the liquid phase, ε_g the holdup of the dispersed phase, k an empirical coefficient depending on the optical properties of the system, and a'_L the interfacial area per unit liquid plus gas volume. Otake *et al.* (1981) plotted the experimental information obtained by them and other authors and reported that $k = 0.125$ for $\mu_{\text{eff},v}$, μ_v , and a'_L in the same units (cm^{-1}) best fits the experimental data.

Another correlation is proposed by Yakota *et al.* (1981), in which the effective attenuation coefficient is a function of the attenuation coefficient in the liquid phase, the bubble diameter, and the gas holdup. This correlation can be expressed as

$$\mu_{\text{eff},v} = \mu_v(1 - h\varepsilon_g) \quad (8.2)$$

and

$$h = \left(\frac{3.6}{d_b} \right)^{0.66}, \quad (8.3)$$

where d_b is the bubble diameter in mm for μ_v , and μ_{eff} , v is expressed in m^{-1} . Both Eqs. (8.1) and (8.2) may be used for μ_v smaller than 40 m^{-1} . When μ_v is greater than 40 m^{-1} , the dispersion effect of radiation due to the presence of bubbles may normally be neglected.

It is clear from this discussion that the design of mechanically agitated photochemical reactors requires a knowledge of ϵ_g , d_b , and a_L . These parameters can be estimated from the correlations reported in Section II. For the multilamp reactor, the effects of internals on ϵ_g , d_b , and a'_L should be appropriately evaluated. No similar, reliable design procedures have yet been developed for solid-fluid photocatalytic reactors.

C. CHEMICAL VAPOR DEPOSITION REACTORS

A CVD reactor system for depositing thin film materials must provide the following functions:

- (1) control flow of diluent and reactant gases entering the reactor;
- (2) provide heat to the site of reaction, namely, the substrate material being coated, and control this temperature by automatic feedback to the heat source; and
- (3) remove the by-product exhaust gases from the deposition zone and safely dispose of them.

The reactor system should be designed to fulfill these three primary functions with maximum effectiveness and simplicity of construction. It must consistently yield films of high quality, good thickness, and compositional uniformity from run to run, and of high purity with a minimum of structural imperfections such as pinholes, cracks, and particulate contaminants.

1. Rotary Vertical Batch Reactors

Chemical vapor deposition in semiconductor processing applications is usually conducted in resistance- or induction-heated quartz tube furnaces. In this type of furnace, it is difficult to achieve uniform deposits consistently, especially if several substrate wafers are processed simultaneously. Part of the difficulty is due to changes in the composition of the reactant gas mixture as it passes through the tube. The creation of uniform turbulence in the gas mixture is also difficult.

Rotary vertical batch reactors used to form dielectric films by chemical vapor deposition reactions in the temperature range of 250–500°C overcome these problems. The substrate wafers lie on a hot plate covered by a glass chamber. A mixture of reactant and diluent gases passes over them. On contact with the heated substrates, the gases react, forming a deposit. The apparatus is used for the controlled deposition of silicon dioxide from silane and oxygen. The binary and ternary silicate glasses can also be deposited. Typical examples of the uniformity of film thickness that can be achieved on polished silicon wafers are: silicon dioxide deposited over a 1.5-inch diameter substrate measured $6,000 \pm 200 \text{ \AA}$; a thick layer of borosilicate deposited over a 1.3-inch diameter substrate measured $72,300 \pm 1,500 \text{ \AA}$. The advantages of this reactor are briefly summarized in Table XXX. The details of the apparatus are given by Kern (1968).

Kern (1975) also described a simple and inexpensive modified single rotation unit, which is schematically illustrated in Fig. 41. In this apparatus, five wafers of 5cm diameter, each $1 \mu\text{m}$ thick ($\pm 2\%$) can be obtained if the nitrogen diluent flow is properly balanced. The reactor is capable of having a high deposition rate (up to $1 \mu\text{m}/\text{min}$).

A commercial rotary, resistance-heated vertical reactor system for semi-continuous operation (Rotox-60) is sold by Unicorp, Inc., CA. It features pre-mixed gas input through four tubes inside the conical deposition chamber for uniform distribution, and has separate stations on a carrier disk for wafer loading/unloading, preheating, deposition, and cool-down. As many as seven 5 cm wafers can be accommodated per station. The maximum oxide deposition rate is $1,700 \text{ \AA}/\text{min}$, with a conservatively estimated overall uniformity of $\pm 5\%$ (Kern, 1975).

An oxide reactor featuring two planetary systems arranged concentrically was described by Wollam (1971). In this complex reactor, the driver element is a cylinder rotating within an annular spacing between a circular inner resistance-heated block and an outer heat ring. The gases are dispensed in a

TABLE XXX

ADVANTAGES OF ROTARY VERTICAL BATCH REACTORS

-
- Provide uniform films because of planetary substrate rotation. The rotation tends to smooth out substrate temperature differences and gas flow differences near the substrate surface.
 - Temperature flexibility—the substrates can be brought to higher temperatures.
 - Flexibility in the method for gas introduction; this offers greater versatility in optimizing specific conditions for a given application.
 - Absence of a fritted glass disk, which has a tendency toward clogging and contamination.
 - Uniform gas distribution over the substrate because the gas exit opening of the reaction chamber is circularly symmetric.
-

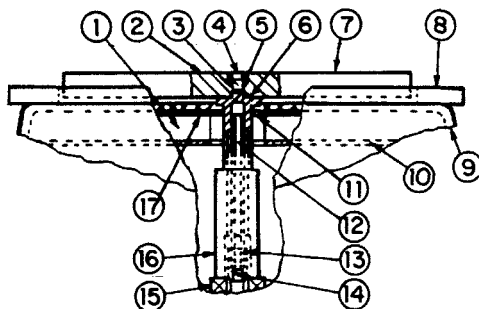


FIG. 41. Modified single rotation unit. 1, heater assembly with cut-out clearance hole for shaft; 2, aluminum alloy rotating disk (1.5 cm \times 21 cm); 3, centering insert of ceramic support pedestal; 4, centering recess on both sides of disk; 5, bushing; 6, ceramic support pedestal and sleeve drive; 7, surface of rotating disk for substrates; 8, transit reaction chamber support plate; 9, pyroceram hot-plate top; 10, backing plate; 11, output for heating element; 12, steel tubing centering shaft; 13, Boston sleeve coupling (# GR4); 14, hexagonal socket heat cap screw; 15, thrust bearing (Aetna F-1); 16, stainless steel sleeve-drive to motor shaft; 17, mica insulation with cut-out clearance hole for shaft. (After Kern, 1975.)

counter-rotating array to ensure good mixing of the gas flows, resulting in a thickness uniformity of $\pm 1.5\%$.

Vertical CVD reactor systems with rotating gas feed over a stationary, resistance-heated plate are manufactured by Phoenix Materials Corporation, Phoenix (500 and 1500 series Vapor Deposition Systems). Units for processing either 26 or 70 5 cm wafers are available (Kern, 1975).

D. SUMMARY

The basic purpose for mechanical agitation in the special-purpose reactors outlined here is similar to that in the ones described in earlier sections. In PC or RE electrochemical reactors, the rotation of the electrochemical cell aids convective transport. As shown in Table XXIX, better results are obtained when the convective transport is enhanced in a selective manner. In photochemical reactors, a large effective attenuation coefficient requires low gas holdup. A small number of very fine bubbles, which gives a low ϵ_g but a high gas-liquid mass-transfer coefficient, is desirable. Intense agitation causing extreme nonuniform gas distribution should be avoided. Design procedures for fluid-solid photocatalytic reactors need to be developed. Finally, in rotating batch CVD reactors, the rotation provides enough agitation to create uniform concentration distribution, which is required to create a uniform

film thickness. More work is, however, needed to determine the optimum rotation speed of the disk for a rotary vertical batch reactor, a modified single rotation unit, and a commercial rotary, resistance-heated vertical reactor system. The optimum speed for the rotating gas feed in a vertical CVD reactor system is similarly needed.

E. FUTURE WORK

Mechanically agitated reactors should find more usefulness in electrochemical, photochemical, and materials (CVD) industries. Future work should include

- application of the pump cell (PC) for various mass-transfer-controlled electrochemical reactions;
- methods for scale-up of the PC reactor;
- more efficient design and scalesup of the multilamp mechanically agitated photochemical reactor, particularly for multiphase systems; and
- design and scale-up of the continuous rotary reactor.

IX. Experimental Methods for Parameter Estimations

In previous sections, we examined the design parameters for gas-liquid, gas-solid, liquid-liquid, gas-liquid-solid, biological polymerization, and special types of mechanically agitated reactors. In this section we present a brief review on available techniques for the measurement of various mixing and transport parameters for a mechanically agitated vessel. Both physical and chemical techniques are examined.

A. GAS HOLDUP

The simplest method for determining gas holdup ε_g is the measurement of the heights of the aerated liquid, L_a , and the nonaerated liquid, L . The average gas holdup ε_g is then

$$\varepsilon_g = \frac{L_a - L}{L_a}. \quad (9.1)$$

This method is not time-consuming, but it is not very accurate (15–20%) when waves or foams exist on top of the dispersion. Reith *et al.* (1968) and

Burgess and Calderbank (1975) used a more accurate manometric technique to measure the height of the dispersion. In this technique, the clear liquid height in the dispersion is measured through successive pressure tapping (e.g., with a manometer) on the side of the vessel. The gas holdup is related to the pressure drop as

$$\varepsilon_g = \frac{\Delta P - \Delta P_a}{\Delta P}, \quad (9.2)$$

where ΔP and ΔP_a are the pressure drops without and with gas, respectively, between two tappings.

An electric technique to measure the gas holdup was implemented by Linek and Mayrhoferova (1969). In this method, the surface elevation of the gas-liquid interface of the nonaerated and aerated liquid in the vessel is detected at certain selected points by means of an electrical probe. The height is determined by the vertical position of the probe at which the sum of contact times equals one-half of the measurement period. The gas holdup is then calculated from the total surface elevation, the cross-section of the reactor, and the liquid volume. The accuracy of the measured value of the total surface elevation is claimed by the authors to be ± 0.2 mm.

A gamma-ray transmission technique was used by Calderbank (1958) to determine the point gas holdup. The application to holdup measurements depends on the relationship

$$\ln \frac{I_0}{I} = \lambda \rho s \quad (9.3)$$

for gamma-ray absorption, where I_0/I is the intensity ratio between incident (I_0) and transmitted (I) radiation, λ is the absorption coefficient (Cameron, 1957, gives values for most atoms), ρ is the density to be measured, and s is the thickness of the absorbing medium. Holdup is obtained simply from the measurements of density of aerated and nonaerated liquid. Calderbank (1958) used a cesium-137 source together with a scintillation counter and a scaler. The gamma radiation transmitted through the empty reactor, the reactor filled with liquid, and the reactor containing the dispersion were taken at various positions. The point gas holdup was calculated by

$$\varepsilon_g = \frac{\log t_2/t_1}{\log t_0/t_1}, \quad (9.4)$$

where t_0 , t_1 , and t_2 , respectively, are the times for a fixed number of counts for the reactor empty, filled with liquid, and containing the dispersion.

B. BUBBLE SIZE, INTERFACIAL AREA, AND VOLUMETRIC MASS-TRANSFER COEFFICIENT

1. *Physical Methods*

With a knowledge of ε_g , the mean bubble size and the gas-liquid interfacial area can be obtained with the knowledge of one of the two latter parameters because

$$a_L = \frac{6\varepsilon_g}{d_{sv}}, \quad (9.5)$$

where

$$d_{sv} = \frac{\sum_i n_i d_B^3}{\sum_i n_i d_B^2}. \quad (9.6)$$

Here, a_L is the gas-liquid interfacial area and d_{sv} is the volume-surface mean diameter or Sauter mean diameter. All bubbles are assumed to be spherical; d_B is the bubble diameter and n_i the number of bubbles of size d_{Bi} . The value of d_{sv} can be directly evaluated through a statistical analysis of high speed photomicrographs performed in the dispersion (Calderbank and Rennie, 1962; Vermeulen *et al.*, 1955; Porter *et al.*, 1966; Akita and Yoshida, 1973; Ashley and Haselden, 1972). Photographs have been taken through the walls of a transparent vessel or in the interior of a reactor with the aid of an intrascope (Koetsier and Thoenes, 1972).

Kawecki *et al.* (1967) employed a sampling apparatus for a photographic technique that avoided wall effects or perturbations normally encountered in the above techniques. Samples of bubbles were taken from the vessel containing the dispersion by a tube connected to a small square test-section column through which a continuous flow of liquid and bubbles occurred. The mean residence time of the bubbles in the vessel was kept constant by choosing a high flow rate. The bubbles in the test section were photographed, and from an analysis of these photographs, average bubble diameters were determined. Todtenhaft (1971) used a different sampling method where bubbles extracted from the dispersion were photographed as they passed through a calibrated capillary tube.

The photographic technique for bubble size usually gives just local values. It does not take into account large bubbles and is applicable only for small gas holdup (i.e., at a low gas velocity). Several measurements in different zones of the vessel are generally needed.

a. Interfacial Area

The local interfacial contact area may be determined directly by either light transmission or reflection techniques. In the former, a parallel beam of light is

passed through the dispersion onto a photocell placed at a large distance from the sample. The photocell only records that part of the incident beam that is not scattered while passing through the dispersion. Calderbank (1958) showed that the scattering cross-section is equal to its projected area when bubbles are large in comparison with the wavelengths of light. He also showed that the total interfacial area per unit volume of the dispersion equals four times the projected area per unit volume, or

$$\ln \frac{I_0}{I} = \frac{a'_L L}{4} = \ln \frac{t}{t_0}, \quad (9.7)$$

where L is the optical path length, and t and t_0 are the times for a given quantity of light to pass through the dispersion and the liquid, respectively. This technique holds for values of $a'_L L < 25$ when multiple scattering is negligible and the bubble diameters are larger than $50 \mu\text{m}$. Landau *et al.* (1977b) extended this technique to situations in which the light source and photocell are placed outside the column and multiple scattering is taken into account. An interesting empirical correlation based on anisotropic scattering in all six mutually perpendicular directions is

$$\frac{a'_L L}{4} = \ln(I_0/I)I - \Phi, \quad (9.8)$$

with

$$\Phi = 1 - 6.59 \frac{1 - \exp(-0.233\tau)}{\tau}, \quad (9.9)$$

which is valid for $a'_L L$ up to 100. This represents a fourfold increase of the range of applicability of the light attenuation technique. The interfacial area is measurable in a range up to 8 cm^{-1} with fractions of light transmitted less than 0.02.

The physical technique just described directly measures the local surface area. The determination of the overall interfacial area in a gas-liquid or a liquid-liquid mechanically agitated vessel requires the application of this technique at various positions in the vessel because of variations in the local gas (or the dispersed-phase) holdup and/or the local Sauter mean diameter of bubbles or the dispersed phase. The accuracy of the average interfacial area for the entire volume of the vessel thus depends upon the homogeneity of the dispersion and the number of carefully chosen measurement locations within the vessel.

An optical technique involves the measurement of the attenuation of a light beam passing through a gas-liquid dispersion. The light that hits a bubble is partially reflected by the gas-liquid interface, so that a lower light intensity is received at the end of the optical path. Calderbank (1958) proposed a very

simple relationship between light attenuation and the interfacial area that is valid for low gas holdups (less than 10%). Other researchers (Landau *et al.*, 1977a) modified this relationship empirically and were able to measure values of a'_L up to 800^{-1} .

b. $k_L a_L$ Determination

A widely employed method for $k_L a_L$ determination is the transient absorption method. The method can be applied to the absorption of a pure component or a component from a mixture.

The experimental technique involves batch gas absorption (by surface aeration) in a liquid. The pressure of the enclosed gas phase in the reactor decreases with time because of the absorption. This decrease in pressure with time allows the estimation of the mass-transfer rate and the volumetric mass-transfer coefficient, $k_L a_L$. The total pressure decrease until equilibrium is reached gives the equilibrium solubility C^* . The relevant equations for the calculations of C^* and $k_L a_L$ are derived by Albal *et al.* (1983), Deimling *et al.* (1985), and Karandikar *et al.* (1986). These can be expressed as

$$C^* = \frac{V_G}{V_L} \frac{1}{RT} (\bar{P}_1 - \bar{P}_2) \quad (9.10)$$

and

$$k_L a_L t = \frac{\bar{P}_2 - \bar{P}_0}{\bar{P}_1 - \bar{P}_0} \ln \left(\frac{\bar{P}_1 - \bar{P}_2}{\bar{P} - \bar{P}_2} \right). \quad (9.11)$$

This method becomes inaccurate when the stirring rate is very high and the transient time is very small.

For a semi-batch reactor, a widely employed method for $k_L a_L$ determination is the gassing-out gassing-in method. The method consists in creating a step decrease or increase of the absorbing component in the inlet gas and monitoring the change in the liquid concentration of the transferring component with time. Assuming perfect mixing of the gas and liquid phases, for sparging by soluble gases, $k_L a_L$ can be obtained from the expression

$$\ln \frac{C_g/\text{He} - C_{\ell}}{C_g/\text{He} - C_{\ell f}} = -k_L a_L t (V/V_{\ell}). \quad (9.12)$$

The method is usually adopted when the transferring component is O_2 , since it is possible to monitor the dissolved oxygen concentration with a polarographic electrode (Clark cell). The method requires some precautions. The probe has an intrinsic "time constant" τ_p (the time needed to attain 63% of the reading after a stepwise concentration change) so that its output is not directly related to the actual concentration, especially when the concentration in the liquid phase changes rapidly. Indeed the measurement may be

significantly in error if τ_p is of the same order of magnitude or greater than $1/k_L a_L$. Commercial electrodes with $\tau_p = 2$ or 3 s can give reliable measurements up to $k_L a_L = 0.1$ s. For higher $k_L a_L$ values, the dynamic characteristics of the probe needs to be considered, and more complicated models proposed by Heinekin (1970, 1971), Linek (1972), and Linek *et al.*, (1973) need to be used. The time constant of the electrode can be increased when the probe is placed in regions of the vessel where the liquid circulation is slow. The lack of turbulence in such regions allows the formation of a transfer boundary layer on the membrane that delays the instrument response. When the electrode is placed in the impeller discharge, this boundary layer has a negligible effect on the instrument readings. When solids are used, this technique is useful only when no adsorption on gas or solid occurs. When appreciable volumetric uptake occurs, such as for CO_2 and acetylene (Tamhankar and Chaudhari, 1979), $k_L a_L$ can be related to volume uptake.

In continuous reactors, for perfect mixing in each phase a measurement of the difference in concentration between outlet and inlet permits determination of $k_L a_L$. In practice, this method can be used for a reacting system when the liquid-phase concentration is maintained at a low value. Mukhopadhyay and Ghose (1976) employed this technique in large fermenters, where they measured gas-phase concentrations of oxygen at the inlet and outlet and the liquid-phase concentration in the fermenter using polarographic electrodes.

The methods for both semi-batch and continuous reactors are generally restricted to the O_2 -aqueous system because of the limitations of the analytical technique for the direct measurement of liquid-phase concentration. Novel agitated vessels for measurement of transient absorption rates are described by Danckwerts and Kennedy (1954), Oishi *et al.* (1965) and Govindam and Quinn (1964).

2. Chemical Methods

The overall interfacial area for the whole reactor can be determined by chemical techniques. These techniques, however, must be used with restrictions. For example, chemical methods are difficult to use for fast-coalescing systems, since the presence of a chemical compound may reduce coalescence rates. Furthermore, in fast-coalescing systems, the specific area may depend strongly on the position in the reactor, which complicates the interpretation of an average value obtained with chemical methods. Indeed, both physical and chemical techniques should be used together to describe the phenomena that occur within gas-liquid reactors. While chemical methods allow the determination of the much-needed average interfacial area, information on the variations of the interfacial parameters, such as a_L and d_{sv} , within the reactor, which is important for scale-up, cannot be obtained by this method.

The chemical technique has been widely used over the past two decades. This technique relies on the measurement of absorption rates where the absorbing gas undergoes a chemical reaction with precisely known kinetics. The nature of the measurements depends on the nature of the reaction regime (i.e., slow, fast, or instantaneous). If a gas A is absorbed into a liquid and there undergoes a reaction with a dissolved reactant B as



then by suitably choosing the solubility, the concentration of the reactants, and the rate of reaction, it is possible to deduce the mass-transfer coefficients, the interfacial area, or both groups of parameters from the overall rate of absorption (Sharma and Danckwerts, 1970). Generally, but not always, a steady flow of each phase through the reactor is assumed.

a. Determination of the Volumetric Mass-Transfer Coefficient $k_L a_L$,
Using a Slow Irreversible Reaction

$k_L a_L$ can be evaluated using a solution that reacts with the dissolved gas in the slow reaction regime, i.e., the reaction is too slow to affect the rate of absorption directly, but it is fast enough to reduce the bulk concentration of dissolved gas effectively to zero. If the reaction is irreversible and m th-order with respect to A and n th-order with respect to B, for a slow reaction,

$$k_L a_L \ll \varepsilon_L k_{mn} (C_A^*)^{m-1} (C_{BL})^n, \quad (9.14)$$

and for the reaction to occur in the bulk rather than the film,

$$\text{Ha}^2 = \frac{2}{m+1} \frac{D_A k_{mn} (C_A^*)^{m-1} (C_{BL})^n}{k_L^2} \ll 1. \quad (9.15)$$

It may not be possible to satisfy both conditions (9.14) and (9.15) simultaneously. If $k_{mn} (C_{BL})^n$ is large to satisfy the condition (9.14) (i.e., $C_{AL} = 0$), it may be too large for the condition (9.15) to be satisfied (no reaction in the film). When only the condition (9.15) is satisfied, one obtains

$$\phi = k_R a_L C_A^*, \quad (9.16)$$

with

$$\frac{1}{k_R a_L} = \frac{1}{k_L a_L} + \frac{1}{k_{mn} (C_{AL})^{m-1} C_{BL}^n \varepsilon_L}$$

If $k_{mn} (C_{BL})^n$ is varied, keeping $k_L a_L$ constant, a plot of $1/k_R a_L$ against $1/k_{mn} (C_{BL})^n$ will be a straight line with a slope of $1/(C_{AL})^{m-1} \varepsilon_L$ and an intercept $1/k_L a_L$. This procedure allows the determination of $k_L a_L$ when it is not possible to satisfy condition (9.15).

Some chemical systems identified by Charpentier (1981) as suitable for the determination of $k_L a_L$ in the slow reaction regime are presented in part A of Table XXXI.

Determination of the Volumetric Coefficient $k_L a_L$ Using an Instantaneous, Irreversible chemical reaction For an irreversible instantaneous reaction,

$$\Phi = k_L a_L C_A^* E_i = k_L a_L C_A^* \left[1 + \frac{D_B}{z D_A} \frac{C_{BL}}{C_A^*} \right]. \quad (9.17)$$

Also for an instantaneous reaction, $Ha > 10 E_i$. If, in addition, $C_{BL} \gg C_A^*$, then the rate of absorption is

$$\Phi = k_L a_L \frac{C_{BL}}{z} \frac{D_B}{D_A}. \quad (9.18)$$

The rate of absorption is independent of the concentration of component A as well as the residence-time distribution in the gas phase. In practice, the use of Eq. (9.17) is valid when $E_i > 4$. Some suitable chemical systems for the determination of $k_L a_L$ in the instantaneous reaction regime are presented in part B of Table XXXI.

b. Determination of the Gas-Liquid Interfacial Area, a_L

When the reaction between components A and B in the liquid phase is m th order in A and n th-order in B, and the concentration of component B is the same throughout the vessel ($k_{mn}(C_{BL})^n$ is constant), the reaction is said to be rapid pseudo- m th-order in A. The condition for this situation is $3 < Ha \ll E_i$. The rate of absorption is then expressed by

$$\Phi = E k_L a_L C_A^* = H a k_L a_L C_A^* = a_L \left[\frac{2}{m+1} k_{mn} D_A (C_A^*)^{m+1} (C_{BL})^n \right]^{1/2}. \quad (9.19)$$

Thus, the rate of absorption is independent of k_L , that is, of the hydrodynamic conditions. Consequently, if the average specific rate of absorption,

$$\Phi' = \frac{\Phi}{a_L} = \left[\frac{2}{m+1} k_{mn} D_A (C_A^*)^{m+1} (C_{BL})^n \right]^{1/2}, \quad (9.20)$$

is known and C_A^* and C_{BL} are effectively the same in all parts of the system, the specific interfacial area may be determined directly from a measurement of the rate of absorption Φ .

It is not always necessary to know the kinetics of the reaction in order to determine Φ . Indeed, the values of Φ may be measured by absorbing the component A into the same solution in a stirred cell. The agitation speed or the flow rate should be varied to confirm that Φ is really independent of k_L and ϵ_L . Some suitable aqueous, organic, and viscous chemical systems for

TABLE XXXI
REACTION SYSTEMS FOR CHEMICAL METHODS

A. Slow Reactions		
Solute Gas A	Reactant B	Catalyst in the Absorbent
CO ₂ O ₂ diluted with air O ₂ butadiene	K ₂ CO ₃ + HKCO ₃ CuCl, Na ₂ SO ₃ glucose molten maleic anhydride	NaClO CuSO ₄ , CaSO ₄ glucose oxidase
B. Instantaneous Reactions		
Solute Gas A	Reactant B	
NH ₃ SO ₂ , Cl ₂ , HCl H ₂ S, HCl, CO ₂ O ₂ diluted with air	H ₂ SO ₄ NaOH amines Na ₂ S ₂ O ₄	
C. Rapid Pseudo-<i>m</i>th-Order Regime		
Solute Gas A	Reactant B	Catalyst
CO ₂ diluted with air	Na ₂ S LiOH-NaOH KOH-Ba(OH) ₂ cyclohexylamine in cyclohexanol monoethanolamine in aqueous di- or polyethylene glycol	As (OH) ₂ O-, ClO-
Cl ₂	<i>p</i> -cresol dissolved in dichlorobenzene	
O ₂ in air	Na ₂ S ₂ O ₃ Na ₂ SO ₃	CoSO ₄ , CuSO ₄
H ₂	edible oil	Ziegler-Natta
isobutylene in C ₄ fraction or air	H ₂ SO ₄	
D. Systems for $k_g a_L$ Determination—Instantaneous Reactions		
Solute Gas A	Insoluble Gas Diluent	Reactant B
SO ₂	Air	NaOH, Na ₂ SO ₃ , <i>N</i> , <i>N</i> -dimethylaniline
Cl ₂	Air, Freon 12, 22, 114	NaOH
NH ₃	Air, Freon 12, 22, 114	H ₂ SO ₄
I ₂	Air	NaOH
propylene, CO	Air	cuprous amine complex solution
E. Systems for k_L and a_L Determinational Using Surface Renewal Theory		
Solute Gas A	Reactant B	Catalyst
CO ₂ dilute with air O ₂ in air	HNaCO ₃ - Na ₂ CO ₃ CuCl, Na ₂ SO ₃	Arsenite, Hypochlorite CoSO ₄

the determination of a_L in the pseudo- m th-order regime are presented in part C of Table XXXI.

c. Determination of the Gas-Side Volumetric Mass-Transfer Coefficient, $k_g a_L$

If the resistance to transfer of component A is entirely in the gas phase ($\text{He} k_g a_L \ll k_L a_L$), the rate of absorption per unit volume of a gas-liquid system in the absence of a chemical reaction is

$$\Phi = k_g a_L (\bar{p} - \bar{p}_i) \quad (9.21)$$

where \bar{p} and \bar{p}_i are the pressure in the bulk of the gas and at the gas-liquid interface, respectively.

For an instantaneous reaction,

$$\Phi = k_g a_L (\bar{p} - \bar{p}_i) = k_L a_L C_A^* \left[1 + \frac{D_B}{z D_A} \frac{C_{BL}}{C_A^*} \right] = k_L a_L C_A^* E_i. \quad (9.22)$$

This equation is valid when $\text{Ha} > 10E_i$. When this is the case, the reaction plane is now at the interface (surface reaction, $\bar{p}_i = C_A^* = 0$), so

$$\Phi = k_g a_L \bar{p} = k_L a_L \frac{D}{z D_A} C_{BL}. \quad (9.23)$$

The transfer process in this case is controlled by diffusion in both phases. Moreover, if at all points in the reactor the following condition is satisfied,

$$k_g a_L \bar{p} - k_L a_L \frac{D_B}{z D_A} C_{BL} < 0, \quad (9.24)$$

the rate of absorption remains equal to $k_g a_L \bar{p}$, but the interfacial concentration of component B is greater than zero. Equation (9.24) insures that the absorption process is entirely controlled by the transport of component A across the gas film. Thus,

$$\Phi = k_g a_L \bar{p}. \quad (9.25)$$

In all cases, the calculation of $k_g a_L$ should be based on analysis of the gas stream, as a small error in the analysis of the liquid stream can lead to large errors in the calculated value of $k_g a_L$. Some chemical systems suitable for the determination of $k_g a_L$ in the instantaneous reaction regime are presented in part D of Table XXXI.

d. Simultaneous Measurements of Volumetric Mass Transfer Coefficients and Interfacial Area

In certain situations, the mass-transfer resistances in both phases may be appreciable, so that both $k_g a_L$ and $k_L a_L$ must be determined. Moreover, for the

purpose of calculating the effect of a chemical reaction on the rate of absorption of a gas, the parameters k_L and a_L must each be known. These separate mass-transfer parameters can be determined by chemical methods with either the pseudo-first-order or the instantaneous reaction regimes using not only the two-film model, but also the surface renewal model.

According to Charpentier (1981), the condition needed to satisfy pseudo-first-order in component A using the Danckwerts model is

$$\sqrt{1 + \text{Ha}^2} \ll \sqrt{\frac{D_A}{D_B}} + \sqrt{\frac{D_B}{D_A} \frac{D_{BL}}{zC_A^*}} = E_i \sqrt{\frac{D_A}{D_B}}. \quad (9.26)$$

When the mass-transfer resistances exists in each phase,

$$\Phi = \bar{p} \left[\frac{1}{k_g a_L} + \frac{\text{He}}{k_L a_L \sqrt{1 + \text{Ha}^2}} \right]^{-1}. \quad (9.27)$$

Two important cases arise depending on whether k_L and a_L , or k_g and a_L , are needed.

e. Simultaneous Determination of k_L and a_L

When the gas-phase resistance is negligible, the rate of absorption is given by,

$$\Phi = \frac{\bar{p}}{\text{He}} k_L a_L \sqrt{a_L + \text{Ha}^2} = a_L C_A^* \sqrt{D_A k_2 D_{BL} + k_L^2}. \quad (9.28)$$

If the rate of absorption is measured for different values of $k_2 C_{BL}$ and the hydrodynamics remain constant, a plot of ϕ^2 against $k_2 C_{BL}$ gives a straight line with slope $D_A a_L^2 (C_A^*)^2$ and intercept $(k_L a_L C_A^*)^2$. If C_A^* and D_A are known, both $k_L a_L$ and a_L can be determined.

In order to use this method, it is necessary to ensure that the physical properties of the system do not alter as $k_2 C_{BL}$ is changed. For this reason, sometimes it is convenient to use a catalytic reaction and to change k_2 by adding small amounts of catalyst. If the catalyst is sufficiently active, the reaction rate can be varied over a wide range without substantially altering the concentration of the solution. The rate of absorption then becomes

$$\Phi = a_L C_A^* \sqrt{D_A k_c C_{cat} + k_L^2}. \quad (9.29)$$

The concentration C_{cat} of the catalyst can be varied and a_L and k_L determined by plotting Φ^2 against C_{cat} . Suitable chemical systems for the determination of k_L and a_L by this method are presented in part E of Table XXXI.

f. Simultaneous Determination of k_g and a_L

If it is not possible to keep the gas-side resistance negligible, it is still possible to determine k_g and a_L by use of a fast, irreversible pseudo- m th-order reaction

($Ha \gg 1$ so that $\sqrt{1 + Ha^2} = Ha$). Thus, the rate of absorption becomes

$$\Phi = \bar{p} \left[\frac{1}{k_g a_L} + \frac{He}{k_L a_L Ha} \right]^{-1}, \quad (9.30)$$

where

$$\frac{\bar{p}}{\Phi} = \frac{1}{a_L} \left[\frac{1}{k_g} + \frac{He}{k_L Ha_L} \right] = \frac{1}{a_L} \left[\frac{1}{k_g} + \frac{He}{\left(\frac{2k_{mn}}{m+1} D_A (C_A^*)^{m-1} (C_{BL})^n \right)^{1/2}} \right]. \quad (9.31)$$

Thus, if $k_{mn} c_{BL}$ is varied, a plot of \bar{p}/Φ against

$$\frac{He}{\left[\frac{2k_{mn}}{m+1} D_A (C_A^*)^{m-1} (C_{BL})^n \right]^{1/2}}$$

will give a straight line of intercept $(1/k_g a_L)$ and slope $(1/a_L)$. Thus, a_L and k_g can be calculated simultaneously. Convenient systems for this method are the absorption of dilute CO_2 into aqueous solutions of $NaOH$ or amines.

In summary, the determination of $k_L a_L$, $k_g a_L$, and a_L by chemical method requires the knowledge of the following:

- (1) the kinetics of the chosen chemical system;
- (2) the diffusivities of the soluble gas or gases and the reactant or reactants in the liquid phase;
- (3) the solubility of the gas or gases in the liquid phase; and
- (4) mathematical relations that describe the prevailing reaction regime and associated absorption rate

g. Determination of $k_L a_L$ for Three Phase Systems

The volumetric mass transfer coefficient is also determined for three-phase (gas-liquid-solid) systems using both physical and chemical methods described above. A summary of these studies is given in Table XXXII.

3. Gradientless Gas-Liquid Reactor

Levenspiel and Godfrey (1974) developed a gradientless gas-liquid reactor to study mass transfer with reaction. Some key features of this reactor are outlined in Table XXXIII. In this type of contactor, the gas-liquid interface is flat (unbroken), and independent stirring of gas and liquid phases is provided. The major advantages of this reactor are that it is flexible enough to allow independent manipulation of the variables, operation in all kinetic regimes, and simple direct interpretation of results without becoming involved in the complications of changing compositions through the system and uncertain

TABLE XXXII

SUMMARY OF THE LITERATURE ON $k_L a_L$ MEASUREMENTS IN THREE-PHASE AGITATED VESSELS

System	Major Parameters	Agitation System	Method Utilized	Reference
(He-N ₂)-kerosene-(polypropylene, sugar, glass beads)	Solids concentration (0-40 vol %)	Standard Rushton turbine with $d_i/d_T = \frac{1}{3}$	Dynamic gassing-out method	Joosten <i>et al.</i> (1977a, 1977b)
CO ₂ -Ba (OH) ₂ -BaCO ₃ (solids); CO ₂ -diethylamine-CaCO ₃ (solids); CO ₂ -Na ₂ CO ₃ -NaHCO ₃ (solids); CO ₂ -Na ₂ CO ₃ -CaCO ₃ (solids)	Solids concentration (0-9 wt %)	Vessels of various sizes ($d_T = 0.12-0.7$ m) with various turbines and d_i/d_T ratios	Absorption with slow chemical reaction	Mehta and Sharma (1971)
Air-water-(glass beads)	Power-to-volume ratio (0.1-10 kW m ³); solids concentration (0-50 wt %) and solids particle size (300-480 μ m)	Gas-sparged vessel with one standard turbine; suction aeration and surface aeration systems with two impellers	Physical system	Wiedmann <i>et al.</i> (1981)
O ₂ -(glucose solution)-(activated carbon, quartz sand)	Stirrer speed (100-500 rev min ⁻¹) and solids concentration (0-20 kg m ⁻³)	Standard Rushton turbine with $d_i/d_T = \frac{1}{3}$	O ₂ absorption and use of O ₂ concentration measuring probe	Alper <i>et al.</i> (1980)
O ₂ -(sodium sulfide solution)-(activated carbon)	Carbon loading (0-2 wt %) and stirrer speed (800-2000 rev min ⁻¹)	Standard Rushton turbine with $d_i/d_T = \frac{1}{3}$	Absorption with chemical reaction	Chandrasekharan and Sharma (1977)
O ₂ -(fermentation media)-CaCO ₃	Solids concentration (0-14 $\times 10^3$ kg m ⁻³)	Four-blade propellers with $d_i/d_T = \frac{1}{2}$	Measurements of transfer rate using O ₂ concentration measuring probe	Elstner and Onken (1981)
O ₂ , CO ₂ , and H ₂ in water (glass beads)	Stirrer speed 600-100 rpm solids concentration (10-25 wt %)	Conventional and unconventional vessels turbine with six blades	Dynamic absorption method	Albal <i>et al.</i> (1983)
H ₂ , CO, CH ₄ , CO ₂ in F-T liquid (glass beads) and F-T liquid saturated with water	Stirrer speed 800-1,000 rpm solids concentration (5-30 wt %)	Conventional vessel turbine stirrer	Dynamic absorption method	Albal <i>et al.</i> (1984) Deimling <i>et al.</i> (1985) Karandikar <i>et al.</i> (1986)

TABLE XXXIII
KEY FEATURES OF THE GRADIENTLESS GAS-LIQUID CONTACTOR

-
1. The reactor is used for the gas-liquid reaction, but it can be used for gas-liquid-solid reactions, where the solid is a reactant.
 2. The compositions of both gas and liquid phases are uniform.
 3. The reactor can be operated isothermally.
 4. It extends the concept of a gradientless gas-solid reactor to the gas-liquid reaction systems. Reliable mass-transfer coefficients can be obtained.
 5. The major difference between this reactor and other gas-liquid reactors such as the wetted-wall column, the laminar-jet absorber, the disk contactor, and the stirred cell is that the experimenter has independent control of the physical factors, such as individual film resistances and interfacial area.
 6. In general, the rate is found without the need to worry about changing gas and/or liquid composition through the reactor, with all its uncertainties.
 7. The reactor is used for second-order gas-liquid reaction. All three regimes, i.e., slow, fast, and instantaneous, have been examined.
-

flow modeling. There is also an independent control over the gas-side mass-transfer coefficient. The mass-transfer coefficients obtained from reacting ($\text{NH}_3\text{-H}_2\text{SO}_4$) and unreacting ($\text{NH}_3\text{-H}_2\text{O}$) systems obtained from this reactor compare well with each other. The reactor can be used for gas-liquid, gas-liquid-solid, or liquid-liquid systems. The gradientless contactor of Levenspiel and Godfrey was subsequently improved by Danckwerts and Alper (1975), Sridharan and Sharma (1976), and Yadav and Sharma (1979).

C. DETERMINATION OF THE LIQUID-SOLID MASS-TRANSFER COEFFICIENT

1. *Physical Methods*

In a batch slurry reactor, the liquid-solid mass-transfer coefficient can be measured by dissolving a sparingly soluble solid in liquid. The concentration of dissolved solid in liquid (B_ℓ) can be measured as a function of time, preferably by a continuous analytical device. Systems such as the dissolution of benzoic acid, β -naphthol, naphthalene, or KMnO_4 in water can be used. A plot of B_ℓ as a function of time and the slope of such plot at time $t = 0$ can give k_s as

$$k_s = \frac{\rho_p d_p}{6wB_s} \left(\frac{dB_\ell}{dt} \right)_{t=0}, \quad (9.32)$$

where B_s is the saturation solubility of the solid species expressed as moles/cm³.

The liquid–solid mass-transfer coefficient can also be measured by the reverse process, namely adsorption on a solid from solution. Furusawa and Smith (1973) studied adsorption of benzene from aqueous solution on to activated carbon particles. The concentration of benzene in the liquid was monitored by a gas chromatograph. The liquid–solid mass-transfer coefficient from such a dynamic adsorption method can be obtained from the expression (Furusawa and Smith, 1973)

$$\frac{B_\ell}{B_{\ell i}} = \frac{1}{1 + wK'_A} + \frac{wK'_A}{1 + wK'_A} \exp \left[-\frac{(1 + wK'_A)k_s a_s t}{wK'_A} \right], \quad (9.33)$$

where

$$K'_A = \frac{1}{w} \left[\frac{B_{\ell i}}{B_{\ell \infty}} - 1 \right]. \quad (9.34)$$

Here, $B_{\ell i}$ and $B_{\ell \infty}$ are the initial and final concentrations of solute in the liquid phase. $k_s a_s$ can be obtained from a plot of

$$\ln \left[\left(\frac{B_\ell}{B_{\ell i}} \right) - \frac{1}{(1 + wK'_A)} \right]$$

versus time. In evaluating $k_s a_s$, the data at shorter times should be preferred, because at longer times intraparticle diffusion may become important.

2. Chemical Methods

For a semi-batch operation, the liquid–solid mass-transfer coefficient can also be obtained by monitoring a reaction between the dissolving solid B and a liquid reactant C. If this reaction is instantaneous, the enhancement factor for the reaction is

$$E = \sqrt{\frac{D_B}{D_C}} + \frac{C_{\text{avg}}}{zB_s} \sqrt{\frac{D_C}{D_B}}. \quad (9.35)$$

Here, D_B and D_C are the diffusivities of B and C in the liquid phase, z the stoichiometric coefficient for the reaction, C_{avg} the average concentration of C in the reactor, and B_s the saturation solubility of the solid species in the liquid. The change in the concentration C is measured as a function of time. k_s can be obtained from the expression

$$k_s = \frac{\rho_p d_p}{6wEB_s} \left(\frac{dC}{dt} \right)_{t=0}. \quad (9.36)$$

This method can be applied to systems such as the dissolution of benzoic acid, boric acid, and salicylic acid in sodium hydroxide (Blasinski and Puc, 1975).

Sano *et al.* (1974) and Harriott (1962) used an ion-exchange process. Sano *et al.* (1974) showed that k_s can be calculated from

$$k_s a_s = - \left(\frac{dy_b}{dt} \right)_{t=0}, \quad (9.37)$$

where y_b is the mole fraction of hydrogen ions in the liquid.

In order to determine the relative importance of mass-transport processes in gas-liquid-solid-reactions, it is recommended to measure the global reaction rate as function of catalyst concentration w (keeping all other operating variables constant). With the assumption of spherical catalyst particles, the specific surface of the catalyst can be calculated as

$$a_s = \frac{6w}{\rho_s d_p} \quad [\text{m}^2/\text{m}^3 \text{ suspension}], \quad (9.38)$$

where the catalyst load w is given in kilograms per cubic meter of suspension, and ρ_s is the density of the solid. Furthermore, if it is assumed that gas bubbles also behave as spheres, as assumption that seems to be justified with small enough bubbles, the specific gas-liquid interface can be calculated as

$$a_L = \frac{6\varepsilon_g}{d_b} \quad [\text{m}^2/\text{m}^3 \text{ suspension}]. \quad (9.39)$$

In the case of a simple first-order reaction with respect to the gaseous reactant (assuming that the liquid reactant is not limiting), the effective global reaction rate can be formulated as

$$\frac{1}{r_{\text{eff}}} = \frac{1}{C_A^*} \left[\frac{1}{k_L a_L} + \frac{1}{k_s a_s} + \frac{1}{k a_s \eta} \right], \quad (9.40)$$

with C_A^* the equilibrium concentration of the gaseous reactant A in the suspension and k the specific first-order rate constant with respect to catalyst surface [ms^{-1}]. In case of completely suspended, nonporous catalyst particles, Eq. (9.40) can be converted (using Eqs. (9.38) and (9.39)) into

$$\frac{1}{r_{\text{eff}}} = \frac{1}{C_A^*} \left(\frac{d_b}{k_L 6\varepsilon_g} + \frac{\rho_s d_p}{6w} \left[\frac{1}{k_s} + \frac{1}{k\eta} \right] \right). \quad (9.41)$$

Therefore, if C_A^*/r_{eff} is plotted against $1/w$, a straight-line plot at a given temperature can be obtained. The slope and the intersection on the ordinate of such a figure can be used to determine transport parameters. These parameters are functions of other operating parameters such as temperature, etc. It should be noted that if gas-liquid mass transfer controls the process, the lines will be horizontal, and if the gas-liquid mass transfer is negligible, the lines will go through the origin.

It is interesting to note the dependence of slope in the just-described plot on d_p . The term $\rho_s d_p / 6k_s \propto d_p^{1.7-2.0}$, whereas $1/k_\eta$ would either change with d_p (if intraparticle resistance is significant) or be independent of d_p (if intraparticle diffusional resistance is absent). Thus, a study of the exponent dependency of the slope on d_p gives insight into the controlling step for the reaction. For small d_p , when the slope is independent of d_p , both intraparticle and liquid-solid mass-transfer resistances may be assumed to be negligible.

When the reaction is nonlinear with respect to A, a nonlinear plot of C_A^*/r_{eff} vs. $1/w$ is obtained. A linear extrapolation of the plot for $n \neq 1$ can lead to significant errors in $k_L a_L$ values. In obtaining kinetic data for nonlinear systems, the intraparticle resistances should be eliminated with the use of a smaller particle size. If a plot of rate vs. catalyst loading shows a positive intercept on the x-axis, a certain w_{minimum} is required for the reaction to occur. The experimental data in such cases should be related to $w - w_{\text{minimum}}$.

Ruether and Puri (1973) presented another method, which separates $k_s a_s$ by examining the catalytic gas-liquid-solid reaction at low (i.e., limiting) concentrations of the liquid reactant, C_{BL} , as a function of the inverse of the partial pressure of the gaseous reactant. In this case, C_{AL} , the concentration of the gaseous reactant in the suspension, is always at equilibrium with the gas phase, not only at the gas-liquid interface but also at the catalyst surface, i.e.,

$$r_{\text{eff}} = k_s a_s (C_{\text{BL}} - C_{\text{BS}}) = \eta r(C_{\text{BS}}, C_A^*), \quad (9.42)$$

where C_{BL} and C_{BS} are the concentrations of the liquid reactant in the bulk of the liquid phase and on the catalyst surface. In order to arrive at a linear plot of C_A^*/r_{eff} vs. $1/w$, r_{eff} should be linearly dependent on C_{BS} (or C_{BL} should be very large compared with C_{BS} , i.e., film transport limitation, so that $k_s a_s$ can be determined directly as $k_s a_s = r_{\text{eff}}/C_{\text{BL}}$). But at low concentrations of C_{BL} , even in the case of Langmuir-Hinshelwood kinetics, one can approximate the hyperbolic rate equation by a potential rate law, leading (probably only in case of strong pore-diffusion limitation) to the desired pseudo-linear dependency,

$$r_{\text{eff}} = k' \cdot C_A^* \cdot C_{\text{BS}}, \quad (9.43)$$

with k' as the apparent rate constant with respect to the catalyst load m . By a combination of Eqs. (9.42) and (9.43), one gets

$$\frac{1}{r_{\text{eff}}} = \frac{1}{C_{\text{BL}}} \left(\frac{1}{k_s a_s} + \frac{1}{k' C_A^*} \right) = \left(\frac{1}{C_{\text{BL}}} \right) \left(\frac{1}{k_s a_s} + \frac{\text{He}}{k' C_{\text{AG}}} \right), \quad (9.44)$$

where C_{AG} is the gas phase concentration of the gaseous reactant and He its Henry's law constant. Hofmann (1983) used this method to determine the relative importance of the individual transport and reaction steps during hydrogenation of an aqueous glucose solution over Raney nickel in the

temperature range of 80–130°C, at hydrogen pressures of 10–30 bar and under variable stirrer speeds.

D. MEASUREMENT OF MIXING TIME

The mixing time θ is the time required for the mixer to achieve the desired degree of homogeneity. The knowledge of the mixing time is therefore only relevant with respect to the definition of the degree of homogeneity. The degree of homogeneity and associated mixing time are commonly evaluated by either the *schlieren* method or the chemical decolorization method. In the *schlieren method*, two liquids having different refractive indices are mixed; the complete homogenization of the liquids is indicated by the disappearance of the streaks (*schlieren*). In the *chemical decolorization method*, the first liquid, which contains one reaction component, is added to the second liquid, containing the second reaction component, as the stirring begins, and the time at which the color of an indicator disappears is measured. (Common reaction systems include a sulfuric acid/alkali solution with a phenolphthalein indicator, and thiosulfate/iodine with a starch indicator.) The degree of homogeneity at the point of decoloration depends on the excess of the added reaction component (Danckwerts, 1957). Because this method is simple and versatile, its details are briefly described below. Chemical decolorization methods fail for extremely short mixing times. In such cases, a consecutive dye reaction (diazotization) is used, in which the degree of mixing (i.e., micromixing) can be determined from the selectivity of the reaction.

1. Danckwerts Method (Danckwerts, 1957)

This method examines the degree of mixing of two fluids on the molecular scale by observing the rate of a second-order reaction in the mixture. The method gives the mean square concentration of component A in a nonhomogeneous mixture of A and B and the actual distribution of deviations from the mean concentration in the mixture.

The mixture consists of two aqueous solutions, A and B. A contains n molal NaOH, while B contains ny molal HCl. If A and B are mixed such that on the molecular scale they are in proportions $a, (1 - a)$, the local composition can be characterized as

$$\text{alkaline if } a > y(1 - a), \quad \text{or} \quad a > \frac{y}{1 + y}, \quad (9.45)$$

and

$$\text{acid if } a < y(1 - a), \quad \text{or} \quad a < \frac{y}{1 + y}. \quad (9.46)$$

If a suitable indicator (e.g., phenolphthalein) is added to one or the other of the solutions, three cases may be considered:

(1) *Phenolphthalein in concentration x added to solution A.* The solution is red in the alkaline regions; in an alkaline region in which the proportion of A is a , the concentration of phenolphthalein in the red form will be xa . The average concentration of phenolphthalein in the red form, x_R , can be expressed as

$$\frac{(1+y)^3}{xy} \frac{dx_R}{dy} = -f\left(\frac{y}{1+y}\right). \quad (9.47)$$

Here, the proportion of A that lies between a and $a + da$ is $f(a)da$. Thus, by varying y and measuring the corresponding color density of the mixture, it is possible to determine the fraction of the volume of the mixture that contains A and B mixed on the molecular scale in any given proportion. In a mixture with a high degree of segregation, $f(a)$ will have high values at $a = 0$ and $a = 1$ and will be low at intermediate values of a . When mixing is complete, $f(a)$ will be small at $a = 0$ and $a = 1$ and will pass through a minimum at a value equal to the volume fraction of A in the entire mixture.

(2) *Phenolphthalein in concentration x added to solution B.* By a similar argument, in this case,

$$\frac{(1+y)^3}{x} \frac{dx_R}{dy} = -f\left(\frac{y}{1+y}\right). \quad (9.48)$$

a can be determined by varying y , and the color is developed only in the regions in which molecular mixing has taken place. This case allows color measurements more easily than case (1), and it also provides a better visual demonstration of the progress of molecular mixing, particularly when $y = 0$.

(3) *Both solutions contain phenolphthalein in concentration x .* In this case,

$$\frac{(1+y)^2}{x} \frac{dx_R}{dy} = -f\left(\frac{y}{1+y}\right). \quad (9.49)$$

There is a sharp boundary separating regions in which $a > y/(1+y)$ and the concentration of red phenolphthalein is uniformly equal to x , from regions in which $a < y/(1+y)$ and the solution is colorless. This case is thus particularly suitable for the study of macroscopic mixing processes.

2. Methods for Viscous Liquids

The mixing time in viscous liquids has been determined by a variety of methods, and the results vary considerably (Nagata *et al.*, 1957; Gray, 1963; Jensen and Talton, 1965). This may be a result of differences both in measuring technique and in definition of mixing time.

Different tracers are used, depending upon the method to be applied, viz.,

- (1) the conductivity or pH method;
- (2) the thermal method;
- (3) the color addition method; and
- (4) the decoloration method.

In method (1) the conductivity or pH is higher after each test and eventually the entire vessel contents have to be renewed. This is not the case in (2). Hoogendoorn and Den Hartog (1967) added a small quantity (1–2%) of heated (20–40°C) liquid in their liquid mixtures; during homogenization, the temperature was measured with thermocouples located at several positions in the vessels. This yielded quantitative information on the progress of mixing at these locations.

In order to evaluate the mixing process visually throughout the vessel, methods (3) and (4) are preferred. Addition of a dye (3) to a clear liquid allows one to follow the mixing process very clearly in the initial stages. However, in the final stages, nearly the whole vessel contents are colored and further changes are difficult to visualize. This can explain the discrepancy in mixing times measured by Gray (1963), Nagata *et al.* (1957), and Hoogendoorn and Den Hartog (1967). For good observation of the final stages, it is better to use a decoloration method (4). For this purpose, a fast chemical reaction in the presence of an indicator can be used. For example, as mentioned before, the acid–base reaction with phenolphthalein as an indicator or the reaction between iodine and sodium thiosulfate in the presence of a starch solution are good case studies. In the decoloration method, say with a starch solution, it is first necessary to add the iodine to the liquid to color it. The iodine must be homogeneously mixed with the liquid; otherwise, possible stagnant zones will not be colored and they will remain undetected in the subsequent decoloration stage.

In order to define mixing time, it is necessary to state the required degree of homogeneity. In general, one would like to define the mixing time $\theta_{r,p}$ as the time beyond which the concentration of the tracer (or the temperature) in $r\%$ of the batch volume differs from the final concentration (or temperature) by less than $\pm(100 - p)\%$ of the total concentration (temperature) step. With methods (1) and (2) it is, however, only possible to find θ_p , which holds for the degree of homogeneity reached at the locations actually measured. From the thermal response curve obtained by method (2), one can derive mixing times such as, say, θ_{75} , which is the time beyond which, at all measuring locations, the differences between the temperatures measured and the final temperature will remain smaller than $\pm 25\%$ of the total temperature step. An advantage of the thermal method is that for the positions measured, it gives a uniquely defined quantitative value of the mixing time.

With the decoloration method, it is not possible to reach equally well-defined values for the mixing time. In order to approach this as closely as possible one can, however, add a well-measured excess of decolorizing agent to the batch. Decoloration then occurs at places where the concentration is differed by only, say, $\pm 25\%$ from the final step. In this way it is also possible to find mixing times θ_{75} , being the time required for the bulk of the liquid to be decolorized. There are, however, parts of the liquid near fixed walls that often do not decolorize, which makes the decolorization method somewhat subjective. However, it can be said that the θ_p value approaches the desired value $\theta_{r,p}$, with $r = p$, rather closely, because to bring the concentration in the bulk of the liquid to within $\pm(100 - p)\%$ of the final value, the tracer has to be spread over at least $p\%$ of the vessel volume.

Hoogendoorn and Den Hartog (1967) found that the value of θ_{75} obtained by the decoloration technique was in good agreement with that from the thermal method, except in cases where large stagnant zones occurred. This shows that in general, the different techniques yield the same mixing time results if a well-defined, unique mixing-time definition is used.

E. MEASUREMENT OF RESIDENCE-TIME DISTRIBUTION (RTD)

The RTD for a mechanically agitated vessel is commonly measured by a stimulus-response technique wherein a tracer input (step, pulse, etc.) is introduced in the reactor and the time response in the effluent (or the reactor) is measured. The RTD for each phase is generally measured separately. For the liquid phase, the tracer should be nonvolatile and nonadsorbing on solids when solids are present. The gas-phase tracer should have a low solubility in the liquid phase. Generally used liquid-phase tracers are inorganic salts or acids such as NaCl, KCl, H_2SO_4 ; organic dyes such as methylene blue; or radioactive tracers such as I and Br. For the gas phase, highly insoluble gases such as helium, krypton, argon, and hydrogen and radioactive tracers such as Ar are used. Additional details on tracers and their measurement devices as well as methods for response analysis are given by Shah (1979).

F. MEASUREMENT OF POWER

When measuring power, in addition to the mixing power P , the motor drive of a stirrer must also account for the power losses in the gearbox and the seals. In order to determine the mixing power P , the torque M_d and the rotational speed N of the stirrer must be known: $P = M_d\omega$, where $\omega = 2\pi N$ is the angular velocity. The torque can be measured using, for example, a torsion shaft with strain gauges, electrically with eddy-current torque transducers, or

mechanically with a swiveling motor. The speed of rotation can be measured using mechanical, electrical (photocell), or optical (stroboscope) instruments.

The pumping capacity of the stirrer or the liquid throughput of the stirrer is the liquid flow rate that is displaced through the area swept by the stirrer. For axial flow stirrers, q' is determined from the circulation time of particles with $\Delta\rho \approx 0$. For radial flow stirrers, it is obtained from the integral value of the measured velocity distribution of the flow.

G. MEASUREMENT OF DROP SIZE AND COALESCENCE RATE IN LIQUID-LIQUID SYSTEMS

The drop-size distributions and coalescence frequencies for a wide range of energy input in flow vessels for a liquid-liquid system are also measured by a flash photomicrographic method and a modified dye-light transmittance technique. A schematic of the apparatus used for this purpose is described by Coulaloglou and Talvarides (1976). This apparatus measured flow rates of feed streams, oil (dispersed phase) drop-size distribution in the impeller and circulation regions, and dispersion light transmittance \bar{I}_0 , \bar{I}_a , and \bar{I}_b . Where \bar{I}_0 = initial average transmittance prior to dye addition, \bar{I}_a and \bar{I}_b = average light transmittance at steady state when the dispersed phase streams are not premixed and are premixed.

The photographic system consisted of a photomicrographic probe assembly, a light probe, and an electronic flash unit. Photographs of the dispersion were taken by using high-contrast Kodak film at locations 12.3 and 2.54 cm from the vessel top plate with dye-free dispersed phase. The light transmittance system included a light source, a photomultiplier, a photomultiplier housing, and a detection unit.

The average Sauter mean diameter of droplets is calculated from

$$d_{sv} = \frac{d_{sv}^i V^i + V^c d_{sv}^c}{V_T}, \quad (9.50)$$

where d_{sv}^i , d_{sv}^c , and the Sauter mean droplet diameters for the impeller and the circulation regimes V^i , V^c , and V_T are the volumes of the impeller region, the circulation region, and the total reactor, respectively. The coalescence frequency for the drop can be obtained from the relation

$$\frac{\log \frac{\bar{I}_a}{\bar{I}_0}}{\log \frac{\bar{I}_b}{\bar{I}_0}} = \frac{2 + \omega\tau}{2(1 - \phi_f)c_1\beta\bar{d}} \ln \left(1 + \frac{2(1 - \phi_f)c_1\beta\bar{d}}{2 + \omega\tau} \right), \quad (9.51)$$

where ϕ_f is the fraction of dispersed feed stream containing dye, τ the nominal residence time of continuous and dispersed feed, c_1 the dye concentration in one of the streams of dispersed phase (steady state), \bar{d} the average drop diameter, β the extinction coefficient of the dye, and \bar{w} the coalescence frequency.

H. SUMMARY

Experimental methods for the design parameters outlined here contain both physical and chemical techniques. The gas holdup can be accurately measured by the techniques described here except when pronounced foaming occurs. In the presence of foam, the gas holdup is best measured by photographic or pressure-drop methods. The bubble size can be measured by photographic methods; however, this method contains inherent inaccuracies, as outlined earlier.

The gas-liquid interfacial area measured from the physical techniques is generally about 35% higher than the one measured by the chemical technique. The chemical technique is generally more accurate than the physical technique. The reaction systems described in Table XXXI are reliable for the gas-liquid system. For gas-liquid-solid systems, the method is not reliable even when solids are inert, because of possible adsorptions of gas and/or liquid on the solid surface.

The physical methods for the measurement of $k_L a_L$ in batch, semi-batch, and continuous systems described earlier are accurate. The main limitation for the semi-batch and continuous systems is the availability of the analytical technique for the measurement of the gas concentration in the liquid phase. For gas-liquid-solid systems, Eq. (9.41) can be used to measure both k_g and k_L simultaneously. The liquid-solid mass-transfer coefficient can also be measured using the method of Ruether and Puri (1973) or the physical methods outlined earlier.

The mixing time is measured by the schlieren or chemical decolorization method. For short mixing times, consecutive dye reaction can be used. For viscous liquids, the decoloration or thermal methods are recommended. The RTD measurement requires a good choice of tracer.

Power measurements require the measurement of the torque and the rotational speed. The torque can be measured using a torsion shaft with strain gauges, electrically with eddy-current torque transducers, or mechanically with a swiveling motor. The speed of rotation can be measured using mechanical, electrical (photocell), or optical (stroboscope) instruments.

For liquid-liquid systems, drop-size distributions and coalescence frequencies can be measured by a flash photomicrographic method and a modified dye-light transmittance technique. Both of these methods are accurate

over a wide range of liquid-liquid systems. Both gas-liquid and liquid-liquid mass-transfer coefficients can also be measured using the gradientless contactor of either Levenspiel and Godfrey (1974) or Doraiswamy and Sharma (1984). The liquid-liquid mass-transfer coefficient can also be obtained using a chemical technique similar to the ones for gas-liquid systems. Some useful chemical reactions for this purpose are outlined by Laddha and Degaleesan (1978).

Heat-transfer parameters for mechanically agitated gas-liquid, gas-liquid-solid, and liquid-liquid systems are measured by the standard techniques described in any textbook on heat transfer.

I. FUTURE WORK

Future work on the development of experimental methods for the measurement of design parameters should include

- nonintrusive techniques for the measurements of phase holdups in both axial and radial directions;
- techniques (nonintrusive if possible) to measure RTD for organic liquid systems;
- simple techniques to measure the gas-liquid mass-transfer coefficient in multicomponent systems;
- further development of techniques to measure coalescence rate under a wide variety of reaction conditions; and
- development of techniques to carry out direct measurements of the gas-liquid interfacial area and gas-liquid and liquid-solid mass-transfer coefficients under actual reaction conditions, particularly at high temperature and pressure.

Nomenclature

A heat transfer area (m^2)	b paddle height (m)
A interfacial area (m^2) (Section VI)	(Section V)
a gap between two electrochemical plates (m)	b radius of entrance tube (m) (Section VIII)
a_L gas-liquid interfacial area (m^2/m^3)	C constant in Eq. (6.10)
a_L' interfacial area per unit liquid + gas volume (cm^{-1})	C^* solubility of gas ($\text{kg mol}/\text{m}^3$)
Ar Archimedes number (dimensionless)	C_1, C_2 constants in Table XX
B thickness of baffles (m)	C_L concentration of gas in the liquid phase ($\text{kg mol}/\text{m}^3$)
	C_p specific heat of fluid ($\text{J}/\text{kg } ^\circ\text{C}$)

d_b, d_b	bubble diameter (m)	H_i	height of impeller from the bottom of the vessel (m)
ΔC	concentration driving force (kg/m ³)	H_{icr}	value of H_i when vortex reaches the upper impeller blades (m)
D	molecular diffusivity (m ² /s)	H_L, H	liquid level (m)
Deb	Deborrah number (dimensionless)	K	consistency coefficient (Pa · s)
d_i	impeller diameter (m)	\bar{k}	thermal conductivity of fluid (J/m°C s)
d_p	particle diameter (m)	k	empirical coefficient in Eq. (8.1) depending on the optical properties of the system
d_{sv}	Sauter mean bubble or drop size (m)	k	fluid consistency index (Pa · s)
d_T	vessel diameter (m)	k'_s	rate constant for the first-order heterogeneous surface reaction (s ⁻¹)
E	enhancement factor (dimensionless)	k_g	gas-side mass-transfer coefficient (kmol/skN)
e	energy consumption per unit volume (kW/m ³)	$k_g a_L$	gas-side volumetric gas-liquid mass-transfer coefficient (1/s)
E^*	dimensionless efficiency number defined by Eq. (6.42)	k_L	gas-liquid mass-transfer coefficient (m/s)
E_i	enhancement factor for an instantaneous reaction (dimensionless)	$k_L a_L$	liquid-side volumetric gas-liquid mass-transfer coefficient (1/s)
E_z	axial dispersion coefficient in the liquid phase (m ² /s)	k_{mn}, k_R	reaction rate constants (1/s)
E_T	total energy input (kW)	k_s	liquid-solid mass-transfer coefficient (m/s)
f	functionality (dimensionless)	L	axial length (m)
Fr	Froude number (dimensionless)	L	dimensionless distance along the solid surface
Fr'	Froude number corresponding to N_m (dimensionless)	l	distance between two successive disks (m)
G	mass flux (kg/m ² s)	L, L_a	unaerated liquid height (m)
g, g_c	gravitational acceleration (m/s ²)	L_i	distance between two blades in an impeller (m)
Ga	Galileo number (dimensionless)	m	flow index behavior constant
Gr	Grashoff number (dimensionless)	m	power law index
H	height of liquid (m)	m, n	order of reaction
h	parameter defined by Eq. (8.3)	N	stirrer speed (r/s)
H^*	liquid height above the stirrer (m)	n	number of mixed tanks
h, h_0, h_i, h_c	convective heat transfer coefficients (J/m ² °C s)	n	number of moles
Ha	Hatta number (dimensionless)	N_A	aeration number (Q_g/Nd_i) or (u_g/Nd_i^3) (dimensionless)
H_B	height of baffles from the vessel bottom (m)		
He	Henry's law constant (Pa · m ³ /Kg mole)		

N_c	critical stirrer speed for gas entrapment (r/s)	$Q_g, Q_l, Q_{\mathcal{L}}$	gas and liquid flowrates (m^3/s)
N_{cY}	critical stirrer speed for onset of gas induction (r/s)	R	universal gas constant ($82.05 \text{ cm}^3 \text{ atm/gm mol K}$)
Ne	Newton or power number (dimensionless)	Re'	modified Reynolds number (dimensionless)
N_G	minimum impeller speed for surface aeration (in presence of gas) (r/s)	$Re, Re^*, Re_M, Re_F, Re_m, Re', Re_{eff}$	Reynolds numbers
N_m	minimum stirrer speed for complete dispersion (r/s)	r_{eff}	effective reaction rate ($\text{kg mol/m}^3 \cdot \text{s}$)
N_0	critical stirrer speed for homogeneous dispersion (r/s)	Sc	Schmidt number (dimensionless)
n_p	number of impeller paddles	\overline{Sh}	average Sherwood number along solid surface (dimensionless)
N_{Pr}, Pr	Prandtl number (dimensionless)	Sh	Sherwood number (dimensionless)
N_s	minimum impeller speed for surface aeration (in absence of gas) (r/s)	St	Stanton number (dimensionless)
n_s	number of stages	T	temperature (K)
Nu	Nusselt number (dimensionless)	t	time (s)
N_{vi}	viscosity ratio, μ_w/μ (dimensionless)	u	peripheral velocity (m/s)
\bar{P}	partial or total pressure (Pa)	u_{AM}	stirrer tip velocity (m/s)
\bar{P}_2	exit pressure (bars)	u_b	bubble velocity (m/s)
P	power input to the vessel (kW)	u_{bo}	terminal bubble rise velocity (m/s)
Pe	Peclet number (dimensionless)	u_g	gas velocity (m/s)
P_g	power input in the presence of gas (kW)	u_l	liquid velocity (m/s)
P_l	power input in the absence of gas (kW)	u_s	gas velocity at sparger exit (m/s)
Pr	Prandtl number (dimensionless)	V	volume of the reactor fluid (m^3)
P_T	total power input (Eq. (2.3)) (kW)	V, V_T	volume of reactor (liquid) (m^3)
Q	volumetric flow rate of gas (m^3/s)	V_c	circulation velocity (m/s)
q	liquid flow through the vessel (m^3/s)	V_f	velocity in feed pipe (m/s)
Q'	dimensionless pumping capacity (q'/Nd_1^3) (dimensionless)	V_G	volume of gas (m^3)
q'	pumping capacity of stirrer (m^3/s)	V_L, V_L'	liquid volume in the reactor (m^3)
q_g	gas flow rate or gas induction rate (m^3/s)	w	angular velocity of rotation (radians/second)
		w	mass velocity (kg/s)
		w'	weight of solids or catalyst (kg)
		We	Weber number (dimensionless)
		w_i	width of impeller (m)
		x	axial distance (m)
		x	mole fraction

Y	characteristic distance in Y direction	y	mole fraction (dimensionless)
Y	sorption number defined by Eq. (6.39) (dimensionless)	z	number of blades
		z	stoichiometric coefficient

Greek Letters

ε	phase holdup (dimensionless)	η	efficiency defined by Eq. (6.27)
$\langle \varepsilon_L \rangle$	radially average liquid holdup (dimensionless)	λ	parameter in Eq. (6.18)
$\bar{\eta}$	parameter defined by Eq. (6.36)	λ	shear rate (s^{-1})
α	thermal diffusivity (m^2/s)	λ	thermal conductivity ($J/m^\circ C s$)
δ	liquid film thickness (m)	μ	viscosity of fluid ($Pa \cdot s$)
$\mathcal{D}, \mathcal{D}_A$	molecular diffusivity of species (A) (m^2/S)	π	total pressure
$\mathcal{D}a$	Damköhler number (Eqs. (4.2) and (4.3)) (dimensionless)	θ	angular position
ΔP	pressure drop in absence of gas (Pa/m)	θ	mixing time (s)
ΔP_s	pressure drop in presence of gas (Pa/m)	$\bar{\theta}_T$	average residence time (s)
ΔP_{stat}	static pressure drop (bar)	ρ	density of fluid (kg/m^3)
$\Delta \rho$	difference in gas and liquid density (kg/m^3)	ρ_p	particle density (kg/m^3)
Δt	contact time of every film element (s)	σ	surface tension (N/m)
Φ	parameter defined by Eq. (3.39)	τ	shear stress (Pa)
ϕ	parameter defined by Eq. (9.37)	τ_p	response time (s)
Φ'	parameter defined by Eq. (3.42)	τ_p	dissipation energy (kW)
ϕ_v	volume fraction of solid (dimensionless)	ν	kinematic viscosity of fluid (m^2/s)
η	effectiveness factor	ω_c	critical rotational speed ($1/s$)
		ψ_s	weight fraction (dimensionless)
		μ	viscosity of fluid (Pa/s)
		μ_{app}	apparent viscosity of fluid (Pa/s)
		$\mu_{eff, v}$	effective attenuation coefficient of the liquid phase (cm^{-1})
		μ_v	attenuation coefficient of the liquid phase (cm^{-1})

Subscripts

1, 2	initial and final	a, app	apparent or ambient conditions
a	refers to air	avg	average value
A, B, C	refer to species A, B, and C		

c	continuous phase (generally liquid)	ℓ, L	refers to liquid
d	dispersed phase (generally gas)	n	refers to impeller
eff	effective	0	reference condition
F	fluid	p	particle
f	feed condition	s	refers to solid
g, G	refers to gas	s'	refers to slurry
G, H	species G and H	T	refers to vessel
′	initial condition	w	refer to water
		w	wall condition

Superscript

i gas-liquid interface

References

- Abichandani, J. S., Weiland, J. H., Shah, Y. T., and Cronauer, D. C., *AIChE J.* **30**, 295 (1984a).
 Abichandani, J. S., Weiland, J. H., Shah, Y. T., and Cronauer, D. C., *AIChE J.* **30**, 304 (1984b).
 Akita, K., and Yoshida, F., *Ind. Eng. Chem. Process Design and Dev.* **12**, 76 (1973).
 Albal, R. S., Shah, Y. T., Schumpe, A., and Carr, N. L., *Chem. Eng. J.* **27**, 61 (1983).
 Albal, R. S., Carr, N. L., Shah, Y. T., and Bell, A., *Chem. Eng. Sci.* **39**(5), 905 (1984).
 Alcorn, W. R., Elliot, G. E., and Cullo, L. A., *Prepr. Pap.—Am. Chem. Soc. Div. Fuel Chem.* **23**(1), 11 (1974).
 Alper, E., Wichtendahl, T., and Deckwer, W. D., *Chem. Eng. Sci.* **35**, 217 (1980).
 Andrews, S. P. S., *Trans. Inst. of Chem. Engrs.* **60**, 3 (1982).
 Arbiter, N., Harris, C. C., and Yap, R. F., *Trans. AIME* **244**, 134 (1969).
 Ashley, M. J. and Haselden, G. G., *Trans. Inst. of Chem. Engrs.* **50**, T119 (1972).
 Aunins, J. G., Woodson, B. A., Hale, T. K., and Wang, D. I. C., "Effect of Paddle Geometry and Power Input and Mass Transfer in Small Scale Animal Cell Culture Vessels," *Biotechnology and Bioengineering* **34**, 1127–1132 (1989).
 Baird, M. H. I., Glovne, A. R., and Meghani, M. A. N., *Can. J. Chem. Eng.* **46**, 249 (1968).
 Baldi, G., "Hydrodynamics and Gas-Liquid Mass Transfer in Stirred Slurry Reactors," Ch. 14 in "Multiphase Chemical Reactors; Theory, Design, Scale-up" (A. Gianetto and P. L. Silveston, eds.). Hemisphere Publ. Co., New York, 1986.
 Baldi, G., Conti, R., and Alaria, E., *Chem. Eng. Sci.* **33**, 21 (1978).
 Baldi, G., Conti, R., and Gianetto, A., *AIChE J.* **27**(6), 1017 (1981).
 Barrett, D., *Trans. Inst. Chem. Eng.* **49**, 80 (1971).
 Bates, R. L., Fondy, P. L., and Corpstein, R. R., *Inc. Eng. Chem. Process Design Dev.* **2**, 310 (1963).
 Bates, R. L., Fondy, P. L., and Fenic, J. G., *Mixing, Vol. I* [2]. Academic Press, New York, 1966.
 Beckner, J. L., and Smith, J. M., *Trans. Inst. Chem. Engrs.* **44**, T236 (1965).
 Beenackers, A. C. M. "Chemical Reaction Engineering—Houston," ACS Symposium Series 65 (V. W. Weekman and D. Luss, eds.), p. 327. ACS, Washington, D.C., 1978.
 Belevi, H., Bourne, J. R., and Rys, P., *Chem. Eng. Sci.* **36**, 1649 (1981).

- Bender, E., Berger, R., Leuckel, W., and Wolf, D., *Chem. Eng. Tech.* **51**, 192 (1979).
- Bennett, C. O., Cutlip, M. B., and Yang, C. C., *Chem. Eng. Sci.* **27**, 2255 (1972).
- Bern, L., Lidefelt, J. O., and Schoon, N. H., *J. Am. Oil Chem. Soc.* **53**, 463 (1976).
- Berty, J. M., *Chem. Eng. Prog.* **70**(5), 78 (1974).
- Berty, J. M., *Catalysis Review—Science and Engineering* **20**, 75 (1979).
- Bhattacharjee, S., Tierney, J. W., and Shah, Y. T., *Ind. Eng. Chem. Process Design and Dev.* **25**, 117 (1986).
- Bhavaraju, S. M., Russell, W. F., and Blanch, H. W., *AIChE J.* **24**, 454 (1978).
- Bibaud, R. E., and Treybal, R. E., *AIChE J.* **12**, 472 (1966).
- Biggs, R. D., *AIChE J.* **9**, 636 (1963).
- Blasinski, H., and Puc, K., *Int. Chem. Eng.* **15**, 73 (1975).
- Blenke, H., *Chem. Ing. Tech.* **39**, 109 (1967).
- Boon-Long, S., Laguerie, C., and Coudere, J. P., *Chem. Eng. Sci.* **33**, 813 (1978).
- Bourne, J. R., Kozicki, F., and Rys, P., *Chem. Eng. Sci.* **36**, 1643 (1981a).
- Bourne, J. R., Kozicki, F., Moergelli, V., and Rys, P., *Chem. Eng. Sci.* **36**, 1655 (1981b).
- Brauer, H., *Chem. Eng. (Rugby, England)* **381**, 224 (1982).
- Brauer, H., and Sucker, D., *Ger. Chem. Eng.* **2**, 77–86 (1979).
- Brennan, D. J., and Lehrer, I. H., *Trans. Inst. of Chem. Engrs.* **54**, 139 (1976).
- Brisk, M. L., Day, R. L., Jones, M., and Warren, J. B., *Trans. Inst. Chem. Eng.* **46**, 3 (1968).
- Brown, C. E., Ph.D. Thesis, University of Connecticut, 1969.
- Bruijn, W., Van't Reit, K., and Smith, J. M., *Trans. Inst. Chem. Engrs.* **52**, 88 (1974).
- Bruxelman, M., *Proc. Int. Symp. on Mixing, 21st–24th February, Mons, Belgium* (1978).
- Bryant, J., and Sadeghzadeh, S., *Proc. 3rd European Conf. on Mixing, April 4th–6th, York, U.K.* (1979).
- Burgess, J. M., and Calderbank, P. H., *Chem. Eng. Sci.* **30**, 743 and 1107 (1975).
- Calderbank, P. H., *Trans. Inst. Chem. Engrs.* **36**, 443 (1958).
- Calderbank, P. H., "Mass Transfer" in "Mixing: Theory and Practice" (V. W. Uhi and I. B. Gray, eds.), Academic Press, New York, 1967.
- Calderbank, P. H., and Moo-Young, M., *Chem. Eng. Sci.* **16**, 39 (1961).
- Calderbank, P. H., and Rennie, J., *Trans. Inst. Chem. Eng.* **40**, 3 (1962).
- Caldwell, L., *Appl. Catalysis* **8**, 199 (1983).
- Cameron, J. F., "Fluid Density Measurements in Enclosed Systems," *Int. Conf. on Radio Isotopes in Scientific Research*, **1**, 426 (1957).
- Carberry, J. J., *Ind. Eng. Chem.* **56**, 39 (1964).
- Carberry, J. J., Tipnis, P., and Schmitz, R. A., *Chem. Technology*, p. 316 (May, 1985).
- Carra, S., and Morbidelli, M., "Gas-Liquid Reactors," Ch. 9 in "Chemical Reaction and Reactor Engineering" (J. J. Carberry and A. Varma, ed.), p. 545. Marcel Dekker Inc., New York, 1987.
- Cassano, A. E., Alfano, O. M., and Romero, R. L., "Photoreactor Engineering: Analysis and Design," Ch. 8 in "Concepts and Design of Chemical Reactors" (S. Whitaker and A. E. Cassano, eds.), Vol. 3 (J. J. Ulbrecht, ed.), Gordon and Breach Science Publishers, New York (1986).
- Chandrasekharan, K., and Calderbank, P. H., *Chem. Eng. Sci.* **36**, 819 (1981).
- Chandrasekharan, K., and Sharma, M. M., *Chem. Eng. Sci.* **32**, 669 (1977).
- Chapman, C. M., Nienow, A. W., and Middleton, J. C., *Trans. Inst. Chem. Engrs.* **59**, 134 (1981).
- Chapman, C. M., Gilbilaro, L. G., and Nienow, A. W., *Chem. Eng. Sci.* **37**, 891 (1982).
- Charpentier, J. C., "Mass Transfer Rates in Gas-Liquid Absorbers and Reactors" in (Editors) "Advances in Chemical Engineering," Vol. II, (Drew and Vermeulen, eds.), Academic Press, New York, 1981.
- Chaudhari, R. V., and Ramachandran, P. A., *AIChE J.* **26**, 177 (1980).
- Chaudhari, R. V., Shah, Y. T., and Foster, N. R., *Catal. Rev.—Sci. and Eng.* **28**(4), 431 (1986).

- Cooper, R. G., and Wolf, D., *Can. J. Chem. Eng.* **46**, 94 (1968).
- Costa, E. C., and Smith, J. M., *AIChE J.* **17**, 947 (1971).
- Coulaloglou, C. A., and Talvarides, L. L., *AIChE J.* **22**(2), 289 (1976).
- Danckwerts, P. V., *Chem. Eng. Sci.* **7**, 116 (1957).
- Danckwerts, P. V., and Alper, E., *Trans. Inst. Chem. Eng.* **53**, 34 (1975).
- Danckwerts, P. V., and Kennedy, A. M., *Trans. Inst. of Chem. Engrs.* **32**, 553 (1954).
- Davidson, J. F., *Trans. Inst. Chem. Engrs. L.* **37**, 131 (1959).
- De Barnardes, E. R., Claria, M. A., and Cassono, A. E., "Analysis and Design of Photoreactors," Ch. 13 in "Chemical Reaction and Reactor Engineering" (J. J. Carberry, and A. Varma, eds.), Marcel Dekker Inc., New York, 1987.
- Deimling, A., Karandikar, B. M., Shah, Y. T., and Carr, N. L., *Chem. Eng. J.* **29** (3), 127 (1985).
- Dierendonck, L. L., Fortuin, J. M. F., and Vanderbos, D., *Proc. 4th Eur. Symp. Chem. Reaction Engineering, Sept. 9-11, Brussels, Belgium* (1968).
- Doraiswamy, L. K., and Sharma, M. M. "Heterogeneous Reactions: Analysis, Examples and Reactor Design," Vols. 1 and 2. John Wiley & Sons, New York, 1984.
- Doraiswamy, L. K., and Tajbl, D. G., *Catalysis Review—Science and Engineering* **10**, 177 (1974).
- Dudukovic, M., Chemical Reaction Engineering Laboratory, June 1, 1988–May 31, 1989, School of Engineering and Applied Science, Washington University, St. Louis, Missouri (1989).
- Edney, H. G., and Edwards, M. F., *Trans. Inst. Chem. Engrs.* **54**, 160 (1976).
- Edwards, D.C., M.Sc. Thesis, Dept. of Chemical Engineering, The Ohio State University, Columbus, Ohio (1961).
- Edwards, M. F., and Wilkinson, W. L., *Chem. Engr. (London)* No. 264, 310–319 (1972).
- Einenkel, W. D., *VDI—Forschungsh.*, 595 (1977).
- Einenkel, W. D., *VT* **11**, 9 (1979).
- Einsele, A., and Finn, R. K., *Ind. Eng. Chem. Process Design and Dev.* **19**, 600 (1980).
- Elstner, F., and Onken, V., *Ger. Chem. Eng.* **4**, 84 (1981).
- Endesz, K., Ringer, D., and Mazumdar, A. S. "Transport Processes in Vibro-Fluidized beds," in "Transport in Fluidized Particle Systems" (L. K. Doraiswamy and A. S. Mazumdar, eds.), p. 317. Elsevier Science Publishers B. V., The Netherlands, 1989.
- Engasser, J. M., *Chem. Eng. Sci.* **43**, 1739 (1988).
- Erickson, L. E., and Stephanopoulos, G., "Biological Reactors," in "Chemical Reaction and Reactor Engineering" J. J. Carberry and A. Varma, (eds.), Marcel Dekker, Inc., New York, 1987.
- Euzen, J. P., Trambouze, P., and Van Landeghem, H., in "Chemical Reaction Engineering—Houston (D. Luss and V. W. Weekman, eds.), ACS Symposium Series, 153 (1978).
- Exxon Research and Development Co., Linden, New Jersey, personal communication (1989).
- Falch, E. A., and Gaden, E. L., *Biotech. Bioengineering* **11**, 927 (1969).
- Faust, V., and Sittig, W., *Adv. Biochem. Eng.* **17**, 63 (1980).
- Feres, V., and Roubicek, R., U.S. Patent No. 4, 717, 669 (Jan. 5, 1988).
- Ford, F. E., and Perlmutter, D. D., *Chem. Eng. Sci.* **19**, 371 (1964).
- Fort, I., Podivinska, J., and Baloun, R., *Collect. Czech. Chem. Commun.* **34**, 959 (1969).
- Foster, N. R., Wilson, M. A., Weiss, R. G., and Clark, K. N., *Ind. Eng. Chem. Prod. Res. and Development* **22**, 478 (1983).
- Foster, N. R., Weiss, R. G., Young, M. M., and Clark, K. N., *Fuel* **63**, 66 (1984a).
- Foster, N. R., Young, M. M., Clark, K. N., and Weiss, R. G., *Fuel* **63**, 716 (1984b).
- Furusawa, T., and Smith, J. M., *Ind. Eng. Chem. Fundamentals* **12**, 197 and 360 (1973).
- Gal-Or, B., and Resnick, W., *Ind. Eng. Chem. Process Design and Development* **5**, 15 (1966).
- Ganguli, K. L., Chem. Eng. Thesis, Technische Hogeschool Delft, Delft, The Netherlands (1975).
- Gelain, C., *Chim. Ind. Genie Chim.* **102**, 984 (1969).
- Geranin, V. I., Kirkchi, V. M., and Minachev, K. M., *Kinet. Katal.* **8**, 605 (1967).

- Germain, A., Doctoral Thesis, University de Liege, Belgium (1973).
- Gerrens, M., "Flow to Select Polymerization Reactors," Part II, *Chemtech*, p. 434 (July, 1982).
- Govindan, T. S., and Quinn, J. A., *AIChE J.* **10**, 35 (1964).
- Gramlich, H., and Lamade, S., *Chem. Ing. Tech.* **45**(3), 116 (1973).
- Grau, R. J., Cassano, A. E., and Baltanas, M. A., *Ind. Eng. Chem. Res.* **26**, 18 (1987).
- Gray, D. J., Treybal, R. E., and Barnett, S. M., *AIChE J.* **28**, 195 (1982).
- Gray, J. B. "Batch Mixing of Viscous Liquids," *Chem. Eng. Progr.* **59**, 55 (1963).
- Haering, E. R., and Syverson, A., *J. Catalysis* **32**(3), 396–414 (1974).
- Halladay, J. B., and Mrazek, R. V., *J. Catalysis* **28**, 221 (1973).
- Hanhart, J., Kraemers, H., and Westerterp, K. R., *Chem. Eng. Sci.* **18**, 503 (1963).
- Harriott, P., *AIChE J.* **8**, 93 (1962).
- Hassan, I. T. M., and Robinson, C. W., *AIChE J.* **23**, 48 (1977).
- Hassan, I. T. M., and Robinson, C. W., *Chem. Eng. Sci.* **35**, 1277 (1980a).
- Hassan, I. T. M., and Robinson, C. W., *Can. J. Chem. Eng.* **58**, 198 (1980b).
- Heinekin, F. G., *Biotech, and Bioengineering* **12**, 145 (1970).
- Heinekin, F. G., *Biotech, and Bioengineering* **13**, 599 (1971).
- Henzler, H. J., *VDI—Forschungsh.* 587 (1978).
- Henzler, H. J., *Chem. Ing. Tech.* **52**, 643 (1980).
- Henzler, H. J., *Chem. Ing. Tech.* **54**(5), 461–476 (1982).
- Henzler, H. J., and Kauling, J., *Proc. 5th European Conf. on Mixing, Würzburg, Germany* (June 10–12, 1985).
- Herringe, R. A., *Proc. 3rd Eur. Conf. on Mixing, April 4–6, York, United Kingdom* (1979).
- Hicks, R. W., and Gates, L. E., *Chem. Eng.*, p. 141 (July 19, 1976).
- Hinze, J. O., *AIChE J.* **1**, 189 (1955).
- Hixon, A. W., and Baum, S. J., *Inc. Eng. Chem.* **33**(4), 478 (1941).
- Hocker, H., and Langer, G., *Rheol. Acta* **16**, 412 (1962).
- Hocker, H., Langer, G., and Werner, V., *Ger. Chem. Eng.* **4**, 51 (1981).
- Hofmann, H., "Reaction Engineering Problems in Slurry Reactor" in "Mass Transfer with Chemical Reaction in Multiphase Systems," Vol. II (E. Alper, ed.) NATO ASI Series, Martinus Nijhoff Publishers, The Hague, 1983.
- Holmes, D. B., Voncken, R. M., and Decker, J. A., *Chem. Eng. Sci.* **20**, 264 (1964).
- Hoogendoorn, C. J., and Den Hartog, A. P., *Chem. Eng. Sci.* **22**, 1689 (1967).
- Hovas, G., Deak, A., and Swinsky, J., *Chem. Eng. J.* **23**, 161 (1982).
- Hubbard, D. W., Wierenga, M. K., and Lehto, J. A., "Gas–Liquid Mass Transfer and Scale-up for Reactors Continuing non-Newtonian Liquids," a paper presented at the AIChE meeting, San Francisco, California (Nov. 5–10, 1989).
- Hughmark, G. A., *Ind. Eng. Chem. Process Design and Dev.* **19**, 638 (1980).
- Jansson, R. E. W., *Electrochimica Acta.* **23**, 1345 (1978).
- Jansson, R. E. W., Marshall, R. J., and Rizzo, J. E., *J. Appl. Electrochem.* **8**, 281 (1978).
- Jeffreys, G. V., and Mumford, C. J., *Process Eng.* **11**, 73 (1974).
- Jensen, W. P., and Talton, R. T., Jr., *Design of Viscous-Material Mixers*, Paper 10.8, AIChE-1, Chem. E. Joint Meeting, London (1965).
- Joosten, G. E. H., Schilder, J. G. M., and Broere, A. M., *Trans. Inst. of Chem. Engrs.* **55**, 20 (1977a).
- Joosten, G. E. H., Schilder, J. G. M., and Jansen, J. J., *Chem. Eng. Sci.* **32**, 563 (1977b).
- Joshi, J. B., *Chem. Eng. Commun.* **5**, 213 (1980).
- Joshi, J. B., and Kale, D. D., *Chem. Eng. Commun.* **3**, 15 (1979).
- Joshi, J. B., and Sharma, M. M., *Trans. Inst. Chem. Eng.* **54**, 42 (1976).
- Joshi, J. B., and Sharma, M. M., *Can. J. Chem. Eng.* **55**, 683 (1977).
- Joshi, J. B., Shah, Y. T., Sharma, M. M., Singh, C. P. P., Ally, M., and Klinzing, G. E., *Chem. Eng. Commun.* **6**(4–5), 257 (1980).

- Joshi, J. B., Pandit, A. B., and Sharma, M. M., *Chem. Eng. Sci.* **37**, 813 (1982).
- Joshi, J. B., Shah, Y. T., and Parulekar, S. J., *Indian Chemical Engineer XXVII* (2), 3–37 (1985).
- Judat, H., *Fortschr. Verfahrenstechnik* **B15**, 141–159 (1977).
- Judat, H., *Ger. Chem. Eng.* (English Translation) **5**, 357–363 (1982).
- Juvekar, V. A., Ph.D. (Tech.) Thesis, University of Bombay, India (1976).
- Karandikar, B. M., and Kale, D. D., personal communication (1981).
- Karandikar, B. M., Shah, Y. T., Morsi, B. I., and Carr, N. L., *Chem. Eng. J.* **33**(3), 157 (1986).
- Kargi, F. and Rosenberg, M. Z., *Biotechnology Progress* **3**(1), 1 (March, 1987).
- Karr, A. E., and Lo, T. C., *Chem. Eng. Progress* **72** (11), 68 (1976).
- Kato, K., Shiozawa, Y., Yamada, A., Nishida, M. K., and Noguchi, M., *Agr. Biol. Chem.* **36**(6), 899–902 (1972).
- Kawecki, W., Reith, T., Van Heuven, J. W., and Beek, W. J., *Chem. Eng. Sci.* **22**, 1519 (1967).
- Keller, R. M., M.Sc. Thesis, Dept of Chemical Engineering, The Ohio State University, Columbus, Ohio (1962).
- Kern, W., *RCA Review* **39**, 525 (1968).
- Kern, W., *Solid State Technol.* **18**, 25 (1975).
- Kim, J. H., Sudol, E. D., El-Aasser, M. S., and Vanderhoff, J. W., *Chem. Eng. Sci.* **43**(8), 2025 (1988).
- Kneule, F., and Weinspach, P. M., *Verfahrenstechnik (Mainz)* **1**(12), 531 (1967).
- Koen, E., and Pingaud, B., *Proc. 2nd European Conf. on Mixing, Paper F5, March 30–April 1, Cambridge, United Kingdom* (1977).
- Koetsier, W. T., and Thoenes, D., *Proc. Symp. on Chem. Reaction Eng., Paper B3-15, May, Amsterdam, The Netherlands* (1972).
- Kolar, V., *Coll. Cz. Chem. Commun.* **32**, 526 (1967).
- Komiyama, H., and Smith, J. M., *AIChE J.* **21**, 664 (1975).
- Komori, S., and Murakami, Y., *AIChE J.* **34**, 932 (1988).
- Kuriyama et al., *J. Chem. Eng. Japan* **14**(4), 323 (1981).
- Kurpiers, P., Steiff, A., and Weinspach, P. M., *Chem. Ing. Tech.* **57**(1), 62–63 (1985).
- Kurten, H., and Zehner, P., *Ger. Chem. Eng.* **2**, 220 (1979).
- Kurz, W. G. W., and Constabel, F., "Plant Cell Suspension Cultures and Biosynthetic Potential," in *"Microbial Technology, (H. J. Peppelerand, and D. Perlman, eds.), Vol. 1, pp. 389–416. Academic Press, New York, 1979.*
- Laddha, G. S., and Degaleesan, T. E., "Transport Phenomena in Liquid Extraction," Tata McGraw-Hill Publ. Co. Ltd., New Delhi, 1978.
- Laddha, G. S., Degaleesan, T. E., and Kannappan, R., *Can. J. Chem. Eng.* **56**, 137 (1968).
- Laity, D. S., and Treybal, R. E., *AIChE J.* **3**(2), 176 (1957).
- Lakshmanan, R., and Rouleau, D., *Can. J. Chem. Eng.* **47**, 45 (1969).
- Lakshmanan, R., and Rouleau, D., J., *Appl. Chem.* **20**, 213 (1970).
- Lamade, S., *Verfahrenstechnik (Mainz)* **11**(2), 72 (1977).
- Landau, J., and Houlihan, R., *Can. J. Chem. Eng.* **52**, 334 (1974).
- Landau, J., Boyle, J., Gomma, H. G., and Al Taweel, A. M., *Can. J. Chem. Eng.* **55**, 13 (1977a).
- Landau, J., Goma, H. G., and Al Taweel, A. M., *Trans. Inst. Chem. Engrs.* **55**, 212 (1977b).
- Le Lan, A., and Angelino, H., *Chem. Eng. Sci.* **27**, 1969 (1972).
- Lee, J. C., Ali, S. S., and Tasakorn, P., *4th BHRA Eur. Conf. on Mixing, 27th–29th April, Noordwijkerhout, The Netherlands* (1982).
- Lee, S. S., and Wang, D. I. C., "The Effects of Mixing on Highly Viscous Xanthan Gum Fermentation," paper presented at the AIChE meeting, San Francisco (Nov. 5–10, 1989).
- Levenspiel, O., and Godfrey, J. H., *Chem. Eng. Sci.* **29**, 1723 (1974).
- Levins, D. M., and Glastonbury, J. R., *Trans. Inst. Chem. Engrs.* **50**, 32 (1972).
- Lim, B. Y., and Yoo, Y. J., "Mixing Effects in the Fermentation of Xanthan Gum," paper presented at the AIChE meeting, San Francisco (Nov. 5–10, 1989).

- Lindsay, K., and Yeoman, M. M., *J. Exp. Botany* **34**, 1055–1065 (1983).
- Linek, V., *Chem. Eng. Sci.* **27**, 627 (1972).
- Linek, V., and Mayrhoferova, J., *Chem. Eng. Sci.* **24**, 481 (1969).
- Linek, V., Mayrhoferova, J., and Mosnerova, J., *Chem. Eng. Sci.* **25**, 1033 (1970).
- Linek, V., Sobotka, M., and Prokop, A., *Biotech. and Bioeng. Symp.* **4**, 429 (1973).
- Loiseau, B., Midoux, N., and Charpentier, J. C., *AIChE J.* **23**, 931 (1977).
- Lombrana, Z. I., Varona, F., Mijangos, F., Pardo, A., and Diaz, M., *Preprints of 5th Int. Conf. on Solid Wastes, Sludges and Residual Materials: Characterization, Technology, Management, Public Policy*, p. 353, Rome, Italy (1989).
- Long, R., Roubicek, R., Creed, J., and Holbrook, S., *Bioprocess Engineering* **3**, 73–77 (1988).
- Loucaides, R., and McManamey, W. J., *Chem. Eng. Sci.* **28**, 2165 (1973).
- Luong, H. T., and Volesky, B., *AIChE J.* **25**, 893 (1979).
- Macarus, D. P., and Syverson, A., *Inc. Eng. Chem. Process Design and Dev.* **5**, 397 (1966).
- Maerteleire, E. De., *Chem. Eng. Sci.* **33**, 1107 (1978).
- Magelli, F., Fajner, D., and Pasquali, G., *Chem. Eng. Sci.* **41**, 2431 (1986).
- Mahoney, J. A., Robinson, K. K., and Myers, E. C., *Chem. Tech.* **8**, 758 (1978).
- Mann, U., Zinzuwadia, H., and Forester, C. C., "Enhanced Performance of Agitated Gas–Liquid Reactors," paper presented at the AIChE meeting, San Francisco (Nov. 8, 1989).
- Manor, Y., and Schmitz, R. A., *Ind. Eng. Chem. Fundamentals* **23**, 243 (1984).
- Marr, R., *Chem. Eng. Tech.* **50**, 337 (1978).
- Martin, G. Q., *Ind. Eng. Chem. Process Design & Development* **11**, 397 (1972).
- Maruoka, Y., Dissertation (Technische Universität Berlin), Federal Republic of Germany (1982).
- Matsumura, M., Masunga, H., and Kobayashi, J., *J. Ferm. Tech.* **55**, 338 (1977).
- Matsumura, M., Masunga, H., Haraya, K., and Kobayashi, J., *J. Ferm. Tech.* **56**, 128 (1978).
- Mazumdar, A. S., "Frontiers in Chemical Reaction Engineering," Vol. II (L. K. Doraiswamy and R. A. Mashelkar, eds.), p. 419. Wiley Eastern Ltd., New Delhi, 1984.
- McManamey, W. J., *Trans. Inst. Chem. Engrs.* **58**, 271 (1980).
- Mehta, V. D., Ph.D. (Tech.) Thesis, University of Bombay, India (1970).
- Mehta, V. D., and Sharma, M. M., *Chem. Eng. Sci.* **26**, 461 (1971).
- Mersmann, A., personal communication (1988).
- Mersmann, A., and Grossmann, H., *Chem. Ing. Tech.* **52**(8), 621 (1980).
- Mersmann, A. et al., *Chem. Ing. Tech.* **47**(23), 953 (1975).
- Metzner, A. B., and Otto, R. E., *AIChE J.* **3**(1), 3 (1957).
- Michel, B. I., and Miller, S. A., *AIChE J.* **8**, 262 (1962).
- Middleman, S., "Fundamentals of Polymer Processing." McGraw-Hill, New York, 1977.
- Middleton, J. C., *Proc. 3rd Eur. Conf. on Mixing, April 4th–6th, York, United Kingdom* (1979).
- Midoux, N., and Charpentier, J. C., *Proc. 3rd Eur. Conf. on Mixing, April 4th–6th, York, United Kingdom* (1979).
- Miller, D. N., *AIChE J.* **20**, 448 (1974).
- Miller, D. N., *Ind. Eng. Chem. Process Design and Dev.* **10**, 365 (1971).
- Miller, T., "Kinetics of Co-Processing," M. S. Thesis, University of Pittsburgh, Pittsburgh, Pennsylvania (1987).
- Molerus, O., and Latzel, W., *Chem. Eng. Sci.* **42**(6), 1431 (1987).
- Moo-Young, M., "Design of Multiphase Reactors for Biological Processes," Ch. 18 in "Multiphase Chemical Reactors: Theory, Design, Scale-up" (A. Gianetto and P. L. Silveston, eds.). Hemisphere Publ. Co., Washington, D.C., 1986.
- Moo-Young, M., Binder, A., and Van Dedem, G., *Biotech. Bioengineering* **21**, 593 (1979).
- Moser, A., *Biotech. Bioengineering, Symp. Series* **4**, 399 (1973).
- Mukhopadhyay, S. N., and Ghose, T. K., *J. Ferm. Technol.* **54**, 406 (1976).
- Muller, W. and Rysall, D., *Chem. Ing. Tech.* **58**, (6), 508 (1986).

- Mumford, C. J., and Thomas, R. J., *Process Eng.* **12**, 54, 57 (1972).
- Murakami, Y., Fujimoto, K., Kakimoto, S., and Sekino, M., *J. Chem. Eng. Japan* **5**(3) 257 (1972).
- Mützenburg, A. B., *Chem. Eng.* **72**(19), 175 (1965).
- Nagata, S., "Mixing." John Wiley and Sons, New York, 1975.
- Nagata, S., Yokogama, T., and Yaragimoto, M., *J. Chem. Eng. Japan* **21**, 278 (1957).
- Nagel, O. H., Kürten, H., and Hegner, B., *Chem. Ing. Tech.* **45**, 913 (1973).
- Nagel, O. H., Hegner, B., and Kürten, H., *Chem. Ing. Tech.* **50**, 934 (1978).
- Narayanan, S., Bhatia, V. K., Guha, D. K., and Rao, M. N., *Chem. Eng. Sci.* **24**, 223 (1969).
- Newman, A. B., *AIChE Trans.* **27**, 310 (1931).
- Nienow, A. W., *Chem. Eng. Sci.* **23**, 1453 (1968).
- Nienow, A. W., *Chem. Eng. J.* **9**, 153 (1975).
- Nienow, A. W., Wisdom, D. J., and Middleton, J. C., *Proc. 2nd Eur. Conf. on Mixing, Paper F2, March 30th–April 1st, Cambridge, United Kingdom* (1977).
- Niiyama, H., Vemura, Y., and Echigoya, E., *J. Chem. Eng. Japan* **11**, 465 (1978).
- Nijiribeako, A., Silveston, P. L., and Hudgins, R. R., *Preprints of the 5th Canadian Symposium on Catalysis*, p. 170 (1977).
- Nishikawa, M., Nakamura, M., and Hashimoto, K., *J. Chem. Eng. Japan* **14**, 227 (1981).
- Nishikawa, M., Nishioka, S., and Kayama, T., *J. Chem. Eng. Japan* **17**(5), 541 (1984).
- Norwood, K. W., and Metzner, A. B., *AIChE J.* **6**, 432 (1960).
- Oguz, H., and Brehm, A., *Chem. Eng. Sci.* **43**, 1416 (1988).
- Oguz, H., Brehm, A., and Deckwer, W. D., *Chem. Eng. Sci.* **42**, 1815 (1987).
- Oishi, T., Yamaguchi, I., and Nagata, S., *Mem. Factly. Engng., Kyoto Univ.* **27**, 317 (1965).
- Oldshue, J. Y., *Chem. Eng. Progress* **76**, 60 (1980).
- Oldshue, J. Y., "Fluid Mixing Technology." McGraw-Hill Publications, New York, 1983.
- Oldshue, J. Y., Mechler, D. O., and Grinnell, D. W., *Chem. Eng. Progr.*, 68 (May, 1982).
- Olney, R. B., *AIChE J.* **10**, 827 (1964).
- Opara, M., *Verfahrenstechnik (Mainze)* **9**(9), 446 (1975).
- Otake, T., Tone, S., Higuchi, K., and Nakao, K., *Kagaku Ronbunshu* **7**, 57 (1981).
- Oyama, Y., and Endoh, K., *Chem. Eng. Tokyo* **19**, 2 (1955).
- Paca, J., Etter, P., and Greg, V., *J. Appl. Chem. Biotech.* **26**, 309 (1976).
- Pal, S. K., Sharma, M. M., and Juvekar, V. A., *Chem. Eng. Sci.* **37**, 327 (1982).
- Pavlushchenko, Y., *J. Appl. Chem. USSR* **30**, 1235 (1957).
- Pawlowski, J., and Zlokarnik, M., *Chem. Ing. Tech.* **44**(16), 982 (1972).
- Penny, W. R., and Bell, K. J., *Ind. Eng. Chem.* **59**(4), 47 (1967).
- Perez, J. F., and Sandall, O. C., *AIChE J.* **20**(4), 770 (1974).
- Perry, R. H., and Chilton, C. H., "Chemical Engineers Handbook," 5th Ed. McGraw-Hill, New York, 1973.
- Platzer, N., *Ind. Eng. Chem.* **62**, 6 (1970).
- Poggemann, R., Steiff, A., and Weinspach, P. M., *Ger. Chem. Eng. (Engl. Translation)* **3**, 167–174 (1980).
- Pohorecki, R., and Baldyga, J., *Chem. Eng. Sci.* **43**, 1949 (1988).
- Porter, K. E., King, M. B., and Vershney, K. C., *Trans. Inst. Chem. Eng.* **44**, T274 (1966).
- Prause, J. J., *Plastic Technology*, No. 2 **14**, 29 (1968).
- Prochazka, J., and Landau, J., *Coll. Czech. Chem. Commun.* **26**, 2961 (1961).
- Ramachandran, P. A., and Choudhary, R. V., "Three Phase Catalytic Reactors." Gordon and Breach, New York, 1983.
- Ramanarayanan, K. A., and Sharma, M. M., *Ind. Eng. Chem. Process Design and Dev.* **21**, 355 (1982).
- Ramaswamy, V., and Doraiswamy, L. K., unpublished material, National Chemical Laboratory, Poona, India (1973).

- Ranade, V. R., and Ulbrecht, J. J., *Proc. 2nd Eur. Conf. on Mixing, March 30–April 1, Cambridge, United Kingdom* (1977).
- Rao, K. B., and Murthy, P. S., *Ind. Eng. Chem. Process Design and Dev.* **12**, 190 (1973).
- Ravekar, D. D., and Kale, D. D., *Chem. Eng. Sci.* **36**, 399 (1981).
- Regenass, W., "Thermal and Kinetic Design Data from a Bench Scale Heat Flow Calorimeter," In "Chemical Reaction Engineering—Houston," ACS Symposium Series (D. Luss and V. W. Weekman, eds.), p. 37 (1978).
- Reher, E. O., *Techn. (Leipzig)* **21**(1), 14 (1969).
- Reichert, K. H. and Moritz, H. V., "Continuous Polymerization of Vinyl Acetate in Suspension," *J. Applied Polymer Science, Applied Polymer Symposium* **36**, 151–164 (1981).
- Reissinger, K. M., and Schröter, J., *Chem. Eng.* **85**(25), 109 (1978).
- Reith, T., *British Chem. Eng.* **15**, 1559 (1970).
- Reith, T. and Beek, W., *Proc. 4th European Symp. Chem. Reaction Eng., 9th, 11th Sept., Brussels, Belgium* (1968).
- Reith, T., Renken, S., and Israel, B. A., *Chem. Eng. Sci.* **23**, 619 (1968).
- Relyea, D. L., and Perlmutter, D. D., *Ind. Eng. Chem. Process Design and Dev.* **7**, 261 (1968).
- Rieger, F., Dittl, P., and Novak, V., *Chem. Eng. Sci.* **34**, 393–403 (1979).
- Rod, V., *Proc. 4th Int'l 6th European Symp. Chem. Reaction Eng.*, p. 271 (1976).
- Rosenbaum, J. B., George, D. R., and May, J. T., U. S. Department of Interior, Bureau of Mines Information Circular 8502 (1971).
- Ruether, J. A., and Puri, P. S., *Can. J. Chem. Eng.* **51**, 545 (1973).
- Rushton, J. H., and Bimbinet, J. I., *Can. J. Chem. Eng.* **46**, 16 (1968).
- Rushton, J. H., Costich, E. W., and Everett, H. J., *Chem. Eng. Progress* **46**, 395 (1950).
- Sabbarao and Taneja (1979) Table VII
- Sahai, O. P., and Shuler, M. L., *Can. J. Bot.* **60**, 692–700 (1982).
- Sano, Y., and Usui, H., *J. Chem. Eng. Japan* **18**(1), 47 (1985).
- Sano, Y., Yamaguchi, N., and Adachi, T., *J. Chem. Eng. Japan* **7**(4), 255 (1974).
- Sawant, S. B., and Joshi, J. B., *Chem. Eng. J.* **18**, 87 (1979).
- Schmidt, C. V., and Reichert, K. H., *Chem. Eng. Sci.* **43**(8), 2133 (1988).
- Schrauwen, F. J. M., and Thoenes, D., *Chem. Eng. Sci.* **43**(8), 2189 (1988).
- Schügerl, K., *Adv. Biochem. Eng.* **19**, 71 (1981).
- Schügerl, K., *Int. Chem. Eng.* **22**, 591 (1982).
- Schümmer, P., *Chem. Ing. Tech.* **42**(5), 322 (1970).
- Schütz, J., *Chem. Eng. Sci.* **43**(8), 1975 (1988).
- Selker, A. H., and Sleicher, C. A., *Can. J. Chem. Eng.* **43**, 298 (1965).
- Shah, Y. T., "Gas–Liquid–Solid Reactor Design." McGraw Hill Book Co., New York, 1979.
- Shah, Y. T., and Sharma, M. M., Ch. 10 in "Chemical Reaction and Reactor Engineering" (J. Carberry and A. Varma, eds.), pp. 667–733. Marcel Dekker Inc., New York, 1986.
- Shah, Y. T., Montagna, A., and Wilson, J., *Indian Journal of Technology* **15**(12), 505 (1977).
- Shah, Y. T., Joshi, J. B., and Sharma, M. M., Ch. 12 in "Chemical Reactors," ACS Symposium Series 168 (H. S. Fogler, ed.), p. 243. ACS, Washington, D.C., 1981.
- Shah, Y. T., Kelkar, B. G., Godbole, S. P., and Deckwer, W. D., *AIChE J.* **28**, 353 (1982).
- Sharma, M. M., and Danckwerts, P. V., *British Chem. Eng.* **15**, 522 (1970).
- Shinn, J., Chevron Research Corp., San Francisco, personal communication (1982).
- Shinnar, R., and Church, J. M., *Ind. Eng. Chem.* **52**, 253 (1960).
- Sicardi, S., Conti, R., Baldi, G., and Franzino, L., *Chem. Ing. Tech.* **53**, 67 (1981).
- Sicardi, S., Conti, R., and Baldi, G., *Proc. 3rd Austrian–Italian–Yugoslav Chem. Eng. Congress, 14th–16th September, Graz, Austria* (1982).
- Sideman, S., Hortacsu, H., and Fulton, J. W., *Ind. Eng. Chem.* **58**, 32 (1966).
- Simek, M. and Rousar, I., *Coll. Cz. Chem. Comm.* **49**, 1122 (1984).

- Skelland, A. H. P., "Non-Newtonian Flow and Heat Transfer." John Wiley, New York, 1968.
- Skelland, A. H. P. and Seksaria, R., *Ind. Eng. Chem. Proc. Design and Dev.* **17**(1), 56–61 (1978).
- Slesser, C. G. M., Allen, W. T., Cumming, A. R., Pawlowsky, V., and Shields, J., *Chem. Reaction Eng.—Proceedings of the Fourth European Symposium at Brussels, Belgium*, p. 41 (1968).
- Smith, J. M., *Proc. 2nd World Congress of Chemical Eng., October, Montreal, Canada* (1981).
- Smith, J., Van't Riet, K., and Middleton, J., preprint, Second European Conf. on Mixing (March 30–April 1), Cambridge, United Kingdom (1977).
- Smith, W. D., paper presented at Symposium on Progress Towards Gradient less Reactors in Catalysis, 63rd Annual AIChE Meeting, Chicago (1970).
- Sprow, F. B., *Chem. Eng. Sci.* **22**, 345 (1967).
- Sridhar, T., and Potter, O. E., *Inc. Eng. Chem. Fundamentals*, **19**, 21 (1980).
- Sridharan, K., and Sharma, M. M., *Chem. Eng. Sci.* **31**, 767 (1976).
- Steiff, A., and Weinspach, P. M., *Ger. Chem. Eng.* **1**, 150 (1978).
- Steiff, A., Poggemann, R., and Weinspach, P. M., *Ger. Chem. Eng.* **4**, 30 (1981).
- Sterbecsek, Z., Kubanek, V. and Sterbackova, M., in "Recent Trends in Chemical Reaction Engineering," Vol. 1, (B. D. Kulkarni, R. A. Mashelkar, and M. M. Sharma, eds.), p. 324. Wiley Eastern Ltd., New Delhi, 1987.
- Stichlmayr, J., "Grundlagen der Dimensionierung des Gas/Flüssigkeit—Kontaktapparates Bodenkolonnen." Verlag Chemie, Weinheim, 1978.
- Stiegel, G. J., Shah, Y. T., and Sharma, M. M., *AIChE J.* **24**(3), 369 (1978).
- Stolk, R. D., and Syverson, A., in "Chemical Reaction Engineering," ACS Symposium Series 65 (V. W. Weekman and D. Luss, eds.), p. 50. ACS, Houston, 1978.
- Stuber, N. P., and Tirrell, M., *Polymer Process Engineering* **3**, 71 (1985).
- Subbarao, D., and Taneja, V. K., Third European Conference on Mixing (April, 1979).
- Sullivan, G. A. and Treybal, R. E., *Chem. Eng. J.* **1**, 302 (1972).
- Sunderland, P., Ph.D. Thesis, University of Leeds, United Kingdom (1974).
- Sunderland, P., and El Kanzi, E. M. A., "A Vibration Mixed Reactor for Chemical Kinetics in Gas/Solid Catalyzed Reactions," in "Chemical Reaction Engineering—II," ACS Symposium Series 133 (H. M. Hulburt, ed.), p. 3. Washington D.C., 1974.
- Tadmor, Z., and Klein, I. "Engineering Properties of Plastics Extrusion." Van-nostrand-Reinhold, New York, 1970.
- Taguchi, H., and Miyamoto, S., *Biotech Bioengineering* **8**, 43 (1966).
- Tai, Z. G., Wannenmacher, N., Haider, A. and Levenspiel, O., "How to Narrow the RTD of Fluids in Laminar Flow in Pipes," paper presented at the AIChE meeting in San Francisco, (Nov. 5–10, 1989).
- Tajbl, D. G., Simmons, J. B., and Carberry, J. J., *Ind. Eng. Chem. Fundamentals* **5**, 171 (1966).
- Tajbl, D. G., Feldkirchner, H. L., and Lee, A. L., *Adv. Chem. Ser.* **69**, 166 (1967).
- Takeda, K., Hoshino, T., Taguchi, H., and Fijii, T., *Kagaku Kogaku* **32**, 376 (1986).
- Tamhankar, S. S., and Chaudhari, R. V., *Ind. Eng. Chem. Fundamentals* **18**, 406 (1979).
- Tanaka, H., *Biotechnology Bioengineering* **23**, 1203–1218 (1981).
- Tebel, K. H., Zehner, P., Langer, G., and Main, W., *Chem. Ing. Tech.* **58**(10) 820 (1986).
- Teramoto, M., Tai, S., Nishi, K., and Teranishi, H., *Chem. Eng. J.* **8**, 223 (1974).
- Teshima, H., and Ohashi, Y., *J. Chem. Eng. Japan* **10**, 70 (1977).
- Thomas, F. B., Ramachandran, P. A., Dudukovic, M. P., and Jansson, R. E. W., *Chem. Eng. Sci.* **43**, 2013 (1988).
- Tikhonov, G. F., Shestov, G. K., Temkin, O. N., and Flid, R. M., *Kinet. Katal.* **7**, 914 (1966).
- Tipnis, P. R., and Carberry, J. J., AIChE Annual Meeting, Paper 18C, San Francisco (Nov., 1984).
- Todd, D. B., and Irving, H. F., *Chem. Eng. Progress* **65**(9), 84 (1969).
- Todtenhauf, E. K., *Chem. Ing. Tech.* **43**, 336 (1971).
- Trotter, I., Ph.D. Thesis, Princeton University, Princeton, New Jersey (1960).
- Uhl, V. W., and Gray, J. B., "Mixing," Vol. I. Academic Press, New York, 1966.

- Uhl, V. W., and Voznick, H. P., *Chem. Eng. Progress* **56**(3), 72–77 (1960).
- Van de Vusse, J. G., *Chem. Eng. Sci.* **17**, 507 (1962).
- Van Dierendonck, L. L., Fortuin, J. M. F., and Vanderbox, D., *Proc. 4th Eur. Symp. Chem. Reaction. Eng., September 9th–11th, Brussels, Belgium* (1968).
- Van Heuven, J. W., and Beek, W. J., *Ingenieur (Utrecht)* **82**(44), Ch. 51–60 (1970).
- Van't Riet, K., *Ind. Eng. Chem. Process Design and Dev.* **18**, 357 (1979).
- Van't Riet, K., and Smith, J. M., *Chem. Eng. Sci.* **28**, 1031 (1973).
- Van't Riet, K., and Smith, J. M., *Chem. Eng. Sci.* **30**, 1093 (1975).
- Van't Riet, K., Boom, J. M., and Smith, J. M., *Trans. Inst. Chem. Engrs.* **54**, 124 (1976).
- Vermeulen, T., Williams, G. M., and Langlois, G. E., *Chem. Eng. Progr.* **51**, 85 (1955).
- Vijayraghvan, K., and Gupta, J. P., *Ind. Eng. Chem. Fundamentals* **21**, 333 (1982).
- Voit, H., and Mersmann, A., *Ger. Chem. Eng. (English Translation)* **9**, 101 (1986).
- Walstra, P., *Neth. Milk Dairy J.* **23**, 290 (1969).
- Warmoeskerken, M., Feijen, J., and Smith, J. M., *I. Chem. E. Symp. Ser.* **63**, 1 (1981).
- Warwick, G. C. I., *Chem. Ind.*, 5th May, p. 403 (1973).
- Weekman, V. W., *AIChE J.* **20**, 833 (1974).
- Weetman, R. J., and Coyle, C. K., "The Use of Fluid Foil Impellers in Viscous Mixing Applications," paper presented at the AIChE annual meeting, San Francisco (Nov. 5–10, 1989).
- Weinspach, P. M., *Chem. Ing. Tech.* **39**(516), 231 (1967).
- Wentzheimer, W. W., Ph.D. Thesis, University of Pennsylvania (1969).
- Westertep, K. R., Van Dierendonck, L. L., and de Kraa, J. A., *Chem. Eng. Sci.* **18**, 157 (1963).
- Whitehurst, D. D., and Michell, T. O., in "Liquid Fuels from Coal" (R. T. Ellington, ed.), p. 153. Academic Press, New York, 1977.
- Widmer, F., in "Polymerization Kinetics and Technology," Adv. in Chem. Ser. 128 (N. A. J. Platzer, ed), p. 51. ACS, Washington, D. C., 1973.
- Wiedmann, J. A., Steiff, A., and Weinspach, P. M., *Ger. Chem. Eng.* **3**, 303 (1980).
- Wiedmann, J. A., Steiff, A., and Weinspach, P. M., *Ger. Chem. Eng.* **4**, 125 (1981).
- Wilson, G., "Continuous Culture of Plant Cells Using the Chemostat Principle," in "Advances in Biochem Engineering" (A. Fletcher, ed.), Vol. 16, pp. 1–25. Springer-Verlag, New York, 1980.
- Winfield, M. E., *Aust. J. Chem.* **6**, 221 (1953).
- Wisniak, J., Stefanovic, S., Rubin, E., Hofmann, Z., and Talmon, Y., *J. Amer. Oil Chem. Soc.* **48**, 379 (1971).
- Wollam, J., *Solid State Technol.* **14**(12), 72 (1971).
- Yadav, G. D., and Sharma, M. M., *Chem. Eng. Sci.* **34**, 1423 (1979).
- Yagi, H., and Yoshida, F., *Ind. Eng. Chem. Process Design and Dev.* **14**, 488 (1975).
- Yakota, T., Iwano, T., Deguchi, H., and Tadaki, T., *Kagaku Koyaku Ronbunshu* **7**, 156 (1981).
- Yamane, T., and Yoshida, F., *J. Chem. Eng. Japan* **5**, 381 (1972).
- Yamane, T., Sada, E., and Takamatsu, T., *Biotechnol. Bioengineering* **19**, 801 (1977).
- Yoshida, Y. and Miura, Y., *Ind. Eng. Chem. Process Design and Dev.* **2**, 263 (1963).
- Yung, C. N., Wang, C. W., and Chang, C. L., *Can J. Chem. Eng.* **57**, 672 (1979).
- Zehner, P., *Ger. Chem. Eng.* **2**, 220 (1979).
- Zlokarnik, M., *Chem. Ing. Tech.* **38**, 357 (1966a).
- Zlokarnik, M., *Chem. Ing. Tech.* **38**(7), 717–723 (1966b).
- Zlokarnik, M., *Chem. Ing. Tech.* **39**(9/10), 539 (1967).
- Zlokarnik, M., *Chem. Ing. Tech.* **41**, 1195–1202 (1969).
- Zlokarnik, M., *Chem. Ing. Tech.* **42**(15), 1009 (1970).
- Zlokarnik, M., *Chem. Ing. Tech.* **43**(18), 1028 (1971).
- Zlokarnik, M., in "Ullmann's Encyclopädie der technischen Chemie," 4th Ed., Vol. 2. Verlag Chemie, Weinheim, 1972.

- Zlokarnik, M., *Adv. Biochem. Eng.* **8**, 133 (1978).
- Zlokarnik, M., *Adv. Biochem. Eng.* **11**, 157 (1979).
- Zlokarnik, M., *Korrespondenz Abwasser* **27**(1), 157 (1980).
- Zlokarnik, M., "Biotechnology," Vol. 2, Ch. 23. VCH Verlagsgesellschaft, Weinheim, 1985.
- Zlokarnik, M., *Ger. Chem. Eng. (English Translation)* **9**, 314–320 (1986).
- Zlokarnik, M., and Judat, H., *Chem. Ing. Tech.* **39**(20), 1163 (1967).
- Zlokarnik, M., and Judat, H., *Chem. Ing. Tech.* **41**(23), 1270 (1969).
- Zlokarnik M., and Judat, H., "Stirring," in "Ullmann's Encyclopedia of Industrial Chemistry," 5th Ed. Vol. B2 (1988).
- Zundeleovich, Y., *AIChE J.* **25**, 763 (1979).
- Zwietering, T. N., *Chem. Eng. Sci.* **8**, 244 (1958).

PARTICULATE FLUIDIZATION: AN OVERVIEW

Mooson Kwauk*

Institute of Chemical Metallurgy, Academia Sinica
Beijing, People's Republic of China

I. The Fluidized State

A. THE FLUIDIZED STATE AND HOW IT IS ACHIEVED

Fluidization refers to the process by which a fluidlike state is imparted to granular solid particles by the application of appropriate external forces. The fluidity of a liquid or a gas has its origin in the mobility against one another of the constituent molecules. Solid particles may be pushed apart from one another to acquire this mobility by the steady upflow of a liquid or a gas at sufficient velocity. When this fluid flow starts at a relatively low velocity through a static bed of solid particles, the interstitial pores among the particles offer sufficient resistance to the fluid to create a corresponding drop in pressure in the direction of flow. As the rate of flow increases, this pressure drop increases correspondingly until at some flow rate, this pressure drop equals the weight of the granular solids, and the solid particles start to lose contact with their neighbors. As the rate of fluid flow increases further, the particles, which are now suspended, cannot offer greater resistance because of their limited masses. Instead, the flowing fluid pushes the particles farther apart to make way for the increased flow, and the pressure drop remains constant at the same level corresponding to the solids weight: that is,

$$\Delta P = (\rho_s - \rho_f)(1 - \varepsilon_{mf})L_0,$$

where ρ_s is the density of the solid particles; ρ_f is the density of the fluid; ε_{mf} is the voidage, or fraction void, in the granular solids bed at minimum fluidization; and L_0 is the height of fixed solids bed before fluidization starts.

While practice and convention have generally regarded upward fluid flow as the only motivating force for fluidizing solid particles, the fluidized state also

* The author wishes to express his gratitude to Virginia Polytechnic Institute and State University for inviting him as a visiting professor for the 1986–87 academic year during which the initial draft of this overview was written in the Department of Chemical Engineering.

can be achieved by vertical oscillation of the fluid without net flow. Conditions can be identified under which oscillation produces higher resistance to the solid particles for the upstroke than for the downstroke—e.g., asymmetric oscillation. Solid particles can also be fluidized by mechanical vibration, or in the case of ferromagnetic particles, by application of an appropriate alternating magnetic field. Thus, the achievement of the fluidized state ought to be considered in terms of all possible motivating forces or the combination of these forces, rather than being limited to upward fluid flow alone. Linking the fluidized state to a variety of possible motivating forces often opens the way to new applications and new processes—for instance, for cases in which solids need to be fluidized while no, or insufficient, fluidizing gas is available.

B. NATURE OF HYDRODYNAMIC SUSPENSION

Fluid flow tends to carry a particle in the direction of the surrounding flowing fluid. There is a layer of fluid around the particle that transmits the shear produced by the moving fluid to act on the particle being pushed. When the rate of flow is high, the fluid also carries a kinetic pressure against those parts of the particle that present a frontal area facing the flowing fluid.

The sum of these forces can be represented for the simplified case of a sphere of diameter d_p :

$$F = \underbrace{\pi(d_p/2)^2}_{\text{frontal area}} \cdot \underbrace{C_D}_{\text{drag coef.}} \cdot \underbrace{\rho_f u_f^2/2g}_{\text{kinetic pressure}}$$

For the case of a single sphere in a large volume of flowing fluid of practically any kind, liquid or gas, the drag coefficient can be correlated to the Reynolds number, $Re = d_p u_f \rho_f / \mu$.

If extra turbulence is created in the fluid, the value of C_D has been noted to rise or fall in a rather unpredictable manner, as shown by the data of Clift and Gauvin (1971) in Fig. 1. Also, the presence of a neighboring sphere tends to lower the value of C_D to an extent that depends on the proximity and angular position of the second sphere (of the same size, for the present consideration), as shown in Fig. 2 (Brauer, 1971). Blockage of flow by the neighboring sphere forces the flow streamlines to converge, thus creating a zone of relatively high velocity between the spheres. This high-velocity region induces a reduction of pressure, thus pinching the spheres together. Since closer approach between the spheres increases the resistance to fluid flow, thus reducing its velocity, there is always an equilibrium position between the two spheres. In the case of two bubbles rising in a fluid, or in a fluidized bed, the pressure reduction between them often induces their coalescence into a larger bubble.

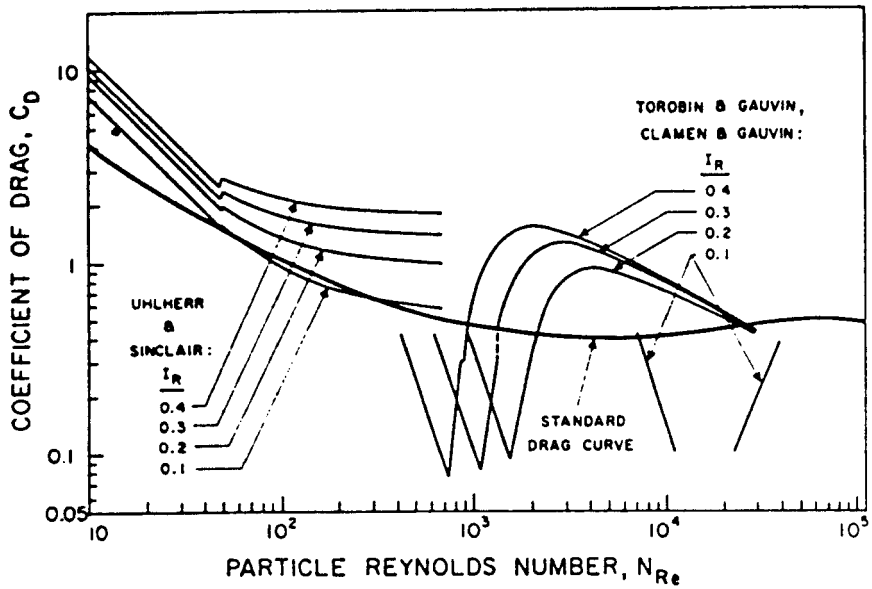


FIG. 1. Variation of drag coefficient with extra turbulence in fluid. [After Clift and Gauvin, 1971.]

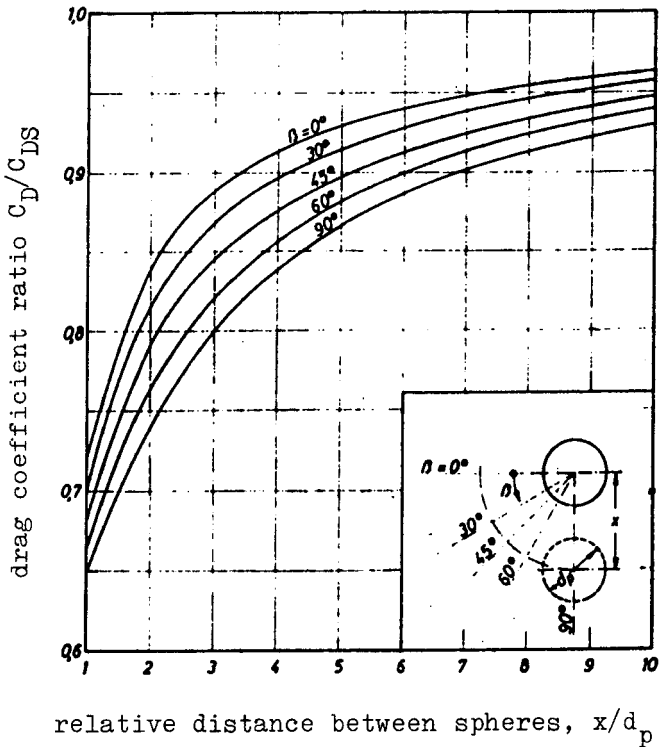


FIG. 2. Variation of drag coefficient with the presence of a neighbor. [After Brauer, 1971.]

Particles may also be induced otherwise to coalesce, thus presenting less resistance to the surrounding fluid. For instance, in a vertical magnetic field, ferromagnetic particles in a fluidized bed are polarized to form individual dipoles that line up in chains in the direction of the magnetic field (Ma and Kwauk, 1983). These chains permit a higher fluidizing velocity because of the reduction in drag.

C. PARTICLE-PARTICLE FORCES

Other forces existing between particles often operate against hydrodynamic drag that produces fluidization. Thus, when particles touch one another, there exists a London-van der Waals force of a molecular nature at the point of contact. This force looms in proportion when gravity and drag forces diminish as a particle becomes smaller. For a small particle, the surface force of adhesion may often be thousands of times greater than its weight.

Particles may also be held together by the presence of a liquid at the point of contact. This liquid may consist of a film due to adsorbed moisture, may result from liquid exudate from the particle during processing—such as liquid sulfur from galena during roasting—or may be a low-melting component of the particle itself or the product of solid-solid reaction, such as sodium metavanadate in roasting a vanadous ore or coal ash with salt or soda ash. Also, a solid bond may be formed at the interparticle point of contact through any of the sintering mechanisms well known in powder metallurgy—bulk diffusion, boundary diffusion of atoms, or vaporization-condensation. Pseudo bonding of particles may occur from abnormal growths on the solid surfaces, such as metallic iron whiskers from the gaseous reduction of iron oxide. These extremely fine spikes of submicron diameters cause the parent particles to be interlocked with one another. Points of contact of the whiskers are sites of high surface energy because of the small radii of curvature, thus offering even greater potential for sintering to follow.

Particle-particle forces may cause particles to gather together into larger agglomerates that need higher fluid velocities to fluidize. The agglomerates may be of unequal sizes, leaving the larger ones unfluidized. These, being now immobile, tend to consolidate and attract the medium- or small-sized ones into these defluidized colonies, thus forming smaller and contracting zones for the fluidizing gas to channel through regions hardly inundated by the main stream.

On the other hand, adhesion, especially for particles of mixed sizes, may lead to the formation of a coating of fine powders on the surface of coarse particles, facilitating the fluidization of these otherwise hard-to-fluidize particles by virtue of the acquisition of this lubricating layer of roller-bearing-like surface deposit.

D. SPECIES OF FLUIDIZATION

In applications and in basic studies of fluidization, it is not only desirable but often necessary to give full consideration to the multitude of operating forces between fluid and particles on the one hand, and between particles and particles on the other.

But an even more significant factor lies in the distinction among the fluidizing media. Fluidization of solid particles was likened to a fluid when the particles were made mobile with respect to one another under the motivating force of the fluidizing medium. While the fluidity of either a liquid or a gas is attributed to the mobility of the constituent molecules, liquid possesses considerably higher viscosity because of the constraint on the mobile molecules caused by their proximity to one another, as compared to the much longer mean free path of the molecules of a gas. Thus, liquids and gases can be considered to belong to two broad classes of fluids, differing greatly in density and viscosity.

	Gases	Liquids
Density, g/cm ³	<0.01	>0.5
Viscosity, cP	<0.1	>0.1

Fluids with intermediate values in density and viscosity are rarely encountered in nature or in ordinary manufacturing processes, except in the laboratory where fluids near their critical conditions could be prepared.

Fluidization of solid particles with these two widely different classes of fluids—liquids and gases—leads to vastly different phenomena of solids behavior, as shown in Fig. 3. For L/S fluidization, as liquid velocity increases beyond the incipient fluidization point, the solids bed continues to expand as if it were an elastic continuum stretching under the dynamic forces of augmented flow, until, near the terminal velocity of the particles, the solid particles can be noted to be suspended sparsely. Throughout this process of liquid-velocity increase, the solid particles are dispersed quite uniformly, fully exhibiting their discrete behavior, essentially independent of one another. Therefore, L/S fluidization was named “particulate.”

For G/S systems, on the other hand, especially when relatively coarse solid particles with close size distributions are used, fluid velocity increment beyond incipient fluidization is accompanied by the formation of bubbles, or rising cavities with hardly any solid particles in them, as shown in the top row of Fig. 3. In general, gas flow beyond incipient fluidization mostly reports to bubble flow, thus implying that gas velocity through the surrounding dense

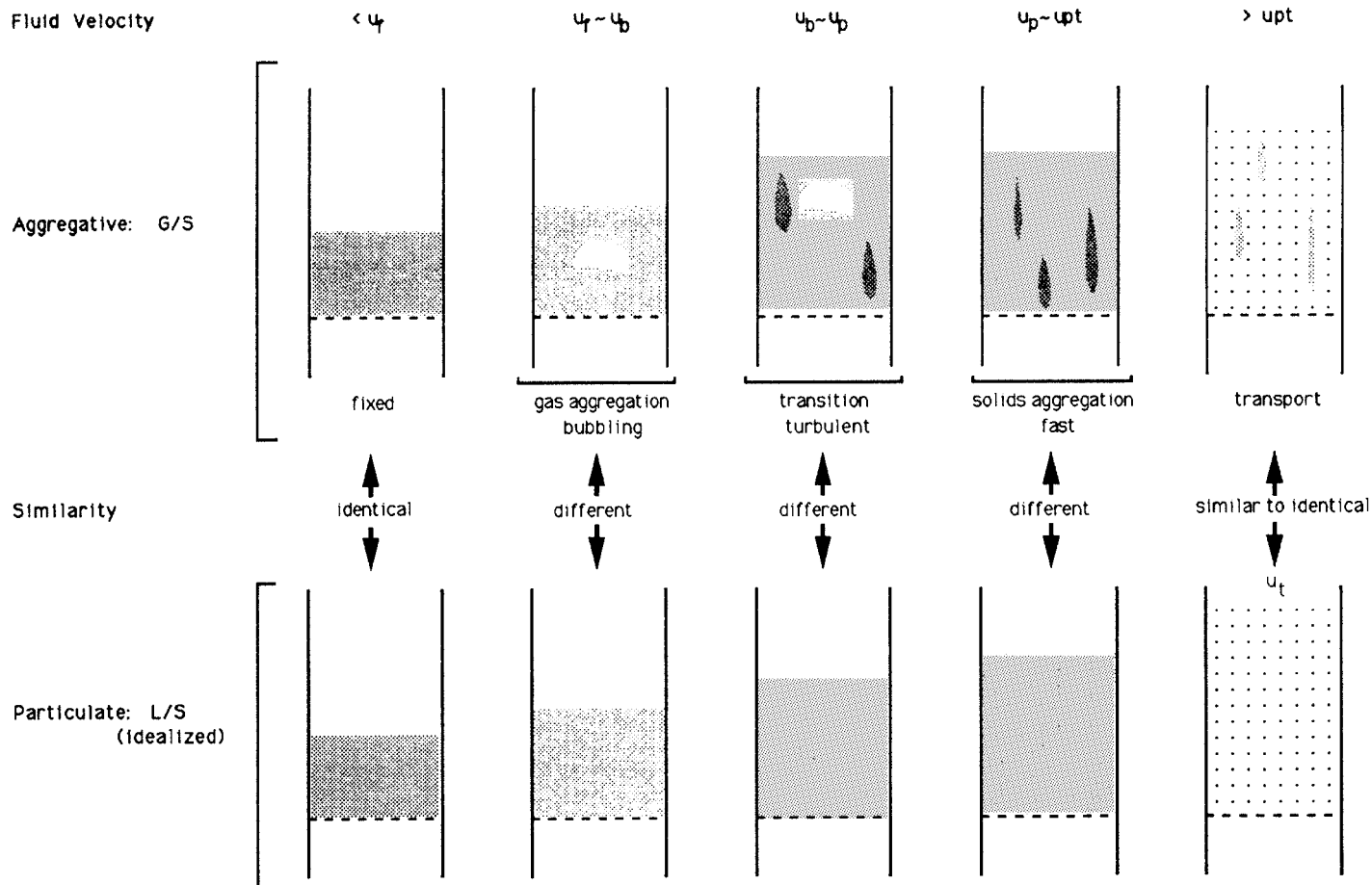


FIG. 3. Phenomenological discrimination between G/S and L/S systems.

G/S bed remains essentially at the value for incipient fluidization. With an increase in gas velocity, the size of the bubbles increases, and so does the velocity of their rise, until at some velocity most of the solid particles are all of a sudden blown out of the vessel top, with those that remain forming a dilute G/S phase much similar to the L/S system at high liquid velocities. Aggregation of solid particles into a dense continuous phase, making room for the passage of most of the gas in excess of incipient fluidization through a bubbling discontinuous phase, bespeaks the two-phase nature of G/S fluidization. Such a phenomenon of G/S systems was designated "aggregative."

Bubbling means gas bypassing and thus is detrimental to efficient G/S contact. Attempts were thus initiated to improve the "quality of fluidization" by reducing the size or altering the shape of bubbles, etc., through the installation of internals in fluidized beds. It was only in the rather recent past that attention was turned to the nature of the solid particles themselves. If the solid particles were made with smoother surfaces and graded in size, especially with the incorporation of fines, their fluidization quality was found to improve. For instance, FCC catalyst has for many years been made of essentially spheroidal particles with strict requirements on particle size distribution, so that it is possible to realize particulate fluidization through a short velocity range above incipient fluidization before any bubble appears. Also, at the higher-velocity end of the bubbling range, it is possible to alter the shape of the bubbles so much, especially with recycling of solids from the top to the bottom of the fluidized bed, that a new two-phase structure is produced with strands or clusters of solids, as a discontinuous phase dispersed in a dilute continuous phase of sparse solid particles population. Aggregation of solid particles into these strands or clusters is highly transient—the strands and/or clusters dart and jump in their dilute-phase surrounding, only to dissolve and reform over and over again, thus resulting in improved G/S contact as compared to the conventional bubbling mode of G/S fluidization. This new high-velocity phenomenon, realizable only with suitable solid materials, is associated with the relatively new mode of G/S contacting called "fast fluidization."

This sequence of transition is depicted in the upper row of insets of Fig. 3. Apparently, there is a phase inversion from the bubbling mode, where gas aggregates into rising cavities, to the "fast" mode, where solids aggregate into strands or clusters. Thus, the original concept of aggregative fluidization is resolved into gas aggregation at low velocities and solids aggregation at high velocities. The transition from one mode to the other, or the "phase inversion" in aggregative fluidization, is diffuse rather than definitive, accompanied by a high degree of deformation of bubbles with simultaneous dissection of the dense phase sporadically into primordial strands or clusters. This transition corresponds to what is often referred to as "turbulent fluidization."

At the high-velocity end of fast fluidization, the transition from dense to dilute phase operation noted for coarse solid particles is still possible, though the better the solid material is designed for improved fluidization quality, the less sudden the transition will be.

E. REGIMIZATION OF THE FLUIDIZED STATE

Design of solid materials capable of encompassing all the four regimes of the fluidized state (particulate, bubbling, fast, and transport) opens up vast possibilities for answering processing needs. However, except for those that are fabricated, such as the catalyst noted above, not all solid materials can be designed, and also there exist processes for which good fluidizing quality may not be essential. It is therefore desirable to describe the phenomenological distinctions of Fig. 3 in terms of descriptors of particle behavior, as shown in Fig. 4. These descriptors will be dealt with in greater detail in Section X on powder classification. The following two sets of descriptors will be introduced at this moment, to aid in early orientation.

Geldart (1972, 1973) classified powders into four categories:

- Group A: quite fine, aeratable, with appreciable range between minimum bubbling u_{mb} and incipient fluidization u_{mf} ($u_{mb}/u_{mf} > 1$);
- Group B: intermediate size, bubbles at incipient fluidization ($u_{mb}/u_{mf} = 1$), detectable to short-range fast regime;
- Group C: fine, cohesive, channels upon fluidization;
- Group D: coarse, readily spoutable.

ICM classification (Yang *et al.*, 1985) according to the bed-collapsing curve of a fluidized powder, in which three characteristic stages have been identified:

- (1) bubble escape;
- (2) hindered sedimentation;
- (3) solids consolidation.

Depending on the presence or absence of the above stages, a three-digit qualitative designation has been formulated:

- 100: bubble-escape stage only;
- 123: three stages: bubble escape, hindered sedimentation, and solids consolidation;
- 020: hindered sedimentation only;
- 023: hindered sedimentation plus solids consolidation.

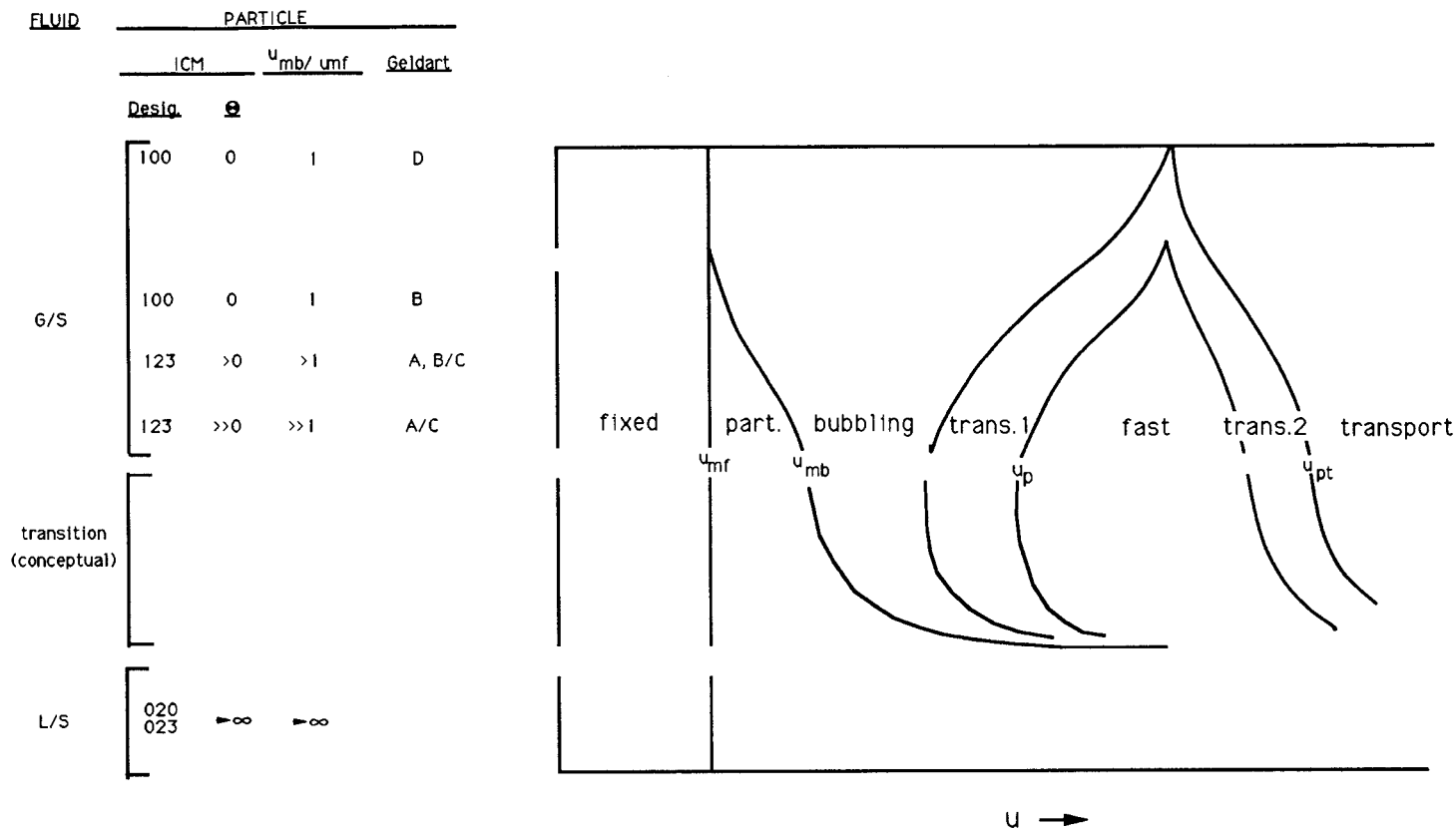


FIG. 4. Conceptualized phenomenological regimization of the fluidized state.

Also, the fluidizing quality of a powder can be quantified by using a dimensionless time Θ , ranging from 0 to ∞ ; the higher the value of Θ , the better the powder. It should be noted from Fig. 4 that a powder with good fluidizing quality is identified by the following characteristics:

- high range for both particulate and fast fluidization;
- short range for bubbling fluidization;
- postponed occurrence of dilute-phase transport.

Liquid–solid fluidization is essentially all particulate throughout the velocity range, except for large, heavy particles. Between the G/S and L/S systems, the expectation for provision of experimental evidence for diminishing bubbling and fast regimes lies in the use of fluids having properties bridging the gap between gases and liquids, e.g., fluids at their critical points. Figure 4 shows that considering the interplay of the fluidizing media and the solid particles being fluidized, it is logical to divide fluidization into three classes.

Class	Fluid	Particles	Regimes
1	liquid	all	1: particulate
2	gas	fine, graded	4: particulate, bubbling, fast, and transport
3	gas	coarse, uniform	2: bubbling and transport

II. Idealization of the Fluidizing Process: Empirical Deductions from L/S Systems

When applied to fluidization, the empirical correlation between the drag coefficient C_D and the Reynolds number Re needs to be extended to account for the automatic adjustment in particle array that results in a regular increase in the fraction void ε in the interstitial spaces with increased fluid flow—that is,

$$f(C_D, Re, \varepsilon) = 0. \quad (2.1)$$

Variation of voidage ε with fluid velocity u was first studied by Hancock (1937, 1942) and demonstrated by Wilhelm and Kwauk (1948) to be linear on log–log plots (Fig. 5), that is,

$$u = \varepsilon^n u_t. \quad (2.2)$$

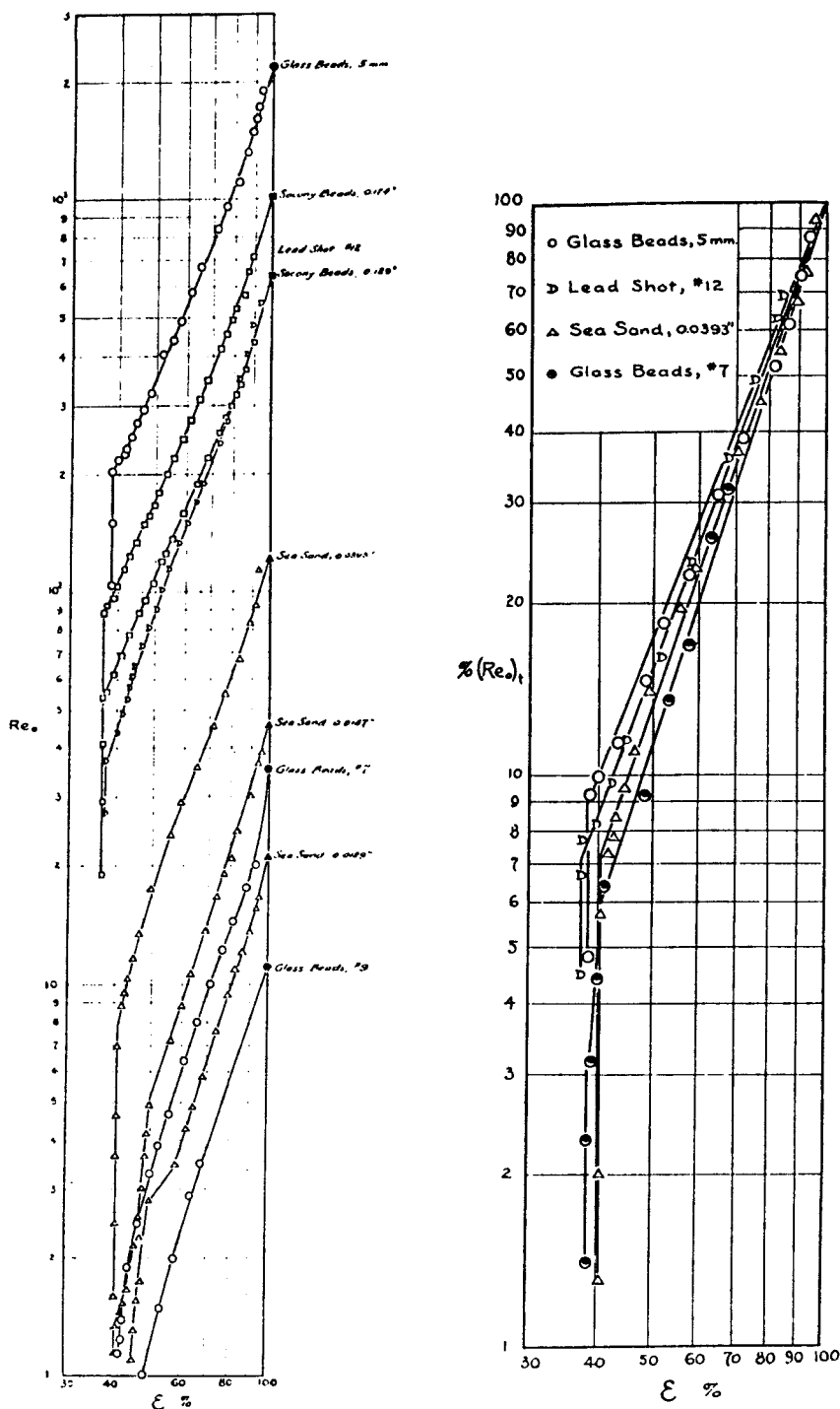


FIG. 5. Relation between voidage ϵ and velocity u for L/S systems. [Whilhelm and Kwauk, 1948.]

Richardson and Zaki (1954) formulated sectionwise correlations of the exponent n to the terminal Reynolds number $Re = d_p u_t \rho_f / \mu$.

The range of the voidage change extends from that for the single particle in an infinite volume of fluid, $\varepsilon = 1$, to the lower limit for the fixed bed, ε_0 . At this point, Eq. (2.1) would still be valid, although it possesses a different physical meaning: Instead of particles suspended by the fluid, this relation now signifies a fixed bed with pressure drop less than that required to balance the particles in the suspended state:

$$f(C_D, \Delta P, Re, \varepsilon_0) = 0. \quad (2.3)$$

The choice of dimensionless groups is a matter of convenience and can always be made to suit the need of the user by combination (Kwauk, 1958; Kwauk and Chong, 1963). For instance, for a given fluidizing medium and a given solid to be fluidized, it is often most desirable to calculate u , d_p , and ε , and, when a fixed bed is formed, ΔP . However, in Eqs. (2.1) and (2.3), both C_D and Re involve d_p and u at the same time, making their independent determination from the graph difficult. If Re/C_D is used, the Lyashenko number is formed, extricating u from d_p :

$$Ly = Re/C_D = u^3 \rho_f / \mu g \Delta \rho, \quad (2.4)$$

where $\Delta \rho = \rho_s - \rho_f$. In order to see the linear change of u , the cube root of the Lyashenko number is often used:

$$Ly^{1/3} = u [\rho_f / \mu g \Delta \rho]^{1/3}. \quad (2.4a)$$

Similarly, d_p can be divorced from u by forming the Archimedes number,

$$Ar_{\Delta \rho} = Re^2 C_D = d_p^3 \rho_f g \Delta \rho / \mu^2 \quad (2.5)$$

Its cube root linearizes d_p :

$$Ar^{1/3} = d_p [\rho_f g \Delta \rho / \mu^2]^{1/3}. \quad (2.5a)$$

From the preceding manipulations on dimensionless numbers, it can be seen that, if the fixed and fluidized beds are to be considered comprehensively, functional plots of $Ar - Re$ with ε as the curve parameter are most desirable, as shown in Fig. 6. If only the fluidized state is of interest, then the $Ar^{1/3} - Ly^{1/3}$ plot will facilitate independent evaluation of d_p and u , as shown in Fig. 7. It has already been observed that the family of curves shown in Figs. 6 and 7 is filled in by using the relation given by Eq. (2.2). Instead of the sectionwise correlations of Richardson and Zaki, n has been correlated to Re , empirically as a continuous function, as shown in Fig. 8.

As for the fixed bed, the pressure drop at any velocity can be prorated from that at incipient fluidization by means of the relation

$$\Delta P / L_0 (1 - \varepsilon_0) = \Delta P (u / u_{mf})^m, \quad (2.6)$$

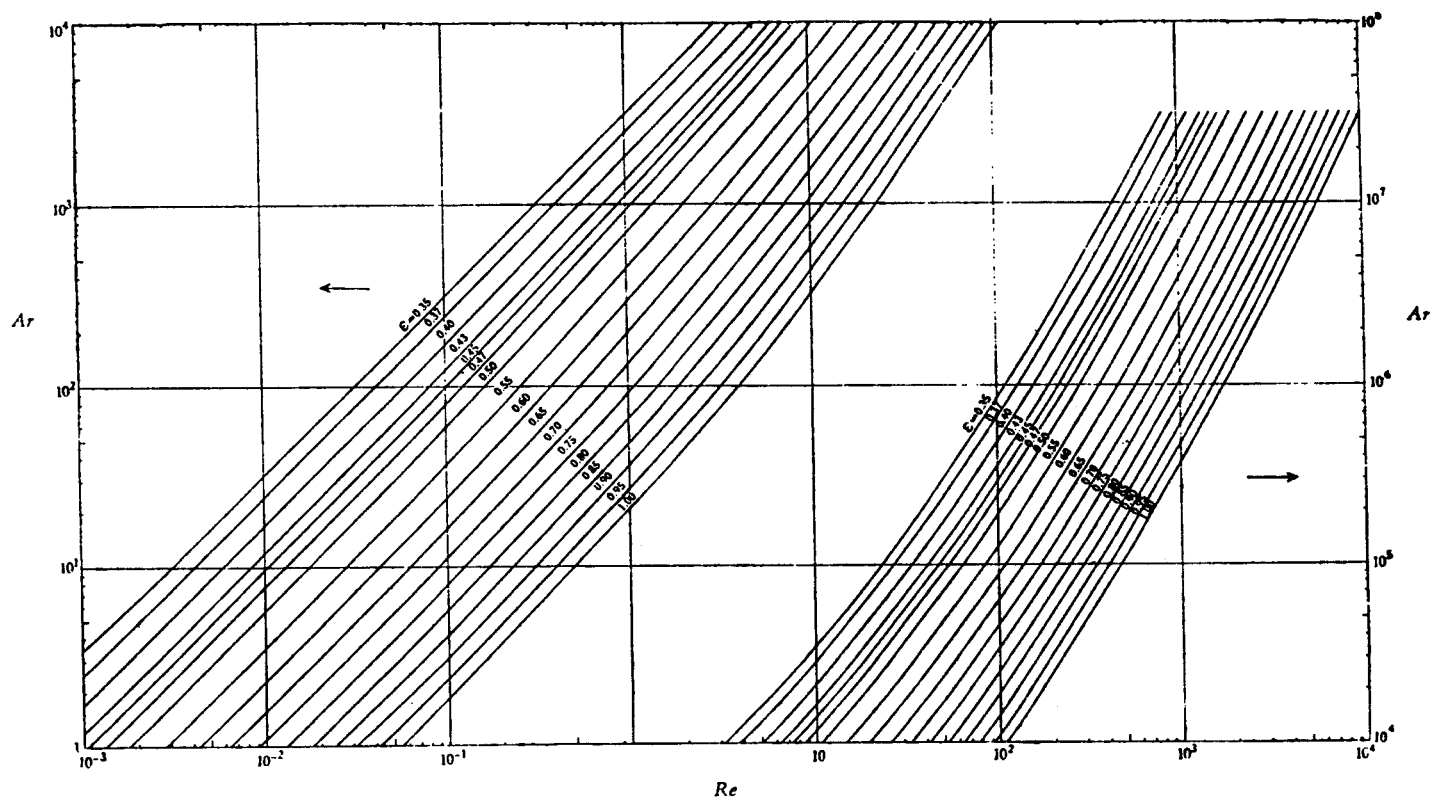


FIG. 6. $Ar-Re$ plot. [After Kwauk, 1958, 1963.]

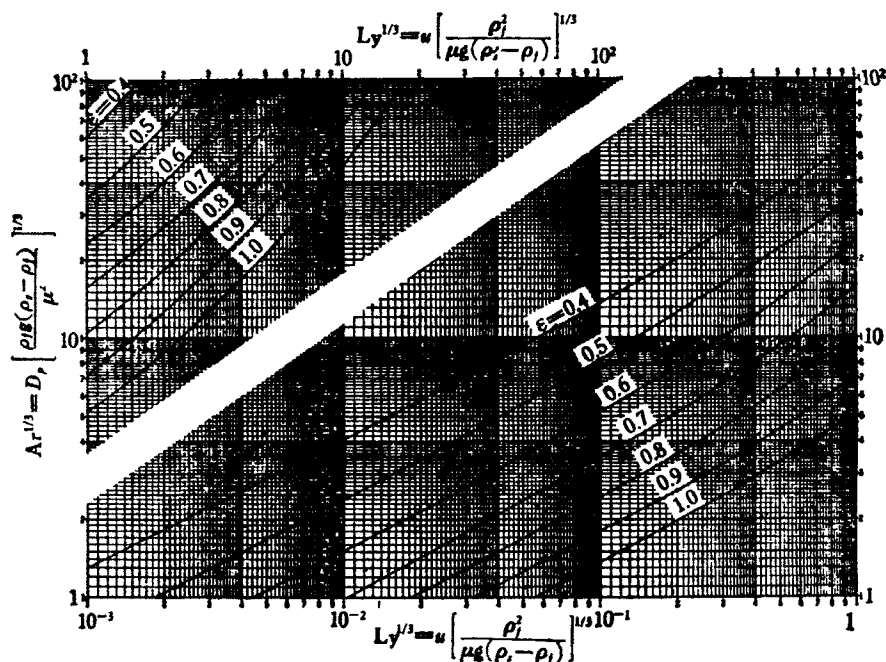


FIG. 7. $Ar^{1/3} - Ly^{1/3}$ plot. [After Kwauk, 1958, 1963.]

for which the value of the exponent m has also been correlated as an empirical function of Re_i and ϵ_0 , as shown in Fig. 9 (Kwauk, 1963a, Kwauk and Chong, 1963).

Data reported in Figs. 6, 7, 8, and 9 were compiled (Kwauk and Chong, 1963) after judicious choice and comparison from a number of sources (Beranek and Sokol, 1959; Goroshko *et al.*, 1958; Pavloshenko, 1956; Bena *et al.*, 1961; Elgin and Foust, 1950; Lewis and Bowerman, 1952; Lewis *et al.*, 1949; Loeffler and Ruth, 1958; Maude, 1958; Oliver, 1961; Steinour, 1944) and have been put to practical use in these forms for some 30 years.

For all the experimental data that have been thus correlated, however, even under the most favorable conditions, particulate fluidization in L/S systems is by no means completely homogeneous. Closely fractioned glass beads ranging in diameter from 0.57 to 4.0 mm were fluidized in glass tubes at approximately equal tube-to-particle diameter ratios, D_t/d_p , with water flowing at such velocities as to yield approximately equal voidages. The various tubes were photographed, and the negatives were enlarged to give prints with essentially equal particle diameters (Kwauk, 1973). Comparison of these four photographs indicates that if the particle diameter is used as a standard of

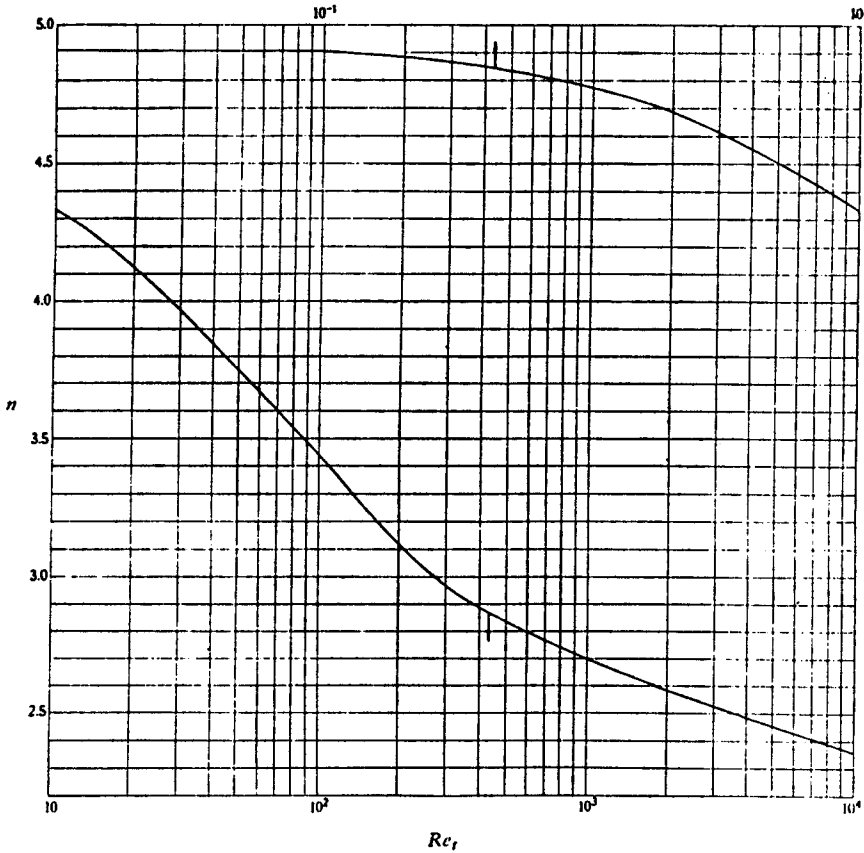


FIG. 8. Empirical correlation between n and Re_t . [After Kwauk, 1963.]

measure, essentially the same degree of particle clustering exists for all these glass beads having such great disparity in size. Because of the rather weak resolving power of the unaided eye, however, the smaller the glass beads, the oftener it creates the false impression of a high degree of homogeneity.

Be that as it may, it is yet possible to conceive of an idealized fluidized system with complete homogeneity (Kwauk, 1973), as characterized by the following factors:

- (1) A definite incipient fluidizing velocity, such that fluidization begins at $u = u_{mf}$ and the solid particles revert to fixed bed as soon as $u < u_{mf}$.
- (2) A stable, well-defined upper surface of the solid bed.
- (3) For a bed having a fixed solids inventory, the pressure drop of the bed at

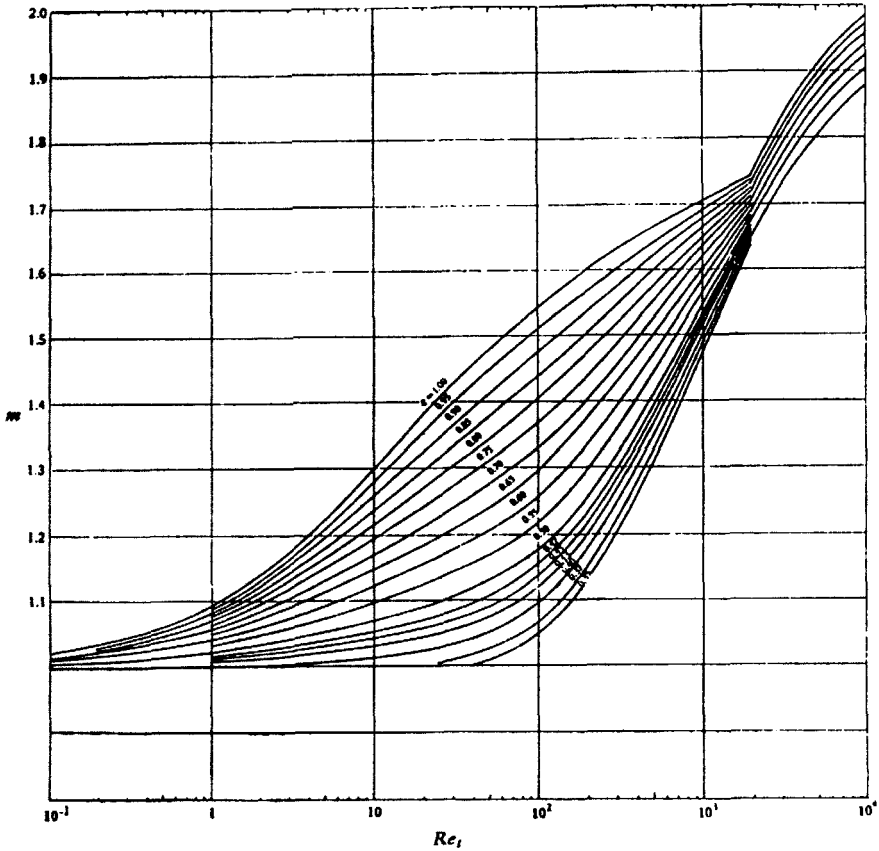


FIG. 9. Empirical correlation among m , Re_t , and ε . [After Kwauk, 1963.]

$u > u_{mf}$ is a constant, equal to the weight of the solids upon unit cross-sectional area—that is,

$$\Delta P = L\Delta\rho(1 - \varepsilon).$$

- (4) The voidage of the fluidized bed at any velocity $u > u_{mf}$ possesses a uniform representative value, definable by the relationship $u = \varepsilon^n u_t$, in which the exponent n is a universal empirical function of Re_t .
- (5) In the state of a fixed bed for $u < u_{mf}$, the pressure drop can be prorated from that at incipient fluidization by the relation $\Delta P = L_0 \Delta\rho(1 - \varepsilon_0)(u/u_{mf})^m$, in which the exponent m is another universal empirical function of Re_t and ε_0 .

The concept of idealized fluidization, possessing the characteristics outlined above, can be utilized, analogously to the concept of an ideal gas, in the analysis of many engineering problems, as will be exemplified in the following sections of this overview.

III. Generalized Fluidization

Fluidized systems generally refer to beds possessing fixed solids inventories—that is, only the flowing velocity of the fluidizing medium needs to be considered, whereas the solids velocity due to feed and discharge is by comparison so small that it can be neglected. This is the case for catalytic reactors and for solids processing calling for relatively long residence time. Such fluidized systems will be called classical fluidization.

On the contrary, it is often necessary to deal with those vertical systems in which the net fluid and solids velocities are of similar magnitudes, and neither should be neglected. This is true for L/S systems, in which the liquid, on account of its much higher density as compared to that of a gas, travels with much lower linear velocity for the same mass flow rate; for standpipes, where minimal fluid flow is often desired for a given solids transport duty; and for transport reactors and the newly developed fast fluidization processes, where solids are recycled at linear velocities approaching those of the fluidizing gases. These systems can be differentiated according to the relative direction of flow of the solids and the fluid, and the direction of flow of the solids with respect to gravity.

		Particles	Fluid
I. Co-up	cocurrent countergravity	↑	↑
II. Co-down	cocurrent cogravity	↓	↓
III. Counter-down	countercurrent cogravity	↓	↑

In liquid–liquid extraction, for instance, when a light liquid is the discontinuous phase, the rising droplets are actually fluidized by the heavy liquid flowing downward, forming an inverted fluidized bed of liquid droplets (Blanding and Elgin, 1942). Similarly, the rise of bubbles in liquid can be treated as sedimentation in a reversed sense.

The distributor plate for fluidized solids is often a necessary stabilizing component—that is, for most fluidized systems, when the distributor is removed, the entire solids bed may fall off from its active region. Under certain

conditions, however, fluidization can take place freely in a vessel without the presence of a distributor plate. Therefore, each of the above three cases of particle–fluid motion may operate in the “restrained” or “free” mode, depending on the presence or absence of a distributor. Accordingly, there can exist eight types of generalized fluidization, as shown in Fig. 10.

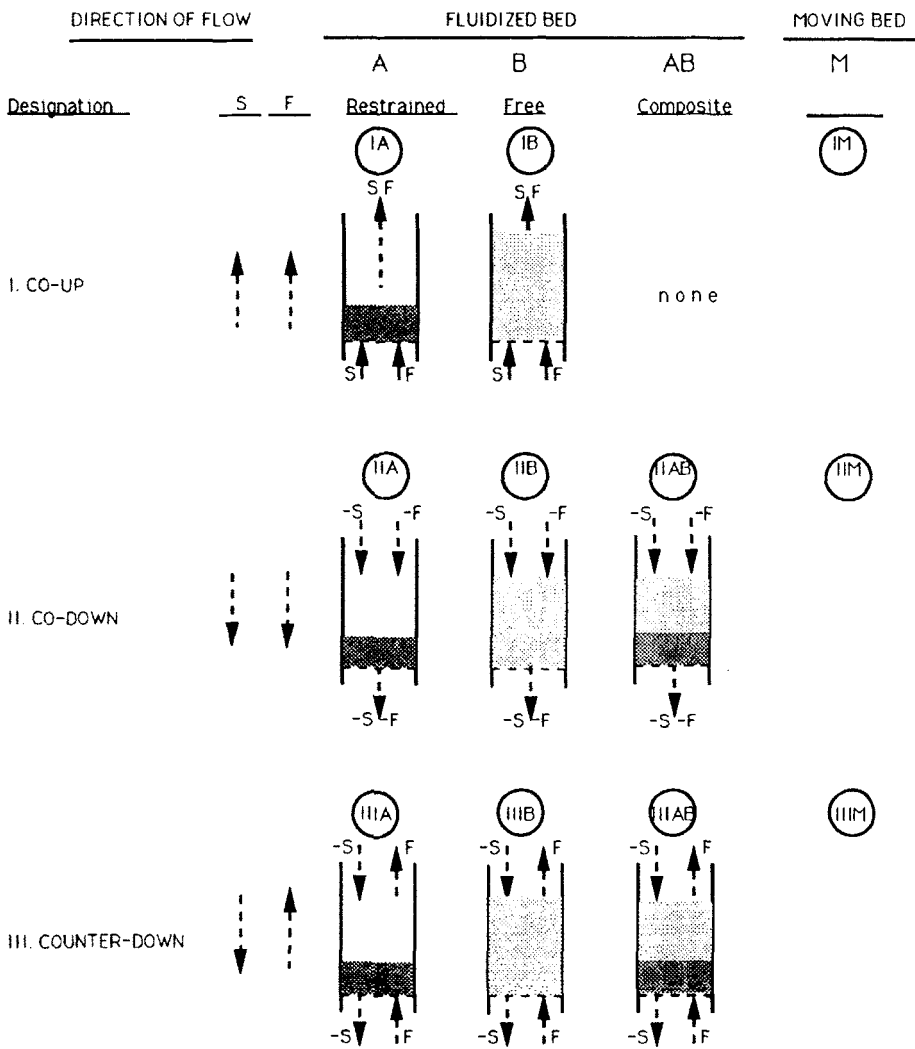


FIG. 10. Modes of operation in generalized fluidization.

The moving bed can also operate according to three cases of relative particle–fluid motion.

IM. Co-up	moving bed uptransport
IIM. Co-down	moving bed downtransport
IIIM. Counter-down	shaft furnaces, etc.

Hindered sedimentation can operate in two modes: when the fluid is essentially at standstill, and when an equal volume of fluid is displaced by the descending solids, such as for batch operation.

Generalized fluidization refers to the overall field of particle–fluid motion represented by the 11 modes of operation shown in Fig. 10, the two types of hindered sedimentation just described, plus classical fluidization when the solids inventory possesses hardly any net motion up or down, totalling altogether 14 cases. It shall be described in the context of the concept of idealized fluidization (Kwauk, 1958, 1963a, 1973; Kwauk and Chong, 1963).

A. STEADY-STATE MOTION

Various aspects of simultaneous particle–fluid motion in the vertical direction were studied experimentally and analyzed theoretically, in a quite exhaustive manner, during the 1950s and 1960s, mostly for L/S systems, by Elgin and Foust (1950), Wilhelm and Valentine (1951), Mertes and Rhodes (1955), Lapidus and Elgin (1957), Price *et al.* (1959), Struve *et al.* (1958), Hoffman, *et al.* (1960), Quinn *et al.* (1960), and Finkelstein *et al.* (1971). These rather coordinated studies afforded sufficient evidence to allow the following statement to be proposed in light of the classical theory of fluidization (Kwauk, 1958, 1963a; Kwauk and Chong, 1963):

If the relative velocity between the particles and the fluid is substituted for velocity u of classical fluidization, the general correlations of classical fluidization can be extended to include the entire realm of generalized fluidization.

Somewhat different approaches to the problem were presented by Zenz (1953) and Zenz and Othmer (1960), though fundamentally for G/S systems, and even more generally by Wallis (1969).

Now, the actual linear velocity with respect to the retaining vessel of a fluid flowing through a fluidized bed of voidage ε is u_0/ε , where u_0 is the superficial fluid velocity, that is, the volumetric fluid flow rate divided by the horizontal cross-sectional area of the otherwise empty retaining vessel, being positive for the upward direction. Similarly, the actual linear velocity of the particles with respect to the retaining wall is $u_d/(1 - \varepsilon)$, where u_d is the solid mass flow rate

divided by the density of the particles ρ_s and the horizontal cross-sectional area of the otherwise empty vessel. Therefore, the actual relative velocity between the particles and the fluid is

$$u_{sa} = u_0/\varepsilon - u_d/(1 - \varepsilon). \quad (3.1)$$

But since the general correlation of classical fluidization is based upon the superficial fluid velocity, the actual relative velocity needs the following conversion to a superficial value:

$$u_s = u_{sa}\varepsilon. \quad (3.2)$$

Substitution of Eq. (3.2) into Eq. (3.1) yields

$$u_s = u_0 - u_d\varepsilon/(1 - \varepsilon). \quad (3.3)$$

According to this statement, this superficial relative velocity u_s will be substituted into Eq. (2.2) of the classical theory to yield the following relation among voidage, particle velocity, and fluid velocity for simultaneous particle–fluid motion:

$$u_t\varepsilon^n = u_0 - u_d\varepsilon/(1 - \varepsilon). \quad (3.4)$$

It would be convenient to convert the velocity terms into reduced quantities, $u'_0 = u_0/u_t$ and $u'_d = u_d/u_t$, so that Eq. (3.4) may become dimensionless:

$$\varepsilon^n = u'_0 - u'_d\varepsilon/(1 - \varepsilon). \quad (3.5)$$

Equation (3.5) will be referred to as the equation of generalized fluidization for steady-state motion. Of the four quantities in this equation, n is an empirical function of Re_t , and the remaining three dimensionless variables are determined by operation and can be represented graphically for any constant value of n , as shown in Fig. 11 for $n = 2.36$, which corresponds to $Re = 10^4$.

Figure 11 will be described in the following order:

- (1) points;
- (2) lines that join points; and
- (3) regions that are demarcated by the lines.

1. Points and Lines

- | | |
|---------|---|
| Point A | stands for a downward-moving bed with voidage ε in still fluid $u'_0 = 0$. |
| Point B | is the incipient fluidizing point u_{mf} for classical fluidization. |
| Point C | stands for the suspension of a single particle in a fluidizing medium of infinite extent: $\varepsilon = 1$, $u'_d = 0$, $u'_0 = 1$. |
| Point D | stands for co-up moving-bed transport with voidage ε_0 and at terminal fluid velocity $u'_0 = 1$. |

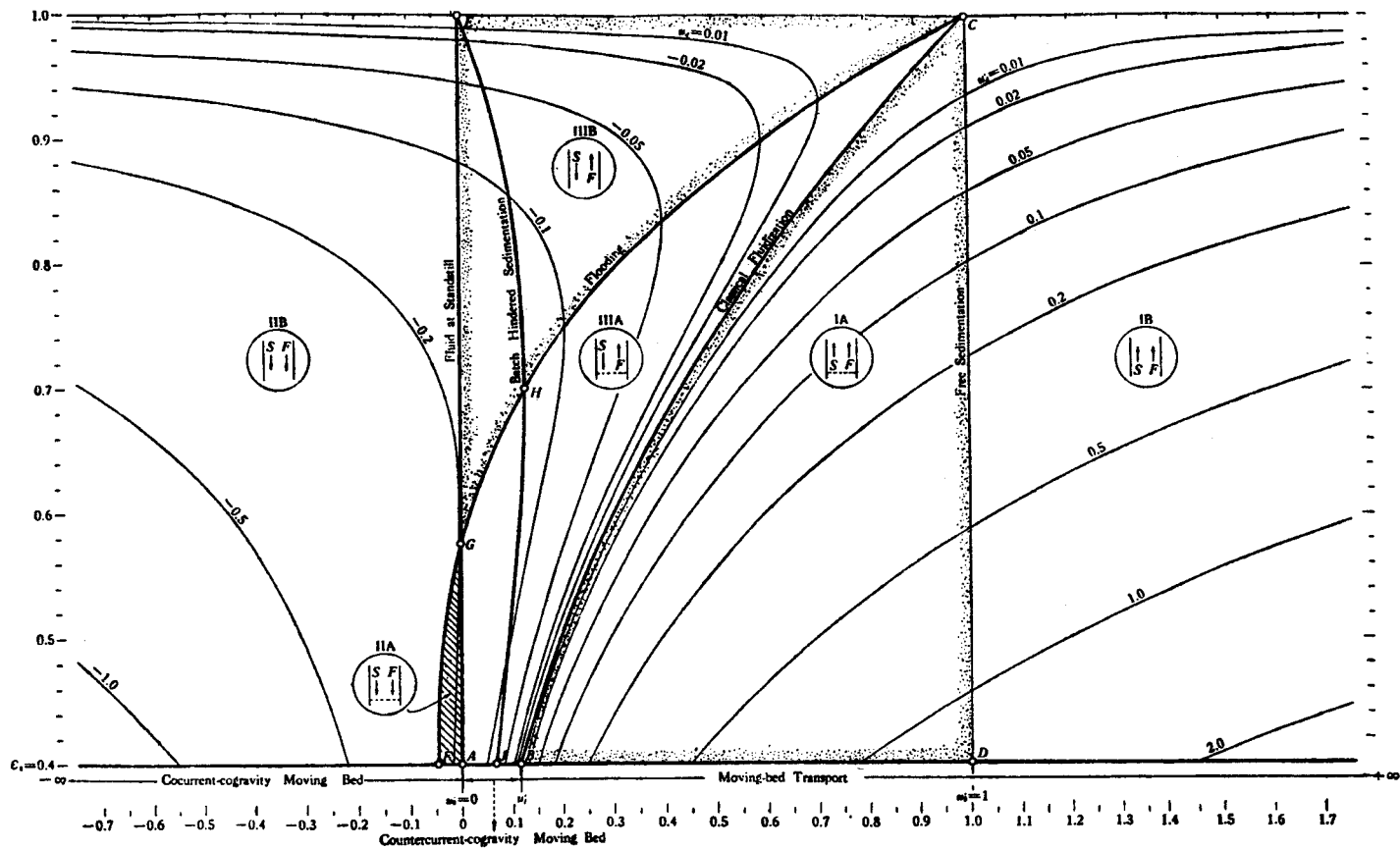


FIG. 11. Constant- n chart for generalized fluidization. [After Kwauk, 1963.]

- Point E is the empty vessel with neither fluid flow nor particle throughput, $\varepsilon = 1$, $u'_0 = 0$, $u'_d = 0$.
 Line BC is for classical fluidization, $u'_d = 0$, $u'_0 = \varepsilon^n$.
 Line FGHC is the flooding line which can be defined by either of the following criteria:

$$[\partial u'_0 / \partial \varepsilon]_{u'_d} = 0,$$

$$[\partial u'_d / \partial \varepsilon]_{u'_0} = 0.$$

- Point F is the flooding point for co-down moving bed.
 Point G is the intersection of the flooding line with the zero fluid velocity axis $u'_0 = 0$, and thus marks the maximum particles throughput for continuous sedimentation.
 Line EHJ is for batch-hindered sedimentation for which an equal volume of fluid is displaced by the descending solids.
 Point H represents the maximum particles throughput in batch-hindered sedimentation.
 Point J represents the maximum solids throughput in batch moving-bed sedimentation at $\varepsilon = \varepsilon_0$.

The locations of the points and lines enumerated above, and related formulae for their computation, are summarized in Table I.

2. Regions

Broadly speaking, the area enclosed by points A, E, C, and B are for countercurrent operation, and the area between the flooding line FGHC and the $u'_0 = 1$ axis CD is for restrained systems. The lines also divide the constant- n chart into regions representing the modes of operation listed in Fig. 10. Of practical significance for these different regions is whether voidage increases or decreases with the fluid or solids throughput—that is, whether the algebraic sign of the following partial derivatives is positive or negative:

$$\partial \varepsilon / \partial |u'_0| = + \text{ or } - \text{ (before the slant sign in the following listing);}$$

$$\partial \varepsilon / \partial |u'_d| = + \text{ or } - \text{ (after the slant sign).}$$

- Region IA: Co-up, restrained, area BCD,
 voidage change $+/-$;
 example: hydraulic uptransport.
 Region IB: Co-up, free, area toward the right of line CD,
 voidage change $+/-$;
 same application as for IA.
 Region IIA: Co-down, restrained, area FGA,
 voidage change $-/+$;
 rarely found in practice.

TABLE I
POSITION OF POINTS AND LINES IN CONSTANT- n CHART (AFTER KWAIK, 1963)

		ε	u'_0	u'_d
<i>Point A</i>	Moving bed with no fluid flow	ε_0	0	$-(1 - \varepsilon_0)\varepsilon_0^{n-1}$
<i>Point B</i>	Incipient fluidization for fixed particles inventory	ε_0	u'_f	0
<i>Point C</i>	Suspension of single particle or free sedimentation	1	1	0
<i>Point D</i>	Moving-bed transport at terminal fluid velocity	ε_0	1	$\left(\frac{1 - \varepsilon_0}{\varepsilon_0}\right)(1 - \varepsilon_0^n)$
<i>Point E</i>	Empty retaining vessel	1	0	0
<i>Point F</i>	Flooding, co-down moving bed	ε_0	$-[n(1 - \varepsilon_0) - 1]\varepsilon_0^n$	$-n(1 - \varepsilon_0)^2\varepsilon_0^{n-1}$
<i>Point G</i>	Flooding in still fluid	$\frac{n-1}{n}$	0	$-\left(\frac{n-1}{n}\right)^n\left(\frac{1}{n-1}\right)$
<i>Point H</i>	Maximum particles throughput in batch-hindered sedimentation	$\frac{n}{n+1}$	$\left(\frac{n}{n+1}\right)^n\left(\frac{1}{n+1}\right)$	$-\left(\frac{n}{n+1}\right)^n\left(\frac{1}{n+1}\right)$
<i>Point J</i>	Maximum particles throughput in batch moving-bed sedimentation	ε_0	$(1 - \varepsilon_0)\varepsilon_0^n$	$-(1 - \varepsilon_0)\varepsilon_0^n$
<i>Line BC</i>	Classical fluidization for fixed particles inventory	—	ε^n	0
<i>Line FGHC</i>	Flooding	—	$-[n(1 - \varepsilon) - 1]\varepsilon^n$	$-n(1 - \varepsilon)^2\varepsilon^{n-1}$
<i>Line EHJ</i>	Batch-hindered sedimentation	—	$(1 - \varepsilon)\varepsilon^n$	$-(1 - \varepsilon)\varepsilon^n$

- Region IIB: Co-down, free, area toward the left of FGE,
voidage change $+/-$;
example: tubular L/S reactor.
Composite IIAB possible for u'_0 between zero and point F.
- Region IIIA: Counter-down, restrained, area AGHCB,
voidage change $+/+$;
example: fluidized leaching and washing; heavy phase dispersed in light phase for liquid-liquid extraction.
- Region IIIB: Counter-down, free, area GEC,
voidage change $-/-$;
same application as for IIIA.
Composite IIIAB often encountered in practice.

Location of the above regions in the constant- n chart and the direction of voidage change are summarized in Table II. Table III gives the ranges of variables for these regions and some important lines in the constant- n chart. Flooding is defined by either of the derivatives, used in describing the regions, equal to zero:

$$\partial \varepsilon / \partial |u'_0| = 0,$$

$$\partial \varepsilon / \partial |u'_d| = 0.$$

TABLE II
REGION LOCATION FOR CONSTANT- n CHART AND DIRECTION OF
VOIDAGE CHANGE^a

Designation	S	F	A Restrained	B Free
I. Co-up	↑	↑	IA BCD +/-	IB right of CD +/-
II. Co-down	↓	↓	IIA FGA -/+	IIB left of FGE +/-
III. Counter-down	↓	↑	IIIA AGHCB +/+	IIIB GEC -/-

^a Signs in table: $\frac{\partial \varepsilon}{\partial |u'_0|} / \frac{\partial \varepsilon}{\partial |u'_d|}$.

TABLE III
RANGE OF VARIABLES IN GENERALIZED FLUIDIZATION

		ε	u'_0	u'_d
1. <i>Line BC</i>	Classical fluidization with fixed particles inventory	$\varepsilon_0 < \varepsilon < 1$	$u'_f < u'_0 < 1$	$u'_d = 0$
2. <i>Region IA</i>	Cocurrent-countergravity restrained system	$\varepsilon_0 < \varepsilon < 1$	$u'_f < u'_0 < 1$	$0 < u'_d < \left(\frac{1-\varepsilon_0}{\varepsilon_0}\right)(1-\varepsilon_0^n) = D$
3. <i>Region IB</i>	Cocurrent-countergravity free system	$\varepsilon_0 < \varepsilon < 1$	$1 < u'_0 < \infty$	$0 < u'_d < \infty$
4. <i>Region IIA</i>	Cocurrent-cogravity restrained system	$\varepsilon_0 < \varepsilon < \frac{n-1}{n} = G$	$F = -[n(1-\varepsilon_0)-1]\varepsilon_0^n < u'_0 < 0$	$F = n(1-\varepsilon_0)^2\varepsilon_0^{n-1} < u'_d < (1-\varepsilon_0)\varepsilon_0^{n-1} = A$
5. <i>Region IIB</i>	Cocurrent-cogravity free system	$\varepsilon_0 < \varepsilon < 1$	$-\infty < u'_0 < 0$	$-\infty < u'_d < 0$
6. <i>Region IIIA</i>	Countercurrent-countergravity restrained system ^a	$\varepsilon_0 < \varepsilon < 1$ (use the smaller of the two ε values)	$0 < u'_0 < 1$	$G = -\left(\frac{n-1}{n}\right)^n \left(\frac{1}{n-1}\right) < u'_d < 0$
7. <i>Region IIIB</i>	Countercurrent-countergravity free system ^a	$\varepsilon_0 < \varepsilon < \frac{n-1}{n} = G$ (use the larger of the two ε values)	$0 < u'_0 < 1$	$G = -\left(\frac{n-1}{n}\right)^n \left(\frac{1}{n-1}\right) < u'_d < 0$
8. <i>Line EHJ</i>	Batch-hindered sedimentation	$\varepsilon_0 < \varepsilon < 1$	$0 < u'_0 < \left(\frac{n}{n+1}\right)^n \left(\frac{1}{n+1}\right) = H$ \parallel $-u'_d$	$-H = -\left(\frac{n}{n+1}\right)^n \left(\frac{1}{n+1}\right) < u'_d < 0$ \parallel $-u'_0$
9. <i>Line BD to</i>	Moving-bed transport	$\varepsilon = \varepsilon_0$	$u'_f < u'_0 < \infty$	$0 < u'_d < \infty$
10. <i>Line AB</i>	Countercurrent-countergravity moving bed	$\varepsilon = \varepsilon_0$	$0 < u'_0 < u'_f$	$A = -(1-\varepsilon_0)\varepsilon_0^{n-1} < u'_d < 0$

^a Can be used in rise of bubbles or light liquid drops in a heavier liquid after reversal of vector signs for u'_0 and u'_d .

B. Moving Bed

All moving-bed operations are compressed into the single line for the abscissa of $\varepsilon_0 = 0.4$ in the constant- n chart shown in Fig. 11. This one-dimensional representation in the diagram needs to be developed into two dimensions for more lucid exposition.

Moving-bed operations in which the particles are poised by hydrodynamic drag against gravity to the point of incipient fluidization is represented by Eq. (3.5) when ε_0 is substituted for ε :

$$\varepsilon_0^n = u'_0 - u'_d \varepsilon_0 / (1 - \varepsilon_0). \quad (3.5m)$$

This is true for moving-bed uptransport, located on the $\varepsilon_0 = 0.4$ line toward the right of point B in Fig. 11. Should u'_0 be less than that required by Eq. (3.5m), then the solid particles would not be hoisted by the flowing fluid. On the other hand, should u'_0 exceed the value specified by Eq. (3.5m), then the solid particles would be fluidized. Moving-bed uptransport is thus a meta-stable operation. Equation (3.5m) shows that u'_d is linear with u'_0 , and therefore, if u'_d is plotted against u'_0 , as shown in Fig. 12, a straight line is obtained with a slope of $\varepsilon_0/(1 - \varepsilon_0)$ and intercept on the u'_0 -axis of ε_0^n .

For the counter-down moving bed, such as shaft furnaces, and shown by the AB segment of the $\varepsilon_0 = 0.4$ line in Fig. 11, fluid velocity can be assigned any value from zero to the point of incipient fluidization, B. The counter-down moving bed can be operated at fluid velocity less than that specified by Eq. (3.5m), resulting, however, in a pressure gradient less than that for incipient fluidization, $L_0 \Delta \rho (1 - \varepsilon_0)$. This reduced pressure gradient can be prorated in accordance with the theory for idealized fluidization:

$$\Delta P = L_0 \Delta \rho (1 - \varepsilon_0) (u/u_{mf})^m,$$

in which the fluid velocity u obviously needs the following substitution for simultaneous particle-fluid motion:

$$u = u_t [u'_0 - u'_d \varepsilon_0 / (1 - \varepsilon_0)],$$

and the incipient fluidization velocity u_{mf} is to be expressed in terms of voidage,

$$u_{mf} = u_t \varepsilon_0^n.$$

Thus,

$$\frac{\Delta P}{L_0 \Delta \rho (1 - \varepsilon_0)} = \left(\frac{u'_0 - u'_d \varepsilon_0 / (1 - \varepsilon_0)}{\varepsilon_0^n} \right)^m = Q_0^m, \quad (3.6)$$

where Q_0 may be called a deviation factor to signify departure of the pressure gradient from the point of balancing the particles against gravity. Equation

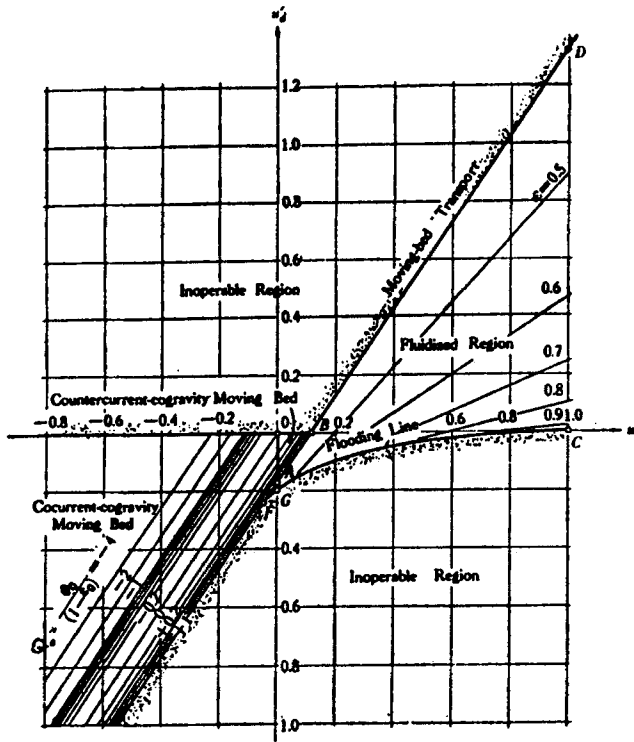


FIG. 12. Moving-bed operation in generalized fluidization. [After Kwauk, 1963.]

(3.6) can then be restored to the same format as Eq. (3.5):

$$Q_0 \varepsilon_0^n = u'_0 - u'_d \varepsilon_0 / (1 - \varepsilon_0). \quad (3.6)$$

Area AOB in Fig. 12 shows the counter-down moving-bed operation described above, with the value of $Q_0 = 0$ for no fluid flow to $Q_0 = 1$ at incipient fluidization.

Co-down moving-bed operation is shown on the $\varepsilon_0 = 0.4$ line to the left of point A. Extension of line ABD in Fig. 12 toward the lower left indicates the critical operation in which the relative particle-fluid velocity is high enough to balance the particles against gravity at incipient fluidization, creating a positive pressure gradient as in normal fluidization. To achieve this state, it is obvious, as can be seen from this line in Fig. 12, that the particles have to move faster than the fluid. As the value of Q_0 is decreased toward zero by reducing fluid flow, this pressure gradient diminishes correspondingly to zero. When

$Q_0 = 0$, the fluid is simply carried down by the particles in their interstices at an equal velocity. It is possible to increase solids throughput by increasing fluid rates to yield values of $Q_0 < 0$, thus producing a negative pressure gradient, as shown by the family of lines in the lower left quadrant of Fig. 12.

To summarize, the deviation factor Q_0 possesses the following range of values for different modes of moving bed operations:

co-up	$Q_0 = 1$ (metastable);
counter-down	$0 < Q_0 < 1$;
co-down	$-\infty < Q_0 < 1$.

C. ACCELERATIVE MOTION

Prorating of pressure drop for idealized fluidization, Eq. (2.6), which has just been applied to moving beds, Eq. (3.6), has also been found useful in formulating the frictional drag between fluid and particles in accelerative motion. Thus, Eq. (3.6) is generalized to any voidage for particles in motion (Kwauk, 1964a):

$$\begin{aligned}\Delta P/z &= \Delta\rho(1-\varepsilon)\left(\frac{u'_0 - u'_d E/(1-\varepsilon)}{\varepsilon^n}\right)^m \\ &= \Delta\rho(1-\varepsilon)Q^m.\end{aligned}\quad (3.6a)$$

It was noted that the deviation factor Q assumes the value of unity when particles are poised in balance against gravity by the frictional drag of the upflowing fluid. When these particles are accelerated upward, additional drag is required, thus increasing the value of Q beyond unity, whereas for particles decelerating downward in the same upflowing fluid, Q is less than unity.

Equation (3.6a) is now introduced into the following set of constitutive equations for simultaneous accelerative one-dimensional particle-fluid motion in the vertical direction (Kwauk, 1964):

$$\left\{ \begin{array}{l} \text{particle} \\ \text{continuity} \\ \text{fluid} \end{array} \right. \quad \begin{cases} u'_p \frac{\partial \varepsilon}{\partial z'} + \frac{\partial \varepsilon}{\partial \theta'} = (1-\varepsilon) \frac{\partial u'_p}{\partial z'}, \\ u'_1 \frac{\partial \varepsilon}{\partial z'} + \frac{\partial \varepsilon}{\partial \theta'} = -\varepsilon \frac{\partial u'_1}{\partial z'}, \end{cases} \quad (3.7)$$

$$(3.8)$$

$$\begin{array}{l}
 \text{momentum} \left\{ \begin{array}{l}
 \text{particle} \quad \underbrace{\left[u'_p \frac{\partial u'_p}{\partial z'} + \frac{\partial u'_p}{\partial \theta'} \right]}_{\text{inertia, particles}} - \underbrace{\frac{\rho_f}{\rho_s} \left[u'_1 \frac{\partial u'_1}{\partial z'} + \frac{\partial u'_1}{\partial \theta'} \right]}_{\text{inertia, displaced fluid}} + \underbrace{Z_0}_{\text{net gravity, particles}} \underbrace{\left\{ 1 + \left[\frac{u'_1 - u'_p}{\varepsilon^{n-1}} \right]^m \right\}}_{\text{frictional drag on particles}} = 0, \\
 \\
 \text{fluid} \quad \underbrace{\left[u'_1 \frac{\partial u'_1}{\partial z'} + \frac{\partial u'_1}{\partial \theta'} \right]}_{\text{inertia, fluid}} - \underbrace{\frac{\rho_s}{\rho_f} Z_0 \left\{ \frac{\partial \Phi_0}{\partial z'} + (1 - \varepsilon) \left[\frac{u'_1 - u'_p}{\varepsilon^{n-1}} \right]^m \right\}}_{\substack{\text{pressure gradient in fluid} \\ \text{net gravity in fluid} \\ \text{frictional drag by fluid}}} = 0,
 \end{array} \right.
 \end{array}
 \quad (3.9)$$

$$\quad (3.10)$$

in which

$$\begin{aligned}
 u_p &= u_t u'_p, & u'_p &= u'_d / (1 - \varepsilon), \\
 u_1 &= u_t u'_1, & u'_1 &= u'_0 / \varepsilon \\
 z &= z_0 z', \\
 \Phi_0 &= \Delta P / z_0 \Delta \rho = z_0 \theta' / u_t, \\
 Z &= \Delta \rho g z_0 / \rho_s u_t^2.
 \end{aligned}$$

Many other investigators, also have studied accelerative particle-fluid motion in general, notably the consistent work of Soo (1962), later summarized in books (1982, 1967, 1990); of Jackson (1963), summarized in a chapter on stability of fluid-particle systems (1985); and also of Arastoopour and his colleagues (1974, 1979, 1986).

These equations are highly descriptive of phenomena related to particle-fluid motion at large, but they find application only in simpler circumstances with additional constraints. For instance, when particles and fluid are fed at constant rates to a system of constant cross-sectional area, the operation can be considered steady, and solutions have been worked out (Kwauk, 1964).

D. POLYDISPERSE SYSTEMS

A considerable amount of work has been carried out on the behavior in fluids of particles differing in density and/or size—for example, the investigations initiated by Rowe *et al.* (1965, 1972a, 1972b), carried on by

Nienow and Chiba (1981), and finally well summarized by the latter authors (1985). Misek (1971) described the hydrodynamics, entrainment, and partial flooding of fluidized systems consisting of nonuniform particles. Kennedy and Bretton (1966) studied the axial dispersion of nonuniform spheres fluidized with liquids, followed by investigations on size segregation carried out by Al-Dibouni and Garside (1979).

However, most such work has been concerned with classical fluidization, and relatively little has been devoted to the simultaneous motion of particles in vertically flowing fluids.

The simplest case for polydisperse systems is a binary mixture of a coarse and a fine size fraction of the same material, each considered to be uniform in size. The generalized fluidization equation for the coarse particles, with subscript 1, is (Kwauk, 1975; Huang *et al.*, 1982)

$$\underbrace{u_0/\varepsilon}_{\text{actual velocity of fluid flow through a bed of coarse and fine particles}} - \underbrace{u_{d1}/(1 - \varepsilon_1)}_{\text{actual velocity of the coarse particles}} = \underbrace{u_{t1}\varepsilon^{\pi_1-1}}_{\text{voidage function for idealized fluidization based on the coarse particles}} \quad (3.11)$$

Similarly, for the fine particles, with subscript 2, it is

$$u_0/\varepsilon - u_{d2}/(1 - \varepsilon_2) = u_{t2}\varepsilon^{\pi_2-1}. \quad (3.12)$$

The overall particles volume fraction is evidently the sum of those of the two individual components, that is,

$$(1 - \varepsilon) = (1 - \varepsilon_1) + (1 - \varepsilon_2). \quad (3.13)$$

For polydisperse systems, the above relations can be generalized to the i th component:

$$u_0 - u_{di}\varepsilon/(1 - \varepsilon_i) = u_{ti}\varepsilon^{\pi_i}, \quad (3.14)$$

$$(1 - \varepsilon) = \varepsilon_i^i(1 - \varepsilon_i). \quad (3.15)$$

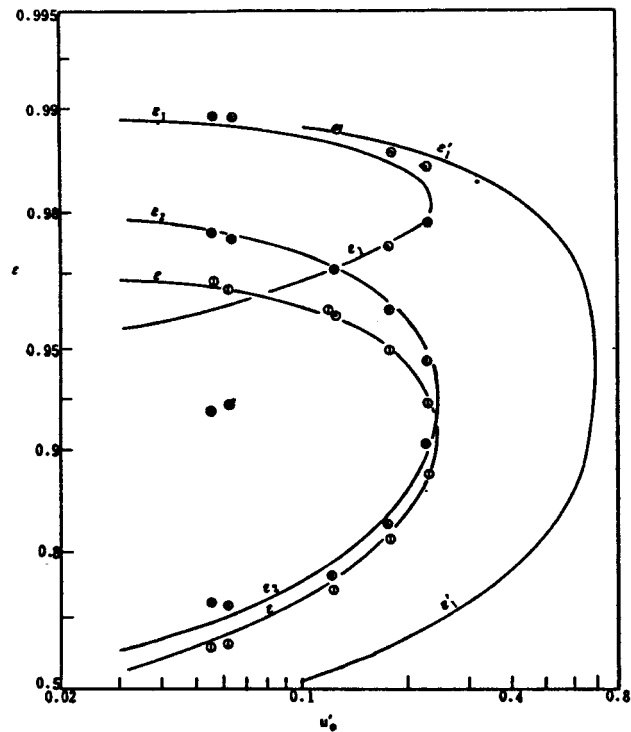
For convenience of computation, the fluid velocity, the terminal velocity, and solids throughput of the individual fractions are expressed as ratios to the terminal velocity of the coarsest particle d_{p1} :

$$u'_0 = u_0/u_{t1},$$

$$u'_{di} = u_{di}/u_{t1},$$

$$M_i = u_{ti}/u_{t1},$$

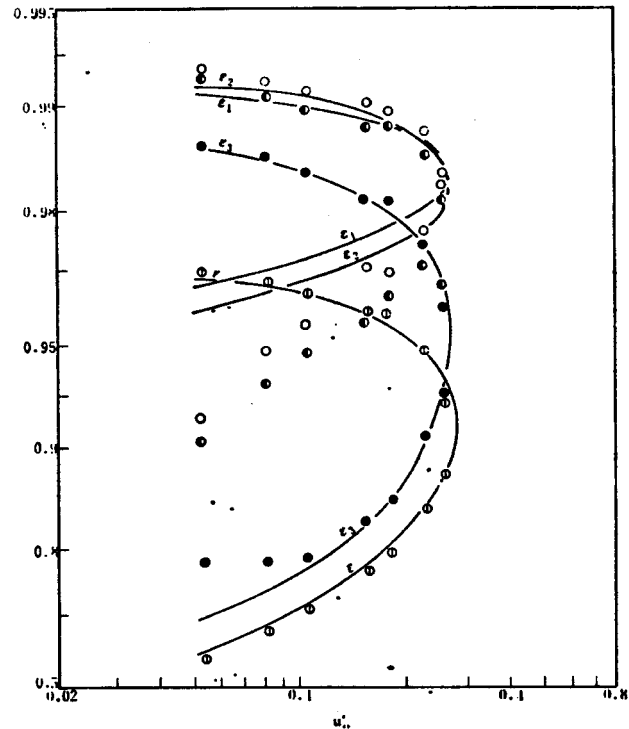
$$\beta_i = u_{di}/u_{d1}.$$



BIDISPERSE

$$u'_{d1} = -0.01$$

$$u'_{d2} = -0.01$$



TRIDISPERSE

$$u'_{d1} = -0.008$$

$$u'_{d2} = -0.006$$

$$u'_{d3} = -0.006$$

FIG. 13. Counter-down (mode III) operation of (a) bidisperse ($u'_{d1} = -0.01$; $u'_{d2} = -0.01$) and (b) tridisperse ($u'_{d1} = -0.008$; $u'_{d2} = -0.006$; $u'_{d3} = -0.006$) generalized fluidization. Curves computed; points experimental for water/sand. [After Huang *et al.*, 1982.]

Thus, Eq. (3.14) can be written in the dimensionless form:

$$u'_0 - \beta_i u_{di} \varepsilon / (1 - \varepsilon_i) = M_i \varepsilon^n i. \quad (3.14a)$$

Figure 13 presents results of computation for a bidisperse and a tridisperse system, including experimental points taken from water and sea sand. The fair check between theory and practice corroborates the concept behind the mathematical model represented by the generalized equations (3.14) and (3.15).

Analytical solutions have been obtained for the following special cases:

- motion of a single component through a stationary layer of the other;
- flooding;
- hindered sedimentation;
- incipient fluidization; and
- continuous classification.

E. COMPUTER SOFTWARE

Computer software is being developed to facilitate calculations dealing with various aspects of generalized fluidization.

IV. Fluidized Leaching and Washing

The equations derived in Section III for idealized fluidization may be applied to nonideal G/S systems with suitable corrections, much in the manner of the van der Waals corrections to the ideal gas law, as will be shown in Section IX. Direct use of the equations in Section III is for L/S systems, as exemplified by fluidized leaching and washing.

A. CHARACTERISTICS

Conceivably, any granular solid containing a soluble component disseminated in an inert matrix could be leached rather efficiently in the fluidized state to separate the soluble from the insoluble. And the leached pulp, or slurry, could again be washed in the fluidized state for removal of the solution lodged in intraparticular enclaves and occupying interparticular spaces.

In extractive metallurgy, for instance, certain low-grade copper ores could be leached with acid or ammoniacal solution advantageously in the fluidized state; cupriferous iron ores, after sulfatizing roasting, could have their copper values recovered selectively by leaching with a very dilute acid (Yu *et al.*, 1964);

calcined bauxite has been leached in fluidized columns with strong alkali solutions (Shangtung Aluminum Plant, 1967); pyrite cinders containing non-ferrous elements have been leached in the fluidized state after chloridizing roasting (Institute of Chemical Metallurgy, 1965; Joint SFL Task Group, 1967); in proposed processes for the hydrometallurgical winning of iron from its ores, hydrochloric acid leaching could also be carried out in fluidized columns. Certain brown coals rich in wax content could be leached in the fluidized state with a proper hydrocarbon solvent; in the production of active carbon, crude char could also be treated in the fluidized state with acid and then washed with water; oil-bearing seeds as well as medicinal herbs, after proper size preparation, could also be leached in fluidized apparatus for the recovery of their valuable ingredients; and supercritical "extraction" could also be carried out in fluid-bed columns under pressure.

Figure 14 illustrates a typical fluidized leacher/washer (Kwauk, 1979a, p. 4). A slurry containing the solid particles to be leached and/or washed is fed at the top through a hydraulic distributor into an enlarged settling head, where preliminary removal of excess liquor is accomplished. Solid particles then fall countercurrently against a rising stream of liquor into the fluidized leaching/washing section, in which there is normally a dilute-phase region surmounting a dense-phase region, both regions fluidized, with a more or less well-defined interface between the two. Fresh leaching/washing liquor enters through special spargers located at the bottom of the dense-phase region. Below the dense-phase region, the solid slurry enters a compression zone in which as much liquor is removed as possible in order to discharge a highly densified underflow.

By comparing this simple diagram with the conventional continuous countercurrent decantation circuit, it is easy to deduce the following characteristics for fluidized leaching and washing:

- (1) complete hydraulic operation without any mechanical parts;
- (2) continuous countercurrent operation in a single vertical column where a longitudinal concentration gradient could be established;
- (3) adaptability to extremely low flowing liquid-to-solid ratios, so that it is possible to obtain a relatively concentrated solution from a relatively lean solid parent material;
- (4) low space requirement; and
- (5) ease of automation.

Rickles (1965) reviewed various methods for contacting granular solids with liquids, including an account of pulsed fluid beds. Polinszky (1966) reported on the fluidized washing of pigments, while Yakubovich *et al.* (1970) described fluidized washing columns, and Korsunski *et al.* (1970) and Burovoi *et al.* (1971) wrote on fluidized leaching of zinc calcine. A more recent review on

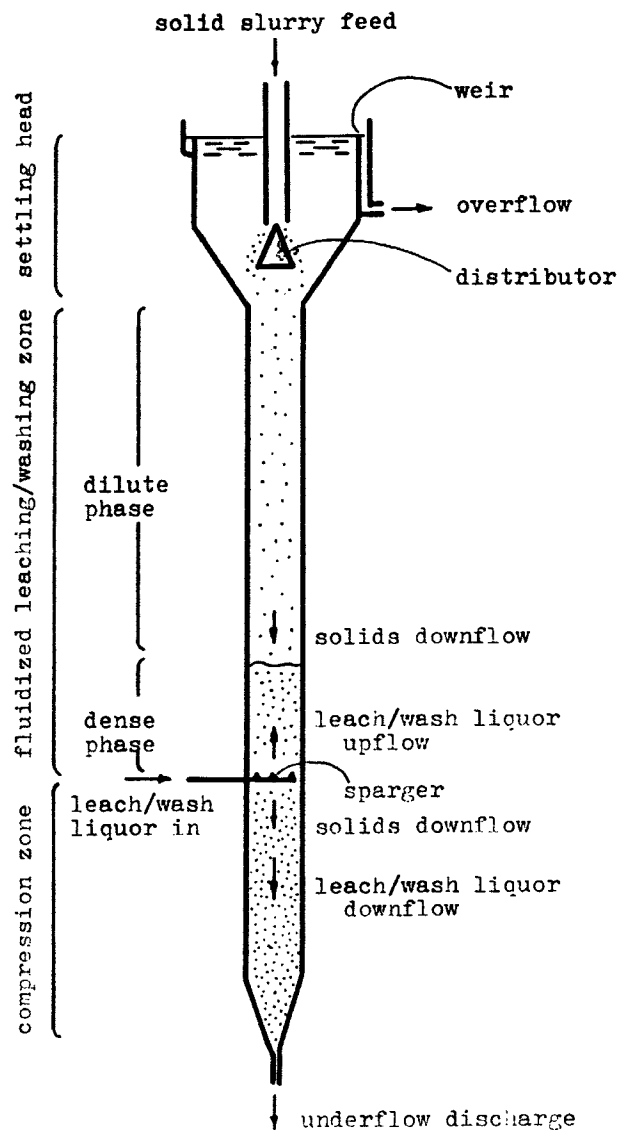


FIG. 14. A typical fluidized leacher/washer. [After Kwauk, 1973, 1979a; Kwauk and Wang, 1981.]

continuous countercurrent contactors for liquids and particulate solids was given by Slater (1969), although his main emphasis was on ion exchange. Among the more recent patents should be mentioned those by Mouret (1971), Rodriguez (1972), and Lloyd and White (1973). Investigations on fluidized leaching and washing started in the People's Republic of China in the late 1950s (Institute of Chemical Metallurgy, Division III, 1959), including analysis on the dynamics of solid-liquid systems (Kwauk, 1961; Kwauk and Chong, 1963), as well as development studies that led to the use of certain industrial equipment up to 1.5 m in diameter.

B. UNIFORM PARTICLES

Fluidized leaching and washing belong to counter-down, or mode III, operation for simultaneous particle-fluid motion. A basic case for uniform particle size will be established, and it will then be extended to mixed particle sizes.

The equation for generalized fluidization, Eq. (3.5), can be rewritten in terms more adapted to the practitioner—that is, solids and fluid at their respective weight rates, S and L , added to the fluidized leacher/washer having a cross-sectional area of A :

$$\frac{L}{\rho_f A} + \frac{S\varepsilon}{\rho_s A(1 - \varepsilon)} = \varepsilon^n u_t. \quad (4.1)$$

Denote the superficial liquid-solids velocity ratio $(L/\rho_f A)/(S/\rho_s A)$ by N , and let $(S/\rho_s u_t) = A_t$, which is the minimal cross-sectional area if the solids were to flow at their terminal velocity u_t in the absence of fluid flow, and can therefore be called terminal cross-sectional area. Then Eq. (4.1) can be reduced to a dimensionless form in terms of a reduced area A' defined as follows:

$$A' = \frac{A}{A_t} = \frac{A}{S/\rho_s u_t} = \frac{N(1 - \varepsilon) + \varepsilon}{\varepsilon^n(1 - \varepsilon)} = \frac{1}{u_d^n}. \quad (4.2)$$

Equation (4.2) is plotted in the upper diagram of Fig. 15 as A' versus ε with N as a parameter. The equation shows that corresponding to any value of N , there exists a minimum value of A' at which the fluidized leacher/washer possesses the least cross-sectional area or the maximum throughput. This minimum A' corresponds to the flooding point characteristic of all counter-down systems and can be calculated by setting the derivative $dA'/d\varepsilon = 0$, thus yielding

$$\varepsilon_{\min} \text{ from } N(1 - \varepsilon) + \varepsilon = \varepsilon/n(1 - \varepsilon), \quad (4.3a)$$

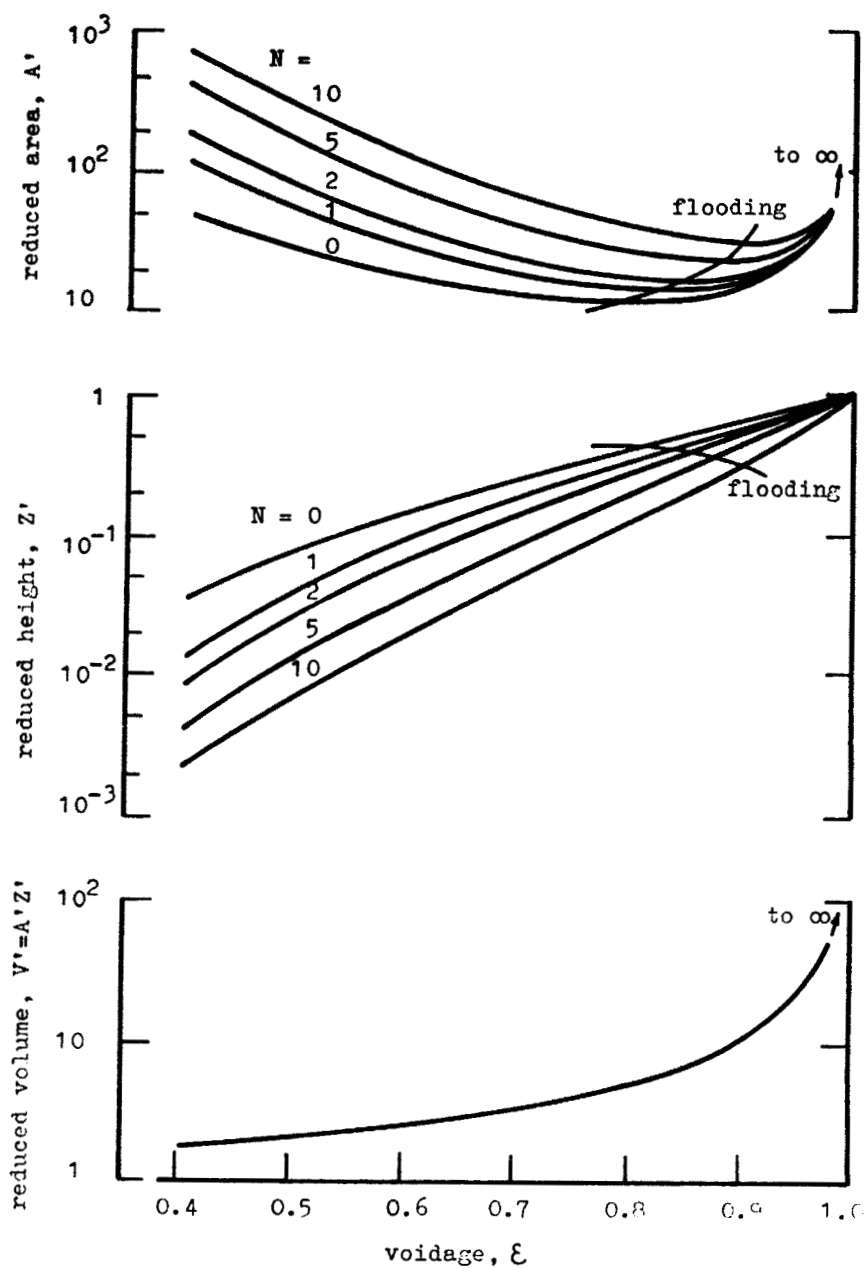


FIG. 15. Fluidized leaching and washing of uniform particles—reduced vessel parameters. [After Kwauk, 1973, 1979a; Kwauk and Wang, 1981.]

$$N_{\min} = \frac{\varepsilon[1 - n(1 - \varepsilon)]}{n(1 - \varepsilon)^2}, \quad (4.3b)$$

$$A'_{\min} = \frac{1}{n(1 - \varepsilon)^2 \varepsilon^{n-1}}. \quad (4.3c)$$

If the leaching or washing of the solids needs an average residence time θ , the required height of the fluidized solids bed can be calculated from

$$\theta = \frac{ZA(1 - \varepsilon)\rho_s}{S}.$$

Substitution of Eq. (4.2) for A and defining terminal height $Z_t = \theta u_t$ give the reduced fluidized bed height,

$$Z' = \frac{Z}{Z_t} = \frac{Z}{\theta u_t} = \frac{\varepsilon^n}{N(1 - \varepsilon) + \varepsilon} = \frac{u'_d}{1 - \varepsilon}. \quad (4.4)$$

Computation indicated that Z' is always less than unity, signifying the fact that the congregation of particles in fluidization reduces the rate of fall of the particles, thus prolonging their residence time. At the point for minimum cross-sectional area A' , the corresponding bed height is

$$Z'_{\min} = n(1 - \varepsilon)\varepsilon^{n-1}, \quad (4.3d)$$

and a reduced volume can be defined as

$$V' = A'Z' = 1/(1 - \varepsilon). \quad (4.5)$$

This equation shows that the smallest volume can be realized only at the lowest possible voidage.

C. MIXED PARTICLES

If the particles treated are not of the same size, some kind of an average particle diameter \bar{d}_p could be adopted, so that the procedure outlined for uniform particles might be followed.

For narrow particle-size cuts, a more convenient method is recommended that consists of calculating the required cross-sectional area on the basis of the smallest particles having diameter d_{p2} , and computing the necessary height to insure the required residence time for the largest particles with diameter d_{p1} . Thus, one can be sure that the smallest particles will not be carried out by the liquid on the one hand, and that the largest particles will not suffer incomplete leaching or washing on the other. According to this so-called two- d_p method, it can be shown that the following expressions for cross-sectional area, height,

and volume ensue:

$$A' = \frac{A}{S/\rho_s u_{t1}} = \left[\frac{N(1 - \varepsilon) + \varepsilon}{\varepsilon^{n_1}(1 - \varepsilon)} \right] \left\{ \frac{1}{M\varepsilon^{\Delta n}} \right\}, \quad (4.2m)$$

$$Z' = \frac{Z}{\theta u_{t1}} = \left[\frac{\varepsilon^{n_1}}{N(1 - \varepsilon) + \varepsilon} \right] \left\{ 1 + N \left(\frac{1 - \varepsilon}{\varepsilon} \right) (1 - M\varepsilon^{\Delta n}) \right\}, \quad (4.4m)$$

$$V' = A'Z' = \left(\frac{1}{1 - \varepsilon} \right) \left\{ \frac{1}{M\varepsilon^n} \left[1 + N \left(\frac{1 - \varepsilon}{\varepsilon} \right) (1 - M\varepsilon^{\Delta n}) \right] \right\}. \quad (4.5m)$$

Comparison of these three equations with their corresponding parent equations for uniform particles reveals that A' , Z' , and V' calculated from the larger particles of d_{p1} need to be corrected, because of the presence of the smaller particles, by factors shown in the large braces of these equations, all involving the factor $M\varepsilon^{\Delta n}$ in which $M = u_{t2}/u_{t1}$ and $\Delta n = n_2 - n_1$.

If the particle size distribution is sufficiently wide, as often occurs for crushed ores or other disintegrated material products, it should be realized that the volumetric utilization of the leaching/washing apparatus would be rather poor, especially when the value of $M\varepsilon^{\Delta n}$ is down to below 0.2. For this reason, leaching or washing could be carried out in parallel columns operating at successively reduced fluid velocities. This principle of the so-called staged fluidized leaching (SFL) is illustrated in Fig. 16. Each leaching or washing column, or stage, together with its entrance region at the top, also serves as a hydraulic classifier. With this provision, the largest particles are treated in the first column or stage, having the highest fluid velocity, so that they may descend slowly in a rather concentrated state, and the required high residence time on account of the larger particle size may be guaranteed without the need of inappropriate height. The smallest particles are leached or washed in the last column or stage of the series, operating with the lowest fluid velocity, so that they may descend through the fluid at their characteristically low velocity without being carried over. Since this fraction of the smallest particles usually constitutes only a small portion of the solid feed material, the cross-sectional area devoted to their use would be far less than when all the fractions were treated *en masse* in a single vessel. Computations have indicated that division of the leaching or washing duty into several stages often resulted in a saving of apparatus volume by a factor amounting to as much as two orders of magnitude.

Detailed method has been developed for designing SFL. Typical results were provided for a 1.5-m diameter industrial washer for leached uranium ore, which was split into 27 particle size fractions, thus resulting in 28 simultaneous equations (Zhang and Zheng, 1982).

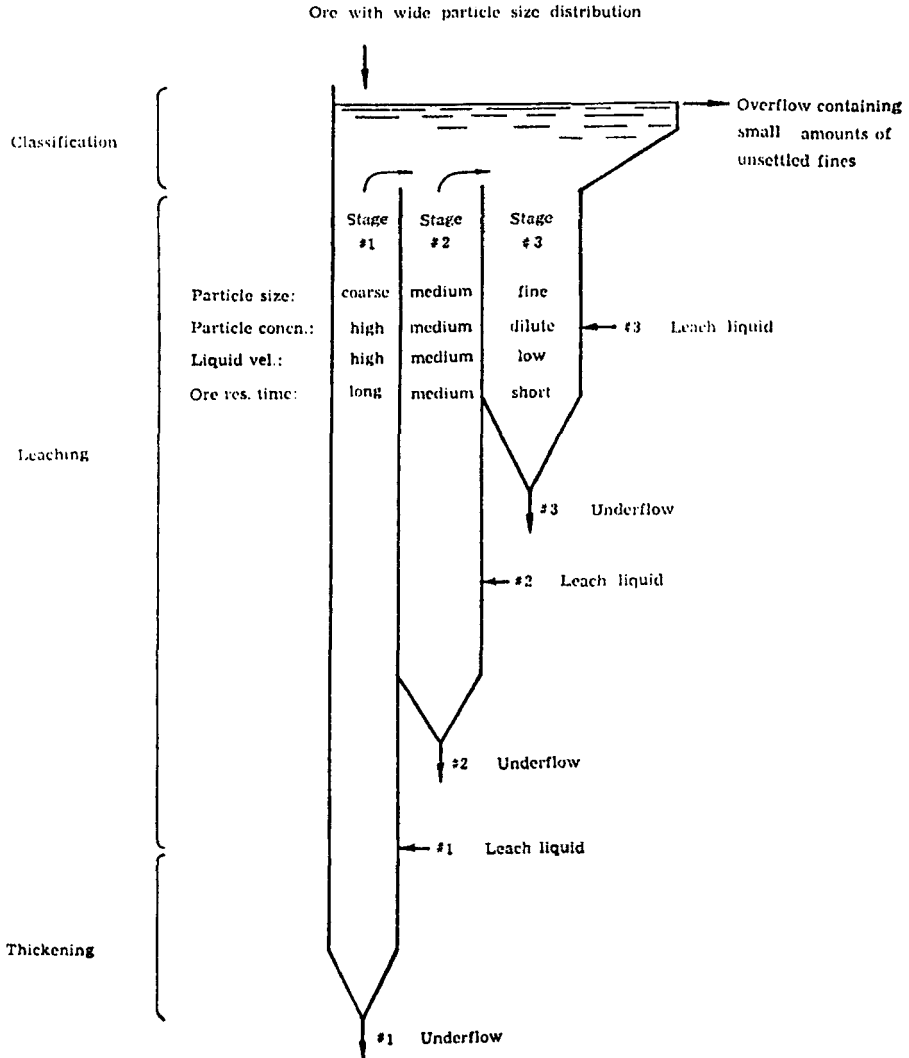


FIG. 16. Staged fluidized leaching/washing. [After Kwauk, 1973.]

D. EXPERIMENTAL FINDINGS

Laboratory experiments were performed in a set of three fluidized columns, each made of unsegmented brass tubing 42 mm in inside diameter. Sea sand, 2.5 g/cm^3 in density and with a broad size distribution, was employed as the

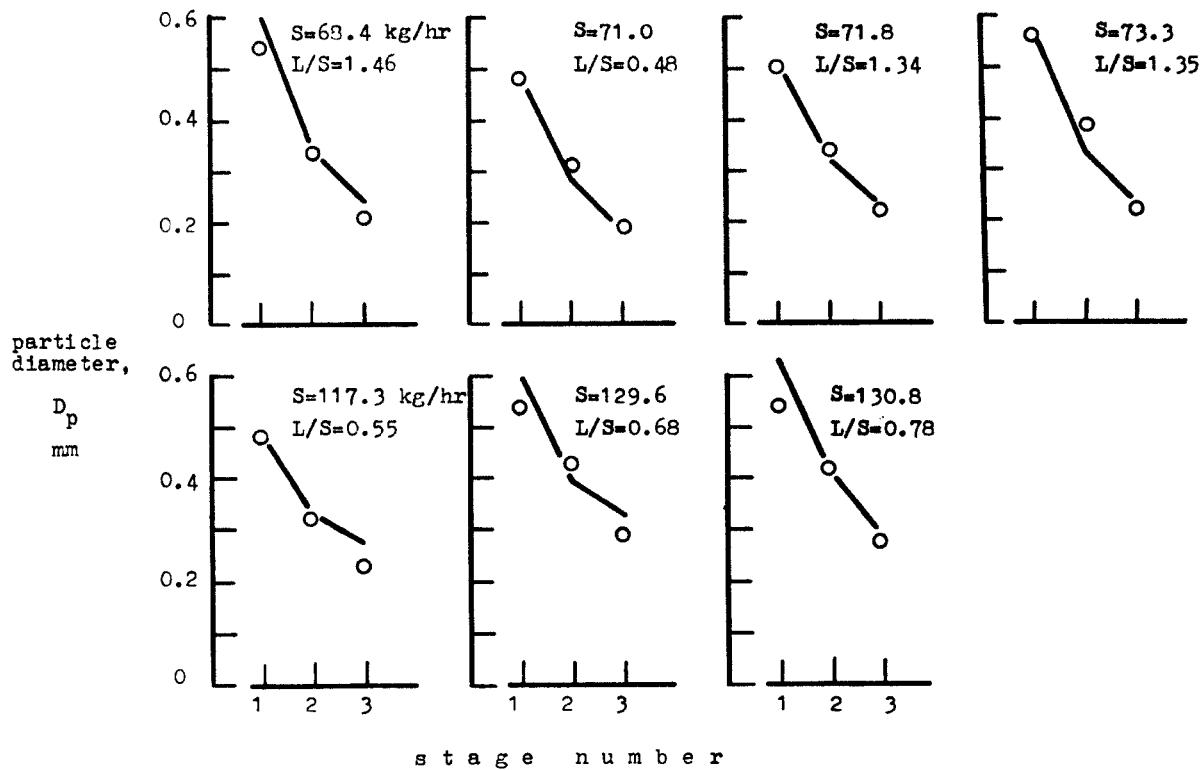


FIG. 17. Flow model study for a three-stage fluidized leacher—comparison of computed particle size (solid lines) with experimental results (open circles). [After Kwauk and Wang, 1981.]

test solid material, and water was used as the fluidizing medium. Figure 17 illustrates some typical experimental results (Yu *et al.*, 1964), in which the average particle size for each stage is shown to check rather closely the computed value.

Figure 18 shows a pilot-scale fluidized washer for stripping nickel from a pulp of fine laterite ore with ammonia liquor (Kwauk, 1979a, p. 19). The washer measures 1 m in diameter and 14.5 m in height, with a 1.6-m diameter settling head at the top for dewatering the rather lean pulp feed, and a

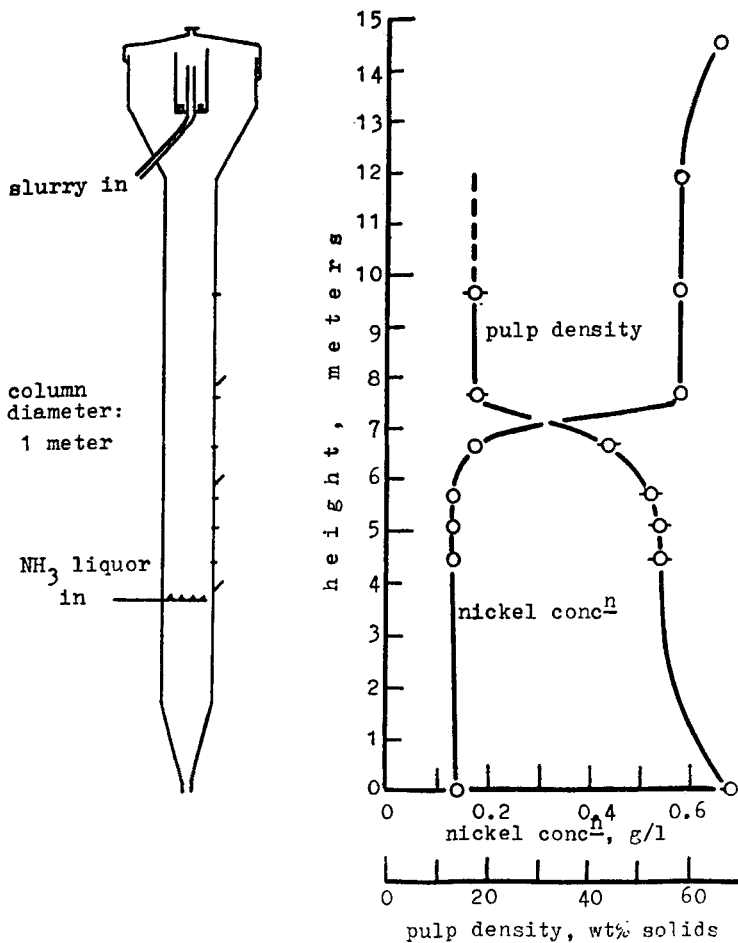


FIG. 18. Results from a pilot-scale fluidized washer. [After Kwauk, 1979a; Kwauk and Wang, 1981.]

thickening section below the ammonia wash liquor entry for delivering a dense underflow. The curves on the right-hand side of Fig. 18 stand for the pulp density and nickel concentration profiles in the column. It can be seen that the dense-phase fluidized bed with a pulp density of 50% by weight is surmounted by an 18% dilute phase, and followed below by a thickening section that ultimately discharges a 65% underflow. At the column height of 6 to 7 m, there is evident a more or less abrupt transition from the dense to the dilute phase, which defines a somewhat diffuse interface. Of interest is the fact that nickel concentration experiences a more or less sudden change at this same interfacial region, from a high value of 0.6 g/l in the dilute phase to a low value of 0.14 g/l in the dense phase. These curves show little variation in either pulp density or nickel concentration in the dilute phase or in the dense phase itself. This is attributed to intense intraphase backmixing, in either the dilute-phase region or the dense-phase region. However, the sharp drop in nickel concentration at the interfacial region between the dilute and dense phases, on the other hand, could be interpreted as the lack of interphase mixing.

For coarser particles, however, a concentration profile could be easily established, and concentration reduction in washing to the order of 1/100 is not uncommon. Unfortunately, available data have not been made public.

E. STAGING

The lack of concentration gradient in either the dilute or dense phase, when small particles are leached or washed, is due to backmixing. Attempts have been made to cut down such backmixing by installing internals varying from vertical baffles to horizontal structures composed of various configurations of slanting surfaces (Kwauk, 1979a). Probably because of the small resistance such internals can offer to the slow convective currents, few seem to have proven themselves effective.

The sharp concentration gradient in the interfacial region between the dilute phase at the top and the dense phase at the bottom has also been demonstrated in visualization studies in laboratory investigations using colored tracers.

The existence of this interfacial barrier between the dilute and dense phases is exploited in the vertical staging of fluidized leaching and washing, with a view to forming as many interfaces as there are stages, each possessing two nonmixing compartments. Figure 19 shows a variety of multistage L/S fluid beds.

For successful operation of a multistage fluidized leacher/washer, the downcomer to transfer solids from any stage to the one below needs to offer sealing power against liquid bypassing and to insure steady flow of the

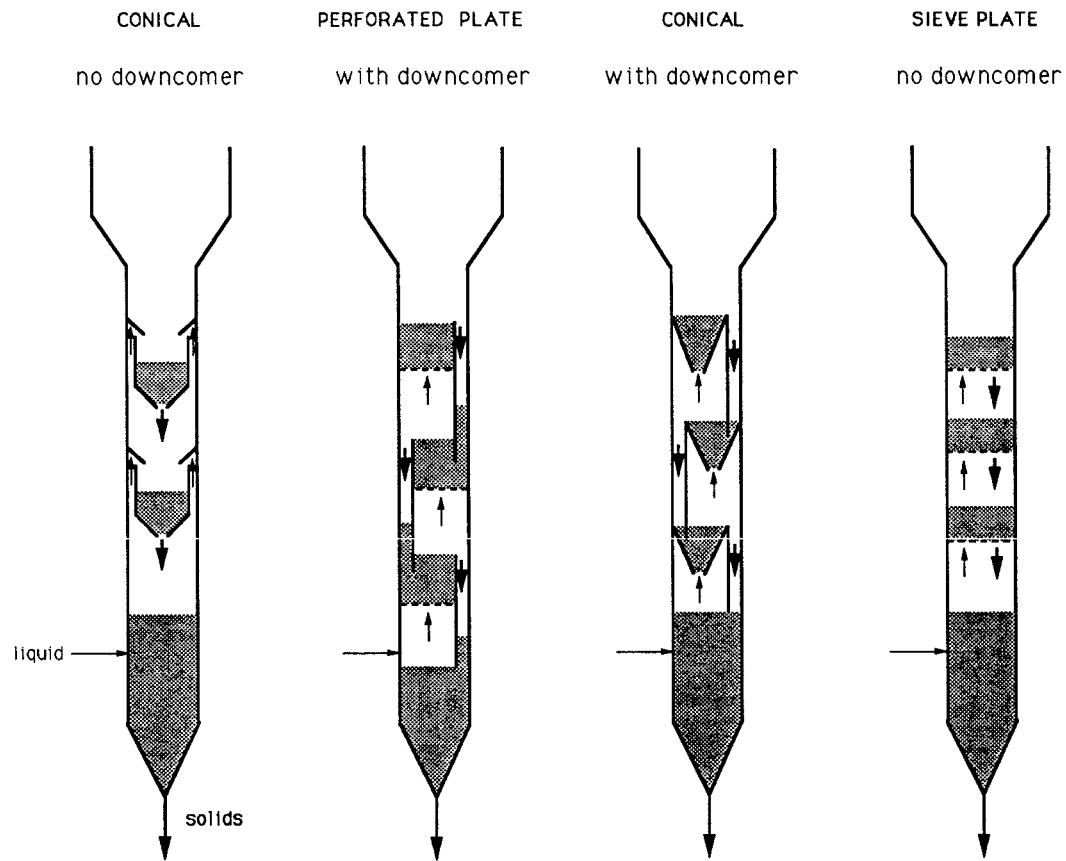


FIG. 19. Multistage fluidized leacher/washer. [After Kwauk, 1979a.]

descending solid particles. For fine particles, however, if they do not dewater easily, they will flow as a slurry for which no hydrodynamic seal is possible. If the downcomer is designed to offer sufficient residence time for the solid particles to dewater, its dimension may be inordinately large compared to that of the leacher/washer, or else, as is often the case, the fine particles may continue to thicken or consolidate after defluidization, thus inducing sporadic solids flow or leading even to plugging.

One solution is the autosiphon-operated fluidized leacher/washer shown in Fig. 20 (Kwauk, 1979a, p. 89; 1981). Each stage is designed with a conical bottom having a large hole in the center for admitting the fluidizing liquor and for letting down solids periodically. Each stage receives its solids feed from discharge through the conical aperture of the compartment above. When sufficient solids have collected in this stage, the increased pressure drop across the fluidized solids bed actuates a siphon associated to this stage that bypasses the fluidizing liquid through a passage in the siphon box to the stage above, so that the solid particles in this stage, now deprived of their fluidizing liquid, fall through the same central hole that has admitted the fluidizing liquor, down to its neighbor below. The descending solids level in the stage that is discharging solids reduces the pressure drop across the solids bed, until when it has fallen to some predetermined level fixed by the autosiphon design, the siphon breaks automatically, thus restoring the main fluidizing stream to the central conical aperture to reactivate the remaining solids in the stage into the fluidized state. When this stage has received sufficient solids from its neighbor above, the cycle repeats itself. This periodic operation is hydrodynamically actuated by the gravity head of the falling solid particles, without interruption of the normal constant flow of the fluidizing liquid.

F. RATE MEASUREMENT FOR SOLIDS LEACHING AND WASHING

Rational design of fluidized leaching or washing columns calls not only for adequate knowledge of the dynamics of solid-liquid systems, but also for data on the rate of leaching or washing of the particles. An apparatus, called the differential leacher/washer cell (Kwauk, 1972; Institute of Chemical Metallurgy, 1973, 1975), has been designed for measuring the unsteady-state decrease of solute concentration in a thin layer of particles being leached or washed, as shown schematically in Fig. 21. The differential cell, approximately the size of a thimble, is first filled with the solid particles concerned, generally as a slurry, which are then leached or washed by passing a leach or wash liquor from beneath the particulate layer at a velocity sufficient to fluidize the solids. The change in solute concentration is monitored conductometrically by an electrode placed either inside the solids bed or as a thin tubular conduit through which the overflow passes, as shown in Fig. 22.

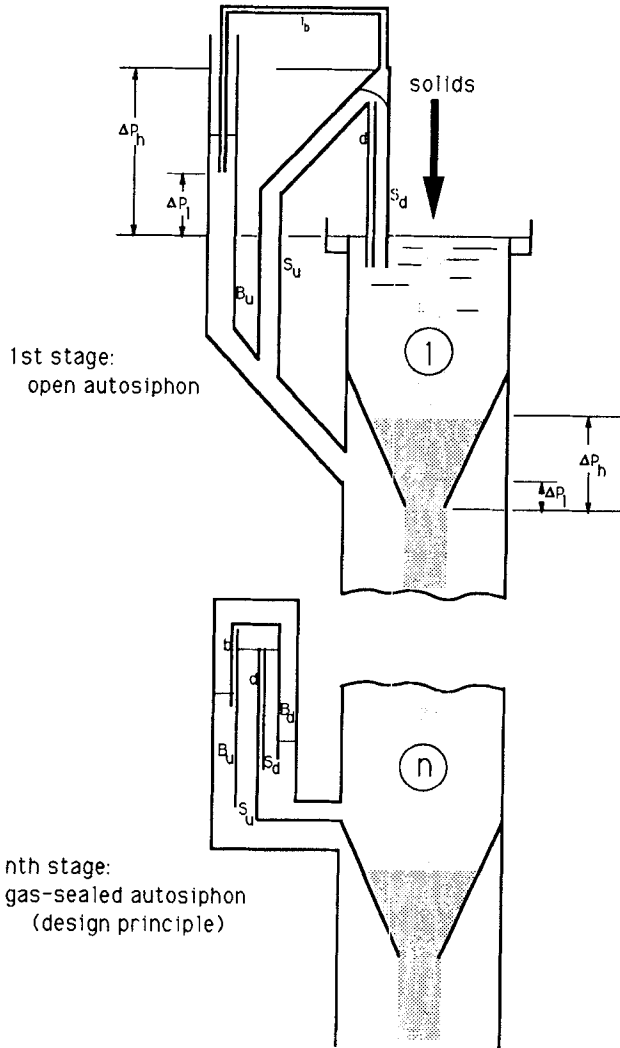


FIG. 20. The autosiphon-operated fluidized leacher/washer. [After Kwauk, 1981.]

Mathematical modeling of the differential leacher/washer resulted in the following equation:

$$\frac{y}{y_0} = \left[1 + \frac{K(\beta - 1)}{K + \gamma} \right] e^{-\gamma\theta} - \left[\frac{K(\beta - 1)}{K + \gamma} \right] e^{K\theta}, \quad (4.9)$$

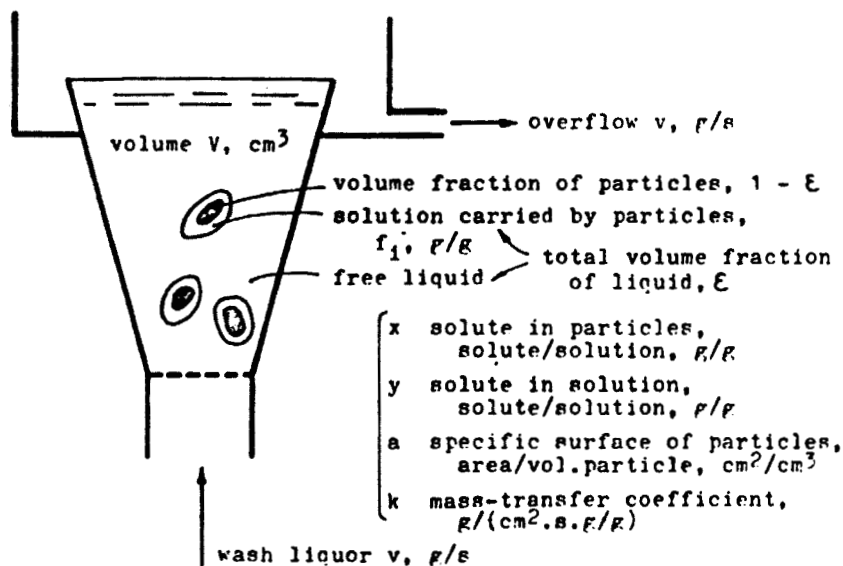


FIG. 21. Principle of the differential leacher/washer cell. [After Kwauk, 1979a; Kwauk and Wang, 1981.]

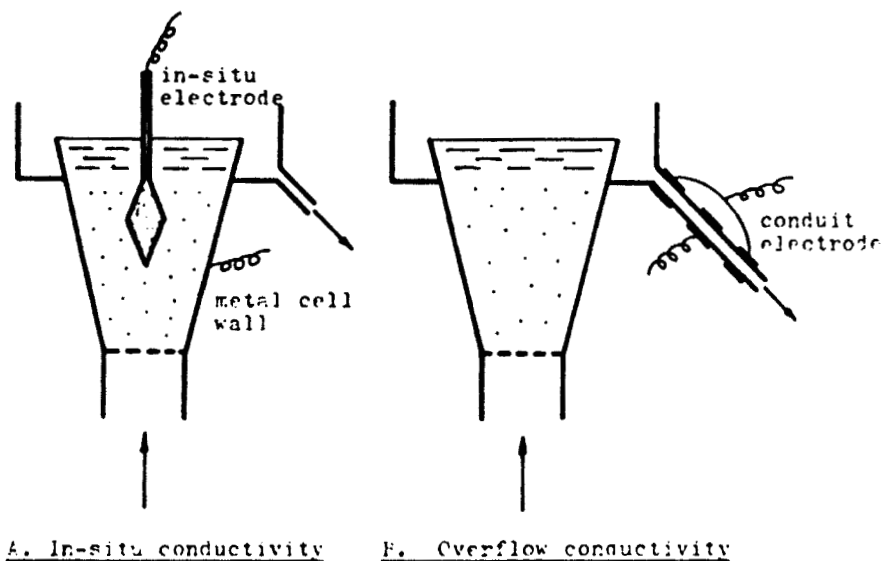


FIG. 22. Two kinds of differential leacher/washer cell: (a) in-situ conductivity; (b) overflow conductivity.

where

$$K = -\frac{\alpha\beta + \gamma}{2} + \left[\left(\frac{\alpha\beta + \gamma}{2} \right)^2 - \alpha\gamma \right]^{1/2}$$

$$a = \frac{ka}{\rho_s f_i}$$

$$\beta - 1 = \frac{(1 - \varepsilon)\rho_s f_i}{\varepsilon\rho_f - (1 - \varepsilon)\rho_s f_i}$$

$$\gamma = \frac{v}{V[\varepsilon\rho_f - (1 - \varepsilon)\rho_s f_i]}$$

Experimentally, the solute concentration is correlated empirically to the conductometric reading, and then $\ln(y/y_0)$ is plotted against time θ , as shown in Fig. 23. Typically there is a sharp initial drop in solute concentration, followed by a slow first-order decay. The first stage is represented by the first term on the

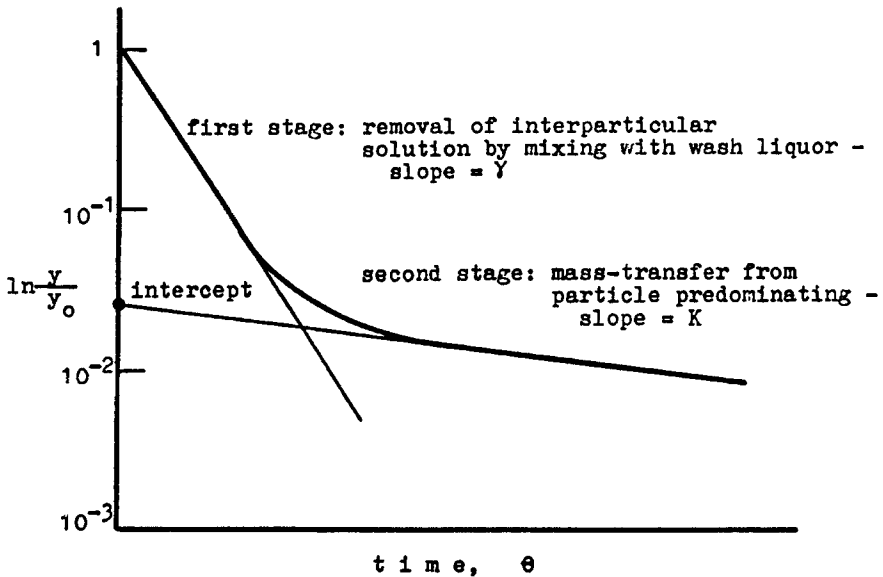


FIG. 23. Treatment of data for the differential leacher/washer cell. First stage: removal of interparticular solution by mixing with wash liquor; slope = γ . Second stage: Mass transfer from particle predominating; slope = K . [After Kwauk, 1979a; Kwauk and Wang, 1981.]

right-hand side of Eq. (4.9), and it signifies the loss of solute from the cell by mixing of the leach or wash liquor with interparticle solution, with a slope equal to γ . The second term on the right-hand side of Eq. (4.9) stands for the slow second stage dominated by mass transfer from the particles, with a slope equal to K and an intercept of $-K(\beta - 1)/(K + \gamma)$, on the ordinate at zero time. From values for the two slopes and the intercept, by solving the related expressions, all parameters listed in Fig. 21 can be computed.

V. Solids Mixing and Segregation

Solids in particle-fluid systems in motion tend to segregate from their dissimilar neighbors and to coexist with their kin under similar conditions. Once segregated, however, they tend to disperse into enclaves occupied by those dissimilar neighbors by a mechanism similar to diffusion. In the case of G/S systems, this dispersion process is augmented on further larger scales by mixing brought about by gas bubbling.

May (1959) was among the earlier workers studying solids mixing in fluidized-bed reactors. A succession of studies was carried out at University College, London (Rowe and Sutherland, 1964; Sutherland *et al.*, 1961; Rowe *et al.*, 1965, 1972a, 1972b, 1978; Gibilaro and Rowe, 1974; Cheung *et al.*, 1974; Nienow, *et al.*, 1978), mostly for G/S systems. These studies were further carried on by Nienow and Chiba (1981, 1985) and continued in Japan by Chiba and his associates (Tanimoto *et al.*, 1980; Naimer *et al.*, 1982; Moritomi *et al.*, 1982, 1985, 1986; Chiba *et al.*, 1986). Chiba's work in collaboration with Moritomi was concerned with L/S systems. Modeling was proposed in England by Gibilaro and Rowe (1974), among others, and in Japan by applying the method of Horio *et al.* (1986). Other workers in solids mixing/segregation include Littman (1964), Jinescu *et al.* (1966), Kang and Osberg (1966), Borlai *et al.* (1967), Highley and Merrick (1972), Leschonski (1981), Somer (1981), Lloyd (1981), Ghar and Gupta (1981), and Valkenburg *et al.* (1986).

Complex as this joint process of mixing and segregation is, the mechanism is best understood by studying the simplest case of a binary mixture of two kinds of solid particles having dissimilar properties, e.g., density and/or particle size.

The general problem of solids mixing and segregation can thus be resolved into three aspects:

1. How would the two segregated phases of the particle-fluid mixture be juxtaposed with respect to each other—which on top and which below?
2. How would the mixing process across the phases take place, in the absence of bubbles, the dispersive force balanced against that of segregation?

3. How would the macro effect of bubbling augment or alter the mixing process?

Quantitative analysis could readily be made in the light of idealized fluidization, to deal with the first two aspects of the mixing/segregation process (Kwauk, 1962, 1963b).

A. PHASE JUXTAPOSITION

Hydrostatic considerations would specify *a priori* that the heavier particle-fluid phase would occupy the lower position in a vertical array of the two phases. Let the heavier particles with effective density $\Delta\rho_1 = \rho_{s1} - \rho_f$ be designated particles #1, which are expanded under the prevailing flow conditions to a voidage ε_1 , thus creating a particle-fluid phase of bulk density $\rho_{B1} = \Delta\rho_1(1 - \varepsilon_1)$. Should this bulk density exceed that of the other particles #2, then particles #1 would occupy the lower position.

Dynamic stability would suggest that a lower-voidage phase should also occupy the lower position: Should a particle from above stray into the lower region, the higher interstitial fluid velocity would no doubt return it to its place of origin where the local velocity is lower. However, a higher-voidage phase may exist in a lower position, provided its bulk density exceeds that of the effective density of the particles in the upper phase. For instance, if the heavier particles #1 are smaller, they would be expanded by the flowing fluid to a voidage greater than that of the lighter particles ε_2 . They may occupy the lower zone provided

$$\rho_{B1} \equiv \Delta\rho_1(1 - \varepsilon_1) > \Delta\rho_2, \quad (5.1)$$

whereby a straying particle #2 would be buoyed back into the upper zone by the higher overall particle-fluid bulk density.

These two criteria, density and voidage, can specify only four combinations:

$\rho_{B1} : \rho_{B2}$	$\varepsilon_1 : \varepsilon_2$	Operation
>	<	IA
>	>	(IB)
<	<	((IIA)) impossible
<	>	IIB

Operation ((IIA)), in double parentheses, is mathematically untenable, because

$$\begin{aligned} \text{if } \Delta\rho_1 > \Delta\rho_2 \quad \text{and} \quad \varepsilon_1 < \varepsilon_2, \\ \text{then } \rho_{B1} \equiv \Delta\rho_1(1 - \varepsilon_1) > \Delta\rho_2(1 - \varepsilon_2) \equiv \rho_{B2}. \end{aligned}$$

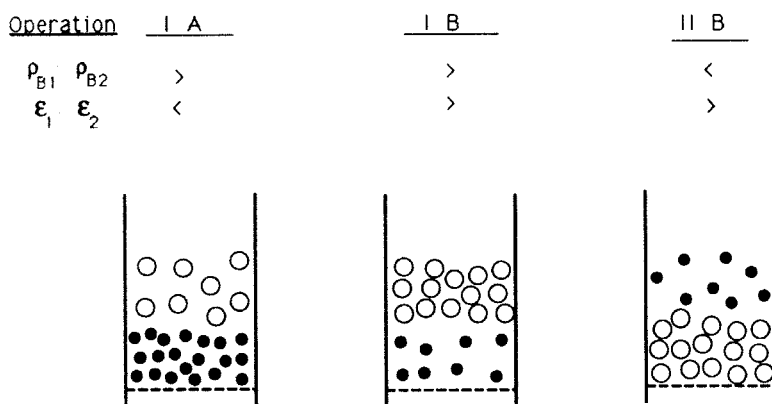


FIG. 24. Juxtaposition of binary phases. Solid circles: particle #1; open circles: particle #2.

Of the three remaining operations, (IB), in parentheses, is stable only subject to the stipulation of Eq. (5.1).

Figure 24 illustrates these three operations.

B. OPERATION SHIFTS

The operations listed in Fig. 24 may shift from one mode to the other as the fluid velocity changes. Such a shift depends on the relative magnitudes of the two incipient fluidization velocities u_{f1} and u_{f2} and of the two terminal velocities u_{t1} and u_{t2} , and on whether the bulk-density-vs.-velocity (as well as the voidage-vs.-velocity) curves of the two kinds of particles are parallel or cross each other. That is, put more succinctly:

$$u_{f1} > \text{or} < u_{f2},$$

$$u_{t1} > \text{or} < u_{t2},$$

$$\rho_B - u \text{ curves } \parallel \text{ or } \times,$$

$$\epsilon - u \text{ curves } \parallel \text{ or } \times.$$

When an operation shifts, phases may change their relative positions. Such operation shifts, predicted theoretically from particulate fluidization in the early 1960s, was recently described in experimental detail by Moritomi *et al.* (1982).

The modes of operation shift were analyzed in terms of the relation between the Archimedes number and the Reynolds number explained in Section II and are summarized in Fig. 25. A search of possible $\rho_B - u$ and $\epsilon - u$ curves, in

$$AS_1 > AS_2$$

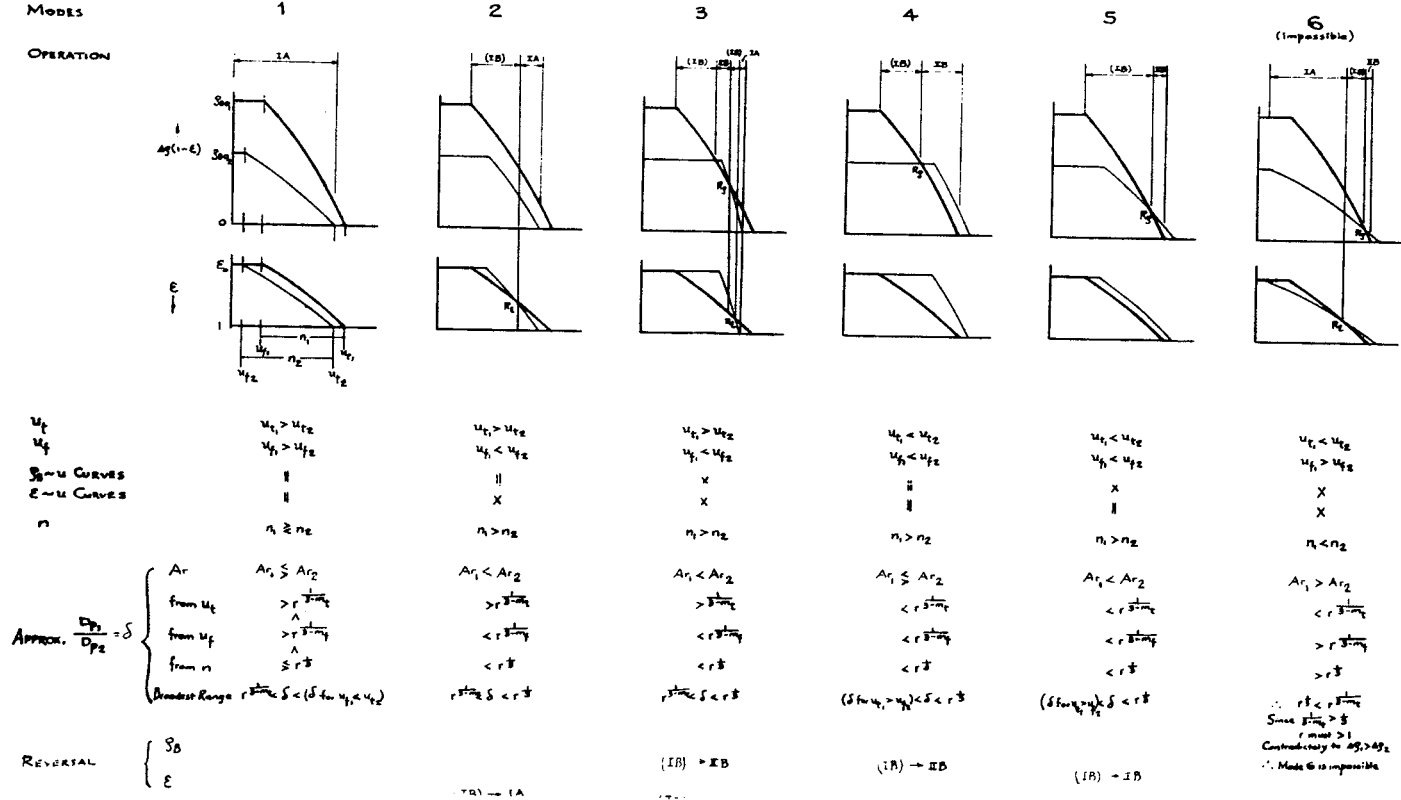


FIG. 25. Modes of operation shifts for binary particle mixtures (heavy lines for denser particles). [After Kwauk, 1962.]

combination with u_t and u_i comparisons, led to the six modes of operation shifts shown in this figure. Mode I has the particles ratio $\delta = d_{p1}/d_{p2}$ unspecified. But evidently it has to be bounded by the requirement $u_{t1} > u_{t2}$. Modes 4 and 5 are similar except for the location of the density reversal point—fluidized for particles #2 in mode 5, and fixed-bed for mode 4. This analysis showed that mode 6 is physically not possible. So, essentially there remain only three types of operation shifts, viz., modes 2, 3, and 4/5.

C. REVERSAL POINTS

As indicated in the last two rows of explanation, Fig. 25 shows two types of operation shifts: a cross in the ρ_B-u curves, or ρ_B -reversal; and a cross in the $\varepsilon-u$ curves, or ε -reversal. The former occurs for modes 3 and 4/5, and the latter for modes 2 and 3. At the ρ_B -reversal point, the bulk densities of the two phases are equal, that is,

$$\rho_{B1} \equiv \Delta\rho_1(1 - \varepsilon_1) = \Delta\rho_2(1 - \varepsilon_2) \equiv \rho_{B2}. \quad (5.2)$$

It was shown that for reversal, the ratios $\delta = d_{p1}/d_{p2}$ and $r = \Delta p_2/\Delta p_1$ are related to each other in a characteristic way.

D. DEGREE OF SEGREGATION

Although heavy-below-light is the irrefutable rule of hydrostatics for phase juxtaposition for binary particles mixtures, the heavier particles in the lower region tend to wander into the lighter phase above, only to return to their point of origin because of insufficient buoyancy in the lighter surroundings, and the lighter particles also tend to wander into the heavier phase below for a similar transient sojourn. In general, this counterdiffusion between the heavier and lighter particles is illustrated in inset A of Fig. 26. If the two particles were completely mixed, they would define a voidage ε_m , constant throughout the height of the solids bed, as shown in the ε -diagram of Fig. 26. If these were completely segregated, without any intermixing at the interphase junction, then there would be two separate voidages, ε_{s1} and ε_{s2} , each determined by the terminal velocity of its member particles at the common prevailing fluid flow rate u . For all practical cases, there would exist a certain degree of intermixing between the two juxtaposed phases, thus creating a voidage curve ε_a that lies between the two extremes of complete mixing and complete segregation.

These characteristic voidage curves would create their corresponding pressure gradient curves as shown in the P' -diagram, all expressed in

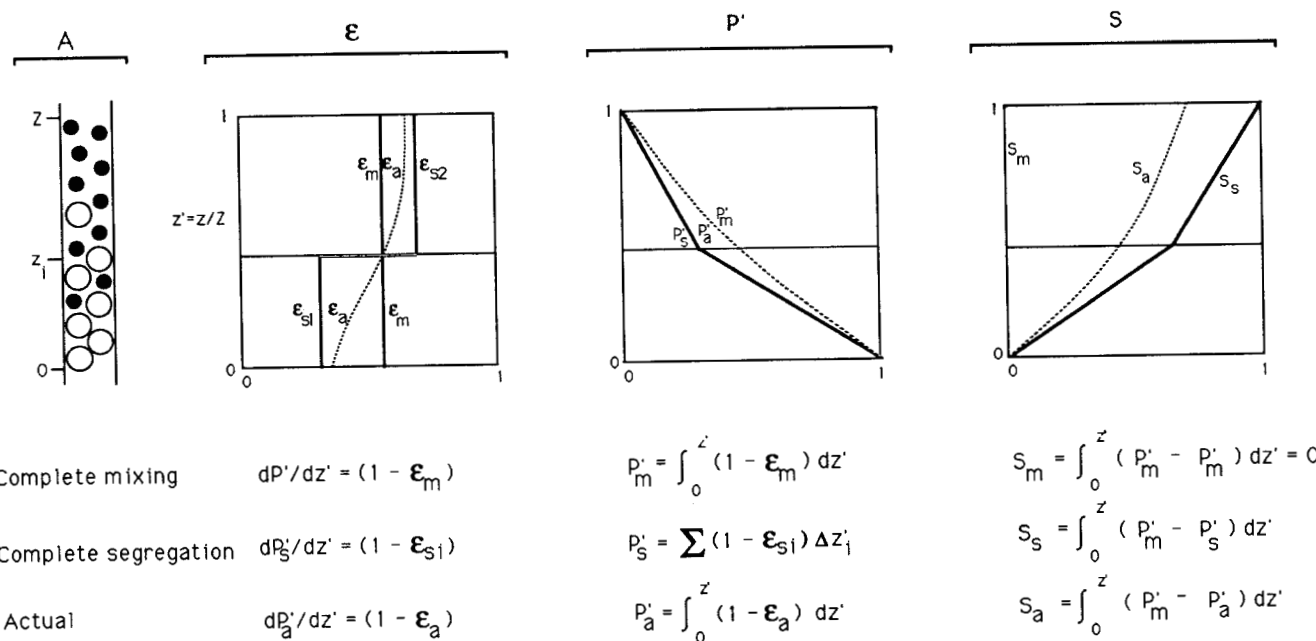


FIG. 26. Degree of segregation for binary particle mixtures.

dimensionless head:

$$\text{complete mixing} \quad P'_m = \int_0^{z'} (1 - \varepsilon_m) dz', \quad (5.3m)$$

$$\text{complete segregation} \quad P'_s = \sum_i^2 (1 - \varepsilon_{si}) z'_i, \quad (5.3s)$$

$$\text{actual case} \quad P'_a = \int_0^{z'} (1 - \varepsilon_a) dz'. \quad (5.3a)$$

The P' curves, transposed from the ε diagram, are all displaced to the left of the P'_m curve for complete mixing, with a maximum position occupied by that for complete segregation, P'_s . Thus, departure from the P'_m curve, which is the diagonal in terms of reduced quantities, is a measure of the amount of particle size segregation, from the completely mixed case. For the entire height of the solids bed, a cumulative measure of this departure is the area between an operating P'_a curve and the P'_m diagonal for complete mixing. These corresponding areas are defined as

$$\text{complete mixing} \quad S_m = \int_0^{z'} (P'_m - P'_m) dz' = 0, \quad (5.4m)$$

$$\text{complete segregation} \quad S_s = \int_0^{z'} (P'_m - P'_s) dz', \quad (5.4s)$$

$$\text{actual case} \quad S_a = \int_0^{z'} (P'_m - P'_a) dz'. \quad (5.4a)$$

Combination of the corresponding Eqs. (5.3) and (5.4) gives

$$S_m = \iint_0^{z'} (\varepsilon_m - \varepsilon_m) dz' dz' = 0, \quad (5.5m)$$

$$S_s = \iint_0^{z'} |(\varepsilon_{si} - \varepsilon_m)| dz' dz', \quad (5.5s)$$

$$S_a = \iint_0^{z'} |(\varepsilon_a - \varepsilon_m)| dz' dz'. \quad (5.5a)$$

From the P' diagram of Fig. 26, it is easy to see that the maximum deviation from complete mixing is represented by complete segregation S_s . Thus, it is desirable to specify the degree of mixing S' as a reduced quantity

$$S' = S_a/S_s$$

so that the range of S' is

$$\underbrace{0}_{\text{complete mixing}} < S' < \underbrace{1}_{\text{complete segregation}}$$

E. MIXING SEGREGATION EQUILIBRIUM

The axial voidage distribution resulting from mixing of dissimilar particles, as shown in Fig. 26, will now be examined in the light of the dynamics of these particles at the interfacial boundary between the properly juxtaposed phases of a binary particle mixture (Lou, 1964; Kwauk, 1973). Both the lighter particles at the top and the heavier particles at the bottom share the same tendency of invading the region occupied by the other. This behavior conforms to the concept of random walk, for which Fick's law can be adapted to describe the macroscopic diffusion flux of the smaller particles #2:

$$J_{m2} = -\mu_2 \frac{d[\rho_s(1 - \varepsilon_2)]}{dz} = \mu_2 \rho_s \frac{d\varepsilon_2}{dz}, \quad (5.6)$$

in which μ_2 represents the pseudo-Fick's constant, and ε_2 the voidage attributable to the smaller particles #2. As these smaller particles #2 diffuse into a lower region mainly populated by the larger particles #1, the average voidage ε at this region of the mixed particles is doubtlessly smaller than the voidage ε_2^* that the smaller particles #2 would possess were they to exist alone, and the smaller particles #2 will therefore experience a buoyancy force proportional to the particle concentration difference $[\Delta\rho(1 - \varepsilon) - \Delta\rho(1 - \varepsilon_2^*)]$, which tends to return them to where they were. This upward reversion, or segregation flux, will also be proportional to the concentration $(1 - \varepsilon_2)$ of the smaller particles #2 themselves, that is,

$$J_{s2} = \sigma_2 [\Delta\rho(1 - \varepsilon) - \Delta\rho(1 - \varepsilon_2^*)](1 - \varepsilon_2), \quad (5.7)$$

in which the proportionality constant σ_2 can be called the segregation constant. For a batch process, the opposite tendencies of diffusion and segregation of the smaller particles #2 are in a state of equilibrium:

$$J_{m2} = -J_{s2}.$$

Therefore, combining Eqs. (5.6) and (5.7) and defining an exchange coefficient $Q_2 = \sigma_2 \Delta\rho / \mu_2 \rho_s$, we get

$$\frac{d\varepsilon_2}{dz} = Q_2(\varepsilon - \varepsilon_2^*)(1 - \varepsilon_2). \quad (5.8a)$$

Similarly, for the larger particles #1,

$$\frac{d\varepsilon_1}{dz} = Q_1(\varepsilon - \varepsilon_1^*)(1 - \varepsilon_1). \quad (5.8b)$$

Combination of Eqs. (5.8a) and (5.8b) yields

$$Q_1 dz = \frac{d\varepsilon_1}{(\varepsilon - \varepsilon_1^*)(1 - \varepsilon_1)} = \frac{Q_1}{Q_2} \frac{d\varepsilon_2}{(\varepsilon - \varepsilon_2^*)(1 - \varepsilon_2)}. \quad (5.9)$$

The unmixed voidages ε_1^* and ε_2^* can be written in terms of their terminal velocities according to idealized fluidization:

$$\varepsilon_1^* = (u/u_{t1})^{1/n_1}, \quad \varepsilon_2^* = (u/u_{t2})^{1/n_2}.$$

Also, the total concentration of particles is the sum of those for the larger particles #1 and smaller particles #2:

$$(1 - \varepsilon) = (1 - \varepsilon_1) + (1 - \varepsilon_2).$$

Substitution into Eq. (5.9) gives

$$Q_1 dz = \frac{d\varepsilon_1}{(\varepsilon_1 + \varepsilon_2 - 1 - \varepsilon_1^*)(1 - \varepsilon_1)} = \frac{Q_1}{Q_2} \frac{d\varepsilon_2}{(\varepsilon_1 + \varepsilon_2 - 1 - \varepsilon_2^*)(1 - \varepsilon_2)}. \quad (5.9a)$$

This nonlinear differential equation admits of no analytical solution except for the special case for $Q_1/Q_2 = 1$.

Experimental testing of the mathematical model was carried out in a Plexiglas two-dimensional vessel measuring 10 mm \times 50 mm in inside dimension and 1,200 mm tall. Typical experimental results for 1.52- and 1.99-mm diameter glass beads are shown in Fig. 27, together with curves computed by using Eq. (5.9a).

The preceding analysis for a binary particles mixture may be generalized to polydisperse systems. Thus, for any j fraction, an equation similar to Eq. (5.8a) can be written

$$\frac{d\varepsilon_j}{dz} = Q_j(\varepsilon - \varepsilon_j^*)(1 - \varepsilon_j). \quad (5.8j)$$

Similarly, the total solids concentration is the sum of the individual fractions,

$$(1 - \varepsilon) = \sum_{j=1}^J (1 - \varepsilon_j).$$

Thus a set of differential equations similar to Eq. (5.18a) can be written, which can be solved on a computer.

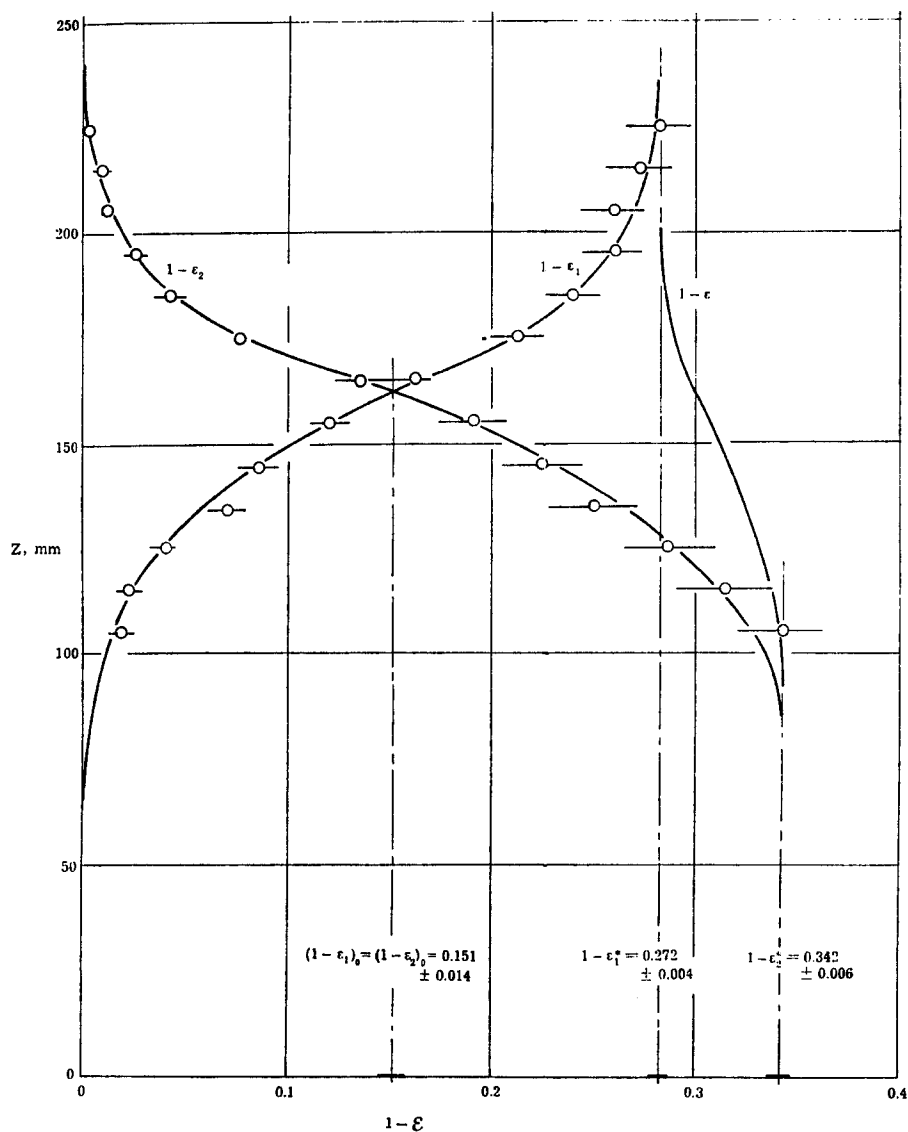


FIG. 27. Particle-size segregation for 1.52- and 1.99-mm glass beads fluidized with water. Lines for computation; points for experimental results, with horizontal dashes to show deviations in data. [After Kwauk, 1973.]

F. GENERALIZED FLUIDIZATION OF POLYDISPERSE SYSTEMS

For generalized fluidization, the diffusion flux J_{m2} of Eq. (5.6) and the segregation flux J_{s2} of Eq. (5.7) will not be equal, their difference being the net flow rate of particles #2:

$$J_{m2} + J_{s2} = u_{d2},$$

or

$$\frac{d\varepsilon_2}{dz} = Q_2(\varepsilon - \varepsilon_2^*)(1 - \varepsilon_2) + \frac{u_{d2}}{\mu_2\rho_s}. \quad (5.8g)$$

And the equilibrium voidage ε_2^* will be determined by Eq. (3.4),

$$u_0 - u_{d2}\varepsilon_2^*/(1 - \varepsilon_2^*) = u_{i2}\varepsilon_2^{*n}. \quad (3.4g)$$

Generalized to the j th fraction, the related system of equations would thus read:

$$\frac{d\varepsilon_j}{dz} = Q_j(\varepsilon - \varepsilon_j^*)(1 - \varepsilon_j) + \frac{u_{dj}}{\mu_j\rho_s}, \quad (5.8g)$$

$$u_0 - u_{dj}\varepsilon_j^*/(1 - \varepsilon_j^*) = u_{ij}\varepsilon_j^{*n},$$

$$(1 - \varepsilon) = \sum_{j=1}^J (1 - \varepsilon_j). \quad (3.4g)$$

For easier computation, an alternate method has also been developed.

VI. Conical Fluidized Beds

Coal can be burnt and gasified more efficiently in fluidized beds confined in conical shells (Clean Fuels from Coal Symposium II, 1975; Schilling *et al.*, 1979; Qader, 1985), and fluid-bed roasters for sulfide ores are conical in shape (Boldt, 1967). Even incineration of waste materials proceeds better in conical vessels (Yaverbaum, 1977). The balling action in conical fluidized beds has been used to produce Portland cement in such beds instead of in rotary kilns (Pyzel, 1959, 1961; Schroth, 1971), in capturing coal dust in the so-called ash agglomerating method in coal gasification, and in coating nuclear fuel particles (Wallroth *et al.*, 1971). The settling cone in ore dressing is another example of the conical fluidized bed, though now in L/S operation.

The decreasing fluid velocity gradient in the direction of flow in a conical vessel possesses the following advantages:

- (1) For polydisperse solids, the higher velocity at the lower section of a cone guarantees adequate fluidization of the coarser particles, while the lower velocity at the top section prevents excessive carry-over of the fines;
- (2) The highly agitated condition of the coarse particles serves to disperse the fluidizing medium as it enters the upper zone for the finer solids, thus performing the function of a normal gas distributor;
- (3) For highly exothermic reactions, the preferential accumulation of coarse particles near the bottom, with their relatively lower specific surface, ameliorates rapid heat release, and the high degree of turbulence due to the higher fluid velocity near the apex of the cone helps heat dissipation.

While fluidization of solid particles in a conical vessel is more complex than that in a cylindrical vessel in which the superficial velocity is constant, minimal knowledge of its operation may be derived by use of the concept of ideal fluidization (Kwauk and Yang, 1964), through adopting the following assumptions:

- uniform particle size;
- uniform radial distribution of fluid velocity;
- absence of friction between the solid particles and the container wall.

The second assumption precludes complications arising from consideration of the momentum of the incoming fluid, such as studied by other authors in the case of G/S systems (Yang *et al.*, 1983, 1986; Massimilla, 1985), or, in the extreme, even for spouted beds.

A. PHENOMENOLOGICAL DESCRIPTION AND PHYSICAL MODELING

At a relatively high fluid rate, all solid particles are fluidized in a conical vessel, as shown in the first figure in Table IV. Under this condition, there is a certain level in the lower region of the vessel at which the fluid velocity is u_t with a corresponding voidage ε of unity. Below this level, no solid particles can exist, and above it, the fluid velocity decreases with height, until at the top of the fluidized particles the fluid velocity $u > u_t$ with voidage $\varepsilon > \varepsilon_0$. When the fluid rate is gradually reduced, the entire solids bed will slowly descend in the conical vessel. If the fluid distributor is located low enough in the cone that it does not interfere with this descent, the lowering of the solids bed will take place in such a manner as to maintain the lower-side velocity always at the

TABLE IV
CONICAL FLUIDIZED BED—SUMMARY OF QUANTITATIVE RELATIONSHIPS AMONG VARIABLES
[AFTER KWAUK, 1973]

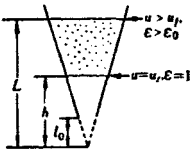
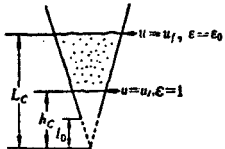
Complete Fluidization, $G_R \geq 1$				
		$G_R > 1$	$G_R = 1$	
				
Fluid Rate, G		—	$G_C = \pi u_f (L_0 L_{RC} \tan \theta)^2$	1
Voidage, ϵ	Fluidized bed	$\epsilon = \epsilon_0 \left(\frac{L_{RC}}{z_R} \right)^{2/n} G_R^{1/n}$	$\epsilon = \epsilon_0 \left(\frac{L_{RC}}{z_R} \right)^{2/n}$	2
Solids inventory, S_R	Fixed bed	0	0	3
	Fluidized bed	$S_R = 1$	$S_R = 1$	4
Velocity, u	Top of fixed bed	—	—	5
	Top of fluidized bed	$u_L = \frac{G}{\pi (L \tan \theta)^2} > u_f$	$u_{L_C} = \frac{G_C}{\pi (L_C \tan \theta)^2} = u_f$	6
	Bottom of fluidized bed	$u_h = \frac{G}{\pi (h \tan \theta)^2} = u_f$	$u_{h_C} = \frac{G_C}{\pi (h_C \tan \theta)^2} = u_f$	7
Liquid height, width band L	Top of fixed bed	—	—	8
	Top of fluidized bed	$L_R = \left[\frac{\left(3 - \frac{2}{n} \right) (1 - \epsilon_0) (1 - l_R^3)}{3 - \frac{2}{n} - 3\epsilon_0 \left(\frac{L_{RC}}{L_R} \right)^{2/n} G_R^{1/n} + \frac{2}{n} \epsilon_0^{3n/2} \left(\frac{L_{RC}}{L_R} \right)^3 G_R^{3/2}} \right]^{1/3}$	$L_{RC} = \left[\frac{\left(3 - \frac{2}{n} \right) (1 - \epsilon_0) (1 - l_R^3)}{3 - \frac{2}{n} - 3\epsilon_0 + \frac{2}{n} \epsilon_0^{3n/2}} \right]^{1/3}$	9
	Bottom of fluidized bed	$h_R = L_{RC} \epsilon_0^{n/2} G_R^{1/2}$	$h_{RC} = L_{RC} \epsilon_0^{n/2}$	10
	Top of fixed bed	—	—	11
	Top of fluidized bed	$L_R^3 = 1 - \epsilon_0 (1 - l_R^3) + \left(\frac{3\epsilon_0}{3 - \frac{2}{n}} \right) L_{RC}^2 G_R^{1/n} [L_R^{3-2/n} - l_R^{3-2/n}]$	$L_{RC}^3 = 1 - \epsilon_0 (1 - l_R^3) + \left(\frac{3\epsilon_0}{3 - \frac{2}{n}} \right) \left[L_{RC}^3 - l_R^3 \left(\frac{L_{RC}}{l_R} \right)^{2/n} \right]$	12
	Bottom of fluidized bed	l_R	l_R	13

TABLE IV (Continued)

		Partial Fluidization, $(G_R)_i < G_R < 1$		Complete Defluidization or Fixed Bed, $G_R < (G_R)_i$	
		Hyperfluidized fixed bed			
Liquid height, width band L	$l_0 < h$	Top of fixed bed	Solve $\begin{cases} L'_{RX} - L'_R = \frac{L_{RC}^{2m} G_R^m}{2m-1} [L_R^{1-2m} - L'_{RX}{}^{1-2m}] \\ \left(3 - \frac{2}{n}\right) [(1 - \epsilon_0)(L_{RX}^3 + l_R^3 - 1) + \epsilon_0 L_R^3] \\ = 3\epsilon_0 L_R^3 \left(\frac{L_{RC}}{L'_R}\right)^{2n} G_R^{1/n} - \frac{2}{n} \epsilon_0^{3n/2} L_{RC}^3 G_R^{3/2} \end{cases}$	1	8
		Top of fluidized bed		—	9
		Bottom of fluidized bed		$h_R = h_{RC} \epsilon_0^{n/2} G_R^{1/2}$	l_R (fixed bed)
	$l_0 < h$	Top of fixed bed	Solve $\begin{cases} L'_{RX} - L'_R = \frac{L_{RC}^{2m} G_R^m}{2m-1} [L_R^{1-2m} - L'_{RX}{}^{1-2m}] \\ \left(3 - \frac{2}{n}\right) [(1 - \epsilon_0)(L_{RX}^3 - 1) + \epsilon_0(L_R^3 - l_R^3)] \\ = 3\epsilon_0 L_{RC}^{2n} G_R^{1/n} [L_R^{3-2n} - l_R^{3-2n}] \end{cases}$	1	11
		Top of fluidized bed		—	12
		Bottom of fluidized bed		l_R	l_R (fixed bed)
Pressure drop, $-\Phi$	$l_0 < h$	Fixed bed	$-\Phi_s = (1 - \epsilon_0)(L'_{RX} - L'_R) \frac{1}{1 - l_R}$	$-\Phi_s = \left(\frac{1 - \epsilon_0}{2m-1}\right) L_{RC}^{2m} G_R^m (l_R^{1-2m} - 1) \frac{1}{1 - l_R}$	14
		Fluidized bed	$-\Phi_t = \frac{L'_R}{1 - l_R} \left[\frac{1 - \frac{2}{n} - \epsilon_0 \left(\frac{L_{RC}}{L'_R}\right)^{2n} G_R^{1/n} + \frac{2}{n} \epsilon_0^{3/2} \left(\frac{L_{RC}}{L'_R}\right) G_R^{3/2}}{1 - \frac{2}{n}} \right]$		15
	$l_0 > h$	Fixed bed	$-\Phi_s = \frac{1 - \epsilon_0}{1 - l_R} (L_{RX} - L'_R)$	$-\Phi_s = \left(\frac{1 - \epsilon_0}{2m-1}\right) \frac{L_{RC}^{2m} G_R^m}{1 - l_R} (l_R^{1-2m} - 1)$	16
		Fluidized bed	$-\Phi_t = \frac{L'_R - l_R}{1 - l_R} - \frac{\epsilon_0 L_{RC}^{2n} G_R^{1/n}}{1 - l_R} \left[\frac{L_R^{1-2n} - l_R^{1-2n}}{1 - \frac{2}{n}} \right]$		17
		C		D	

constant value of u_t , whereas the velocity at the top of the bed will decrease continually until, at some certain fluid rate, it reaches the incipient fluidization velocity u_f with the corresponding critical voidage ε_0 . At this point, the top of the bed is under incipient fluidization, while all the solids below the top surface are actively fluidized, with increasing voidage, up to $\varepsilon = 1$ at the bottom of the solids bed. The fluid rate corresponding to this critical condition is designated complete-fluidization rate G_c . The phenomenon described above for complete fluidization belongs to the first type of conical fluidized bed operation.

If the fluid rate is further decreased, the fluid velocity at the top of the bed falls below u_f , and some solids become defluidized. With still further decrease in fluid rate, the defluidized zone becomes deeper, until at some fluid rate, the last solids layer immediately above the fluid distributor loses fluidization. The fluid rate that produces this second critical condition is known as initial-fluidization rate G_i . During the transition from complete fluidization to initial fluidization, the total integrated pressure drop in the defluidized zone balances its weight. To accomplish this, in view of the varying fluid velocity, the defluidized bed is divided into two regions. In the bottom region, the gradient of the pressure drop exceeds the apparent density of the solids, thus exerting an overall thrust upward to support the top region, where the pressure gradient, because of reduced fluid velocity, is less than the apparent density of the solids and is therefore insufficient to balance the solids in this region. Thus, there exist two complementary actions in these two regions of the defluidized zone: The bottom region supports the top region, and the top region suppresses the fluidization of solid particles in the bottom region, where the prevailing fluid velocity $u > u_f$. This bottom region of the defluidized zone is said to exist in a state of hyperfluidization. It is thus evident that at the lower side of this bottom region, the fluid velocity may be appreciably greater than u_f . Consequently, the voidage of the fluidized bed immediately below the lower side of this bottom region is greater than the critical voidage ε_0 , while above this lower side, the voidage has the constant value of ε_0 throughout the defluidized zone. Thus, across this interface, the bed voidage experiences a discontinuity, while the fluid velocity change is by all means continuous in consideration of bed geometry. The phenomenon related to this state of partial fluidization belongs to the second type of conical fluidized bed operation.

The third type of conical bed operation belongs obviously to the condition of total defluidization, or the common fixed bed, at fluid rates less than G_i .

The appearance of these three phenomena is affected by the location of the fluid distributor, l_0 above the lower apex of the cone. If l_0 is higher than the level h at which $u = u_t$, then the region for $\varepsilon = 1$ does not exist in the bed but lies at an imaginary level below l_0 .

Table IV summarizes the results of a quantitative analysis based on the

just-discussed physical model of conical fluidized bed operation, by applying the concept of ideal fluidization. The contents of Table IV are explained in the following sections.

B. THE BASIC PARAMETERS

The fundamental relation between voidage and velocity given by Eq. (2.2) in Section II will be made amply use of:

$$u/u_t = \varepsilon^n, \quad u_t/u_t = \varepsilon_0^n \quad (2.2)$$

A number of reduced quantities will be adopted in order to put the relations between parameters, which are defined graphically in Table IV, on a dimensionless basis:

$$\begin{aligned} \text{height:} \quad & l_R = l/L_0, \quad h_R = h/L_0, \quad L_R = L/L_0, \\ & L_{RC} = L_C/L_0, \text{ etc.,} \end{aligned}$$

$$\text{fluid rate:} \quad G_R = G/G_C,$$

$$\text{solids inventory:} \quad S_R = S/S_0.$$

Geometry of the conical vessel defines the following relation between fluid rate G and fluid velocity u at any position z :

$$G = \pi u(z \tan \theta)^2. \quad (6.1)$$

At the point of complete fluidization, the top of the bed L_C , which is at incipient fluidization, is at fluid velocity u_t :

$$G_C = \pi u_t(L_C \tan \theta)^2 = \pi u_t(L_0 L_{RC} \tan \theta)^2 \quad (6.1a, B-1)$$

In addition to its numbering, each equation derived will be cross-referenced to its coordinate charted in Table IV, e.g., B-1 for Eq. (6.1a).

C. THE FULLY FLUIDIZED STATE

The first type of conical fluidized bed operation for complete fluidization will be analyzed with respect to bed height and pressure drop.

The inventory of solids, S , will be described in terms of the amount added and of the amount enumerated from the varying voidage in the fluidized bed:

$$S_0 = \underbrace{\int_{l_0}^{L_0} \pi \rho_s (z \tan \theta)^2 (1 - \varepsilon_0) dz}_{\text{solids added}} = \underbrace{\int_h^L \pi \rho_s (z \tan \theta)^2 (1 - \varepsilon) dz}_{\text{solids in completely fluidized bed}}.$$

Substitution of the expressions for the basic parameters gives

$$S_0 = \int_h^L \pi \rho_s (z \tan \theta)^2 [1 - \varepsilon_0 (L_C/z)^{2/n} G_R^{1/n}] dz.$$

Integration and substitution of the appropriate expression for h gives

$$L_R^3 = \frac{(3 - 2/n)(1 - \varepsilon_0)(1 - l_R^3)}{3 - 2/n - 3\varepsilon_0(L_{RC}/L_R)^{2/n} G_R^{1/n} + (2/n)\varepsilon_0^{3n/2}(L_{RC}/L_R)^3 G_R^{3/2}}. \quad (6.2, A-9)$$

The differential pressure drop for the completely fluidized bed can be written in terms of the effective solids density ($\rho_s - \rho_f$) and voidage ε :

$$-(dP)_f = (\rho_s - \rho_f)(1 - \varepsilon) dz.$$

Define the dimensionless pressure gradient as

$$\begin{aligned} -\Phi_f &= - \int_h^L \frac{(dP)_f}{(L_0 - l_0)(\rho_s - \rho_f)} \\ &= \frac{1}{L_0 - l_0} \int_h^L (1 - \varepsilon) dz. \end{aligned}$$

Substitution of the expressions for the basic parameters gives

$$-\Phi_f = \frac{1}{L_0 - l_0} \int_h^L [1 - \varepsilon_0 (L_C/z)^{2/n} G_R^{1/n}] dz.$$

Integration and substitution of the appropriate expression for h gives

$$\begin{aligned} -\Phi_f &= \frac{L_R}{(1 - l_R)(1 - 2/n)} [1 - 2/n - \varepsilon_0 (L_{RC}/L_R)^{2/n} G_R^{1/n} \\ &\quad + (2/n)\varepsilon_0^{n/2} (L_{RC}/L_R) G_R^{1/n}]. \end{aligned} \quad (6.3, A-15)$$

At the critical condition for complete fluidization, $G_R = 1$ and $L_R = L_{RC}$, and Eq. (6.3) is simplified to

$$-\Phi_f = \frac{L_R}{(1 - l_R)(1 - 2/n)} [1 - 2/n - \varepsilon_0 + (2/n)\varepsilon_0^{n/2}]. \quad (6.3a, B-15)$$

D. WITH HYPERFLUIDIZED FIXED BED

The inventory of solids, S , of a partially fluidized conical bed consists of two parts, one in the fluidized bed from level h to L' , and the other in the fixed bed

from L' to L'_x :

$$\begin{aligned}
 S_0 &= \underbrace{\int_{l_0}^{L_0} \pi \rho_s (z \tan \theta)^2 (1 - \varepsilon_0) dz}_{\text{solids added}} \\
 &= \underbrace{\int_h^{L'} \pi \rho_s (z \tan \theta)^2 (1 - \varepsilon) dz}_{\text{solids in fluidized bed}} + \underbrace{\int_{L'}^{L'_x} \pi \rho_s (z \tan \theta)^2 (1 - \varepsilon_0) dz}_{\text{solids in fixed bed}}.
 \end{aligned}$$

As before, substitution of the appropriate expression for ε , integration, and substitution of the appropriate expression for h yield

$$\begin{aligned}
 &(3 - 2/n)[(1 - \varepsilon_0)(L'_R{}^3 + l_R^3 - 1) - \varepsilon_0 L'_R{}^3] \\
 &= 3\varepsilon_0 L'_R{}^3 (L_{RC}/L_R)^{2/n} G_R^{1/n} - (2/n)\varepsilon_0^{3n/2} L_{RC}^3 G_R^{3/2}. \quad (6.4, C-9)
 \end{aligned}$$

The differential pressure drop across the fixed bed is, according to Eq. (2.6) of Section II,

$$-(dP)_x = (\rho_s - \rho_f)(1 - \varepsilon_0)(u/u_f)^m dz.$$

The very concept of hyperfluidization as described in Section VI.A calls for the overall pressure drop across the entire fixed-bed zone to balance the weight of the solids it contains:

$$(\Delta P)_x = (\rho_s - \rho_f)(1 - \varepsilon_0)(L'_x - L').$$

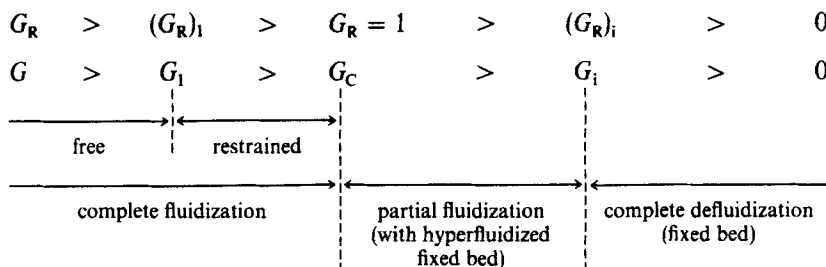
Expressed in dimensionless form, the above equation becomes

$$\begin{aligned}
 -\Phi_x &= \frac{(\Delta P)_x}{(L_0 - l_0)(\rho_s - \rho_f)} \\
 &= \frac{(1 - \varepsilon_0)(L'_R{}^x - L'_R)}{1 - l_R} \quad (6.5a, C-14, C-16)
 \end{aligned}$$

E. RANGES FOR CONICAL FLUIDIZED BED OPERATIONS

The minimal fluid rate for the existence of the hyperfluidized bed is reached when the fluidized zone has shrunk to zero height, that is, when L' reaches the fluid distributor at l_0 . Under this condition, all solids inventory resides in the fixed bed, and the upper bed level coincides with that for the solids added.

The range of fluid rates for various types of conical fluidized bed operation can therefore be summarized as follows:



F. CHARTING CONICAL FLUIDIZED BED OPERATION AND EXPERIMENTAL VERIFICATION

Figure 28 compares curves computed from the equations derived in the preceding sections and summarized in Table IV with experimental results (Chong and Bao, 1962; Kwauk, 1973). Experiments were carried out in an accurately fabricated conical bed made of copper with a diameter of 100 mm at the top and a total height of 1,000 mm. The solids used were three kinds of closely sized glass beads having diameters of 0.60–0.75, 0.63–0.75, and 1.10–2.35 mm. Solids concentrations at various levels inside the conical bed were measured with a regular Geiger–Muhler counter on the attenuation of radiation from a ^{75}Se source placed at a diametrically opposite location, the measurement assembly being placed on a platform movable in the vertical direction.

Figure 28 shows the computed and experimental results for the 0.63–0.75 mm glass beads fluidized with water and with the fluid distributor located at $l_R = 0.283$. As fluid velocity increases from the lowest value shown at A, the pressure drop rises along line AD in a manner typical of any fixed bed, with the top and bottom levels of the fixed bed maintained constant along lines A'D' and A''D'', respectively. When fluid rate reaches the initial fluidization point $(G_R)_i = 0.27$, the pressure drop reaches a maximum of $-\Phi = (1 - \epsilon_0) = 0.58$, at which fluidization starts from the bottom of the solids bed. With a further increase in fluid rate, the top level of the fixed bed rises along D'B', while the bottom level of the fluidized bed remains constant at $l_R = 0.283$, although the voidage there increases along line D''B''. At the same time, pressure drop $-\Phi$ drops from D to B, until at point B, where the fluid rate reaches the critical value for complete fluidization, $G_R = 1$, and $-\Phi$ has dropped to a new value of 0.46. While fluid rate increases from D to B, the interface between the fixed

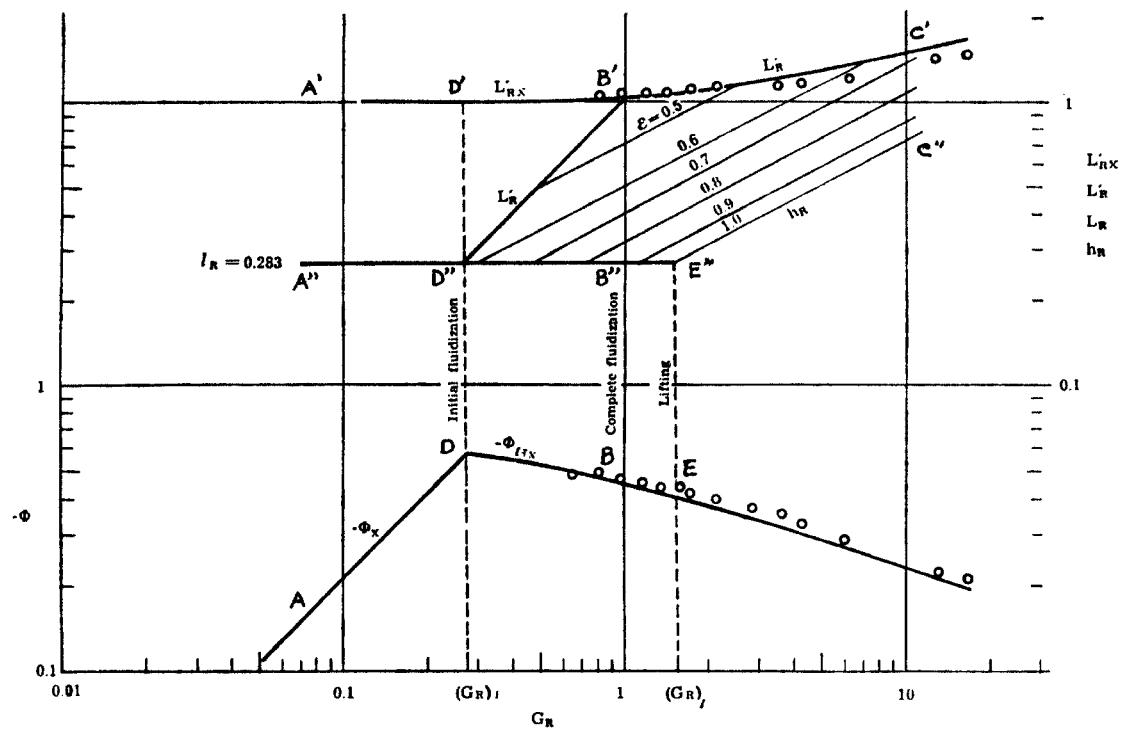


FIG. 28. Conical fluidized bed: 0.63–0.75 mm glass beads in water. Lines calculated; points experimental. [After Kwauk, 1973.]

bed and the fluidized bed rises along line $D''B'$, shown as L'_R , until at the critical fluid rate of $G_R = 1$ at B' , $L'_R = L'_{Rx} = L'_{RC} = 1.03$. From there on, with a further increase in fluid rate, the solids are completely fluidized until the fluid rate reaches the lifting fluid rate $(G_R)_l = 1.5$ at point E, at which the voidage at the bottom of the fluidized bed has just reached unity, $\varepsilon = 1$, and h_R has arrived at l_R . At fluid rates exceeding $(G_R)_l$, the fluidized bed behaves as a free system, with $h_R > l_R$ rising along line $E''C''$ while the top bed level rises along $B'C'$. Between these two lines, $B'C'$ and $E''C''$, lines of constant voidages are sketched in to show the voidage distribution in the fluidized zone of the conical bed.

G. INSTABILITY

Figure 28 shows that the pressure drop of a conical bed reaches a maximum value at the initial fluidization point $(G_R)_i$, and it drops at higher fluid rates. Inherent in this drooping pressure-drop characteristic lies the instability of conical bed operation, especially with gas as the fluidizing medium, for as soon as fluid rate reaches $(G_R)_i$, the decrease in pressure drop induces higher flow from a compressible medium. As the pressure expends itself, fluid flow drops to even lower values, only to permit reaccumulation of pressure because of reversion to the higher pressure-drop region of the system.

VII. Application of the Moving Bed

The analysis of the principle of moving-bed operation, as described in Section III.B, will be amplified in terms of viable equipment design. Two examples will be given: moving-bed uptransport of granular solids with compressible media that expand as the solids are moved upward, and the solids downcomer with a conical spout in which moving-bed uptransport is balanced against a counter-down fluidized dipleg.

A. MOVING-BED UPTRANSPORT WITH COMPRESSIBLE MEDIA

In moving-bed transport, solid particles are in contiguous contact with one another and are pushed along by the transporting fluid more or less in plug flow, with a voidage equivalent to that of the loosest fixed bed. The velocity of solids movement can be varied from zero to any practical upper limit.

This type of solids transport came into vogue during the 1950s, when bead-type catalyst was used in petroleum processing (Berg, 1951, 1952, 1953, 1954,

1956; Weber, 1952), though the mechanism of the related particle–fluid motion was not amply studied until much later (Kwauk, 1963c; Sandy *et al.*, 1970; Aoki *et al.*, 1973; Kano *et al.*, 1981). More basic investigations of such particulate systems were provided by Delaplaine (1956).

Moving-bed transport is a metastable operation (Kwauk, 1963c; Li and Kwauk, 1989), and the threshold for stability calls for “equal lift” of all particles under transport, so that every particle is supported hydrodynamically by the fluid medium at the point of incipient fluidization. If a positive “lift gradient” exists in the direction of transport, the particles further ahead will tend to move faster than those from coming behind, with the result that voidage pockets will be created upstream in the form of bubbles or slugs. On the other hand, if a negative “lift gradient” exists, then the particles ahead will be pushed mechanically by those coming from behind, thus creating interparticle contact pressure. Such interparticle contact pressure will be transmitted to the conduit wall, giving rise to additional wall friction, which may lead to blockage if its magnitude exceeds a certain prescribed value.

At the point of metastable operation, which will be designated “critical,” the pressure drop for moving-bed uptransport is closely approximated by the head of the particulate solids, not counting the minor contributions of solids acceleration and wall friction against the mobile solids. For a positive lift gradient, instability may be inhibited by restraining devices at the top exit to suppress the formation of voidage pockets—only, however, when the lift gradient does not deviate excessively from the “critical.” Negative lift gradient, if not carried to the point of blockage, is itself a measure against instability. But for both cases, top restraint and induced wall friction increase pressure drop beyond that needed for balancing the column of particulate solids in the uptransport tube, thus increasing additional power expenditure in transporting the solids.

1. Design for Critical Transport

From the preceding discussion, it is evident that the uptransport tube needs to be “contoured” to realize metastable operation of critical transport in order to insure equal lift of all the solid particles.

The general equation of motion for a thin slice of thickness dz for a moving bed, shown schematically in Fig. 29, can be written as

$$\underbrace{[\rho_s(1 - \varepsilon_0) dz] \frac{du_p}{d\theta}}_{\text{acceleration}} + \underbrace{[\Delta\rho(1 - \varepsilon_0) dz] g}_{\text{gravity}} = \underbrace{[\Delta\rho(1 - \varepsilon_0) dz] \left(\frac{u_{sz}}{u_{tz}} \right)^m g}_{\text{hydrodynamic drag}} = dP,$$

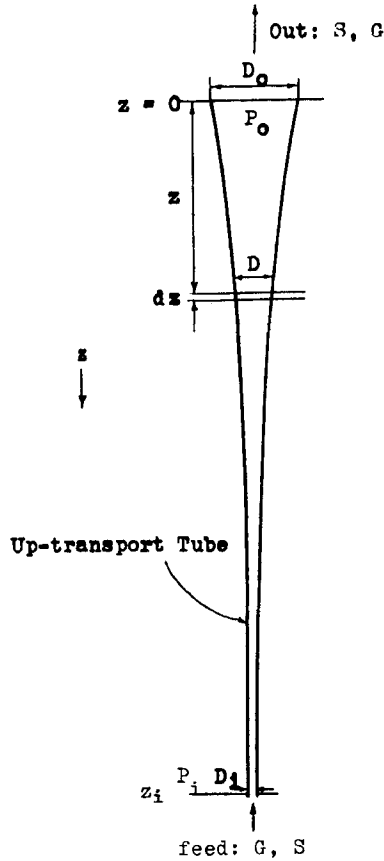


FIG. 29. Schematic representation of a moving-bed uptransport tube. [After Kwauk, 1963.]

where the prorating drag factor $(u_{sz}/u_{tz})^m$, described by Eq. (2.6) of Section II, is based on the *local* state of pressure and flow at a distance z from the top of the tube. This equation can be reduced to the dimensionless form

$$\left(\frac{\rho_s}{\Delta\rho}\right)\frac{1}{g}\frac{du_p}{d\theta} + 1 = \left(\frac{u_{sz}}{u_{tz}}\right)^m = \frac{1}{\Delta\rho(1 - \varepsilon_0)}\frac{dP}{dz} \quad (7.1)$$

by defining the following quantities:

$$\begin{aligned} D' &= D/D_0, & \text{reduced diameter;} \\ P' &= \Delta P/P_0, & \text{reduced pressure drop} \\ & & \text{(measured from top of uptransport tube);} \end{aligned}$$

$z' = \Delta\rho(1 - \varepsilon_0)z/P_0,$	reduced length (measured from top of uptransport tube);
$u'_0 = u_0/u_f,$	reduced gas velocity;
$u'_d = u_d/u_f$	reduced solids velocity;
$r = (S/\rho_s)/GV_0,$	rate-of-flow ratio;
$v = r\varepsilon_0/(1 - \varepsilon_0),$	actual-velocity ratio.

Elaboration on Eq. (7.1) resulted, among others, in three important relations for critical transport:

- (1) a relation between pressure P' and tube diameter D' :

$$\gamma\left(\frac{v}{1-v}\right)^2 \frac{1}{D'^5} dD' = \left(1 - \frac{D'^{2m}(1+P')}{[1/(1-v)]^m[1-v(1+P')]^m}\right) dP'; \quad (7.2)$$

- (2) an approximate expression for the contour of the up-transport tube where particle acceleration is negligible:

$$D'^2 = \frac{1-v(1+P')}{(1-v)(1+P')^{1/m}}; \quad (7.3)$$

- (3) the efficiency for lifting the solids, based on compressing the transporting gas to the bottom pressure of the uptransport tube:

$$\eta = \left(\frac{\rho_s}{\Delta\rho}\right)\left(\frac{k-1}{k}\right) \frac{vz'_1}{[\varepsilon_0 - v(1-\varepsilon_0)(1+z'_1)][(1+z'_1)^{(k-1)/k} - 1]}. \quad (7.4)$$

Figure 30 shows the variation of the efficiency of critical moving-bed uptransport as a function of v and z' .

2. Stability

Equal lift for critical uptransport is predicated upon exact hydrodynamic support of all particles at incipient fluidization. Therefore, the lift gradient is zero, $d^2P/dz^2 = 0$. A positive lift gradient, $d^2P/dz^2 < 0$, creating voidage pockets, is exemplified by cylindrical or rectangular uptransport tubes of constant cross-sectional area, while a negative lift gradient, $d^2P/dz^2 > 0$, generates wall friction, typical for conical or trapezoidal uptransport tubes, for which the wall slope exceeds the contour specified for critical transport.

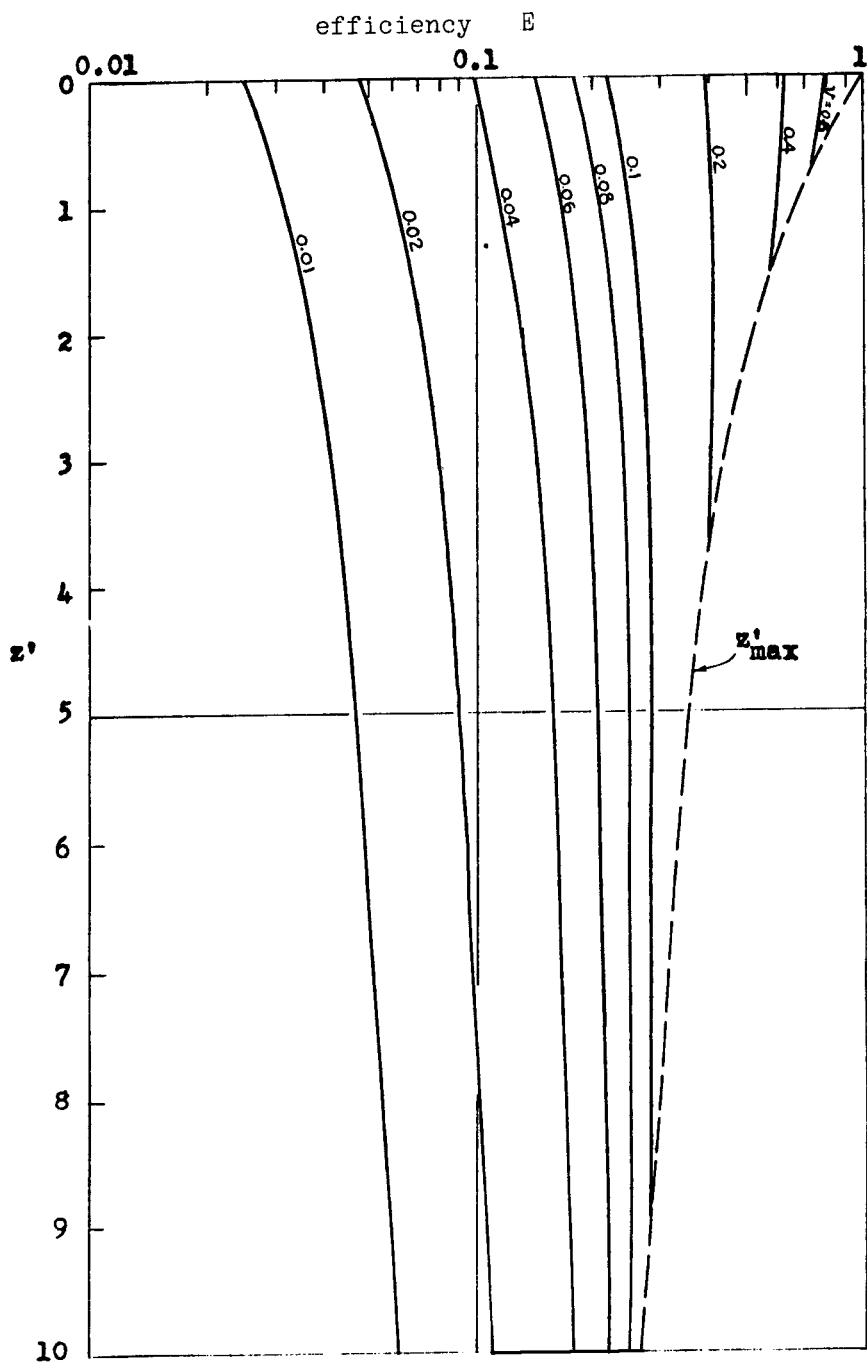


FIG. 30. Efficiency of moving-bed uptransport. [After Kwauk, 1963.]

In summary, the following cases can be differentiated:

Lift	Operation	Definition	Uptransport Tube Shape
Positive	unstable (voidage pockets)	< 0	cylindrical, rectangular
Equal	metastable, $\Delta P = \Delta \rho(1 - \epsilon_0)z$	$= 0$	contoured Eq. (7.3)
Negative	stable, $\Delta P > \Delta \rho(1 - \epsilon_0)z$	> 0	conical, trapezoidal

These three types of moving-bed uptransport are shown in Fig. 31 (Li and Kwauk, 1989), computed for ion-exchange resin at a common solids rate of 100 kg/h through an 8-m-high uptransport tube of the same inlet radius of 23.46 mm, for the configurations cylindrical, critical, and 2°-conical. The advantage in low pressure drop for the critical contour is obvious.

What is more important is the stability of an uptransport tube designed for critical transport and yet operating at different gas and solids rates. For instance, the gas rate u_{00} could deviate from the design value by a factor α , and the rate-of-flow ratio r by a factor β , as summarized below:

	Design	Operating
Gas Velocity	u_{00}	αu_{00}
Rate-of-flow ratio	r	βr
Solids velocity	$u_{d0} = r u_{00}$	$\alpha \beta u_{d0}$
Velocity ratio	$v = \frac{r \epsilon_0}{1 - \epsilon_0}$	βv

Pertinent analysis showed that when

$$\begin{aligned}
 \alpha = 1, \quad d\beta/dz = 0, & \quad \text{metastable operation for} \\
 & \quad \text{critical uptransport;} \\
 \alpha > 1, \quad d\beta/dz < 0, & \quad \text{unstable operation;} \\
 \alpha < 1, \quad d\beta/dz > 0, & \quad \text{stable operation.}
 \end{aligned}$$

It is therefore evident that only when the gas rate is less than the design value can stability of operation be insured. However, under this subcritical operation, excessive wall pressure, and therefore pressure drop, would be incurred.

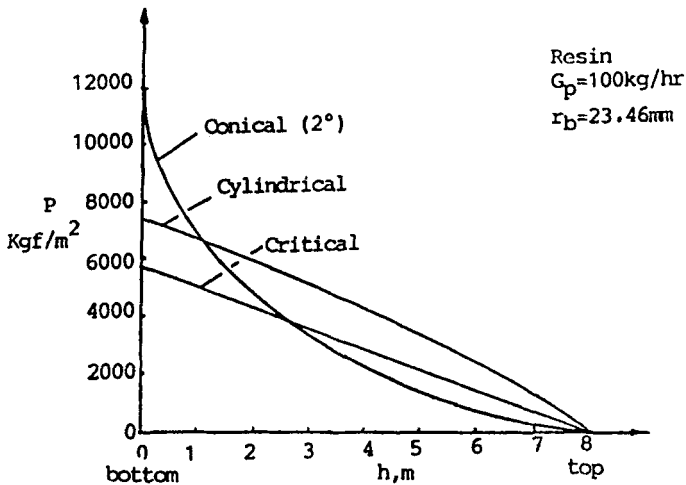


FIG. 31. Types of moving-bed uptransport. [After Li and Kwauk, 1987.]

3. Noncritical Moving-Bed Uptransport

The rather complex problem of noncritical moving-bed uptransport, for which both shear and normal stresses within the particulate mass come into play, will be given the barest cursory review. Experimental measurements in a trapezoidal uptransport tube (rectangular cross section, expanding upward in the direction of flow) yielded the families of pressure drop curves in the upper set of diagrams of Fig. 32 (Li and Kwauk, 1989). These curves are convex upward, indicating unstable transport, which was stabilized, however, by restraining devices at the top exit. Normal stress distribution along the uptransport tube is shown by the families of curves in the lower set of diagrams of Fig. 32. These curves show maxima somewhere in the middle of the tube.

The force balances on an elemental slice in the trapezoidal moving-bed uptransport tube, shown schematically in Fig. 33, and written in terms of quantities convenient for experimental data treatment, are as follows:

$$\frac{d\bar{\sigma}_h}{dh} = \left(\frac{f_i}{1 + f_i(h - h_i)} \left[1 + \frac{E_s D_s}{\tan \alpha} - H_s D_s \right] + \frac{2}{T_0} E_v D_v \right) \sigma_h - \rho_s(1 - \varepsilon) \frac{g}{g_c} - \frac{dP}{dh} + \frac{f_i G_p^2}{g_c \rho_s(1 - \varepsilon) A_i^2 [1 + f_i(h - h_i)]^3}, \quad (7.5)$$

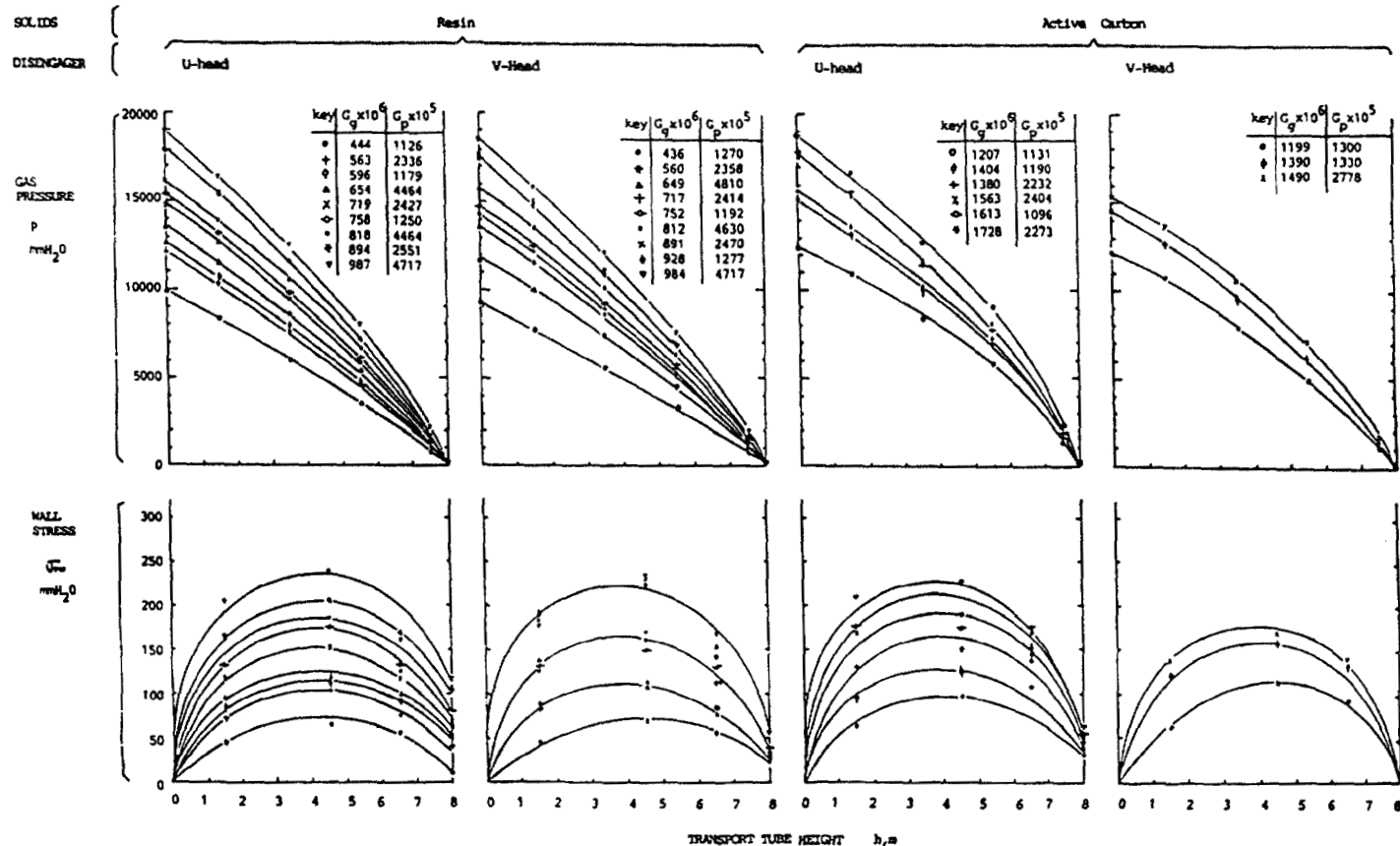


FIG. 32. Measured gas pressure and wall stress along a trapezoidal moving-bed uptransport tube. [After Li and Kwauk, 1987.]

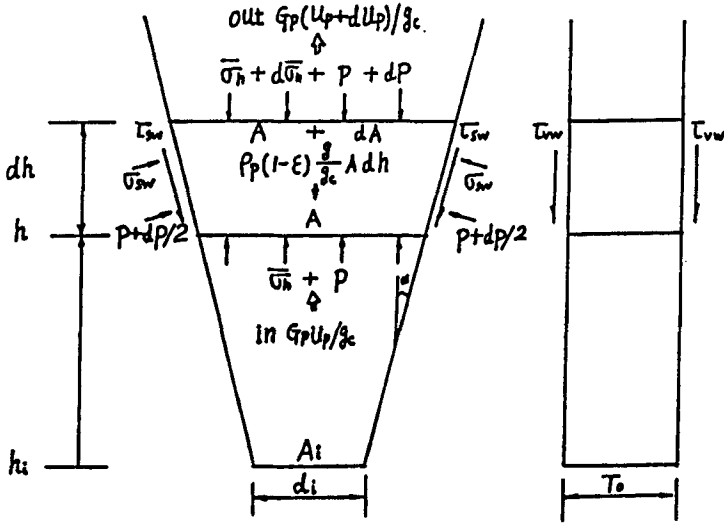


FIG. 33. Force balance for an elemental slice in a trapezoidal moving-bed uptransport tube. [After Li and Kwauk, 1987.]

$$-\frac{dP}{dh} = \rho_s(1 - \epsilon) \frac{g}{g_c} \left(\frac{1}{A_i[1 + f_i(h - h_i)]u_{mf0}} \right)^m \left(\frac{P}{P_0} \right)^{m-1} \left(\frac{G_p RT}{MP_0} - \frac{G_p \epsilon_0}{1 - \epsilon_0} \right)^m, \quad (7.6)$$

where E_v , E_s , H_v , H_s , D_v , and D_s are ratios of stresses determined through analysis based on soil mechanics (e.g., Walker, 1966, 1967; Walters, 1973a, 1973b) and defined below.

	Vertical Wall	Slanting Wall
$\frac{t}{\sigma_h}$	$E_v = \frac{\tau_{vw}}{(\sigma_h)_{vw}}$	$E_s = \frac{\tau_{sw}}{(\sigma_h)_{sw}}$
$\frac{\sigma}{\sigma_h}$	$H_v = \frac{\sigma_{vw}}{(\sigma_h)_{vw}}$	$H_s = \frac{\sigma_{sw}}{(\sigma_h)_{sw}}$
$\frac{\sigma_h}{\bar{\sigma}_h}$	$D_v = \frac{(\sigma_h)_{vw}}{\bar{\sigma}_h}$	$D_s = \frac{(\sigma_h)_{sw}}{\bar{\sigma}_h}$

In the above expressions, τ is shear stress, σ_h is vertical stress over a horizontal section, $\bar{\sigma}_h$ is its mean value, subscript vw denotes the vicinity of the vertical

wall, and sw that of the slanting wall. Together with the experimentally determined distribution along the uptransport tube of wall friction $d\mu/dh$ and of voidage $d\epsilon/dh$, Eqs. (7.5) and (7.6) have been used successfully in computing the curves shown in Fig. 32.

B. THE PNEUMATICALLY CONTROLLED DOWNCOMER

Downcomers (or diplegs, or standpipes) for transferring particulate solids between regions of different pressure levels need to be designed to satisfy the following requirements:

- nonbridging of descending solids;
- positive seal against appreciable gas leakage;
- freedom from instability, notably gas backflow in dilute phase.

From the usual plate-type distillation and absorption columns, it was but natural to attempt to devise stagewise equipment for G/S processing, for better heat economy and better utilization of the contacting media. But instability of the downcomer for solids transfer between stages remained for many years an unsolved hydrodynamic problem, and even to this data, the stable operation of many solids downcomers still depends on mechanical devices.

One recent solution is the pneumatically controlled downcomer shown in Fig. 34 (Kwauk, 1974a; Liu and Kwauk, 1980; Liu *et al.*, 1981), which consists of a fully fluidized dipleg connected at the lower end to a conical spout for uptransport. Fluidization of the dipleg minimizes the bridging of solids that often takes place for moving-bed descent. In view of its unique pressure-drop characteristics, the conical bed affords a positive seal against geysering of solids through gas backflow. In operation, the downcomer is provided with a set gas rate that is only sufficient to insure mild fluidization. With no solids feed, a fixed bed is maintained in the conical spout. As solids are added to the dipleg, the level in it rises until enough pressure is built up near the gas distributor of the dipleg to initiate solids uptransport in the conical spout. The solids level in the dipleg is self-adjusting to accommodate the pressure differential between the solids inlet and outlet, so that the downcomer can enable solids to flow either from a high-pressure region to a low-pressure region, or vice versa. Solids flow rate can be varied from zero to the permissible maximum determined by the part of major resistance for the downcomer assembly. The fluidizing gas for pneumatic control, once set, divides itself between the dipleg and the conical spout in accordance with the solids flow rate: for zero solids flow, most fluidizing gas enters the dipleg, and this portion diminishes as the solids rate increases.

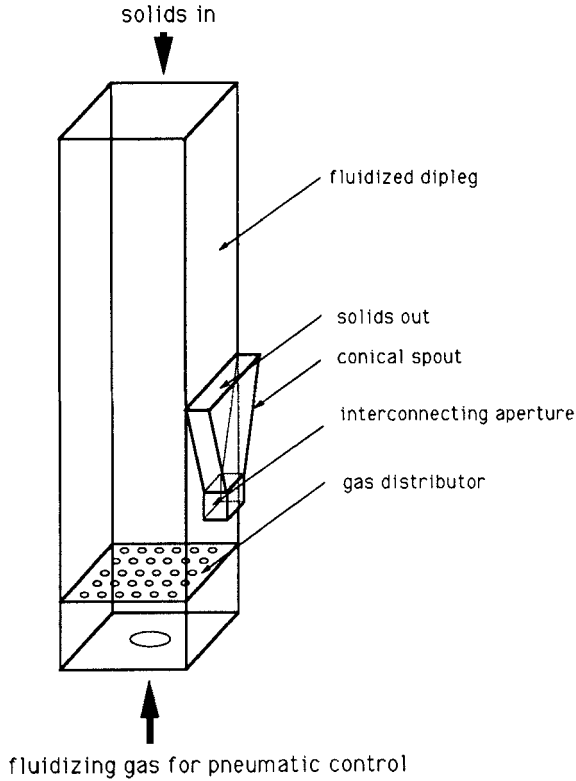


FIG. 34. The pneumatically controlled downcomer. [After Liu and Kwauk, 1980.]

1. Pressure Drop through Spout

The uptransport spout is often designed with a trapezoidal cross-section, as shown in Fig. 34. A simplified analysis (Kwauk, 1974) will be given on the basis that the dipleg operates under the condition of incipient fluidization and the spout in moving-bed uptransport.

By taking into account the pressure gradient in the spout in relation to gas velocity and tube contour, it could be shown that the pressure drop through the spout can be computed by integrating the equation

$$dP/dz = \Delta\rho(1 - \varepsilon_0)[Q_i/(1 + fz)]^m, \quad (7.7a)$$

in which

$$Q_i^m = \frac{(2 - m)(\alpha^2 - 1)}{2(\alpha^{2-m} - 1)}. \quad (7.8)$$

It can be shown that for viscous flow,

$$m = 1, \quad Q_i = \frac{\alpha + 1}{2},$$

and for turbulent flow,

$$m = 2, \quad Q_i = \left(\frac{\alpha^2 - 1}{2 \ln \alpha} \right)^{1/2}.$$

2. Gas Distribution

When the total gas to the downcomer assembly remains constant, the gas to the dipleg decreases linearly with solids rate, with $u'_{o1} = \varepsilon_0^n$ at $u'_{d1} = 0$:

$$u'_{o1} = (\beta/\alpha) Q_i \varepsilon_0^n + u'_{d1} \varepsilon_0 / (1 - \varepsilon_0). \quad (7.9)$$

Also, at $u'_{o1} = 0$, $u'_d = \varepsilon_0^n (1 - \varepsilon_0)^{n-1}$. Thus, a gas distribution diagram for the downcomer assembly can be constructed as given in Fig. 35, showing the total

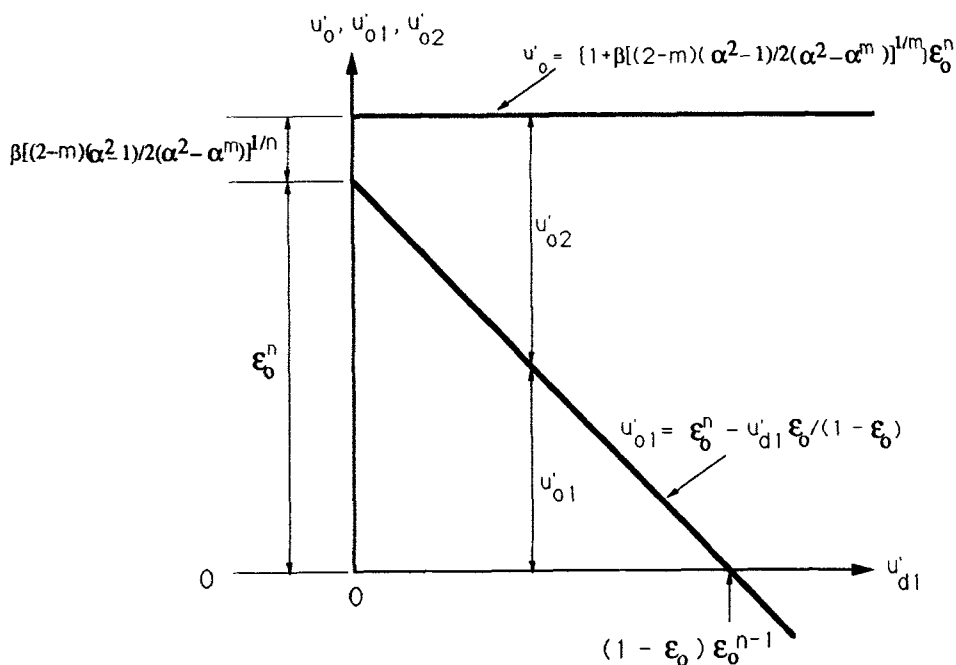


FIG. 35. Gas distribution for the pneumatically controlled downcomer. [After Kwauk, 1974.]

constant gas rate and its split between the dipleg and the downcomer, with expressions for the related intercepts on the abscissa and ordinate.

3. "Self-Flow"

For fine Geldart Group C powders that defluidize slowly, it has been shown experimentally that solids continued to be transported through the downcomer even when the fluidizing gas to the dipleg was turned off. The particulate solids move in the dense phase. This operation will be designated "self-flow" (Kwauk, 1974a). Under this condition, the total gas rate is zero:

$$u'_0 = u'_{01} + u'_{02} = 0.$$

Substitution of Eq. (7.9) into the above relation gives

$$r = \frac{1 + (\beta/\alpha)Q_i \epsilon'^n}{\frac{\epsilon' \epsilon_{01}}{1 - \epsilon' \epsilon_{01}} + \frac{\beta}{\alpha} Q_i \epsilon'^n \left(\frac{\epsilon_{01}}{1 - \epsilon_{01}} \right)}, \quad (7.10)$$

where $\epsilon' = \epsilon_{02}/\epsilon_{01}$ represents the ratio of voidages between the spout and the dipleg.

4. *Pneumatically Started Seal*

The pneumatically controlled downcomer shown in Fig. 34 stops delivering solids only when none are fed to the dipleg. In certain circumstances, it would be desirable to stop and start solids discharge from the spout at will, even when the dipleg is amply supplied with solids. This is exemplified by the two-solids-processing batch reactors in tandem, shown in Fig. 36, operating countercurrently against a common reacting gas (Kwauk, 1978). When the solids in Reactor 1 have reacted to some predetermined extent, Reactor 2 is first discharged and the contents of Reactor 1 need to be transferred as quickly as possible to Reactor 2, without stopping the gas flow.

The dipleg of the downcomer is connected to the gas distributor of Reactor 1 and is followed at its lower end by a spout, which is long enough to seal the solids from flowing to Reactor 2 under the normal operating-pressure differential between the two reactors. At selected locations along the height of the spout are control gas inlets, which serve to unlock the fixed-bed solids inventory, according to the mechanism explained in Fig. 37. Under the normal mode of sealed operation, the solids in the spout are locked by virtue of its conical geometry. Under this condition, the pressure drop from point A to point B (shown in Fig. 36) through the dipleg ΔP_i , needs to be less than the sum of the pressure drops through the spout, ΔP_c , the cyclone, ΔP_{cy} , and

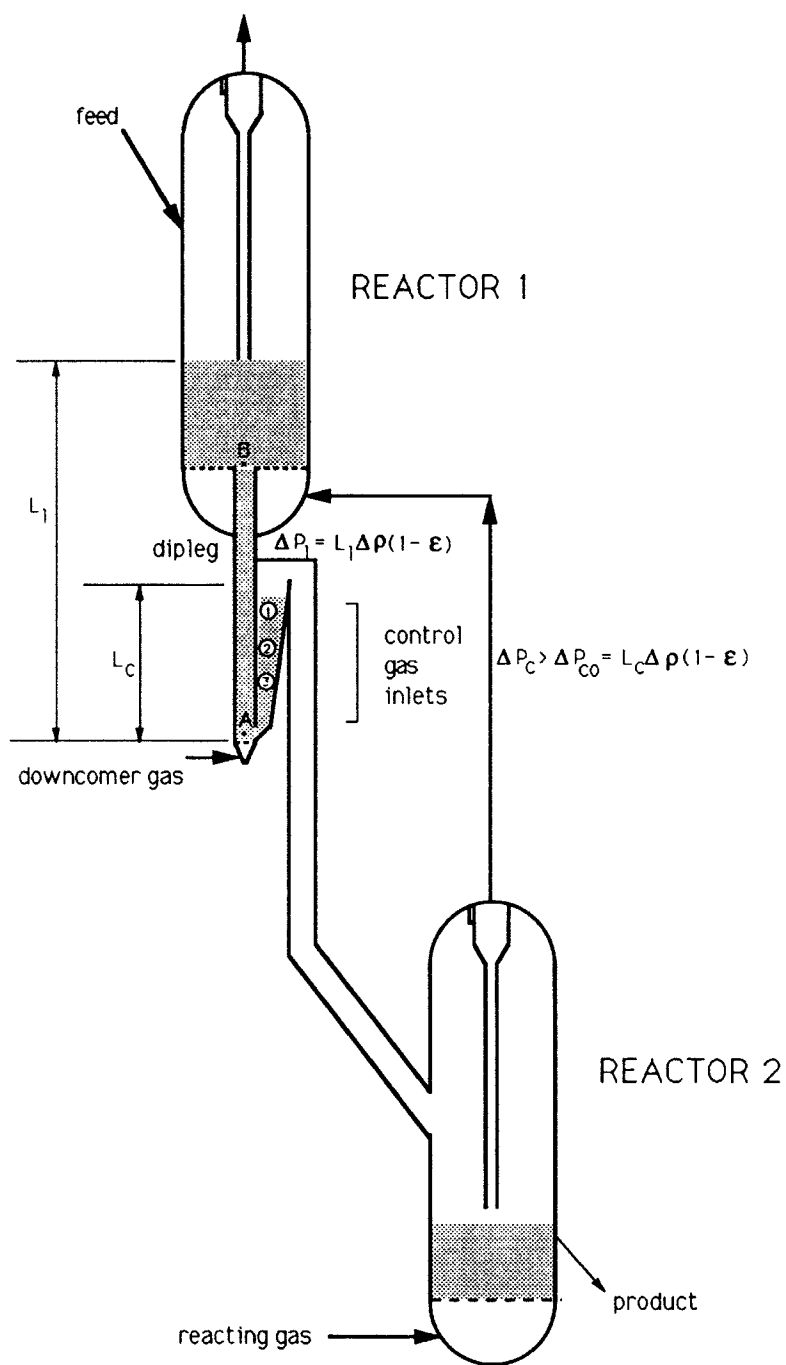


FIG. 36. Pneumatically started seal for tandem batch reactors. [After Kwauk, 1978.]

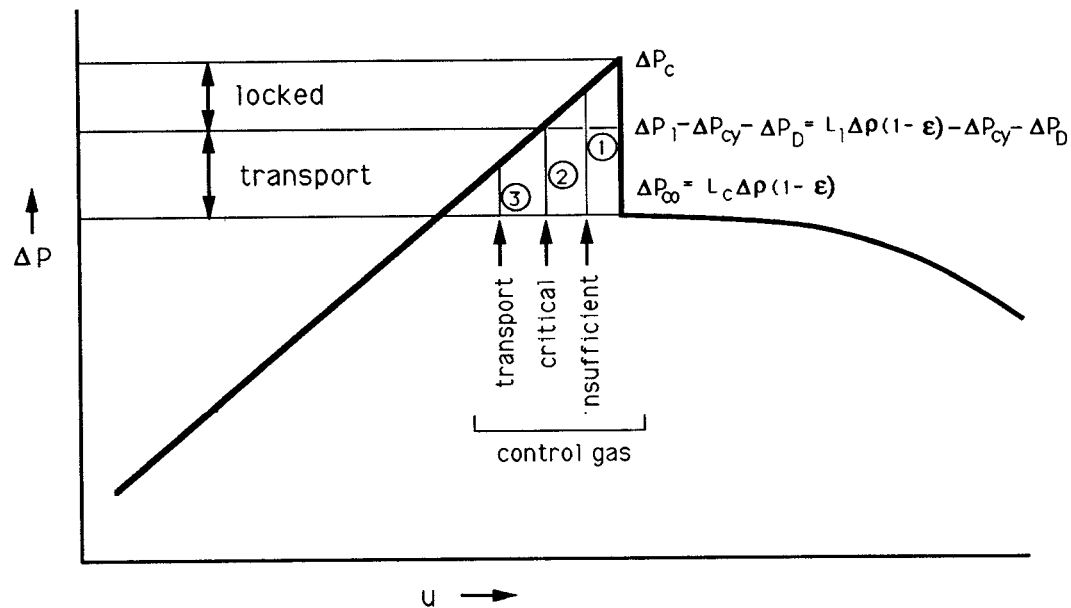


FIG. 37. Unlocking mechanism for a pneumatically started seal. [After Kwauk, 1978.]

the distributor plate, ΔP_D , of Reactor 1; that is,

$$\Delta P_1 < (\Delta P_c + \Delta P_{cy} + \Delta P_D).$$

Or alternately, the pressure drop through the locked solids in the spout has to satisfy the condition

$$\Delta P_c > (\Delta P_1 - \Delta P_{cy} - \Delta P_D). \quad (7.11)$$

If control gas at point 1 in Fig. 37 is admitted to unlock the solids above this point, the ΔP_c peak, shown in Fig. 37, will first be lowered to ΔP_{c1} , which is, however, still above the value $(\Delta P_1 - \Delta P_{cy} - \Delta P_D)$. If the unlocking gas streams at point 2 and point 3 are successively turned on, the new peak P_{c0} is eventually reached, which is below $(\Delta P_1 - \Delta P_{cy} - \Delta P_D)$. The unlocked spout now drops to its normal operating pressure drop ΔP_{c0} for moving-bed uptransport, and the solids of Reactor 1 will now flow rather rapidly to Reactor 2 under the driving force $(\Delta P_1 - \Delta P_{cy} - \Delta P_D) - \Delta P_{c0}$.

A method of computation has been developed for designing the pneumatically started seal.

5. Multistage Fluidized Bed

A significant application of the pneumatically controlled downcomer is for multistage fluidized beds (Kwauk, 1974b; Liu and Kwauk, 1980; Liu *et al.*, 1981). As was already noted, solids bridging and gas backflow have for many years prevented the prevalent adoption of multistaging of fluidized beds. The fully fluidized dipleg of the pneumatically controlled downcomer insures against solids bridging, and the conical spout offers significantly less resistance to forward flow of solids than to backflow, as has been demonstrated experimentally (Li *et al.*, 1982).

Various configurations have been developed for multistaging of fluidized beds using the pneumatically controlled downcomer, as shown in Fig. 38. Figure 38A shows the fundamental concept of multistaging of fluidized beds, with a downcomer between two adjacent beds, each downcomer being supplied with a separate stream of control gas. Consequently, there are as many control gas streams as there are stages.

To reduce the number of control gas streams, duo-beds have been developed, as shown in Fig. 38B-1, B-2, and B-3. Figure 38B-1 shows a bed split in two halves, A and B, with solids flowing alternately between the two, so that each half serves as the downcomer of the other. An alternate design is shown in Fig. 38B-2, in which one half is incorporated concentrically in the other, with all inflow and outflow conical spouts directed inwardly, so that the inner tube may permit easy sliding in thermal expansion as well as complete withdrawal for servicing. Figure 38B-3 shows the essential design of a duo-bed

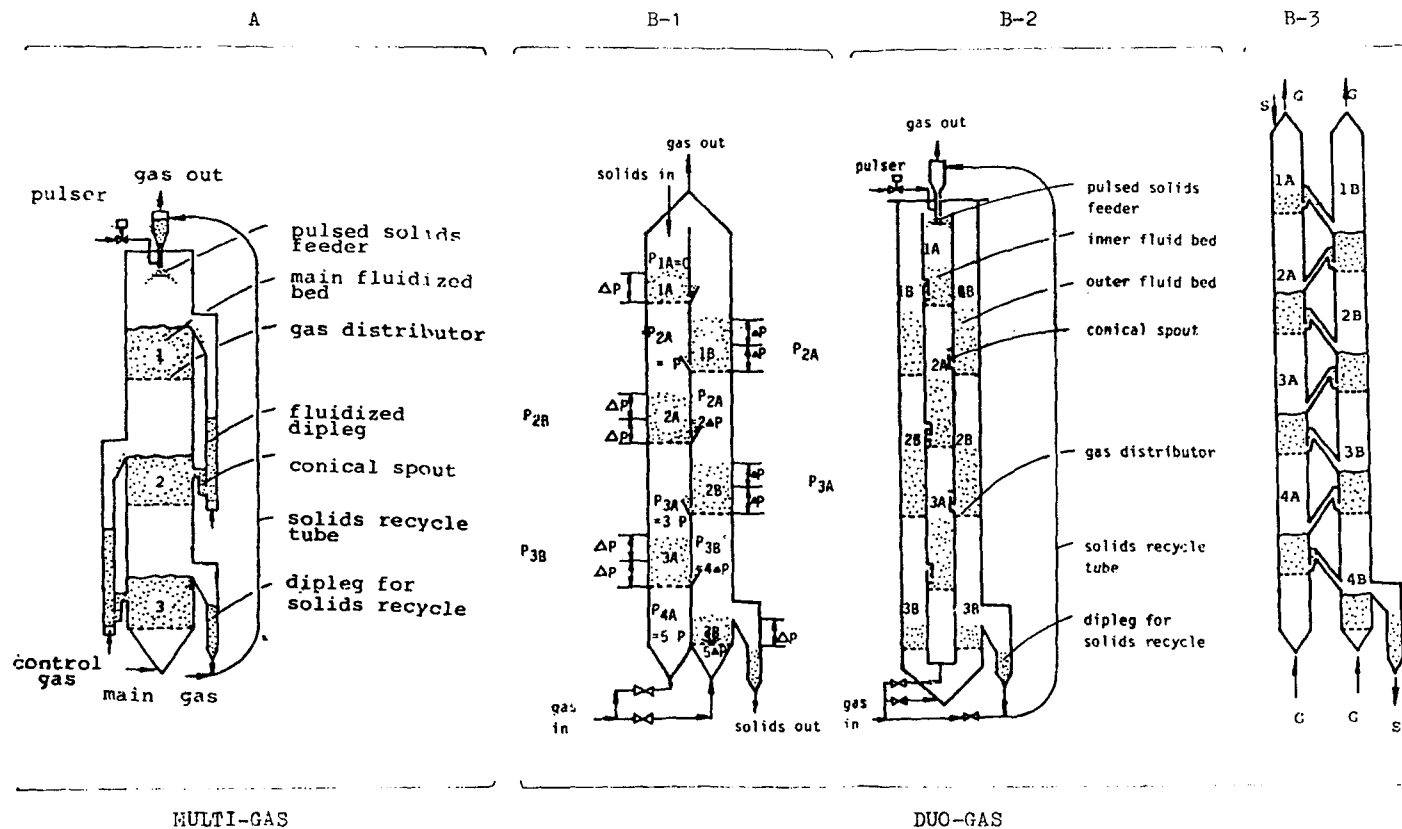


FIG. 38. Configurations for multistage fluidized beds using the pneumatically controlled downcomer. [After Kwauk, 1974; Liu and Kwauk, 1980; Liu *et al.*, 1981.]

with separate columns, A and B, which may be used for repeated solids contacting alternately with two separate gas streams.

Figure 38C shows a multi-bed with a single gas supply, for which a design method has been developed with respect to hydrostatic balancing of stages as well as stability requirements of the gas distributors.

VIII. Systems with Dilute Raining Particles

Certain industrial processes call for rapid G/S contacting, such as the heating or cooling of relatively fine particles or the drying of such fine particles involving only surface moisture evaporation. For these processes, heat and/or mass transport at the particle–fluid interface is the dominant rate-controlling process, and for efficient operation, particle–fluid contact needs to be highly transitory. For such systems, the conventional bubbling fluidized bed suffers considerable disadvantages as compared to other alternate modes of G/S contacting. One of these alternate modes is dilute-phase fluidization, in which solid particles rain down against a rising stream of gas or are entrained by a cocurrently flowing gas stream.

A. BUBBLING FLUIDIZATION AND G/S CONTACTING EFFICIENCY

Figure 39 shows that as a gas stream enters a bubbling fluidized bed, it splits into two paths. One of these leads the gas through the dense solids emulsion with good G/S contacting, while along the other path, the entering gas aggregates into bubbles, almost devoid of solid particles, thus representing rather limited G/S contacting.

Figure 40 (Kwauk and Tai, 1964) collects data taken during the fairly early stages of fluidization research (Kramers, 1946; McCune and Wilhelm, 1949; Kettenring *et al.* 1950; Walton *et al.*, 1952; Hudyakov, 1953; Wamsley and Johanson, 1954; Richardson and Bakhtiar, 1958; Richardson and Ayers, 1959; Sunkoori and Kaparathi, 1960; Richardson and Szekely, 1961) to illustrate the detriment of bubbles to good G/S contacting. Similar figures have since been published (Reh, 1976, 1977). Figure 40 plots the transfer factor, $NuPr^{-1/3}$ for heat transfer and $ShSc^{-1/3}$ for mass transfer, to Re for single particles, fixed beds, and fluidized solids. In this figure, the relatively good G/S contacting for single particles and the fixed bed is clear. The sudden drop of the transfer factor as soon as fluidization sets in, that is, when bubbling starts, is also evident.

In principle, practically all enhancement in convective heat or mass transfer is derived at the expense of increased pressure drop in moving the gas at

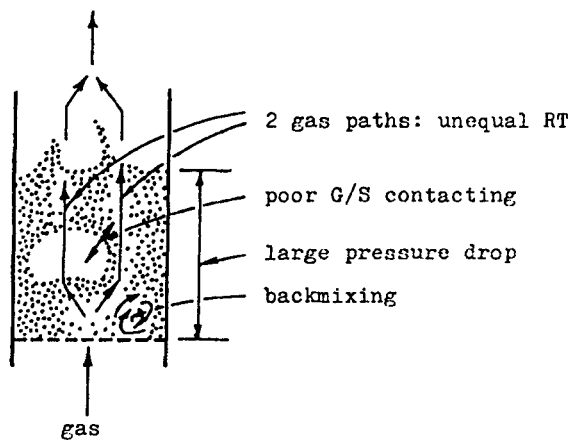


FIG. 39. Split gas flow for a bubbling fluid bed.

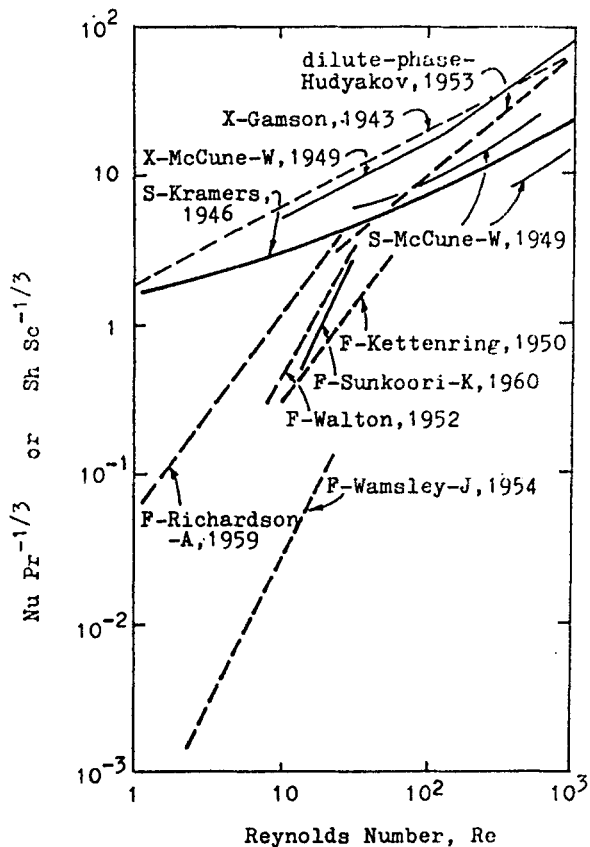


FIG. 40. Comparison of transfer factors for different particle-fluid systems. Heavy solid lines: L/S heat; light solid lines: L/S mass; heavy dashed lines: G/S heat; light dashed lines: G/S mass. S, single particles; F, fluidized bed; X, fixed bed. [After Kwauk and Tai, 1964.]

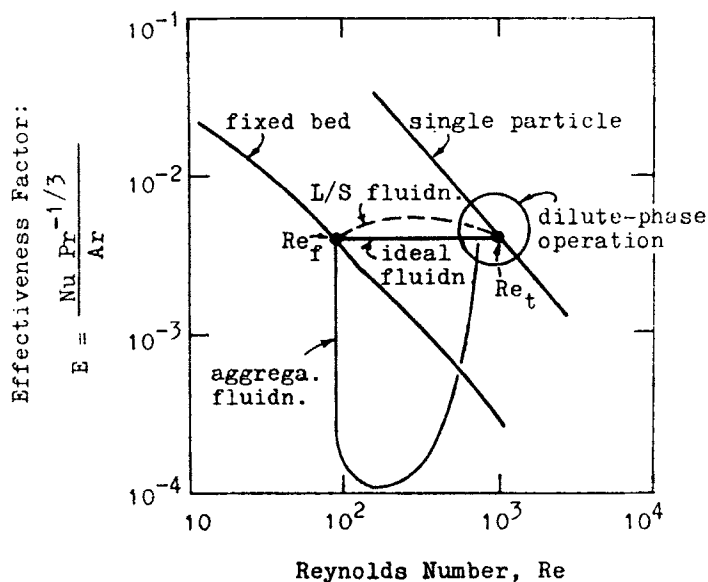


FIG. 41. Effectiveness factor for fluid-particle systems. [After Kwauk and Tai, 1964.]

higher velocities. A measure of the relative benefit of enhanced heat or mass transfer to added expenditure for fluid movement can be approximated by an effectiveness factor E , defined as the ratio of the heat or mass transfer factor, $\text{NuPr}^{-1/3}$ or $\text{ShSc}^{-1/3}$, to a generalized pressure drop, which, in the case of particle-fluid systems, can be represented by the Archimedes number,

$$\text{Ar} = (d_p^3 \rho_f g / \mu^2)(\Delta P / L) \quad \text{for fixed bed,}$$

$$\text{Ar} = (d_p^3 \rho_f g / \mu^2)(\rho_s - \rho_f) \quad \text{for fluidized bed.}$$

Thus,

$$E = \text{NuPr}^{-1/3} / \text{Ar} = \text{ShSc}^{-1/3} / \text{Ar}.$$

This is shown schematically in Fig. 41. The downwardly directed curve on the left-hand side of Fig. 41 for the fixed bed implies that increased flow is by no means sufficient to raise the heat or mass-transfer factor proportionately to the increased pressure drop. Similarly, for single particles, neither a larger particle diameter nor a higher flow rate could compensate for the relatively limited increase in the transfer factor.

Between the fixed-bed and single-particle curves lies the region for fluidized solids. For ideal fluidization, the flow rate can be varied by one to two orders of magnitude without affecting the value of $\text{NuPr}^{-1/3}$ or $\text{ShSc}^{-1/3}$, thus lead-

ing to a constant value of E , as approximated by L/S systems (McCune and Wilhelm, 1949). For G/S fluidization, however, as soon as the particles start to fluidize, gas bypassing caused by the formation of bubbles induces a sudden drop in the effectiveness factor E . As bubbling gives way to turbulent fluidization with increased gas velocity, improvement in G/S contacting is reflected in a gradual arrest in the decreasing value of E . As fluidization further improves with even higher gas velocity while entering the pneumatic transport regime, the value of E will be noted to increase and recover.

It is thus evident that for processes in which resistance at the particle-fluid interface is the dominant rate-controlling step—when the value of hd_p/k_s or $h_D d_p/D_s$ is small—operation near the single-particle region, that is, dilute-phase G/S contacting, is the preferred choice.

B. RAINING-PARTICLES HEAT EXCHANGER

When particles are raining into an upflowing gas stream, or alternately, are carried cocurrently by a flowing gas stream, to be cooled or heated, they exchange heat with the surrounding gas in a manner shown schematically in Fig. 42 (Kwauk and Tai, 1964; Kwauk, 1979b). The left-hand diagram shows solids entering at the top at a temperature of T_0 , to be heated by a gas stream entering at the bottom at a temperature of T'_{v+1} to an exit temperature of T_v at the bottom, while the gas is cooled to a temperature T'_1 at the top. The capacity of this particle-gas heat exchanger can be gauged from the ratio of the temperature rise of the solids to some average value of the temperature difference between the solids and the gas. This concept is expressed in terms of the number of heat transfer stages:

$$N_H = \frac{1}{\gamma} \int_{T_0}^{T_v} \frac{dT_s}{T_g - T_s}. \quad (8.1)$$

Using this concept of N_H , it is convenient to define efficiency of the G/S heat exchanger in terms of the following factors:

unitary heat transfer time	θ/N_H ,	
unitary heat transfer distance	z/N_H ,	(8.2)
unitary heat transfer pressure drop	$\Delta P/N_H$.	

Thus, a low value of θ/N_H means rapid heat exchange, a low value of z/N_H means low equipment height (or length), and a low value of $\Delta P/N_H$ means low pumping cost for the gas.

A further parameter needs to be specified, the fractional heat recovery η . This is defined as the ratio of the actual temperature rise (or drop) of the gas (or

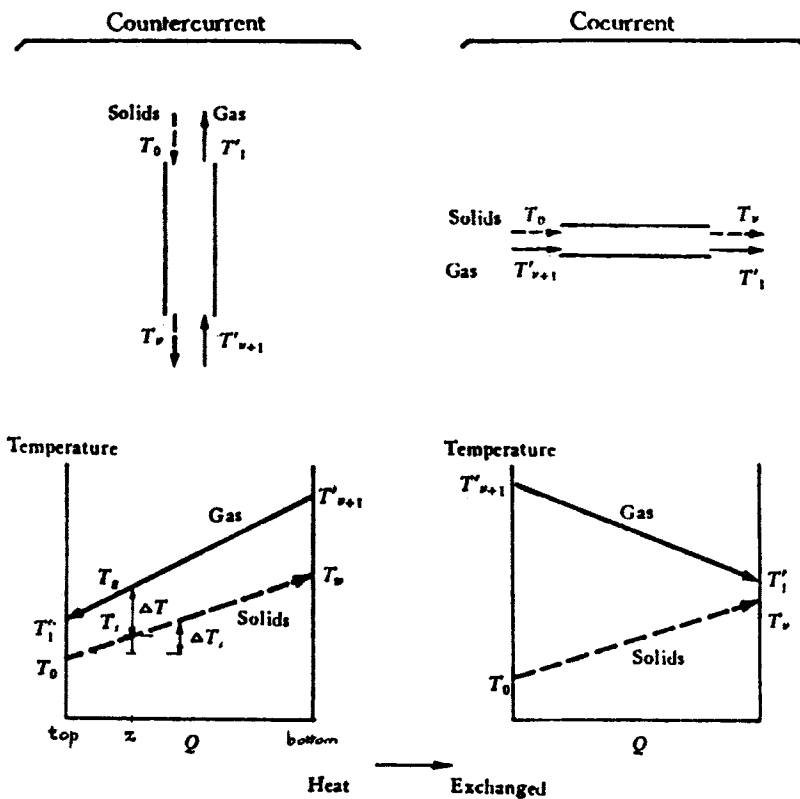


FIG. 42. Continuous particle-gas heat exchange. [After Kwauk and Tai, 1964.]

alternately, the solids) to that for complete heat transfer between the gas and the solids—that is, using the notation of Fig. 42,

$$\eta = \frac{T'_{v+1} - T'_1}{T'_{v+1} - T_0}, \quad (8.3)$$

it can be shown that n and N_H are related to each other:

$$\text{countercurrent} \quad \eta = \frac{1 - e^{-N_H(1-\gamma)}}{1 - \gamma e^{-N_H(1-\gamma)}}, \quad (8.3a)$$

$$\text{cocurrent} \quad \eta = \frac{1 - e^{-N_H(1-\gamma)}}{1 + \gamma}. \quad (8.3b)$$

While raining into a gas stream, the particles are accelerated from some initial velocity to some equilibrium slip velocity with respect to the flowing gas. If the particles fall in a highly dispersed state, they may be treated as behaving individually (Kwauk and Chong, 1963), for which the time of travel and the distance traveled can be expressed in dimensionless forms:

$$\begin{aligned} \text{dimensionless time} \quad \Theta_1 &= \frac{\mu \theta}{d_p^2 \rho_s} = \int_0^{\text{Re}} \frac{d\text{Re}}{\text{Ar}_{\Delta\rho} - f(\text{Re}_0 - \text{Re})^2} \\ &= \int_{\text{Re}_0}^{\text{Re}_0 + \text{Re}} \frac{d\text{Re}_s}{\text{Ar}_{\Delta\rho} - f\text{Re}_s^2}, \end{aligned} \quad (8.5)$$

$$\begin{aligned} \text{dimensionless distance} \quad Z_1 &= \frac{\rho_f z}{d_p \rho_s} = \int_0^{\text{Re}} \frac{\text{Re} d\text{Re}}{\text{Ar}_{\Delta\rho} - f(\text{Re}_0 - \text{Re})^2} \\ &= \int_{\text{Re}_0}^{\text{Re}_0 + \text{Re}} \frac{\text{Re}_s d\text{Re}_s}{\text{Ar}_{\Delta\rho} - f\text{Re}_s^2} - \text{Re}_0 \theta_1, \end{aligned} \quad (8.6)$$

where Re_0 is the Reynolds number for the flowing gas at velocity u_0 , and Re_s , that for the slip velocity between the particle and the gas, $u_0 + u$.

The overall pressure drop can also be expressed in the dimensionless form

$$-\Phi = -\frac{\Delta P}{z \Delta \rho} = \frac{1}{Z_1} \left(\frac{\text{Re}_d}{\text{Re}_f^m} \right) \int_{\text{Re}_0}^{\text{Re}_0 + \text{Re}} \frac{\text{Re}_s^m d\text{Re}_s}{\text{Ar}_{\Delta\rho} - f\text{Re}_s^2}. \quad (8.7)$$

All three of the preceding dimensionless numbers involve the so-called acceleration integral, defined in an abbreviated form as

$$\int F(x) = \int_{\text{Re}_0}^{\text{Re}_0 + \text{Re}} \frac{\text{Re}_s^x d\text{Re}_s}{\text{Ar}_{\Delta\rho} - f\text{Re}_s^2}. \quad (8.8)$$

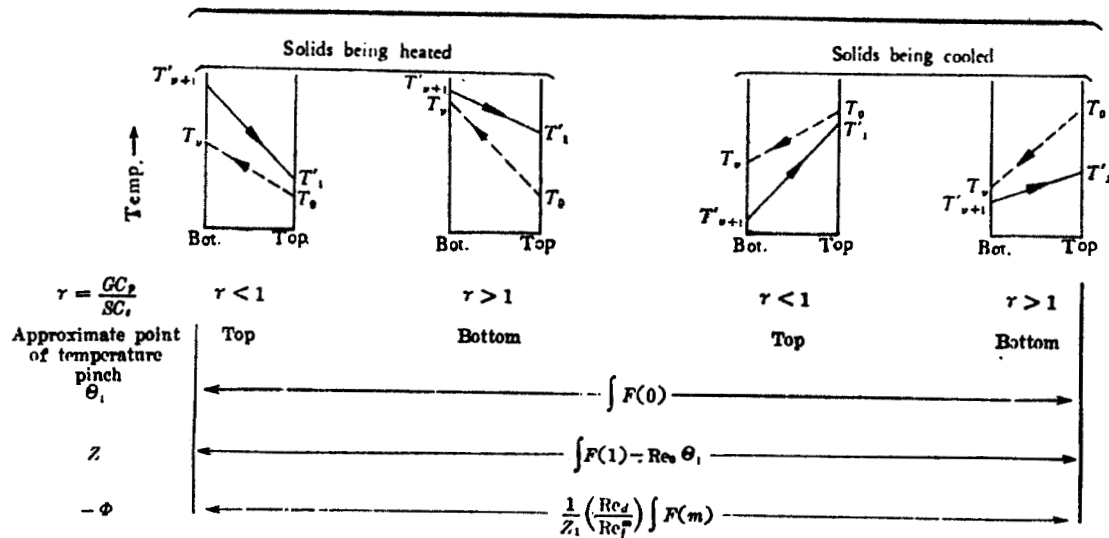
While the particle is undergoing the accelerative motion as described above, heat is being transferred between it and the surrounding gas stream, also in an unsteady state. By using the Nusselt number Nu for evaluating the heat-transfer coefficient h from the slip velocity between the particles and the gas (Kramers, 1964),

$$\text{Nu} = a + b \text{Re}^q, \quad (8.9)$$

the following expression for the number of heat-transfer stages results:

$$N_H = \frac{K}{\gamma} \left(a \int F(0) + b \int F(q) \right). \quad (8.10)$$

countercurrent systems



$$N_H \quad \frac{1}{r} \int_{T_0}^{T_v} \frac{dT_i}{T_0 - T_i} = \frac{1}{1-r} \ln \left[\frac{T'_{v+1} - T_v}{T'_i - T_0} \right] \quad \int_{T_0}^{T_v} \frac{dT_i}{T_0 - T_i} = \frac{1}{1 - \frac{1}{r}} \ln \left[\frac{T'_i - T_0}{T'_{v+1} - T_v} \right] \quad - \frac{1}{r} \int_{T_0}^{T_v} \frac{dT_i}{T_i - T_0} = \frac{1}{1-r} \ln \left[\frac{T_v - T'_{v+1}}{T_0 - T'_i} \right] \quad - \int_{T_0}^{T_v} \frac{dT_i}{T_i - T_0} = \frac{1}{1 - \frac{1}{r}} \ln \left[\frac{T_0 - T'_i}{T_v - T'_{v+1}} \right]$$

$$= \frac{K}{r} \left[a \int F(0) + b \int F(q) \right]$$

$$= K \left[a \int F(0) + b \int F(q) \right]$$

$$= \frac{K}{r} \left[a \int F(0) + b \int F(q) \right]$$

$$= K \left[a \int F(0) + b \int F(q) \right]$$

$$\eta \quad \frac{T'_{v+1} - T'_i}{T'_{v+1} - T_0}$$

$$\frac{T_v - T_0}{T'_{v+1} - T_0}$$

$$\frac{T'_i - T'_{v+1}}{T_0 - T'_{v+1}}$$

$$\frac{T_0 - T_v}{T_0 - T'_{v+1}}$$

$$= \frac{1 - e^{-N_H(1-r)}}{1 - r e^{-N_H(1-r)}}$$

$$= \frac{1 - e^{-N_H(1-\frac{1}{r})}}{1 - \frac{1}{r} e^{-N_H(1-\frac{1}{r})}}$$

$$= \frac{1 - e^{-N_H(1-r)}}{1 - r e^{-N_H(1-r)}}$$

$$= \frac{1 - e^{-N_H(1-\frac{1}{r})}}{1 - \frac{1}{r} e^{-N_H(1-\frac{1}{r})}}$$

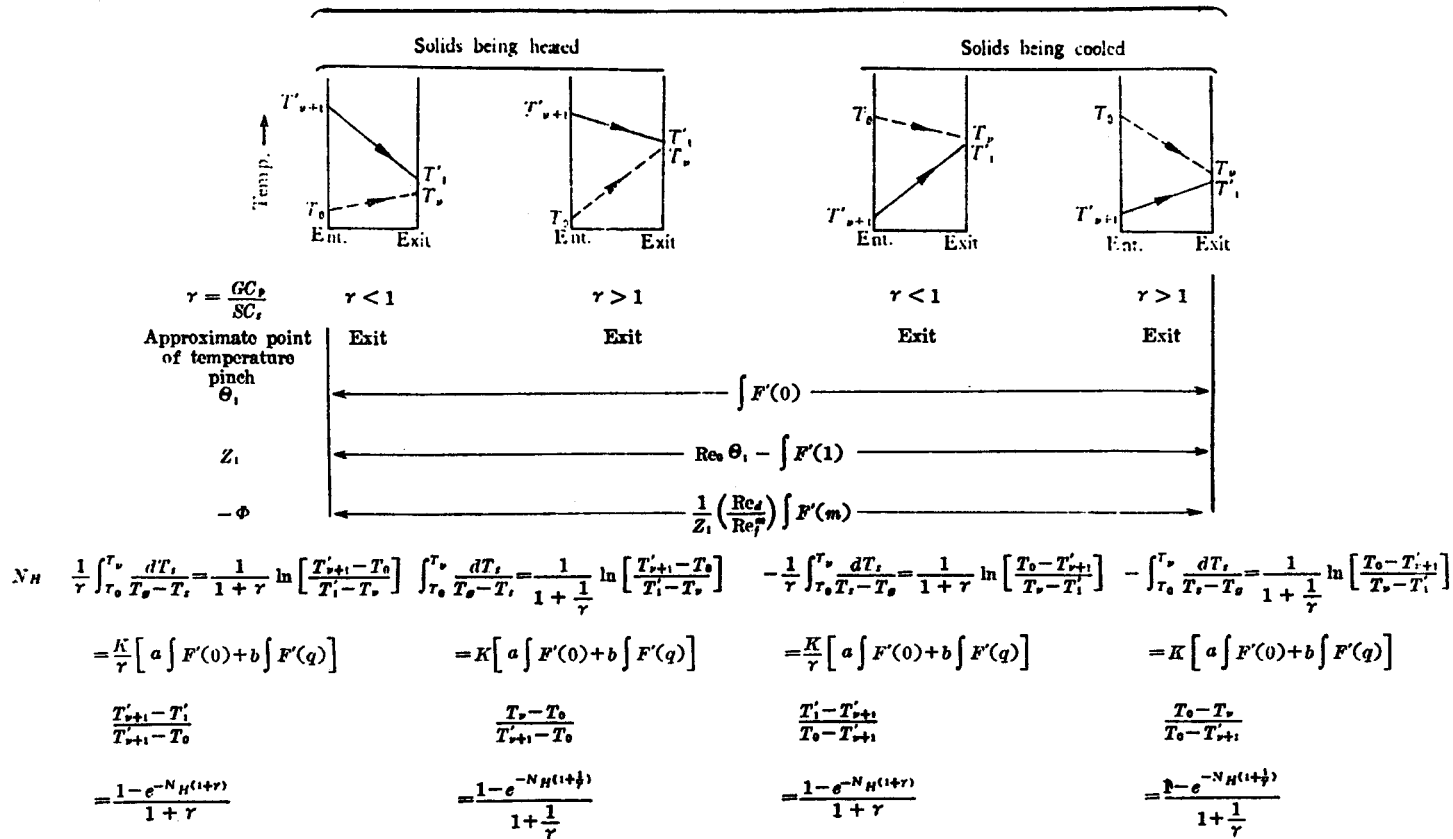


FIG. 43. Number of heat-transfer stages and fractional heat recovery in dilute-phase heat transfer for particles under accelerative motion.

$$\int F(x) = \int_{Re_0}^{Re_0 + Re} \frac{Re_s^* dRe_s}{Ar_{\Delta\rho} - fRe_s^2}; \quad \int F'(x) = \int_{Re_0}^{Re_0 - Re} \frac{Re_s^* dRe_s}{fRe_s^2 - Ar_{\Delta\rho}}; \quad K = \frac{6}{Pr} \left(\frac{C_p}{MC_s} \right)$$

For G/S heat exchange, altogether eight cases can be enumerated, as shown in the tabulation of Fig. 43, according to the following differentiations:

- operation is countercurrent or cocurrent;
- solids are being heated or cooled;
- value of τ is less or greater than unity.

By using the three-dimensionless integrals Θ_1 , Z_1 , and $-\Phi$, the three unitary heat-transfer parameters can now be quantified:

$$\begin{aligned} \text{unitary heat transfer time} \quad \theta/N_H &= \frac{d_p^2 \rho_s}{\mu} \frac{\Theta_1}{N_H}, \\ \text{unitary heat transfer distance} \quad z/N_H &= \frac{d_p \rho_s}{\rho_f} \frac{Z_1}{N_H}, \quad (8.2a) \\ \text{unitary heat transfer pressure drop} \quad \Delta P/N_H &= \Delta \rho z \frac{\Phi}{N_H}. \end{aligned}$$

C. POLYDISPERSE PARTICLES

For polydisperse particles, the larger particles fall faster than the smaller ones, as shown by the isochronous locations in Fig. 44, and yet they need a longer time for heat exchange.

In computation, the dynamics and heat transfer of each particle-size fraction d_{pi} are evaluated separately, and then summated for the entire size spectrum (Kwauk, 1964b). To establish a temperature profile for the apparatus,

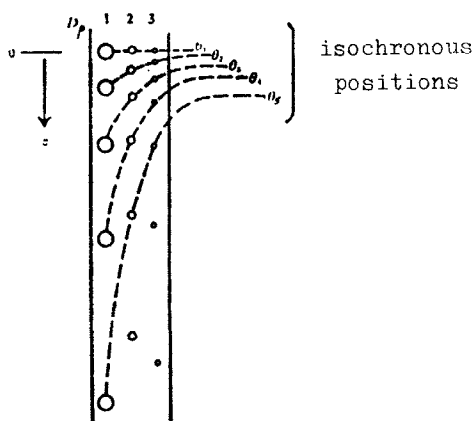


FIG. 44. Accelerative particle motion for polydisperse systems. [After Kwauk, 1979.]

time θ in the unsteady-state heat transfer equation is converted to position z through the relation $d\theta = dz/u_s$, in which u_s is the slip velocity between the particle and the gas, thus giving the differential equation for the i th fraction:

$$dT_{si} = (1/l_i)(T_g - T_{si})dz, \quad (8.11)$$

in which

$$l_i = d_{pi}\rho_s C_s u_s / 6h$$

has the dimension of length and will be called the differential unitary distance, to signify the distance required to achieve $N_H = 1$ for the i th particle-size fraction.

If particles of size d_{pi} represent a weight fraction a_i of the entire polydisperse mixture, then the following set of difference equations can be set up:

$$\text{temperature change for particle } d_{pi} \quad T_{si} = (1/l_i)(T_g - T_{si})z, \quad (8.11a)$$

$$\text{temperature change for gas} \quad T_g = \frac{z}{\gamma} \sum_1^I \frac{a_i}{l_i} (T_g - T_{si}), \quad (8.12)$$

$$\text{average temperature of all particles} \quad \bar{T}_s = \sum_1^I a_i T_{si}, \quad (8.13)$$

where I is the total number of size fractions.

D. EXPERIMENTAL VERIFICATION

Experiments for verifying the efficiency of heat transfer in the dilute phase were carried out in the equipment shown in Fig. 45 (Tai, 1959). It consisted of two vertical heat transfer columns, with an inside diameter of 300 mm for solids heating and 250 mm for solids cooling, both measuring 7.2 m in effective height, with solids circulating between the two by pneumatic transport.

Solids temperatures were measured at different levels by intercepting receptacles, each with a bare fine-wired thermocouple at its center. When in the upright position, the receptacle collected the falling solids, and its thermocouple measured the solids temperature. When the receptacle was turned to dump the solids, the thermocouple was exposed to the surrounding gas and thus measured the gas temperature. The transient behavior of the collected solids in heating the thermocouple was carefully analyzed (Liu and Tai, 1965) to justify the accuracy of the measurement.

Experimental results are shown in Fig. 46 (Kwauk and Tai, 1964) in terms of the unitary heat transfer height z/N_H for different average particle sizes in the millimeter range for both empty columns and columns with internal baffles (Tai, 1959). The various data give a range of N_H values between 2 and 7 for the

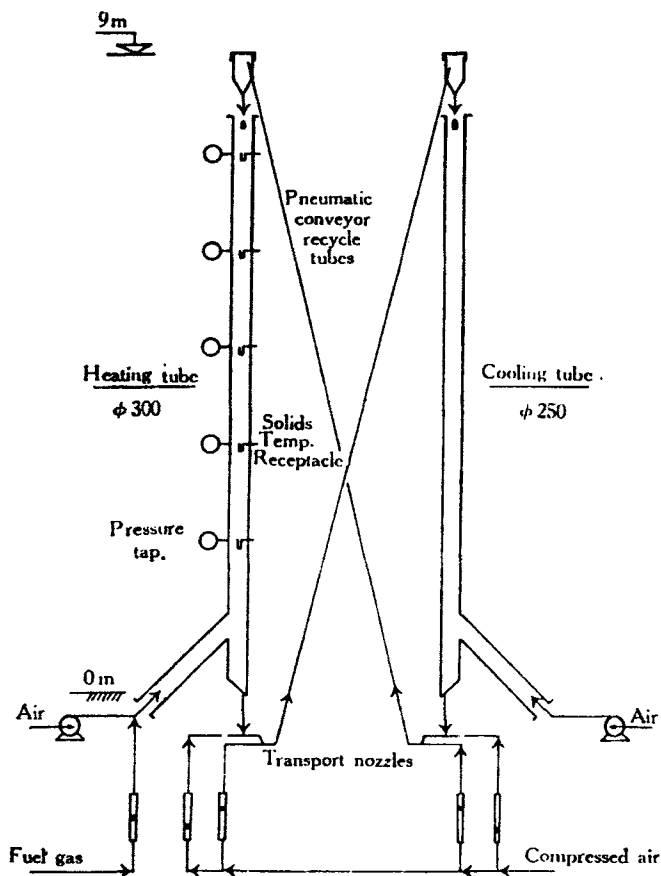


FIG. 45. Experimental setup for dilute-phase heat transfer. [After Kwauk and Tai, 1964.]

7.2-m experimental apparatus, corresponding to particle-gas heat-transfer coefficients between 300 and $1,000 \text{ kcal/m}^2 \text{ h}^\circ\text{C}$. The measured pressure drops for the two columns were of the order of 10 mm water gauge.

E. BAFFLING AND PARTICLES DISTRIBUTION

The disadvantage of employing coarse particles in raining-bed operations due to short retention and insufficient heat exchange is evident from Fig. 44, as described in Section VIII.C. For countercurrent operation, this may be improved by breaking the fall of these particles during their descent by means

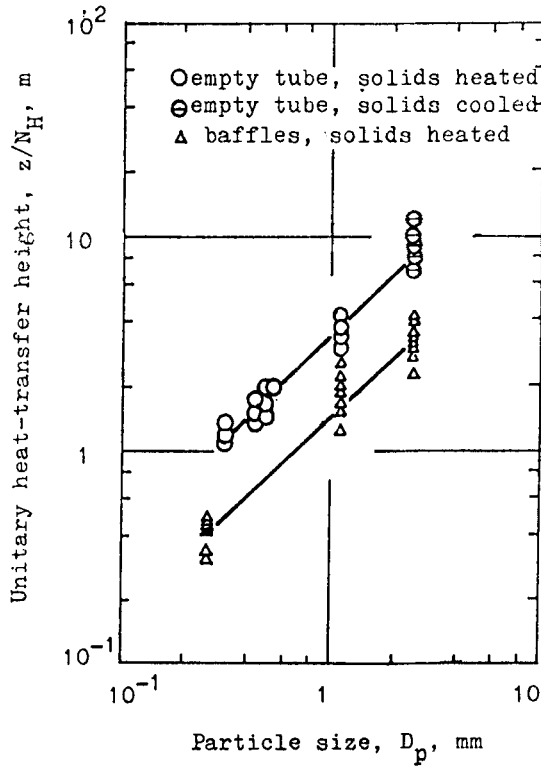


FIG. 46. Experimental values of unitary heat-transfer height. Circles: empty tube, solids heated; circles with bar: empty tube, solids cooled; triangles: baffles, solids heated. [After Kwauk and Tai, 1964.]

of baffles in order to prolong their residence, as shown schematically in Fig. 47. In vacuum, solid particles fall according to the law of gravity, covering distance $z = g\theta^2/2$ in time θ . In gas, the fall is slower because of hydrodynamic drag, and attains the terminal velocity of the particles relative to the flowing gas. This fall may be slowed down further by repeated interception by horizontal baffles. A good baffle needs to cover as near as possible to 100% of the cross-sectional area of the heat exchanger in order to accomplish complete particle interception, and yet to permit oblique passage of the deflected particles and the flowing gas as near as possible to 100% of the time (Kwauk, 1965a). Baffles are also expected to distribute solids laterally in order to give a uniform particle population in the heat transfer apparatus. Conceptually, an ideal baffle plate should consist of a cellular array of deflectors, structurally robust and made of infinitesimally thin sheet materials.

Of prime importance is the initial distribution of solids at the top of the heat-exchanging apparatus. Figure 48 shows the design of the bullet-head solids distributor. Solids fed from a nearly point source fall on a bullet-shaped target, from which they bounce off to land at some distance below on a fall-breaker baffle that either straightens the particles into essentially vertical paths or redistributes them by further deflection. The contour of the bullet head is calculated from the coefficient of restitution K between its material of construction and the solid particles concerned, and from the distance of solids feed point above it, h , and the distance to the fall-breaker baffle below, H .

Figure 49 illustrates the derivation of a criterion for assessing the lateral distribution of solids by baffles. Solid particles fed at a point source are required to be distributed as uniformly as possible throughout a circular area of radius R . The amount of solids fed is designated M , which, when uniformly distributed, will give an average population density of

$$\bar{w} = M/\pi R^2. \quad (8.14)$$

For any circular band of width dr and located at distance r from the center O , the actual density would be w , which differs from the average density \bar{w} . Thus, the difference in the amount of solids collected in this band as compared to the average density \bar{w} is

$$dm = 2\pi r dr |w - \bar{w}|. \quad (8.15)$$

The overall difference from uniform distribution for the entire circle R is therefore the integrated value of dm ,

$$\Delta M = \int dm = 2\pi \int_0^R |w - \bar{w}| r dr. \quad (8.15a)$$

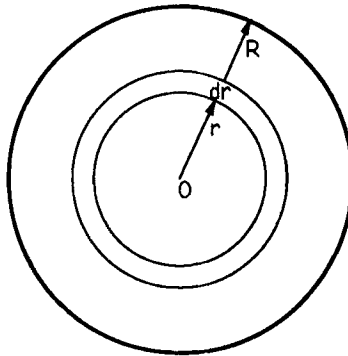


FIG. 49. Assessing lateral solids distribution by baffles.

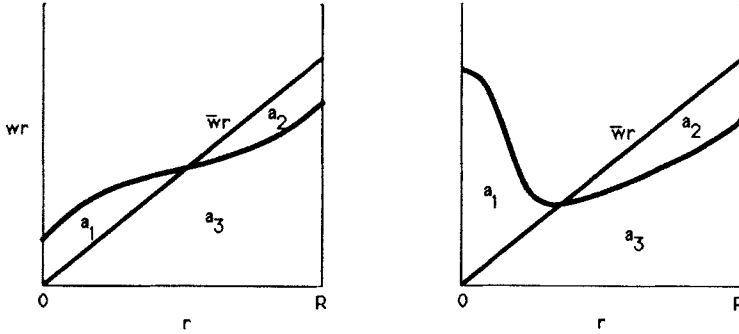


FIG. 50. Nonuniform lateral solids distribution. (a) Good distribution; (b) solids concentrated near source.

When normalized against the total solids added M , this gives a nonuniformity index, defined as

$$H = \frac{\Delta M}{M} = \frac{2\pi}{M} \int_0^R |w - \bar{w}| r dr. \quad (8.16)$$

Figure 50 shows two cases for lateral solids distribution, a fairly uniform distribution illustrated on the left-hand side, and a relatively concentrated distribution near the center source, shown on the right-hand side. It is clear that for both cases, area a_1 represents the excess of solids over the average for \bar{w} near the central feed, at the expense of deficit for area a_2 near the peripheral region. Graphically, the nonuniformity index is thus

$$H = \frac{a_1 + a_2}{a_3 + a_2}. \quad (8.17)$$

Since the actual excess balances the peripheral deficit, that is, $a_1 = a_2$,

$$H = \frac{2a_2}{a_3 + a_2}. \quad (8.17a)$$

It is evident from the figure that for a uniform distribution, $a_2 \rightarrow 0$, and therefore $H \rightarrow 0$, and for solids concentrated at the feed point, $a_3 \rightarrow 0$ and $H \rightarrow 2$. Thus, the limits for H are

$$\underbrace{0}_{\text{perfectly uniform solids distribution}} < H < \underbrace{2}_{\text{solids concentrated at feed point}}$$

F. COUNTERCURRENT STAGING OF CONCURRENT SYSTEMS

In countercurrent raining-particles heat exchange, large particles suffer from short residence time and therefore insufficient heat exchange, as just described, while small particles tend to be carried out by the uprising gas stream and thus put a limit on the throughput of the heat exchanger. Yet these small particles need only a short residence time for adequate heat exchange.

This suggests cocurrent operation for the small particles, in which gas velocities even orders of magnitude greater than the terminal velocity of the particles can be employed, thus leading to a considerable reduction in the size of the heat exchanger. The high particle-to-gas slip velocity during particle acceleration, shortly after they are fed, insures a high degree of heat recovery in a short time and within a small distance.

A higher degree of heat recovery could be achieved by stagewise operation of cocurrent G/S contacting (Kwauk, 1965b). Two modes are possible for linking the stages: solids in series and gas in series, with the two streams flowing countercurrently against each other; or solids in series and gas in parallel, with the latter flowing crosswise against all the solids stages. These two modes will be referred to, for simplicity, as "series-series" and "parallel-series," respectively.

Figure 51 shows the basic stage of a cocurrent particle-gas contactor that

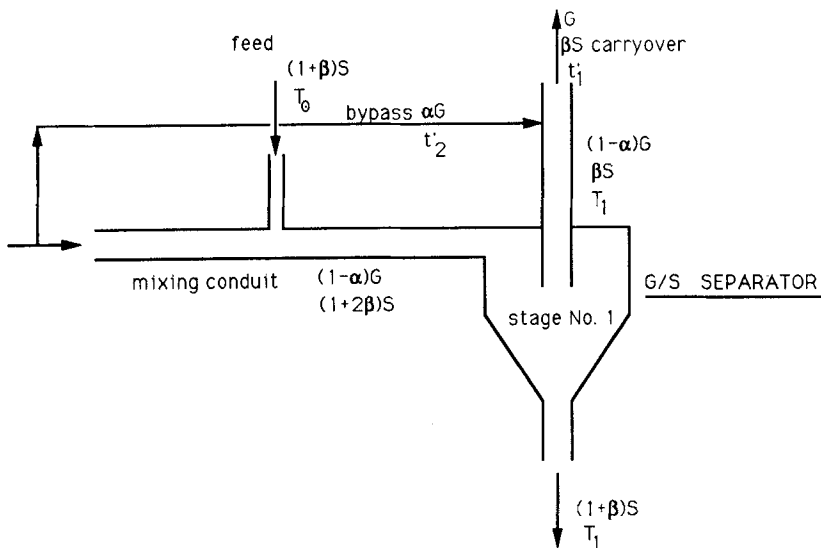


FIG. 51. The basic cocurrent particle-gas contactor. [After Kwauk, 1965.]

consists of a mixing conduit followed by a G/S separator. It should be recognized that the solids and the gas do not reach 100% equilibrium in temperature in the mixing conduit, nor do they experience 100% separation in the G/S separator. Imperfect G/S contacting in the conduit is modeled by splitting the gas stream into two fractions, fraction α totally bypassing the solids, and the remaining $(1 - \alpha)$ fraction reaching thermal equilibrium with the solids. Imperfect G/S separation is modeled by reserving a solids weight fraction β that is carried by the gas leaving the separator. This means that for collecting a unit of solids from the separator, $(1 + \beta)$ units need to be fed to it, of which β units exit with the leaving gas. Detailed analysis led to a tabulation of equations modeling the series-series and the parallel-series operations.

G. PILOT PLANT DEMONSTRATION

Countercurrently staged cyclone G/S heat exchangers have been used in recent years quite extensively in preheating raw meal for rotary cement kilns (Ziegler, 1971), thereby relieving the kilns of much of their heat-transfer duty, to which they are not so well adapted. Countercurrent raining-particles heat exchangers have been developed in the People's Republic of China for processing low-grade ores, as will be described below.

1. Ore Preheating

Figure 52 shows the inside contour of a brick-lined 15-TPD pilot-plant sulfatizing roaster for cupriferous iron ores. It consists of an upper section, i.d. 850 mm, heated by combustion of producer gas and provided with baffles, in which the cupriferous ore, crushed to 0–2 mm, was heated in dilute phase through a fall of 12 meters to the reaction temperature of 500–550°C. The preheated ore was fed pneumatically via an angle-of-repose solids valve into a lower section, where it was sulfatized in a dense-phase fluid bed, i.d. 500 mm, with a gas containing 6–7% SO₂ produced by roasting pyrite concentrate in a separate auxiliary roaster at higher temperatures. Most of the copper and cobalt in the ore was rendered soluble by selective sulfatization, while the iron oxide remained essentially unconverted. With ore preheating, the pyrite consumption was reduced to nearly $\frac{1}{3}$ as compared to autogenous roasting by direct admixture of pyrite with the cold cupriferous iron ore.

An alternate process for winning copper from cupriferous iron ore was segregation roasting, in which the hot ore was mixed with small amounts of common salt and powdered coal, in order to transport the copper content of the ore via gaseous copper chlorides to the coal particles, where they were reduced *in situ* to the metal. The copper-coated char could be concentrated by

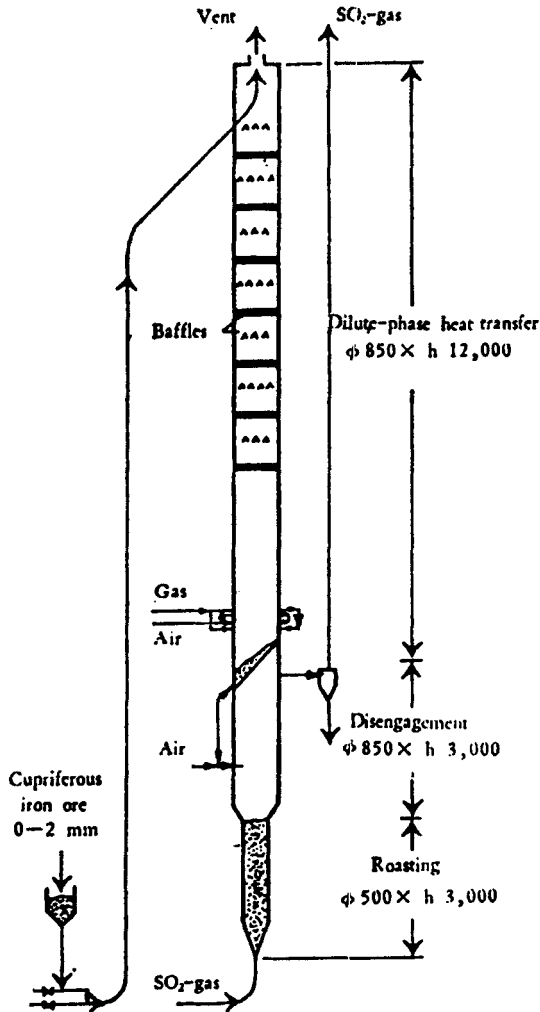


FIG. 52. 15-TPD sulfatizing pilot plant roaster. [After Kwauk and Tai, 1964.]

ore dressing. Figure 53 shows a segregation pilot plant, in which cupriferous iron ore was preheated in a dense-phase fluidized bed by direct injection of powdered coal, and the sensible heat of the hot flue gas was recovered by the incoming ore particles raining down in dilute phase, which was introduced at the top of the roaster by a rotary feeder to a number of radially positioned bullet-head distributors located above two tiers of fall-breaker baffles.

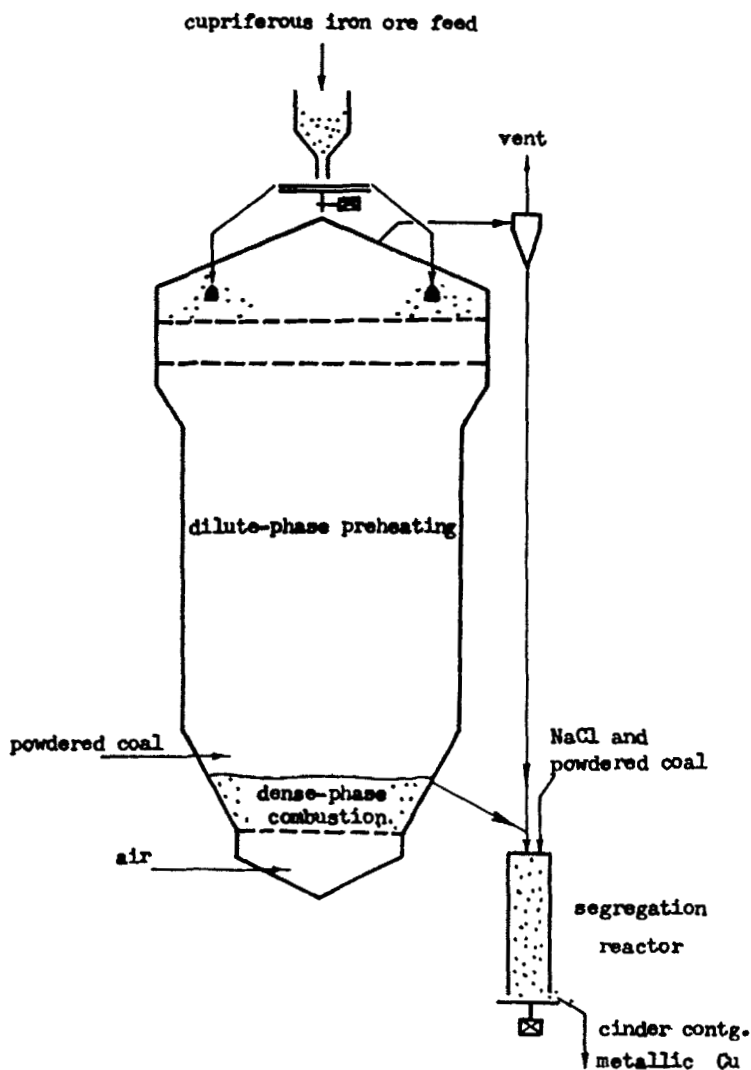


FIG. 53. 250-TPD segregation pilot roaster.

2. Semi-Conveying Magnetizing Roasting

Figure 54 shows diagrammatically the two-phase magnetizing roaster for low-grade iron ores—dilute-phase ore preheating in an upper section of i.d. 1,050 mm, and dense-phase reduction with producer gas in a lower section of i.d. 825 mm. The roasting consisted of a mild reduction with producer gas

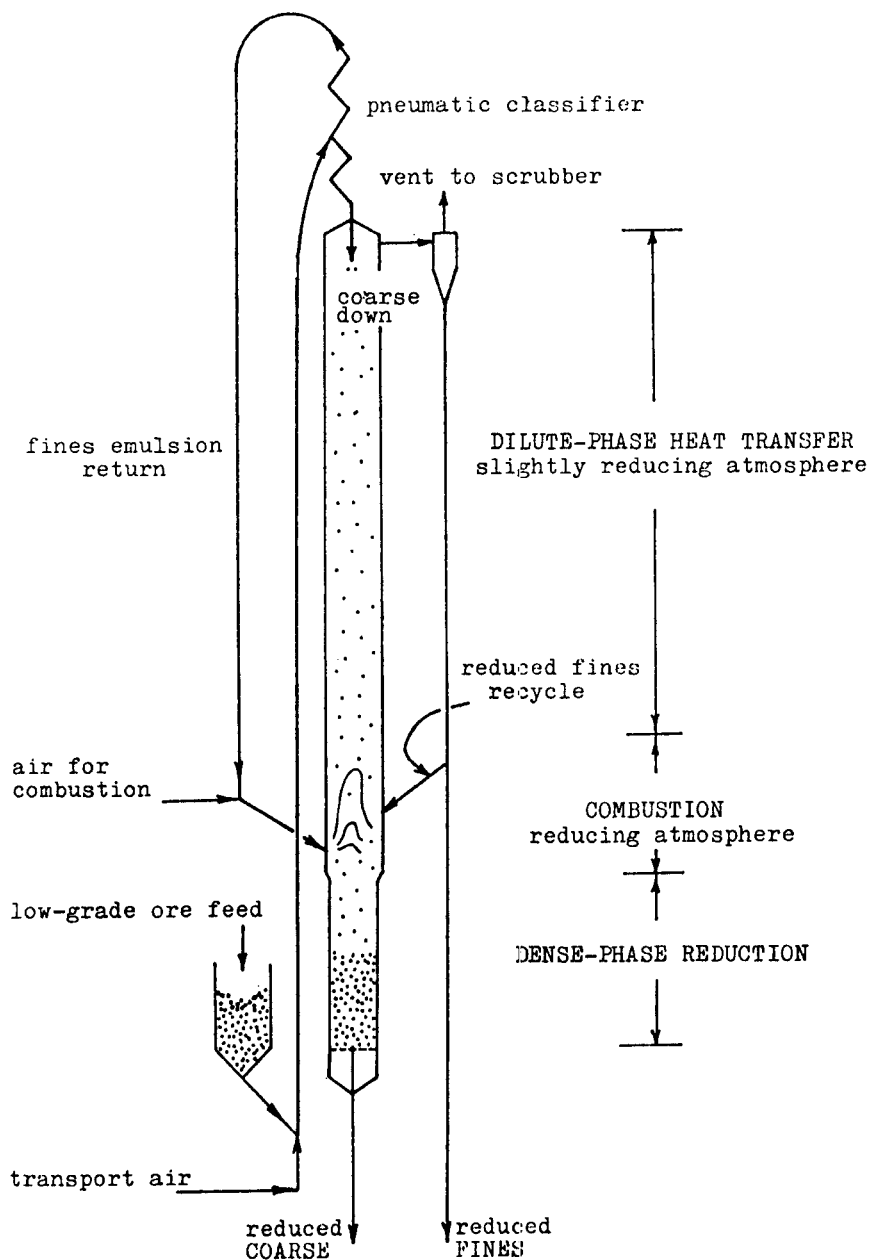


FIG. 54. Semi-conveying two-phase fluid-bed magnetizing roaster.

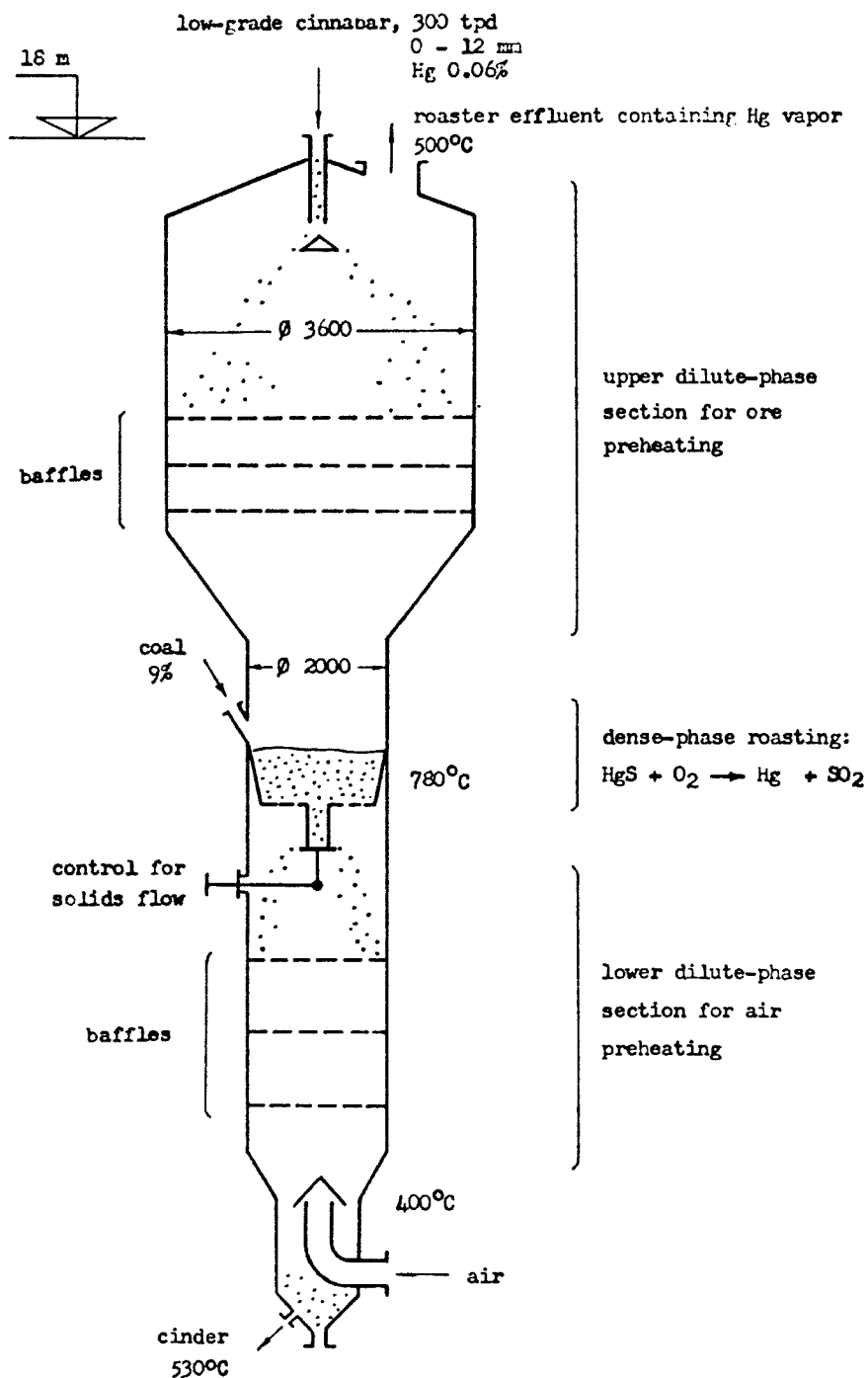


FIG. 55. Double-section two-phase cinnabar roaster.

to convert the iron values to Fe_3O_4 , followed by low-intensity magnetic ore dressing to yield an iron ore concentrate. At the junction of the two sections, approximately one-third of the way from the bottom, air was injected to burn most of the partly spent reducing gas issuing from the dense bed, for heating the ore particles raining from above.

To guard against incomplete reduction of ore fines that would be elutriated prematurely during preheating, the midsection combustion was adjusted to produce a mildly reducing flame containing approximately 4% of $\text{H}_2 + \text{CO}$, and the major portion of the fines present in the ore feed were removed by pneumatic classification in a zigzag tube at the top of the vertical pneumatic transport feed pipe. From there, the remaining coarse portion was fed, as usual, by gravity at the top of the dilute-phase preheating section, while the fines were carried by the same transport air downward again to the combustion zone, where the high-temperature reducing flame converted these minute particles almost instantly to the required magnetite state. The up-flowing emulsion of fines travelled to the top of the roaster, delivering its heat to the falling particles of larger diameters, and the fines, now already reduced, were finally collected in an external cyclone. Thus, part of the ore—the fines—was reduced during upward conveying. Inasmuch as the upflowing heat capacity was augmented by the presence of these fines, the amount of excess combustion air, normally needed to moderate the gas temperature after the midway combustion, could be reduced, thus increasing the roaster capacity.

3. *Heat Recovery from Both Hot Calcine and Hot Flue Gas*

Figure 55 shows a roaster with two sections for dilute-phase heat recovery both from the hot calcine at the bottom and from the hot flue gas at the top. With this design, low-grade cinnabar ore containing as little as 0.06% Hg and crushed to particle sizes as large as 0–12 mm has been successfully roasted at around 800°C for mercury extraction with a coal ratio of 90 kg/t of ore. This design has also been used on a pilot scale to roast low-grade pyrite, containing only 13% sulfur and thus hardly autogenous, to produce a gas containing over 10% SO_2 for use in sulfuric acid manufacture.

IX. Extension of Idealized Fluidization to G/S Systems

In the circulating fluidized bed, solids are removed from the top and recycled to the bottom, to be carried up again by the flowing fluid, thus forming a co-up system. Generalized fluidization predicts a decrease in voidage, as shown in the constant- n chart. The high solids concentration,

through recycling, permits operation at increased gas velocities, thus enhancing G/S contacting.

The ability of small particles to admit high gas velocities, often a hundredfold more than that estimated on the basis of particulate fluidization, was noted even in early studies on fluidization. (Wilhelm and Kwauk, 1948 (discussion by Friend)). At the relatively high velocities for fast fluidization, the fine particles tend to aggregate into transient clusters or strands, thus depriving the surrounding dilute zones of their normal share of solid particles and clearing the way for easier gas passage. However, the practical potentialities of this phenomenon were hardly tapped until the past decade or two. Reh applied (1970, 1971, 1972, 1985) the circulating bed principle commercially to endothermic reactions; Squires (1975a, 1975b, 1975c, 1985) described early attempts at applying fast fluidization to coal processing. In many processes, fast fluidization offers more promising returns as compared to the conventional bubbling-type G/S contacting (Squires *et al.*, 1985; Kwauk, 1983), such as the catalytic conversion of methanol to gasoline (Avidan *et al.*, 1985). Related hydrodynamic studies have been on the increase (e.g., Yerushalmi *et al.*, 1976; Yerushalmi and Cankurt, 1978; Cankurt and Yerushalmi, 1978; Yang and Keairns, 1978; Grace and Tuot, 1979; Li and Kwauk, 1980).

A. MODELING LONGITUDINAL VOIDAGE DISTRIBUTION

The characteristic solids distribution in fast fluidization—dilute at the top and dense at the bottom with a possible point of inflection in the middle (Squires, 1975a; Li and Kwauk, 1980; Weinstein *et al.*, 1983)—could not be accounted for by a one-dimensional analysis based on accelerative motion for particulate fluidization, as described in Section III.C. For discrete fine particles, the acceleration zone would be much shallower than what occurs near the point of inflection, as shown in Fig. 56. This figure gives, on the left-hand side, a typical voidage distribution curve, extending from a low asymptotic voidage ϵ_a at the bottom, through a point of inflection z_i , to a dilute-phase asymptotic voidage ϵ^* at the top.

The right-hand side of Fig. 56 shows the clusters to move upward through a diffusive mechanism from a relatively dense region of the lower section, and then, when they arrive at a higher region, where the average bed density is lower, they tend to fall back to the lower region of their origin by virtue of buoyancy (Kwauk, 1979c; Li and Kwauk, 1980). Dynamic equilibrium calls for equality of the diffusion and buoyancy fluxes, as explained on the lower right-hand corner of Fig. 56. Diffusion is taken to be determined by the gradient of the strands concentration, $\rho_s f(1 - \epsilon_a)$, with ξ as the proportionality

Typical Voidage Distribution

Proposed Physical Model

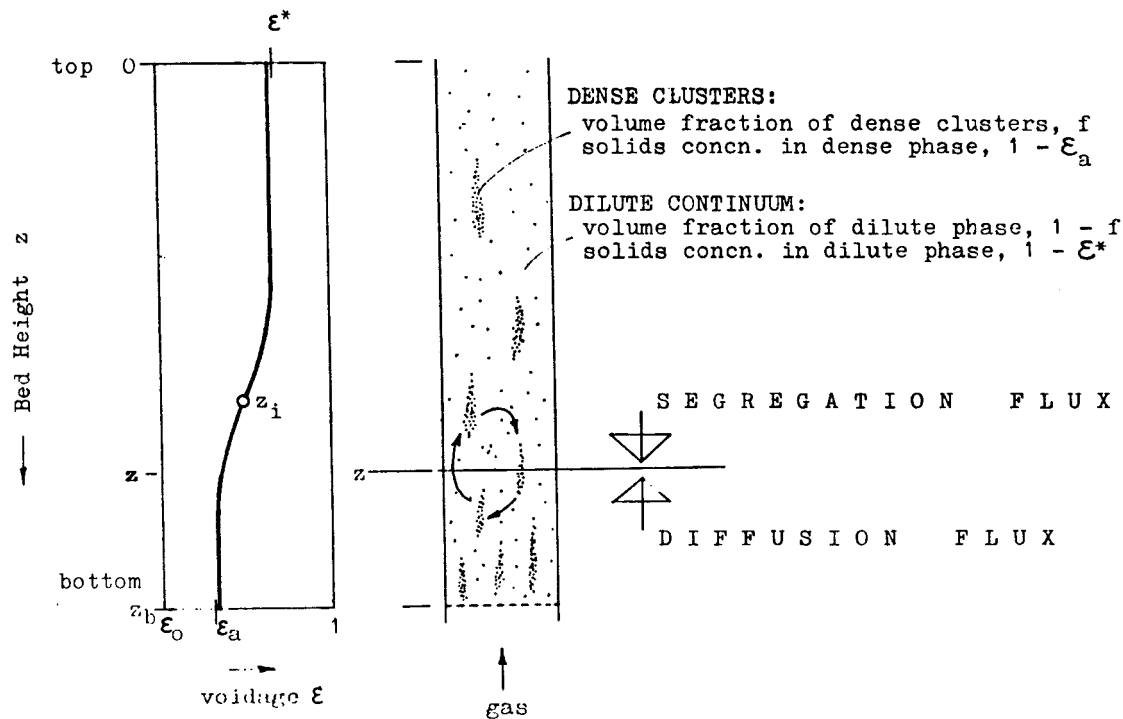


FIG. 56. Modeling for fast fluidization. [After Li and Kwauk, 1980.]

constant, while the upthrown strands, at their volume concentration of $f(1 - \varepsilon_a)$, are subject to a driving force for segregation, represented by the difference in concentration between the average bed, $(1 - \varepsilon)$, and the strands, $(1 - \varepsilon_a)$, with an analogous proportionality constant ω . Thus,

$$\xi \frac{d}{dz} [\rho_s f(1 - \varepsilon_a)] = \omega [\Delta \rho (1 - \varepsilon_a) - \Delta \rho (1 - \varepsilon)] f(1 - \varepsilon_a). \quad (9.1)$$

The average solids concentration, $(1 - \varepsilon)$, is evidently composed of both the strands and the dilute continuum,

$$(1 - \varepsilon) = f(1 - \varepsilon_a) + (1 - f)(1 - \varepsilon^*). \quad (9.2)$$

Integration, using the point of inflection z_i as the origin, results in

$$\frac{\varepsilon - \varepsilon_a}{\varepsilon^* - \varepsilon} = \exp \left[1 - \frac{z - z_i}{Z_0} \right], \quad (9.3)$$

where

$$Z_0 = \frac{\xi \rho_s}{\omega \Delta \rho} \frac{1}{\varepsilon^* - \varepsilon_a}$$

has the dimension of length and will be designated the characteristic length of fast fluidization.

The value of Z_0 represents how rapidly the dense region at the bottom merges into the dilute region at the top. Thus, for $Z_0 \rightarrow 0$, the point of inflection is marked by a horizontal line, indicating a sharp interface between the dense and dilute regions, characteristic of particulate fluidization. For $Z_0 \rightarrow \infty$, uniform voidage prevails throughout the bed, as approximated by long vertical pneumatic transport tubes.

Typical voidage distribution curves computed by using Eq. (9.3) for four kinds of solid materials are shown in Fig. 57 and compared against experimentally determined values.

Equation (9.3) also permits analytical evaluation of the integrated average voidage $\bar{\varepsilon}$ taken through the whole bed height, above the point of inflection z_i for the dilute region at the top, and below z_i for the dense region at the bottom:

$$\text{entire} \quad \frac{\bar{\varepsilon} - \varepsilon_a}{\varepsilon^* - \varepsilon_a} = \frac{1}{Z_0} \ln \left[\frac{1 + \exp(z_i/Z_0)}{1 + \exp(z_i - Z)/Z_0} \right], \quad (9.4)$$

$$\text{upper} \quad \frac{\bar{\varepsilon}_B - \varepsilon_a}{\varepsilon^* - \varepsilon_a} = \frac{1}{z_i/Z_0} \ln \left[\frac{1 + \exp(z_i/Z_0)}{2} \right], \quad (9.4b)$$

$$\text{lower} \quad \frac{\bar{\varepsilon}_A - \varepsilon_a}{\varepsilon^* - \varepsilon_a} = \frac{1}{(z_i - z)/Z_0} \ln \left[\frac{2}{1 + \exp(z_i - z)/Z_0} \right]. \quad (9.4a)$$

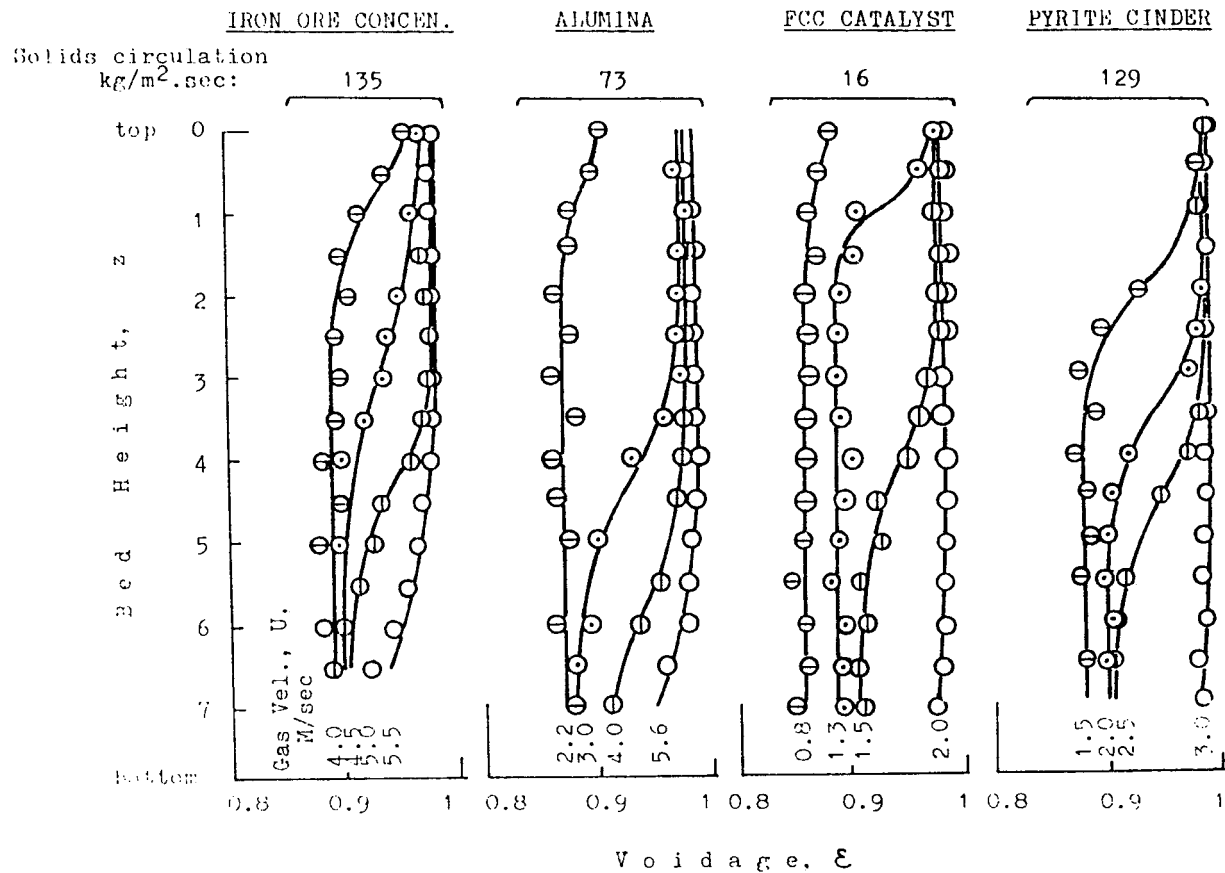


FIG. 57. Vertical voidage distribution in fast fluidization. [After Li and Kwauk, 1980.]

B. EVALUATION OF PARAMETERS

Experimental values for ε^* and ε_a for five kinds of solid materials—FCC catalyst, fine alumina, coarse alumina, pyrite cinder, and iron ore concentrate—ranging in character from Geldart's Group A to weakly Group B, are shown in Fig. 58 (Li *et al.*, 1982, 1981). The correlation could be fitted with the following empirical equations (Kwauk *et al.*, 1985):

$$1 - \varepsilon^* = 0.05547 \left[\frac{18 \text{Re}_s^* + 2.7 \text{Re}_s^{*1.687}}{\text{Ar}} \right] + 0.6222, \quad (9.5)$$

$$\text{where } \text{Re}^* = \frac{d_p \rho_f}{\mu} \left[u_0 - u_d \left(\frac{\varepsilon^*}{1 - \varepsilon^*} \right) \right],$$

$$\text{Ar} = d_p^3 \rho_f g \rho / \mu^2;$$

$$1 - \varepsilon_a = 0.2513 \left[\frac{18 \text{Re}_{sa} + 2.7 \text{Re}_{sa}^{1.687}}{\text{Ar}} \right] - 0.4037, \quad (9.6)$$

$$\text{where } \text{Re}_{sa} = \frac{d_p \rho_f}{\mu} \left[u_0 - u_d \left(\frac{\varepsilon_a}{1 - \varepsilon_a} \right) \right].$$

In accordance with the definition of Z_0 for Eq. (9.3), expressed in meters, it has been correlated to $(\varepsilon^* - \varepsilon_a)$ empirically as

$$Z_0 = 500 \exp[-69(\varepsilon^* - \varepsilon_a)]. \quad (9.7)$$

C. COMPUTING VOIDAGE DISTRIBUTION

The mathematical model for longitudinal voidage distribution, along with the empirical correlations for the four related parameters, provides a means for computing voidage distribution along a fast fluidized column from the physical properties of the solids and of the gas, as well as the operating variables (Wang *et al.*, 1985). Of primary significance is the location of the point of inflection z_i , which is determined by the solids inventory of the solids circulating system—the more solids are contained in the system, the greater is the proportion of the dense region, and the higher is the location of the inflection point z_i .

Balance of static pressures in the various zones of the circulating system led to an independent relation for determining the average bed voidage in addition to that provided by Eq. (9.4):

$$\bar{\varepsilon} = 1 - \frac{I/A - (a/A)C}{(1 + a/A)Z}. \quad (9.8)$$

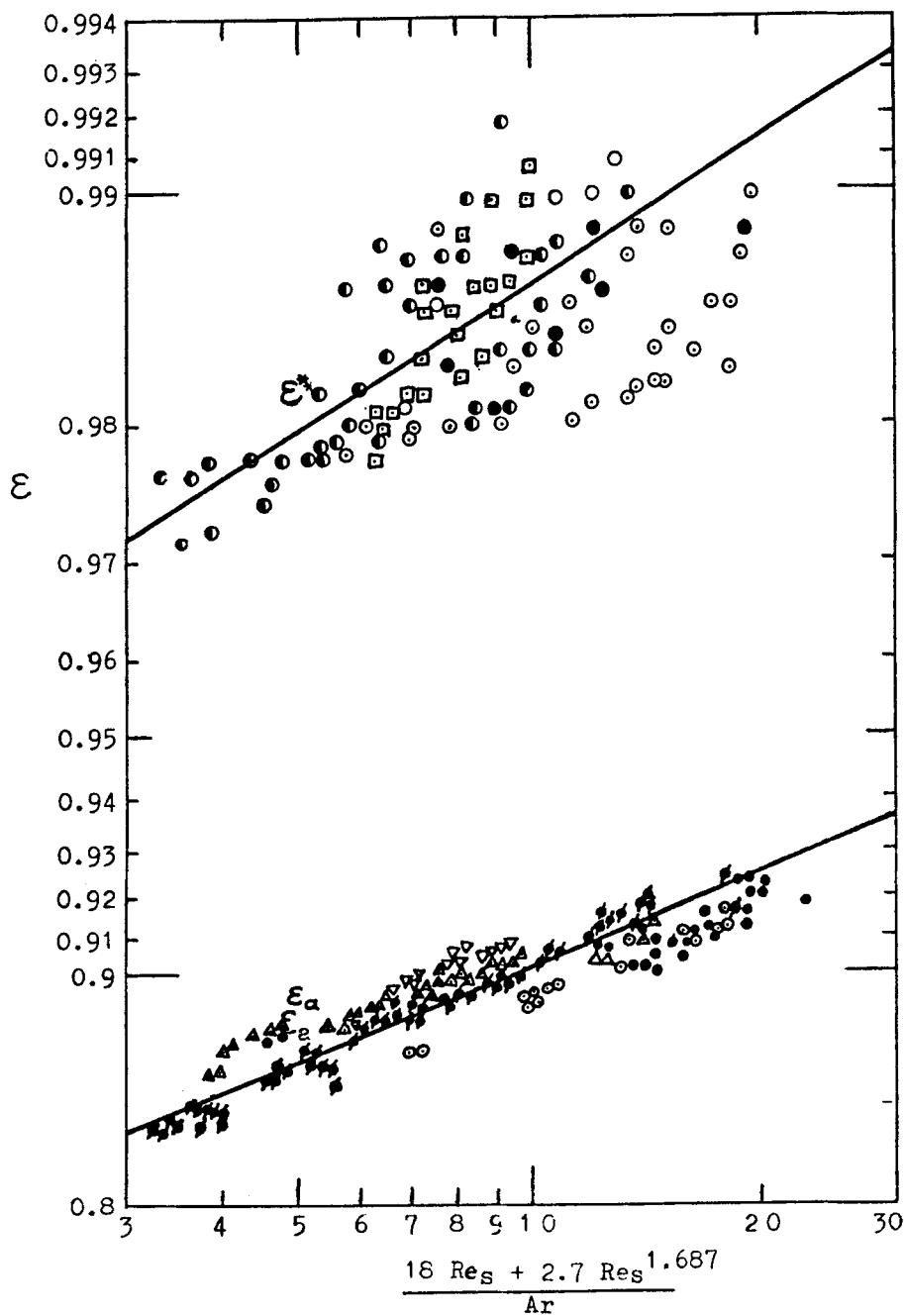
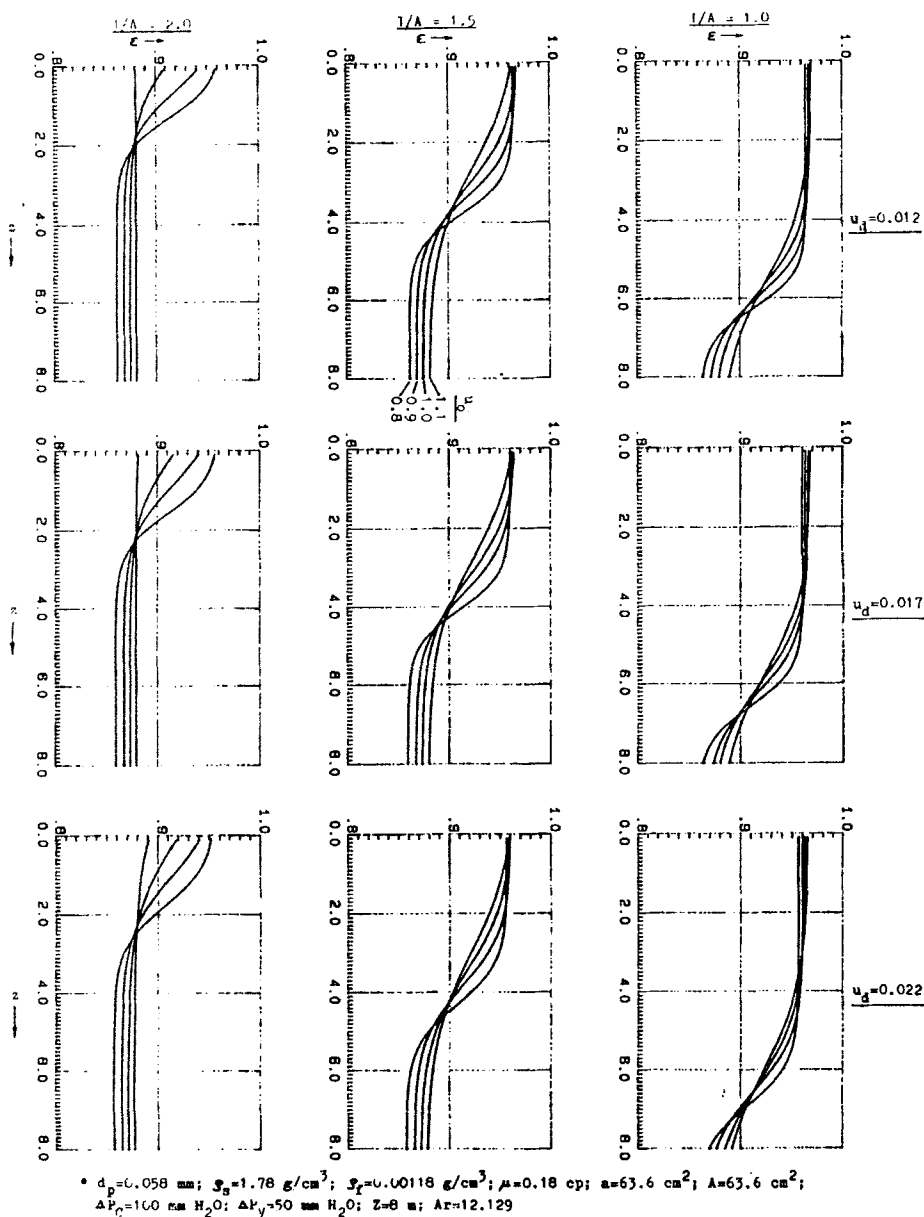


FIG. 58. Empirical correlations for voidages ε^* and ε_a . [After Kwauk *et al.*, 1985.]

FIG. 59. Computerized voidage profiles. [After Wang *et al.*, 1985.]

Substitution of the above expression for $\bar{\varepsilon}$ in Eq. (9.4) gives the following expression, which can be used for determining the point of inflection z_i :

$$\frac{\left(1 - \frac{I/A - (a/A)C}{(1 + a/A)Z}\right) - \varepsilon_a}{\varepsilon^* - \varepsilon_a} = \frac{1}{Z/Z_0} \ln \left(\frac{1 + \exp(z_i/Z_0)}{1 + \exp[(z_i - Z)/Z_0]} \right). \quad (9.9)$$

Typical computations for four values of u_0 , three values of u_d , and three values of I/A , totalling altogether 36 ε - u curves, are shown in Fig. 59. Looking horizontally along any row of the nine plots in Fig. 59, one can see that the point of inflection z_i moves downward as the solids inventory I/A decreases. Looking vertically down along any column of the nine plots, one can see that as the solids circulation rate increases, not only does the dense bed settle downwardly, but also the asymptotic bed voidages, ε^* and ε_a , decrease as a whole. Looking at any family of four curves for each of the nine plots, one can see that as gas velocity decreases, not only does the demarcation between the dense and dilute phases become sharper, but also both asymptotic voidages, ε^* and ε_a decrease as the same time.

D. REGIME DIAGRAM

Figure 60 charts the variation of the average voidages for the dense- and dilute-phase regions, $\bar{\varepsilon}_A$ and $\bar{\varepsilon}_B$, with gas velocity u_0 for fixed rates of solids

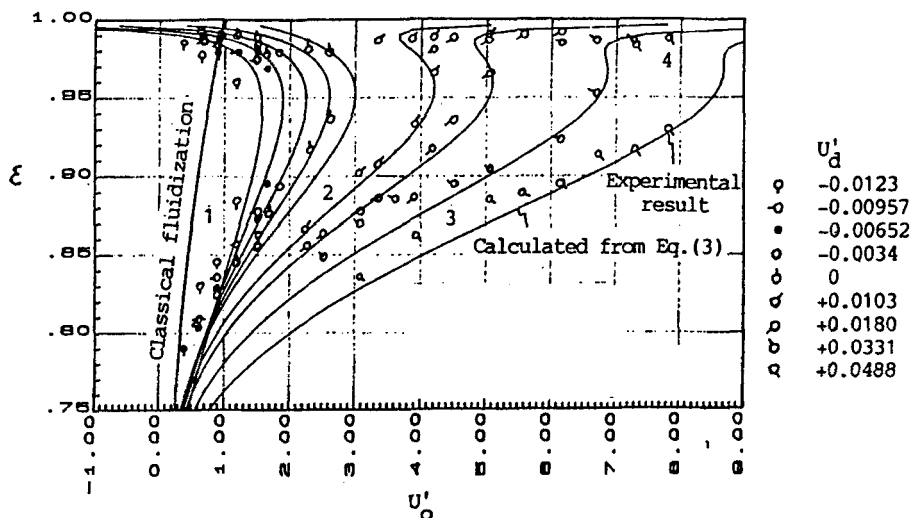


FIG. 60. Regime diagram for Al_2O_3 . 1. bubbling region; 2. turbulent region; 3. fast fluidization region; 4. pneumatic transport region. [After Chen and Kwauk, 1985.]

circulation u_d (Chen and Kwauk, 1985). The diagram shows curves not only of experimentally determined points for the co-up system toward the right, but also of the counter-down system toward the left, the division between these two groups of curves being provided by the $u_d = 0$ line for zero solids throughput. Compared to the constant- n diagram of Section III for ideal fluidization, the G/S line for zero solids flow is shown to bulge characteristically towards the right of the classical line for ideal fluidization. This and the other co-up curves toward the right illustrate the two-region nature of fast fluidization—that is, on any constant- u_d line, for a certain dense-phase voidage $\bar{\epsilon}_A$, there is a corresponding dilute-phase voidage $\bar{\epsilon}_B$. As gas velocity u_0 increases, $\bar{\epsilon}_A$ increases while $\bar{\epsilon}_B$ decreases, much in the manner of the counter-down operation for ideal fluidization, until at some value of u_0 , the $\bar{\epsilon}_A$ curve merges rather rapidly into the $\bar{\epsilon}_B$ curve. This quick reversion of $\bar{\epsilon}_A$ to $\bar{\epsilon}_B$ corresponds to the disappearance of the dense phase and signifies the transition from fast fluidization to pneumatic transport.

The transition from bubbling to fast fluidization is characterized by the replacement of the bubble-in-emulsion structure with the prevalent formation of transient solids clusters or strands in a dilute continuum of sparsely dispersed particles. This transition can be considered a phase inversion—from gas aggregation to solids aggregation—and it usually takes place through a range of gas velocities in an intermediate stage, often referred to as turbulent fluidization, where both bubbles and clusters coexist. This transition has been identified with a bed height z that represents a measure of the thickness of an interface zone lying between the dense- and dilute-phase regions. The greater the value of z is, the further removed is the operation from bubbling fluidization, and the more predominant are the features of fast fluidization with solids clustering.

Analysis has shown that this interface thickness Δz is related to the characteristic length by the simple relation

$$\Delta z = 4Z_0. \quad (9.10)$$

E. GENERALIZED FLUIDIZATION OF NONIDEAL SYSTEMS

The nonideal nature of G/S fluidization, shown as the bulging curve for zero solids flow in the voidage–velocity plot of Fig. 60, is considered to be caused by gas aggregation at low velocities and solids aggregation at high velocities. Alternately, the G/S system may be visualized to be equivalent to a binary mixture of the aggregated gas bubbles with a volume fraction of $(\epsilon - \epsilon_0)$ on the one hand, and of the aggregated solid particles in the form of clusters with a volume fraction of $(1 - \epsilon)$ on the other. At low gas velocities,

solids clusters are so profuse as to form a continuum in which gas is dispersed as bubbles, whereas at high velocities, gas bubbles become so profuse as to form a dilute-phase continuum in which solids clusters are suspended. A gross correction factor $F(\varepsilon, u_d)$ that combines the two tendencies of gas aggregation and solids aggregation has been introduced (Chen and Kwauk, 1985) to modify the generalized relation for ideal fluidization, Eq. (3.5) of Section III, as follows:

$$u'_0 - u'_d \varepsilon / (1 - \varepsilon) = \varepsilon^n [1 + F(\varepsilon, u'_d)]. \quad (9.11)$$

Since the G/S and L/S systems are identical for the fixed bed, as shown in Fig. 3 of Section I, and are essentially the same for dilute-phase transport, the correction factor needs to approach zero for these two boundary states of $\varepsilon \rightarrow \varepsilon_0$ and $\varepsilon \rightarrow 1$, and it has to assume some appropriate positive values for the intermediate range $\varepsilon_0 < \varepsilon < 1$. Among the possible trial functions, the following has been adopted:

$$F(\varepsilon, u'_d) = \alpha [(1 - \varepsilon)(\varepsilon - \varepsilon_0)^\lambda]^\beta. \quad (9.12)$$

At incipient fluidization, $\varepsilon = \varepsilon_0$ and the volume fraction for bubbles ($\varepsilon - \varepsilon_0$) diminishes to zero, and so does the correction factor; at the particle terminal velocity, $\varepsilon = 1$, and the volume fraction of clusters ($1 - \varepsilon$) diminishes to zero, and so does the correction factor.

Relative to the bulged ε - u curves of Fig. 61, the empirical parameters in Eq. (9.12) possess the following physical significances:

- α , amplitude of maximum deviation;
- β , breadth of bulge;
- λ , location of maximum bulge.

Relations for the parameters can be formulated on the basis of the following three datum points, shown schematically in Fig. 61:

	u'_0	ε
Incipient fluidization	u'_f	ε_0
dense phase at u_i	1	ε_i
Maximum bulge	u'_{0m}	ε_m

Thus, the correction factor has been transformed to read

$$F(\varepsilon, u'_d) = \left[\frac{u'_{0m}}{\varepsilon^n} - \frac{u'_d}{\varepsilon_m^n} \left(\frac{\varepsilon_m}{1 - \varepsilon_m} \right) - 1 \right] \left[\left(\frac{1 - \varepsilon}{1 - \varepsilon_m} \right) \left(\frac{\varepsilon - \varepsilon_0}{\varepsilon_m - \varepsilon_0} \right)^\lambda \right]^\beta. \quad (9.12a)$$

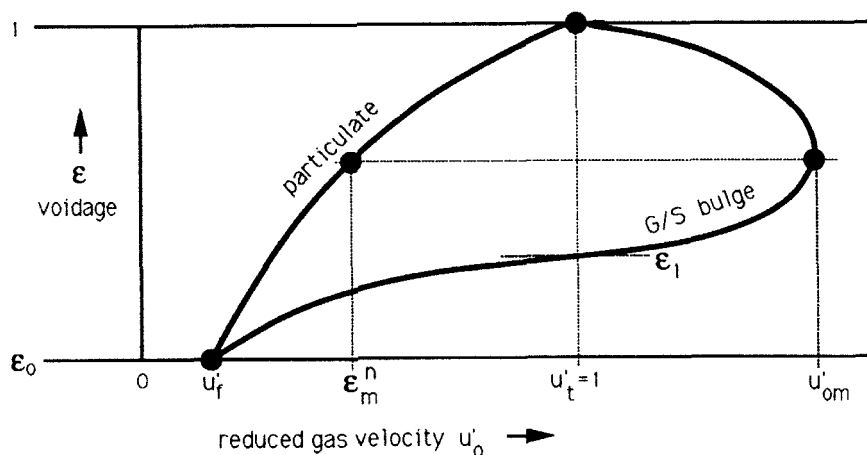


FIG. 61. Scheme for evaluating correction factor $F(\epsilon, u_d)$. [After Kwauk *et al.*, 1985.]

Rather complex forms have been derived analytically (Chen and Kwauk, 1985) to express β and λ in terms of the parameters at the three datum points noted above.

Equations (9.11) and (9.12a) have been tested against experimental data for both co-up and counter-down operations for three solids: FCC catalyst, alumina, and iron ore concentrate. These results are shown in Fig. 62. In this figure, the generalized fluidization charts on the right-hand side are compared with the corresponding bed collapsing curves of the solids (to be explained in Section X) on the left. The fluidizing behaviors of the three powders along the left-hand side are well reflected in the shapes of the families of $\epsilon-u$ curves for G/S generalized fluidization along the right-hand column. Both FCC catalyst and alumina, which are Geldart A, or "123" in nature, exhibit extended ranges for fast fluidization, while for iron ore concentrate, which is weakly Geldart B, or essentially "100," bubbling is followed fairly closely by pneumatic transport in the dilute phase, with a rather short intermediate range of fast fluidization.

X. Powder Classification

The efficiency of particle-fluid contacting in fluidization, popularly described in terms of the quality of fluidization, has its origin not only in the physical properties of the fluidizing medium and of the solid material of which the particles are composed, but also in the particle characteristics and in the group behavior of the particles while in motion. Particle characteristics include size, size distribution, shape, and surface roughness or texture, while

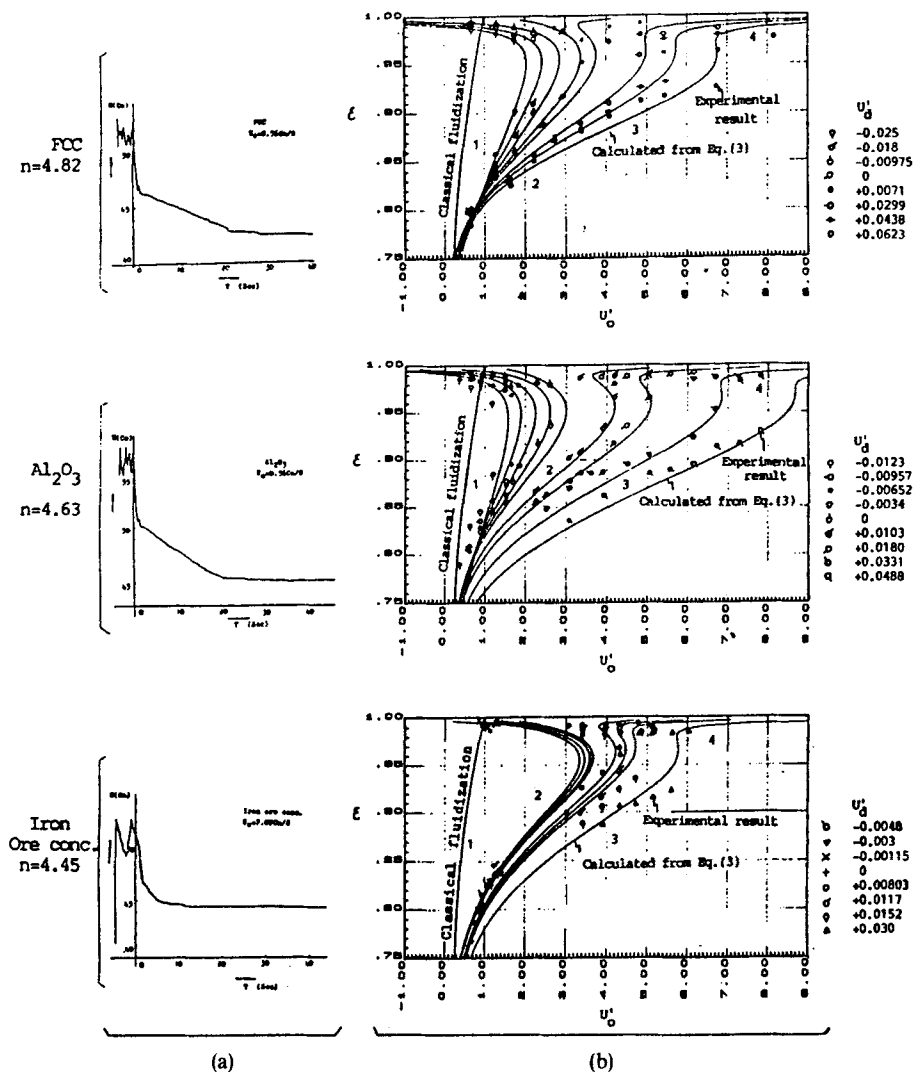


FIG. 62. Charting G/S generalized fluidization against experimental data. (a) Bed collapsing; (b) generalized fluidization. 1. bubbling region; 2. turbulent region; 3. fast fluidization region; 4. pneumatic transport region. [After Chen and Kwauk, 1985.]

particle group behavior refers to the interaction between a particle and its neighbors, as well as the movement of the particles as a group.

Early investigations were concerned mostly with physical properties, somewhat with particle characteristics, but little with particle group behavior. Even so, significant results were obtained—for instance, the distinction

between L/S fluidization and G/S fluidization, viz., "particulate" and "aggregative," and the provision of criteria for such a distinction (Wilhelm and Kwauk, 1948; Harrison *et al.*, 1961; Romero and Johanson, 1962), most of which were based on the Froude number. Other criteria were then proposed involving fluctuating parameters in fluidization (Rietema, 1967), for instance, pressure drop or voidage.

In all these correlations, however, parameters on particle characteristics and particle group behavior were hardly invoked. These investigations did lead, on the other hand, to the solutions of problems of considerable practical importance, such as the careful specification of particle-size distribution for artificially produced fluidizable materials, e.g., catalyst for fluid catalytic cracking, graphite particles for heat treatment of metallic parts in fluid beds (Chen and Song, 1980; Jin, 1980, 1984), etc. Perfection of these artifacts guarantees a small velocity range above incipient fluidization where bubbling is essentially suppressed, and, within this small velocity range, the G/S system can be made to behave comparably to its L/S counterpart.

It was thus gradually recognized that the distinction between particulate and aggregative fluidization had ignored the finer details in regard to the not-so-good particulate fluidization for L/S systems, e.g., large and/or heavy particles, such as lead in water, for which liquid cavities similar to bubbles in G/S systems were observed, on the one hand, and the smoother type of aggregative fluidization for G/S systems, e.g., light and/or fine, especially size-graded particles, which suppressed the formation of large bubbles, on the other. In other words, the particulate-aggregative transition should be viewed as continuous (Tung, 1981; Tung and Kwauk, 1982; Foscolo and Gibilaro, 1984; Geldart and Wong, 1985; Rowe, 1986), rather than abrupt. Fluidization quality in terms of material properties, particle characteristics, and particle group behavior thus needs to be assessed on three scales: the gross scale of the fluidized bed (macro scale), the aggregate scale of gas bubbles and particle clusters (meso scale), and the scale of the discrete, individual particles (micro scale).

According to such methodology, powders can be classified in relation to the regimes in which they tend to perform in the fluidized state, as was mentioned briefly in Section I and shown schematically in Fig. 3.

A. GELDART'S CLASSIFICATION

Geldart (1972, 1973) classified powders with respect to their fluidizing characteristics into four groups, as already mentioned in Section I.E, which are summarized in Table V in terms of typical particle size, particle characteristics, fluidizing behavior, and bubble characteristics.

TABLE V
GELDART'S CLASSIFICATION OF POWDERS

Group	Typical $d_p, \mu\text{m}$	Particle Characteristics	Fluidizing Behavior	Bubble Characteristics
C	20	fine cohesive interparticle forces e.g., flour	channel rather than fluidize pressure drop < particle weight fluidization improved by stirring vibration addition of submicrons anti-electrification	
A	30–100	fine aeratable e.g., cracking catalyst	appreciable range between u_{mf} and u_{mb} , viz., $u_{mb}/u_{mf} > 1$ fluidize nicely	
B	100–800	intermediate size e.g., sand	bubble at incipient fluidization viz., $u_{mb}/u_{mf} = 1$ collapse immediately upon shutoff of gas flow	bubbles have clouds “fast bubbles”
D	1,000	coarse e.g., wheat	can be spouted mix poorly when fluidized appreciable particle attrition rapid elutriation of fines relatively sticky materials can be fluidized	bubbles cloudless “slow bubbles” bubble velocity less than interstitial gas velocity

Geldart found that the above classification could be charted quantitatively by two variables: the effective density of the particles ($\rho_s - \rho_f$), and their average surface–volume diameter d_{sv} , as shown in Fig. 63a. In Geldart's original chart for air, the boundary between Groups A and C is empirically determined and consists of a rather diffuse belt. The boundary between A and B is defined by the relation

$$(\rho_s - \rho_f)d_p = 0.225.$$

The boundary between Groups B and D is

$$(\rho_s - \rho_f)d_p^2 = 1.$$

Grace (1986) improved Geldart's original diagram by incorporating data for gases other than air and for operations at pressures higher than atmospheric. The group boundaries proposed by Grace are based on the

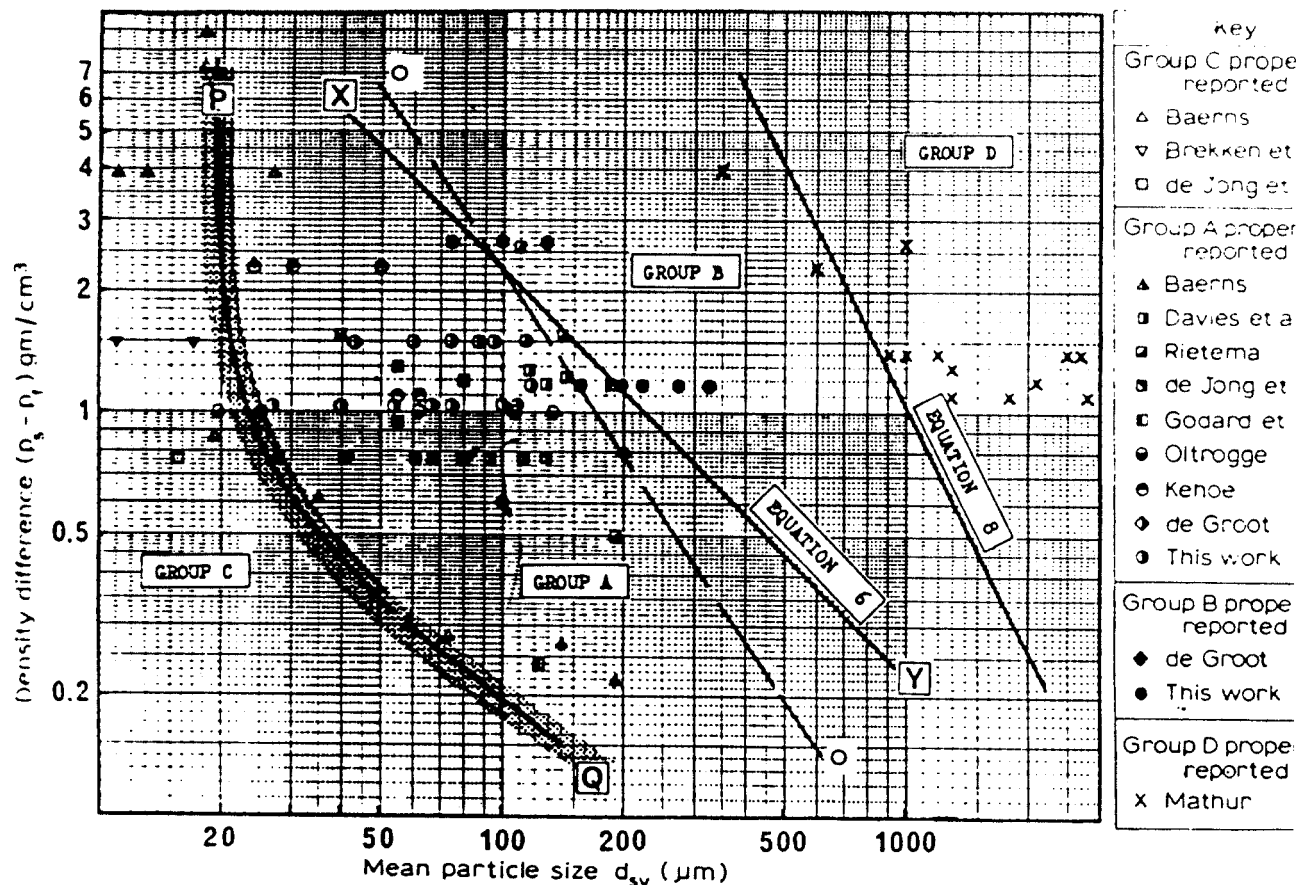


FIG. 63. Geldart's powder classification chart. (a) Geldart's original diagram for air; (b) Grace's improvement on Geldart's diagram, 1986.

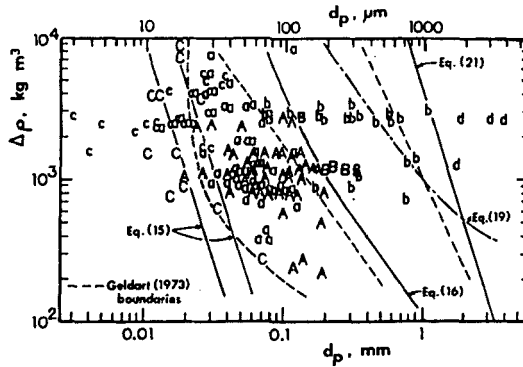


FIG. 63b. (Continued)

Archimedes number, as shown in Fig. 63b:

$$\text{boundary C/A} \quad \text{Ar} = 0.31-1.3$$

$$\text{A/B} \quad \text{Ar} = 1.03 \times 10^6 (\Delta\rho/\rho_f)^{-1.275}$$

$$\text{B/D} \quad \text{Ar} = 1.45 \times 10^6$$

B. POWDER CLASSIFICATION BY BED COLLAPSING

The spectrum of states of transition between particulate and aggregative fluidization calls on the one hand for devising experimental techniques for recording the related phenomenological manifestations, and on the other for developing analytical procedures for quantifying these experimental findings in relation to the properties, characteristics and group behavior of the powders.

Broadly speaking, for G/S systems, three modes of particle-fluid contacting may be recognized to take place simultaneously, as shown in Fig. 64: bubbles containing sparsely disseminated particles, emulsion of densely suspended particles, and defluidized (transient as well as persistent) particles not fully suspended hydrodynamically by the flowing gas. When the gas fluidizing a powder, exhibiting all these modes of contacting, is turned off abruptly, the fluidized bed will collapse and subside in three consecutive stages:

- (1) a rapid initial stage for bubble escape;
- (2) an intermediate stage of hindered sedimentation with constant velocity of the dense emulsion of mobile particles; and
- (3) a final decelerating stage of solids consolidation for the incompletely suspended particles.

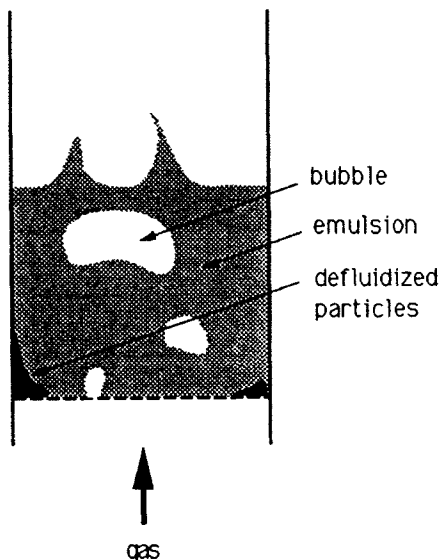


FIG. 64. The three modes of particle-fluid contacting in G/S fluidization.

Thus, the random, spatial distribution of the three modes of particle-fluid contacting is transformed into the ordered, temporal sequence of the three stages of the sedigraph. The bed collapsing method has been used, too, for other objectives in studies on fluidization (Rietema, 1967; Morooka *et al.*, 1973).

C. MODELING THE THREE-STAGE BED COLLAPSING PROGRESS

Figure 65 shows the variation of the solids bed surface with time for the three-stage bed collapsing process. In this figure, (i) shows bubbles dispersed throughout the bed at $t < 0$. After the fluid is shut off, the bubbles ascend through the bed, until at $t = t_b$, a bubble-free dense phase B remains, as shown in (ii) and (iii). The initial stage of rapid bed collapse resulting from the depletion of bubbles is called the *bubble escape* stage. Thereafter, the dense phase B collapses slowly at a constant rate. While layer B descends, the particles near the bottom of the bed begin to pile up, building up the accumulated layer D. This second stage will be called *hindered sedimentation*. The voidage throughout layer B remains constant during this stage, and at $t = t_c$, shown as (v), layer B has just disappeared, all solids now being in layer D. The time that marks the end of this second stage will be denoted as

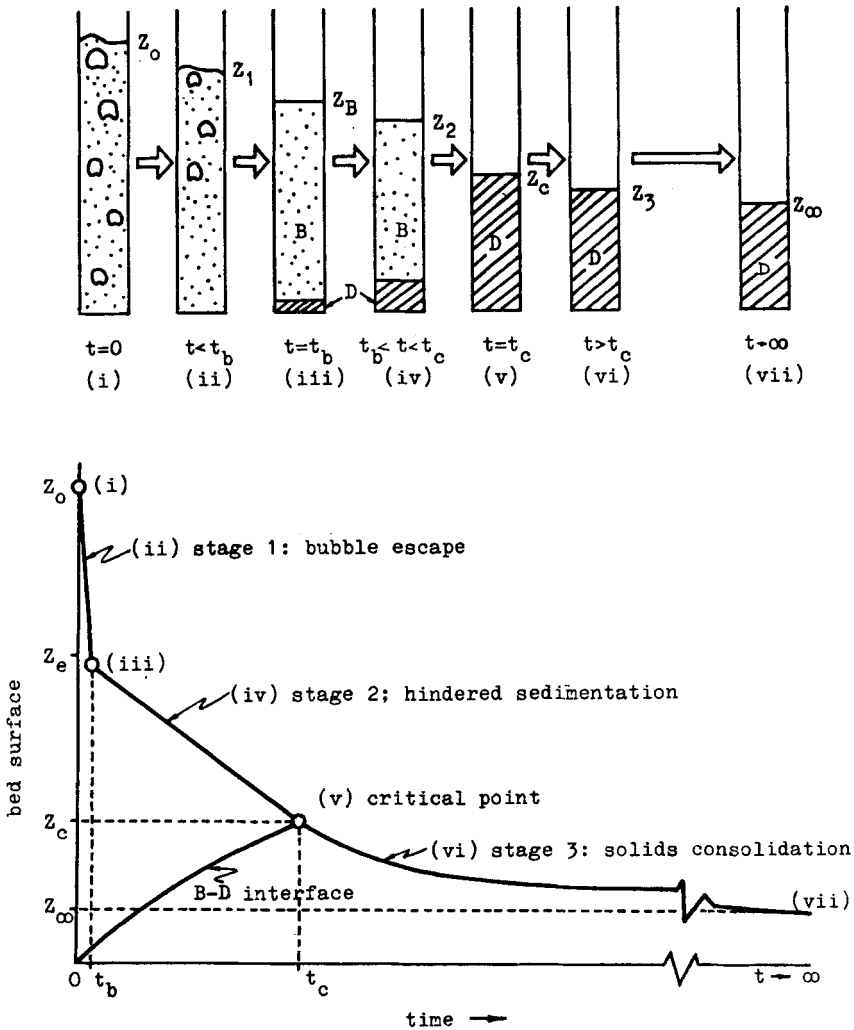


FIG. 65. Modeling the three-stage bed-collapsing process. [After Yang *et al.*, 1985.]

the critical time t_c , and the corresponding voidage, the critical voidage ε_c . Layer D possesses a loose structure, with fluid in the interstitial spaces being slowly expelled by virtue of the weight of the accumulated solids. The rate of solids settling decreases with time, until at $t = \infty$, the ultimate bed height Z_∞ is reached, as shown in (vii). The third stage is called *solids consolidation*.

Results of mathematical modeling of the bed collapsing process follow.

In the bubble escape stage, $0 < t < t_b$, the change of the bed surface is linear with time:

$$Z_1 = Z_0 - u_1 t, \quad (10.1)$$

where

$$u_1 = \frac{f_B(1 + f_w \varepsilon_e)u_B + \varepsilon_e(1 - f_B - f_w f_B)u_e}{(1 - f_B)(1 - \varepsilon_e)}, \quad (10.2)$$

$$f_B = \frac{Z_0 - Z_e}{Z_0}. \quad (10.3)$$

In the hindered sedimentation stage, $t_b < t < t_c$, while layer B settles with a constant velocity,

$$u_2 = dZ_2/dt, \quad (10.4)$$

layer D acquires solids from layer B, and consolidation in layer D is a first-order process with respect to the amount of solids present (Roberts, 1949):

$$-\frac{dZ}{dt} = K(Z_D - Z_\infty), \quad (10.5)$$

where K is a rate constant.

The surfaces of layer B and layer D are, respectively,

$$Z_2 = Z_B = Z_e - u_2 t \quad (10.6)$$

$$Z_D = \left(\frac{Z_\infty}{Z_e - Z_\infty} \right) u_2 t + \left\{ 1 - \exp \left[-K \left(\frac{Z_e - Z_\infty}{Z_e} \right) t \right] \right\} \frac{u_2 Z_e}{(Z_e - Z_\infty) K} \\ \times \left[\frac{1 - \varepsilon_e}{\varepsilon_e - E_0} - \frac{Z_e}{Z_e - Z_\infty} \right]. \quad (10.7)$$

In the solids consolidation stage, $t_c < t < \infty$, according to Eq. (10.5), the rate of descent of the bed surface for layer D is

$$\frac{dZ_3}{dt} = \frac{dZ_D}{dt} = -K(Z_D - Z_\infty), \quad (10.8)$$

which integrates to

$$Z_3 = Z_D = (Z_c - Z_\infty) \exp[-K(t - t_c)] + Z_\infty. \quad (10.9)$$

D. INSTRUMENT FOR AUTOMATIC SURFACE TRACKING AND DATA PROCESSING

Figure 66 shows the instrument (Qin and Liu, 1985) used for automatic tracking of the surface of the collapsing bed, inclusive of a computer for data acquisition and on-line analysis. The fluidized bed is 5 cm in diameter

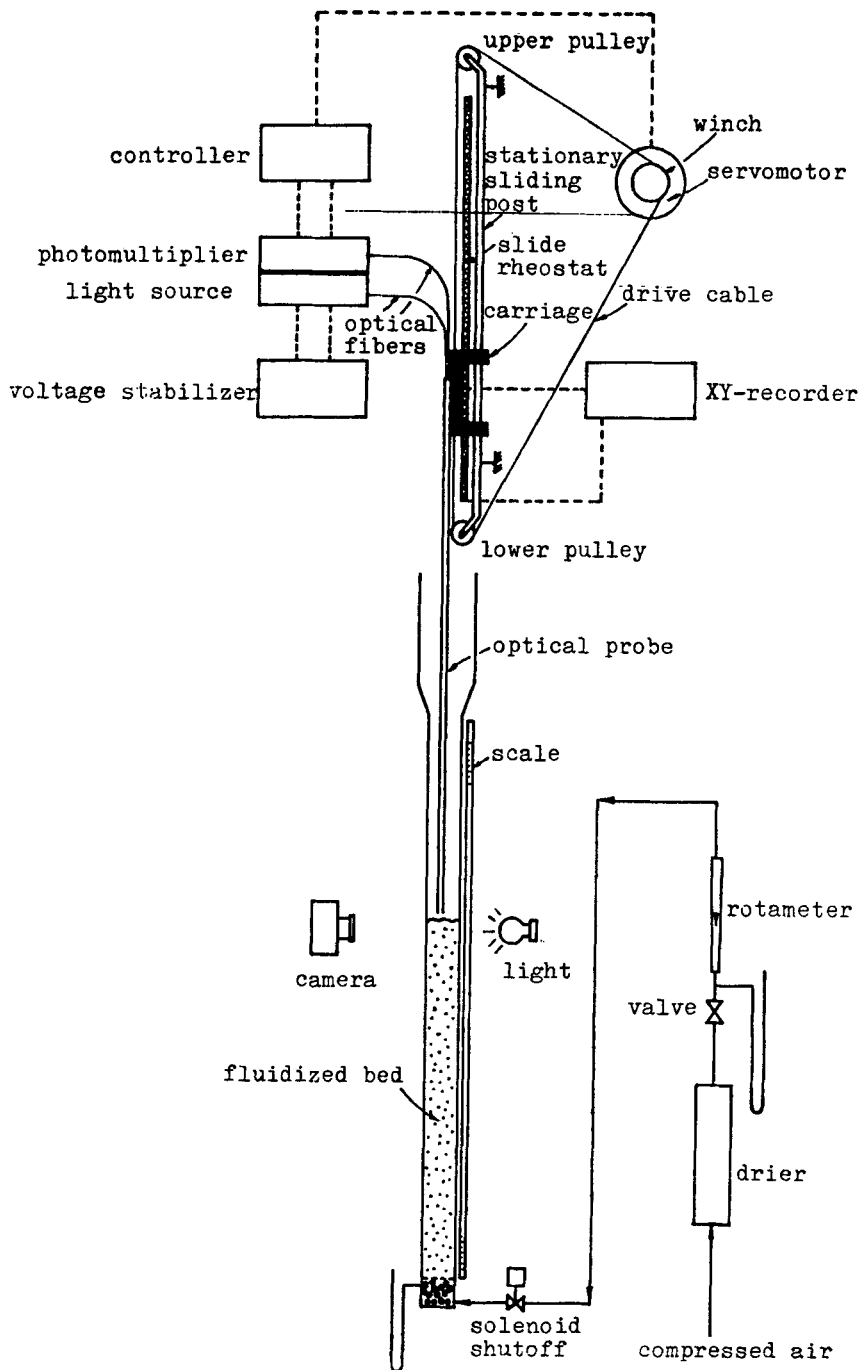


FIG. 66. Instrument for automatic surface tracking and data processing. [After Yang *et al.*, 1985.]

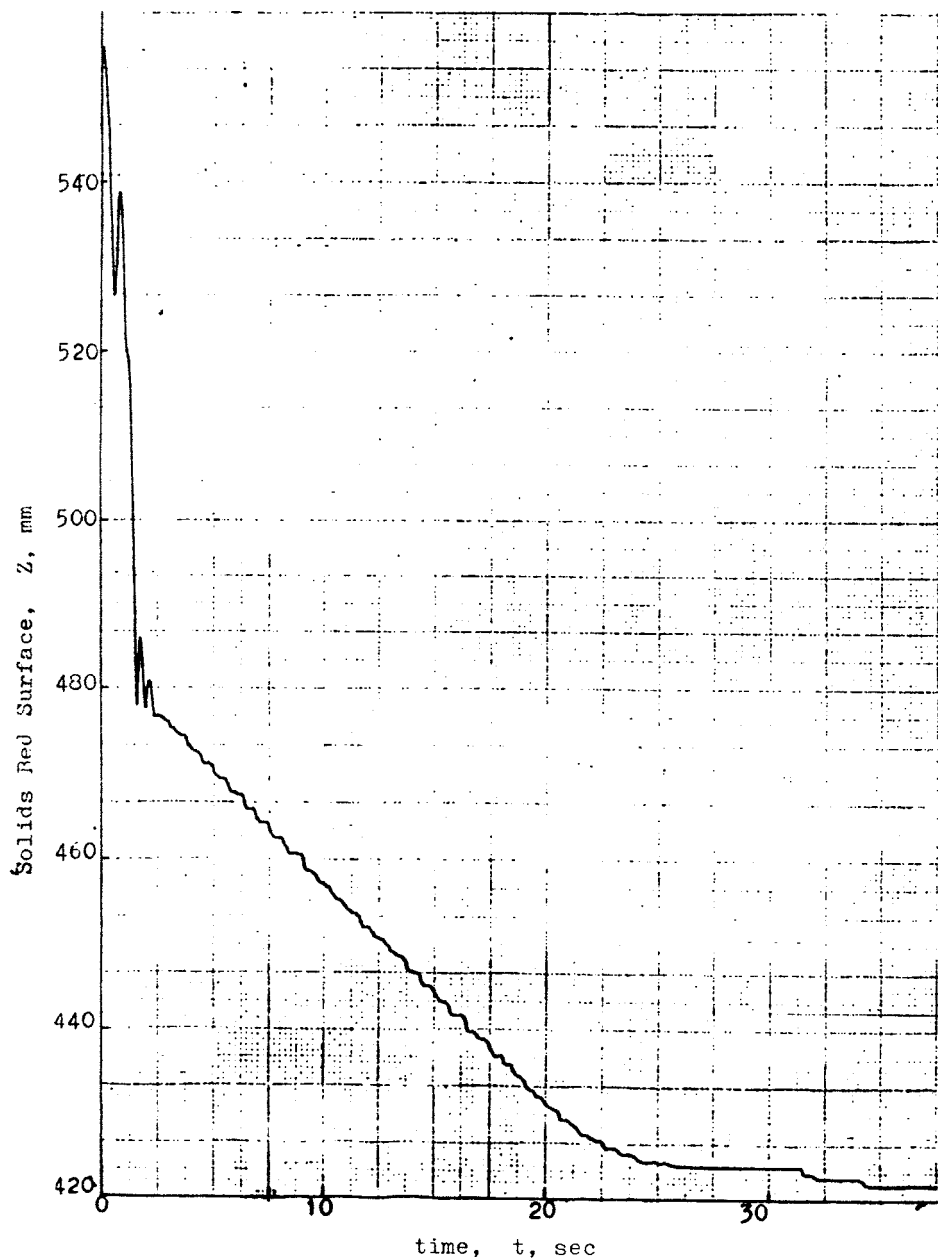


FIG. 67. Typical bed-collapsing curve traced by optical-fiber probe tracking instrument (solids A66, alumina, 140–280 microns). [After Yang *et al.*, 1985.]

and 120 cm high, provided with a high-pressure-drop gas distributor to insure uniform gas flow. Below the distributor is a specially designed knife valve operated by a solenoid for quick gas shutoff.

An optic-fiber probe, consisting of two separate sets of projector and receiver fibers, is used for rapid tracking and recording of the subsiding bed surface.

Figure 67 shows a typical bed collapsing curve traced by the instrument described above.

The entire determination, from gas shutoff to printout from the computer, rarely exceeds 3 to 4 minutes for normal solids. And since all measurements are taken by the instrument, they are not subject to personal error of observation. The size of a solids test sample is of the order of a kilogram or less.

E. QUALITATIVE DESIGNATION FOR BED COLLAPSING

Not all powders exhibit all the three stages described in Section X.C for the bed collapsing process. For G/S systems, the full three-stage curves obtain only for Geldart Group A powders and their like, as shown in Fig. 68. For Geldart Group B and D powders, which fluidize aggregatively at all gas velocities above incipient fluidization, the bed collapsing curve consists only of the first stage, showing that the solids reach their final static bed height as soon as the bubbles are expelled. For L/S systems, on the other hand, the first stage is generally absent. For Geldart B and D powders, neither does the third stage appear.

These powders can be classified qualitatively by assigning appropriate three-digit designations, or descriptors, in accordance with the presence or absence of particular stages in the bed collapsing test, as shown in Table VI.

F. QUANTIFYING FLUIDIZING CHARACTERISTICS OF POWDERS

The three-digit designation affords a convenient descriptive classification of powders in terms of their bed collapsing behavior, but an additional criterion is desirable to show the entire spectrum of continuous transition of fluidized states from particulate to aggregative.

Examination of the multitude of bed-collapsing curves obtained experimentally led to the recognition of the significance of a number of variables, viz., the difference between the height of the dense phase and the bed height at the critical point ($Z_c - Z_c$), which defines the extent of particulate contraction after bubbles have escaped; the rate of hindered sedimentation u_2 ; and certain physical properties of the solids and the fluid involved. These factors are

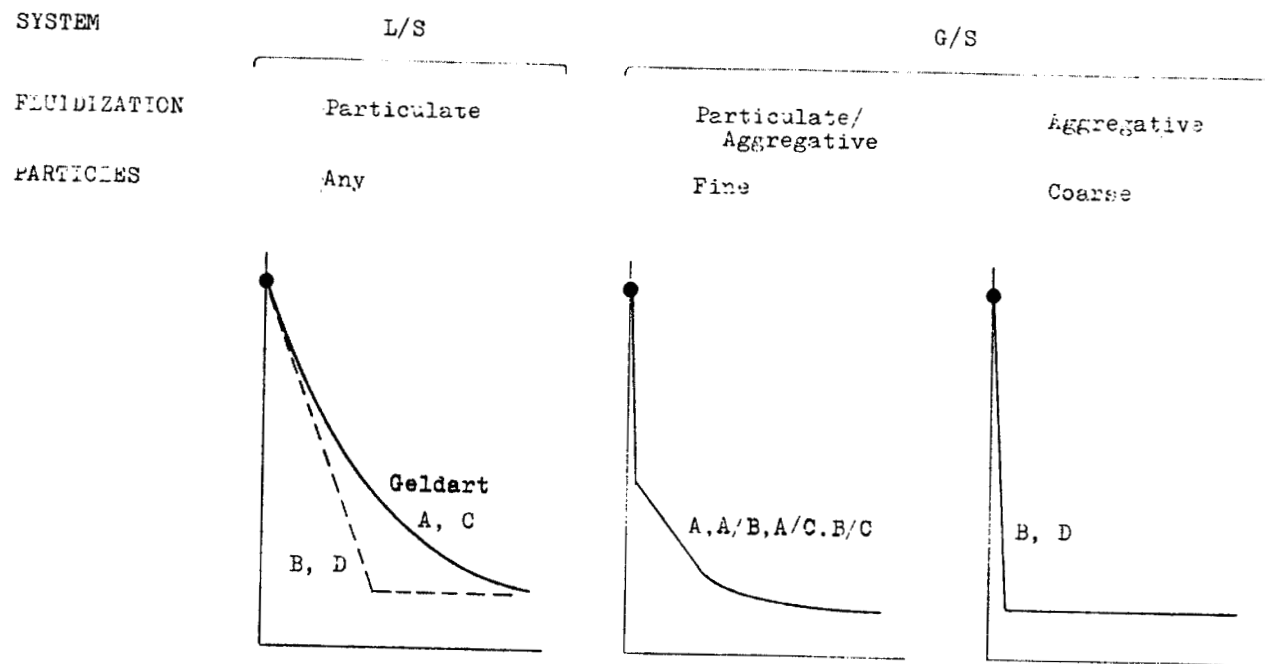


FIG. 68. Essential types of bed-collapse curves.

TABLE VI
THREE-DIGIT DESIGNATION OF BED COLLAPSING CURVES

System		G/S				L/S		
Geldart's group		D, B	B/A	A	C	D	B	A, C
ICM designation		100	120	123	123	120	020	023
		rare				ideal		
Stage in bed collapse	1. Bubble escape	x	x	x	x	x		
	2. Hindered sedimentation		x	x	x	x	x	x
	3. Solids consolidation			x	x			x
Fluidization characteristics	Particulate			x	x	x	x	x
	Bubbling	x		x	x			
	Channeling				x			x
Value of Θ	High						x	x
	Medium			x	x			
	Low		x		x			
	Near zero	x	x					

organized into a dimensionless number

$$\Theta = \frac{d_p g}{u_t u_2} \left(\frac{Z_c - Z_c}{Z_\infty} \right). \quad (10.10)$$

This dimensionless number, designated as the dimensionless subsidence time of a power, portrays its dynamic behavior in relation to the overall bed collapsing process, inclusive of the significant variables Z_∞ and t_c .

To test the viability of Θ in quantifying fluidizing characteristics, it is plotted against the ratio of incipient bubbling velocity to incipient fluidization velocity, u_{mb}/u_{mf} , the latter being calculated after Geldart. Figure 69 shows that a linear relation exists between $\ln(u_{mb}/u_{mf})$ and $\Theta^{1/4}$, as represented by the empirical relation

$$\ln(u_{mb}/u_{mf}) = 4\Theta^{1/4}. \quad (10.11)$$

The straight line starts from $\Theta = 0$ and $u_{mb}/u_{mf} = 1$ and extends without limit towards the upper right-hand corner. The value of $u_{mb}/u_{mf} = 1$ obviously signifies aggregative fluidization. The corresponding value of Θ is zero, that is, t_c approaches zero, indicating that stages 1 and 2 of the bed collapsing process take place almost instantaneously. As the fluidizing characteristics improve, the value of u_{mb}/u_{mf} becomes progressively greater than unity, signifying particulate expansion. The corresponding value of Θ also increases, showing a slower bed-collapsing process accompanied by a large value for t_c . As the

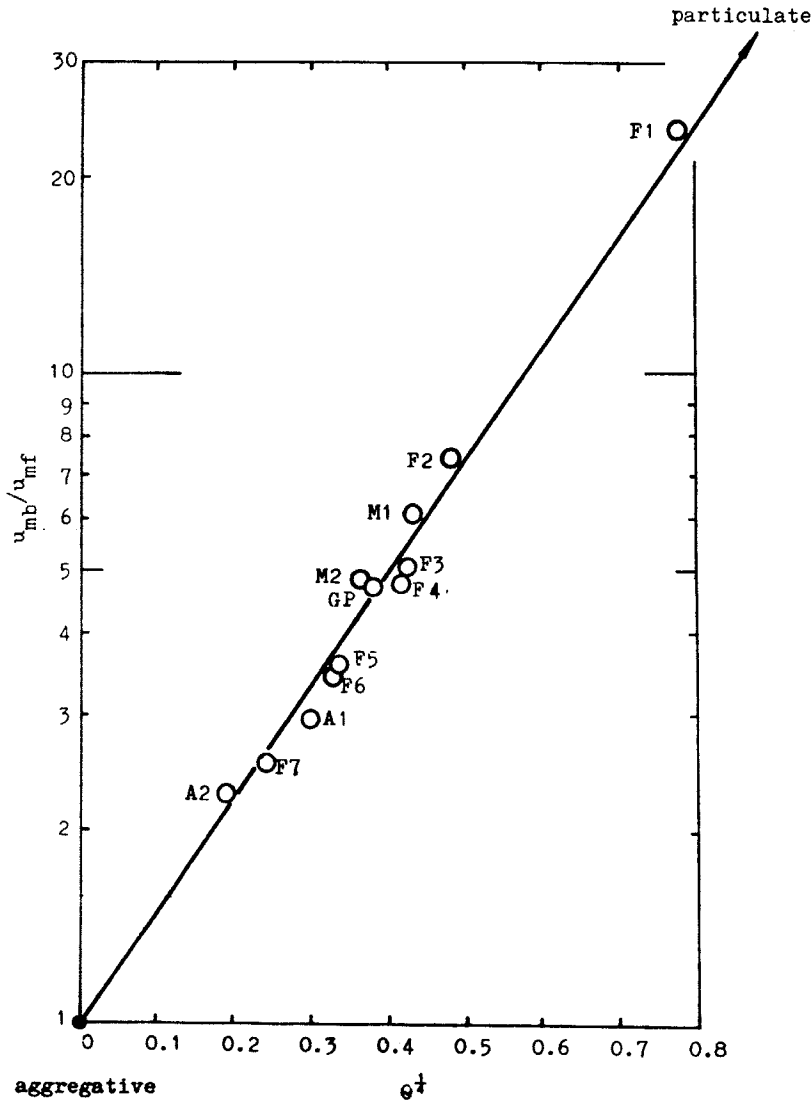


FIG. 69. Plot: u_{mb}/u_{mf} vs. $\theta^{1/4}$ [After Yang *et al.*, 1885.]

curve tends toward even larger values of Θ , the characteristics of particulate fluidization become more predominant.

G. IMPROVING FLUIDIZATION BY PARTICLE-SIZE ADJUSTMENT

It was mentioned earlier in the chapter that catalyst powders with carefully specified particle-size distribution have been prepared to insure good fluidization characteristics. It is well known that even addition of fine particles to a powder of coarser particles tends to improve its fluidization characteristics. Experiments were thus conducted on binary particle mixtures, each consisting of a fairly close particle size distribution (Yang, Z., 1982).

Figure 70 shows a set of bed-collapsing curves for a Geldart Group A–A binary solids mixture, two closely sized alumina powders of average particle diameters 104 and 66 microns, respectively. The curve on the extreme left with 0% fines represents the pure coarse component, which is barely Group A in fluidizing characteristics, as can be seen from its very brief stage 2. The curve on the extreme right, representing the 100% fine component, demonstrates pronounced Group A, or “123,” fluidizing characteristics with a long stage 2. Curves with intermediate compositions are shown in their ordered locations between the purely coarse and purely fine components.

Figure 71 illustrates the fluidizing characteristics of a set of Group B–A mixtures of relatively coarse (212 microns) polyethylene spheres mixed with a relatively fine (27 microns) FCC catalyst. The pure polyethylene spheres, shown as the 0% curve, demonstrates the “100” fluidizing characteristics typical of a Group B powder. As the fine FCC catalyst is added, there is a progressive predominance of the Group A fluidizing characteristics of the finer component.

Figure 72 shows the effect of adding talc (7 microns), Group C, to a coarse sea sand (165 microns), Group B. The beneficial effect of the fines on the fluidizing characteristics is shown to increase to a fines composition of around 25%, and then it diminishes with further fines addition.

Figure 73 plots the dimensionless subsidence time Θ for the six sets of Group A–A and Group B–A binary mixtures for different compositions x_f , showing that the improvement of fluidizing characteristics by addition of fine particles increases monotonically with increasing percentage of the fines.

Figure 74 is a similar plot, but for the 10 sets of Group B–C mixtures. Most curves show that the values of Θ for Group B–C binaries give maxima at certain intermediate compositions. The presence of these maxima suggests that not only may fine particles belonging to Group C improve the fluidizing characteristics of such coarse solids as Group B, but the coarse particles may

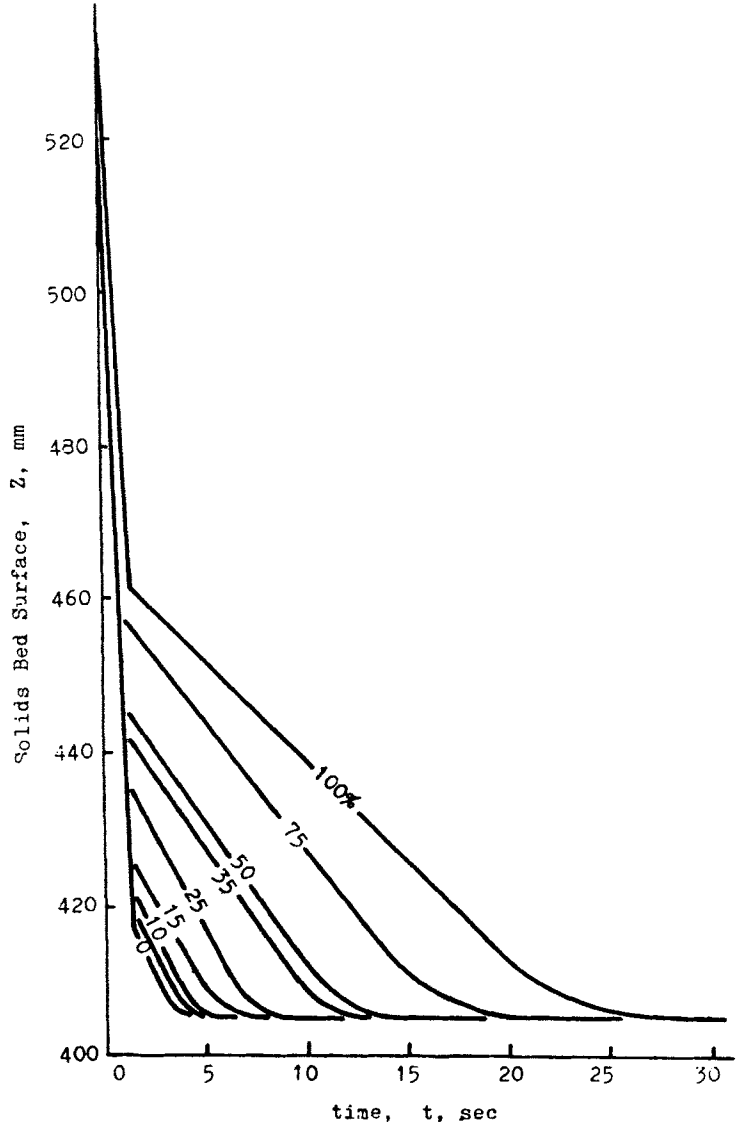


FIG. 70. Bed-collapse curves for a group A-A solid pair: solids A104/A66. [After Yang *et al.*, 1985.]

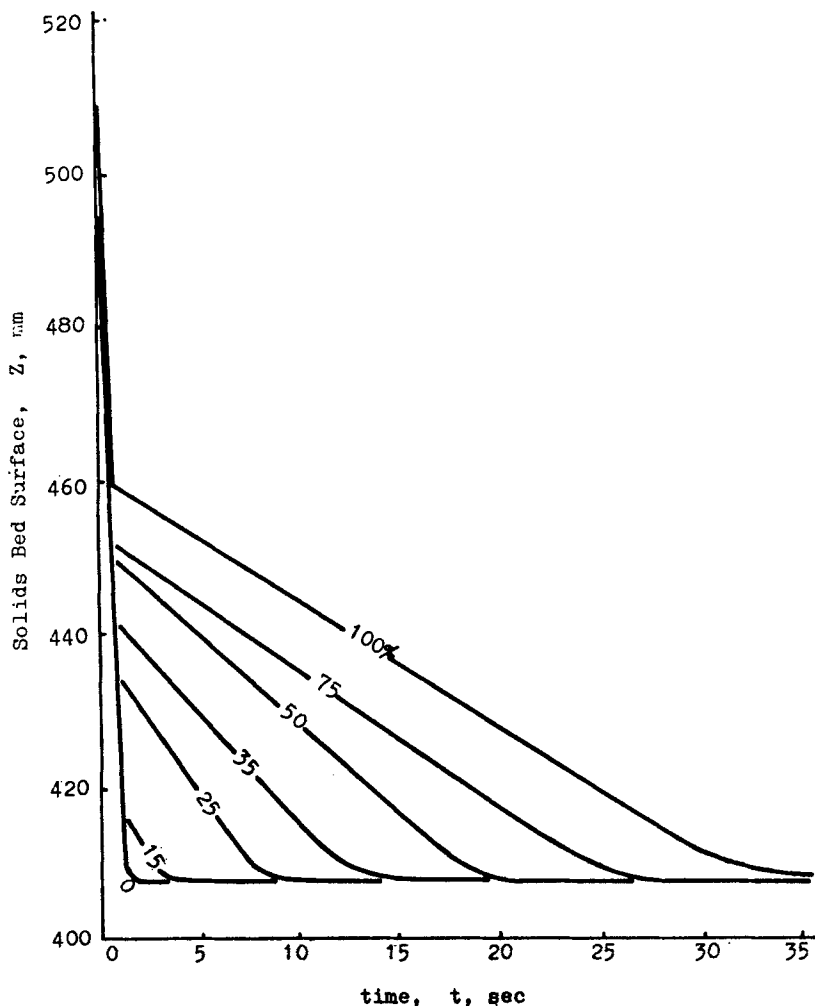


FIG. 71. Bed-collapse curves for a group B-A solid pair, solids PE212/F27. [After Yang *et al.*, 1985.]

also improve the fluidizing characteristics of the fine particles, which possess a notorious tendency towards channelling before fluidization sets in.

This synergism (Yang, Z., 1982; Kwauk, 1984, 1986) of Group B-C mixtures testifies to the significance of particle-size selection and particle-size distribution design, in order to tailor a solid particulate material to certain desired fluidizing characteristics.

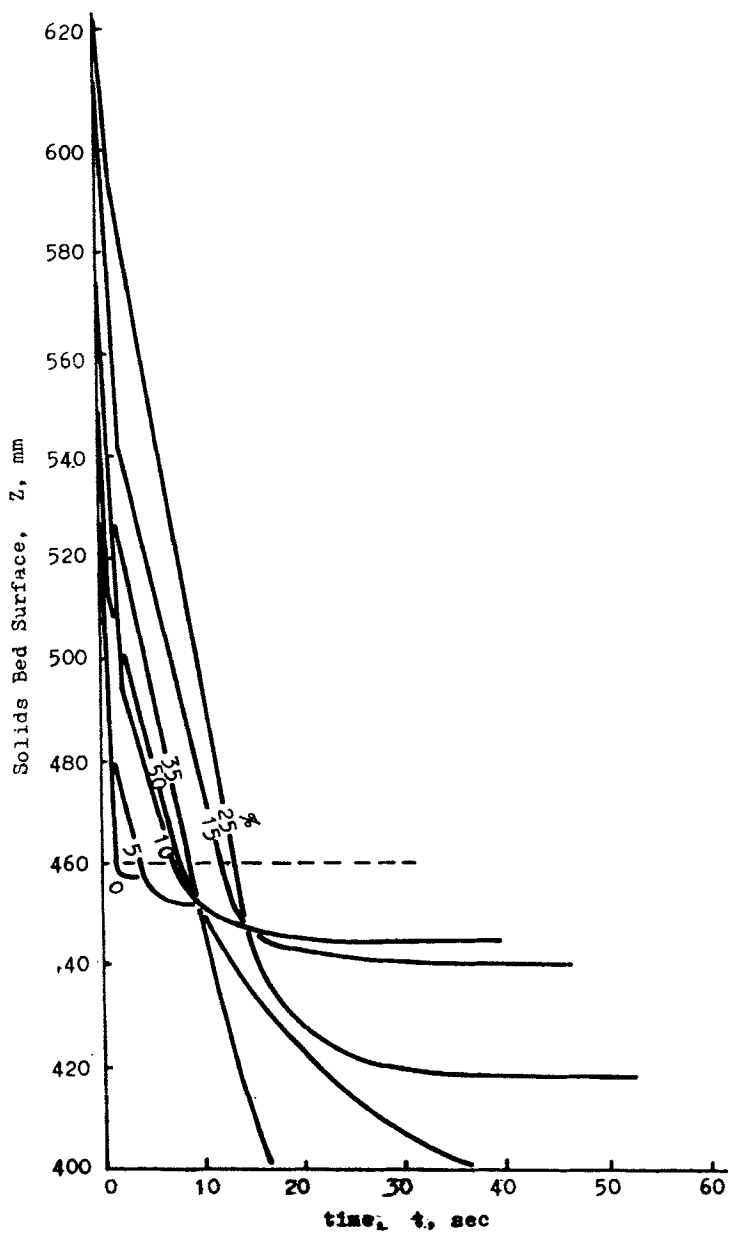


FIG. 72. Bed-collapse curves for a group B-C solid pair: solids SA165/T7. [After Yang *et al.*, 1985.]

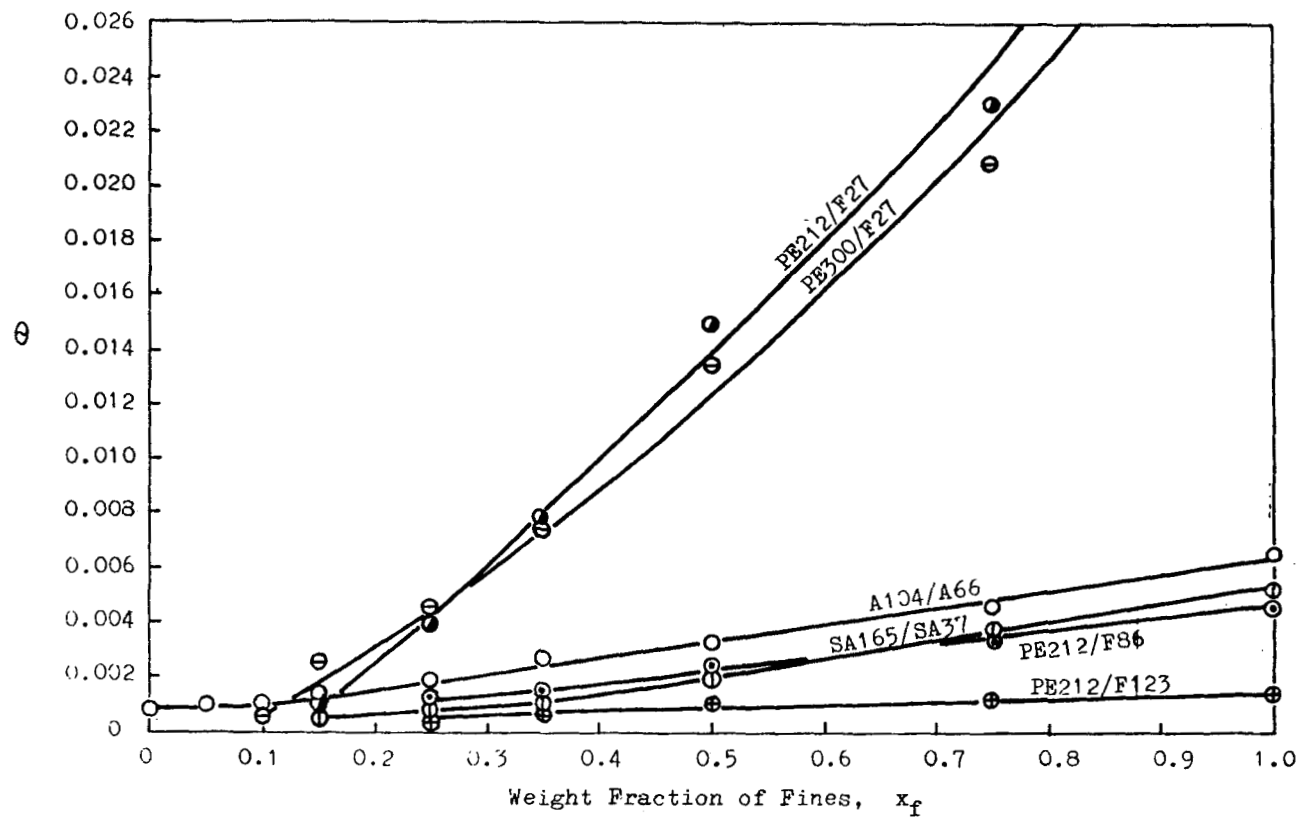


FIG. 73. Improving fluidizing characteristics by fines addition, solid groups A-A and B-A. [After Yang *et al.*, 1985.]

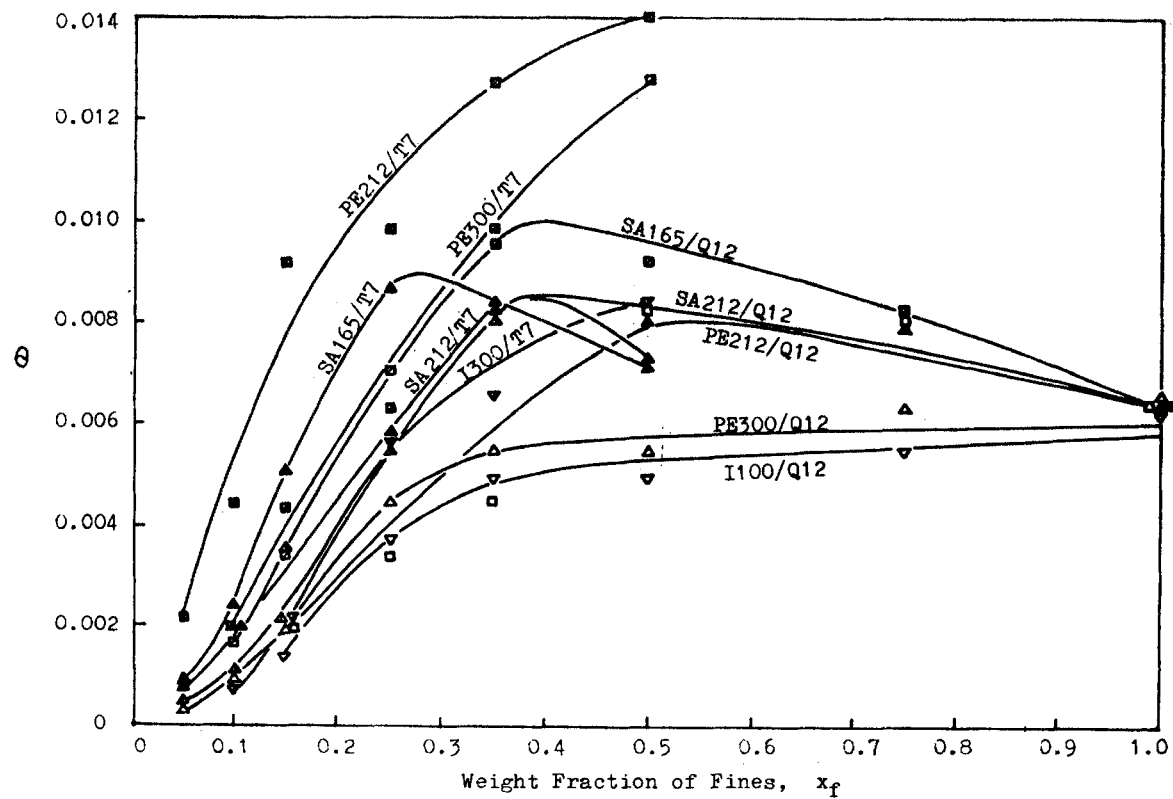


FIG. 74. Improving fluidizing characteristics by fines addition, solid group B-C. [After Yang *et al.*, 1985.]

H. FLUIDIZING QUALITY AND PARTICLE-PARTICLE INTERACTION

In order to understand the two types of results in Group A-A and B-A binaries on the one hand, and Group B-C binaries on the other, these binaries were first examined, on micro-meso scales, under a scanning electron microscope, and then were followed by a TV camera through a microscope when they were fluidized (Xia and Kwauk, 1985). It was seen that for all Group A-B combinations, the particles behave independently of one another, whereas whenever a Group C powder was added, the C particles were noticed to adhere to the surface of the coarse particles. Additional experiments were carried out to observe the process of fines deposition when a Group C powder was entrained by a flowing gas stream past a sessile Group B particle (see Fig. 75). Fines deposition starts from the polar regions, north and south, with a denuded equatorial belt that first diminishes with increased fines deposition as increased gas velocity carries more fines towards the sessile coarse particle. With a further increase in gas velocity, however, the denuded equatorial belt widens as increased drag carries away the deposits from the surface of the coarse particle. The receding deposit first disappears at the south pole, and a final cap is left at the north pole at the highest gas velocity used.

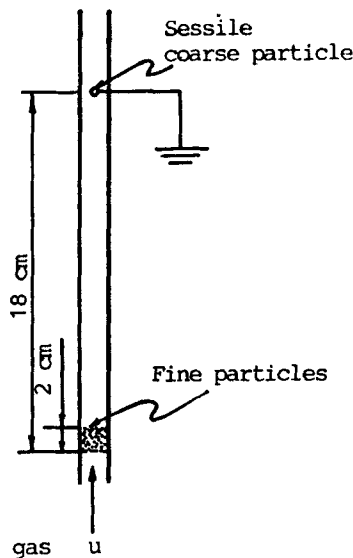
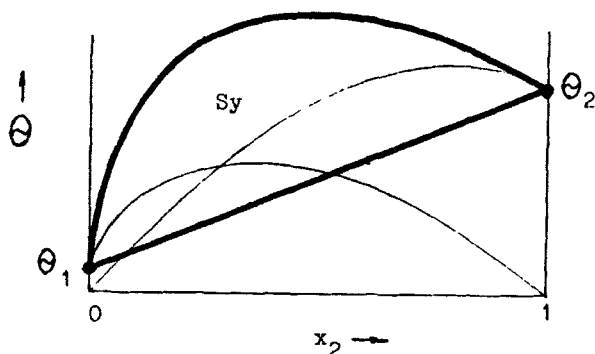


FIG. 75. Experimental setup for deposition of fine particles on a sessile coarse particle. [After Xia and Kwauk, 1985.]

SYNERGISM

$$\Theta = \underbrace{\Theta_1 (1 - x_2)}_{\text{contribution of coarse}} \underbrace{(1 + x_2)^{n_1}}_{\text{interaction of fine}} + \underbrace{\Theta_2 x_2}_{\text{contribution of fine}} \underbrace{(1 + (1 - x_2))^{n_2}}_{\text{interaction of coarse}}$$

$$\begin{aligned} \text{Sy} &= \left[\int_0^1 \Theta \, dx_2 - \frac{1}{2} (\Theta_1 + \Theta_2) \right] / (\Theta_1 + \Theta_2) \\ &= \Theta_1' \left[\frac{2^{n_1+2} - n_1 - 3}{(n_1 + 2)(n_1 + 1)} \right] + \Theta_2' \left[\frac{2^{n_2+2} - n_2 - 3}{(n_2 + 2)(n_2 + 1)} \right] - \frac{1}{2} \\ \Theta_1' &= \Theta_1 / (\Theta_1 + \Theta_2) ; \quad \Theta_2' = \Theta_2 / (\Theta_1 + \Theta_2) \end{aligned}$$

FIG. 76. Measure of synergism for binary particle mixtures. [After Kwauk, 1984, 1986.]

Regardless of the nature of the adhesive force (Krupp, 1967; Ranada, 1986) holding the fines onto the surface of the coarse particle, an analysis of force balance on the fine particle between adhesion, hydrodynamic drag, and gravity (Kwauk, 1984, 1986; Xia and Kwauk, 1985) lent support to the phenomena enumerated above on the varying degree of surface coverage of the coarse particle by the fine particles.

I. MEASURE OF SYNERGISM FOR A BINARY PARTICLE MIXTURE

A mathematical model has been proposed to account for the mutual synergistic action of either particle component on the other in increasing the value of the dimensionless time Θ as shown in Fig. 74, resulting in an overall dimensionless time Θ for the binary system consisting of the algebraic sum of the contributions from the component particles:

$$\Theta = \Theta_1(1 - x_2)(1 + x_2^{n_1}) + \Theta_2 x_2[1 + (1 - x_2)^{n_2}]. \quad (10.12)$$

Mutual synergism of binary mixtures containing fine particles can be quantified in terms of the departure of the Θ - x_2 curve from a linear tie line, which signifies absence of synergism, joining Θ_1 and Θ_2 , as shown in Fig. 76. A convenient measure of this departure is the shaded area lying between the Θ - x_2 curve and the linear tie line. This can be derived analytically from Eq. (10.12) in terms of what will be called the synergism number Sy , normalized with respect to $\Theta_1 + \Theta_2$ of both the coarse and the fine particles:

$$\begin{aligned} Sy &= \frac{1}{\Theta_1 + \Theta_2} \left[\int_0^1 \Theta dx - \frac{1}{2}(\Theta_1 + \Theta_2) \right] \\ &= \frac{1}{(n_1 + 1)(n_1 + 2)} + \frac{\Theta_2/\Theta_1}{(n_2 + 1)(n_2 + 2)}. \end{aligned} \quad (10.13)$$

The larger the value of Sy , the stronger the mutual synergistic interaction between the coarse and fine particles. Also, an effective fine particle additive to improve the fluidizing characteristics of coarse particles calls for a large value of Θ_m produced with minimal amount of the fine material, that is, a small value of x_2 .

Figure 77 shows more computer-generated curves (Qian and Kwauk, 1986) showing synergism for different binary particle mixtures.

XI. Future Prospects

Idealization of particulate fluidization provides the essential concept towards a basic understanding of fluid-particle systems in terms of the most significant factors, L/S in particular and G/S after appropriate corrections. The nature of fluid-particle motion cannot be properly understood, e.g., the preferential arrays of particles, L/S versus G/S , without supplementary studies of the basic mechanisms. Of immediate interest from a practical point of view is how to adapt the relatively simple relations derived for ideal fluidization to G/S systems, as already exemplified for fast fluidization. For polydisperse systems, the problem was oversimplified to the binary case, and

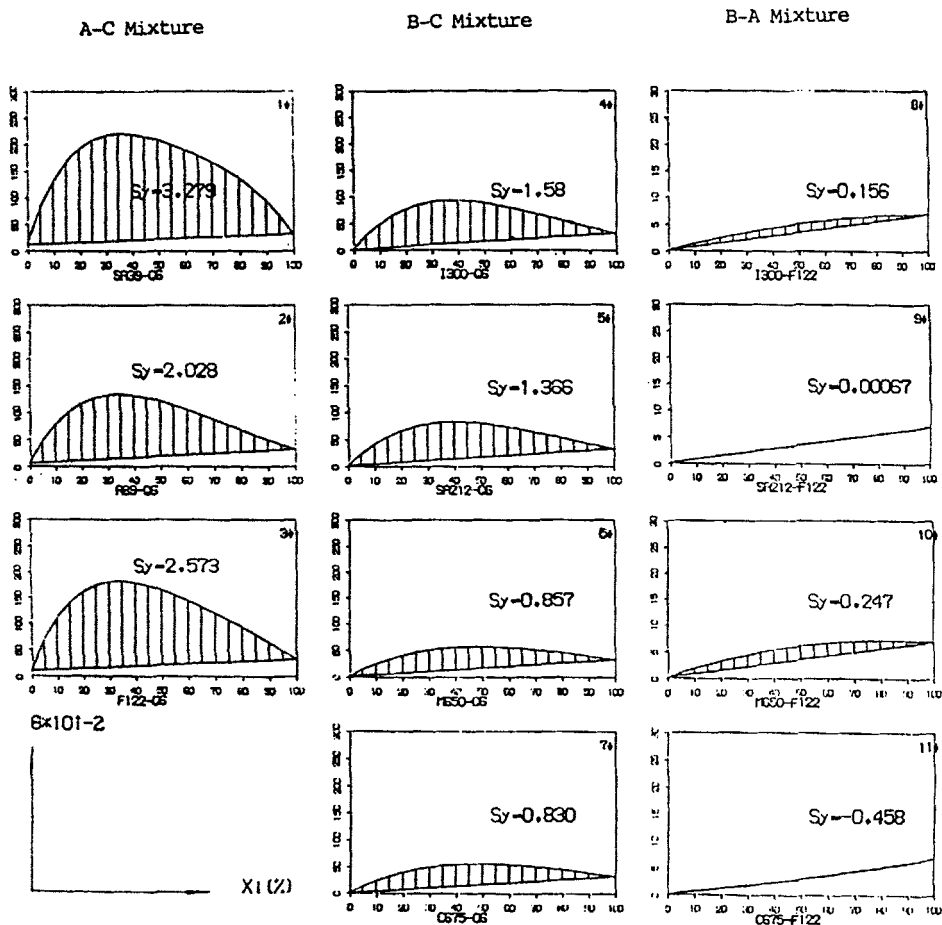


FIG. 77. Computer-generated curves showing synergism for different binary particle mixtures. [After Qian and Kwauk, 1986.]

for particle sizes exceeding two, the summation method needs revision to reflect more sophisticated expressions for size distribution. Liquid/solid systems, to which the idealized relations generally find direct application, often need intensification with respect to increased mass-transport rate across the fluid-particle boundary, and suppression of backmixing through the design of new internals or better vessel configuration including staging, especially where small and/or light particles are involved. Forces other than drag may even be invoked, e.g., magnetic forces, in order to improve contacting efficiency.

Certain existing L/S process operate, or could operate, more efficiently in the fluidized state, for which basic information can be derived from the correlations derived for ideal fluidization:

- hydraulic classification of particles differing in size or density (Anon., 1965; Ullmann, 1972; Kwauk, 1979a);
- mixing of particles differing in size or density;
- leaching and washing (Kwauk, 1979a; Kwauk and Wang, 1981);
- continuous ion-exchange or adsorption processes involving solids recycling (Higgins, 1969; Stevens, 1970; Bennett *et al.*, 1970; George and Rosenbaum, 1970; Haines, 1978; Martinola and Siegers, 1984);
- water treatment for clean water supply as well as for pollution control (Tesarik and Vostreil, 1962; Mican and Tesarik, 1960; Cooper and Atkinson, 1981; Cooper, 1986);
- fluid-bed electrolysis, especially for dilute solutions (Le Goff *et al.*, 1969; Flett, 1972; Roats *et al.*, 1977);
- biochemical reactions involving solid particles of immobilized enzymes or cells (Bailey and Ollis, 1986; Webb, 1986);
- supercritical extraction of fluidizable solids.

Notation

a_i	fraction of solids, dimensionless	F	force, g-wt.
A	area; cross-sectional area, cm^2	f	friction factor, dimensionless
A_x	frontal area of particle, cm^2	F_{H12}	adhesion force between two particles, g-wt
Ar	$= d_p^3 \rho_f g \Delta \rho / u^2$, Archimedes number, dimensionless	F_D	drag force on particle, g-wt
A_i	cross-sectional area based on particle terminal velocity, cm^2	g	$= 980 \text{ cm/s}^2$, acceleration of gravity
A'	$= A/A_i$, reduced area, dimensionless	G	fluid rate for conical bed, cm^3/s
Bi	$= hd_p/k_s$, Biot number, dimensionless	G_s	solids rate, $\text{gm/cm}^2 \text{ s}$
C	concentration, g/cm^3	h	lower height of conical fluid bed at $u = u_i$, cm; heat-transfer coefficient between particle and fluid, $\text{cal/s cm}^2 \text{ }^\circ\text{C}$
C_D	drag coefficient, dimensionless	h_D	mass-transfer coefficient between particle and fluid, cm/s
C_{Ds}	drag coefficient for single particle, dimensionless	H	nonuniformity index, dimensionless
d_p	particle diameter, cm	I	solids inventory in circulating fluidized bed, g
D_i	molecular diffusion coefficient, cm^2/s	j	$= \text{NuPr}^{-1/3}/\text{Re}$ or $\text{ShSc}^{-1/3}/\text{Re}$, j -factor, dimensionless
E	$= \text{NuPr}^{-1/3}/\text{Ar}$ or $\text{ShSc}^{-1/3}/\text{Ar}$, effectiveness factor, dimensionless		

J_m	particles mixing flux, g/cm ² s	S	mass velocity of solids, g/cm ² s
J_s	particles segregation flux, g/cm ² s	S_m, S_s, S_a	segregation number, dimensionless
k	constant	Sc	$= \mu/\rho_t D_s$, Schmidt number, dimensionless
k_g	thermal conductivity of gas, cal/cm s °C	Sh	$= h_D d_p/D_s$, Sherwood number, dimensionless
k_s	thermal conductivity of solid, cal/cm s °C	Sy	synergism number, dimensionless
l	underflow mass velocity of liquid, g/cm ² s; location of distributor plate in conical fluid bed, cm	T	temperature, °C
l_i	differential unitary distance for particle heat transfer, cm	u	velocity, cm/s
L	height, cm; mass velocity of liquid, g/cm ² s	u_0	superficial fluid velocity, cm/s
L_0	height of fixed solids bed before fluidization starts, cm	u_d	superficial solids velocity, cm/s
Ly	$= u^3 \rho_t^2 / \mu g \Delta \rho$, Lyashenko number, dimensionless	u_{mb}	superficial fluid velocity at incipient bubbling, cm/s
m	fixed-bed pressure-drop exponent, dimensionless	u_f, u_{mf}	superficial fluid velocity at incipient fluidization, cm/s
M_i	$= u_{ti}/u_{t1}$, terminal velocity ratio, dimensionless	u_f	actual velocity of fluid, cm/s
n	fluidized bed expansion exponent, dimensionless	u_p	actual velocity of particle, cm/s
N	$= (L/\rho_t A)(S/\rho_s A)$, liquid-solids velocity ratio, dimensionless	u_s	relative velocity between particle and fluid, cm/s
N_H	number of heat transfer stages, dimensionless	u_{sa}	actual relative velocity between particle and fluid, cm/s
Nu	$= h d_p/k_g$, Nusselt number, dimensionless	u_t	terminal particle velocity, cm/s
p, P	pressure, g-wt/cm ²	u'	$= u/u_t$, reduced velocity, dimensionless
ΔP	pressure drop, g-wt/cm ²	U_{pt}	minimum velocity for dilute-phase transport, cm/s
ΔP_{ss}	pressure drop for steady-state motion, g-wt/cm ²	U_{BT}	minimum velocity for turbulent fluidization, cm/s
P'	dimensionless head (pressure ratio)	U_{TF}	minimum velocity for fast fluidization, cm/s
Pr	$= C_p \mu/k_g$, Prandtl number, dimensionless	V'	$= A'Z'$, reduced volume, dimensionless
Q	deviation factor, dimensionless	w	width, cm; particle population density, g/cm ²
Q_0	deviation factor for fixed bed, dimensionless	x_f	weight fraction of fines in binary particle mixture, dimensionless
Q_1, Q_2	exchange coefficient in particle mixing-segregation, dimensionless	y	solute concentration, g/cm ³
r	$= \Delta \rho_2 / \Delta \rho_1$, effective density ratio for two particles, dimensionless	z	distance, cm
Re	$= d_p u \rho_t / \mu$, Reynolds number, dimensionless	z_1	location of point of inflection for fast fluidization, cm
		Z	height of fluidized bed, cm
		Z_0	dimensionless distance in accelerative motion of particle; characteristic length for fast fluidization voidage profile, cm

Z_1	height based on particle terminal velocity, cm	ε_{mf}	voidage at incipient fluidization, dimensionless
Z_1	dimensionless distance in heat transfer	ε_0	voidage of fixed bed, dimensionless
z'	$= z/Z$, reduced distance, dimensionless	ε_{ss}	voidage for steady-state motion, dimensionless
α	fraction of solids, dimensionless; solids ratio bypassing a cyclone, dimensionless; empirical constant for nonideal fluidization, signifying maximum deviation, dimensionless	η	fractional heat recovery, dimensionless
β	solids ratio uncollected in a cyclone, dimensionless; empirical constant for nonideal fluidization, signifying breadth of bulge in $\varepsilon-u$ curve, dimensionless	θ	time, s
β_i	$= u_{di}/u_{d1}$, particle velocity ratio, dimensionless	Θ	dimensionless time in accelerative particle motion; dimensionless time in particle-fluid heat transfer; dimensionless subsidence time in bed-collapsing test
β_r, β_t	coefficient for Archimedes-Reynolds correlation, dimensionless	γ	empirical constant for nonideal fluidization, signifying location of maximum bulge in $\varepsilon-u$ curve, dimensionless
γ	$= GC_p/SC_s$, flowing heat capacity ratio, dimensionless	μ	viscosity, g/cm s
δ	$= d_{p1}/d_{d2}$, particle diameter ratio, dimensionless	ρ_s	density of solid, g/cm ³
ε	voidage or void fraction, dimensionless	ρ_f	density of fluid, g/cm ³
		$\Delta\rho$	$= \rho_s - \rho_f$, effective density
		σ	shear stress, g-wt/cm ²
		Φ_0	dimensionless pressure drop in accelerative particle motion
		Φ_x, Φ_t	dimensionless pressure drop for conical fluid bed

References

- Al-Dibouni, M. R., and Garside, J., "Particle Mixing and Classification in Liquid Fluidized Beds," *Trans. Instn. Chem. Engrs.* **57**(2), 94 (1979).
- Anon., "Classifying Sand by Elutriation," *Cement, Lime and Gravel* **40**(4), 123 (1965).
- Aoki, R., Tsunakawa, H., Nishizawa, T., and Moizumi, M., *J. Res. Assoc. Powd. Technol.* **10**(9), 616 (1973).
- Arastoopour, H., "Pneumatic Transport of Solids," Chap. 11 in "Encyclopedia of Fluid Mechanics," Vol. 4 (N. P. Cheremisinoff, Ed.). Gulf Pub. Co., Houston, TX, 1986.
- Arastoopour, H., and Gidaspow, D., "Vertical Pneumatic Conveying Using Four Hydrodynamic Models," *Ind. Eng. Chem. Fund.* **18**(2), 123 (1974).
- Arastoopour, H., and Gidaspow, D., "Vertical Countercurrent Solids-Gas Flow," *Chem. Eng. Sci.* **34**, 1063 (1979).
- Avidan, A. A., Gould, R. M., and Kam, A. Y., "Operation of a Circulating Fluid-Bed Cold Flow Model of the 100 B/D MTG Demonstration Plant," *Proc. First Intern. Conf. Circulating Fluidized Bed, Halifax, Canada*, pp. 287-296 (1985).
- Bailey, J. E., and Ollis, D. F., "Biochemical Engineering Fundamentals." McGraw-Hill, New York, 1986, pp. 614-617.

- Bena, J. V., Ilavsky, J., Kossaczky, E., and Neuzil, L., "Zmeny Charakteru Prúdenia vo Vrstve Zrnitého Materiálu," Konferenz uber Wirbelschichttechnik, Praha, 1961, Vortrag Nr. 7, 1961.
- Bena, J. V., *et al.*, "Zmeny Charakteru Prúdenia vo Vrstve Zrnitého Materiálu," Konferenz uber Wirbelschichttechnik, Praha, 1961, Vortrag Nr. 7, 1961.
- Bennett, B. A., Cloete, F. L. D., and Streat, M., "A Systematic Analysis of the Performance of a New Continuous Ion-Exchange Technique," in "Ion Exchange in the Process Industries," pp. 131–139. Soc. Chem. Ind., 1970.
- Beranek, Y., and Sokol, D., "Theory of the Fluidized Bed" (in Russian), *Khim. Prom.* **1959**(1), 62 (1959).
- Berg, C., "Hypersorption Design—Modern Advancements," *Chem. Eng. Prog.* **47**, 585–590 (1951).
- Berg, C., "Hydroforming—Newest Development in Refining," *Petr. Ref.* **31**(12), 131 (1952).
- Berg, C., "New Gas Lift for Solids," *Chem. Eng.* **60**(5), 138 (1953).
- Berg, C., "Conveyance of Granular Solids," U.S. Pat. 2,684,867; 2,684,868; 2,584,870; 2,684,873; 2,684,930 (1954).
- Berg, C., in "Fluidization" (D. F. Othmer, ed.), p. 161. Reinhold Pub. Corp., New York, 1956.
- Blanding, F. H., and Elgin, J. C., "Limiting Flow in Liquid–Liquid Extraction Columns," *Trans. A. I. Ch. E.* **38**, 305 (1942).
- Boldt, J. R., Jr., "The Winning of Nickel—Its Geology, Mining and Extractive Metallurgy," figures inset, pp. 320–321. Longmans Canada Ltd., Toronto, 1967.
- Borlai, O., Hodany, L., and Blickle, T., "Investigation into the Mixing in Fluidized Beds," *Proc. Intern. Symp. Fluidization, Eindhoven*, pp. 433–441 (1967).
- Brauer, H., "Grundlagen der Einphasen- und Mehrphasenströmungen," Verlag Sauerländer, Frankfurtam Main 1971.
- Burovoi, I. A., Dracheva, T. V., and Ibraev, A. Kh., "Semi-Industrial Testing of the Fluidized-Bed Acid Leaching of Zinc Calcine," *Tsvet. Metal.* **44**(10), 16 (1971); *Chem. Abs.* **76**, 36,301 (1972).
- Cankurt, N. T., and Yerushalmi, J., "Gas Backmixing in High Velocity Fluidized Beds," *Second Intern. Conf. Fluidization, Cambridge*, pp. 387–393 (1978).
- Chen, B., and Kwauk, M., "Generalized Fluidization of Non-Ideal Systems," *Proc. First Intern. Conf. Circulating Fluidized Bed, Halifax, Canada*, pp. 127–132 (1985).
- Chen, M., and Song, T., "Fluidized Graphite-Particle Furnace," Second National Fluidization Conference, Beijing, Dec. 1980, proceedings, pp. 119–122 (in Chinese) (1980).
- Cheung, L., Nienow, A. W., and Rowe, P. N., "Minimum Fluidization Velocity of a Binary Mixture of Different Sized Particles," (*Shorter Commun.*) *Chem. Eng. Sci.* **29**, 1301–1303 (1974).
- Chiba, T., Chiba, S., and Nienow, A. W., "Prediction of the Steady State Segregation Pattern in Gas Fluidized Beds with Particles in Throughflow," *Fifth Intern. Conf. Fluidization, Elsinore, 1986*, pp. 185–192 (1986).
- Chong, Y., and Bao, M., "Particulately Fluidized Conical Bed" (in Chinese, unpublished). Inst. Chem. Metall., 1962.
- Clean Fuels from Coal Symposium II, June 23–27, 1975, IIT, Chicago, pp. 196, 361 (1975).
- Clift, R., and Gauvin, W. H., "Motion of Entrained Particles in Gas Streams," *Can. J. Chem. Eng.* **49**(4), 439–448 (1971).
- Cooper, P. F., "The Two Fluidized Bed Reactor for Wastewater Treatment," Chap. 11 in "Process Engineering Aspects of Immobilized Cell Systems," pp. 179–204. Instn. Chem. Engrs. (London), 1986.
- Cooper, P. F., and Atkinson, B., "Biological Fluidized Bed Treatment of Water and Wastewater." Ellis Horwood, Chichester, W. Sussex. England, 1981.
- Delaplaïne, J. W., "Forces Acting in Flowing Beds of Solids," *A.I.Ch.E.J.* **2**, 127–138 (1956).

- Elgin, J. C., and Foust, H. C., "Countercurrent Flow of Particles through Moving Continuous Fluid—Pressure Drop and Flooding in Spray-Type Liquid Towers," *Ind. Eng. Chem.* **42**, 1127 (1950).
- Finkelstein, E., Letan, R., and Elgin, J. C., "Mechanics of Vertical Moving Fluidized Systems with Mixed Particle Sizes," *A.I.Ch.E.J.* **17**, 867 (1971).
- Flett, D. S., "The Fluidized-Bed Electrode in Extractive Metallurgy," *Chem. and Ind.* **1972**(24), 983 (1972).
- Foscolo, P. U., and Gibilaro, L. G., "A Fully Predictive Criterion for the Transition between Particulate and Aggregative Fluidization," *Chem. Eng. Sci.* **39**, 1667–1675 (1984).
- Geldart, D., "The Effect of Particle Size and Size Distribution on the Behavior of Gas-Fluidized Beds," *Powder Technol.* **6**, 201–205 (1972).
- Geldart, D., "Types of Fluidization," *Powder Technol.* **7**, 285–290 (1973).
- Geldart, D., and Wong, A. C. Y., "Fluidization of Powders Showing Degrees of Cohesiveness—I. Bed Expansion, II. Experiments on Rates of De-aeration," *Chem. Eng. Sci.* **39**, 1481–1488 (1984); **40**, 653–661 (1985).
- George, D. R., and Rosenbaum, J. B., "New Development and Applications of Ion-Exchange Techniques for the Mineral Industry," in "Ion Exchange in the Process Industries," pp. 155–161. Soc. Chem. Ind., 1970.
- Ghar, R. N., and Gupta, P. Sen, "Mixing of Solids in Fluidized Beds," POWTECH '81, Mixing, paper S2/I (1981).
- Gibilaro, L. G., and Rowe, P. N., "A Model for a Segregating Gas Fluidized Bed," *Chem. Eng. Sci.* **29**, 1400–1412 (1974).
- Goroshko, V. D., *et al.*, "Approximate Law for the Hydraulically Suspended Layer and Hindered Sedimentation" (in Russian), *Neft. i Gaz* **1958**(1), 125 (1958).
- Grace, J. R., "Contacting Modes and Behavior Classification of Gas-Solid and Other Two-Phase Suspensions," *Can. J. Chem. Eng.* **64**, 353–363 (1986).
- Grace, J. R., and Tuot, J., "A Theory for Cluster Formation in Vertically Conveyed Suspensions of Intermediate Density," *Trans. Instn. Chem. Engrs.* **57**, 49–54 (1979).
- Haines, A. K., "The Development of Continuous Fluidized Bed Ion Exchange in South Africa, and Its Use in the Recovery of Uranium," *J. S. Afr. Min. Metall.* **78**(12), 303 (1978).
- Hancock, R. T., "The Law of Motion of Particles in a Fluid," *Trans. Instn. Min. Engrs. (London)* **94**, 114–121 (1937).
- Hancock, R. T., "Interstitial Flow," *Mining Mag.* **67**, 179–186 (1942).
- Harrison, D., Davidson, J. F., and deKock, J. W., "On the Nature of Aggregative and Particulate Fluidization," *Trans. Instn. Chem. Engrs.* **39**, 202 (1961).
- Higgins, I. R., "Continuous Ion Exchange of Process Water," *Chem. Eng. Prog.* **65**(6), 59 (1969).
- Highley, J., and Merrick, D., "Effect of the Spacing between Solid Feed Point on the Performance of a Large Fluidized-Bed Reactor," *A.I.Ch.E. Symp. Ser.* **62**(116), 219–227 (1972).
- Hoffman, R. F., Lapidus, L., and Elgin, J. C., "The Mechanics of Vertical-Moving Fluidized Systems—IV. Application to Batch-Fluidized Systems with Mixed Particle Size," *A.I.Ch.E.J.* **6**, 321 (1960).
- Horio, M., Takada, M., Ishida, M., and Tanaka, N., "The Similarity Rule of Fluidization and Its Application to Solid Mixing and Circulation Control," *Fifth Intern. Conf. Fluidization, Elsinore, 1986*, pp. 151–158 (1986).
- Huang, X., He, T., Wang, Y., and Kwauk, M., "Generalized Fluidization of Polydisperse Systems," *Proc. CIESC/AIChE Joint Meet. Chem. Eng., Sept. 19–22, 1982, Beijing, China*, p. 354 (1982).
- Hudjakov, G. N., "O Tseploobiene b Gazobzbeci," *Izvet. Akad. Nauk. CCCP, Otd. Tech. Nauk.* **1953**(2), 265 (1953).

- Institute of Chemical Metallurgy, Division III, "Leaching in Conical Fluidized Beds," 1959-9 (1959).
- Institute of Chemical Metallurgy, Division III, "Staged Fluidized Leaching of Products of Chloridizing Roasting of Pyrites Cinder—Preliminary Process Design" (in Chinese, unpublished), 1965-7-31 (1965).
- Institute of Chemical Metallurgy, Division III, "The Differential Leacher/Washer Cell" (in Chinese, unpublished), 1973-8 (1973).
- Institute of Chemical Metallurgy, Division III, "The Differential Leacher/Washer Cell—Supplementary Experiments" (in Chinese, unpublished), 1975-3 (1975).
- Jackson, R., "The Mechanics of Fluidized Beds," *Trans. Instn. Chem. Engrs.* **41**, 13 (1963).
- Jackson, R., "Hydrodynamic Stability of Fluid-Particle Systems," Chap. 2 in "Fluidization," 2nd Ed. (Davidson, J. F., Clift, R., and Harrison, D., eds). Academic Press, New York, 1985.
- Jin, H., "Particles and Distributor for Fluid-Bed Heat Treatment Furnace," (in Chinese) *Proc. Soc. Nat. Fluidization Conf.*, Beijing, Dec. 1980, p. 109.
- Jin, H., "Fluidized Electric Furnace for Heat Treatment," (in Chinese) *Proc. Third Nat. Fluidization Conf.*, Taiyuan, Apr. 1984, p. 336.
- Jinescu, G., Teoreanu, I., and Ruckenstein, E., "The Mixing of Solid Particles in a Fluidized Bed," *Can. J. Chem. Eng.* **44**, 73-76 (1966).
- Joint SFL Task Group (Nanjing Iron and Steel Mill, Institute of Chemical Metallurgy and Metallurgical Research Institute), "Staged Fluidized Leaching of Products of Chloridizing Roasting of Pyrites Cinder—A Report on Pilot-Plant Tests" (in Chinese, unpublished), 1967-5 (1967).
- Kang, W. K., and Osberg, G. L., "Longitudinal Particle Mixing in a Screen-Packed Gas-Solid Fluidized Bed," *Can. J. Chem. Eng.* **44**, 142-147 (1966).
- Kano, T., Takeuchi, F., Yamazaki, E., and Tsuzuki, H., "Reduction of Power Consumption for Pneumatic Conveying of Granular Materials," *Kagaku Kogaku Ronbunshu* **7**(2), 126 (1981).
- Kennedy, S. C., and Bretton R. H., "Axial Dispersion of Spheres Fluidized with Liquids," *A.I.Ch.E.J.* **12**(1), 24 (1966).
- Kettenring, K. N., Manderfield, E. L., and Smith, J. M., "Heat and Mass Transfer in Fluidized Systems," *Chem. Eng. Prog.* **46**, 139-145 (1950).
- Korsunski, V. I., D'yachko, A. G., and Svetozarova, G. I., "Calculation of the Fluidized-Bed Leaching of Zinc Sinters with Consideration of Mixing of the Solid Phases," *Tsvet. Metal.* **43**(5), 21 (1970); *Chem. Abs.* **73**, 37,665 (1970).
- Kramers, H., "Heat Transfer from Spheres to Flowing Media," *Physica* **12**, 61 (1946).
- Krupp, H., "Particle Adhesion: Theory and Experiment," *Adv. Colloid Interface Sci.* **1**, 111 (1967).
- Kwauk, M., "Application of Fluidization Technology in Chemical Metallurgy" (in Chinese). Science Press, Beijing, 1958.
- Kwauk, M., "Fluidized Leaching" (in Chinese, unpublished). *Inst. Chem. Metall.*, 1961-4-10 (1961).
- Kwauk, M., "A Preliminary Note on Particle Segregation in Fluidized Systems" (unpublished), *Inst. Chem. Metall.*, 1962-40-20 (1962).
- Kwauk, M., "Generalized Fluidization, I. Steady-State Motion," *Scientia Sinica* **12**(4), 587 (1963a).
- Kwauk, M., "A Note on Particle Segregation in Fluidized Systems" (unpublished), *Inst. Chem. Metall.*, 1963-6-3 (1963b).
- Kwauk, M., "A Tentative Analysis of Moving-Bed Transport of Granular Materials with Compressible Media" (unpublished), *Inst. Chem. Metall.*, 1963-7-2 (1963c).
- Kwauk, M., "Generalized Fluidization, II. Accelerative Motion with Steady Profiles," *Scientia Sinica* **13**(9), 1477 (1964a).

- Kwauk, M., "Fluidized Calcination of Aluminum Ore for Pre-Desilication" (unpublished), Inst. Chem. Metall., 1964-11-6 (1964b).
- Kwauk, M., "Design of Internals for Aggregative Fluidization" (in Chinese, unpublished), Inst. Chem. Metall., 1965-10-5 (1965a).
- Kwauk, M., "Countercurrent Staging for Cocurrent Dilute-Phase Heat Exchange" (in Chinese, unpublished), Inst. Chem. Metall., 1965-1-26 (1965b).
- Kwauk, M., "The Differential Leacher/Washer Cell and its Mathematical Modeling" (in Chinese, unpublished) Inst. Chem. Metall., 1972-12-31 (1972).
- Kwauk, M., "Particulate Fluidization in Chemical Metallurgy," *Scientia Sinica* **16**, 407 (1973).
- Kwauk, M., "Dense-Phase Transport Downcomers" (in Chinese, unpublished), Inst. Chem. Metall., 1974-1-9, rev. 1977-2-13 (1974a).
- Kwauk, M., "Pneumatically Controlled Multi-Stage Fluidized Beds" (in Chinese, unpublished), Inst. Chem. Metall., 1974-3-7 (1974b).
- Kwauk, M., "Generalized Fluidization of Bidisperse Particles" (in Chinese, unpublished), Inst. Chem. Metall., 1975-9-21 (1975).
- Kwauk, M., "Pneumatically Started Seals" (in Chinese, unpublished), Inst. Chem. Metall., 1978-6-24 (1978).
- Kwauk, M., "Fluidized Leaching and Washing" (in Chinese). Science Press, Beijing, 1979a.
- Kwauk, M., "Fluidized Roasting of Oxidic Chinese Iron Ores," *Scientia Sinica* **22**, 1265 (1979b); repr. *Intern. Chem. Eng.* **21**, 95-115 (1981).
- Kwauk, M., "Fast Fluidization," in three parts on mathematical modeling (in Chinese, unpublished), Inst. Chem. Metall. (1979c).
- Kwauk, M., "Multi-Stage Fluidized Beds—L/S Fill and Dump Type," (unpublished) Inst. Chem. Metall., 1981-1-22 (1981).
- Kwauk, M., "Bubble-less Gas-Solid Contacting," exchange-scholar lecture, Japan Soc. Promotion of Sci. (1983).
- Kwauk, M., Behavior of Binary Particulates, Note 1, 84-11-1; Note 2, 86-10-20 (1984, 1986) (unpublished).
- Kwauk, M., and Chong, Y. O., "Fluidization—Dynamics of Uniform Spheres in Fluids" (in Chinese). Science Press, Beijing, 1963.
- Kwauk, M., and Tai, D.-W., "Transport Processes in Dilute-Phase Fluidization as Applied to Chemical Metallurgy. I. Transport Coefficient and System Pressure Drop as Criteria for Selecting Dilute-Phase Operations; II. Application of Dilute-Phase Technique to Heat Transfer" (in Chinese, with English abstract), *Acta Metallurgica Sinica* **7**, 264-280; 391-408 (1964).
- Kwauk, M., and Wang, Y., "Fluidized Leaching and Washing," *I. Chem. E. Symp. Ser. No. 63*, paper D4/BB/1-21 (1981).
- Kwauk, M., and Yang, J., 1964, "Particulate Fluidization in a Conical Bed" (in Chinese, unpublished), Inst. Chem. Metall., 1964-1 (1964).
- Kwauk, M., Wang, N., Li, Y. Chen, B., and Shen, Z., "Fast Fluidization at ICM," *Proc. First Intern. Conf. Circulating Fluidized Bed, Halifax, Canada*, pp. 33-62 (1985).
- Lapidus, L., and Elgin, J. C., "Mechanics of Vertical-Moving Fluidized Systems," *A.I.Ch.E.J.* **3**, 63 (1957).
- Le Goff, P., Vergenes, F. Coeuret, F., and Bordet, J., "Application of Fluidized Beds in Electrochemistry," *Ind. Eng. Chem.* **61**(10), 8 (1969).
- Leschonski, K., "Recent Development in the Theory and Practice of Particle Classification," POWTECH '81, paper D2/M (1981).
- Lewis, E. W., and Bowerman, E. W., "Fluidization of Solid Particles in Liquids," *Chem. Eng. Prog.* **48**, 603 (1952).
- Lewis, W. K., Gilliland, E. R., and Bauer, W. C., "Characteristics of Fluidized Particles," *Ind. Eng. Chem.* **41**, 1104 (1949).

- Li, H., and Kwauk, M., "Vertical Pneumatic Moving-Bed Transport. I. Analysis on Flow Dynamics," *Chem. Eng. Sci.* **44**, 249 (1989a).
- Li, H., and Kwauk, M., "Vertical Pneumatic Moving-Bed Transport. II. Experimental Findings," *Chem. Eng. Sci.* **44**, 261 (1989b).
- Li, X., Liu, D., and Kwauk, M., "Pneumatically Controlled Multi-Stage Fluidized Beds II," *CIESC-AIChE Joint Meet. Chem. Eng., Beijing, China*, p. 382 (1982).
- Li, Y., and Kwauk, M., "The Dynamics of Fast Fluidization," *Third Intern. Conf. Fluidization, Henniker, New Hampshire, U.S.A.*, pp. 537–544 (1980).
- Li, Y., Chen, B., Wang, F., and Wang, Y., "Hydrodynamic Correlations for Fast Fluidization," *First China-Japan Symp. Fluidization, Hangzhou, China*, pp. 124–134 (1982).
- Li, Y., Chen, B., Wang, F., Wang, Y., and Kwauk, M., "Rapid Fluidization," *Intern. Chem. Eng.* **21**, 670–678 (1981).
- Littman, H., "Solids Mixing in Straight and Tapered Fluidized Beds," *A.I.Ch.E.J.* **10**, 924–929 (1964).
- Liu, D., and Kwauk, M., "Pneumatically Controlled Multi-Stage Fluidized Bed," *Third Intern. Conf. Fluidization, Henniker, New Hampshire, U.S.A.*, pp. 485–492 (1980).
- Liu, D., Li, X., and Kwauk, M., "Pneumatically Controlled Multi-Stage Fluidized Bed and Its Application in Solvent Recovery from a Plant Waste Gas," *Selec. Pap., J. Chem. Ind. Eng.* **1**, 1 (1981).
- Liu, S., and Tai, D.-W., "Temperature Measurement for Dilute-Phase Heat Transfer" (in Chinese, unpublished), *Inst. Chem. Metall.* (1965).
- Lloyd, P. J., "The Evaluation of Powder Mixtures," *POWTECH '81, Mixing*, paper S2/K (1981).
- Lloyd, P. J., and White, D. A., "Contacting Liquid with Solids in Fluidized Beds with Countercurrent Flow," *S. African Pat.* 71 08,233 (Feb. 5, 1973).
- Loeffler, A. L., and Ruth, B. F., "Particulate Fluidization and Sedimentation of Spheres," *A.I.Ch.E.J.* **5**, 310 (1958).
- Lou, J., "Particles Segregation and Mixing in Particulate Fluidization" (in Chinese, unpublished), *Tsinghua University and Inst. Chem. Metall.* 1964–7 (1964).
- Ma, X., and Kwauk, M., "Particulate Fluidization of Ferromagnetic Particles in Uniform Magnetic Field," *Fine Particle Society Pacific Region Meeting*, Aug. 1–5, 1983, Honolulu, Hawaii, U.S.A. (1983).
- Martinola, F., and Siegers, G., "Experience Data with Liftbed and Rinsebed Process," in "Ion Exchange Technology" (Naden, D., and Streat, M., eds.), pp. 127–137. *Soc. Chem. Ind.*, 1984.
- Massimilla, L., "Gas Jets in Fluidized Beds," Chap. 4 in "Fluidization," 2nd Ed. (Davidson, J. F., Clift, R., and Harrison, D., eds.) Academic Press, New York, 1985.
- Maude, A. D., "A Generalized Theory of Sedimentation," *Brit. J. App. Phys.* **9**, 477 (1958).
- May, W. G., "Fluidized-Bed Reactor Studies," *Chem. Eng. Prog.* **55**, 49 (1959).
- McCune, L. K., and Wilhelm, R. H., "Mass and Momentum Transfer in Solid-Liquid System. Fixed and Fluidized Beds," *Ind. Eng. Chem.* **41**, 1124–1134 (1949).
- Mertes, T. S., and Rhodes, H. B., "Liquid Particle Behavior, Part I," *Chem. Eng. Prog.* **51**, 427; "Part II," *Chem. Eng. Prog.* **51**, 517 (1955).
- Mican, V., and Tesarik, I., "The Packed Water Treatment Station Developed by the Institute of Hydrodynamics of the Czechoslovak Academy of Sciences," *Aqua* **1960**(4), 17 (1960).
- Misek, T., "Behavior of Polydisperse Phase in Column-Type Apparatus—I. Hydrodynamics, Entrainment and Partial Flooding," *Coll. Czech. Chem. Commun.* **32**, 4018 (1967).
- Moritomi, H., Iwase, T., and Chiba, T., "A Comprehensive Interpretation of Solid Layer Inversion in Liquid Fluidized Beds," *Chem. Eng. Sci.* **37**, 1751–1757 (1982).
- Moritomi, H., Yamagishi, T., and Chiba, T., "Prediction of Solid Mixing in Liquid Fluidized Beds of Binary Solid Particles," *Proc. Second China-Japan Symp. Fluidization, April, 1985*, pp. 238–249 (1985).

- Moritomi, H., Yamagishi, T., and Chiba, T., "Prediction of Complete Mixing in Liquid-Fluidized Binary Solid Particles," *Chem. Eng. Sci.* **41**, 297–305 (1986).
- Morooka, S., Nishinaka, M., and Kato, Y., "Sedimentation Velocity and Expansion Ratio of the Emulsion Phase in a Gas-Solid Fluidized Bed" (in Japanese), *Kagaku Kogaku* **37**, 485 (1973).
- Mouret, P., "Installation et procede de traitement a contre courant de mineraux," *Fr. Pat.* 70.18978, 2.087,585 (Dec. 6, 1971).
- Naimer, N. S., Chiba, T., and Nienow, A. W., "Parameter Estimation for a Solid Mixing/Segregation Model for Gas Fluidized Beds," *Chem. Eng. Sci.* **37**, 1047–1057 (1982).
- Nienow, A. W., and Chiba, T., "Solids Mixing and Segregation in Gas-Fluidized Beds," *POWTECH '81*, Mixing, paper S2/F (1981).
- Nienow, A. W., and Chiba, T., "Fluidization of Dissimilar Materials," Chap. 10 in "Fluidization," 2nd Ed. (Davidson, J. F., Clift, R., and Harrison, D., eds.). Academic Press, New York, 1985.
- Nienow, A. W., Rowe, P. N., and Cheung, L. Y.-L., "A Qualitative Analysis of the Mixing of Two Segregating Powders of Different Density in a Gas-Fluidized Bed," *Powd. Technol.* **20**, 89–97 (1978).
- Oliver, D. R., "The Sedimentation of Suspensions of Closely-Sized Spherical Particles," *Chem. Eng. Sci.* **15**, 230 (1961).
- Pavloshenko, I. S., "Free Motion of Single Particles in Unlimited Surrounding" (in Russian), *Zh. Priklad. Khim.* **28**, 885 (1956).
- Polinsky, K., "Use of the Fluidized Layer Method for Washing and Concentration of Pigment Suspension," *Zh. Prikl. Khim.* **39**(1), 225 (1966); *Chem. Abs.* **64**, 12,225 (1966).
- Price, B. G., Lapidus, L., and Elgin, J. C., "Mechanics of Vertical-Moving Fluidized Systems—II. Application to Countercurrent Operation," *A.I.Ch.E.J.* **5**, 93 (1959).
- Pyzel, R., "Hydraulic Cement Process," U.S. Pats. 2,874,950 (1959); 2,977,105 (1961).
- Qader, S. A., "Natural Gas Substitutes from Coal and Oil," *Elsevier*, pp. 239, 243, 257, 260 (1985).
- Qian, Z., and Kwak, M., "Computer Application in Characterizing Fluidization by the Bed Collapsing Method," Tenth Intern. CODATA Conf., Ottawa, July, 1986.
- Qin, S., and Liu, G., "Automatic Surface Tracking for Collapsing Fluidized Bed," *Sec. China-Japan Fluidization Symp., Kunming, 1985*, p. 468. Elsevier, 1985.
- Quinn, J. A., Lapidus, L., and Elgin, J. C., "The Mechanics of Vertical-Moving Fluidized Systems—V. Concurrent Cogravity Flow," *A.I.Ch.E.J.* **7**, 260 (1960).
- Ranada, M. B., "Adhesion and Removal of Fine Particles on Surfaces," *Aerosol Sci. Technol.* (1986) preprint.
- Reh, L., "Calcination von Aluminumhydroxid in einer zirkulierenden Wirbelschicht," *Chem.-Ing.-Tech.* **42**, 447–451 (1970).
- Reh, L., "Fluidized Bed Processing," *Chem. Eng. Prog.* **67**, 58–63 (1971).
- Reh, L., "Calcining Aluminum Trihydrate in a Circulating Fluid Bed, a New Technique of High Thermal Efficiency," *Metallurges. Rev. Activ.* **1972**(15), 58–60 (1972).
- Reh, L., "The Circulating Fluid Bed Reactor—A Key to Efficient Gas-Solid Processing," *Proc. First Intern. Conf. Circulating Fluidized Bed, Halifax, Canada*, pp. 105–118 (1985).
- Reh, L., "Auswahlkriterien für Gas/Feststoffreaktionssysteme," *Erzmetall* **29**, 402–410 (1976).
- Reh, L., "Trends in Research and Industrial Application of Fluidization. Part 1. Research," *Verfahrenstechnik* **11**, 381–384 (1977).
- Richardson, J. F., and Ayers, P., "Heat Transfer between Particles and a Gas in a Fluidized Bed," *Trans. Instn. Chem. Engrs.* **37**, 314 (1959).
- Richardson, J. F., and Bakhtiar, A. G., "Mass Transfer Fluidized Particles and Gas," *Trans. Instn. Chem. Engrs.* **36**, 283 (1958).
- Richardson, F., and Szekeley, J., "Mass Transfer in a Fluidized Bed," *Trans. Instn. Chem. Engrs.* **39**, 212 (1961).

- Richardson, J. F., and Zaki, W. N., "Sedimentation and Fluidization," *Trans. Instn. Chem. Engrs.* **32**, 35 (1954).
- Rickles, R. N., "Liquid-Solid Extraction," *Chem. Eng.* **72**(6), 157 (1965).
- Rietema, K., "The Effect of Interparticle Forces on the Expansion of a Homogeneous Gas-Fluidized Bed," *Proc. Intern. Symp. Fluidization, Toulouse*, pp. 28-40 (1967).
- Roats, C. M. S., Boon, H. F., and Eveissens, W., "Wirbelbettelektrolyse zur Entfernung von Metallen aus verdünnten Lösungen," *Erzmetall* **30**(9), 365 (1977).
- Roberts, E. J., "Thickening—Art or Science?" *Min. Eng. & Min. Trans.* **1**, 61 (1949).
- Rodriguez, J., "Leaching Process," U.S. Pat. 3,695,846 (Oct. 3, 1972).
- Romero, J. B., and Johanson, L. N., "Factors Affecting Fluidized Bed Quality," *Chem. Eng. Prog. Symp. Ser.* **58**(38), 28-37 (1962).
- Rowe, P. N., "A Rational Explanation for the Behavior of Geldart Type A and B Powders when Fluidized," Dept. Chem. & Biochem. Eng., Univ. Coll. London, April 1986.
- Rowe, P. N., and Sutherland, K. S., "Solids Mixing Studies in Gas Fluidized Beds, Part II: The Behavior of Deep Beds of Dense Materials," *Trans. Instn. Chem. Engrs.* **42**, T55 (1964).
- Rowe, P. N., Partridge, B. A., Cheney, A. G., Henwood, G. A., and Lyall, Z., "The Mechanisms of Solids Mixing in Fluidized Beds," *Trans. Instn. Chem. Engrs.* **43**, 271 (1965).
- Rowe, P. N., Nienow, A. W., and Agbim, A. J., "The Mechanism by Which Particles Segregate in Gas Fluidized Beds—Binary Systems of Near-Spherical Particles," *Trans. Instn. Chem. Engrs.* **50**, 310 (1972a).
- Rowe, P. N., Nienow, A. W., and Agbim, A. J., "A Preliminary Quantitative Study of Particle Segregation in Gas Fluidized Beds—Binary Systems of Near-Spherical Particles," *Trans. Instn. Chem. Engrs.* **50**, 324 (1972b).
- Sandy, C. W., Daubert, T. E., and Jones, J. H., "Vertical Dense-Phase Gas-Solids Transport," *Chem. Eng. Prog. Symp. Ser.* **66**(105), 133-142 (1970).
- Schilling, H.-D., Bonn, B., and Krauss, U., "Kohlenvergasung: Eine Basisstudie über bestehende Verfahren und neue Entwicklungen," English translation, pp. 93, 198, 227, 233. Verlag Gluckauf GmbH, Essen, 1979.
- Schroth, G., "Pyzel Process zum Klinkerbrennen," *Zement-Kalk-Gips* **24**, 571-3 (1971).
- Shangtung Aluminum Plant, Research Institute, Fluidization Group, "Fluidized Leaching of Aluminum Ore Sinter—A Report on Laboratory Investigations and Bench-Scale Tests" (in Chinese, unpublished), 1967-5-23 (1967).
- Slater, M. J., "A Review of Continuous Countercurrent Contactors for Liquids and Particulate Solids," *Brit. Chem. Eng.* **14**(1), 41 (1969).
- Somer, K., "Mechanism of Powder Mixing and Demixing," POWTECH '81, Mixing, paper S1/A (1981).
- Soo, S. L., "Boundary Layer Motion of a Gas-Solid Suspension," *Proc. Symp. Interaction between Fluids and Particles, Instn. Chem. Engrs.*, 1962, p. 50 (1962).
- Soo, S. L., "3. Gas-Solid Systems," in "Handbook of Multiphase Systems" (Hestroni, G., eds.). Hemisphere Pub. Corp., Washington, 1982.
- Soo, S. L., "Fluid Dynamics of Multiphase Systems." Blaisdell, 1967; 2nd Ed., Science Press, Beijing, 1990.
- Squires, A. M., "Applications of Fluidized Beds in Coal Technology," lecture, Intern. School on Heat and Mass Transfer Problems in Future Energy Production, Dubrovnik, Yugoslavia (1975a).
- Squires, A. M., "Gasification of Coal in High-Velocity Fluidized Beds," *loc. cit.* (1975b).
- Squires, A. M., "The City College Clean Fuels Institute: Programs for I. Gasification of Coal in High-Velocity Fluidized Beds, II. Hot Gas Cleaning," Symp. Clean Fuels from Coals, I. G. T., Chicago (1975c).
- Squires, A. M., "The Story of Fluid Catalytic Cracking: The First Circulating Fluid Bed," *Proc. First Intern. Conf. Circulating Fluidized Bed*, pp. 1-19 (1985).

- Squires, A. M., Kwauk, M., and Avidan, A. A., "Fluid Beds: At Last, Challenging Two Entrenched Practices," *Science* **230**, 1329–37 (1985).
- Steinour, H. H., "Rate of Sedimentation," *Ind. Eng. Chem.* **36**, 618 (1944).
- Stevens, D. G., "Development of a Continuous Ion-Exchange Process," in "Ion Exchange in the Process Industries," p. 114–119. Soc. Chem. Ind., 1970.
- Struve, D. L., Lapidus, L., and Elgin, J. C., "The Mechanics of Vertical-Moving Fluidized Systems—III. Application to Cocurrent Countergravity Flow," *Can. J. Chem. Eng.* **36**, 141 (1958).
- Sunkoori, N. R., and Kaparthi, R., "Heat Transfer Studies between Particles and Liquid Medium in a Fluidized Bed," *Chem. Eng. Sci.* **12**, 166–174 (1960).
- Sutherland, K. S., "Solids Mixing Studies in Gas Fluidized Beds—Part I: A Preliminary Comparison of Tapered and Non-tapered Beds, *Trans. Instn. Chem. Engrs.* **39**, 188–194 (1961).
- Tai, D.-W., "Experimental Studies on Dilute-Phase Heat Transfer," *Inst. Chem. Metall.*, 1959–9–21 (1959).
- Tanimoto, H., Chiba, S., Chiba, T., and Kobayashi, H., "Mechanism of Solid Segregation in Gas Fluidized Beds," *Third Intern. Conf. Fluidization, Henniker, New Hampshire, 1980*, pp. 381–388 (1980).
- Tesarik, I., and Vostreil, J., "Fluidization of Granular and Floccular Beds," *Aqua Ind.* **4**(19), 25 (1962).
- Tung, Y., "Dynamics of Bed Collapse for Fluidization Systems," M.S. Thesis, *Inst. Chem. Metall.* (1981).
- Tung, Y., and Kwauk, M., "Dynamics of Collapsing Fluidized Beds," in *China–Japan Fluidization Symp., Hangzhou, April 4–9, 1982*, pp. 155–166. Science Press, Beijing and Gordon Breach, 1982.
- Ullmann Enzy. tech. Chemie, 4. Aufl., Bd. 2, Verfahrenstechnik I (Grundoperationen), s. 70, Aufstromklassierer (1972).
- Valkenburg, P. J. M., Schouten, J. C., and van den Bleek, C. M., "The Non-Steady State Segregation of Particles in Gas Fluidized Beds," *Fifth Intern. Conf. Fluidization, Elsinore, 1986*, pp. 193–200 (1986).
- Walker, D. M., "An Approximate Theory for Pressures and Arching in Hoppers," *Chem. Eng. Sci.* **21**, 975–997 (1966).
- Walker, D. M., and Blanchard, M. H., "Pressures in Experimental Coal Hoppers," *Chem. Eng. Sci.* **22**, 1713–1745 (1967).
- Wallis, G. B., "One Dimensional Two-Phase Flow." McGraw-Hill, New York, 1969.
- Wallroth, C. F., Gyarmati, E., and Nickel, H., "Modelluntersuchungen an konischen Fließbetten zur Beschichtung von Kernbrennstoffteichen," *Chem.-Ing.-Tech.* **43**, 1298 (1971).
- Walters, J. K., "A Theoretical Analysis of Stresses in Silos with Vertical Walls," *Chem. Eng. Sci.* **28**, 13–21 (1973a).
- Walters, J. K., "A Theoretical Analysis of Stresses in Axially-Symmetric Hoppers and Bunkers," *Chem. Eng. Sci.* **28**, 779–789 (1973b).
- Walton, J. S., Olson, R. L., and Levenspiel, O., "Gas–Solid Film Coefficients of Heat Transfer in Fluidized Coal Beds," *Ind. Eng. Chem.* **44**, 1474–1480 (1952).
- Wamsley, W. W., and Johnson, L. N., "Fluidized Bed Heat Transfer," *Chem. Eng. Prog.* **50**, 347 (1954).
- Wang, N., Li, Y., Zheng, X., and Kwauk, M., "Voidage Profiling for Fast Fluidization," *First Intern. Conf. Circulating Fluidized Beds, Halifax, Canada* (1985).
- Webb, C., "Biomass Holdup in Immobilized Cell Reactors," Chap. 8 in "Process Engineering Aspects of Immobilized Cell Systems," pp. 117–133. *Instn. Chem. Engrs. (London)*, 1986.
- Weber, G., "New Lift Technique," *Oil & Gas J.*, 75 (1952).
- Weinstein, H., Graff, R. A., Meller, M., and Shao, M. J., "The Influence of the Imposed Pressure

- Drop across a Fast Fluidized Bed," *Proc. Fourth Intern. Conf. Fluidization, Kashikojima, Japan*, pp. 299–306 (1983).
- Wilhelm, R. H., and Kwauk, M., "Fluidization of Solid Particles," *Chem. Eng. Prog.* **44**, 201–218 (1948).
- Wilhelm, R. H., and Valentine, S., "The Fluidized Bed—Transition State in the Vertical Pneumatic Transport of Particles," *Ind. Eng. Chem.* **43**, 1199 (1951).
- Xia, Y., and Kwauk, M., "Micro-Visualization of Fluidizing Behavior of Binary Particle Mixtures," *Intern. Symp. Heat Transfer, Beijing, 1985*, Hemisphere (1985).
- Yakubovich, I. A., Tyuftin, E. P., and Tolkachev, V. A., "Separation and Washing of Sediments in a Column Containing a Fluidized Bed," *Khim. Neft. Mashinstr.* **1970**(9), 14; *Chem. Abs.* **73**, 132, 482 (1970).
- Yang, W. C., and Keairns, D. L., "Design of Recirculating Fluidized Beds for Commercial Operation," *A.I.Ch.E. Symp. Ser.* **74**(176), 218–228 (1978).
- Yang, W. C., Revay, D., Anderson, R. G., Chelan, E. J., Keairns, D. L., and Cicero, D. C., "Fluidization Phenomena in a Large-Scale, Cold-Flow Model," *Fourth Intern. Conf. Fluidization, Kashikojima, 1983*, pp. 77–84 (1983).
- Yang, W. C., Ettedadieh, B., Anestis, T. C., Gizzie, R. E., and Haldipur, G. B., "Fluidization Phenomena in a Large Jetting Fluidized Bed," *Fifth Intern. Conf. Fluidization, Elsinore, 1986*, pp. 95–102 (1986).
- Yang, Z., "Effect of Particle Size Distribution on Fluidization Quality," M. S. Thesis, Inst. Chem. Metall. (1982).
- Yang, Z., Tung, Y., and Kwauk, M., "Characterizing Fluidization by the Bed Collapsing Method," *Chem. Eng. Commun.* **39**, 217–232 (1985).
- Yaverbaum, L., "Fluidized Bed Combustion of Coal and Waste Materials," *Noyes Data*, p. 206 (1977).
- Yerushalmi, J., and Cankurt, N. T., "Flow Regimes in Vertical Gas–Solid Contact Systems," *A.I.Ch.E. Symp. Ser.* **74**(176), 1–13 (1978).
- Yerushalmi, J., Turner, D. H., and Squires, A. M., "The Fast Fluidized Bed," *Ind. Eng. Chem., Process Des. Dev.* **15**, 47 (1976).
- Yu, M. X., Zhang, H. Z., and Chong, Y. O., "Staged Fluidized Leaching—Laboratory Investigations" (in Chinese, unpublished), Inst. Chem. Metall., 1964–10 (1964).
- Zenz, F. A., "Visualizing Gas–Solid Dynamics in Catalytic Processes," *Petr. Ref.* **32**(7), 123 (1953).
- Zenz, F. A., and Othmer, D. F., "Fluidization and Fluid–Particle Systems," p. 136. Reinhold, 1960.
- Zhang, F., and Zheng, X., "Polydisperse Behavior of Leached Uranium Ore in Fluidized Classifying and Washing Column," *Proc. China–Japan Fluidization Symposium, April 4–9, 1982, Hangzhou, China* (1982).
- Ziegler, E., "Stand der Zement-Brennverfahren—Ofen, Vorwarmer, Kuhler, Feurungen," *Zement-Kalk-Gips* **24**, 543–553 (1971).

INDEX

B

- Baffling and particle distribution, 302
- Bed-collapsing
 - instrument for surface tracking, 332
 - modeling, 330
 - powder characterization by, 329
 - qualitative designation for, 335
- Biological reactors, conventional, 110, 113
 - design parameter estimations, 115
 - mass-transfer
 - gas-liquid, 117
 - liquid-solid, 120, 182, 183
 - power consumption, 115
- Bubbling fluidization and G/S contacting efficiency, 292

C

- Catalytic reactor, 68, 70
 - adsorber for transient studies, 79
 - ball-mill and traveling-grate, 79
 - basket-type, 72
 - fluidized bed with agitation, 78
 - internal recycle, 75
 - rotating packed-bed, 82
 - vibration-mixed, 80
 - wiper-blade, 75
- Conical fluidized beds, 264
 - basic parameters, 270
 - carting, 273
 - fully fluidized state, 270
 - hyperfluidization, 271
 - instability, 275
 - modeling, 265
 - phenomenological description, 265
 - ranges for operation, 272

- Contactors, gas-inducing, 25
 - critical impeller speed, 27
 - gas-liquid mass-transfer, 28
 - heat transfer, 29
 - rate, 27
- Countercurrent staging of concurrent dilute G/S systems, 307
- Cyclone spray reactor, 29

F

- Fluidization
 - fast, 313
 - evaluation of parameters, 318
 - regime diagram, 321
 - voidage distribution
 - longitudinal, 314
 - computing, 318
 - generalized, 223
 - accelerative motion, 234
 - nonideal systems, 322
 - polydisperse systems, 235, 264
 - steady-state motion, 225
 - idealization, 216
 - improving by particle size adjustment, 339
 - species, 211
- Fluidized beds, multistage, 290
- Fluidized leaching and washing, 238
 - characteristics, 238
 - experimental findings, 245
 - mixed particles, 243
 - rate measurement, 250
 - staged, 248
 - uniform particles, 241
- Fluidized state, 207
 - regimization, 214

G

Gas-liquid reactors, 10, 11
 conventional mechanically agitated, 10
 critical impeller speed, 13
 gas-liquid mass-transfer, 17
 correlations for $k_L a_L$
 gradientless, 180
 heat transfer, 20
 hydrodynamics, 11
 mixing and RTD, 15
 power consumption, 14

H

Heat recovery from calcine and flue gas, 313
 Hydrodynamic suspension, nature of, 208

L

Liquid-liquid reactors, 84
 dispersions, 95
 mass-transfer, 99
 scale-up, 98
 stirrer power, 97
 industrial, 100
 columns agitated with rotating stirrers, 105
 extractors
 centrifugal, 107
 vibrating-plate, 107
 measurement of drop size and coalescence rate, 190
 mixer-settler, 102
 pulsed column, 106
 pump, 105
 reciprocating sieve-plate column, 106
 Liquid-solid mass-transfer coefficient, determination, 182-3
 L/S systems, empirical deductions from, 216

M

Magnetizing roasting, 310
 Miscible liquids, mixing of two, 85
 correlation of mixing time, 85
 power consumption, 88

pumping capacity of stirrers, 91
 vortex depth in unbaffled stirred tanks, 93

Mixing-segregation equilibrium, 261

Mixing time, measurement, 186
 Danckwerts method, 186
 for viscous liquids, 187

Moving-bed

application, 275
 in generalized fluidization, 232
 upstart
 compressible media with, 275
 design for critical, 276
 noncritical, 281
 stability, 278

Multidisks reactor, 154

Multistage mechanically agitated reactors, 22
 mass-transfer, 24
 mixing, 23
 power consumption, 23

N

Novel reactors, 155, 159
 for polymerization reactions, 155
 for waste treatment, 132
 horizontal agitated contractors, 136
 rotating disk, 137
 rotating bubble column biological, 138
 surface aerators, 132
 UNOX oxygenation, 135
 Novel bioreactor designs, 122
 centrifugal film fermenter, 124
 plug flow processing, 130
 reciprocating, 129
 rotating disk, three-stage, 126
 stagnation jet, 127

O

Ore preheating, 308

P

Parameter estimations, experimental
 methods, 169
 bubble size, 171, 174
 gas holdup, 169

interfacial area, 171, 176
 volumetric mass-transfer coefficient, 178,
 179
 gas-side, 178
 and interfacial area, 178
 Particle-particle
 force, 210
 interaction and fluidizing quality, 345
 Particulate fluidization
 future prospects, 347
 notation, 349
 references, 351
 Polymerization reactors, 141
 fluid rheological considerations, 143
 gas-liquid mass-transfer, 147
 heat transfer, 148
 hydrodynamics and stirrer power in
 non-newtonian fluids, 144
 mixing and RTD, 145
 Propeller loop reactor, 154
 Pneumatically controlled downcomer, 284
 gas distribution, 286
 pressure drop, 285
 self-flow, 287
 Pneumatically started seal, 287
 Powder characterization by bed-collapsing,
 329
 Powder classification, 324
 Geldart's, 326
 Powder, quantifying fluidizing
 characteristics of, 335
 Power, measurement, 189

R

Raining-particles heat exchanger, 295
 experiments, 301
 pilot plants, 308
 for polydisperse particles, 300
 Reaction calorimeter, 149
 Reactor internals, 4
 Residence-time distribution (RTD),
 measurement, 189
 Rotating-cylinder reactor, 150
 Rotating packed-bed reactor, 82

S

Screw reactor, 153
 Segregation, degree, 258

Slurry reactor, 32, 33
 adiabatic, 58
 gas-induced agitated, 61
 mechanically agitated, 34
 aerated suspension, 47
 gas holdup, 49
 gas-liquid mass transfer, 53
 heat transfer, 58
 hydrodynamics, 35
 liquid-solid mass transfer, 57
 mixing, 51
 particle suspension, 42, 48
 power consumption, 38
 multiple-agitator, 60
 novel catalytic, 62
 cup-and-cap, 62
 falling-basket, 63
 with induction heaters, 64
 microreactors, 65
 rapid-injection, 64
 Solids mixing and segregation, 254
 operation shifts, 256
 reversal points, 258
 Special purpose reactors, 161
 chemical vapor deposition, 166
 rotary vertical batch, 166
 photochemical, 163
 rotating disk electrochemical, 161
 Stirrers, 5
 anchor, 6
 axial motion, 6
 helical ribbon, 7
 MIG and INTERMIG, 7
 paddle and propeller, 6
 blade, 6
 cross-beam, 6, 7
 grid, 6
 hollow, 8
 impeller, 6
 rotor-stator, 7
 turbine, 6
 Suspension culture reactors, magnetically
 stirred plant-cell, 121
 Synergism of binary particle mixtures, 347
 Systems with dilute raining-particles, 292

T

Thin-film reactors, 151

This Page Intentionally Left Blank